OCS Study
MMS 2000-052

FINAL REPORT

ENVIRONMENTAL SURVEY OF POTENTIAL SAND RESOURCE SITES: OFFSHORE NEW JERSEY

Volume I: Main Text

Prepared by:

Applied Coastal Research and Engineering, Inc.
766 Falmouth Road, Suite A-1
Mashpee, MA 02649

In Cooperation With:

Continental Shelf Associates, Inc.
Barry A. Vittor & Associates, Inc.
Aubrey Consulting, Inc.

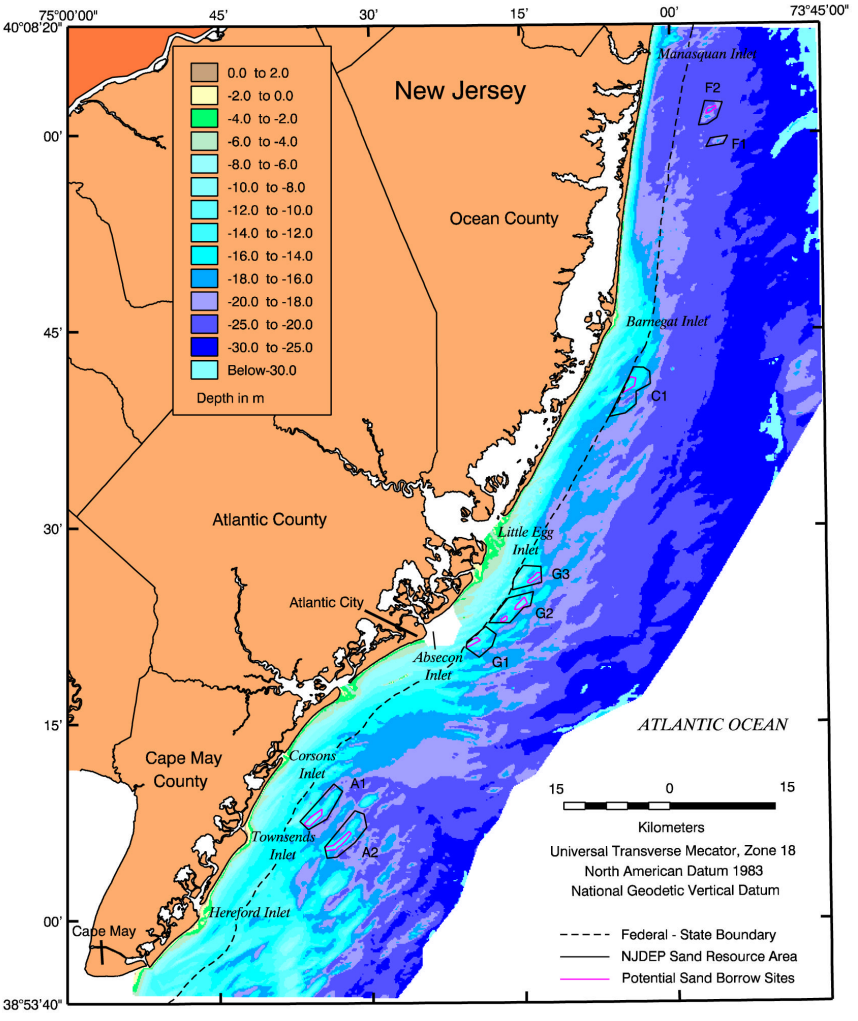

Prepared for:

U.S. Department of the Interior
Minerals Management Service
International Activities and Marine Minerals Division (INTERMAR)

Funded Under Contract Number 14-35-01-97-CT-30864

DISCLAIMER

This report has been reviewed by the Minerals Management Service and approved for publication. Approval does not signify that the contents necessarily reflect the views and policies of the Service, nor does mention of trade names or commercial products constitute endorsement or recommendation for use.

SUGGESTED CITATION

Byrnes, M.R., R.M. Hammer, B.A. Vittor, J.S. Ramsey, D.B. Snyder, J.D. Wood, K.F. Bosma, T.D. Thibaut, N.W. Phillips, 2000. Environmental Survey of Potential Sand Resource Sites: Offshore New Jersey. U.S. Department of the Interior, Minerals Management Service, International Activities and Marine Minerals Division (INTERMAR), Herndon, VA. OCS Report MMS 2000-052, Volume I: Main Text 380 pp. + Volume II: Appendices 291 pp.

FINAL REPORT

Environmental Survey Of Potential Sand Resource Sites: Offshore New Jersey

December 2000

Mark R. Byrnes
Physical Processes Project Manager, Co-Editor
(Applied Coastal Research and Engineering, Inc.)

Richard M. Hammer
Biological Component Project Manager, Co-Editor
(Continental Shelf Associates, Inc.)

With Contributions From:

Barry A. Vittor
Barry A. Vittor & Associates, Inc.

John S. Ramsey
Applied Coastal Research and Engineering, Inc.

David B. Snyder
Continental Shelf Associates, Inc.

Jon D. Wood
Applied Coastal Research and Engineering, Inc.

Kirk F. Bosma
Aubrey Consulting, Inc.

Tim D. Thibaut
Barry A. Vittor & Associates, Inc.

Neal W. Phillips
Continental Shelf Associates, Inc.

Prepared by:
Applied Coastal Research and Engineering, Inc.
766 Falmouth Road, Suite A-1
Mashpee, MA 02649

Prepared for:
U.S. Department of Interior
Minerals Management Service
International Activities and Marine Minerals Division (INTERMAR)
381 Elder Street, MS 4030
Herndon, VA 22070

In Cooperation With:
Continental Shelf Associates, Inc.
Barry A. Vittor & Associates, Inc.
Aubrey Consulting, Inc.

Contract Number 14-35-01-97-CT-30864

ACKNOWLEDGMENTS

Numerous people contributed to the project titled *Environmental Survey of Potential Sand Resource Sites: Offshore New Jersey*, which was funded by the U.S. Department of the Interior, Minerals Management Service (MMS), International Activities and Marine Minerals Division (INTERMAR). Mr. Barry S. Drucker provided assistance and direction during the project as the MMS Contracting Officer's Technical Representative. Ms. Jane Carlson served as the MMS Contracting Officer. Mr. Barry Drucker and Mr. Roger Amato of the MMS reviewed the draft document.

Dr. Mark R. Byrnes of Applied Coastal Research and Engineering, Inc. (Applied Coastal) served as Project Manager; Physical Processes Component Manager; authored Sections 1.0 (Introduction), 2.1 (Offshore Sedimentary Environment), 7.1 (Offshore Sand Resource Areas), 7.4.1 (Historical Sediment Transport Patterns), and Section 3.0 (Regional Geomorphic Change); co-authored with Dr. Richard M. Hammer Sections 7.7 (Potential Cumulative Effects), 8.0 (Conclusions); and was Co-Editor of the report. Dr. Richard M. Hammer of Continental Shelf Associates, Inc. (CSA) served as the Biological Component Manager, authored Sections 7.5.1 (Effects of Offshore Dredging on Benthic Fauna) and 7.5.2 (Recolonization Rate and Success), and was Co-Editor of the report.

Other Applied Coastal personnel who participated in the project included Mr. John S. Ramsey who led the nearshore sediment transport modeling component of the study. Mr. Ramsey authored Sections 2.2.5 (Nearshore Sediment Transport), 5.2.2 (Nearshore Sediment Transport Modeling), and 7.4.3 (Nearshore Sediment Transport Trends). Mr. Jon D. Wood authored Sections 5.1.1 (Historical Data Analysis), 5.1.2 (Summary of Flow Regimes at Offshore Borrow Sites), 7.3 (Currents and Circulation), and co-authored Section 2.2 (General Circulation). Ms. Feng Li was responsible for shoreline and bathymetry change data compilation and surface modeling. Ms. Jessica M. Côté assisted with data analysis and report preparation related to currents and circulation, and nearshore sediment transport modeling. Ms. Elizabeth A. Wadman was responsible for report compilation and editorial assistance during production of the report.

Additional CSA personnel who contributed to the project included Mr. David B.Snyder who served as Chief Scientist during Biological Field Survey 2; authored Sections 2.3.1.2 and 7.5.4 (Atlantic Surf Clam), 2.3.2.1 and 7.6.1 (Zooplankton), 2.3.2.2 and 7.6.2 (Squids), and 2.3.2.3 and 7.6.3 (Fishes); and incorporated sections from other authors concerning infauna, epifauna and demersal fishes, and discussion into the remainder of Section 6.0 (Biological Field Surveys) that he authored. Dr. Alan D. Hart led the sampling design and statistical analyses for the biological data. Dr. Neal W. Phillips wrote Sections 2.3.2.4 and 7.6.4 (Sea Turtles) and 2.3.2.5 and 7.6.5 (Marine Mammals). Mr. Paul S. Fitzgerald served as Chief Scientist during Field Survey 1 and Scientist for Survey 2. Mr. Thomas Quinney served as Scientist during Survey 1. Mr. Frederick B. Ayer, III directed the field surveys and pre-plotted the station locations. Mr. Lynwood R. Powell, Jr. produced the field survey post-plot figures. Ms. Melody Powell provided editorial assistance and supervised CSA support staff during production of the report.

Personnel from Aubrey Consulting, Inc. who contributed to the project included Mr. Kirk F. Bosma who led the wave transformation numerical modeling effort and co-authored Sections 4.0 (Wave Transformation Numerical Modeling), 5.1.3 (Wave-Induced Bottom Currents), 5.1.4 (Wave-Generated Currents), 5.2.1 (Sediment Transport at Borrow Sites), 7.2 (Wave Transformation), and 7.4.2 (Sediment Transport at Potential Borrow Sites). Mr. Steven Jachec provided technical assistance on Sections 4.0 (Wave Transformation Numerical Modeling) and 5.2.1 (Sediment Transport at Borrow Sites). Ms. Nadine Sweeney provided editorial assistance for the ACI portion of the report. Mr. Ken Israel and Dr. Dave Cacchione provided technical assistance on Section 5.1 (Currents and Circulation).

Personnel from Barry A. Vittor & Associates, Inc. (BVA) who contributed to the project included Dr. Barry A. Vittor, who served as Manager of BVA's responsibilities for the field surveys and report. Mr. Tim D. Thibaut authored Sections 2.3.1.1 and 6.3.3 (Infauna), 2.3.1.3 and 6.3.4 (Epifauna and Demersal Fishes), 6.4 (Discussion), and 7.5.3 (Predictions Relative to the Sand Resource Areas) of the report, with assistance from Dr. Vittor. Mr. J. Dobbs Lee served as Scientist during both field surveys. Mr. Joie M. Horn served as Scientist during Survey 2. Ms. Linda W. Sierke supervised personnel associated with taxonomic identifications. Mr. Felix Fernandez served as Manager for BVA's benthic infaunal data entry and analysis.

Dr. Wayne C. Isphording, from the University of South Alabama, was responsible for the laboratory grain size analyses. Dr. Rober J. Diaz and Mr. G. Randall Cutter Jr., from the Virginia Institute of Marine Science, conducted the sediment profiling camera aspects of the project.

TABLE OF CONTENTS

APPENDICES

LIST OF FIGURES

LIST OF TABLES

LIST OF ABBREVIATIONS

µ	micron
ACI	Aubrey Consulting, Inc.
ASTM	American Society for Testing Materials
BVA	Barry Vittor & Associates, Inc.
CEQ	Council on Environmental Quality
CERC	Coastal Engineering Research Center
CETAP	Cetacean and Turtle Assessment Program
CHL	Coastal Hydraulics Laboratory
cm	centimeter
CRC	Coastal Research Center
CSA	Continental Shelf Associates, Inc.
DEC	Division of Engineering and Construction
DGPS	Differential Global Positioning System
EA	Environmental Assessment
EEZ	Exclusive Economic Zone
EFH	Essential Fish Habitat
EIS	Environmental Impact Statement
ESA	Endangered Species Act
FMP	Fishery Management Plan
ft	feet
ha	hectare
INTERMAR	International Activities and Marine Minerals Division
km	kilometers
kts	knots
LEO	Long-Term Ecosystem Observatory
LPIL	Lowest Practical Identification Level
m	meter
MAB-NURC	Mid-Atlantic Bight National Undersea Research Center
MAFMC	Mid-Atlantic Fisheries Management Council
MARMAP	Marine Monitoring, Assessment, and Prediction Program
MCM	million cubic meters
MCY	million cubic yards
mi	statute mile
mm	millimeter
MMS	Minerals Management Service
MSL	Mean Sea Level
MWL	Mean Water Level
NAD	North American Datum
NEFMC	New England Fisheries Management Council
NEPA	National Environmental Policy Act
NGDC	National Geophysical Data Center
NGVD	National Geodetic Vertical Datum
NJDEP	New Jersey Department of Environmental Protection
NJGS	New Jersey Geological Survey
NMFS	National Marine Fisheries Service
NOAA	National Oceanic and Atmospheric Administration
OCS	Outer Continental Shelf
OCSLA	Outer Continental Shelf Lands Act
ODFS	Offshore Demersal Fishing Sampling
Ppt	parts per thousand
REF/DIF S	Refraction/Diffraction Model for Spectral Wave Conditions
sec	second
USACE	U.S. Army Corps of Engineers
USC & GS	U.S. Coast and Geodetic Survey
USDOI	U.S. Department of the Interior
USFWS	U.S. Fish and Wildlife Service
UTM	Universal Transverse Mercator
WIS	Wave Information Study
WISWAVE	Wave Information Study Wave Model
yd	yard
yr	year

1.0 INTRODUCTION

The coastal zone is a unique geological, physical, and biological area of vital economic and environmental value. Houston (1995) discusses the value of beaches to America's economy and their maintenance through beach nourishment. Not only are beaches the dominant component of most coastal economies, but they also provide a measured level of protection against high winds and waves associated with storms. This is particularly true in New Jersey where coastal development has flourished since the early 1900s. In fact, some of the earliest beach erosion control structures along the coast of New Jersey were built in the 1890s, and beach nourishment became an important component of coastal engineering and management in New Jersey in the 1960s (Wiegel and Saville, 1996). Miller (1993) stresses the importance of coastal and marine tourism as the world's largest industry and its continual rise over the past 50 years. As such, beaches are key elements of coastal tourism because they represent the leading tourist destination.

Coastal community master plans are being developed and revised to address concerns associated with population growth, storm protection, recreation, waste disposal and facilities management, and zoning (Williams, 1992; e.g., New Jersey Department of Environmental Protection (NJDEP) Shore Protection Master Plan and the U.S. Army Corps of Engineers New Jersey Shore Protection Study). Often, problems stemming from these issues are in direct conflict with natural coastal processes. Some of the more direct problems are related to coastal erosion and storm protection. The practice of replenishing beaches with sand from upland and nearshore sources as protection for community infrastructure has increased in direct relation to population growth. As coastal and nearshore borrow areas become depleted, and our knowledge of environmental effects of coastal sand mining develop, alternate sources of aggregate and beach fill must be evaluated for offshore sites to meet specific societal needs. In many cases, sand resource extraction from the Outer Continental Shelf (OCS) may prove environmentally preferable to nearshore borrow areas due to potential changes in waves and currents as large quantities of sand are dredged the seafloor.

Denmark, Japan, The Netherlands, and United Kingdom have been actively involved in marine mining of sand and gravel for the past few decades. The U.S. recognizes the potential benefits of sand and gravel mining on the OCS, as well as the potential for environmental impacts. The U.S. Department of the Interior (USDOI), Minerals Management Service (MMS) is responsible for managing the exploration and development of sand and gravel resources on the OCS seaward of State boundaries. In 1983, the MMS established the Office of Strategic and International Minerals for evaluating the prospects for and conditions under which sand and gravel mining would develop in the U.S. In 1991, the Office of International Activities and Marine Minerals (INTERMAR; now referred to as the International Activities and Marine Minerals Division) was created to develop strategies for addressing specific concerns regarding offshore sand and gravel mining operations (Hammer et al., 1993).

The MMS has significant responsibilities with respect to the potential environmental impacts of sand and gravel mining. Existing regulations governing sand and gravel mining provide a framework for comprehensive environmental protection during operations. Specific requirements exist for evaluations and lease stipulations that include appropriate mitigation measures (Hammer et al., 1993; Woodworth-Lynas and Davis, 1996). Guidelines for protecting the environment stem from a wide variety of laws, including the OCS Lands Act (OCSLA), National Environmental Policy Act (NEPA), Endangered Species Act, Marine Mammals Protection Act, and others. Regulations require activities to be conducted in a manner which prevents or minimizes the likelihood of any occurrences that may cause damage to the

environment. The MMS takes a case-by-case approach in conducting environmental analyses, as required by NEPA and the Council on Environmental Quality (CEQ) regulations.

In recent years, there has been increasing interest in sand and gravel mining on the OCS. Currently, eight Federal-State task forces, several cooperative agreements, at least five negotiated agreements, and six environmental surveys exist to ensure substantive government and public involvement and attention to regional, State, and local concerns regarding leasing, engineering, economic, and environmental aspects of sand and gravel mining (to obtain specific information regarding these activities, visit http://www.mms.gov/intermar/marineac.htm). Under the OCSLA, the MMS is required to conduct environmental studies to obtain information useful for decisions related to negotiated agreements and lease activities. As such, the MMS pursues its responsibilities for management of offshore sand and gravel mining vigorously by:

- Protecting ocean and coastal environments by ensuring that all OCS sand and gravel mining activities are environmentally acceptable;
- Ensuring the OCS sand and gravel activities are compatible with other uses of the ocean;
- Involving coastal States in all aspects of sand and gravel mining activities; and
- Evaluating the potential of the OCS as a domestic source for sand and gravel resources.

To this end, the MMS initiated four environmental studies along the Atlantic and Gulf coasts in FY97 to provide information for programmatic marine mining decisions at MMS Headquarters and OCS Regional Offices. This report presents the results of the second of four environmental studies administered through INTERMAR. Entitled “Environmental Study of Identified Sand Resource Areas: Offshore New Jersey”, this program was initiated by Aubrey Consulting, Inc. (ACI) in September 1997 under MMS Contract No. 14-35-01-97-CT-30864. This report was prepared by Applied Coastal Research and Engineering, Inc. (Applied Coastal) in cooperation with Continental Shelf Associates, Inc. (CSA), ACI, and Barry A. Vittor & Associates, Inc. (BVA).

1.1 STUDY AREA AND BORROW SITE CHARACTERISTICS

The inshore portion of the continental shelf, seaward of the Federal-State OCS boundary and within the New Jersey Exclusive Economic Zone (EEZ), encompasses the project study area (Figure 1-1). The seaward limit of the study area is generally within about 20 km of the shoreline. Sand resource areas are located on the New Jersey OCS between the 10- and 20-m depth contours. The continental shelf surface within the study area contains many first-, second-, and third-order morphologic features formed during the Holocene transgression (McKinney et al., 1974; Figure 1-1). Sand ridges 2- to 5-m high and 0.5- to 1.5-km apart represent second-order features that are the primary sand resource targets of this study.

Eight potential sand resource areas were defined within the study area through a Federal-State cooperative agreement between MMS-INTERMAR and the New Jersey Geological Survey (NJGS) (Figure 1-1). Uptegrove et al. (1995, 1997) describe program goals and accomplishments for the first two years of the program. Based on regional variations in coastal erosion trends and the availability of existing geologic data, the area offshore Townsends Inlet was selected for detailed sand resource evaluation in Phase II of the MMS/NJGS cooperative. Smith (1996) used existing and newly acquired shallow seismic and vibracore data to characterize the sand resource potential for Resource Areas A1 and A2. The remaining six sand resource areas currently are being evaluated by the NJGS in cooperation with the Institute of

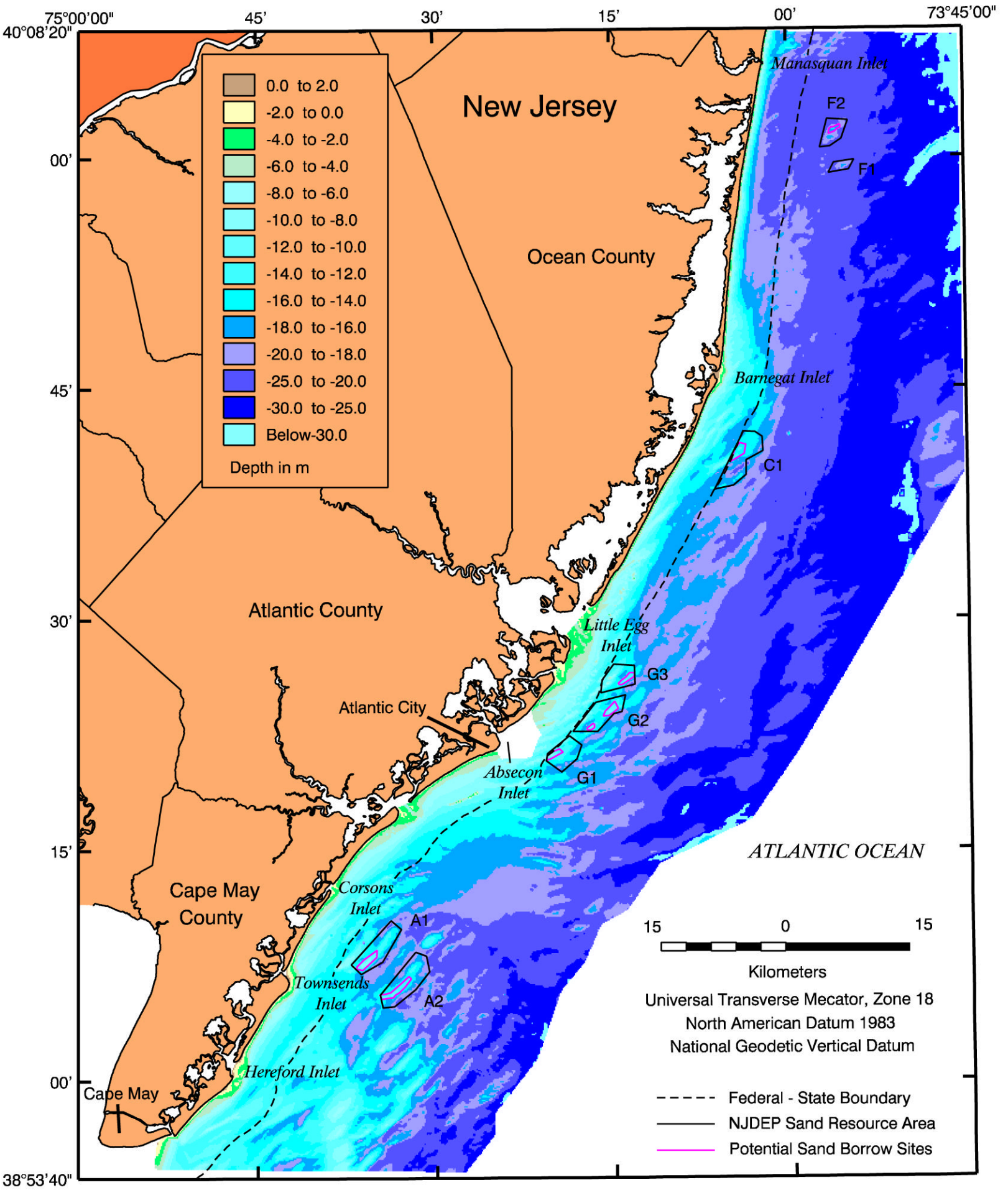

Figure 1-1. Location diagram illustrating sand resource areas and the Federal-State boundary relative to the 1934/77 bathymetry.

Marine and Coastal Sciences, Rutgers University, using new vibracore and shallow seismic data. Eight potential sand resource areas within the study region were evaluated to determine the potential impacts of offshore sand mining for beach replenishment (see Section 7.0). Areas A1, A2, G1, G2, G3, C1, and F2 contain borrow sites with the greatest potential for use in the future. Sand Resource Area F1 was not included in the physical processes analysis because the quantity of sand available for beach nourishment is small (<1 million cubic meters [MCM]) relative to basic replenishment needs, and water depths are greatest in this region, making potential dredging operations more complicated and costly.

For sand resource areas on the New Jersey continental shelf, maximum shoal relief is on the order of 5 m, and average shoal relief is about 3 m. Although modern beach replenishment practice varies depending on geographic location and level of funding for the New Jersey coast, it is reasonable to expect multiple replenishment events over the next 50 years from the designated sand resource areas. As such, shoal deposits were selected as potential borrow sites for each of the sand resource areas based on geological characteristics (Tables 1-1 and 1-2). A maximum excavation depth was determined for each site. In Area A1, a 2.21×10^6 m^2 borrow site was defined based on shoal morphology (Figure 1-1). Bathymetric data and geological samples indicate a maximum excavation depth of 4 m, resulting in a 8.8 MCM extraction scenario; median grain diameter for the deposit is 0.35 mm (Table 1-1). The same procedure was used for selected borrow sites at the other six sand resource areas. The borrow site in Area A2 encompassed 2.60×10^6 m^2 of seafloor to a depth of 3 m, resulting in 7.8 MCM of sand. The borrow site for Area G1 covers 1.12×10^6 m^2 of seafloor to a maximum excavation depth of 4 m. The borrow site contains 4.5 MCM of sand. For the borrow site in Areas G2 and G3, surface areas encompassed 1.44×10^6 and 1.09×10^6, respectively. Maximum excavation depth for each ridge was 3 m, resulting in 4.3 and 3.3 MCM of sand, respectively. The potential borrow site in Area C1, seaward of Long Beach Island, included 2.04×10^6 m^2 surface area, a 3-m excavation depth, and a 6.1 MCM extraction scenario. The northernmost resource area (F2) contains the smallest borrow site (0.69×10^6 m^2). With an excavation depth of 3 m, 2.1 MCM of sand and gravel would be available for beach replenishment purposes. The sand volume at each of these borrow sites is at least equal to the quantity of sand available for any single expected replenishment event, so all analyses were used to estimate potential cumulative effects of multiple extraction scenarios.

Table 1-1. Sand Resource Characteristics at Potential Borrow Sites in Resource Areas Offshore New Jersey.

Resource Area	Sand Volume (MCM)	Excavation Depth (m)	D10 (mm)	D50 (mm)	D90 (mm)	% Sand & Gravel
A1	8.8	4	0.6	0.35	0.21	100
A2	7.8	3	1.6	0.62	0.30	100
G1	4.5	4	0.85	0.41	0.19	100
G2	4.3	3	1.4	0.66	0.30	100
G3	3.3	3	0.9	0.51	0.26	100
C1	6.1	3	0.4	0.20	0.14	100
F1	Too small	Too shallow	-----	-----	-----	-----
F2	2.1	3	2.4	0.46	0.27	100

D10 = grain diameter above which 10% of the distribution is retained; D50 = median grain diameter; D90 = grain diameter above which 90% of the distribution is retained

Table 1-2. UTM Coordinates defining borrow site polygons offshore New Jersey.

UTM Coordinates (Zone 18, NAD83, meters)	Borrow Site in Area A1	Borrow Site in Area A2	Borrow Site in Area G1	Top Borrow Site in Area G2
	536032.8 4332649.5	539873.1 4329460.7	556555.0 4355987.6	564718.5, 4362615.3
	534475.3 4331494.5	538814.6 4328536.9	556489.1 4355463.0	565141.0, 4361760.6
	533589.7 4330606.1	537692.6 4327510.5	557069.7 4355744.5	564416.6, 4361186.9
	533650.7 4330339.6	536972.8 4327305.2	558455.2 4356486.7	563994.1, 4360882.5
	534322.6 4330221.1	536358.9 4327264.1	558033.0 4356896.1	563330.0, 4360847.4
	536002.3 4331761.1	536612.9 4326709.9	557201.6 4356550.6	563535.3, 4361409.4
	536032.8 4332649.5	537226.8 4326853.6	556555.0 4355987.6	564102.7, 4361959.6
		537967.8 4326874.1		564718.5, 4362615.3
		538306.5 4327264.1		564718.5, 4362615.3
		538708.8 4327510.5		565141.0, 4361760.6
		539407.4 4328167.4		564416.6, 4361186.9
		540148.3 4329214.4		
		539873.1 4329460.7		
	Bottom Borrow Site in Area G2	Borrow Site in Area G3	Borrow Site in Area C1	Borrow Site in Area F2
	562074.4 4359922.5	566467.9, 4366055.3	578604.8, 4391437.7	591822.8, 4432075.9
	561398.2 4359395.7	567060.5, 4366045.7	579250.1, 4393066.7	591667.7, 4432062.2
	561398.2 4359184.9	567040.7, 4365739.2	579770.7, 4393773.4	591216.5, 4431802.4
	561675.9 4359138.1	566951.8, 4365547.7	580499.5, 4393571.5	591075.5, 4431706.7
	562086.4 4359302.0	565628.4, 4364637.9	580326.0, 4392460.9	590779.4, 4431720.4
	562255.5 4359465.9	565243.2, 4364637.9	579215.4, 4391787.9	590553.8, 4431529.0
	562231.3 4359828.8	565144.4, 4364772.0	578604.8, 4391437.7	590469.2, 4431296.6
	562074.4 4359922.5	565509.9, 4365135.9	578604.8, 4391437.7	590426.9, 4430941.1
		566053.1, 4365538.1	579250.1, 4393066.7	590835.8, 4431105.1
		566467.9, 4366055.3		591146.0, 4431228.2
		566467.9, 4366055.3		591611.3, 4431624.7
		567060.5, 4366045.7		591851.0, 4431679.4
				591822.8, 4432075.9

1.2 STUDY PURPOSE

The primary purpose of this study was to address environmental concerns raised by the potential for dredging sand from the OCS offshore the State of New Jersey for beach replenishment and to document the findings in a technical report. The primary environmental concerns focused on biological and physical components of the environment. To this end, seven study objectives were identified:

- Compile and analyze existing oceanographic literature and data sets to develop an understanding of baseline environmental conditions offshore New Jersey and the ramifications of dredging operations at selected sand borrow sites;

- Design and conduct biological and physical field data collection efforts to supplement existing resources;
- Analyze the physical and biological field data sets to address basic environmental concerns regarding potential sand dredging operations;
- Use physical processes data sets and wave climate simulations to predict wave transformation under natural conditions and in the presence of proposed dredging activities;
- Determine existing coastal and nearshore sediment transport patterns using historical data sets, and predict future changes resulting from proposed sand dredging operations;
- Evaluate the potential environmental effects of multiple dredging scenarios; and
- Develop a document summarizing the information generated to assist with decisions concerning preparation of an Environmental Assessment/Impact Statement to support a negotiated agreement.

In meeting these objectives, this document should provide invaluable information regarding environmental concerns examined relative to proposed future sand dredging in support of beach replenishment needs from offshore New Jersey.

1.3 STUDY APPROACH

Biological and physical processes data were collected and analyzed to assess the potential impacts of offshore dredging activities within the study area to minimize or preclude long-term adverse environmental impacts at potential borrow sites and along the coastline landward of resource areas. In addition, wave transformation and sediment transport numerical modeling were employed to simulate the physical environmental effects of proposed sand dredging operations to ensure that offshore sand resources are developed in an environmentally sound manner.

Five primary study elements were outlined in Task 1 (Data Collection and Analysis) of the Request for Proposals for addressing environmental concerns associated with offshore sand dredging for beach replenishment. They included:

- Assessment of baseline benthic ecological conditions, using existing data sets and data collected from field work, in and around the proposed sand borrow areas;
- Evaluation of the benthic infauna present in the proposed borrow areas, and assessment of the potential effects of offshore sand dredging on these organisms, including an analysis of the potential rate and success of recolonization following dredging;
- Development of a schedule of best and worst times for offshore sand dredging in relation to transitory pelagic species;
- Evaluation as to the potential modification to waves that propagate within the study area due to offshore sand dredging within the proposed sand borrow areas; and
- Evaluation of the impact of offshore dredging and consequent beach replenishment in terms of potential alteration to sediment transport patterns, sedimentary environments, and impacts to local shoreline processes.

The first three study elements focused primarily on biology and associated ecological impacts relative to potential sand dredging operations. The final two elements concentrated on potential alterations to physical processes and sedimentary environments, as well as potential shoreline response to incident waves and currents resulting from dredging operations. The scientific approach used to address each of the study elements is presented below. The remaining study tasks (2-14) focused on document preparation and project management requirements.

1.3.1 Baseline Ecological Conditions

The goal of this study element was to assess baseline benthic ecological conditions in and around the eight sand resource areas. This phase of the study primarily focused on field data collection efforts conducted in May and September 1998 (presented in detail in Section 6.0). However, existing literature and data were compiled and summarized to characterize the ecological environment and to form the foundation upon which field surveys were designed. Biological field surveys were conducted to characterize infauna, epifauna, demersal fishes, sediment grain size, and water column parameters.

1.3.2 Benthic Infaunal Evaluation

The goal of this study element was to assess the potential effects of offshore dredging on benthic infauna and analyze the potential rate and success of recolonization following cessation of dredging activities. Existing literature and data on dredging effects were searched and synthesized then combined with results from the biological field surveys to examine potential benthic effects and recolonization in the sand resource areas.

1.3.3 Project Scheduling

The goal of this study element was to determine the best and worst times for offshore dredging relative to pelagic species. Environmental windows are temporal constraints placed on dredging activities to protect biological resources from potentially detrimental effects (Dickerson et al., 1998). Existing information was collected and summarized concerning the seasonal occurrence of pelagic species and potential impacts from dredging. Project scheduling considerations for pelagic species then were analyzed based on this information.

1.3.4 Wave Modifications

The goal of this study element was to perform wave transformation numerical modeling to predict the potential for adverse modification of waves resulting from sand dredging operations. Changes in bathymetry in sand resource areas can cause wave energy focusing resulting in substantial alterations in sediment transport at the site of dredging operations, as well as along the shoreline landward of borrow sites. Because the purpose of dredging offshore sand from a specific site will be driven by the need for beach replenishment, it is critical to understand the impact of changing wave transformation patterns on shoreline response before potentially exacerbating a problem. Numerical comparisons of pre-and post-dredging impacts provided a means of documenting modifications to waves as they crossed the seven sand resource areas (detailed in Section 4.0).

1.3.5 Sediment Transport Patterns

The goal of this study element was to predict changes in sediment transport patterns resulting from potential sand dredging operations using numerical information generated from wave transformation modeling, combined with existing offshore current data. Sediment transport rates were quantified for sand resource areas using an analytical approach, whereas

transport rates at the shoreline were determined numerically using output from wave transformation numerical modeling (detailed in Section 5.0).

Historical shoreline and bathymetric data were compiled to document regional sediment transport patterns over a 40- to 80-yr time period. Net changes in sediment erosion and deposition on the shelf surface offshore New Jersey provided a direct method for identifying patterns of sediment transport and quantifying net rates of change throughout the potential sand resource areas (detailed in Section 3.0). These data also were used to calibrate numerical results for direction and magnitude of sediment transport.

1.4 DOCUMENT ORGANIZATION

Information presented in this document represents the culmination of a year and a half of work among experts in the fields of biology (CSA and BVA) and coastal processes (Applied Coastal and ACI), under the direction of Mr. Barry Drucker (MMS INTERMAR). This document was organized into nine major sections as follows:

- Introduction
- Environmental Setting
- Regional Geomorphic Change
- Wave Transformation Numerical Modeling
- Circulation and Sediment Transport Dynamics
- Biological Field Surveys
- Potential Effects
- Conclusions
- Literature Cited

The sections are presented in a different order than the list of study elements in the RFP. Because benthic and pelagic biological characteristics are in part determined by spatially varying physical processes throughout the study area, physical processes analyses are summarized first.

In addition to the main document, appendices were prepared in support of many of the analyses presented in each section of the report. Furthermore, an Executive Summary, a Technical Summary, and a Non-Technical Summary will be prepared as separate documents to provide a brief description of study methods and findings for audiences ranging from researchers to non-technical people.

2.0 EXISTING LITERATURE

The outer coastline of New Jersey is approximately 210 km long and represents part of the passive, slowly subsiding eastern North American continental margin (Klitgord et al., 1988; Smith, 1996). Coastal features are represented by a series of barrier beaches and islands, punctuated by inlets that allow the exchange of sediment and water between estuaries and the continental shelf, primarily as a function of tide (Figure 2-1). The project area extends from approximately 40°08'N latitude (Manasquan Inlet) to 38°55'N latitude (Cape May). Although the offshore Federal-State jurisdictional boundary marks the direct landward limit of the study area (see Figure 1-1), the ultimate use of sand extracted from the OCS is for beach replenishment along the New Jersey outer coast. Consequently, a description of the environmental setting from the outer coast to the OCS is pertinent for addressing the overall study purpose.

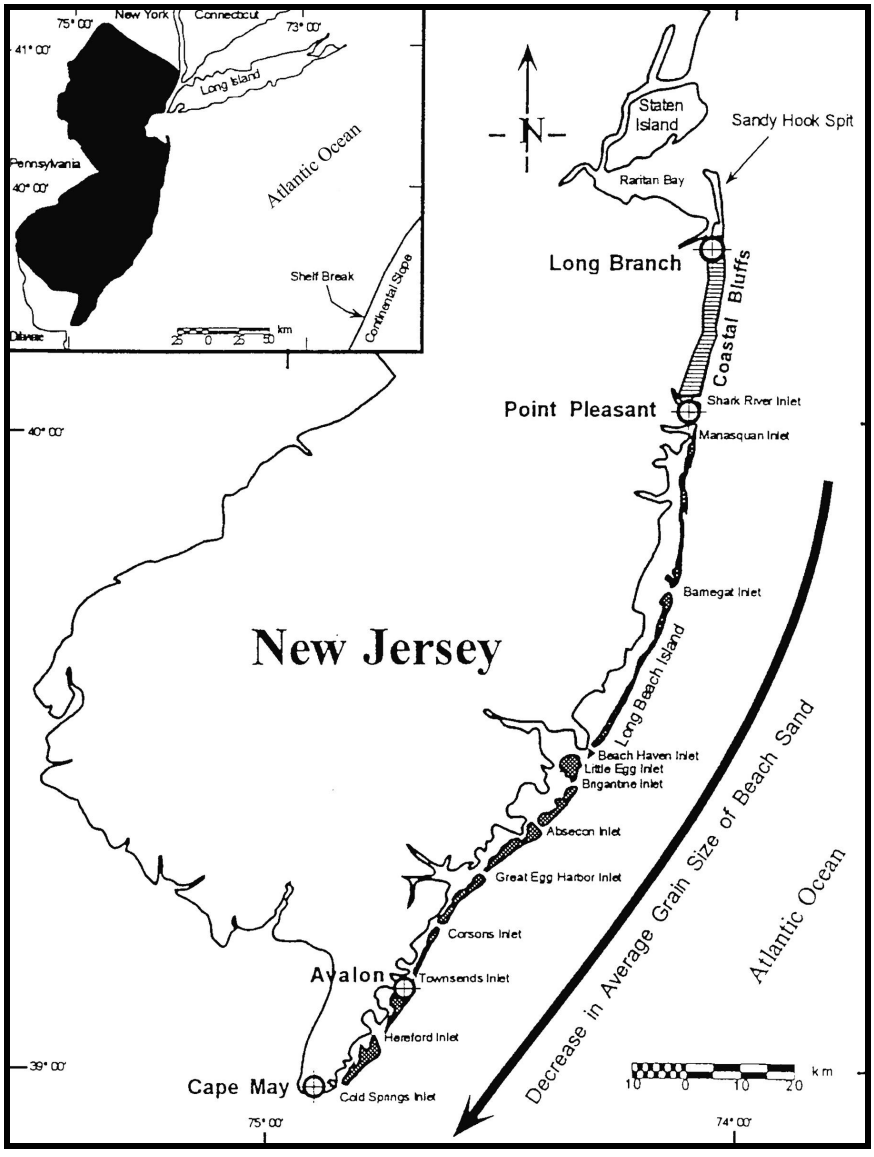

Figure 2-1. Coastal New Jersey and vicinity (from Smith, 1996).

Along the northern portion of the coast, beaches have formed at the base of Cretaceous, Tertiary, and Quaternary bluffs that extend up to 8 m above mean sea level (MSL; Uptegrove et al., 1995). These eroding bluffs are the primary source of coastal sediment to adjacent beaches in northern New Jersey, where wave-generated longshore currents distribute eroding sediment into spit deposits and barrier islands (e.g., Sandy Hook Spit; Figure 2-1). Throughout this area, mean grain size on the beaches decreases with distance from the eroding coastal bluffs and as the mineralogical composition of sand changes south of Long Beach Island (Uptegrove et al., 1995).

Along the barrier island shoreline from Manasquan Inlet south to Cape May, islands within this continuous chain range in length from 8 to 29 km, protecting estuarine and coastal plain environments from direct wave attack. Landward of the barrier islands, estuaries, salt marshes, and tidal channels encompass the Intracoastal Waterway (Smith, 1996). Eleven tidal entrances separate the barrier islands, resulting in complex tidal currents that produce lateral migration and redistribution of sand along adjacent shorelines (Ashley, 1987). To maintain navigability at these inlets, five have been stabilized with parallel rock jetties (Shark River, Manasquan, Barnegat, Absecon, and Cold Springs); three have been partially stabilized with one rock jetty or rock armoring on one shoreline (Great Egg, Townsends, and Hereford); and three inlets have remained natural (Beach Haven/ Little Egg, Brigantine, and Corsons) (Uptegrove et al., 1995). Five of the inlets require regular maintenance dredging, and sand derived from these projects is placed on adjacent beaches as nourishment material in accordance with New Jersey's Rules on Coastal Zone Management (Mauriello, 1991).

Development of beaches for recreational purposes along the coast of New Jersey started in the mid-1800s because of the excellent barrier island beaches and warm climate and ocean water in the summer months. In addition, the beaches were near the metropolitan areas of New York and Philadelphia and accessible by boat, wagon, and later rail (Quinn, 1977). The first developments at the beaches were in Cape May, Long Branch, and Atlantic City (Wicker, 1951). Piers and boardwalks were built, along with shoreline protection structures to combat the forces of ocean waves at the coastline. Beach nourishment has been employed at a number of vulnerable beach erosion "hot spots" to protect upland areas from storm damage and for recreational purposes since the 1950s. The availability of sand to replenish eroding beaches continues to be a concern to local, State, and Federal resource agencies, prompting the exploration and environmental evaluation of offshore resource areas for future use.

2.1 OFFSHORE SEDIMENTARY ENVIRONMENT

Seafloor topography and Holocene sediment distribution on the New Jersey continental shelf reflect a combination of processes, including regression during the late-Pleistocene, reworking of the exposed shelf surface by ancient fluvial systems, and reworking of the exposed shelf surface by coastal processes during the subsequent Holocene rise in sea level (Duane and Stubblefield, 1988). Redistribution of sediment by waves and currents during transgression partially or totally destroyed geomorphic features associated with Pleistocene fluvial environments. Concurrently, these same processes formed modern shelf deposits as subaerial coastal features became submerged and reworked during relative rising sea level. As such, much of the shelf offshore New Jersey is sand (Figure 2-2) (Knebel, 1981).

Sea level rise across the New Jersey continental shelf probably was interrupted by a series of near stillstands followed by rapid rises during the Holocene (Duane and Stubblefield, 1988). This process resulted in a series of shore-parallel features that have been interpreted as old shorelines composed of sand (Figure 2-3; Uchupi, 1968; Knebel and Spiker, 1977; Swift, 1976). Large parts of the New Jersey continental shelf surface contain shoreface sand ridges oriented obliquely to the modern shoreline (Figure 2-4; Swift et al., 1972; Stubblefield et al.,

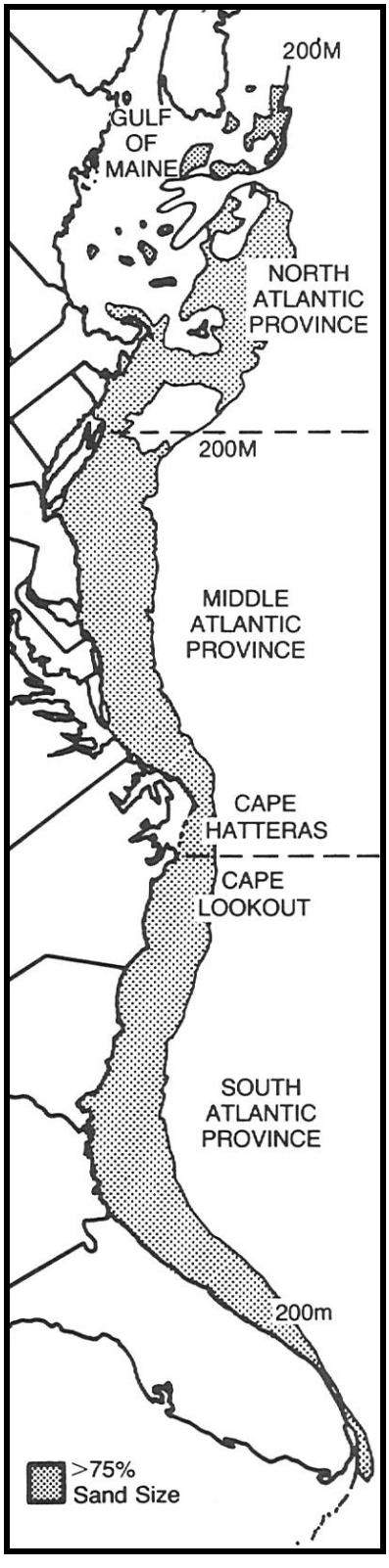

Figure 2-2. Map of the Atlantic continental shelf illustrating the dominant surface sedimentary facies as >75% sand sized material (from Duane and Stubblefield, 1988).

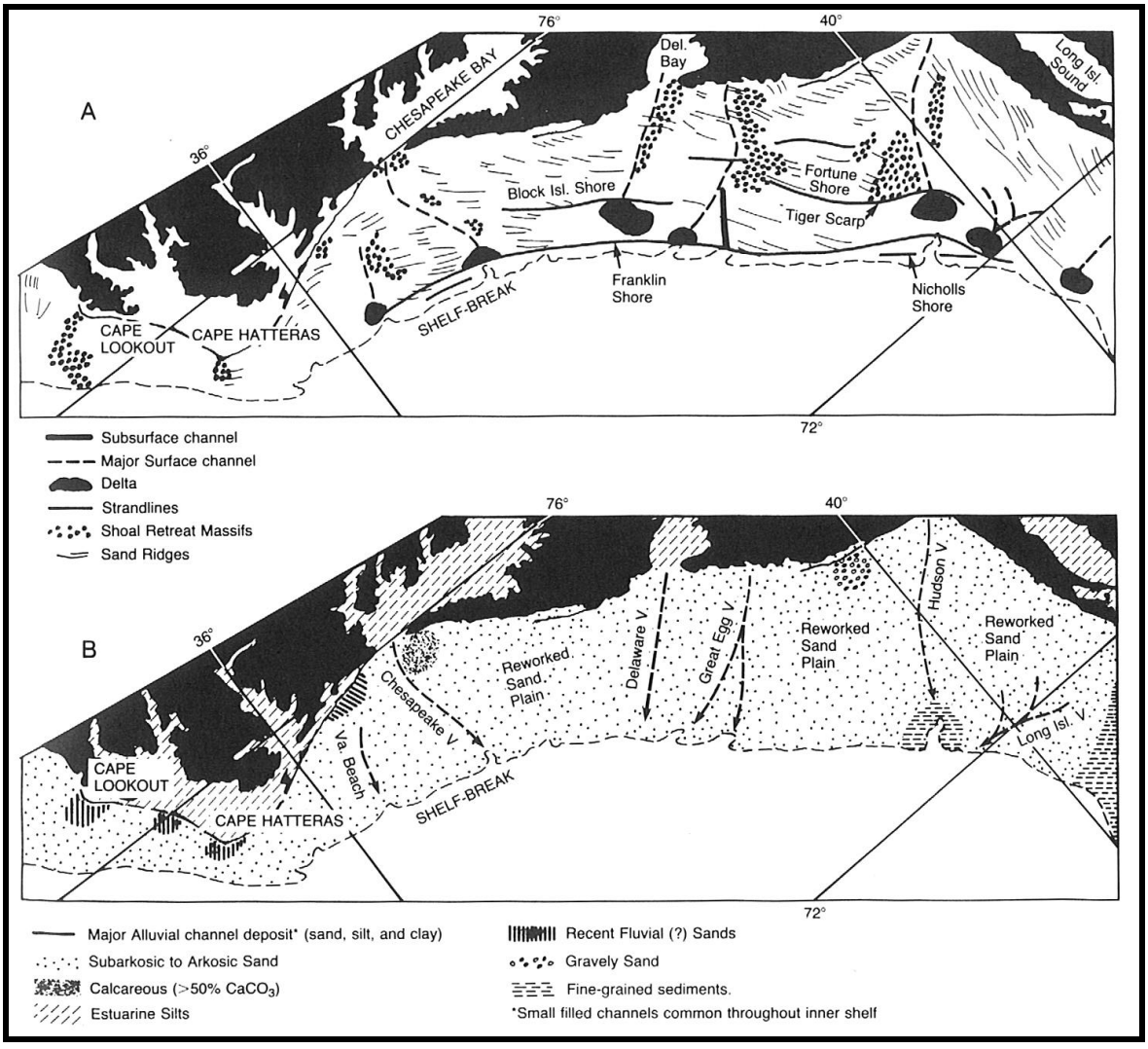

Figure 2-3. A summary of the: A) Pleistocene-Holocene paleoenvironments of the Middle Atlantic Province and B) sedimentary facies for the same area. Data from Emery and Uchupi, 1965; Uchupi, 1968; Swift, 1976. Figure from Duane and Stubblefield (1988).

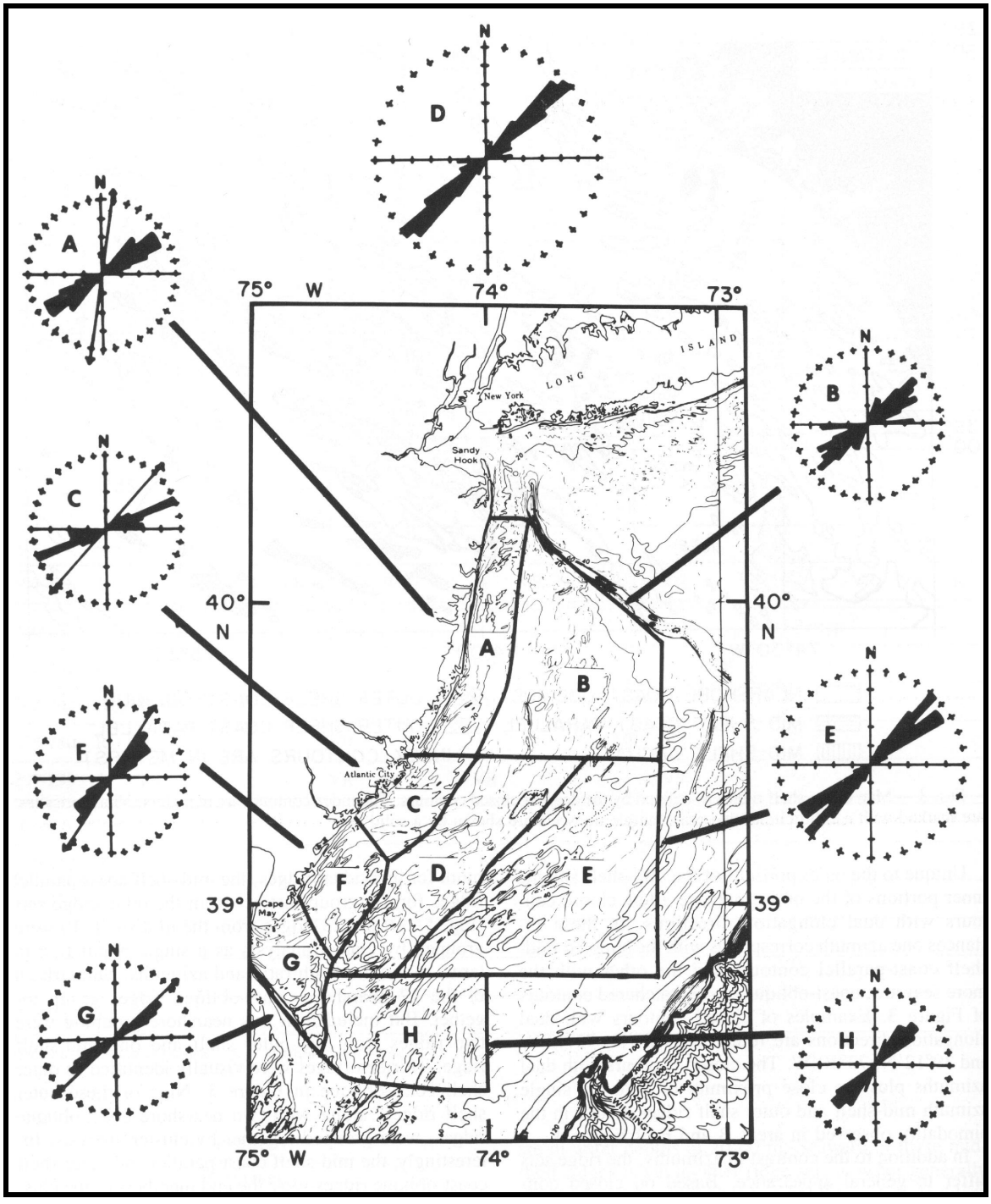

Figure 2-4. Sand ridge orientations for the New Jersey continental shelf. Each division on the x-y axis of the rose diagrams represents a value of two, and the compass rose is divided into 10° units. The study area includes regions A, C, F, and G (from Stubblefield et al., 1984).

1984; McBride and Moslow, 1991). Within the study area, average ridge spacing varies from 1 to 6 km, ridge length varies from 2 to 7 km, and ridges trend approximately 15 to 30° relative to the shoreline. The following sections describe these shoreface deposits in greater detail.

2.1.1 Seabed Morphology

The New Jersey continental shelf can be divided into two regions based on regional seafloor geomorphology. The shelf surface north of Barnegat Inlet is steeper than that seaward of southern beaches, as illustrated by the position of the 18-m depth contour relative to the Federal-State jurisdictional boundary (see Section 3.2 for details on nearshore bathymetry). Bathymetric contours north of Barnegat Inlet are primarily straight and parallel to -18 m, whereas those to the south contain numerous shoreface ridges with oblique orientations to the coast (Stubblefield et al., 1984; McBride and Moslow, 1991; see Figure 1-1). South of Barnegat Inlet, it is rare when the 18-m depth contour exists landward of the Federal-State boundary; however, north of this point, it is rare when the 18-m depth contour resides seaward of the Federal-State boundary.

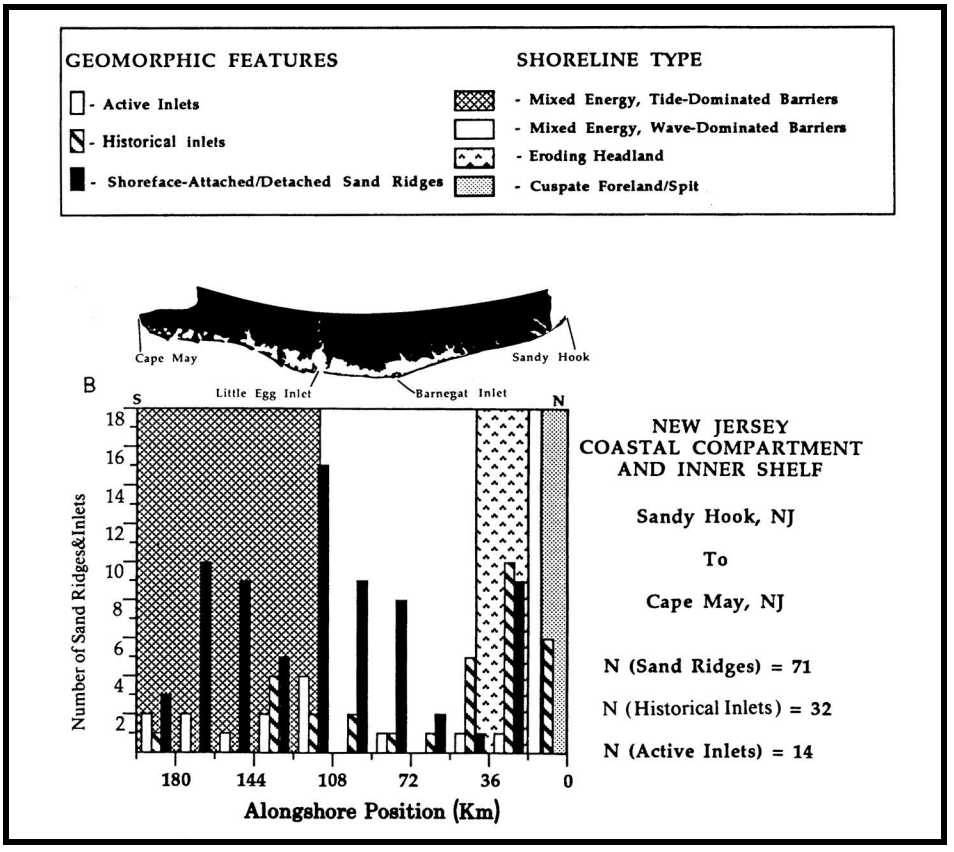

Figure 2-5. Distribution of shoreface sand ridges and tidal inlets for the New Jersey coast (from McBride and Moslow, 1991).

Along the southern New Jersey coast, McBride and Moslow (1991) illustrate that numerous shoreface sand ridges are associated with mixed-energy, wave- and tide-dominated barrier shorelines (Figure 2-5). They show that the number of ridges and inlets per length of coast are identical for these shoreline types. However, inlet morphology associated with wave-dominated barrier beaches consistently migrates to the south, and that associated with tide-dominated beaches remain relatively stationary or migrate north and south with time.

Nearshore, coast-oblique ridges seaward of the southern coast, as defined by Uptegrove et al. (1995), average about 4.2 m high, 2.7 km wide, and 3.4 km apart (Figure 2-6; Stubblefield et al., 1984). The ridges have an average orientation of 58°, and they intersect the coastline at an average of 25 ± 5°.

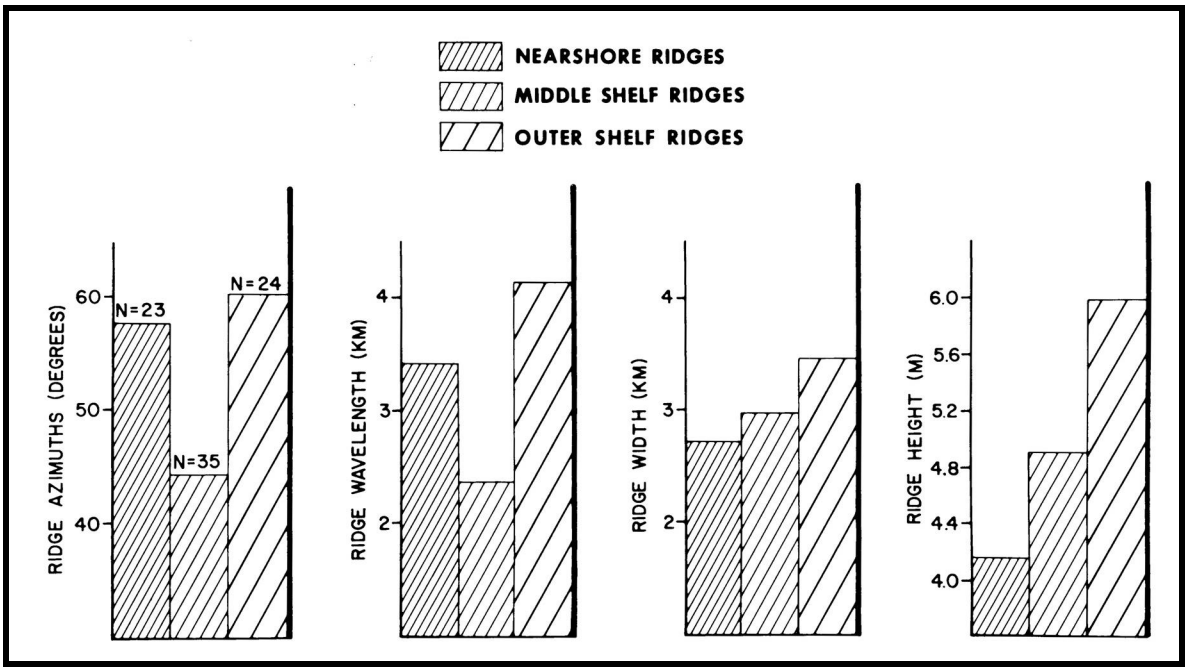

Figure 2-6. Average ridge azimuth (orientation), wavelength (spacing), width, and height for sand ridges on the New Jersey continental shelf (from Stubblefield et al., 1984).

Nearshore sand ridges on the New Jersey continental shelf, as described by Duane et al. (1972), Swift (1976), Meisburger and Williams (1980, 1982), Stubblefield et al. (1984), Duane and Stubblefield (1988), McBride and Moslow (1991), and Smith (1996), provide a primary source of sand-sized sediment for potential beach nourishment activities. Each of the potential sand borrow sites, located in sand resource areas identified by the NJGS (see Figure 1-1), are located on these ridges, except for Resource Areas F1 and F2 that exist southeast of Manasquan Inlet as relict fluvial deposits in 15- to 20-m water depth. Sand Resource Areas C1, G1, G2, and G3 exist just seaward of the Federal-State boundary between Barnegat and Absecon Inlets. Water depth over the ridges ranges from 8 to 12 m, and relief above the surrounding seafloor ranges from 3 to 6 m. To the south and seaward of Townsends Inlet, Sand Resource Areas A1 and A2 contain the largest potential borrow sites and the greatest sand volumes. The sand ridges are continuous throughout the resource areas, water depths over the ridge crests are 8 to 9 m, and relief above the surrounding seafloor is about 5 to 6 m.

Over the past 30 years, numerous hypotheses have been used to explain the origin of shoreface sand ridges. Based on bathymetric analysis and grain size characteristics, McKinney and Friedman (1970) concluded that shoreface sand ridges reflected Pleistocene coastal plain fluvial drainage topography, modified by modern coastal processes. Emery et al. (1967), Uchupi (1970), McClennen and McMaster (1971), and Sanders and Kumar (1975) described sand ridges of the U.S. Middle Atlantic Bight as indicative of overstepped coastlines. Duane et al. (1972), Swift et al. (1972), Field and Duane (1976), and Swift and Field (1981) concluded that shoreface ridges were produced and maintained by post-transgressive wave and current processes. Knebel and Spiker (1977) and Stubblefield et al. (1984) argued that shelf

sand ridges reflect a combination of degraded barrier deposits reworked by shelf currents and post-transgressive deposits. McBride and Moslow (1991) evaluated the geomorphology of hundreds of shoreface sand ridges and determined a genetic link between tidal inlet shoal deposits and sand ridges. They also stated that not all ridges can be explained by their ridge evolution model. Snedden et al. (1994) concluded that the ridge-evolution model of McBride and Moslow (1991) best explained the development of Peahala Ridge (New Jersey), where a combination of long-term transgressive and short-term hydrodynamic factors determined the present morphology and internal structure of the ridge.

Smith (1996) and Uptegrove et al. (1997) document the importance of offshore sand ridges as potential borrow sites for beach-quality sediment. These deposits exist in State and Federal waters, but potential physical environmental impacts for a specific project of set size and extraction requirements are expected to be minimized as distance from shore increases. The abundance of sand ridges on the New Jersey continental shelf (Figures 2-4 and 2-5) provides potential borrow sites to meet sand resource requirements for beach nourishment within the confines of State and Federal environmental regulations.

2.1.2 Surface Sediments

Surface sediments throughout the study area are composed primarily of fine- to medium-grained, quartz sand with varying mixtures of gravel and silt (Milliman, 1972; Knebel, 1981; Poppe et al., 1994; Figure 2-7). The sand typically is unimodal and well sorted, and deposits were formed by glacial, wave, and current processes reworking underlying Coastal Plain formations (Poppe et al., 1994). Although McMaster (1954) defined a southward fining trend in mean grain size along New Jersey beaches (0.4 to 0.5 mm at Sandy Hook to 0.1 to 0.2 mm at Cape May), Meisburger and Williams (1980, 1982) document a relatively consistent medium- to coarse-grained sand on the surface of offshore linear sand ridges between Barnegat and Townsends Inlets. However, Amato (1994) states that gravel content in sediment offshore Monmouth and Ocean Counties is greater than in sediments offshore Atlantic and Cape May Counties. In fact, sediment in Resource Areas F1 and F2 have the coarsest median diameter of any other resource area in the study region (see Appendix D4). Schlee (1964) attributes these gravel deposits to fluvial processes associated with the drowned Hudson River Valley that extends across the continental shelf east of New Jersey (see Poppe et al., 1994).

Frank and Friedman (1973) document the textural variability of surface sediment between southern Long Beach Island and Absecon Inlet, seaward to the shelf break. The mean grain size on the shelf is predominantly medium sand, but the distribution of grain size is irregular (Figure 2-8). Overall, mean grain size decreases offshore, with fine-grained sand being dominant at the shelf break. Donahue et al. (1966) collected surface sediment samples along a northwest-southeast transect from southern Long Beach Island to the shelf edge and identified similar textural trends as Frank and Friedman (1973). Median grain size ranged from 0.2 to 0.5 mm (fine to medium sand), with a fining trend in the offshore direction (Figures 2-9 and 2-10).

Stubblefield and Swift (1981) provide a detailed view of grain size variability across a nearshore and middle shelf sand ridge southeast of Absecon Inlet (Figure 2-11). For the nearshore, coast-oblique ridge, surficial sand grades from coarse on the shoreward flank and ridge crest to fine on the seaward flank of the shoal. Across the middle shelf ridge, the size distribution is approximately symmetrical with the coarsest sand residing near the shoreward flank of the shoal. Overall, the middle shelf ridges are finer-grained and better sorted than nearshore ridges.

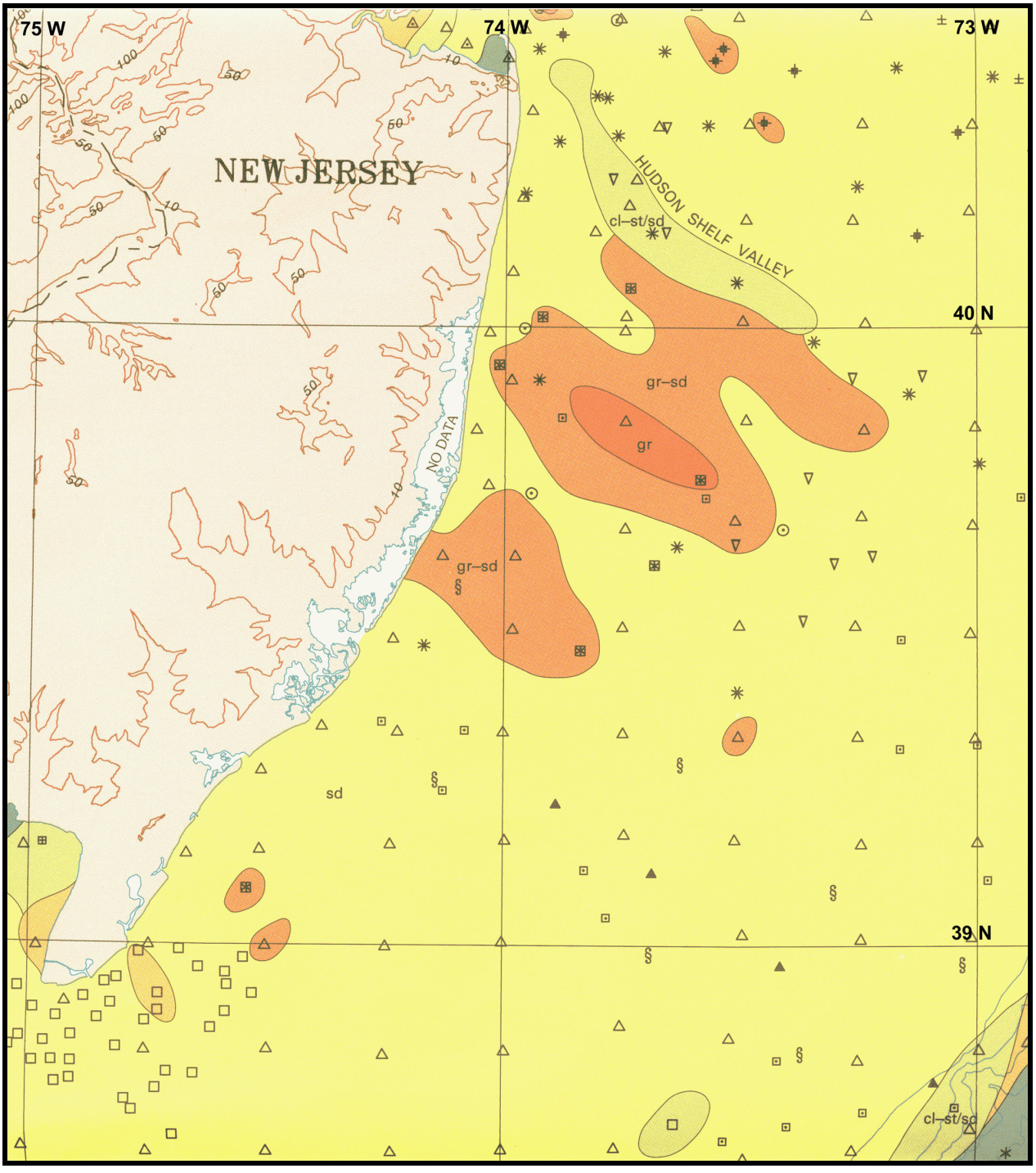

Figure 2-7. Surficial sediment texture on the New Jersey continental shelf (from Poppe et al., 1994). Yellow areas represent sand (sd) and orange areas depict gravelly sand (gr-sd) deposits.

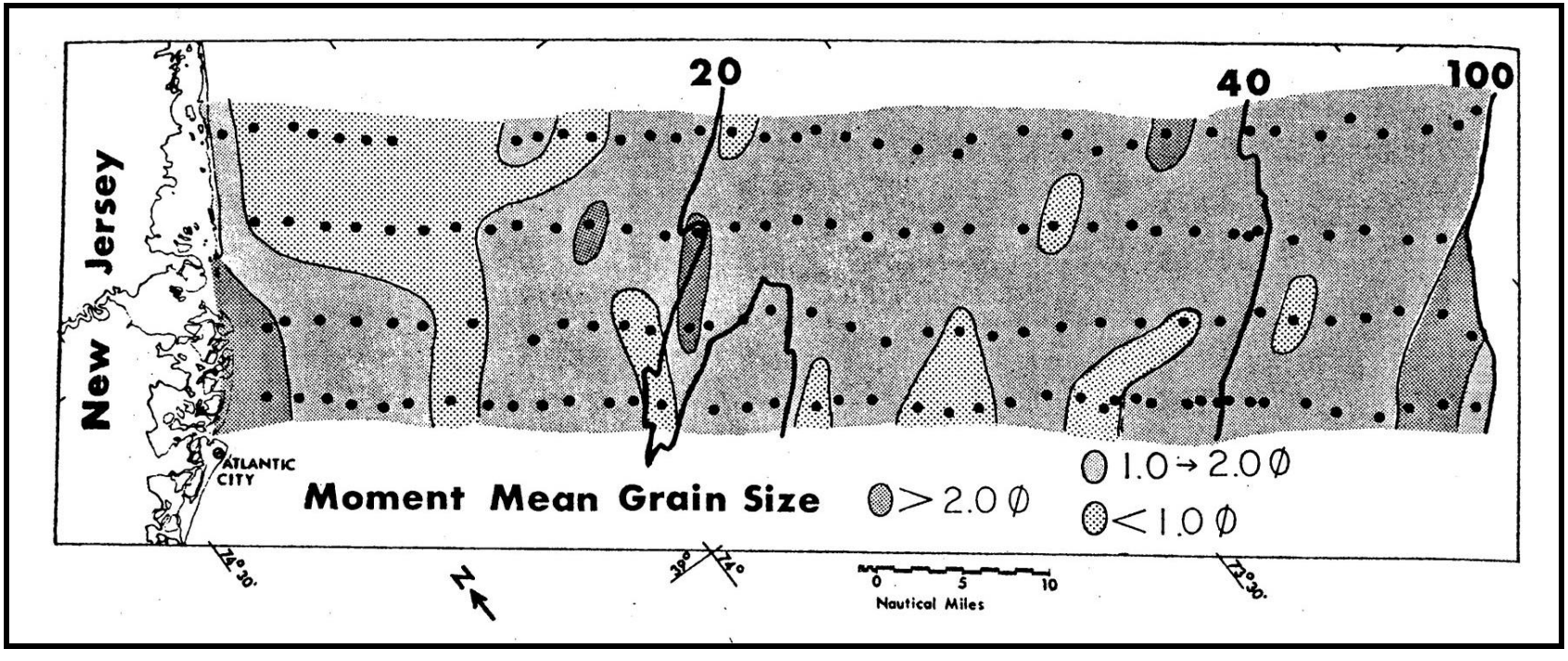

Figure 2-8. Pattern of mean grain size (moment statistic) for offshore sediment between southern Long Beach Island and Absecon Inlet, New Jersey (from Frank and Friedman, 1973). Depth contours are in fathoms.

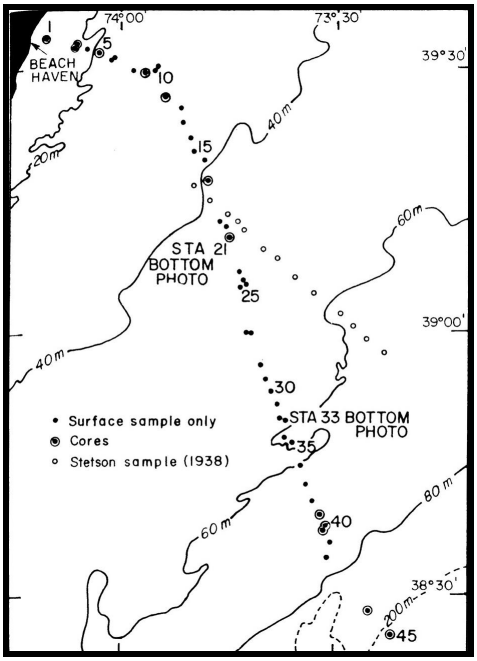

Figure 2-9. Surface sediment sample locations on the New Jersey continental shelf (from Donahue et al., 1966).

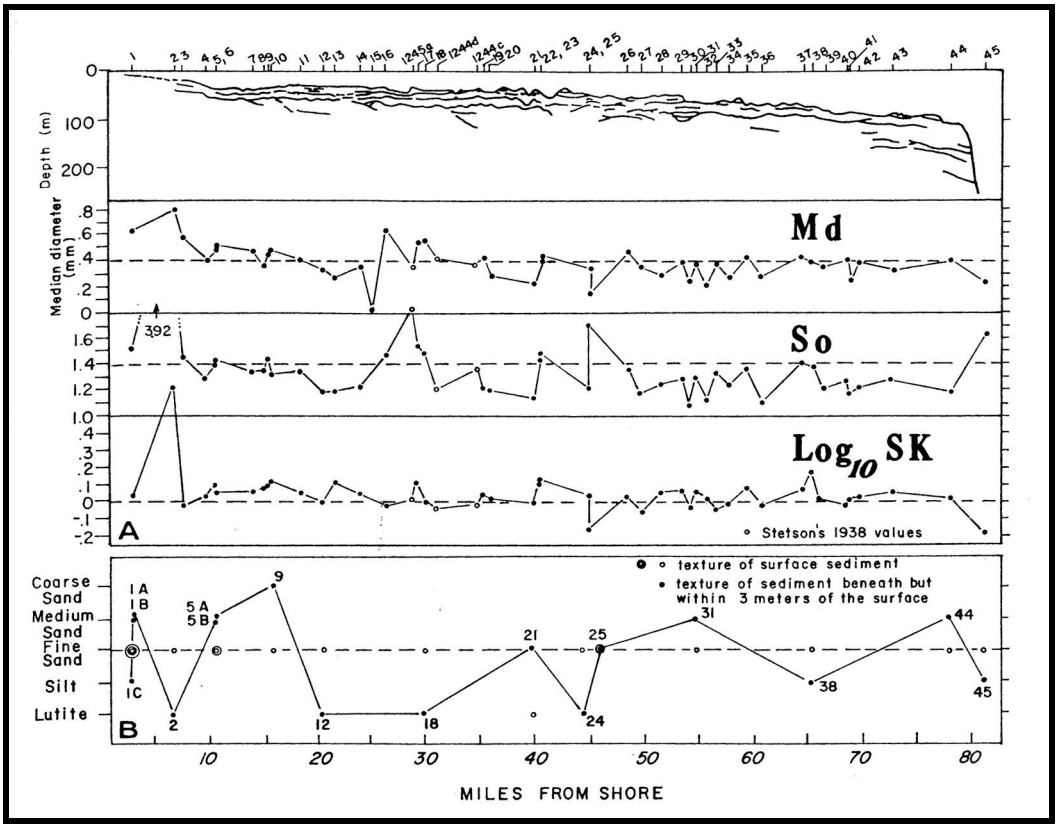

Figure 2-10. Median diameter (Md), grain sorting (So), and $\log_{10}$ skewness (Sk) for surface sediment samples illustrated in Figure 2-8 (from Donahue et al., 1966).

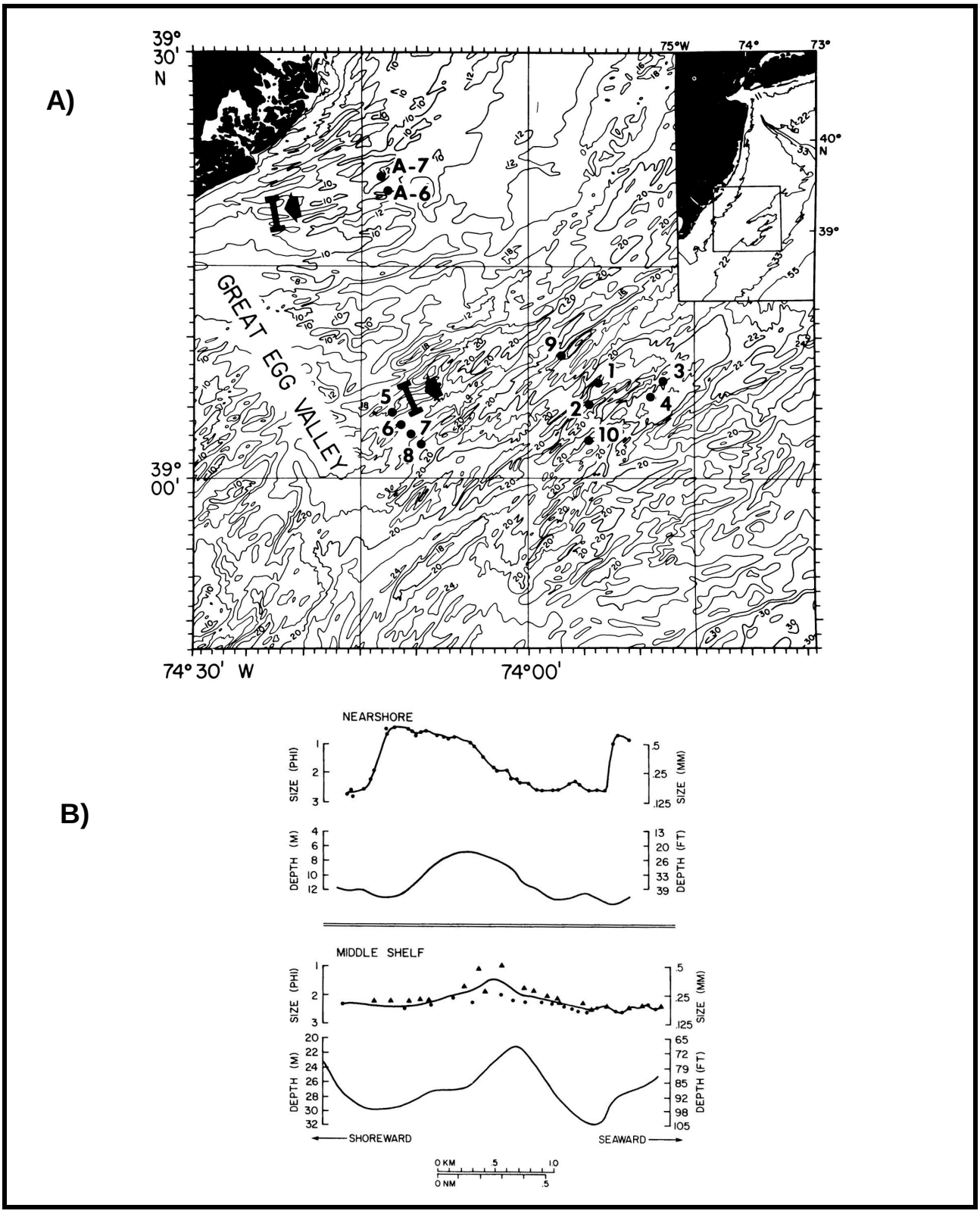

Figure 2-11. A) Index map illustrating two sediment grab sample transects over nearshore and middle shelf sand ridges. B) Plot of mean grain size across the nearshore and middle shelf sand ridge (from Stubblefield and Swift, 1981).

2.1.3 Subsurface Deposits

Uptegrove et al. (1995) identified seven geological studies of continental shelf sedimentation processes within the study area that described the regional character of shelf stratigraphy and sedimentology (Table 2-1). Furthermore, two (2) additional studies document the shallow geology of nearshore and offshore sand ridges for determining the genesis of shoreface ridge deposits. In addition, Smith (1996) provided a detailed description of the geology of shoreface sand ridges seaward of Townsends Inlet and the Federal-State OCS boundary. A description of the studies summarized in Table 2-1 are provided in Stubblefield et al. (1984), Rine et al. (1991), Uptegrove et al. (1995), and Smith (1996).

The geology and geomorphology of shelf deposits in the northern portion of the study area are described by McClennen (1983), Alpine Ocean Seismic Survey (1988), and Ashley et al. (1991). This area of coverage includes NJGS Sand Resource Areas C and F1 and F2 (Figure 2-12). McClennen (1983) conducted a sidescan sonar and seismic reflection survey seaward of the central New Jersey coast to investigate the shallow subsurface character of shelf deposits. Numerous active megaripples were documented across the shelf surface. Shallow seismic data recorded sub-bottom reflectors as deep as 42 m that outlined sediment-filled valleys and buried channels. Alpine Ocean Seismic Survey (1988) collected seismic and vibracore data to characterize offshore areas potentially suitable for sand borrow material. Approximately 55 million cubic yards of sand were identified at the northern margin of the present study area. Ashley et al. (1991) collected shallow seismic and vibracore data seaward of Barnegat Inlet to describe subsurface depositional environments resulting from late-Quaternary sea level rise, including barrier island-lagoon complexes, shoreface sand ridges, and ebb-tidal delta deposits.

Miller et al. (1973) and Meisburger and Williams (1982) collected seismic reflection and vibracore data offshore central New Jersey near Sand Resource Areas C, G1, G2, and G3 (Figure 2-13). Although Miller et al. (1973) focused on characterizing the sand thickness of Beach Haven Ridge related to the proposed siting of an offshore generating station, Meisburger and Williams (1982) described sand and gravel resources between Barnegat Inlet and Avalon (Figure 2-14). After analyzing 1,100 km of high-resolution seismic data and describing 97 vibracores, 15 potential sand resource areas were identified (Figure 2-15). Most areas existed landward of the Federal-State OCS boundary, but significant portions of Resource Areas C, G1, G2, and G3 were described by the authors as suitable for beach fill. An estimated 225 MCY of sand was identified in the 15 sand resource areas.

Meisburger and Williams (1980), Dill and Miller (1982), and Smith (1996) documented shoreface geology offshore southern New Jersey (Figure 2-16). Dill and Miller (1982) used high-resolution seismic and vibracore data to describe sediment characteristics in the upper 20 m of the subsurface seaward of Avalon, New Jersey. The surface unit was defined as a medium-to-fine sand that thins rapidly seaward. These deposits are characteristic of the primary sand resource areas identified by Meisburger and Williams (1980) and Smith (1996). Meisburger and Williams (1982) acquired about 1,200 km of seismic data and 104 vibracores to define 18 sand resource areas (Figure 2-17). Approximately 1.4 billion cubic yards of sand was identified offshore Cape May County. This included potential sand deposits seaward of the Federal-State OCS boundary near Resource Areas A1 and A2. Smith (1996) used these data to further evaluate the resource potential of two shoreface sand shoals seaward of Townsends Inlet.

Table 2-1. Geological studies documenting Holocene sedimentation processes on the New Jersey continental shelf (after Uptegrove et al., 1995).

Author(s) Date	Title	Agency	Description of Data			Biblio	Maps	Tables	Comments
			Seismic Study Area Corners	Vibracores					
				Amount	Data				
Miller, Dill, and Tirey (1973)	Final Report: Geophysical Investigation of Atlantic Generating Station Site and Offshore Region	Alpine Geophysical, Inc.	39° 25' 00" N, 74° 17' 30" W 39° 22' 30" N, 74° 02' 30" W 39° 40' 00" N, 73° 52' 30" W 38° 00' 00" N, 73° 59' 30" W 39° 52' 30" N, 74° 05' 00" W	47	Log	Yes	Yes	No	3.5 kHz sparker profiles, uniboom system also used, max depth 500 ft
Meisburger and Williams (1980)	Sand Resources on the Continental Shelf off the Cape May Region, New Jersey	U.S. Army Corps of Engineers (USACE)	39° 00' N, 75° 00' W 38° 45' N, 75° 00' W 38° 45' N, 74° 30' W 39° 00' N, 74° 30' W	104	Log, Grain size	Yes	No	Yes	Icons Program misc. report, no equipment specified
Dill and Miller (1982)	Bathymetric and Geologic Study of the Proposed Outfall at Avalon, New Jersey	Alpine Geophysical, Inc.	39° 04' N, 74° 38' W 39° 05' N, 74° 40' W 39° 07' N, 74° 34' W 39° 05' N, 74° 37' W	12	Log, Grain size	No	No	No	Max. penetration 100 ft, 3.5 kHz profile
Meisburger and Williams (1982)	Sand Resources on the Inner Continental Shelf off the Central New Jersey Coast	USACE	39° 05' N, 74° 40' W 39° 50' N, 74° 05' W 39° 50' N, 73° 55' W 39° 05' N, 74° 36' W	97	Log, Grain size	Yes	No	Yes	Icons Program limited sidescan sonar
McClennen (1983)	Middle Atlantic Nearshore Seismic Survey and Sidescan Sonar Survey of Potential Geologic Studies on the U.S. Middle and North Atlantic Outer Continental Shelf	United States Geological Survey (USGS)	39° 12' N, 74° 37' W 39° 00' N, 74° 22' W 40° 10' N, 74° 01' W 40° 10' N, 73° 55' W	20	Unknown	Yes	Yes	No	Sidescan sonar geohazard analysis 3.5 kHz uniboom system
Stubblefield et al. (1984)	Recognition of Transgressive and Post-Transgressive Sand Ridges on the New Jersey Continental Shelf	National Oceanic and Atmospheric Administration Marine Ecosystems Analysis Program	39° 30’ N, 74° 30’ W 39° 30’ N, 73° 30’ W 38° 45’ N, 73° 30' W 38° 45’ N, 74° 30’ W	12	Core logs	Yes	Yes	Yes	Genesis of storm-generated shoreface sand ridges
Alpine Ocean Seismic Survey (1988)	Identification and Delineation of Potential Borrow Areas for the Atlantic Coast of New Jersey	Alpine Ocean Seismic Survey, Inc. for the USACE	38° 40' N, 74° 40' W 38° 40' N, 71° 50' W 40° 30' N, 71° 50' W 40° 30' N, 74° 00' W	70	Log, Grain size	No	Yes	Yes	Summary of at least five borrow sites
Ashley et al. (1991)	Clastic Sequences Developed During Late Quaternary Glacio-eustatic Sea-level Fluctuations on a Passive Margin: Example from Inner Continental Shelf near Barnegat Inlet, New Jersey	Sea Grant Program, New Jersey Marine Consortium	39° 40' 00" N, 74° 07' 30" W 39° 40' 00" N, 74° 00' 00" W 39° 47' 00" N, 74° 05' 00" W 39° 47' 00" N, 74° 06' 00" W	12	Core logs, grain size	Yes	Yes	No	100 line-km of ORE Geopulse data; up to 6.1 m long cores
Rine et al. (1991)	Lithostratigraphy of Holocene Sand Ridges from the Nearshore and Middle Continental Shelf of New Jersey	Atlantic Shelf Coring Project (oil industry research consortium)	39° 30’ N, 74° 30’ W 39° 30’ N, 73° 30’ W 38° 45’ N, 73° 30' W 38° 45’ N, 74° 30’ W	13	Core logs, grain size	Yes	Yes	No	General stratigraphic framework of shoreface sand ridges
Smith (1996)	Nearshore Ridges and Upper Pleistocene Sediments on the Inner Continental Shelf of New Jersey	Masters Thesis, Rutgers University	39° 12’ N, 74° 45’ W 39° 12’ N, 74° 25’ W 38° 58’ N, 74° 25' W 38° 58’ N, 74° 45’ W	20	Core logs, grain size	Yes	Yes	Yes	303 line-km of ORE Geopulse shallow seismic records; up to 6.1 m long cores

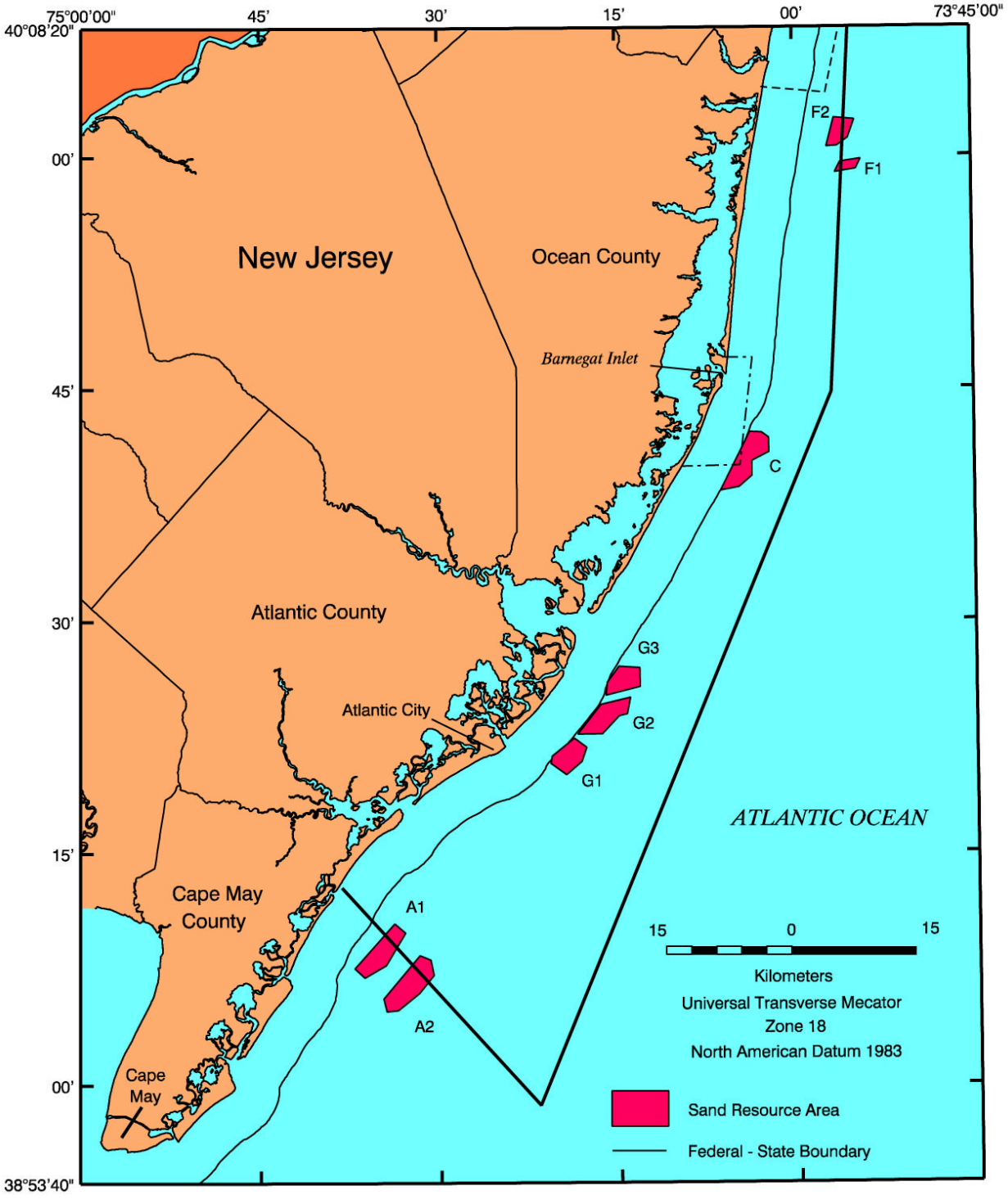

Figure 2-12. Study area locations for McClennen (1983; thick solid line), Alpine Ocean Seismic Survey (1988; dashed line), and Ashley et al. (1991; dash-dot line) (study locations from Uptegrove et al., 1995).

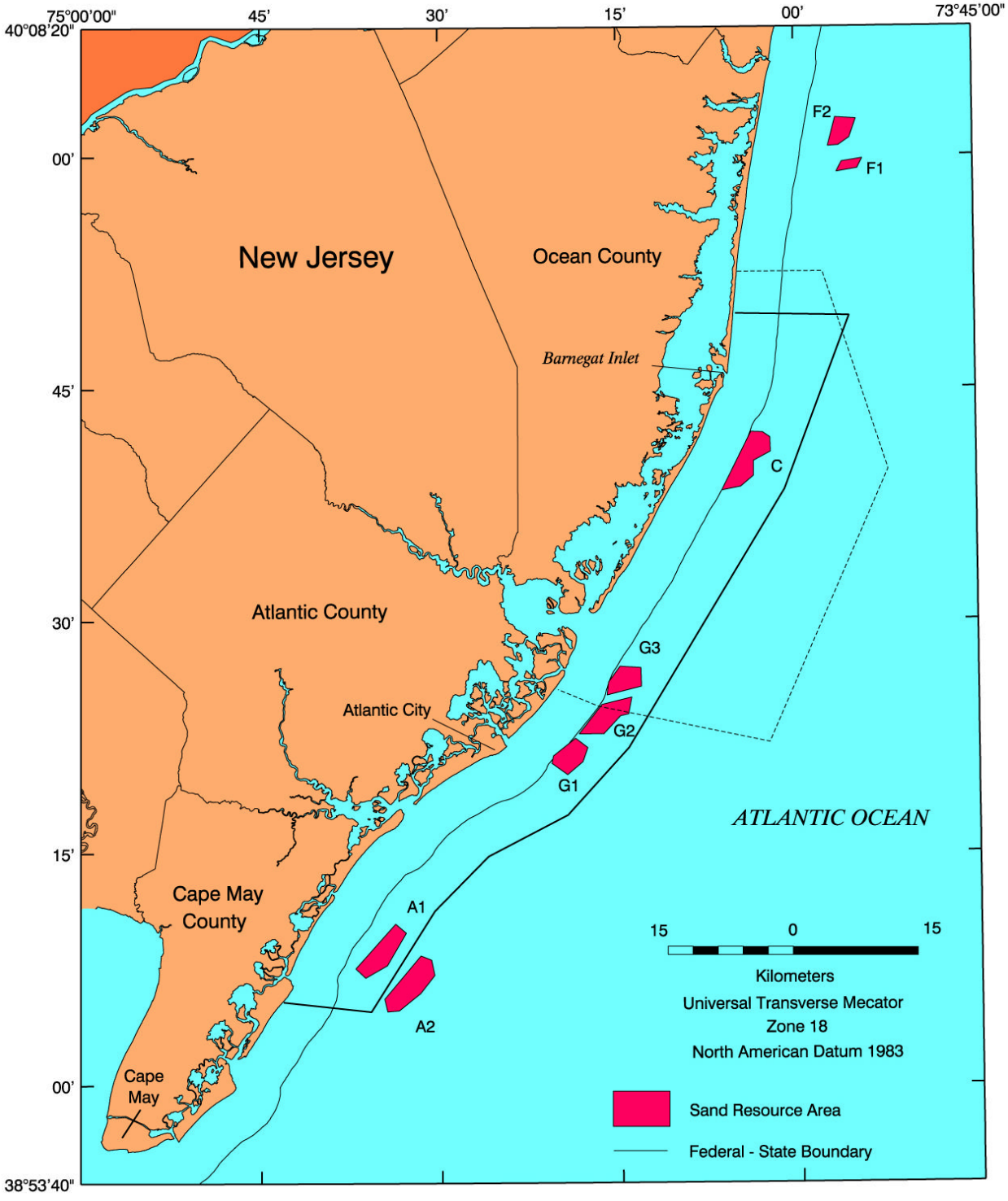

Figure 2-13. Study area locations for Miller et al. (1973; dashed line) and Meisburger and Williams (1982; thick solid line) (study locations from Uptegrove et al., 1995).

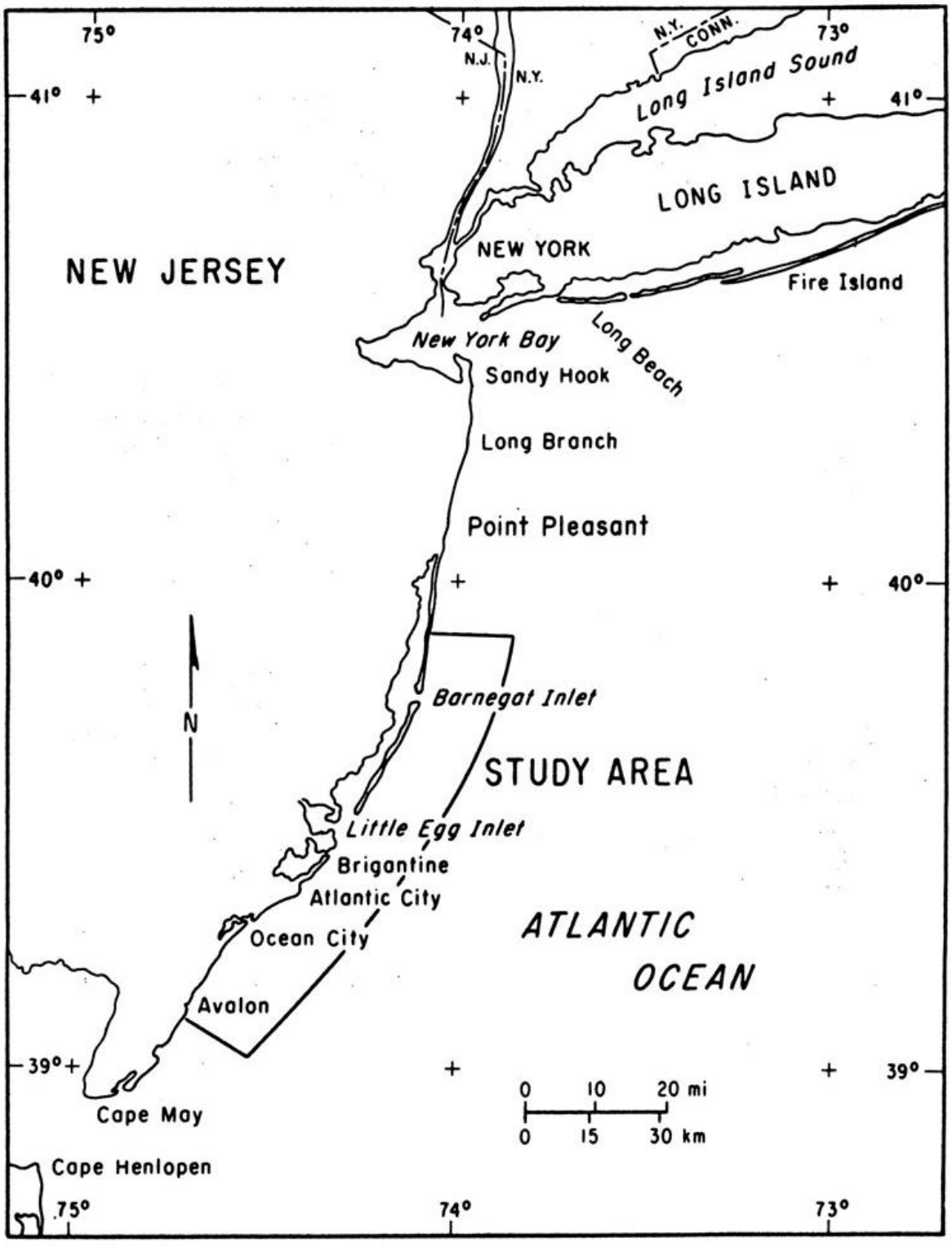

Figure 2-14. General location diagram for U.S. Army Corps of Engineers (USACE) central New Jersey sand resource study area (from Meisburger and Williams, 1982).

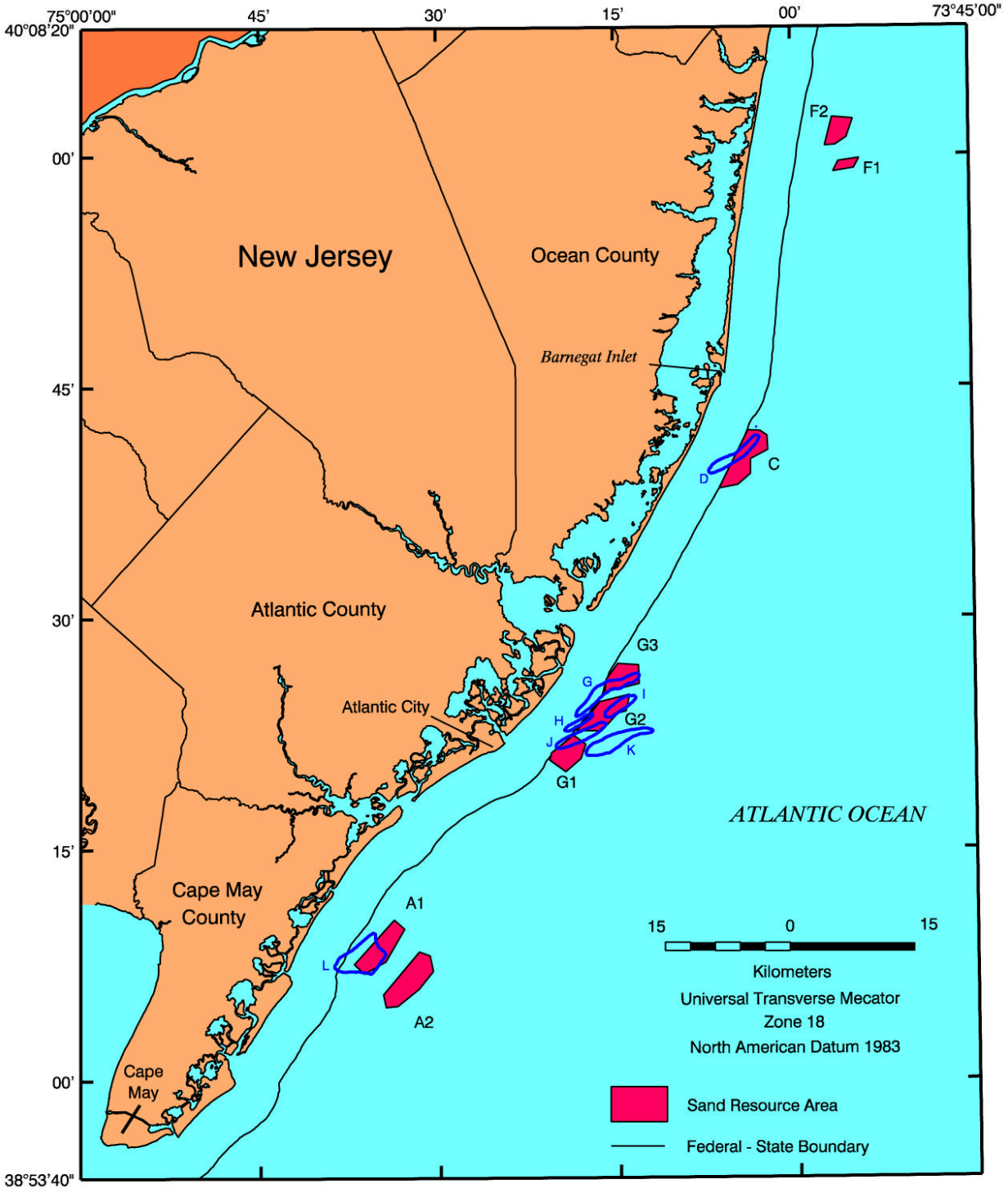

Figure 2-15. Map of U.S. Army Corps of Engineers (USACE) sand resource sites (dark blue lines labeled D, G, H, I, J, K, L) relative to New Jersey Geological Survey (NJGS) sand resource areas (labeled A1, A2, G1, G2, G3, C, F1, F2). Sand resource locations are from Meisburger and Williams (1982) and the NJGS.

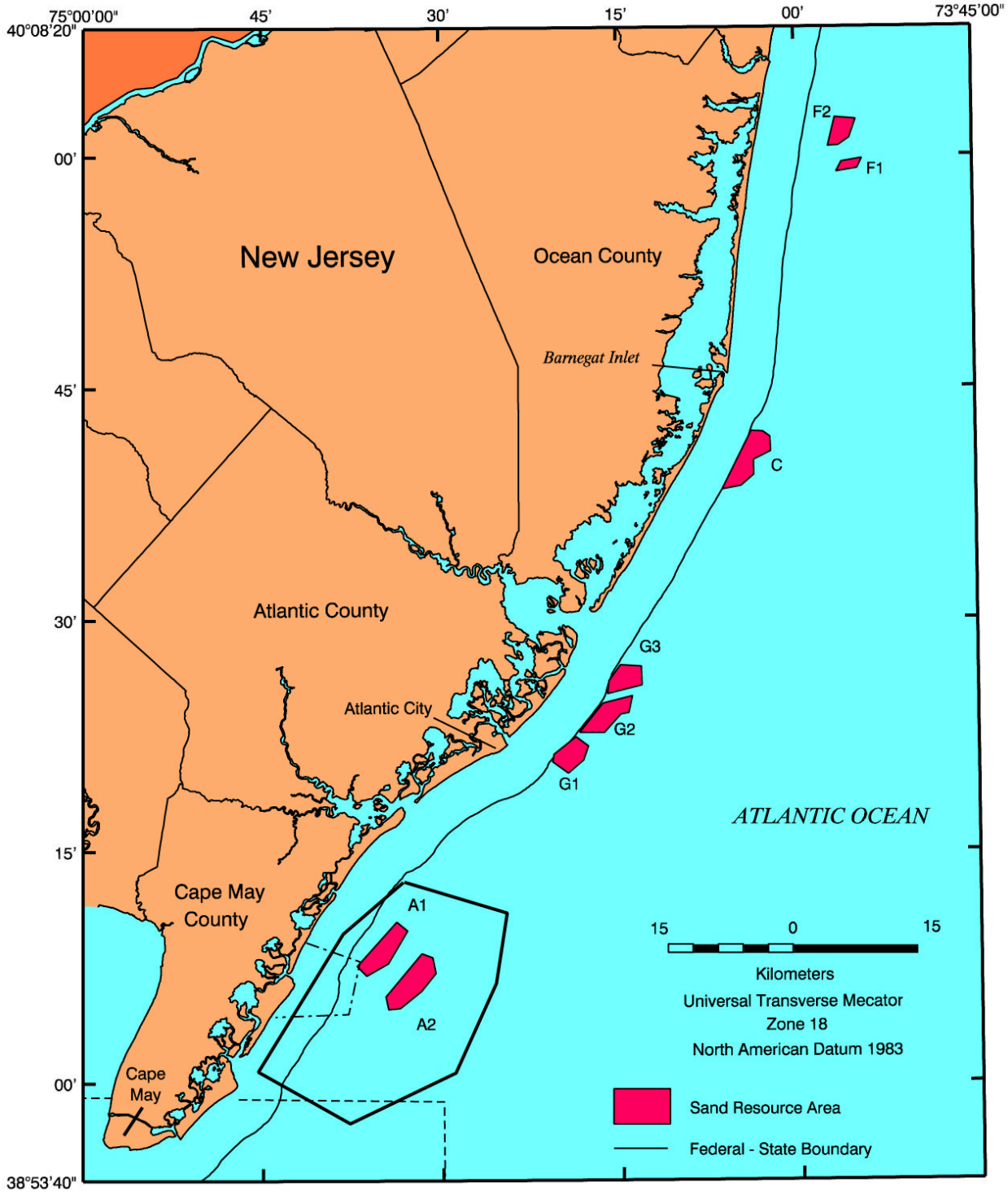

Figure 2-16. Study area locations for Meisburger and Williams (1980; dashed line), Dill and Miller (1982; dash-dot line), and Smith (1996; thick solid line) (study locations from Uptegrove et al., 1995).

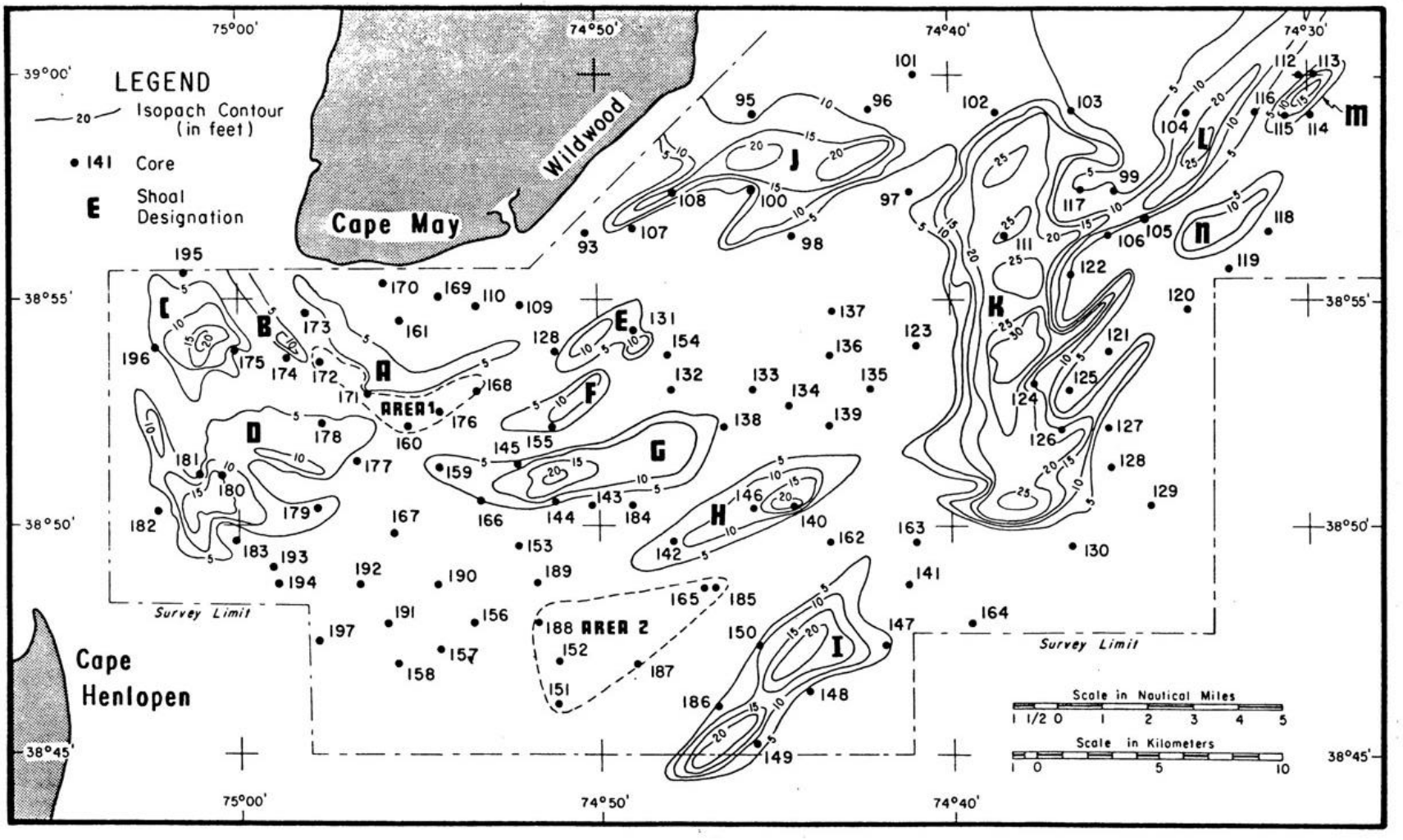

Figure 2-17. Map of U.S. Army Corps of Engineers (USACE) sand resource sites offshore Cape May County, New Jersey, and associated core locations (from Meisburger and Williams, 1980).

2.1.4 Sand Resource Areas

The resource potential of offshore sand deposits within the study area was documented using geological data from Smith (1996), Uptegrove et al. (1997), and Alpine Ocean Seismic Survey (1997). Sand volume estimates for Resource Areas A1 and A2 were determined by Smith (1996) and Uptegrove et al. (1997). Smith (1996) obtained 303 line-km of high-resolution seismic reflection profiles in 1993 offshore southern New Jersey between Corsons Inlet and Hereford Inlet. In 1994, 20 vibracores were obtained from sand ridges evident in the seismic records. Two prominent sand ridges were targeted; Inner Sand Ridge (ISR; Sand Resource Area A1) was characterized using information from five vibracores, and Avalon Shoal (Sand Resource Area A2) was cored in three locations to define sand thickness and extent (Figure 2-18). Avalon Shoal is located approximately 11 to 12 km east of Avalon, New Jersey in 6- to 12-m water depth (relative to the National Geodetic Vertical Datum 1929, NGVD). Ridge periphery was defined by the 5-m contour above the S_1 unconformity surface (Figure 2-19). Sand ridge thickness relative to the underlying S_2 unconformity is up to 7 to 8 m. However, sediment between the S_2 and S_1 surface is unusable fine-grained estuarine sediment (2-m thick), resulting in a maximum sand ridge thickness of 5 to 6 m (Figure 2-20).

Inner Sand Ridge (Sand Resource Area A1) is located approximately 6 km east of Avalon. Water depths over and around the shoal range from 6 to 12 m (NGVD), and sand ridge thickness ranges from 0 to 5 m (Figure 2-21; ISR is defined by the 5-m isopach line). Although sand thickness generally is less at ISR than Avalon Shoal, initial beach quality sand volume estimates were greater for ISR (48 MCM) than Avalon Shoal (37 MCM; Smith, 1996). Further analysis of digital seismic data for these two sites illustrated that potential beach quality sand volumes for ISR and Avalon Shoal are 39 and 57 MCM, respectively (Uptegrove et al., 1997). Mean grain size for both shoals averaged about 0.57 mm, with a range between 0.20 and 2.0 mm. Percent sand and gravel content averaged >99 (Smith, 1996).

As of this report, Resource Areas C, F1, F2, G1, G2, and G3 have not been characterized completely by the NJGS. In August 1997, 20 vibracores were obtained from the above-referenced resource areas (Alpine Ocean Seismic Survey, 1997). These data, along with information from previous studies, were used by the NJGS to define the locations and extent of present resource areas. Figure 2-22 illustrates the location of vibracores relative to defined resource areas. Resource Areas G1, G2, and G3, east and north of Absecon Inlet, can be characterized using the descriptions from nine vibracores. Core G-1 was located on a ridge crest and is composed of approximately 5.6 m of gray to light gray medium sand. Core G-2 is located off the ridge crest and is composed of a light brown to light gray medium sand with shell fragments. Vibracore G-3 is located on a sand ridge crest in Resource Area G2. The core sequence recorded 6 m of light gray to gray medium sand with shell fragments (Alpine Ocean Seismic Survey, 1997). Cores G-4 and G-5 are located off the flank of a shoal in Resource Area G2 and contain 2 to 4 m of medium to coarse sand at the surface. Core G-6 is located on the southern sand ridge in Resource Area G2 (Figure 2-22). It contains approximately 6 m of gray to light brown medium sand with small zones of silty sand. Shell fragments are common in the upper 3.5 m of the sequence.

Resource Area G1 was cored in three locations. Cores G-6A and G-8 were obtained off the main sand ridge but contain substantial quantities of sand (Alpine Ocean Seismic Survey, 1997). The upper 2 m of Core G-6A contains gray, medium-to-coarse sand with some shell fragments. Between 2 and 5.5 m, an increase in silt and clay content is noted on the vibracore log. However, the deepest 0.5 m of the sequence is again described as a clean, medium sand. Core G-8, located just east of the main sand ridge in Resource Area G1, contains coarse-to-medium sand throughout the sequence (6.0 m) with small amounts of shell fragments. Core

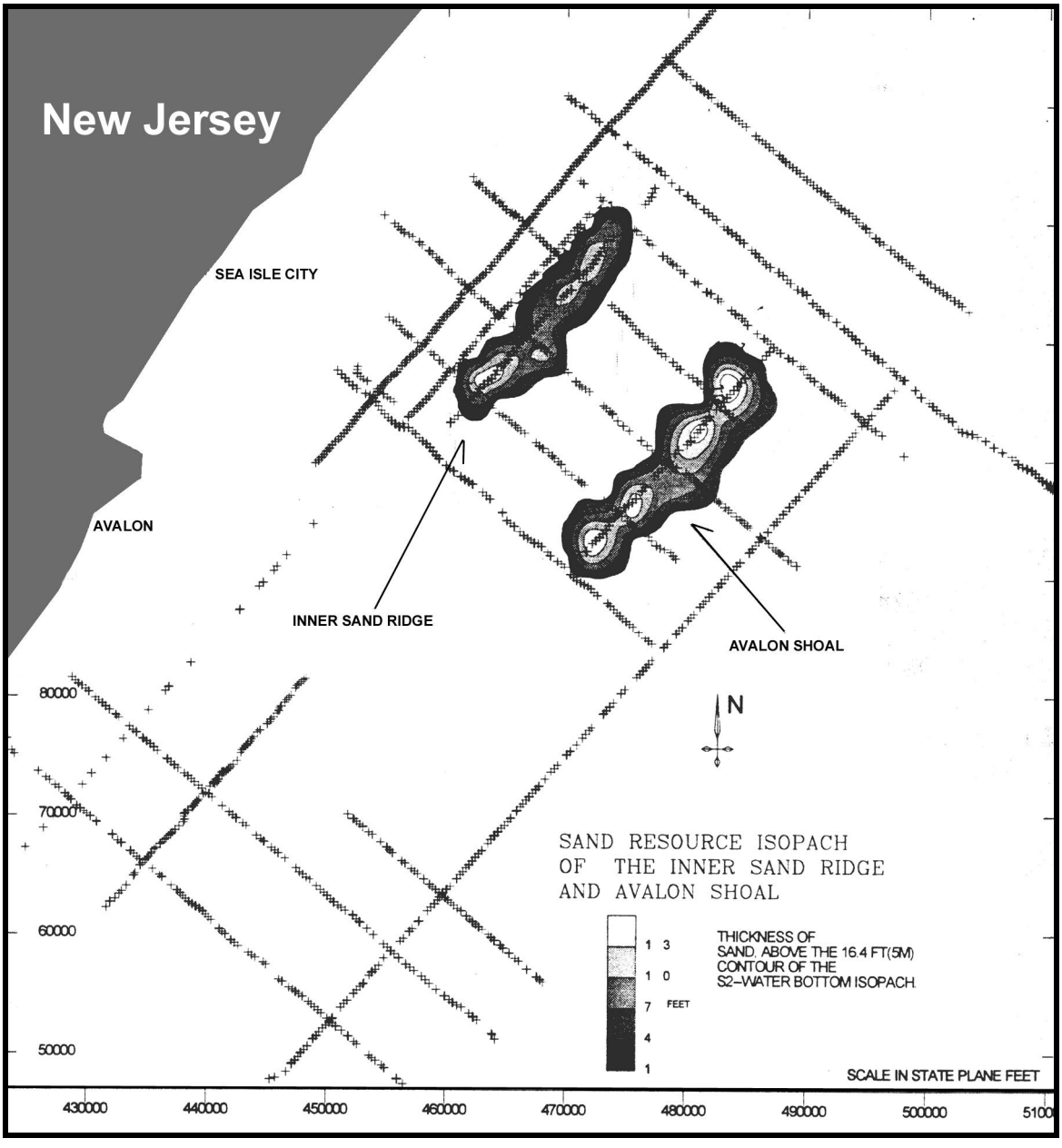

Figure 2-18. Isopach map illustrating sand ridge thickness at Inner Sand Ridge and Avalon Shoal (from Uptegrove et al., 1997).

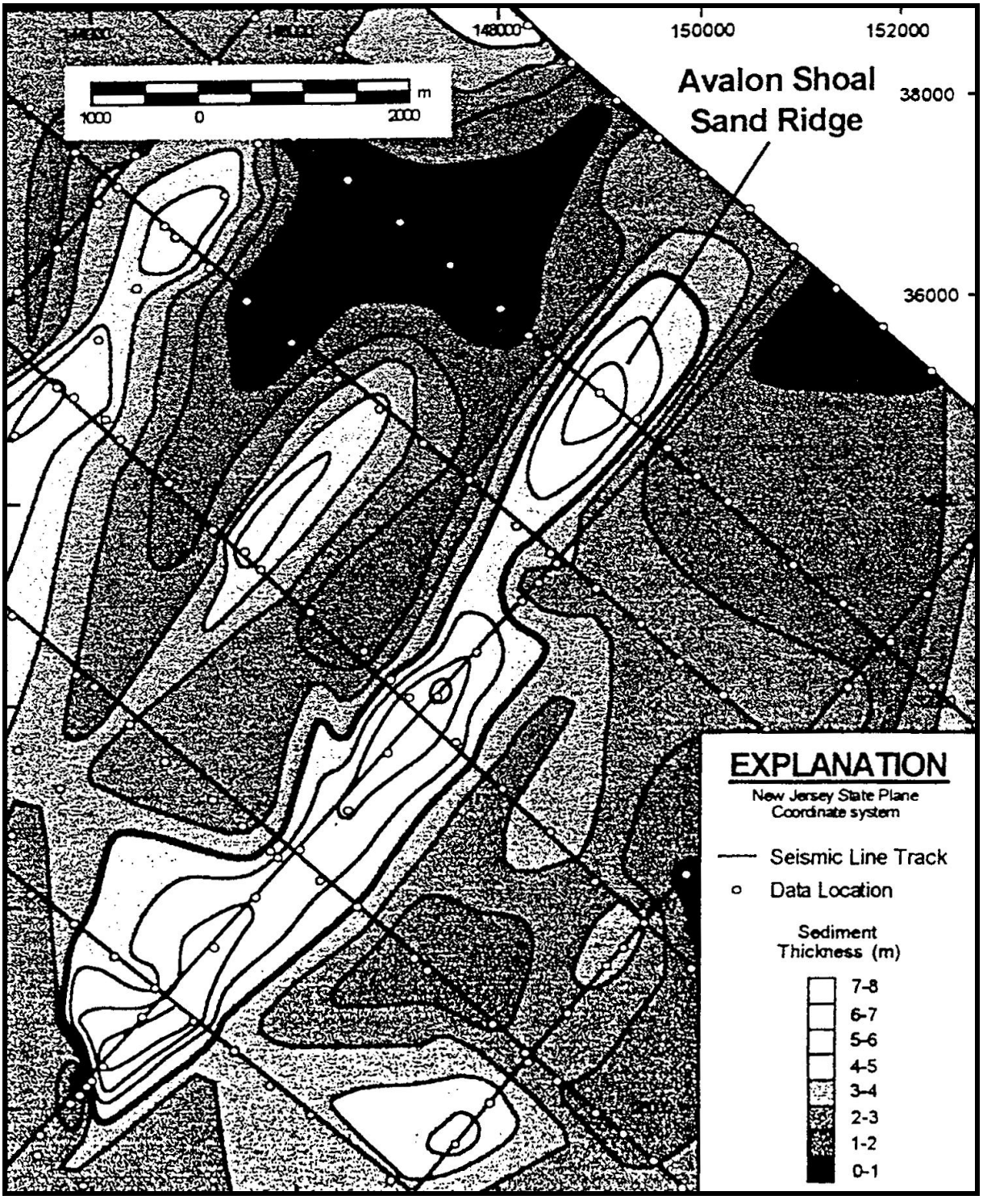

Figure 2-19. Sediment thickness above the S_2 unconformity at Avalon Shoal. The bold line approximates the base of the sand ridge as it exists on top of the S_1 unconformity (from Smith, 1996).

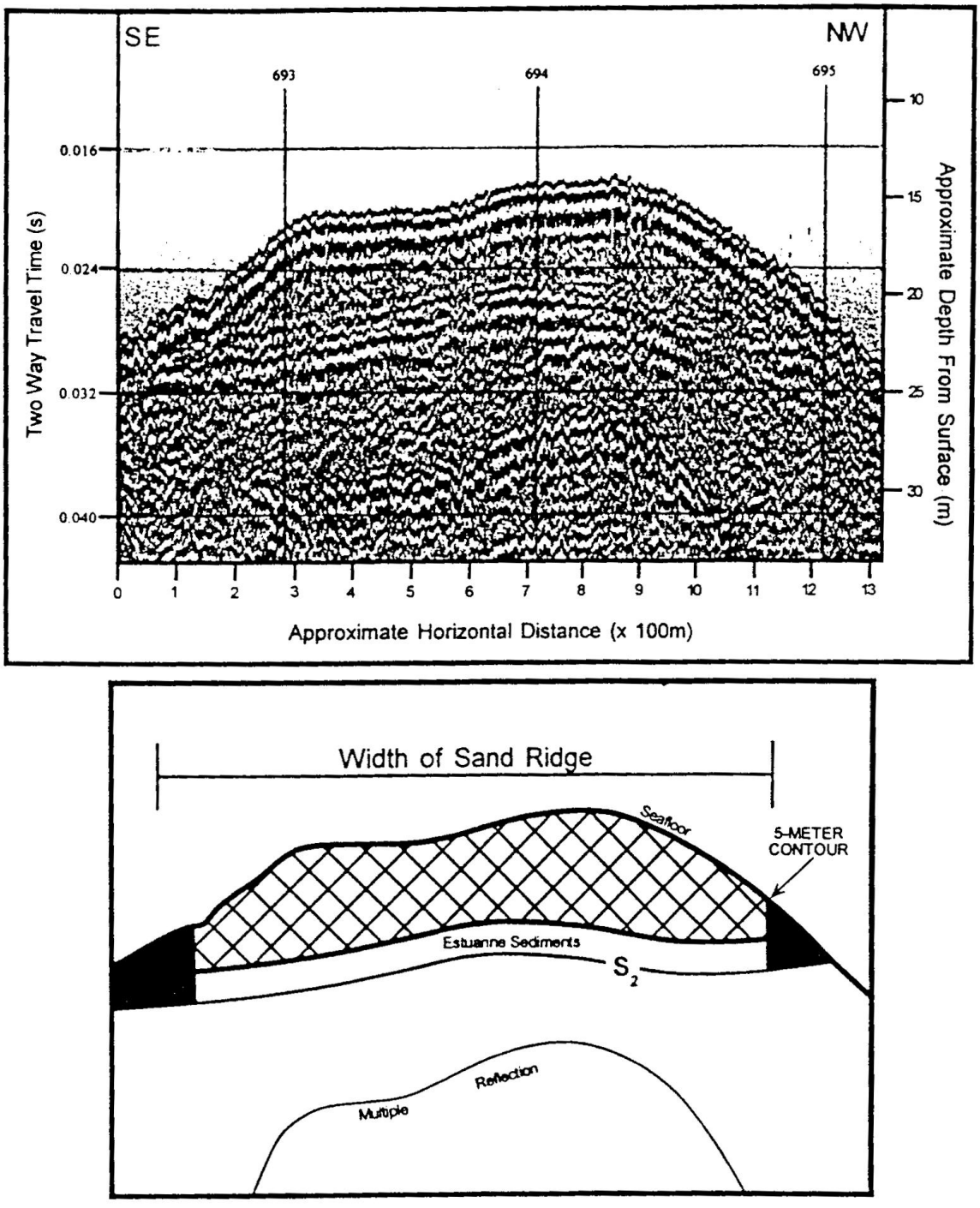

Figure 2-20. Sand ridge volume as calculated using seismic data. Because sand ridge sediment thins away from the ridge crest, a bounding area was defined to calculate ridge thickness. The bounding area was defined by Smith (1996) as the 5-m contour above the regional S_2 boundary. The lower 2 m above the S_2 boundary was considered unusable, fine-grained, estuarine sediment based upon core observations. It was not included in the sand volume calculation (Smith, 1996).

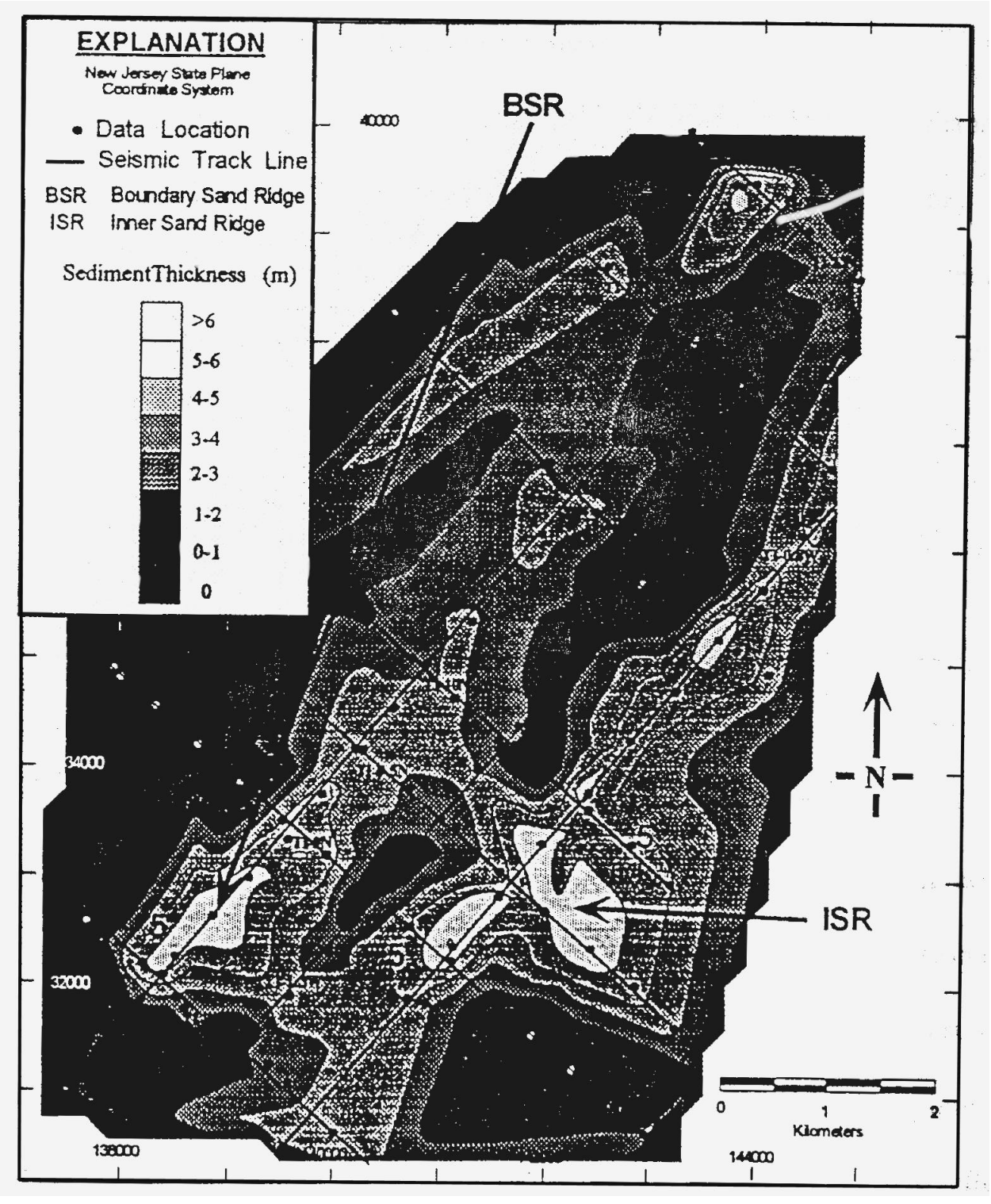

Figure 2-21. Sediment thickness above the S_2 unconformity in the vicinity of Inner Sand Ridge (ISR). The surface expression of the inner ridge is approximated by the 5-m isopach, producing a sand volume estimate of approximately 48 MCM (from Smith, 1996).

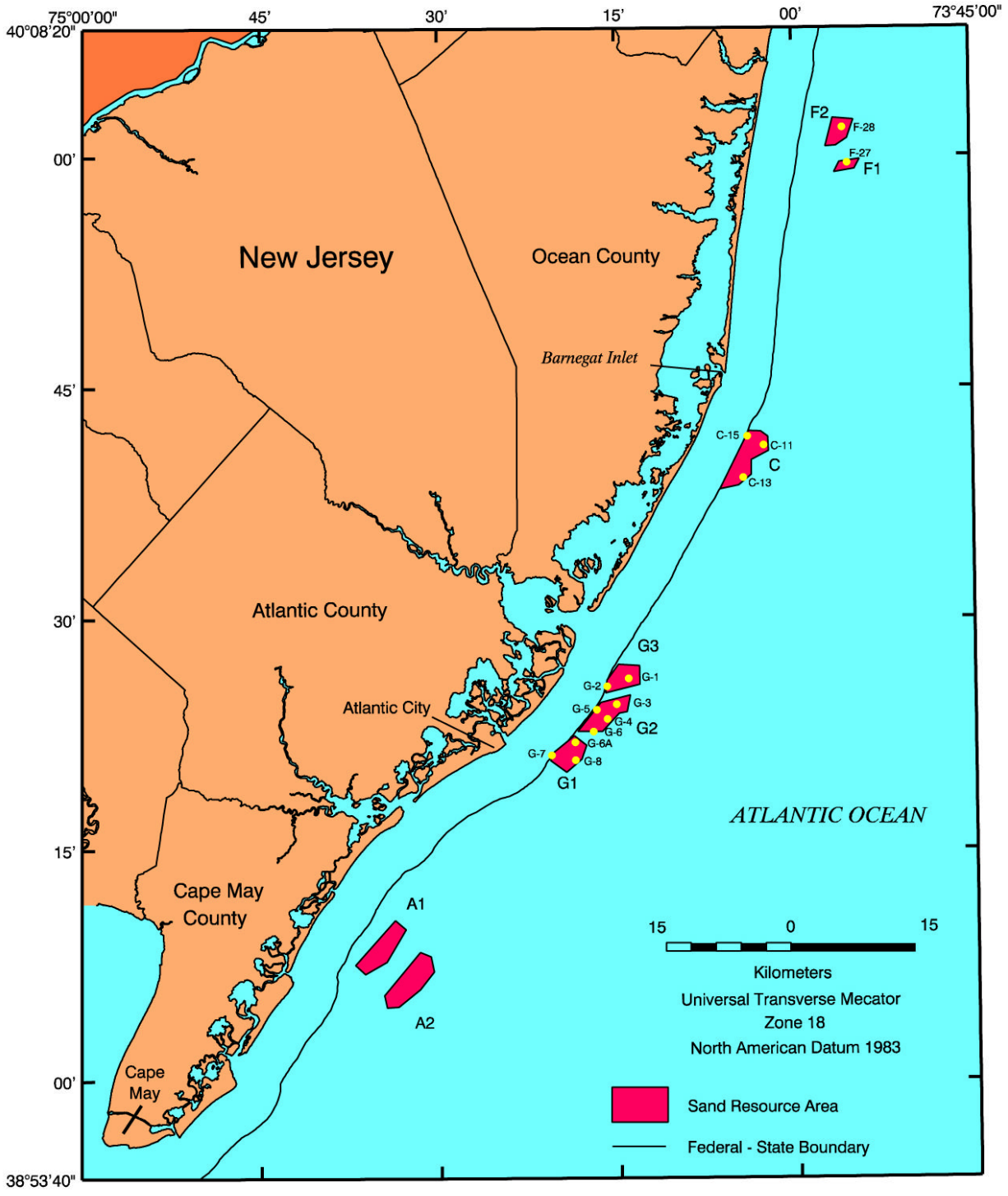

Figure 2-22. Vibracore locations (yellow dots) for samples collected in 1997 at Sand Resource Areas C, G1, G2, G3, F1, and F2 (data from Alpine Ocean Seismic Survey, 1997).

G-7 is located on the main sand ridge crest and contains 6.0 m of clean, gray medium sand. A small area of clay is noted on the core log at about 3.0 m.

Resource Area C is located south and east of Barnegat Inlet, seaward of the Federal-State OCS boundary. The area is characterized using geologic data from cores C-11, C-13, and C-15; all three cores are adjacent to the peak of the main ridge. Core C-11 contains approximately 5.8 m of light gray to light brown, coarse-to-medium sand. Sediment composition changes at C-13, where the top 1.4 m of sand overlays a 1-m thick clay zone. Below 2.4 m in the core, coarse gray sand with shell fragments is present to the base of the core sequence. At core C-15, the top 3.0 m of sediment contains substantial quantities of clay and silt mixed with coarse sand and shell fragments. The next 2.4 m of core sequence contains light gray medium-to-coarse sand. Overall, core sequences off the flanks of the main sand ridge do not appear to provide viable borrow material for beach nourishment; however, sand ridge deposits recorded in core C-11 appear very compatible with beach nourishment needs.

The northernmost resource areas (F1 and F2) are characterized using two cores. Core F-27 is located in Resource Area F1 and grades from a light gray medium sand with some gravel (at the surface) to a light gray gravel with some sand and shell fragments (about 4.3 m deep; Alpine Ocean Seismic Survey, 1997). North of this location at core F-28 (Resource Area F2), the ridge deposit is composed primarily of coarse-to-medium gray sand with gravel and shell fragments. Below 2.4 m in the sequence, sediment color becomes light gray to light brown and grain size becomes coarse-to-very coarse. These data are consistent with the surficial sediment distribution map of Poppe et al. (1994).

Specific beach quality sand volume estimates have not been calculated for Sand Resource Areas C, G1, G2, G3, F1, and F2, but estimates of sand volumes are at a minimum equal to the proposed sand extraction scenarios presented in Section 1.0. The smallest quantity of sediment calculated for any of the proposed sand resource areas was about 500,000 cm for F1. All other sand resource areas contain at least 2 MCM of borrow material for potential beach nourishment activities.

2.2 GENERAL CIRCULATION

The earliest description of the seasonal mean circulation in the Middle Atlantic Bight was given by Bumpus (1973) based on an extensive 10-year program of surface drift bottle and seabed drifter releases and other historical data (sailing and shipping logs, etc.). In the region off New Jersey, Bumpus (1973) found that the mean near-bed along-shelf flow was about 5 cm/s toward the SW. The mean near-bed across-shelf flow was slightly onshore at <1 cm/s.

A summary of the general circulation and other currents in the Middle Atlantic Bight was provided by Beardsley and Boicourt (1981). Based on long-term measurements (>1 year) of currents at many locations in this region, they showed that the annual mean along-shelf flow was towards the southwest near the surface and above the seabed. In about 12-m water depth off southern New Jersey, Beardsley and Boicourt (1981) found that the annual mean currents were toward the southwest at about 4 and 1 cm/s at 4.5- and 10-m water depths, respectively. In water depths <60 m, the mean velocity vectors showed onshore veering with increasing depth, a tendency also found by Bumpus (1973). The slow mean across-shelf flow may be related to the long-term wind-driven circulation (due to seasonal upwelling and downwelling conditions). More detailed discussion of the variability and dynamics in the along-shelf flow on the continental shelf in this region was provided by Noble et al. (1983). This study utilized numerous long-term current meter moorings on the shelf to relate long-term current dynamics to wind and density forcing on the shelf.

General circulation is directly related to regional atmospheric surface pressure and wind stress distributions and to the regional density field along and across the shelf. Regional wind climate is influenced by two dominant pressure systems, the Bermuda High and the Icelandic Low. In summer, the Bermuda High is located over more northerly latitudes, creating generally weak southwesterly winds. In winter, the Bermuda High pressure zone weakens and is depressed to the south, allowing the Icelandic Low to bring stronger northerly and northwesterly winds out of Canada (Louis Berger Group, 1999). Seasonal changes in atmospheric surface pressure and winds significantly affect currents over the entire shelf, and are particularly effective in winter when energetic low pressure storm systems create strong northeast winds on the backside of low pressure centers. These strong winds and pressure gradients accelerate southwest flows over the shelf throughout the water column (Noble et al., 1983).

Louis Berger Group (1999) describes the presence of an elongated cyclonic gyre offshore New Jersey, encompassing most of the Middle Atlantic Bight. This gyre results from strong horizontal shear between the Gulf Stream and shelf waters and stretches from the Nantucket Shoals to Cape Hatteras. The inshore edge of this gyre flows towards the south and may also contribute the average southwesterly flow detected in this region. Williams and Godshall (1977) measured a 5 cm/sec mean flow along the New Jersey coast. The position of this gyre varies with the northern edge of the Gulf Stream, and it may contribute to low frequency current variability on the New Jersey inner shelf.

2.2.1 Tidal Currents

Tidal currents are dominated by the rotary semi-diurnal components in this region, especially the M2 (12.4 hour) component (Mayer, 1982; Moody et al., 1983). The M2 tidal component generally has a maximum amplitude of about 10 to 15 cm/s oriented in the cross-shelf direction over much of the shelf off New Jersey (Moody et al., 1983). The diurnal components are much weaker and largely oriented along-shelf (Moody et al., 1983). Spring-neap tidal current variations have been observed in previous current data. In the inner shelf regions, where water depths are less than 9 m, tidal currents are weak, generally less than 5 cm/sec. These tidal currents contribute little to the overall current variance (Louis Berger Group, 1999).

2.2.2 Monthly Mean Currents

The persistent southwest flow that dominates shelf circulation during most of the year occasionally reverses toward the northeast under the influence of strong and persistent south winds. On the inner shelf, these reversals can occur during summer periods of strong northward winds and low river runoff. This pattern is more common in the region offshore southern New Jersey than further to the north in the Middle Atlantic Bight. Current measurements suggest that this northward flow occurs frequently along the inner shelf (Boicourt, 1981). Off the mouth of Chesapeake Bay, Boicourt (1982) indicated that a narrow, coastal, relatively fresh southward “jet” is flanked on the inner shelf by a northward surface current. The width and vertical structure of the coastal jet and northward inner shelf flow are uncertain.

Available current data indicate that monthly mean near-surface currents throughout the Middle Atlantic Bight are generally stronger during winter than summer. Off southern New Jersey, near-bottom monthly mean currents tend to reverse during one or more winter months, but near-surface currents remain to he southwest (Beardsley and Boicourt, 1981).

2.2.3 Low-Frequency Synoptic-Scale Currents

Low-frequency currents in the synoptic-scale time domain (2 to 10 days) are largely related to atmospheric forcing. Considerable information and analysis of currents in this time

domain is available for the Middle Atlantic Bight, and specifically off New Jersey. In general, the results can be summarized by noting that synoptic-scale current fluctuations have a strong along-shelf component that accounts for about 70 to 90% of the subtidal current variance throughout the Middle Atlantic Bight (Beardsley and Boicourt, 1981). Most previous field studies producing analyses of current fluctuations in this frequency band have shown convincingly that the along-shelf currents and cross-shelf pressure gradient are coherent and in phase (essentially in geostrophic balance). Along-shelf currents are coherent in the mid-shelf region for distances of over 200 km. These same studies have shown that the along-shelf currents generally lag the along-shelf surface wind stress by about 5 to 10 hours in the Middle Atlantic Bight (Flagg, 1977; Chuang et al., 1979; Mayer et al., 1979; Beardsley and Boicourt, 1981). The along-shelf currents are generally not coherent with across-shelf wind stress (Csanady, 1982).

In contrast, across-shelf currents on the inner to outer shelf are incoherent over very short distances (<70 km; Mayer, 1982). However, the Hudson Shelf Valley, which lies to the north of the sand resource areas off New Jersey and transects the shelf, does have significant across-shelf flows that are coherent along the entire thalweg (Mayer et al., 1982). Flows of 10 to 25 cm/s have been recorded within the valley.

2.2.4 Water Level Variations

Tides on the New Jersey shelf are comprised primarily of the M2 semi-diurnal lunar component. The tidal amphodromic point in the North Atlantic shows that the M2 tide rotates counter-clockwise in the western Atlantic, resulting in a tidal wave that propagates southward along the New Jersey coast (i.e., it is high tide at Sandy Hook before it is high tide at Cape May). The S2 (solar semidiurnal) and O1 (diurnal) tides also contribute to overall tidal signatures (Louis Berger Group, 1999). Tides along the New Jersey coast reach a maximum range of approximately 2 m during spring tides and a minimum range of approximately 1 m during neap conditions (NOAA, 2000).

2.2.5 Nearshore Sediment Transport

Nearshore sediment transport is a complex process that governs erosion and accretion on beaches. Sediment is moved alongshore and cross-shore (on and offshore) by physical coastal processes, such as wind, waves, tides, and currents. The time scales of sediment movement and shoreline change vary from the initial formation of headlands and coasts on geologic time scales (thousands of years) to severe coastal erosion over a few days or hours during extratropical storms (northeasters) and hurricanes.

In addition to physical coastal processes, sediment transport patterns are dependent upon the characteristics and supply of sediment. Grain size is the most important characteristic of the sediment. The quantity of sediment moved is inversely proportional to its grain size. Sediment transport rates decrease with increasing grain size, because heavier sediment requires more time and energy to be transported. Sediment density, durability, and shape also affect transport rates. In addition, the supply of sediment governs sediment transport rates, because transport rates are reduced where sediment is in short supply.

When waves break at an angle to the beach, alongshore-directed currents are generated, capable of lifting and moving sediment along the coast. For example, waves approaching most of the New Jersey shoreline from the east tend to move sand alongshore from north-to-south towards Cape May. Superimposed on this regional pattern are the smaller scale reversals in longshore transport direction associated with tidal inlets. Toward the northern portion of New Jersey, the shoreline becomes oriented nearly north-south. In this region, the net sediment transport direction is reversed, where mean wave conditions tend to drive sediment from south-

to-north. Because wave direction changes frequently along the New Jersey coast, sand is moved back-and-forth along the beach. On an annual basis, there typically is a dominant wave direction that drives net sediment transport. Gross sediment transport (the annual transport that occurs in both directions along a beach) may be significantly larger than the net transport if a single wave direction is not dominant. Along the New Jersey shoreline, regional wave conditions exhibit large variations; therefore, some areas show nearly unidirectional longshore sediment transport and other areas exhibit large gross transport, with relatively low net sediment transport.

Past work regarding longshore transport rates for much of the New Jersey coast is limited. According to Ashley et al. (1986), wave-generated longshore currents have the most apparent effect on sediment transport. Although it is generally accepted that the typical north-to-south currents dominate beach transport processes along much of the shoreline, the amount of sediment entrained in the littoral system along the New Jersey coast is not known with confidence. In addition, a sediment transport reversal occurs in the vicinity of Barnegat Inlet (Buteux, 1982), where the net sediment transport north of this region is from south-to-north. However, Buteux (1982) acknowledged that the location of the nodal point was highly variable and migrated between Beach Haven Inlet at the southern end of Long Beach Island to Bradley Beach north of Manasquan Inlet.

The USACE have been responsible for most quantitative estimates of littoral transport rates along the New Jersey shoreline. Caldwell (1966) determined that the total net longshore transport north of the “nodal point” between Manasquan and Barnegat Inlets was to the north. Around Manasquan Inlet, the net transport was estimated to be 74,000 cubic yards annually to the north. Further north, northerly sediment transport increased to a maximum of nearly 500,000 cubic yards annually along the Sandy Hook shoreline.

South of Barnegat Inlet, the shoreline becomes oriented nearly southwest-to-northeast, and wave-induced transport becomes more southerly. The USACE performed a Feasibility Study (USACE, 1996) for the shoreline region between Brigantine Inlet and Great Egg Harbor Inlet which computed a net sediment transport rate along Brigantine Island to be approximately 100,000 cubic yards annually to the south. Another Feasibility Study for the shoreline between Townsends Inlet and Cape May Inlet (USACE, 1997) concluded that the net transport rate in the vicinity of Townsends Inlet was 385,000 cubic yards annually to the southwest.

2.3 BIOLOGY

2.3.1 Benthic Environment

The following subsections provide summaries of the existing literature concerning the benthic environment, including infauna (Section 2.3.1.1), Atlantic surfclam (Section 2.3.1.2), and epifauna and demersal fishes (Section 2.3.1.3), in and around the eight sand resource areas. This information, along with the assessment of ecological conditions from the biological field surveys (see Section 6.0), provides the framework for the evaluation of potential effects from dredging on these organisms (Section 7.5).

2.3.1.1 Infauna

Regional investigations of benthic fauna in the vicinity of the New Jersey sand resource areas primarily have been associated with more widespread sampling in the New York Bight, which includes shelf waters offshore New Jersey. While fewer in number and generally more limited in scope, previous surveys in the immediate vicinity of the New Jersey sand resource areas reveal a consistency with New York Bight benthic surveys in terms of infaunal assemblage composition (Pearce, 1974; Garlo and Saffian, 1976; Pearce et al., 1976; Pearce et

al., 1981; Reid et al., 1991; Kropp, 1995a; Chaillou and Scott, 1997; Versar, Inc., 1997). Infaunal assemblages inhabiting shelf waters offshore New Jersey resemble assemblages common to much of the Middle Atlantic Bight (Wigley and Theroux, 1981). Figure 2-23 shows the location of select benthic investigations of inner shelf sand bottoms offshore New Jersey.

Organisms collected during previous investigations of the New York Bight consist of members of the major invertebrate groups commonly found in sand bottom marine ecosystems, primarily crustaceans, echinoderms, mollusks, and polychaetous annelids. Generally, inner shelf infaunal assemblages are numerically dominated by polychaetes in terms of abundance (Wigley and Theroux, 1981) and numerically dominant taxa (Reid et al., 1991). Other conspicuous members of the coastal New Jersey infaunal community include amphipod crustaceans and bivalves. Infaunal taxa that inhabit inner shelf sand bottoms offshore New Jersey comprise assemblages that exhibit spatial and seasonal variability (Pearce et al., 1976; Pearce et al., 1981; Wigley and Theroux, 1981; MMS, 1989; Reid et al., 1991; Chang et al., 1992).

Large-scale investigations of the New York Bight identified the most common infaunal taxa inhabiting inner shelf waters, including areas offshore New Jersey. Chang et al. (1992) identified infaunal assemblages based on 1980 to 1982 benthic data from the New York Bight. One widespread group of infaunal taxa identified by this study was determined to be a basic, natural assemblage for the Bight. Common taxa in this widespread assemblage are predominantly polychaetes, including *Aricidea catherinae*, *Goniadella gracilis*, *Mediomastus ambiseta*, *Monticellina dorsobranchialis*, *Parougia caeca*, *Scoletoma acicularum*, *S. hebes*, and *Tharyx acutus*. Other taxa include the amphipods *Ampelisca agassizi*, *Byblis serrata*, *Corophium crassicorne*, *Erichthonius fasciatus*, *Leptocheirus pinguis*, and *Unciola* spp., the bivalve *Nucula proxima*, and the echinoid *Echinarachnius parma*. Pearce et al. (1981) summarized and synthesized results from several benthic investigations (1973 to 1976) of the Bight inner shelf. Common infaunal taxa censused during those investigations, including areas offshore New Jersey, include the amphipods *Protohaustorius wigleyi* and *Unciola irrorata*, the bivalves *N. proxima*, *Spisula solidissima*, and *Tellina agilis*, the echinoid *E. parma*, and the polychaetes *Glycera dibranchiata*, *G. gracilis*, *Nephtys bucera*, *N. picta*, *Pherusa affinis*, *Spiophanes bombyx*, and *T. acutus*.

Reid et al. (1991) summarized infaunal data collected during 1980 to 1985 in the New York Bight, including the contents of grab samples collected from several stations in the central portion of the New Jersey inshore (depths <30 m) subarea (Figure 2-23). Cluster analysis using this infaunal data determined patterns of infaunal similarity among samples collected from New Jersey stations. The study presented the consistently dominant taxa (i.e., those that were in the top 10 of numerical abundance in ≥50% of the samples) within sample groups formed by cluster analysis of the 1980 to 1985 data collected from inshore New Jersey stations. The numerically dominant taxa contained in these sample groups predominantly were polychaetes (15 taxa), especially *G. gracilis*, and bivalves (*Astarte castanea*, *S. solidissima*, and *T. agilis*). Other common taxa included the amphipod *Pseudunciola obliquua*, the echinoid *E. parma*, the tanaid *Tanaissus liljeborgi* (= *psammophilus*), and unidentified rhynchocoels.

Sampling associated with the proposed Atlantic Generating Station occurred in an area of inner shelf waters from Brigantine Island to Long Beach Island and 8 km seaward of New Jersey (Garlo and Saffian, 1976). Clam dredge and grab samples were used to survey infaunal assemblage composition and the abundance and distribution of infaunal populations. Common taxa collected during this investigation included the amphipod *U. irrorata*, the bivalves *Ensis directus*, *N. proxima*, and *T. agilis*, and the polychaetes *G. gracilis*, *M. ambiseta*, *N. picta*, *Paranaitis speciosa*, *S. bombyx*, and*T. acutus*.

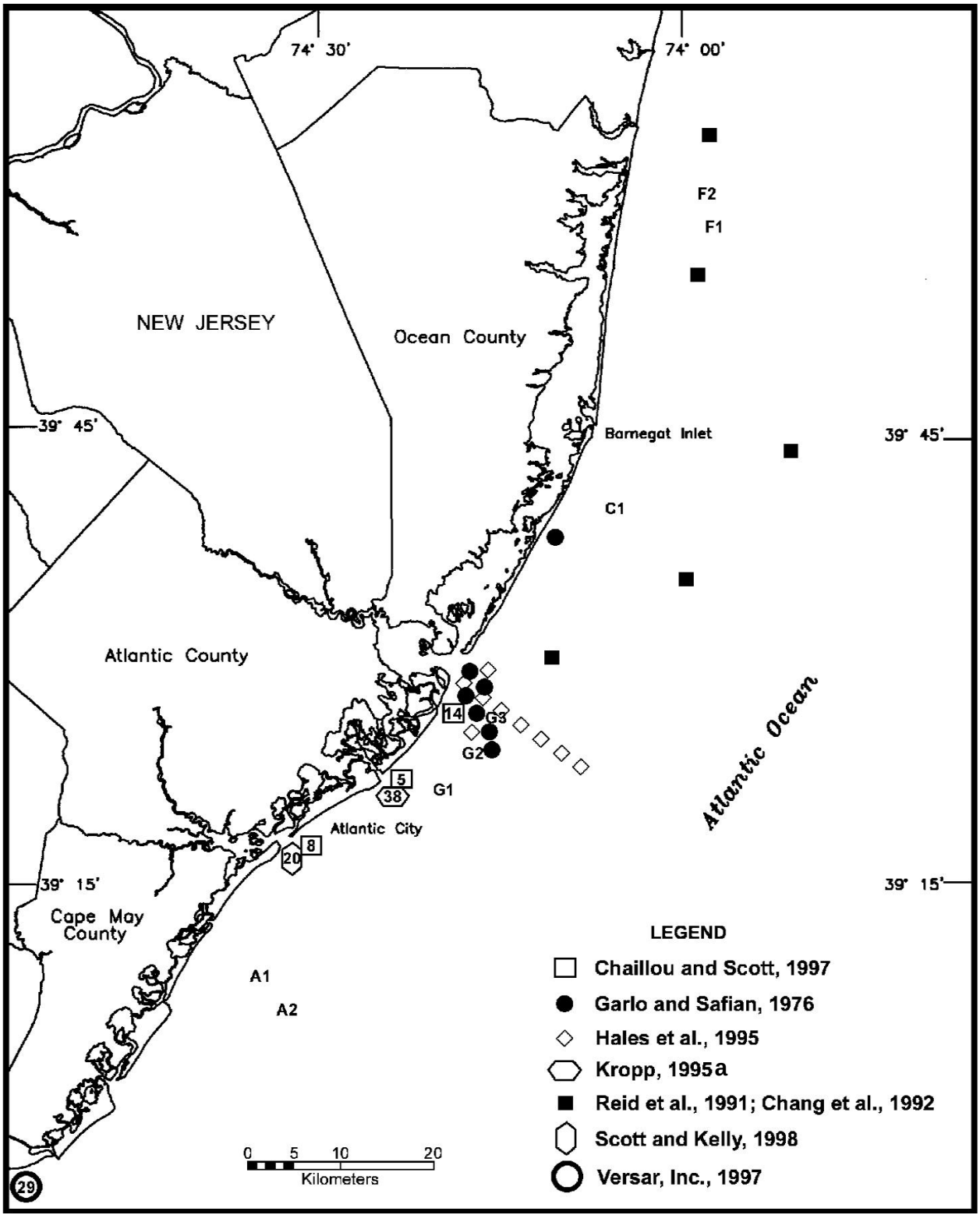

Figure 2-23. Approximate locations of benthic sampling stations for previous biological surveys offshore New Jersey relative to the eight sand resource area locations (A1, A2, C1, F1, F2, G1, G2, G3). Numbers inside symbols indicate multiple stations.

More recently, Versar, Inc. (1997) identified infauna collected with benthic grabs offshore Cape May Meadows, New Jersey. Numerically dominant infauna collected in this investigation included the amphipod *Parahaustorius longimerus*, the bivalves *Petricola pholadiformis*, *S. solidissima*, and *T. agilis*, the gastropod *Turbonilla interrupta*, the annelids *Caulleriella* sp., oligochaetes, *Parapionosyllis longicirrata*, and *Polycirrus eximius*, and the archiannelid *Polygordius* sp. The archiannelid *Polygordius* was found in great abundance in the Versar, Inc. (1997) survey, in some areas with mean densities of nearly 11,000 individuals/m^2. *Polygordius* also occurred in high densities in nearshore waters off New Jersey during the study by Kropp (1995a). Scott and Kelly (1998) surveyed the infaunal community at a sand borrow site 3 km offshore Great Egg Harbor, New Jersey and identified the numerically dominant taxa. The most abundant taxa at the borrow site included the amphipods *Acanthohaustorius millsi*, *P. longimerus*, and *Protohaustorius* cf. *deichmannae*, the bivalves *Donax variabilis* and *S. solidissima*, the isopod *Chiridotea tuftsi*, and the polychaete *Dispio uncinata* (Scott and Kelly, 1998).

The distribution and abundance of infaunal populations inhabiting New Jersey inner shelf communities are affected by abiotic environmental parameters that influence the composition and distribution of infaunal assemblages. Spatially variable factors such as water depth and sediment type influence benthic assemblages and the extent of numerical dominance of those assemblages by various infaunal groups.

Wigley and Theroux (1981) reported that highest infaunal densities in the New York Bight occurred at relatively shallow depths. With increasing water depth, abundance of each of the major taxonomic groups (e.g., bivalves) generally decreases, although not uniformly across taxonomic groups. At depths less than 24 m, polychaetous annelids are numerically dominant (1,120 individuals/m^2), followed by bivalves (590/m^2) and amphipod crustaceans (487/m^2). At depths from 25 to 49 m in New York Bight waters, amphipods (459/m2) are the most common group, followed by polychaetes (137/m2) and bivalves (51/m^2).

The effect of water depth upon benthic assemblages in some cases may be defined more precisely as an effect of depth-related environmental factors, including parameters that vary with increasing depth, such as current regime, dissolved oxygen, sedimentary regime, and temperature. Surficial sediments tend to be well sorted at shallow depths, due primarily to the mixing of shelf waters by storms. In broad terms, inner shelf waters are less depositional in nature than outer shelf or slope waters due to a dynamic current regime, but shallow areas near an area affected by estuarine outflow may experience episodic deposition of fine materials, and thereby influence benthic community structure. Although existing descriptions of depth-related differences in benthic assemblages have encompassed geographically broad areas (Wigley and Theroux, 1981), local variability in bathymetric relief can result in habitat heterogeneity within an area of relatively minor depth differences. Trough features, especially those that are bathymetrically abrupt, can dissipate current flow along the bottom. Reduction of current flow can result in deposition of fine materials, including organic material. The presence of fine sediments and organics in bathymetric depressions can support benthic assemblages that are distinct from nearby areas without depressions (Boesch, 1972).

Certain infaunal populations are distributed in approximately equal numbers from shallow waters to the edge of the shelf (e.g., the polychaete *S. bombyx*), while others occur mostly on the inner shelf (e.g., the bivalve *S. solidissima*) or midshelf to outer shelf (e.g., the polychaete *Scalibregma inflatum*) (Pearce et al., 1981). Although there is a negative correlation between infaunal abundance and water depth, it is unclear whether such faunal distributions are affected mostly by sedimentary regime, or whether factors such as water depth, hydrology, and seasonality override any effects of sediment particle size and type on infaunal assemblages.

Previous sampling efforts in northwestern Atlantic shelf waters have demonstrated the importance of sediment type in determining infaunal population densities. Coarse-grained sediments generally support greatest numbers of infauna, while fine-grained sediments support the fewest (MMS, 1989). In a report based on over 1,000 quantitative samples of benthic fauna collected from Maine to northern New Jersey between 1956 and 1965, Theroux and Wigley (1998) summarized the relationship between sediment type and infaunal abundance. Amphipods are found in all sedimentary habitats, though densities are highest in sand. Greater bivalve densities are found in silt-clay sediments relative to coarser particles and bivalve abundance generally decreases with increasing sediment particle size, although shell fragment habitats can support moderately high bivalve numbers. Gravel bottoms support the lowest densities of bivalves, while gastropod densities are highest on shell or gravel bottoms, with these coarse sediments being more suitable for locomotion by broad-footed prosobranch and opisthobranch mollusks. Polychaetes occur in all sediment types, although greatest abundances are found in sand and gravel bottoms and least in silt-clay habitats (Theroux and Wigley, 1998).

Sediment particle size has a qualitative effect on the species composition of benthic assemblages, as well. Pearce et al. (1981) confirmed the findings of other studies that found sediment type a reliable predictor of the distribution of certain infaunal taxa inhabiting inner shelf sediments of the New York Bight. Although many infaunal species inhabit a variety of sediment types, many of these taxa tend to predominate in specific sedimentary habitats. Offshore New Jersey, the medium- to coarse-grained sand community commonly is represented by *E*. *parma*, *N*. *bucera*, *Protohaustorius* spp., *S*. *bombyx*, *S*. solidissima, *T*. *agilis*, and *U*. *irrorata*. *Polygordius* commonly is associated with sand habitat, although it also is common in shell or shell hash habitats (Barry A. Vittor & Associates, 1985). Sedimentary habitats with finer materials support relatively high densities of taxa such as the amphipods *Ampelisca agassizi* and *U*. *irrorata*, the bivalve *N*. *proxima*, and the polychaetes *Mediomastus* and *T*. *acutus* (Pearce et al., 1981; Chang et al., 1992).

Certain taxa are well adapted to inhabiting gravel bottoms, due to anchoring, locomotion, or feeding methods. Blue-ribbed mussel (*Mytilus edulis*) have byssal threads to attach to hard or fixed objects, and gravel bottoms provide a suitable substratum for such an anchoring method. Marine gastropod densities generally are highest on shell or gravel bottoms, with these coarse sediments suitable for their method of crawling locomotion, as opposed to relatively unstable sands. Many scale-worm polychaetes (e.g., *Harmothoe* spp.) are interstitial predators that are abundant in cracks and crevices that exist between gravel-sized particles (Pettibone, 1963).

Infaunal assemblages are composed of taxa that are adapted to particular sedimentary habitats through differences in behavioral, morphological, physiological, and reproductive characteristics. Feeding is one behavioral aspect most closely related to sedimentary habitat (Sanders, 1958; Rhoads, 1974). In general, coarse sediments in high water current habitats, where organic particles are maintained in suspension in the water column, favor the occurrence of suspension-feeding taxa that strain food particles from the water column. Coarse sediments also facilitate the feeding of carnivorous taxa that consume organisms occupying interstitial habitats (Fauchald and Jumars, 1979). At the other extreme, habitats with fine-textured sediments and little or no current are characterized by the deposition and accumulation of organic material, with these habitats supporting surface and subsurface deposit feeding taxa. In between these habitat extremes are a variety of habitat types that differ with respect to various combinations of sedimentary regime, depth, bathymetry, and hydrological factors. These different habitats tend to support particular infaunal assemblages that often vary with time.

2.3.1.2 Atlantic Surfclam

The Atlantic surfclam (*Spisula solidissima*) inhabits sandy substrate on the continental shelf from Maine to North Carolina. It ranges from nearshore to at least 80-m water depths and is restricted to water temperatures of 25°C or less. Individuals occur in "beds" or aggregations over the sandy shelf, where they are harvested by commercial fishers using hydraulic dredges (Mid-Atlantic Fishery Management Council, 1988).

The Atlantic surfclam grows to a shell length of about 20 cm as an adult and is one of the largest bivalves known from the northeastern continental shelf (Weinberg, 1998a). Shell growth varies with water depth, temperature, and food availability. Shell growth in inshore waters averages 9.8 cm/yr, whereas shell growth in offshore waters averages 13.3 cm/yr (Jones et al., 1978). Large individuals have been found to be at least 25 years old with some exceeding 30 years (Jones et al., 1978). Growth of individuals appears to be retarded in relation to density within the beds (Weinberg, 1998b). Density-dependent effects on growth were thought to be caused by intraspecific competition for space and food (Weinberg, 1998b).

Male and female Atlantic surfclams reach sexual maturity in their second year. Spawning has been described as a single event and as multiple events from July to early November (Weinberg, 1998a). Within a surfclam bed, spawning is thought to be a synchronous annual event (Mid-Atlantic Fishery Management Council, 1988). The gametes are broadcast into the water column, where fertilization occurs. Distribution and settlement of larvae depend on local circulation patterns and larval behavior. Larvae are planktonic for about 20 days.

Atlantic surfclam abundance varies spatially over the shelf depending upon recruitment patterns, predation, and fishing pressure. Fishery landings data and fishery-independent sampling show that Atlantic surfclams are common on the New Jersey shelf. The National Marine Fisheries Service (NMFS) divides the Middle Atlantic Bight into five subareas for fishery-independent surveys and fishery landings recording. These subareas are Long Island, northern New Jersey, southern New Jersey, Delmarva, and southern Virginia-North Carolina. About 95% of the commercial Atlantic surfclam landings were taken from these collective areas. Since 1984, most of the commercial catch was recorded from northern New Jersey. This area produced a higher proportion of larger clams (>12.7 cm), which in turn produced a better yield (weight of shucked meat per bushel) than other areas such as Delmarva and southern Virginia-North Carolina. The northern New Jersey area continues to produce the highest catches and currently represents 80% of the total surfclam catch in the U.S. (Mid-Atlantic Fishery Management Council, 1998).

To illustrate the distribution and abundance of Atlantic surfclam in relation to the eight sand resource areas, catches from NMFS fishery independent surveys for the years 1977 to 1997 were examined (NMFS, 1998a). These surveys follow a stratified random sampling design and use a hydraulic dredge to collect surfclams. Figure 2-24 gives the location of the hydraulic dredge samples and average catch. Surfclams are widespread over the shelf in water depths that include the sand resource areas. From these data, it is clear that the likelihood of encountering surfclams within the sand resource areas is high.

2.3.1.3 Epifauna and Demersal Fishes

Investigations of the epifaunal and demersal fish communities inhabiting New Jersey inner shelf waters reveal seasonal and spatial variations in the distribution and abundance of taxa. Many numerically dominant epifauna that inhabit the inner shelf may be described more precisely as epibenthic, especially gastropods and decapods, as these taxa routinely are collected along with infauna using grab samplers.

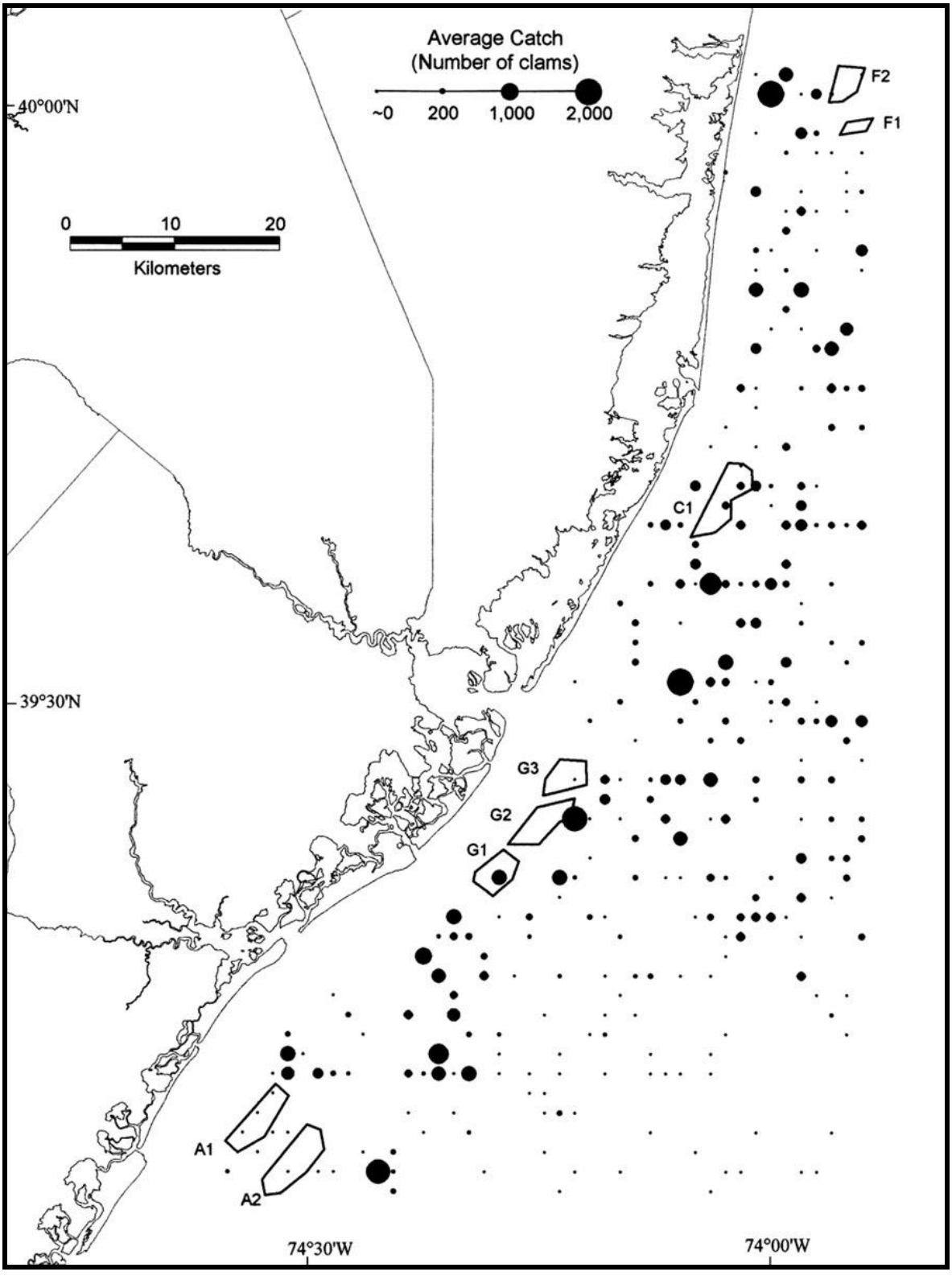

Figure 2-24. Locations and average catches of hydraulic dredge hauls made during National Marine Fisheries Service surfclam/ocean quahog surveys (1977 to 1997) relative to the eight sand resource areas offshore New Jersey.

Certain epifaunal taxa, such as lady crab (*O. ocellatus*), commonly burrow deeply into sediments and adaptive behaviors of this type can complicate efforts to categorize such taxa into a specific, lifestyle-based, invertebrate group. Given this dilemma of ecological classification, however, the taxa discussed below commonly are collected in trawl samplers and, for the sake of comparison and consistency, herein are considered epifauna. Abundant epifauna of the New Jersey inner shelf include crustaceans such as *Pagurus* spp., Atlantic rock crab (*C. irroratus*), and sevenspine bay shrimp (*Crangon septemspinosa*), echinoderms such as the sea star *Asterias forbesi* and sand dollar *E. parma*, and moon snails (*Euspira heros* and *Nevirita duplicata*) (Pearce et al., 1981; Hales et al., 1995; Versar, Inc., 1997; Viscido et al., 1997).

Epifaunal taxa were collected and described during 18 cruises from October 1991 to November 1992 on the inner continental shelf (water depth 8 to 16 m), offshore Great Egg Inlet, New Jersey (Hales et al., 1995; Viscido et al., 1997). Monthly samples were taken with a 2-m beam trawl at and adjacent to the Beach Haven Ridge, an offshore sand shoal. Crustaceans, echinoderms, and mollusks were the most abundant epifauna in trawl collections. Commonly sampled epifauna included the bivalve *S. solidissima*, echinoderms, such as the asteroid *A. forbesi* and the echinoids *E. parma* and *Arbacia punctulata* (sea urchin), and the gastropods *Busycon* spp., *E. heros*, and *N. duplicata*, (Hales et al., 1995). Viscido et al. (1997) reported on epibenthic decapods sampled during the Beach Haven Ridge investigation. The sevenspine bay shrimp was the most abundant decapod found in the study, followed by Atlantic rock crab, lady crab, and spider crab (*Libinia emarginata*). Together with sevenspine bay shrimp, these taxa comprised over 98% of all decapods collected.

Seasonal patterns in abundance were similar for nearly all taxa in the Beach Haven Ridge studies. Abundance of most epifaunal taxa was low in winter, then increased to peak densities in summer and declined in fall (Hales et al., 1995). Exceptions to this seasonal pattern included members of the Gastropoda (including the moon snails *E. heros* and *N. duplicata*), which were most abundant in winter or spring. Temporal variation of the numerically dominant epibenthic decapods was evident in the Viscido et al. (1997) study, as well. Abundance of sevenspine bay shrimp showed two clear peaks, in spring and fall, as did spider crab. Atlantic rock crab and lady crab each showed a single peak in individual density of very small individuals in summer and appeared to use the site for settlement.

Monthly trawl samples for the Beach Haven Ridge investigations were taken at three separate stations (landward of the ridge, on the ridge top, and seaward of the ridge). Among near-ridge collections of epifauna, gastropods and *S. solidissima* were more abundant in deeper waters (depths 12 to 16 m) around the ridge (landward, seaward, or both) than on top of the ridge (depths 8 to 10 m). *S. solidissima* was present seaward of the ridge but was more abundant at deeper sites on the continental shelf. All echinoderm groups occurred near the ridge but were generally abundant in, and characteristic of, deeper sites on the inner continental shelf. Three of the numerically dominant decapods (Atlantic rock crab, lady crab, and sevenspine bay shrimp) exhibited marked spatial heterogeneity in abundance, with many fewer found on the ridge top than at either of the other two stations, while lady crab was not as spatially variable (Viscido et al., 1997). Statistical analyses revealed much less difference in assemblage structure between the landward and seaward stations than was demonstrated between either of these two areas and the ridge top. The most common pattern of distribution found by the Beach Haven sand ridge studies was that epifauna were abundant around (landward and seaward), but not on, the ridge (Hales et al., 1995; Viscido et al., 1997). The observed distribution patterns of epifauna around Beach Haven Ridge may be attributable to a number of factors, including, but not limited to, sediment type and local hydrology.

Demersal fishes inhabiting the New Jersey inner shelf mostly are seasonal migrants (Grosslein, 1976; MMS, 1989). Southern transients found in offshore New Jersey waters during fall include taxa in the families Carangidae, Dasyatidae, Fistulariidae, Mullidae, Priacanthidae, Sciaenidae, Scombridae, Serranidae, and Tetraodontidae. Northern transients collected during winter and spring in waters offshore New Jersey include members of the Clupeidae, Cottidae, Gadidae, and Gasterosteidae (Able and Hagen, 1995). Although there is considerable variation in the abundance and distribution of demersal taxa between both seasons and years, numerical dominants at any one time generally are represented by a relatively small group of fishes. Winter is a time of low abundance and diversity, as most species leave the area for warmer waters offshore and to the south.

Many fishes that commonly are found offshore New Jersey also utilize the estuarine areas along the coast. During spring, increasing numbers of fishes are attracted to the New Jersey coast because of the proximity of the estuaries that these fishes use for spawning and as nurseries. Some fishes that use the bays and inlets include bay anchovy (*Anchoa mitchilli*), red hake (*Urophycis chuss*), spot (*Leiostomus xanthurus*), weakfish (*Cynoscion regalis*), windowpane (*Scophthalmus aquosus*), and winter flounder (*Pseudopleuronectes americanus*).

From 1972 to 1975, a large-scale ecological study was conducted for the proposed Atlantic Generating Station, and included trawl surveys (depths 2 to 19 m) along the New Jersey coast near Little Egg Inlet, in the vicinity of Beach Haven Ridge (Able and Hagen, 1995). Species composition of trawls included 93 taxa from 47 families. Relative abundance of these demersal taxa varied substantially between sampling efforts. The most abundant fishes sampled included resident species such as bay anchovy, red hake, silver hake (*Merluccius bilinearis*), spotted hake (*Urophycis regia*), weakfish, and windowpane. The proximity of Little Egg Inlet to the sampling area was reflected in the numerical dominance of estuarine-related taxa in the trawls.

The Offshore Demersal Fish Sampling (ODFS) is part of an ongoing biological monitoring program offshore New Jersey (Barry A. Vittor & Associates, Inc., 1999a). Sampling efforts for the ODFS use an otter trawl at depths from 12 to 22 m. To date, sampling has been conducted during two time periods (spring and late summer) of each year from 1995 to 1998. Overall, results from the ODFS program indicate substantial annual and seasonal variability in species abundance. For example, the Spring 1995 sampling effort collected 17,161 individuals representing 25 taxa, while the Spring 1996 effort resulted in 2,727 individuals in 18 taxa. Numerical dominance in trawls showed marked variation, as well. Blueback herring (*Alosa aestivalis*) was numerically dominant in three of four spring sampling efforts, comprising as much as 60% of trawl-caught taxa (1995), while various skates (*Raja* spp.) were the most abundant taxa in 1997 spring trawls. The single most dominant species observed in fall collections (1995 to 1998) was butterfish (*Peprilus triacanthus*), representing 33.1, 49.4, 98.8, and 91.8% of the total catch for each year, respectively. Other numerical dominants collected by the ODFS were anchovies (*Anchoa* spp.), hakes (*Urophycis* spp.), sand lance (*Ammodytes hexapterus*), searobins (*Prionotus* spp.), windowpane, and winter flounder.

Much of the diet of Mid-Atlantic fishes consists of other fishes, however, the diet of many of the most common demersal fishes consists of epibenthic and infaunal invertebrates (Grosslein, 1976). The affinity of certain demersal fishes for particular sediment types often is related to the types of prey items supported by those sediments (Rogers, 1977). Species such as butterfish, skates, and winter flounder predominantly are bottom feeders that consume infaunal and epibenthic crustaceans and polychaetes. Amphipods are known to be important in the diets of some demersal fishes, including cod, haddock, and winter flounder. Certain demersal foragers may therefore be attracted to areas of medium to coarse sands, where crustaceans and polychaetes are most abundant (Theroux and Wigley, 1998).

2.3.2 Pelagic Environment

Existing information on the pelagic environment is provided in this section to support discussions in Section 7.6 concerning potential impacts to transitory pelagic species. Ecological characteristics and seasonal distributions of zooplankton (including ichthyoplankton) and nekton (i.e., squids, fishes, sea turtles, and mammals) that occur in nearshore shelf waters of New Jersey are described. Available literature supplied most of the information presented in this section. These studies provide information relevant to the New Jersey shelf as it is included within the larger regions such as the Middle Atlantic Bight or New York Bight.

2.3.2.1 Zooplankton

Zooplankton form essential links in the marine food web between primary producers (phytoplankton and bacteria) and larger marine species such as fishes, birds, and marine mammals. They are relatively weak swimmers that drift with water currents. Zooplankton transport organic matter through the water column by their vertical migration and production of organically rich fecal pellets that sink to the seafloor.

Zooplankton can be functionally divided into holoplankton and meroplankton. Holoplankton spend their entire lives in the water column, whereas meroplankton occur as plankton only during certain stages (generally larval stages) of their life cycle. Many important commercial and recreational fish species have planktonic eggs and larvae. Holoplankton and non-fish meroplankton are discussed together in this zooplankton section. Fish eggs and larvae are discussed separately in the ichthyoplankton section, which occurs after this section.

Major constituents of the zooplankton include chaetognaths, copepods, and gelatinous zooplankton. Other groups include amphipods, cladocerans, euphausiids, heteropods, polychaetes, and pteropods. Middle Atlantic Bight zooplankton assemblages were studied by Judkins et al. (1980), Sherman et al. (1983, 1984), and Grant (1991). All of these large-scale studies included samples collected offshore New Jersey.

Collections by Judkins et al. (1980) in the New York Bight produced 124 taxa including 88 copepods, 10 chaetognaths, and 26 classified as other (either holoplankters or meroplankters). Table 2-2 gives the 20 most abundant taxa collected by Judkins et al. (1980). Copepods numerically dominated samples collected in the New York Bight (Judkins et al., 1980) as well as the entire northeastern continental shelf (Sherman et al., 1983). Copepods composed more than 60% of the zooplankton numbers in samples from the New York Bight and Middle Atlantic Bight. They also were the most frequently occurring taxon. Listed in decreasing order of occurrence, the most frequently occurring species were *Centropages typicus*, *Psuedocalanus* sp., *Calanus finmarchicus*, *Oithona similis*, *Paracalanus parvus*, and *O. atlanticus*. Three species (*Calanus finmarchicus*, *Pseudocalanus minutus*, and *Centropages typicus*) accounted for 75% of the total zooplankton abundance for the entire shelf from Georges Bank to Cape Hatteras (Sherman et al., 1983). Aside from these numerical dominants, most copepod taxa (approximately 60 taxa) were considered uncommon or rare. Many of these rare taxa were coastal or estuarine forms present only in fall samples (Judkins et al., 1980).

Other holoplankters collected in appreciable numbers were pteropods, cladocerans, and urochordates (Judkins et al., 1980). Pteropods contributed 14% of the total zooplankton numbers, cladocerans (Penilia avirostris and Evadne spp.) contributed 10%, and urochordates (doliolods and appendicularians) yielded another 6% of the total zooplankton numbers. Chaetognaths were not abundant, but were frequently collected by Judkins et al. (1980). The following species were most common: *Parasagitta* (=*Sagitta) elegans*, *Serratosagitta (=Sagitta)*

Table 2-2. Seasonal variations in mean abundance (#/m^3) of zooplankton in the New York Bight, 1974 to 1975 (after: Judkins et al., 1980).

	1974		1975			
	Sept	Oct-Nov	Feb-Mar	Apr-May	June-July	Aug-Sept
20 Most Abundant Taxa						
Copepods						
Acartia tonsa	140	14	-	<1	-	132
Calanus fimmarchicus	70	32	12	261	231	173
Centropages typicus	445	606	700	104	1,498	451
Clausocalanus pergens	1	1	21	27	15	21
Metridia lucens	2	4	23	58	15	12
Oithona atlantica	18	31	27	18	14	24
O. similis	3	<1	221	255	227	68
Paracalanus parvus	74	188	299	41	295	784
Pseudocalanus sp.	33	11	374	1,163	900	245
Temora longicornis	3	5	30	204	1,605	16
Chaetognaths						
Sagitta elegans	19	5	9	55	61	19
Others						
Appendicularians	115	6	204	316	60	39
Doliolids	552	1	-	-	4	183
Evadne spp.	127	2	-	306	77	23
Gastropod veligers	<1	<1	431	324	149	2
Medusae	4	16	10	87	33	2
Penilla avirostris	2,278	24	<1	-	-	1,152
Echinoderm plutei	308	90	-	22	1	25
Polychaete larvae	3	1	4	57	12	26
Pteropods	13	8	1,215	937	335	149
Total Zooplankton						
Total Copepods	1,089	986	1,879	2,260	4,930	2,047
Total Chaetognaths	34	31	12	53	94	43
Total Others	3,441	215	1,582	2,138	733	1,662
Grand Total	4,564	1,232	3,473	4,451	5,757	3,752

serratodentata, and *Flaccisagitta (=Sagitta) enflata*. Grant (1991) collected 18 chaetognath species offshore of southern New Jersey and Delamarva. The most frequently occurring species collected during his survey were *Serratosagitta tasmanica*, *Parasagitta elegans*, *Flaccisagitta enflata*, *Mesosagitta minima*, and *Sagitta helenae*. Other holoplankters reported from the New York Bight or Middle Atlantic Bight were euphausiids, heteropods, hyperiid amphipods, medusae, salps, and siphonophores.

Although not abundant, meroplankters were represented in the collections by anthozoan larvae, barnacle cyprises, barnacle nauplii, bivalve veligers, decapod larvae, echinoderm pleutei, ectoproct larvae, gastropod veligers, polychaete larvae, and stomatopod larvae. The most abundant were gastropod veligers, which accounted for 3% of the overall zooplankton abundance (Judkins et al., 1980).

Zooplankton species composition in the Middle Atlantic Bight appears to be persistent over time. Comparisons of zooplankton samples collected over a wide spatial grid annually for 5 years with older studies revealed that species composition and biomass in the northeastern Atlantic (including the Middle Atlantic Bight) have not changed appreciably in 70 years (Sherman et al., 1983, 1984). The seasonal pattern in zooplankton abundance and biomass is an annual low in winter to an autumn high (Sherman et al., 1983, 1984). This pattern was persistent within the Middle Atlantic Bight over the 5-year period (Sherman et al., 1983). Observed seasonal patterns were mostly driven by the numerically dominant copepods (e.g., Kane, 1997).

Ichthyoplankton

The ichthyoplankton assemblage found in the Middle Atlantic Bight and New Jersey shelf waters generally corresponds with the existing adult fish assemblage. This adult fish assemblage consists of some endemic resident species, but many are migrants from northern or southern waters. Northern species migrate south during winter months and southern species migrate north in summer months. This pattern is seen in the occurrence of larval fishes in the Middle Atlantic Bight. Many of the transient species spawn while moving through Middle Atlantic Bight waters, thus contributing to the abundance and diversity of local ichthyoplankton. Because spawning times of adults can be inferred from egg and larval occurrences, this information is given to augment information on temporal patterns of ichthyoplankton occurrence. Table 2-3 provides the spawning times and locations of important species from the region.

Investigations of ichthyoplankton in the Middle Atlantic Bight region have been conducted by the NMFS (e.g., Smith, 1988; Smith and Morse, 1988) primarily through the Marine Monitoring, Assessment and Prediction Program (MARMAP). Under this program, ichthyoplankton samples have been collected at cross-shelf stations throughout the northeastern continental shelf from the Gulf of Maine to Cape Hatteras since the 1970s. Summaries exist for various portions of the program (e.g., Sherman et al., 1984; Smith, 1988; Smith and Morse, 1988; Doyle et al., 1993). MARMAP collections relevant to the shelf and inshore areas of New Jersey were recently summarized by Able and Fahay (1998).

More than 200 taxa of fish eggs and larvae have been recorded from Middle Atlantic Bight waters by MARMAP (Smith and Morse, 1988). Fifty taxa represented most of the fish larvae collected from the entire northeast Atlantic shelf (Doyle et al., 1993). Of these taxa, sand lances (*Ammodytes* spp.) accounted for 30% of the numbers, while hakes (*Urophycis* spp.) and silver hake (*Merluccius bilinearis*) accounted for 7.5 and 5.5%, respectively. Anchovies (Engraulidae) and 12 other species accounted for another 1 to 5% of all fish larvae in the collections. These included Atlantic herring (*Clupea harengus*), lanternfish (*Ceratoscopelus maderensis*),

Table 2-3. Summary of spawning times and location of fishes in the central part of the Middle Atlantic Bight (after: Able and Fahay, 1998).

Species	Spawning Time	Spawning Location	Egg Type
Carcharhinidae			
Mustelus canis	Sp	Estuary/MAB	Live
Anguillidae			
Anguilla rostrata	Sp	SS	Unknown
Clupeidae			
Alosa aestivalis	Sp	FW	Pelagic
Brevoortia tyrannus	Fa, Sp	MAB/SAB	Pelagic
Clupea harengus	Sp	MAB	Demersal
Engraulidae			
Anchoa hepsetus	Su	MAB	Pelagic
A. mitchilli	Su	Estuary/MAB	Pelagic
Synodontidae			
Synodus foetens	Unknown	SAB	Unknown
Gadidae			
Pollachius virens	Fa-Wi	MAB	Pelagic
Phycidae			
Urophycis chuss	Su	MAB	Pelagic
U. regia	Sp-Fa	MAB	Pelagic
U. tenuis	Sp	MAB (Slope)	Pelagic
Ophidiidae			
Ophidion marginatum	Su-Fa	MAB	Pelagic
Syngnathidae			
Hippocampus erectus	Sp-Su	Estuary/MAB	Live
Triglidae			
Prionotus carolinus	Su-Fa	MAB (Estuary?)	Pelagic
P. evolans	Su-Fa	MAB (Estuary?)	Pelagic
Serranidae			
Centropristis striata	Sp-Fa	MAB	Pelagic
Pomatomidae			
Pomatomus saltatrix	Sp-Su	SAB/MAB	Pelagic
Carangidae			
Caranx hippos	Unknown	SAB	Pelagic
Lutjanidae			
Lutjanus griseus	Su	SAB	Pelagic
Sciaenidae			
Bairdiella chrysoura	Su	Unknown	Pelagic
Cynoscion regalis	Sp-Su	Estuary/MAB	Pelagic
Leiostomus xanthurus	Wi	MAB	Pelagic
Menticirrhus saxatilis	Su	MAB	Pelagic
Micropogonias undulatus	Su-Fa	MAB	Pelagic
Pogonias cromis	Su	MAB	Pelagic
Chaetodontidae			
Chaetodon ocellatus	Unknown	SAB	Pelagic
Mugilidae			
Mugil cephalus	Wi	SAB	Pelagic
M. curema	Sp	SAB	Pelagic
Sphyraenidae			
Sphyraena borealis	Sp	SAB	Pelagic
Labridae			
Tautoga onitis	Sp-Fa	Estuary/MAB	Pelagic
Tautogolabrus adspersus	Sp-Fa	MAB	Pelagic
Pholidae			
Pholis gunnellus	Wi	Estuary/MAB	Demersal
Uranoscopidae			
Astroscopus guttatus	Su	Estuary/MAB	Unknown
Stromateidae			
Peprilus triacanthus	Sp-Su	Estuary/MAB	Pelagic
Scophthalmidae			
Scophthalmus aquosus	Sp,Fa	Estuary/MAB	Pelagic
Paralichthyidae			
Etropus microstomus	Sp-Fa	MAB	Pelagic
Paralichthys dentatus	Fa-Wi	MAB	Pelagic
Pleuronectidae			
Pseudopleuronectes americanus	Wi	Estuary/MAB	Demersal

Spawning Time
Fa = Fall.
Sp = Spring.
Su = Summer.
Wi = Winter.

Spawning Location
FW = Fresh Water.
MAB = Middle Atlantic Bight.
SAB = South Atlantic Bight.
SS = Sargasso Sea.

Atlantic cod (*Gadus morhua*), haddock (*Melanogrammus aeglefinus*), bluefish (*Pomatomus saltatrix*), Atlantic mackerel (*Scomber scombrus*), butterfish (*Peprilus triacanthus*), and flatfishes including windowpane (*Scophthalmus aqousus*), Gulf Stream flounder (*Citharichthys actifrons*), smallmouth flounder (*Etropus microstomus*), fourspot flounder (*Paralichthys oblongus*), and yellowtail flounder (*Pleuronectes* [=*Limanda*] *ferrugineus*). The remaining taxa each represented less than 1% of the total numbers of larval fishes collected (Doyle et al., 1993).

A persistent seasonal cycle was documented for eggs and larvae in the Middle Atlantic Bight that reflects the spawning times of the adults (Smith and Morse, 1988). Eggs occur in relatively low numbers during late winter, but by mid-April they were abundant and peak levels were reached in June. Numbers of larvae exhibited a similar seasonal pattern with a peak in summer. Each season's samples were numerically dominated by different larval taxa (Sherman et al., 1984). In winter, sand lances exceeded all taxa in abundance representing over 90% of the numbers collected. In spring, the rank order of abundance was a lanternfish (*Benthosema glaciale*), Atlantic mackerel, sand lance, windowpane, butterfish, and yellowtail flounder. In summer, smallmouth flounder, Gulf Stream flounder, anchovies, bluefish, butterfish, and searobins (*Prionotus* spp.) were numically dominant. By fall, searobins, Atlantic croaker (*Micropogonias undulatus*), hakes (*Urophycis* spp.), Gulf stream flounder, smallmouth flounder, and lefteye flounders (Bothidae) numerically dominated the collections. Cowen et al. (1993) described a summer shelf assemblage of fish larvae for the New York Bight that was numerically dominated by bluefish, hakes, butterfish, and cunner (*Tautogolabrus aspersus*). Able and Fahay (1998) summarized the species composition and monthly occurrence of larval fishes from MARMAP collections made in the central Middle Atlantic Bight that focused on the New Jersey shelf (Table 2-4).

Several species mentioned above that are present as larvae and juveniles in the Middle Atlantic Bight were actually spawned in more southerly waters. This highlights the influence of circulation on the distribution of larval fishes in the region. The role of physical processes in structuring larval fish assemblages was examined in detail by Cowen et al. (1993). They described five spatially distinct summer ichthyoplankton assemblages for the New York Bight. These assemblages were maintained by a combination of physical processes (currents and fronts) and larval behavior. They found larvae of species spawned in waters south of Cape Hatteras often appear offshore in the Middle Atlantic Bight, transported to the area by the Gulf Stream. Many of these taxa, especially those of southern origin, will not survive in the Middle Atlantic Bight due to low water temperatures or other stressors. Two species spawned in southerly waters that do survive are bluefish and butterfish. Larvae and juveniles of these species enter offshore waters of the Middle Atlantic Bight and make their way into inshore waters where they spend their first year of life (Cowen et al., 1993; Rotunno and Cowen, 1997). These species appear to have adapted their cross-shelf migration to the complex circulation of the Middle Atlantic Bight.

Table 2-4. Ranking of the most abundant larval fishes collected in continental shelf waters in the central part of the Middle Atlantic Bight during Marine Monitoring, Assessment and Prediction Program (MARMAP) surveys from 1977 to 1987 (after: Able and Fahay, 1998).

Taxon	Jan	Feb	Mar	Apr	May	Jun	Jul	Aug	Sep	Oct	Nov	Dec
Ammodytes spp.	1	1	1	1	2	--	--	--	--	--	--	4
Gadus morhua	2	3	2	3	7	--	--	--	--	--	--	7
Paralichthys dentatus	3	2	9	--	--	--	--	--	--	5	2	1
Brevoortia tyrannus	4	--	--	--	--	--	--	--	--	--	5	5
Merluccius bilinearis	5	9	--	--	--	7	9	9	--	6	4	2
Maurolicus muelleri	6	--	--	--	--	--	--	--	--	--	--	8
Leiostomus xanthurus	7	--	--	--	--	--	--	--	--	--	--	--
Pollachius virens	8	4	7	--	--	--	--	--	--	--	--	--
Gobiidae	9	--	--	--	--	--	--	--	--	--	8	--
Clupea harengus	10	--	--	--	--	--	--	--	--	--	--	--
Micropogonias undulatus	11	--	--	--	--	--	--	--	--	--	--	--
Pholis gunnellus	--	5	4	11	--	--	--	--	--	--	--	--
Myoxocephalus octodecemspinosus	--	6	3	10	--	--	--	--	--	--	--	--
Paralepididae	--	7	--	--	--	--	--	--	--	--	--	--
Anguilla rostrata	--	8	--	--	--	--	--	--	--	--	--	--
Notolepis rissoi	--	10	10	--	--	--	--	--	--	--	--	--
Pseudopleuronectes americanus	--	--	5	5	--	--	--	--	--	--	--	--
Myoxocephalus aenaeus	--	--	6	9	--	--	--	--	--	--	--	--
Cottidae	--	--	8	7	--	--	--	--	--	--	--	--
Benthosema glaciale	--	--	--	2	9	--	--	--	--	--	--	--
Limanda ferruginea	--	--	--	4	1	1	10	--	--	--	--	--
Liparis spp.	--	--	--	6	5	--	--	--	--	--	--	--
Melanogrammus aeglefinus	--	--	--	8	10	--	--	--	--	--	--	--
Scomber scombrus	--	--	--	--	3	3	--	--	--	--	--	--
Enchelyopus cimbrius	--	--	--	--	4	2	--	--	--	--	10	--
Scophthalmus aquosus	--	--	--	--	6	6	11	--	--	3	3	3
Glyptocephalus cynoglossus	--	--	--	--	8	5	--	--	--	--	--	--
Lophius americanus	--	--	--	--	--	4	7	--	--	--	--	--
Tautogolabrus adspersus	--	--	--	--	--	8	3	7	--	--	--	--
Hippoglossina oblonga	--	--	--	--	--	9	1	2	4	8	--	--
Urophycis chuss	--	--	--	--	--	10	4	--	--	--	--	--
Peprilus triacanthus	--	--	--	--	--	--	2	1	8	--	--	--
Pomatomus saltatrix	--	--	--	--	--	--	5	6	--	--	--	--
Engraulidae	--	--	--	--	--	--	6	8	10	--	--	--
Citharichthys arctifrons	--	--	--	--	--	--	8	4	2	2	6	--
Urophycis spp.	--	--	--	--	--	--	--	3	1	--	--	--
Etropus microstomus	--	--	--	--	--	--	--	5	3	7	--	--
Prionotus carolinus	--	--	--	--	--	--	--	10	5	9	--	--
Ophidion marginatum	--	--	--	--	--	--	--	--	6	--	--	--
Lepophidium profundorum	--	--	--	--	--	--	--	--	7	--	9	--
Centropristis striata	--	--	--	--	--	--	--	--	9	--	--	--
Ophidiidae	--	--	--	--	--	--	--	--	--	4	--	--
Bothus spp.	--	--	--	--	--	--	--	--	--	10	11	--
Urophycis regia	--	--	--	--	--	--	--	--	--	1	1	6
Ceratoscopelus maderensis	--	--	--	--	--	--	--	--	--	--	7	--
Diaphus spp.	--	--	--	--	--	--	--	--	--	--	--	9

Note: Larvae are ranked in the top 10 or 11 taxa per month according to numbers collected per 10 m^2 of sea surface. Dashes indicate few or no collections of that taxon in that month.

2.3.2.2 Squids

Squids (cephalopods) display patchy distributions and periodic vertical and horizontal migrations. Water quality, currents, and temperature principally control the occurrence of squids, while food and population density affect movements within suitable water masses.

Two squid species are common in New Jersey shelf waters: the longfin squid, *Loligo pealei*, and the shortfin squid, *Illex illecebrosus* (Lange and Sissenwine, 1980). These are the squids most likely to occur in or near the eight sand resource areas. The longfin squid, a member of the family Loliginidae, occurs primarily in shelf and shelf edge waters from Newfoundland to the Gulf of Venezuela. Its distribution, determined by fishery independent sampling, is influenced by water temperature, depth, and time of day (Brodziak and Hendrickson, 1999). A general seasonal migratory pattern has been observed for the Middle Atlantic Bight population. Adults move offshore in fall and remain there until April, when adults and young migrate back into shelf waters for the summer (Lange and Sissenwine, 1980). Spawning reportedly occurs year-round with major peaks in spring (April and May) and fall (August and September). The longfin squid grows rapidly and lives about 1 year (Lange and Sissenwine, 1980; Brodziak and Macy, 1996). This species represents an important fishery in the Middle Atlantic Bight with annual landings averaging 18,200 mt (Cadrin, 1998). Commercial fishing for longfin squid takes place from Cape Hatteras to Georges Bank. It is caught with small-mesh trawls, pound nets, and traps (Cadrin, 1998). Fishing effort tracks the seasonal distribution, with offshore (i.e, shelf edge) fishing taking place from October to March and inshore (i.e., middle and inner shelf) fishing taking place from April to September.

The shortfin squid belongs to the family Ommastrephidae, a family consisting entirely of oceanic species. This species is distributed accordingly in oceanic and shelf edge waters from Greenland to Cape Hatteras (Lange and Sissenwine, 1980). It migrates into shallower waters (10 to 50 m) during summer months; in late fall it moves south and offshore in the area from Georges Bank to Cape Hatteras (Lange and Sissenwine, 1980). Spawning occurs from December to June in offshore waters. Most individuals die following spawning. The species lives up to 1 year (Hendrickson, 1998). In Middle Atlantic Bight waters, commercial trawl fisheries are concentrated in outer shelf waters from June to September, when abundance peaks. The 1986 to 1996 annual catch of shortfin squid averaged 12,800 mt (Hendrickson, 1998). Most commercial fishing is conducted in shelf edge waters with small-mesh trawls.

2.3.2.3 Fishes

Common pelagic fishes inhabiting New Jersey shelf waters include herrings such as alewife (*Alosa psuedoharengus*), American shad (*Alosa sapidissima*), Atlantic herring, and Atlantic menhaden (*Brevoortia tyrannus*), as well as Atlantic mackerel, bluefish, and butterfish. Other pelagic species occurring offshore New Jersey, but not mentioned further include anchovies (*Anchoa hepsetus* and *A. mitchilli*), jack crevalle (*Caranx hippos*) and mullets (*Mugil* cephalus and *M. curema*).

All of these pelagic species form schools and migrate seasonally with peaks during various portions of the year. Most of these species are important to recreational and commercial fisheries. As with the demersal fishes, most pelagic species found in the Middle Atlantic Bight are transitory, originating in waters either to the north (Gulf of Maine or Georges Bank) or to the south (south of Cape Hatteras). Their occurrence in

the Middle Atlantic Bight is generally a response to seasonal changes in water temperature, which trigger southerly or northerly movements by species of southern or northern origin, respectively.

The herring species exhibit two basic spawning patterns: the alewife and American shad are anadromous, migrating from the sea into freshwater rivers to spawn, whereas Atlantic menhaden and Atlantic herring spawn in continental shelf waters. The alewife is found along the coast of eastern North America from the Gulf of St. Lawrence to South Carolina (Kocik, 1998a). During autumn, most of the population overwinters in waters near the edge of the continental shelf. In spring, the population moves into shelf waters throughout the region. Adults enter coastal rivers and migrate to freshwater to spawn during spring. The American shad is another anadromous species found in shelf waters during summer and fall (Kocik, 1998b). It moves up rivers to spawn during spring. Water temperature is the key environmental determinant of spawning in this species. Temperature may vary within a season, thus timing of the upstream migration may vary slightly from year to year. Alewife and American shad are important to commercial and recreational fisheries in the region. Commercial catches of alewife averaged about 500 mt for the Middle Atlantic Bight since 1994 (Kocik, 1998a). American shad catches, mostly by gill net, have averaged 1,100 mt since 1980 (Kocik, 1998b).

The Atlantic menhaden occurs in shelf waters, where it forms large schools. The schools in the Middle Atlantic Bight migrate northward in summer and back south in fall to overwinter in warmer waters. Some spawning may occur offshore New Jersey during fall, while the fishes are migrating south. This species is not fished north of Virginia. Atlantic herring is most abundant in northern waters of the Gulf of Maine and Georges Bank. The Georges Bank stock overwinters in the New York Bight from December to April. Spawning occurs year-round with peaks in spring and fall. Adult females lay demersal eggs. Spawning probably does not occur offshore of New Jersey (Able and Fahay, 1998). The primary fisheries for this species occur north of New Jersey on Georges Bank and in the Gulf of Maine.

The Atlantic mackerel occurs in two spawning populations in the northwest Atlantic: a northern population in the Gulf of St. Lawrence that spawns in June and July, and a southern population that spawns in the Middle Atlantic Bight during July and August (Overholtz, 1998a). In the Middle Atlantic Bight, it spends winter months in offshore waters near the shelf edge; in spring it migrates inshore and to the north. Spawning occurs during this migration in shelf waters. This species is sought by commercial and recreational fishers. Commercial fishing occurs primarily from January through May; recreational fishing occurs mostly from April to October (Overholtz, 1998a). Landings in the Middle Atlantic Bight averaged 14,840 mt from 1987 to 1996.

The bluefish is a migratory species occurring in inshore, coastal, and shelf waters. It migrates into the Middle Atlantic Bight during spring, and south or offshore during fall. The bluefish is an important fishery species. Early investigations held that the bluefish spawned during two discrete events, one in the South Atlantic Bight and the other in the Middle Atlantic Bight. New evidence indicates that spawning is a continuous event beginning during spring and ending during late summer in South Atlantic Bight waters (Cowan et al., 1993; Smith et al., 1994). The bluefish spawns during midsummer months in waters south of Cape Hatteras; however, young fish recruit to inshore waters of the Middle Atlantic Bight coast including Long Island Sound (Nyman and Conover, 1988). This species is important to commercial and recreational fisheries of the region. The 1994 to 1996 average commercial landings were 11,400 mt for the eastern U.S.;

recreational landings for the Middle Atlantic Bight were 7,400 mt (Terceiro, 1998). Primary commercial gear for bluefish are otter trawl and gill net.

The Middle Atlantic Bight butterfish population migrates northward and inshore in summer. In winter months, the population moves southward and offshore. The butterfish spawns continuously from late January to at least July in the Middle Atlantic Bight (Rotunno and Cowen, 1997). This species exhibits high natural mortality and serves as prey for many predatory species. It grows rapidly and reaches a maximum age of about 3 years (Rutunno and Cowen, 1997; Overholtz, 1998b). The current Middle Atlantic Bight fishery lands an average of 3,000 mt annually. Otter trawl is the principal gear used in the fishery.

2.3.2.4 Sea Turtles

Four sea turtle species are likely to occur offshore New Jersey: loggerhead (*Caretta caretta*), leatherback (*Dermochelys coriacea*), Kemp's ridley (*Lepidochelys kempii*), and green (*Chelonia mydas*). A fifth turtle species not discussed here is the hawksbill (*Eretmochelys imbricata*), which inhabits tropical/subtropical coral reefs and would be very unlikely to occur off New Jersey.

All sea turtles are protected under the Endangered Species Act of 1973. The leatherback and Kemp's ridley are endangered and the loggerhead is threatened. The green sea turtle is also threatened, except for the Florida breeding population, which is endangered. Due to inability to distinguish between the latter two populations away from the nesting beach, green turtles are considered endangered wherever they occur in U.S. waters (NMFS, 1996).

Loggerheads are the most common turtle in the project area. Although minor loggerhead nesting does occur as far north as New Jersey, most of the turtles found there are juveniles or subadults, which use shallow, coastal waters as benthic foraging grounds during their development. The seasonal window for the presence of turtles in New Jersey waters extends from June through November (NMFS, 1996).

Loggerhead Sea Turtle

The loggerhead sea turtle occurs throughout temperate and tropical waters of the Atlantic, Pacific, and Indian Oceans (Dodd, 1988). In the western North Atlantic, it is found in estuarine, coastal, and shelf waters from South America to Newfoundland. Because it is the most temperate of the sea turtles in nesting habits, it is the species most likely to be present along the Mid-Atlantic coast. The loggerhead was the most abundant turtle species seen during Cetacean and Turtle Assessment Program (CETAP) aerial surveys off the Mid-Atlantic and New England coasts (Winn, 1982).

Most of the loggerhead sightings, strandings, and incidental captures in coastal and estuarine New Jersey waters are juveniles or subadults (NMFS, 1996). These animals are most common during spring and summer months. Benthic immature turtles migrate northward from south of Cape Hatteras during spring, moving south again during fall (Marine Turtle Expert Working Group, 1996a). Loggerhead turtles may be present in New Jersey waters from June through November (NMFS, 1996).

Four nesting subpopulations of loggerhead turtles have been identified (Marine Turtle Expert Working Group, 1996a). These are 1) the northern subpopulation, extending from North Carolina to northeastern Florida; 2) the South Florida subpopulation; 3) the Florida Panhandle subpopulation; and 4) the Yucatan subpopulation. Ninety percent of loggerhead nesting in the U.S. occurs in South Florida.

Only minor loggerhead nesting occurs along the Atlantic coast as far north as New Jersey (Frazier, 1995).

After hatching, loggerheads swim offshore and begin a pelagic existence within *Sargassum* rafts, drifting in current gyres for several years (Marine Turtle Expert Working Group, 1996a). At approximately 40 to 60 cm carapace length, juveniles and subadults move into nearshore and estuarine areas, where they become benthic feeders for a decade or more prior to maturing and making reproductive migrations (Carr, 1987). Loggerheads captured incidentally in New Jersey coastal waters are typically in this size range (NMFS, 1996).

Loggerhead adults and subadults are generalist carnivores feeding primarily on nearshore benthic crustaceans (particularly crabs) and mollusks (Dodd, 1988). Studies in New York waters have shown that these turtles generally feed in water depths of 15 m or less (NMFS, 1996). All of the potential sand resource areas except Area F1 include such shallow depths.

Leatherback Sea Turtle

The leatherback sea turtle is a circumglobal species that inhabits waters of the western Atlantic Ocean from Newfoundland to northern Argentina. The leatherback is the largest living turtle (Eckert, 1995). It is considered the most pelagic of the sea turtles (Marquez, 1990) because of its unique deep-diving abilities (Eckert et al., 1986) and wide-ranging migrations. This species was the second most abundant turtle seen off the Mid-Atlantic coast during CETAP, including numerous sightings in shelf waters despite its reputation as an offshore species (Winn, 1982). Most sightings occurred during summer months.

Leatherbacks nest on coarse-grained, high-energy beaches in tropical latitudes (Eckert, 1995). Florida is the only location in the continental U.S. where significant leatherback nesting occurs. Very little is known of the pelagic distribution of hatchling and/or juvenile leatherback turtles.

Adult leatherbacks feed in the water column, primarily on cnidarians (medusae, siphonophores) and tunicates (salps, pyrosomas) (Eckert, 1995). The turtles are sometimes observed in association with jellyfish, but actual feeding behavior has only occasionally been documented. Foraging has been observed at the surface, but also is likely to occur at depth (Eckert, 1995).

Kemp's Ridley Sea Turtle

The Kemp's ridley is the smallest and most endangered of the sea turtles. Its distribution extends from the Gulf of Mexico to Nova Scotia and Newfoundland (Marine Turtle Expert Working Group, 1996b). Adult turtles are found almost exclusively in the Gulf of Mexico, primarily in shallow coastal waters less than 50 m deep (Byles, 1988).

Kemp's ridleys found along the New Jersey coast are juveniles and subadults that use shallow East Coast waters as developmental habitat. They move northward along the coast in spring with the Gulf Stream to feed in productive, coastal waters between Georgia and New England (NMFS and USFWS, 1992). These migrants then move southward with the onset of cooler temperatures in late fall and winter.

Nesting of Kemp's ridleys occurs almost entirely at Rancho Nuevo beach, Tamaulipas, Mexico, where 95% of the nests are laid along 60 km of beach (NMFS and USFWS, 1992; Weber, 1995). In the U.S., nesting occurs infrequently on Padre and

Mustang Islands in south Texas and in a few other locations (Marine Turtle Expert Working Group, 1996b).

After emerging, Kemp's ridley hatchlings swim offshore to inhabit *Sargassum* mats and drift lines associated with convergences, eddies, and rings. The hatchlings feed at the surface and are dispersed widely by Gulf and Atlantic surface currents. After reaching a size of about 20 to 60 cm carapace length, juveniles enter shallow coastal waters and become benthic carnivores (Marine Turtle Expert Working Group, 1996b). This is the life stage that could be present in the project area. Kemp's ridleys prefer crabs, but also occasionally eat mollusks, shrimps, dead fishes, and vegetation (Mortimer, 1982; Lutcavage and Musick, 1985; Shaver, 1991; Burke et al., 1993; Werner and Landry, 1994).

Green Sea Turtle

The green sea turtle has a circumglobal distribution in tropical and subtropical waters. In the U.S., it occurs in Caribbean waters around the U.S. Virgin Islands and Puerto Rico, and along the mainland coast from Texas to Massachusetts. Adult green turtles are typically found in shallow tropical and subtropical waters, particularly in association with seagrass beds (NMFS and USFWS, 1991).

Green sea turtles along the New Jersey coast are juveniles and subadults, because adults do not migrate from their preferred habitat (tropical/subtropical seagrass beds) except to nest. Juveniles and subadults may use shallow, coastal waters along the Atlantic coast as developmental habitat.

Primary nesting sites in U.S. Atlantic waters are high-energy beaches along the east coast of Florida, with additional sites in the U.S. Virgin Islands and Puerto Rico (NMFS and USFWS, 1991). Hatchlings swim out to sea and enter a pelagic stage in *Sargassum* mats associated with convergence zones.

Adult green turtles commonly feed on seagrasses, algae, and associated organisms, using reefs and rocky outcrops near seagrass beds for resting areas. The major feeding grounds in U.S. waters are located in Florida. In coastal New York waters, green turtles feed mainly on algae and the seagrass *Zostera marina* (Burke et al., 1992). Juveniles go through an omnivorous stage of 1 to 3 years (NMFS and USFWS, 1991).

2.3.2.5 Marine Mammals

Numerous marine mammal species may occur off the New Jersey coast (Winn, 1982). This discussion focuses on species that may occur in and near the sand resource areas. Marine mammals listed as endangered or threatened under the Endangered Species Act of 1973 are discussed first. A subsequent section covers non-listed cetaceans and pinnipeds. All marine mammals are protected under the Marine Mammal Protection Act of 1972.

Listed Species

Three species of endangered cetaceans that may occur offshore of New Jersey are associated primarily with shelf waters (Winn, 1982; NMFS, 1996). They are the fin whale, *Balaenoptera physalus*; humpback whale, *Megaptera novaeangliae*; and northern right whale, *Eubalaena glacialis*. There is no "resident" population of any of these whales in the study area. However, fin and humpback whales may be present during any season, though most likely during winter and spring. Northern right whales would be

present only as transients during spring and fall migrations. One additional cetacean (the harbor porpoise, *Phocoena phocoena*) occurring seasonally in coastal waters has been proposed for listing as a threatened species (62 FR 37562). No critical habitat for listed marine mammals is located in or near the project area.

Fin Whale. Fin whales range from the Arctic to the Greater Antilles. They are among the largest and fastest baleen whales and are usually found inshore of the continental shelf break (Winn, 1982). This species occurs widely in the Mid-Atlantic throughout the year, with concentrations from Cape Cod north in summer and from Cape Cod south in winter. Fin whales are frequently found along the New England coast from spring to fall in areas of fish concentration (Blaylock et al., 1995). It is thought that fin whales migrate north nearshore along the coast during spring and south offshore during winter. The area off the Delmarva peninsula may be important as winter and spring habitat (Winn, 1982). This species feeds on krill, planktonic crustaceans, and schooling fishes such as herring and capelin.

Humpback Whale. Humpback whales range from the Arctic to the West Indies. During summer, there are at least five geographically distinct feeding aggregations in the northern Atlantic (Blaylock et al., 1995). During fall, humpbacks migrate south to the Caribbean where calving and breeding occurs from January to March (Blaylock et al., 1995). Aerial surveys during CETAP detected only a few humpback whale sightings from New Jersey southward during any season (Winn, 1982). However, subsequently there have been numerous sightings and strandings off the Mid-Atlantic coast, particularly during winter and spring (Swingle et al., 1993; Wiley et al., 1995). Most of the stranded animals were juveniles, suggesting that the area may be an important developmental habitat (Wiley et al., 1995). Humpbacks feed largely on euphausiids and small fishes such as capelin, herring, and sand lance, and their distribution has been largely correlated to prey species and abundance (Blaylock et al., 1995). They have not historically used New Jersey waters as a major feeding ground (NMFS, 1996). Critical habitats have been identified in the western Gulf of Maine and the Great South Channel (Massachusetts).

Northern Right Whale. Northern right whales range from Iceland to eastern Florida, primarily in coastal waters. This is the rarest of the world's baleen whales, with a North Atlantic population of between 325 and 350 individuals (Kraus et al., 1993). Coastal waters of the southeastern U.S. (off Georgia and northeast Florida) are important wintering and calving grounds for northern right whales, while the waters around Cape Cod and Great South Channel are used for feeding, nursery, and mating during summer (Kraus et al., 1988; Schaeff et al., 1993). From June to September, most animals are found feeding north of Cape Cod. Southward migration occurs offshore from mid-October to early January (Kraus et al., 1993). Migration northward along the Mid-Atlantic coast takes place during late winter and early spring (NMFS, 1996). Designated critical habitat for the northern right whale includes portions of Cape Cod Bay and Stellwagen Bank and the Great South Channel (off Massachusetts) and waters adjacent to the coasts of Georgia and northeast Florida (59 FR 28793).

Harbor Porpoise. Harbor porpoises are found in cool temperate and subpolar waters of the Northern Hemisphere (Blaylock et al., 1995). Harbor porpoises were the most common odontocete species sighted on the continental shelf during CETAP (Winn, 1982). However, they were primarily concentrated in New England waters, well to the northeast of the New Jersey coastline (Winn, 1982). As the name implies, harbor porpoises are typically found in shallow water, most often in bays and harbors, although they occasionally travel over deeper offshore waters (Jefferson et al., 1993). The Gulf of

Maine population, which would include harbor porpoises occurring off New Jersey, has been proposed for listing as a threatened species (62 FR 37562). During summer, these animals are concentrated in Canada and the northern Gulf of Maine. During fall (October to December) and spring (April to June), they are widely distributed from Maine to North Carolina (Blaylock et al., 1995). Little is known of their distribution during winter (December through March). It is thought that harbor porpoises feed on pelagic schooling fishes such as herring and mackerel (Gaskin, 1992).

Other Listed Species. Three other endangered marine mammals occurring offshore the Mid-Atlantic are rarely seen in near-coastal waters. These are the blue whale, *B. musculus*; sei whale, *B. borealis*; and sperm whale*, Physeter macrocephalus*. Because these large whales prefer deep water well offshore of the continental shelf (Winn, 1982; Roden, 1998), they are unlikely to occur in the project area and are not discussed here.

Non-Listed Species

Numerous non-listed cetacean species may occur in waters off New Jersey. These include one mysticete (the minke whale, *B. acutorostrata*) and a variety of odontocetes (toothed whales and dolphins). The most common odontocetes in Mid-Atlantic shelf waters are bottlenose dolphin (*Tursiops truncatus*) and common dolphin (*Delphinus delphis*), both of which may be present year-round (Winn, 1982; Kenney, 1990). Other odontocetes potentially occurring off the Mid-Atlantic coast but typically in deeper waters (along the shelf edge and beyond) include long-finned pilot whale (*Globicephala melas*), grampus (*Grampus griseus*), northern bottlenose whale (*Hyperoodon ampullatus*), dwarf and pygmy sperm whales (*Kogia simus* and *K. breviceps*), Atlantic spotted dolphin (*Stenella frontalis*), clymene dolphin (*S. clymene*), striped dolphin (*S. coeruleoalba*), spinner dolphin (*S. longirostris*), and rough-toothed dolphin (*Steno bredanensis*) (Winn, 1982; Blaylock et al., 1995; Roden, 1998). Though beaked whales (*Mesoplodon* spp. and *Ziphius cavirostris*) also may occur off the Mid-Atlantic, their distribution at sea is poorly known and they are believed to be principally deep, offshore species. Shelf species potentially occurring in the area but generally found in more northern waters include Atlantic white-sided dolphin (*Lagenorhynchus acutus*), white-beaked dolphin (*L. albirostris*), and the previously discussed harbor porpoise. The killer whale (*Orcinus orca*) also may occur on the shelf or slope (Winn, 1982), but is considered uncommon or rare in U.S. waters (Blaylock et al., 1995).

Five non-listed pinniped species may occur off the New Jersey coast. The harbor seal (*Phoca vitulina*) and gray seal (*Halichoerus grypus*) are most common. Harbor seals normally occur year-round in coastal waters of Canada and New England, moving south to winter (Blaylock et al., 1995). Occurrences off New Jersey would be most likely from November through May. Gray seals (*Halichoerus grypus*) normally range from Labrador to New England (Blaylock et al., 1995), with wintering individuals likely to occur in the New York Bight area during November through May. Three other “ice seals” (the harp seal, *P. groenlandica*; hooded seal, *Cystophora cristata*; and ringed seal, *P. hispida*) are uncommonly found in U.S. waters.

3.0 REGIONAL GEOMORPHIC CHANGE

Nearshore sediment transport processes influence the evolution of shelf sedimentary environments to varying degrees depending on temporal and spatial response scales. Although micro-scale processes, such as turbulence and individual wave orbital velocities, determine the magnitude and direction of individual grain motion, variations in micro-scale processes are considered noise at regional-scale and only contribute to coastal response in an average sense. By definition, regional-scale geomorphic change refers to the evolution of depositional environments for large coastal stretches (10 km or greater) over extended time periods (decades or greater) (Larson and Kraus, 1995). An underlying premise for modeling long-term morphologic change is that a state of dynamic equilibrium is reached as a final stage of coastal evolution. However, the interaction between the scale of response and forces causing change may result in a net sediment deficit or surplus within a system, creating disequilibrium. This process of disequilibrium defines the evolution of coastal depositional systems.

Topographic and hydrographic surveys of coastal and nearshore morphology provide a direct source of data for quantifying regional geomorphology and change. Historically, hydrographic data have been collected in conjunction with regional shoreline position surveys by the U.S. Coast and Geodetic Survey (USC&GS); currently the Coast and Geodetic Survey of the National Ocean Service [NOS], National Oceanic and Atmospheric Administration [NOAA]). Comparison of digital bathymetric data for the same region but different time periods provides a method for calculating net sediment movements into (accretion) and out of (erosion) an area of study. Coastal scientists, engineers, and planners often use this information for estimating the magnitude and direction of sediment transport, monitoring engineering modifications to a beach, examining geomorphic variations in the coastal zone, establishing coastal erosion setback lines, and verifying shoreline change numerical models. The purpose of this portion of the study is to document patterns of geomorphic change throughout the sand resource areas and quantify the magnitude and direction of net sediment transport over the past 100 to 140 years. These data, in combination with wave and current measurements and model output, provide a temporally integrated approach for evaluating the potential physical impacts of offshore sand mining on sediment transport dynamics.

3.1 SHORELINE POSITION CHANGE

Creation of an accurate map is always a complex surveying and cartography task, but the influence of coastal processes, relative sea level, sediment source, climate, and human activities make shoreline mapping especially difficult. In this study, shoreline surveys are used to define landward boundaries for bathymetric surfaces and to document net shoreline movements between specified time periods. Consequently, net change results can be compared with wave model output and nearshore sediment transport simulations to evaluate cause and effect. Integration of results provides a direct method of documenting potential environmental impacts related to sand mining on the OCS.

3.1.1 Previous Studies

Beaches along the New Jersey coast are composed primarily of sand, silt, and gravel reworked from Cretaceous, Tertiary, and Quaternary Coastal Plain sediment (McMaster, 1954). Sediment is eroded from onshore Coastal Plain formations in the northern section of the coast or from submerged coastal plain sediment redistributed along the coast by waves and currents (Uptegrove et al., 1995). The northern limit of the study area is Manasquan Inlet, and the southern limit is Cape May. This length of shoreline encompasses an area referred to by Uptegrove et al. (1995) as the southern coast. Sand reworked from submerged Coastal Plain sediment mixes with southward-directed sediment originating from bluffs along the northern

coast to form a series of barrier islands extending 5 to 18 miles (8 to 29 km) in length. Some of the greatest shoreline changes that occur along the outer coast are the result of inlet processes. Inlets interrupt longshore transport of beach sand, potentially restricting sediment transport at entrances. Furthermore, navigation structures used to control channel migration and shoaling may result in erosional and depositional "hot spots" along beaches adjacent to inlets. Seven inlets along the southern coast have at least one jetty or one shoreline armored with rock to control inlet channel migration (Uptegrove et al., 1995).

Historical shorelines for the entire coast of New Jersey were digitally mapped as part of the New Jersey Historical Map Series (Farrell and Leatherman, 1989). The primary benefit of these data was to document shoreline response since the mid-1800s to natural processes and engineering activities (e.g., beach nourishment, jetty and groin placement). Unfortunately, a regional quantitative assessment of shoreline change was never completed using the map series. Only a cursory analysis has been performed by the USACE using this data set to address site-specific project needs (e.g., USACE, 1996, 1997).

Short-term shoreline and beach volume changes have been monitored by the State since March 1986. The NJDEP's Division of Engineering and Construction (DEC) contracted with the Stockton State College Coastal Research Center (CRC) to assist with planning and implementing the program. In Fall 1986, a survey team collected the first set of measurements at 83 beach profile stations along the Atlantic coast of New Jersey. Since this time, the CRC has collected annual beach profile measurements to document changes in beach sand volume and shoreline position. Uptegrove et al. (1995) provide details regarding these data for the period 1986 to 1992. Between Manasquan and Barnegat Inlets (Ocean County), a balance between beach erosion and accretion is illustrated; however, south of Barnegat Inlet to Little Egg Inlet, beach erosion has been chronic between 1986 and 1992 (Figure 3-1). In Atlantic and Cape May Counties, beach sand volume changes illustrate more variability depending on profile location relative to inlets and beach replenishment activities (Figure 3-2).

3.1.2 Shoreline Position Data Base

For the present study, six outer coast shoreline surveys were used to quantify historical shoreline change (Table 3-1). The first five surveys were conducted by the USC&GS in 1839/42, 1863/86, 1899, 1932/33, and 1950/51. The sixth survey was compiled by the NJGS in 1977 for the coast between Manasquan Inlet (north) and Hereford Inlet. The first three surveys were completed as field surveys using standard planetable techniques, whereas the final three shoreline surveys were interpreted from aerial photography. Data were compiled from historical maps and aerial photography by Farrell and Leatherman (1989). Digital data were provided for this study by the NJGS Geographic Information System Data and Resources group.

When determining shoreline position change, all data contain inherent errors associated with field and laboratory compilation procedures. These errors should be quantified to gauge the significance of measurements used for engineering/research applications and management decisions. Table 3-2 summarizes estimates of potential error for the shoreline data sets used in this study. Because these individual errors are considered to represent standard deviations, root-mean-square error estimates are calculated as a realistic assessment of combined potential error.

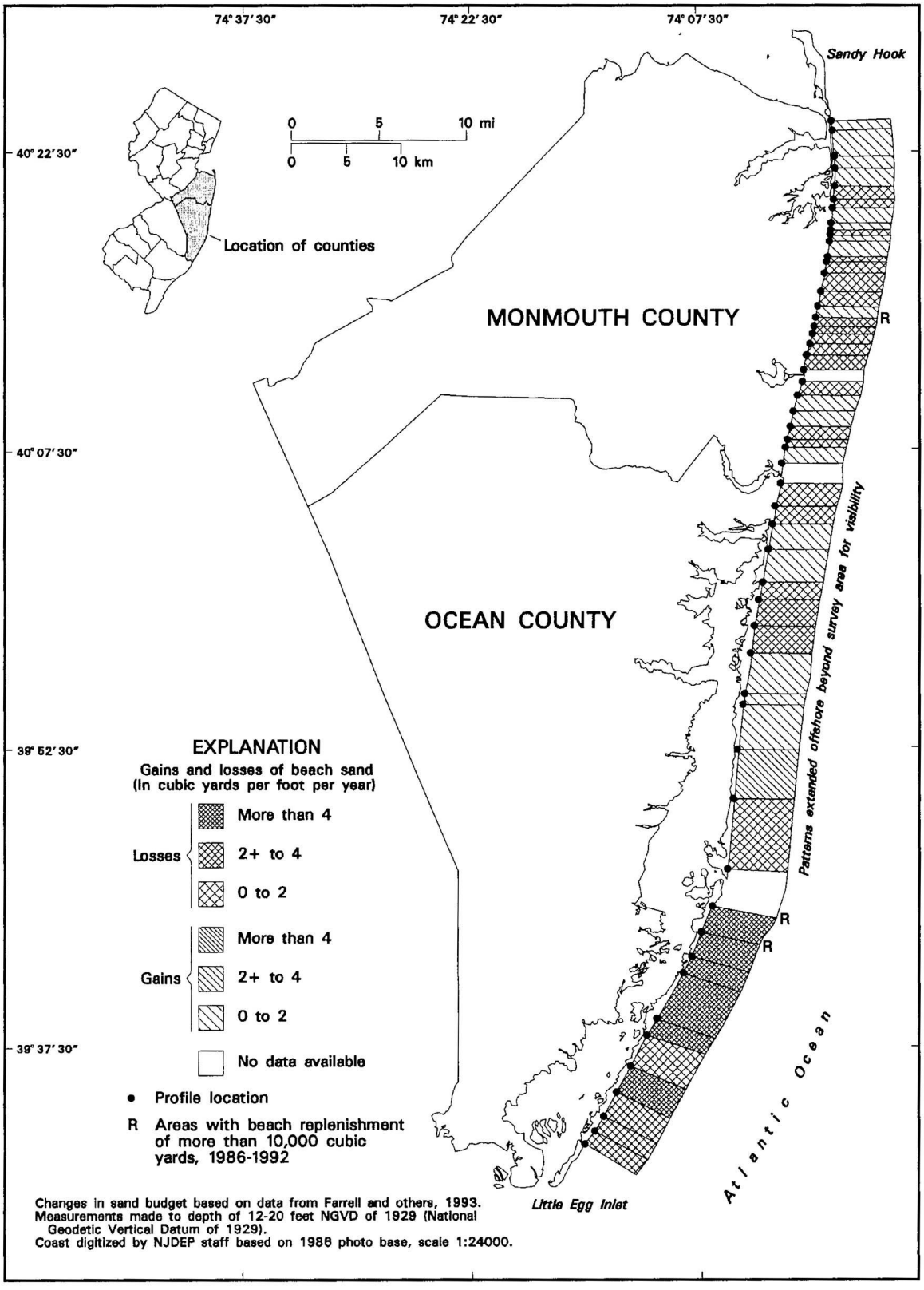

Figure 3-1. Changes in beach sediment volume and beach replenishment volume in Monmouth and Ocean Counties, New Jersey, 1986 to 1992 (from Uptegrove et al., 1995).

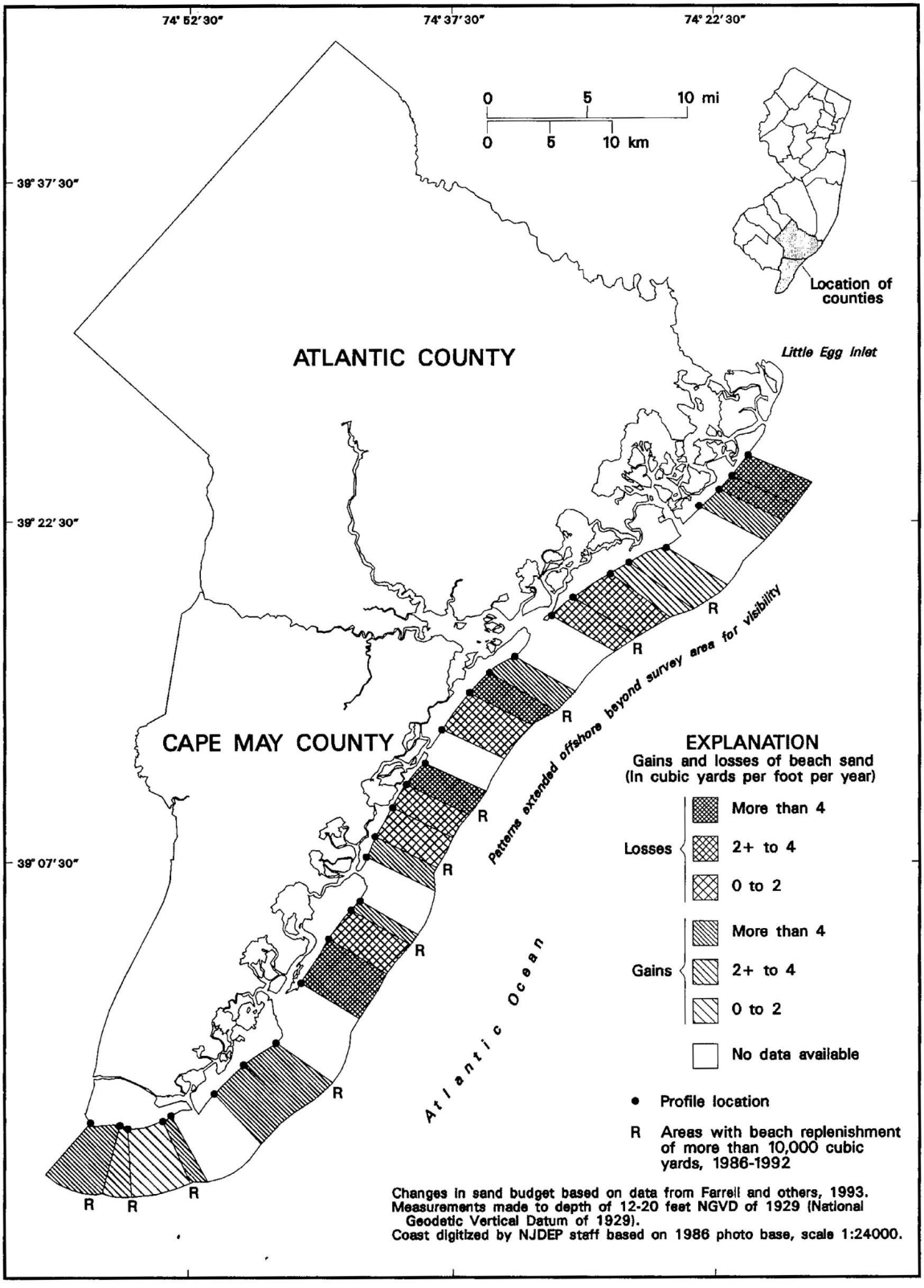

Figure 3-2. Changes in beach sediment volume and beach replenishment volume in Atlantic and Cape May Counties, New Jersey, 1986 to 1992 (from Uptegrove et al., 1995).

Table 3-1. Summary of shoreline source data characteristics for the New Jersey coast between Manasquan Inlet and Hereford Inlet.

Date	Data Source	Comments and Map Numbers
1839/42	U.S. Coast and Geodetic Survey (USC&GS) Topographic Maps 1:20,000 (T-116, T-119, T-120, T-121, T-142, T-143, T-146, T-147)	First regional shoreline survey throughout study area using standard planetable surveying techniques; 1839 - Manasquan Inlet south to central Long Beach Island (T-116, T-120, T-121); 1841 - central Long Beach Island south to Great Egg Inlet (T-119, T-142, T-143); 1842 - Great Egg Inlet south to Hereford Inlet (T-146, T-147).
1863/86	USC&GS Topographic Maps 1:10,000 (T-952) 1:20,000 (T-1084, T-1315a, T-1315b, T-1333, T-1371, T-1407, T-1532, T-1597, T-1744)	Second regional shoreline survey along the seaward coast of the study area using standard planetable surveying techniques; 1863/64 - Brigantine Inlet south to Longport (T-952); 1868 - Manasquan Inlet to northern Barnegat Bay (T-1084); 1871/75 - northern Barnegat Bay south to Little Egg Inlet (T-1315a, T-1315b, T-1333, T-1371, T-1407); 1881/86 - Longport south to Hereford Inlet (T-1532, T-1597, T-1744).
1899	USC&GS Topographic Maps 1:20,000	Third regional shoreline survey along the seaward coast of the New Jersey using standard planetable surveying techniques; Manasquan Inlet to Barnegat Inlet (T-2458, T-2459); Barnegat Inlet to Great Egg Inlet (T-2455, T-2456, T-2457); Great Egg Inlet to Hereford Inlet (T-2452, T-2453, T-2454).
April 1932/ May 1933	USC&GS Topographic Maps 1:10,000	First regional shoreline survey completed using aerial photography; Manasquan Inlet to Barnegat Inlet (T-5097, T-5284, T-5285, T-5286, T-5330); Barnegat Inlet to Great Egg Inlet (T-5099, T-5444, T-5445, T-5635, T-5637, T-5638); Great Egg Inlet to Hereford Inlet (T-5639, T-5642, T-5644, T-5645, T-5646, T-5647).
April 1950/ March 1951 and April 1943	USC&GS Topographic Maps 1:10,000 (T-9483N, T-9483S; T-9498N, T-9498S, T-9499N, T-9501S, T-9502N, T-9502S, T-9504S, T-9505N, T-9505S, T-9507N, T-9507S, T-9508N, T-9509N, T-9509S, T-9828N, T-9828S, T-9830N, T-9830S, T-9831N) 1:20,000 (T-8494)	All maps produced from interpreted aerial photography; April 1943 - Stone Harbor to Hereford Inlet (T-8494); April 1950 - Barnegat Inlet to Townsends Inlet (T-9501S, T-9502N/S, T-9504S, T-9505N/S, T-9507N/S, T-9508N, T-9509N/S); March 1951 - Manasquan Inlet to Barnegat Inlet, and Townsends Inlet to Stone Harbor (T-9483N/S, T-9498N/S, T-9499N, T-9828N/S, T-9830N/S, T-9831N).
1977	New Jersey Geological Survey (NJGS) 1:10,000	All maps produced from interpreted aerial photography; all shoreline information compiled and digitized by New Jersey Geological Survey personnel.

Table 3-2. Estimates of potential error associated with New Jersey shoreline position surveys.

Traditional Engineering Field Surveys (1839/42, 1863/86, and 1899)		
Location of rodded points	±1 m	
Location of plane table	±2 to 3 m	
Interpretation of high-water shoreline position at rodded points	±3 to 4 m	
Error due to sketching between rodded points	up to ±5 m	
Cartographic Errors (all maps for this study)	**Map Scale**	
	1:10,000	1:20,000
Inaccurate location of control points on map relative to true field location	up to ±3 m	up to ±6 m
Placement of shoreline on map	±5 m	±10 m
Line width for representing shoreline	±3 m	±6 m
Digitizer error	±1 m	±2 m
Operator error	±1 m	±2 m
Aerial Surveys (1932/33, 1950/51, 1977)	**Map Scale**	
	1:10,000	1:20,000
Delineating high-water shoreline position	±5 m	±10 m

Sources: Shalowitz, 1964; Ellis, 1978; Anders and Byrnes, 1991; Crowell et al., 1991.

Positional errors for each shoreline can be calculated using the information in Table 3-2; however, change analysis requires comparing two shorelines from the same geographic area but different time periods. Table 3-3 is a summary of potential errors associated with change analyses computed for specific time intervals. As expected, maximum positional errors are aligned with the oldest shorelines (1839/42, 1863/86, and 1899) at smallest scale (1:20,000), but most change estimates for the study area document shoreline advance or retreat greater than these values.

Table 3-3. Maximum root-mean-square potential error for New Jersey shoreline change data.

	1863/86	**1899**	**1932/33**	**1950/51**	**1977**
1839/42	±21.5[1]	±21.5	±17.3	±17.3	±17.3
	(±0.6)[2]	(±0.4)	(±0.2)	(±0.2)	(±0.1)
1863/86		±21.5	±17.3	±17.3	±17.3
		(±0.9)	(±0.3)	(±0.2)	(±0.2)
1899			±17.3	±17.3	±17.3
			(±0.5)	(±0.3)	(±0.2)
1932/33				±11.8	±11.8
				(±0.7)	(±0.3)
1950/51					±11.8
					(±0.5)

[1] Magnitude of potential error associated with high-water shoreline position change (m); [2] Rate of potential error associated with high-water shoreline position change (m/yr).

3.1.3 Historical Change Trends

Regional change analyses completed for this study provide a without-project assessment of shoreline response for comparison with predicted changes in wave-energy focusing at the

shoreline resulting from potential offshore sand dredging activities. It differs from previous qualitative analyses in that continuous measurements of shoreline change are provided at 50-m alongshore intervals for the period 1839/42 to 1977 (see Appendix A). As such, model results (wave and sediment transport) at discreet intervals along the coast can be compared with historical data to develop process/response relationships for evaluating potential impacts. The following discussion focuses on incremental changes in shoreline response (1839/42 to 1863/86, 1863/86 to 1899, 1899 to 1932/33, 1932/33 to 1950/51, 1950/51 to 1977) relative to net, long-term trends (1839/42 to 1977).

3.1.3.1 1839/42 to 1932

Shoreline response along the ocean beaches between Manasquan Inlet and Little Egg Inlet was significant for the period 1839/40 to 1872/74, illustrating large areas of shoreline recession north and south of Barnegat Inlet (up to 10 m/yr), as well as south of Manasquan Inlet (Figure 3-3). The average change rate for this area was about -2.3 m/yr (σ = ±4.0 m/yr); however, average change for areas of shoreline advance and retreat was 2.8 and -4.1 m/yr, respectively. Between 1872/74 and 1899, shoreline recession continued to dominate change trends for this section of coast, but the magnitude of change decreased along the shoreline 15 km north and south of Barnegat Inlet and increased substantially north of Little Egg Inlet. Average shoreline change was -1.8 m/yr (σ = ±3.3 m/yr), and average shoreline advance and retreat was 0.5 and -2.6 m/yr, respectively. Sediment transported alongshore by wave-induced currents created significant southward growth of Long Beach Island across Little Egg Inlet by 1872/74 (2.8 km or a southward migration rate of 85 m/yr). From 1872/74 to 1899, southward migration of Long Beach Island continued at a rate of about 46 m/yr, extending Long Beach Island about 1.2 km. However, shoreline recession of up to 15 m/yr ($\bar{x}$ = -6.5 m/yr) resulted along the coast 10 km to the north (Figure 3-4). The same trend continued between 1899 and 1932; that is, greatest changes occurred adjacent to entrances. Except for the beach south of Barnegat Inlet and the beaches adjacent to Little Egg Inlet, shoreline changes were within ±5 m/yr (Figure 3-5). Average change away from entrances was about -0.20 m/yr; average shoreline advance and retreat for the same area was 0.6 and -0.7 m/yr, respectively.

Shoreline changes along barrier island beaches south of Brigantine Inlet exhibited significantly greater variations than those to the north between 1841/42 and 1864/86. Greatest changes were again associated with inlets (up to 20 m/yr of recession and advance); however, net change between Brigantine and Hereford Inlets was about 1.1 m/yr (Figure 3-6) compared with -2.3 m/yr between Manasquan and Little Egg Inlets for the same time period (Figure 3-3).

The same level of variability in shoreline change rates was illustrated for the period 1864/86 to 1899. However, the average change rate for this section of coast was -0.5 m/yr, indicating that erosive processes and shoreline recession dominate (Figure 3-7). Although the average change rate is small, the variation between shoreline advance and retreat rates is large (18 to 20 m/yr), resulting in a standard deviation of 4.0. The average shoreline advance and retreat rates during this time were 2.6 and -2.8 m/yr, respectively. The most extreme changes again are associated with shorelines adjacent to inlets.

Between 1899 and 1932, overall patterns of shoreline change from Brigantine Inlet to Hereford Inlet remained influenced by inlet location and processes. Like earlier time periods, greatest rates of shoreline change (±10 to 15 m/yr) were adjacent to entrances (Figure 3-8). Average shoreline change for the beaches south of Brigantine Inlet was 0.4 m/yr (σ = ±3.7 m/yr). The large standard deviation value indicates that peaks in shoreline advance and

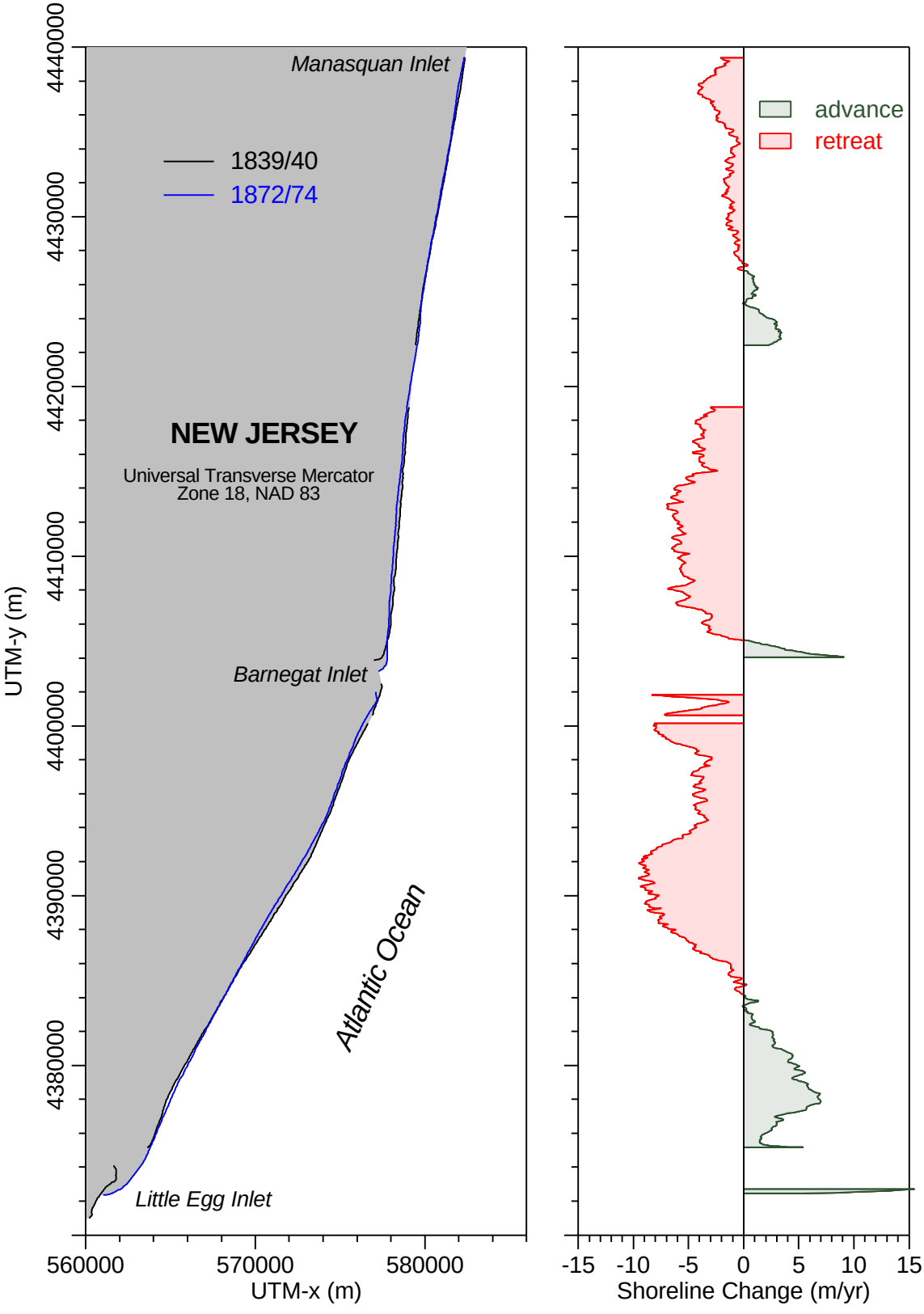

Figure 3-3. Shoreline position and change between Manasquan Inlet and Little Egg Inlet, New Jersey, 1839/40 to 1872/74.

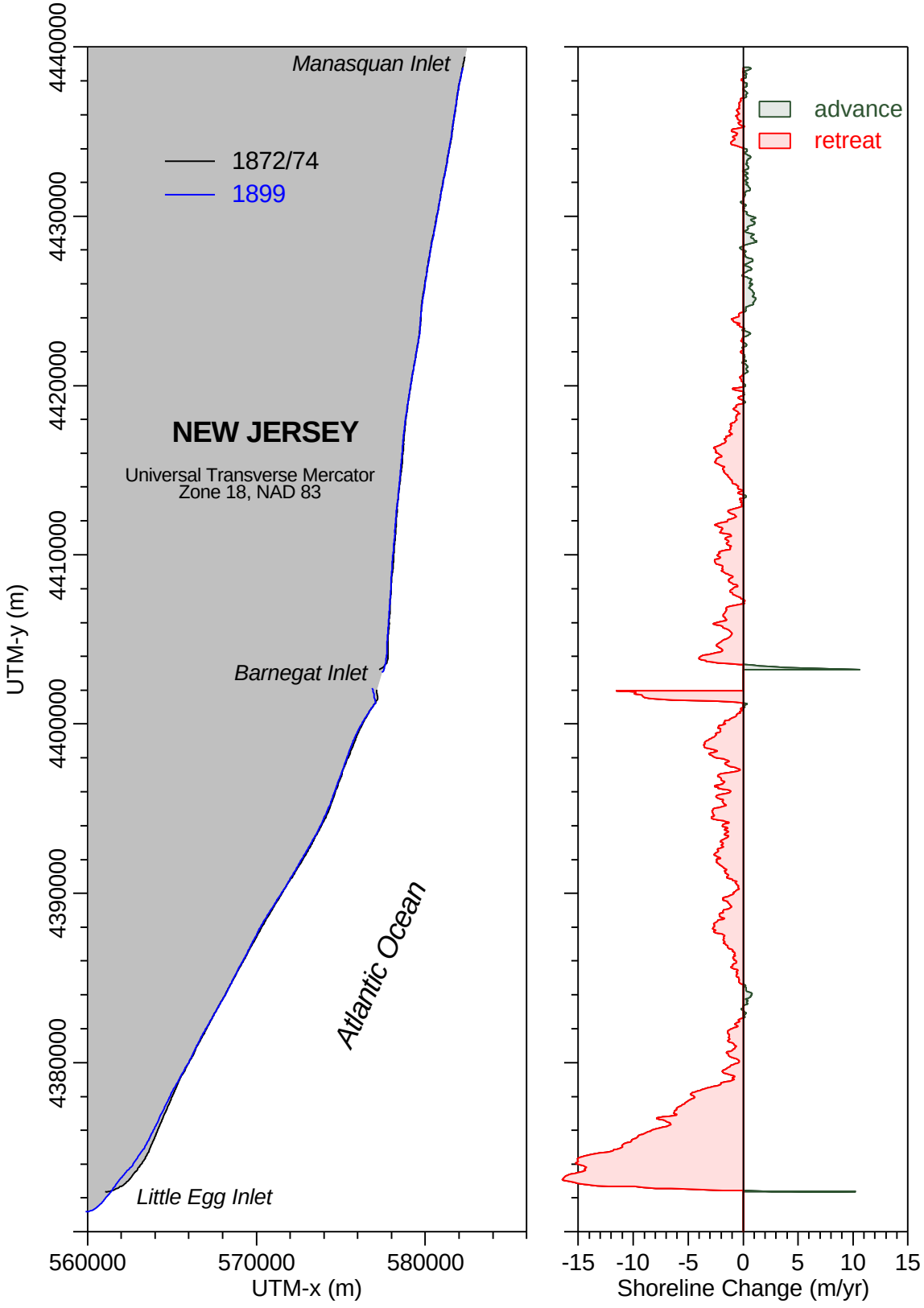

Figure 3-4. Shoreline position and change between Manasquan Inlet and Little Egg Inlet, New Jersey, 1872/74 to 1899.

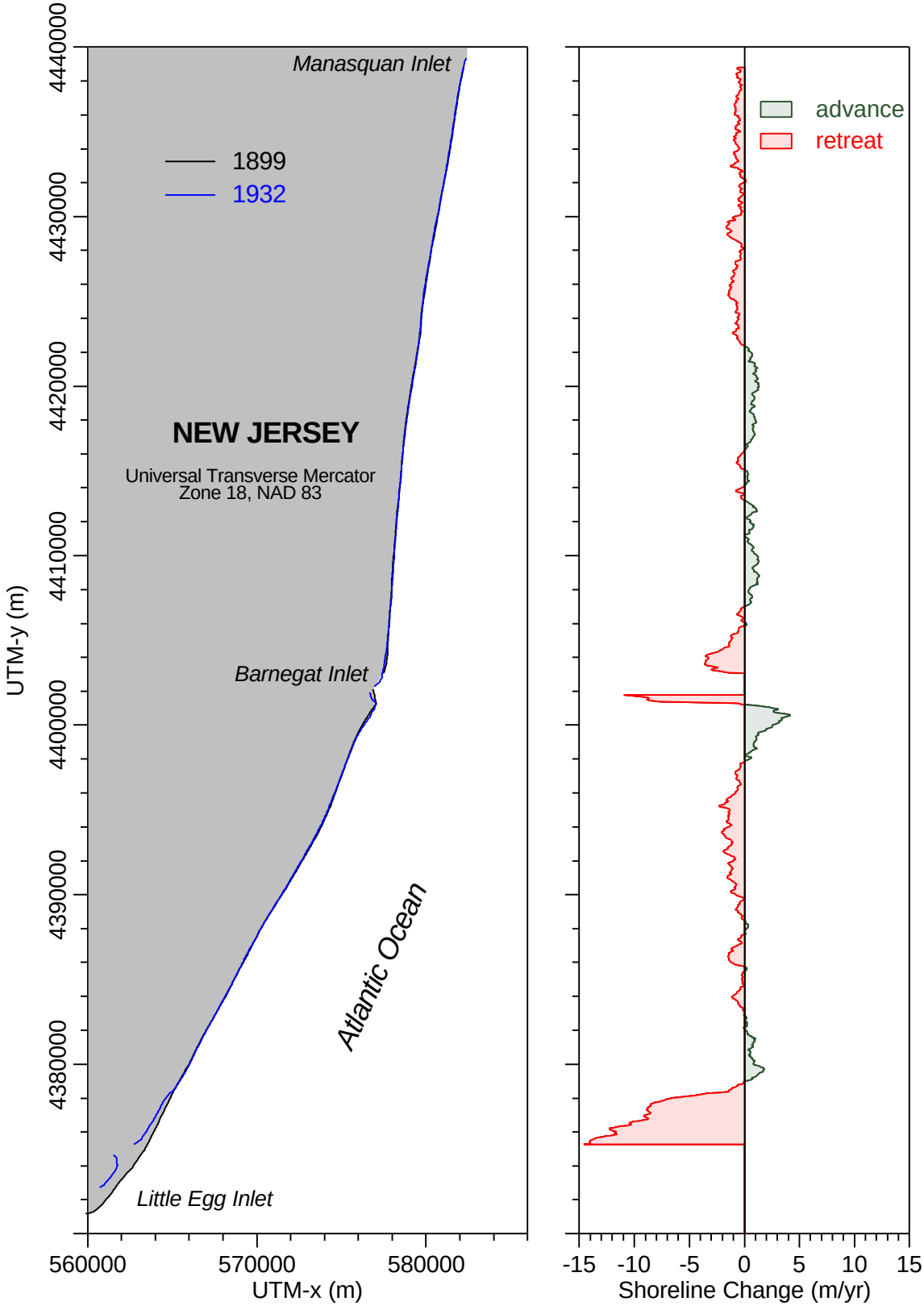

Figure 3-5. Shoreline position and change between Manasquan Inlet and Little Egg Inlet, New Jersey, 1899 to 1932.

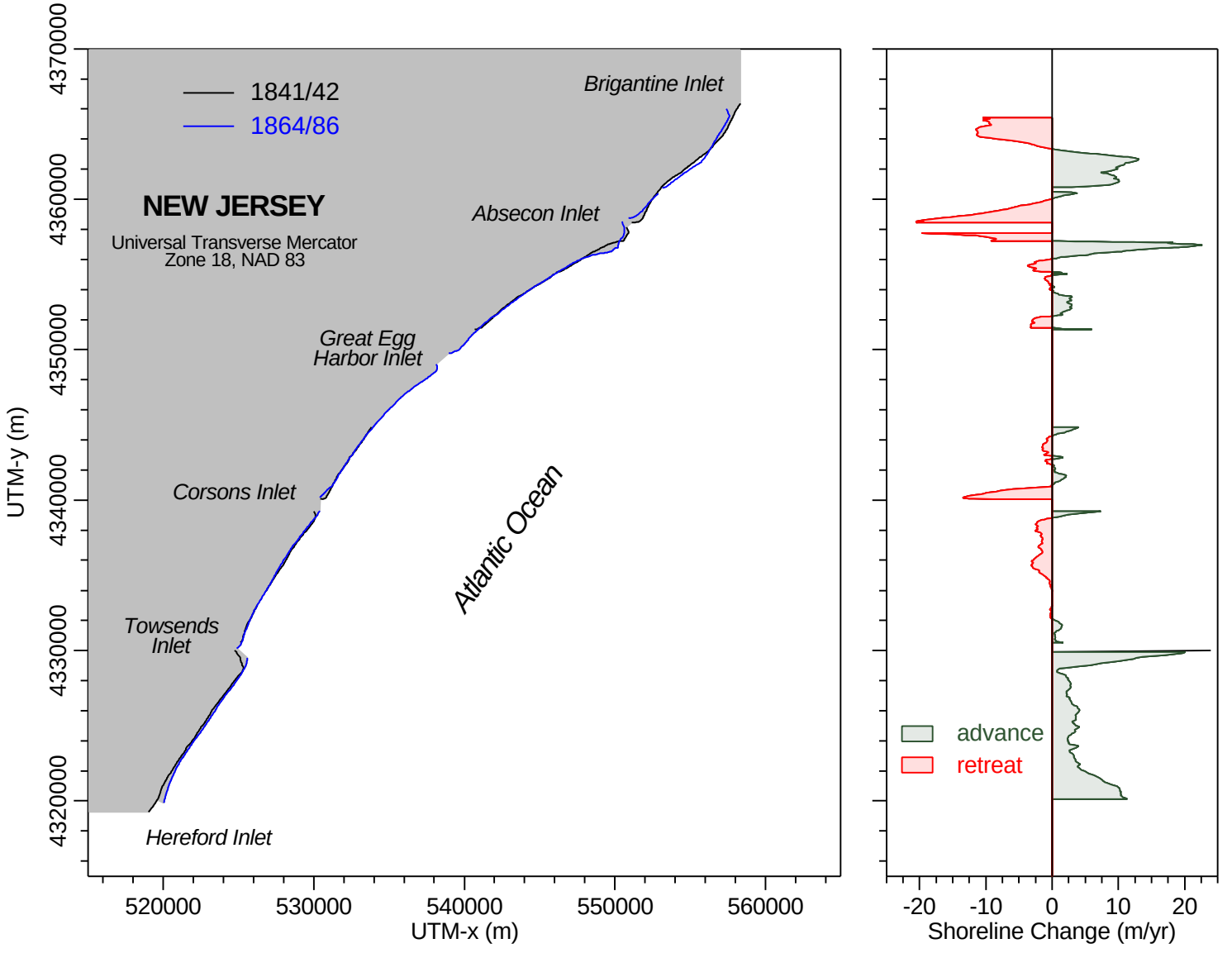

Figure 3-6. Shoreline position and change between Brigantine Inlet and Hereford Inlet, New Jersey, 1841/42 to 1864/86.

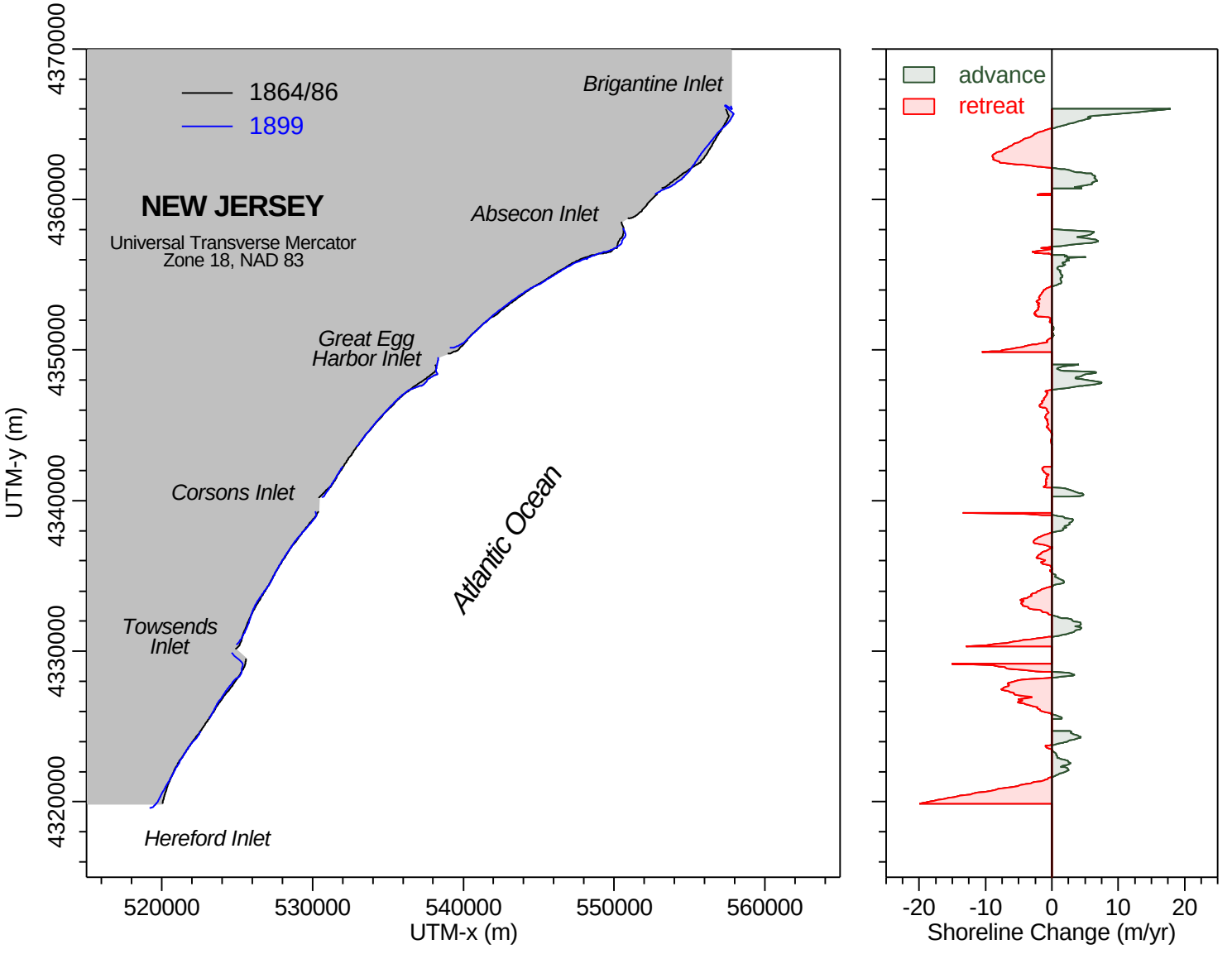

Figure 3-7. Shoreline position and change between Brigantine Inlet and Hereford Inlet, New Jersey, 1864/86 to 1899.

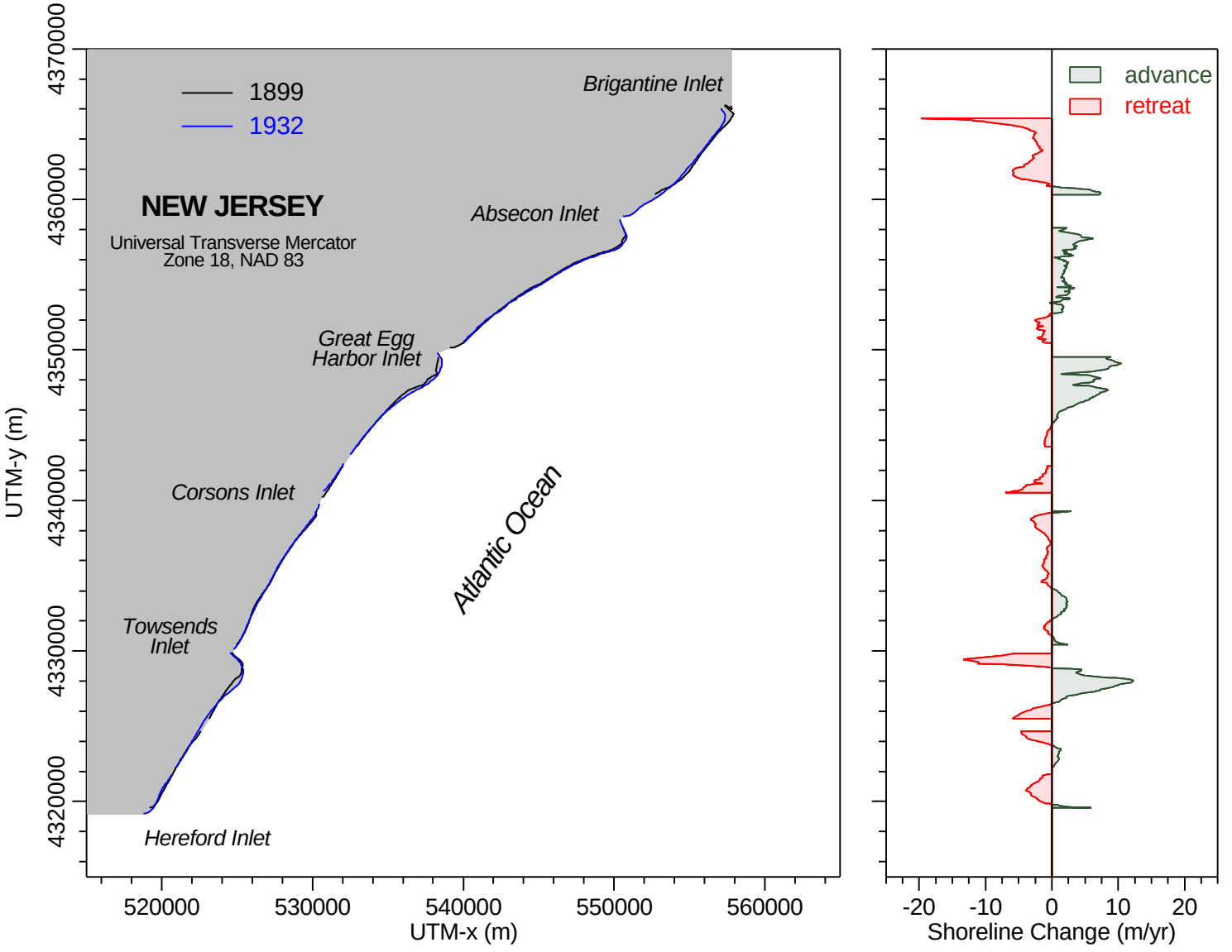

Figure 3-8. Shoreline position and change between Brigantine Inlet and Hereford Inlet, New Jersey, 1899 to 1932.

retreat dominate regional coastal change, whereas average change only summarizes the mathematical balance between these peaks. An independent summary of average shoreline advance (3.0 m/yr) and recession (-2.2 m/yr) documents this trend.

3.1.3.2 1932 to 1977

The period 1932 to 1977 represents the modern time interval for quantifying shoreline change, when aerial photography was used for mapping shoreline position and beach nourishment was active. In 1932, the beach near Little Egg Inlet contained a storm breach that occurred between 1899 and 1932. By 1950/51, the south end of Long Beach Island had migrated 1.1 km to the south (about 60 m/yr; see Figure 3-9). Except at beaches adjacent to inlets, shoreline changes between 1932 and 1950/51 were relatively small (average change = -0.1 m/yr; average shoreline retreat and advance values equal -0.8 and 0.6 m/yr, respectively.). Updrift deposition and downdrift erosion adjacent to Barnegat Inlet recorded the greatest magnitude of change (-12 to 15 m/yr), although the distance over which changes occurred was small.

From 1950/51 to 1977, average shoreline change between Manasquan and Little Egg Inlets was 0.34 m/yr. Except for shoreline movements adjacent to Barnegat and Little Egg Inlets, variations in shoreline movement were relatively small (Figure 3-10). Shoreline recession along the southern shore of Long Beach Island marked the greatest change in the area; however, island growth to the south resulted in 0.9 km of new beach. An apparent cycle of island growth and destruction is illustrated when comparing incremental changes in shoreline position at Little Egg Inlet between 1839/40 and 1977. The rapid rate of southward growth of Long Beach Island indicates a strong southward-directed longshore sediment transport system.

Shoreline changes south of Brigantine Inlet remained quite variable between 1932 and 1950/51. Peaks in shoreline recession and advance on either side of inlets dominate patterns of change; however, significant beach changes between entrances have great impacts on average shoreline change (Figure 3-11). The average rate of change between Brigantine and Hereford Inlets for the period 1932 to 1950/51 is about 0.3 m/yr. Variability in change measurements is reflected by a standard deviation value of ±3.2 m/yr, and average change by direction is -2.4 and 2.3 m/yr. In this case, average change rates for the entire coastal area provide little insight into the processes causing erosion and accretion. Potential beach nourishment activities require an understanding of absolute beach response relative to average change.

For the period 1950/51 to 1977, greatest changes again were associated with beaches adjacent to inlets. Overall, the magnitude of shoreline advance peaks (14 to 20 m/yr) were greater than those related to shoreline recession (-10 to -12 m/yr; Figure 3-12). This trend is reflected in the average shoreline change rate (1.1 m/yr), as well as with average change by direction values (-1.1 to 2.1 m/yr). Between 1986 and 1992, many beaches between Brigantine and Hereford Inlets were nourished with thousands of cubic yards of beach sand (Uptegrove et al., 1995). Between 1950 and 1977, the USACE and the State of New Jersey placed millions of cubic yards of beach fill within this coastal area (e.g., USACE, 1996, 1997). These beach nourishment projects helped stabilize eroding coasts and increased beach width since the 1950s.

3.1.3.3 Cumulative Shoreline Position Change (1839/42 to 1977)

Shoreline position change between 1839/40 and 1977 documents significant shoreline recession along much of the beach between Manasquan and Little Egg Inlets (Figure 3-13). Average shoreline change between Manasquan and Barnegat Inlets was -0.6 m/yr ($\sigma = \pm 0.8$ m/yr). However, for the beaches between Barnegat and Little Egg Inlets, average shoreline

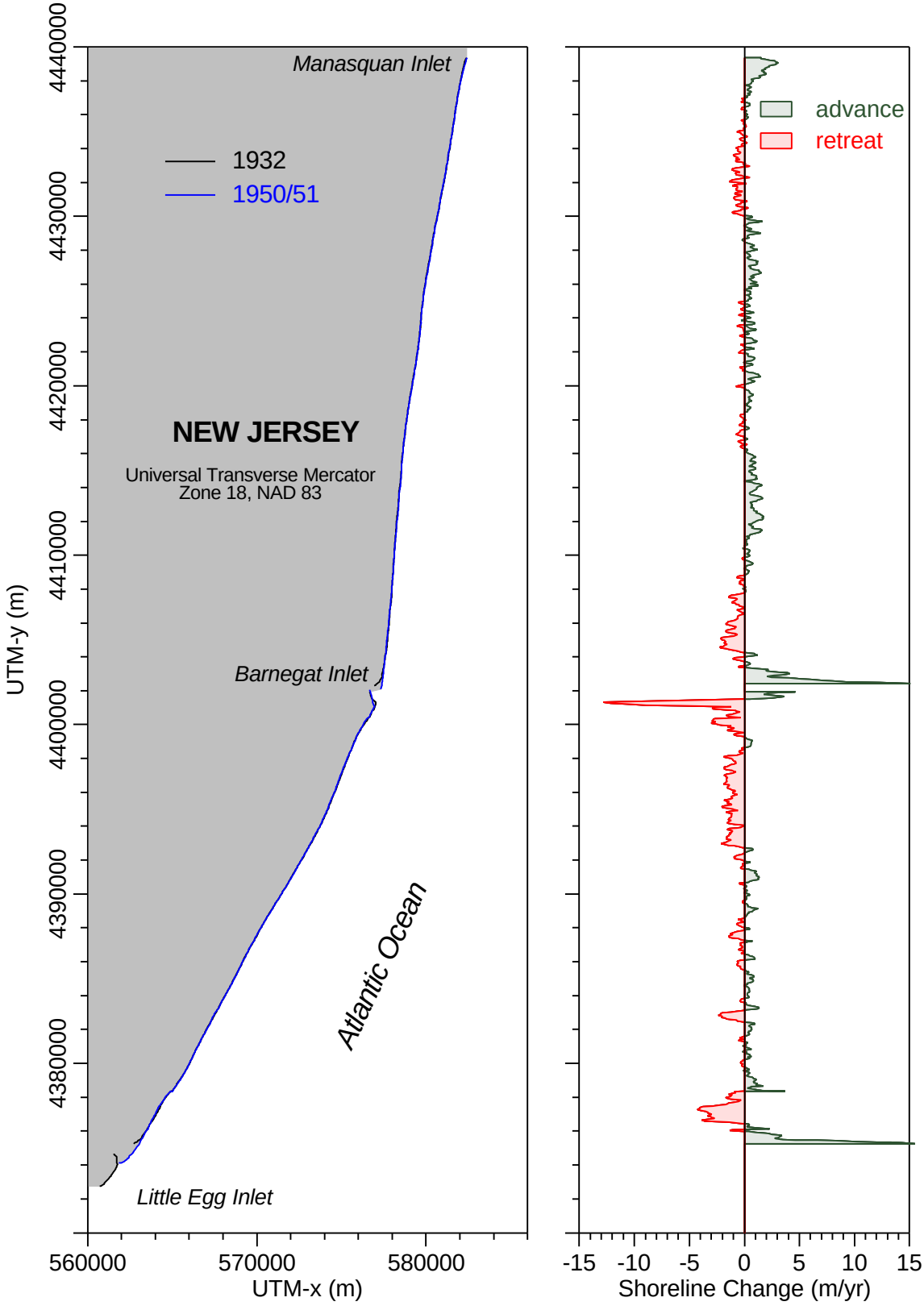

Figure 3-9. Shoreline position and change between Manasquan Inlet and Little Egg Inlet, New Jersey, 1932 to 1950/51.

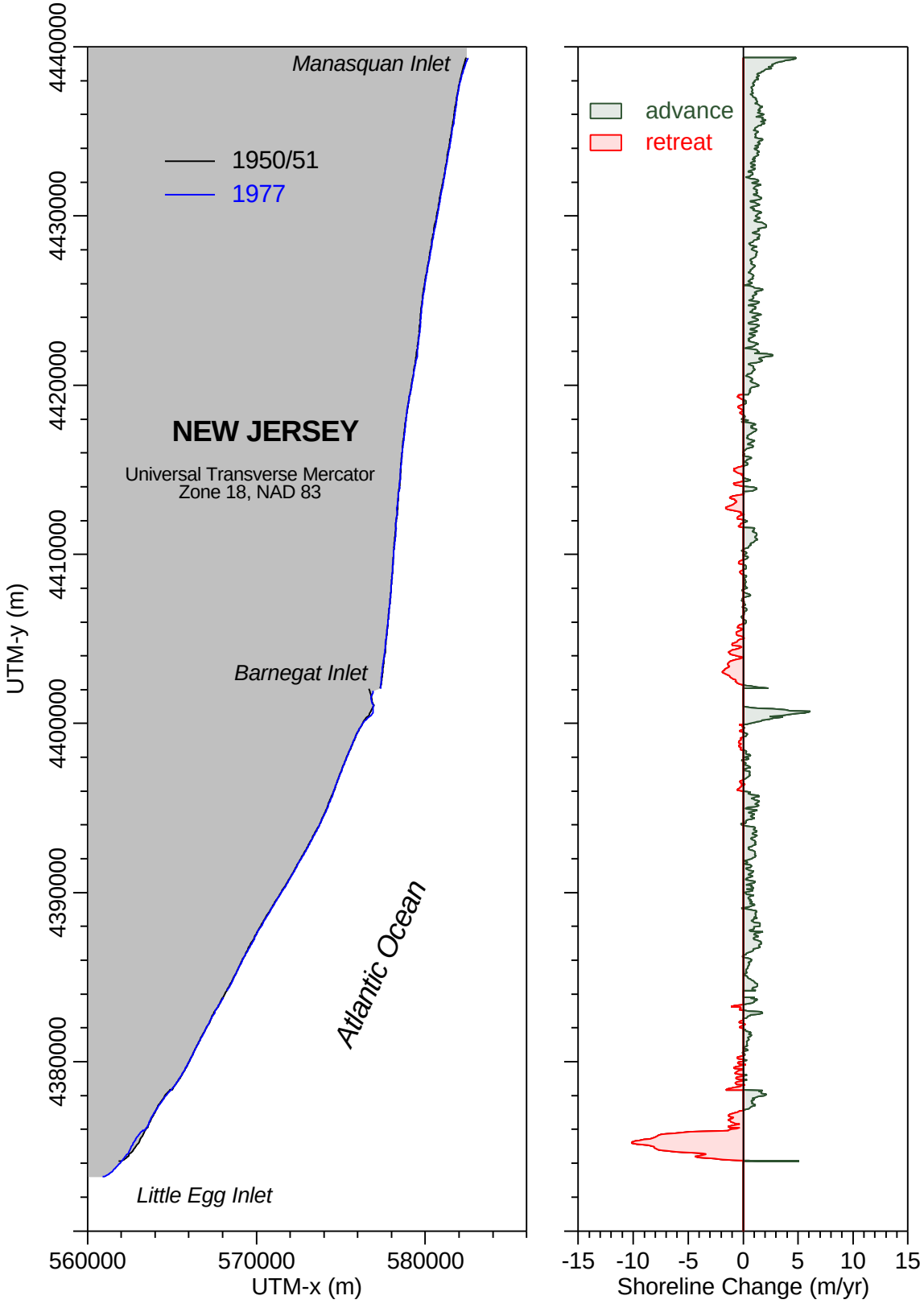

Figure 3-10. Shoreline position and change between Manasquan Inlet and Little Egg Inlet, New Jersey, 1950/51 to 1977.

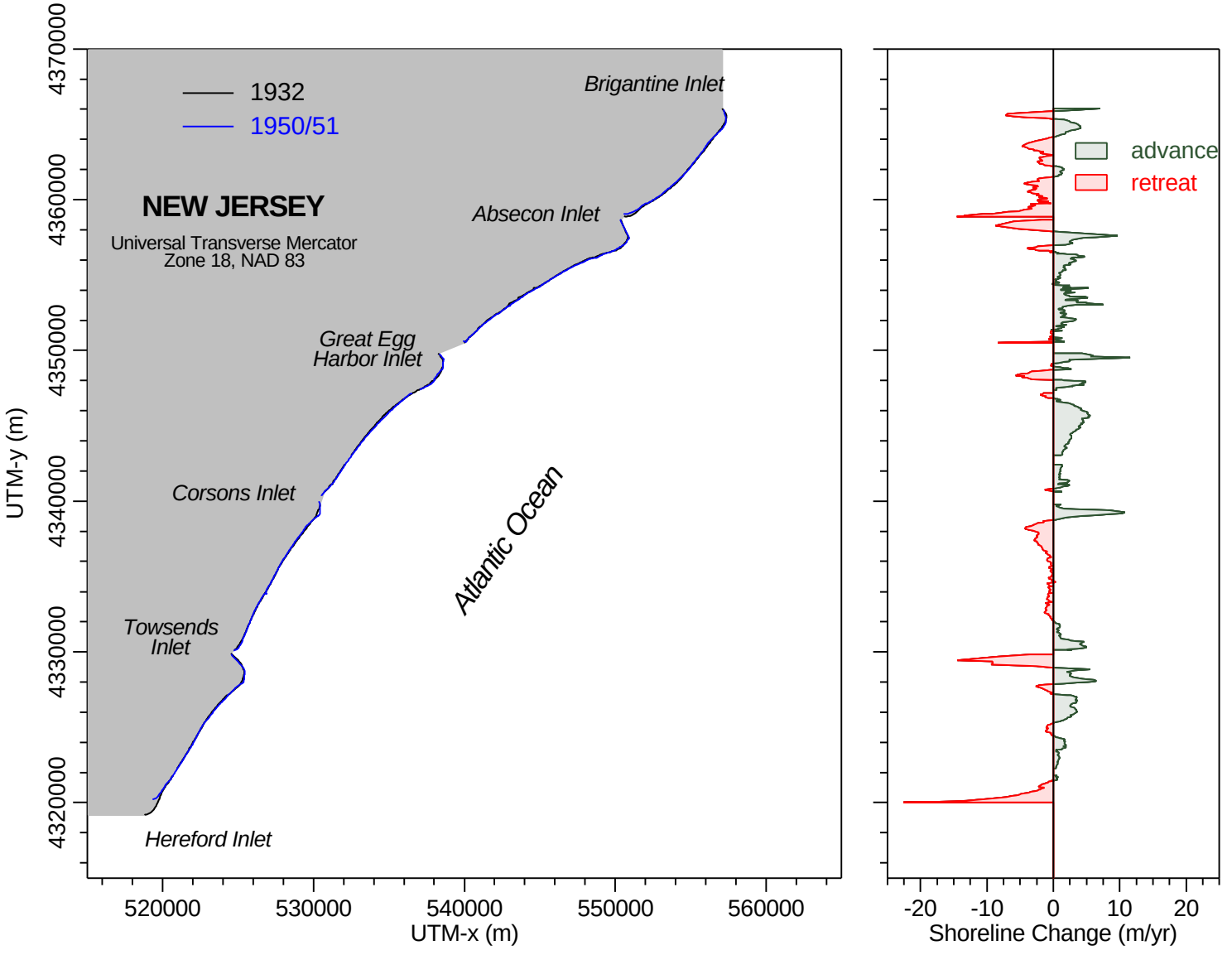

Figure 3-11. Shoreline position and change between Brigantine Inlet and Hereford Inlet, New Jersey, 1932 to 1950/51.

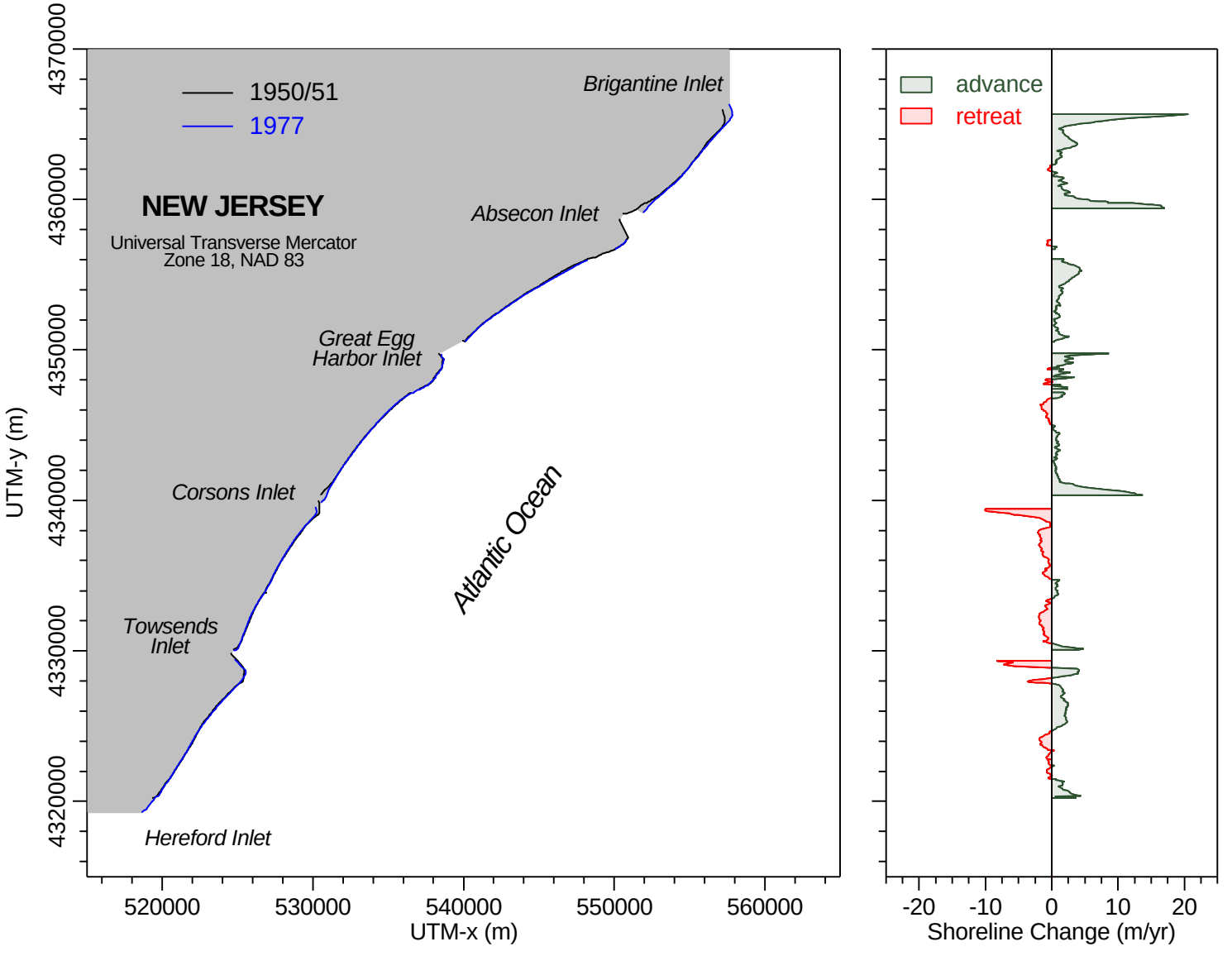

Figure 3-12. Shoreline position and change between Brigantine Inlet and Hereford Inlet, New Jersey, 1950/51 to 1977.

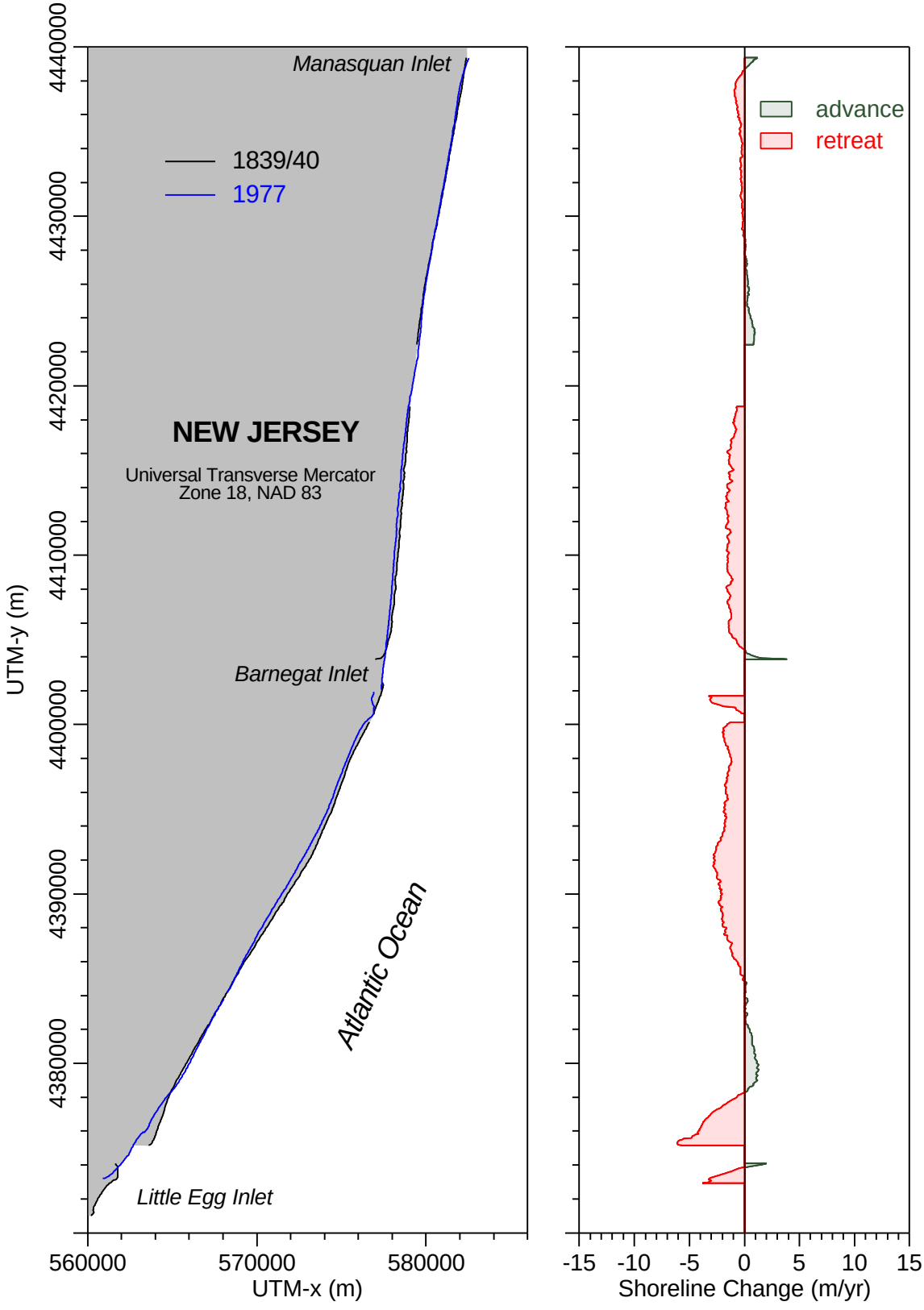

Figure 3-13. Shoreline position and change between Manasquan Inlet and Little Egg Inlet, New Jersey, 1839/40 to 1977.

recession more than doubled to -1.3 m/yr ($\sigma = \pm 1.5$ m/yr). For the entire length of coast, the variability in measurements was relatively low, as indicated by low standard deviation values. Although the southern part of Long Beach Island, north of Little Egg Inlet, showed the greatest net shoreline recession for the 137-yr period of record, the southern terminus of the island grew approximately 1.9 km to the southwest (about 14 m/yr) during this same time period. Sequential shoreline changes recorded between 1839/40 and 1977 suggest that storm events play a primary role in beach and inlet evolution along southern Long Beach Island. In fact, at Barnegat Inlet, Island Beach (north of the inlet) migrated 1.8 km to the south during the same time period. These data indicate that net longshore sediment transport is to the south. The change in shoreline orientation between Island Beach and Long Beach Island may be partially responsible for the increase in shoreline recession south of Barnegat Inlet and the rapid southward growth of Long Beach Island.

South of Brigantine Inlet to Hereford Inlet, net shoreline change was relatively small between 1841/42 and 1977 (Figure 3-14). Greatest changes occurred near the inlets, and net shoreline advance dominated beach response (0.3 m/yr [$\sigma = \pm 1.4$ m/yr]). The trend in shoreline change from north to south was more variable than that to the north, and the magnitude of change was less. This may reflect the addition of numerous beach fills starting in the 1940s. Southward growth of the beaches in southern New Jersey mimic those to the north, illustrating that the dominant direction of longshore sediment transport for the entire coast is to the south.

3.2 NEARSHORE BATHYMETRY CHANGE

3.2.1 Bathymetry Data Base and Potential Errors

Seafloor elevation measurements collected during historical hydrographic surveys are used to identify changes in nearshore bathymetry for quantifying sediment transport trends relative to natural processes and engineering activities. Two USC&GS bathymetry data sets were used to document seafloor changes between 1843/91 and 1934/77. Temporal comparisons were made for an 85-km coastal segment from southern Long Beach Island (2 km north of Little Egg Inlet) to Cold Springs Inlet near Cape May. Data extend offshore to about the 30-m depth contour (about 30 km offshore). The survey sets consist of digital data compiled by the National Geophysical Data Center (NGDC) and analog information (maps) that were compiled in-house using standard digitizing procedures (see Byrnes and Hiland, 1994).

The first regional USC&GS bathymetric survey was conducted in 1843/91 (Table 3-4); data were registered in units of feet. Nearshore surveys were mapped at scales of 1:10,000 and 1:20,000, whereas offshore survey maps focused on regional data coverage at a scale of 1:40,000. The density of points was good for characterizing coastal and shelf topography; however, the most recent survey (1943/77) recorded many more points for describing surface characteristics for the same area. The 1843/91 offshore surveys contained an adequate number of depths along each survey line, and longshore spacing of lines was about 0.5 to 1 km. As such, depth values are reasonable for describing bathymetric features and compared well with the 1943/77 survey set. The 1943/77 bathymetry data are available as digital data from the NGDC.

As with shoreline data, measurements of seafloor elevation contain inherent errors associated with data acquisition and compilation. Potential error sources for horizontal location of points are identical to those for shoreline surveys (see Table 3-2). These shifts in horizontal position translate to vertical adjustments of about ±0.3 to 0.5 m based on information presented in USC&GS and USACE hydrographic manuals (e.g., Adams, 1942). Corrections to soundings for tides and sea level change introduce additional errors in vertical position of ±0.1 to 0.3 m.

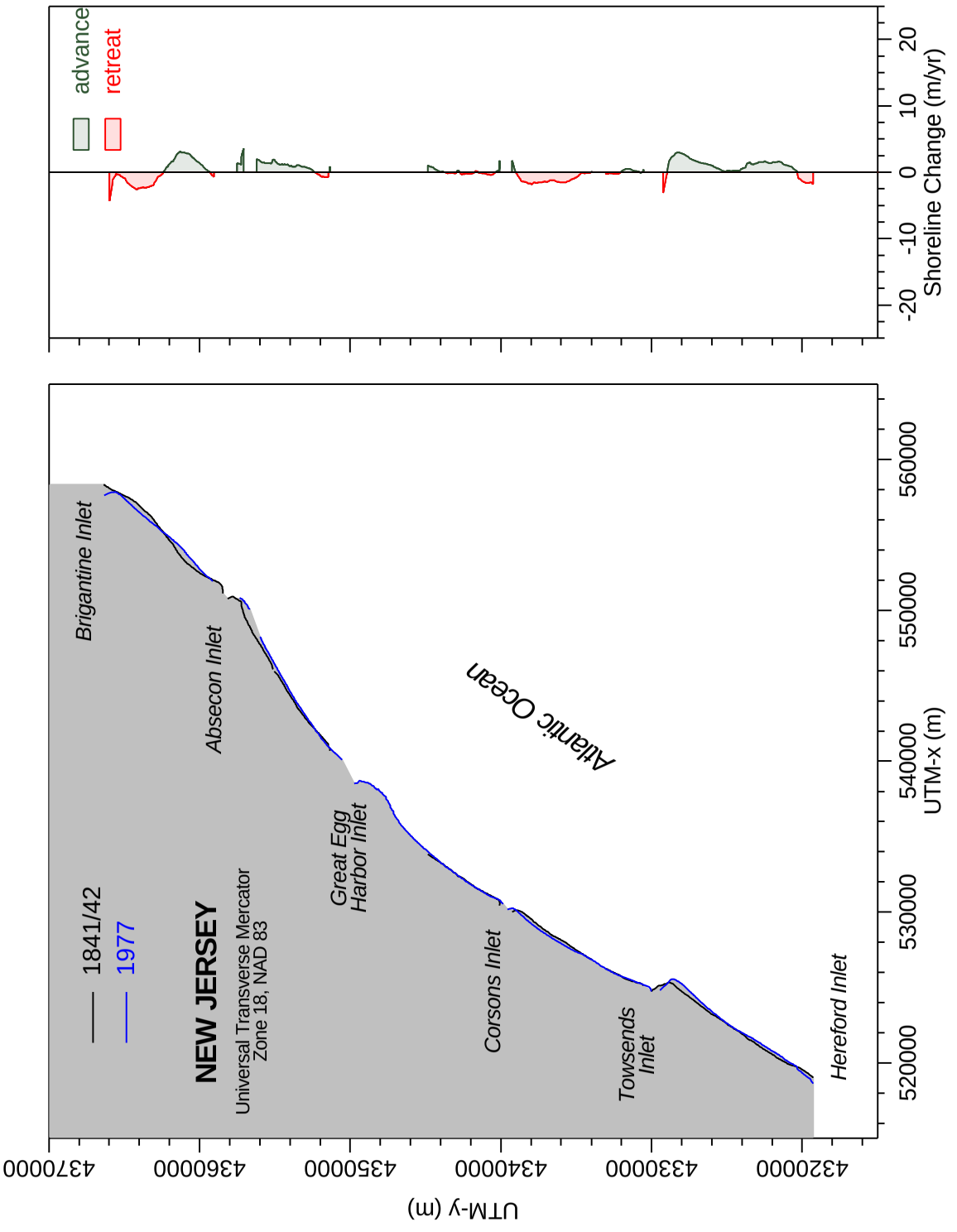

Figure 3-14. Shoreline position and change between Brigantine Inlet and Hereford Inlet, New Jersey, 1841/42 to 1977.

Table 3-4. Summary of bathymetry source data characteristics for the offshore area between Manasquan Inlet and Cape May, New Jersey.

Date	Data Source	Comments and Map Numbers
1843/91	USC&GS Hydrographic Sheets 1:10,000 (H-837, H-1158a, H-1158b, H-1578b, H-2164, H-2166) 1:20,000 (H-2165) 1:40,000 (H-116, H-1533, H-1696)	First regional bathymetric survey for offshore New Jersey; 1843 - offshore area from Little Egg Inlet to Cape May (H-116); 1864 - seaward of Absecon Inlet (H-837); 1872/74 - seaward of Little Egg Inlet and Brigantine Inlet (H-1158a, H-1158b); 1883/91 - Manasquan Inlet to Seaside Heights (H-1578b), Corsons Inlet to Hereford Inlet and offshore (H-1533, H-1696), seaward of Cape May Inlet, Hereford Inlet, and Townsends Inlet (H-2164, H-2165, H2166).
1934/88	USC&GS Hydrographic Sheets 1:10,000 (H-5615, H-6141, H-6145, H-6195, H-6196, H-6232, H-6236, H-6262, H-8219, H-8220, H-8675, H-8676) 1:20,000 (H-6136, H-6225, H-6226, H-6227, H-8222, H-9153, H-9312, H-9699, H-9700) 1:40,000 (H-6188, H-6190, H-6224, H-6271, H-9531, H-9534, H-9452, H-9546, H-9552, H-9573)	Most recent offshore regional bathymetric survey; 1934/40 - Manasquan Inlet to Barnegat Inlet (H-5615, H-6136, H-6141, H-6188, H-6190), Barnegat Inlet to Great Egg Inlet (H-6145, H-6195, H-6196, H-6225, H-6271, Great Egg Inlet to Cape May Inlet (H-6226, H-6227, H-6232, H-6236, H-6262, H-6264); 1954/62 - Surf City to Ocean City (H-8219, H-8220, H-8222, H-8675, H-8676); 1970/77 - offshore New Jersey (H-9153, H-9312, H-9531, H-9534, H-9542, H-9546, H-9552, H-9573, H-9699, H-9700).

Finally, the accuracy of depth measurements adds error that is variable depending on the measurement method. It is estimated that the combined root-mean-square error for bathymetric surface comparisons between 1843/91 and 1943/77 is about $\pm$0.6 m. This estimate was used to denote areas of no significant change on surface comparison maps.

Because seafloor elevations are temporally and spatially inconsistent for the entire data set, adjustments to depth measurements were made to bring all data to a common point of reference. These adjustments include changes in relative sea level with time and differences in reference vertical datums. Vertical adjustments were made to each data set based on the time of data collection. All depths were referenced to NGVD and projected average sea level for 1977. The unit of measure for all surfaces is meters, and final values were rounded to decimeters before cut and fill computations were made.

3.2.2 Digital Surface Models

Historical bathymetry data within the study area provide geomorphic information on characteristic surface features that form in response to dominant coastal processes (waves and currents) and relative sea level change. Comparing two or more surfaces documents net sediment transport patterns relative to incident processes and sediment supply. The purpose for conducting this analysis throughout the study area is to document net sediment transport trends on the shelf surface and to quantify the magnitude of change to calibrate the significance of short-term wave and sediment transport numerical modeling results. Net sediment transport rates on the shelf were determined using historical data sets to address potential infilling rates for sand borrow sites.

3.2.2.1 1843/91 Bathymetric Surface

Bathymetry data for the period 1843/91 were combined with the 1839/42 and 1872/74 shoreline data to create a continuous surface from the shoreline seaward to about the 30-m depth contour (NGVD). The most prominent geomorphic features throughout the study area are the ebb-tidal deltas associated with inlets and the presence of linear offshore sand ridges south of Townsends Inlet (Figure 3-15). A series of well-defined ebb shoals exist for Little Egg, Absecon, Corsons, Townsends, Hereford, and Cold Springs Inlets (data were not available for Great Egg Harbor Inlet, but similar features were likely present at this entrance as well). Shoreline change data for this area indicated dominant southward-directed longshore sediment transport, and the predominance of shallow shoals on the north side of these entrances supports this conclusion.

A series of relatively small linear sand ridges are present southwest of Little Egg Inlet near the Federal-State OCS boundary. These prominent features exist landward of the Federal-State boundary as well and represent a primary offshore sand source for beach nourishment or construction aggregates. The presence and characteristics of these features are best defined south of Corsons Inlet. The continental shelf offshore Sea Isle City, Townsends Inlet, Avalon, Stone Harbor, Hereford Inlet, and Wildwood contain extensive shoreface sand ridges oriented at oblique angles to the modern shoreline. The origin of these sand ridges has been associated with lateral inlet migration along a landward migrating shoreline (McBride and Moslow, 1991), suggesting that sediment associated with offshore sand ridges is compatible with modern beach deposits. Historical shoreline change data illustrate lateral island migration and shoreline retreat between 1839/42 and 1977, providing a mechanism for oblique sand ridge formation on the upper shoreface. Geological data from the NJDEP (Uptegrove et al., 1995) illustrate that shoreface sand ridges are the most viable features for beach sand on the continental shelf.

A little less than half of the study area did not have accurate bathymetric data coverage to create a continuous surface for the 1843/91 timeframe. Historical bathymetry data are available from the NOS for the area between Manasquan Inlet and Little Egg Inlet for this time period. However, after extensive evaluation regarding the reliability of measurements in this area, it was determined that depth values could not be used to accurately describe surface morphology or quantify sediment transport patterns.

3.2.2.2 1934/77 Bathymetric Surface

General characteristics of the 1934/77 bathymetric surface are similar to those of the 1843/91 surface with a couple of exceptions (Figure 3-16). First, the area of coverage includes the offshore zone north of Little Egg Inlet to Manasquan Inlet. Second, geomorphic features are better defined because the number of data points describing the surface is larger. The general shape and position of shoals is consistent for both surfaces. However, the detail associated with shoals along the coast (generally at inlets) and linear sand ridges on the shoreface provides an understanding of the relationship between potential sand resource areas and coastal sedimentation processes. All potential sand resource areas, with the exception of F2, exist on offshore linear sand ridges, which have been linked with ancient inlet deposits during lower sea level (McBride and Moslow, 1991).

With the availability of continental shelf bathymetry data from Manasquan to Cold Springs (Cape May) Inlets, a general trend in shelf morphology emerges. The slope of the shelf surface north of Little Egg Inlet is noticeably steeper than that seaward of the barrier islands in Cape May County (Figure 3-16). For example, the 20-m depth contour seaward of the beaches south of Manasquan Inlet exists approximately 3 km offshore. Seaward of Townsends Inlet (west of Sand Resource Area A2), the same depth contour is about 12 km offshore. As a result, there is

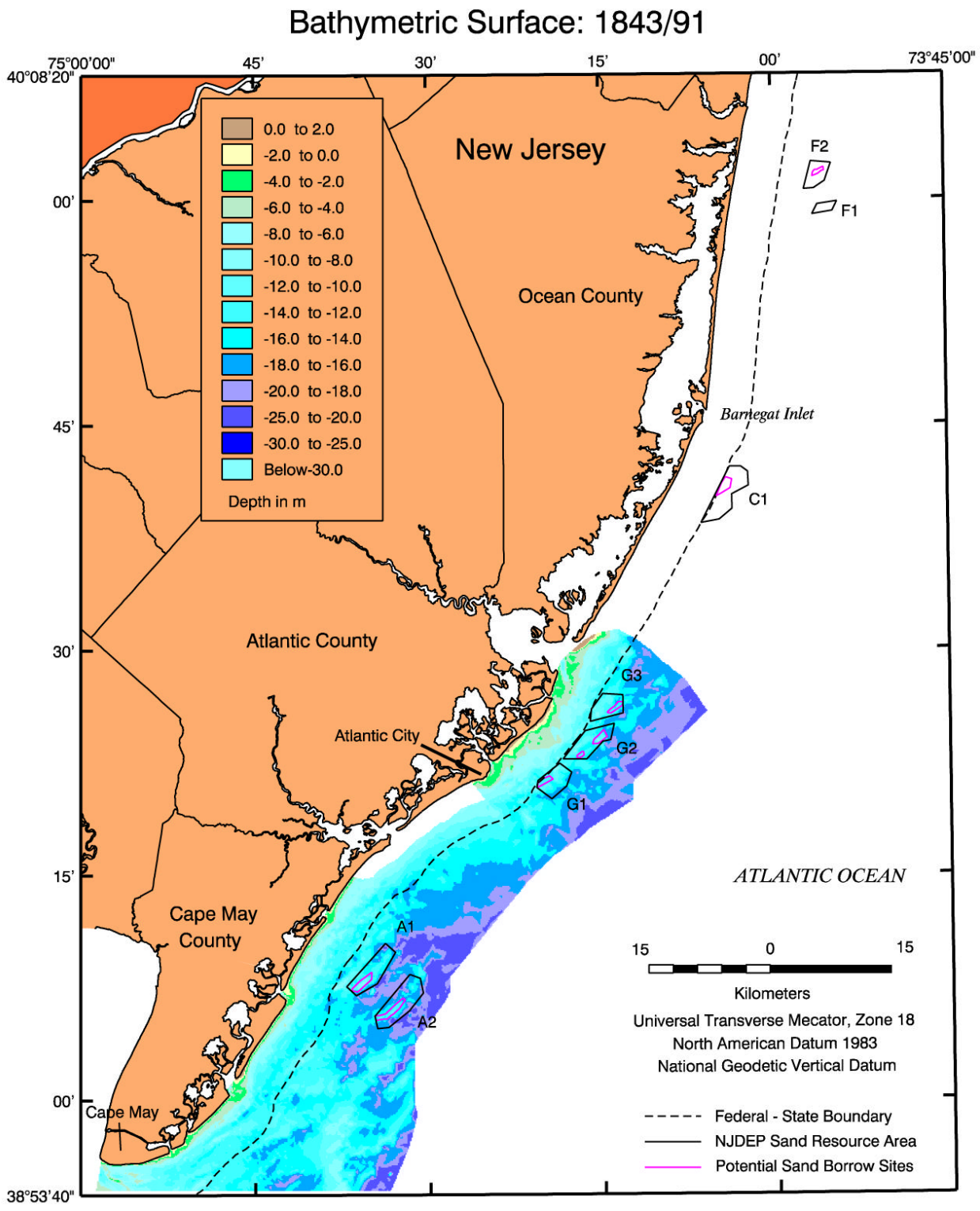

Figure 3-15. Nearshore bathymetry (1843/91) for offshore New Jersey.

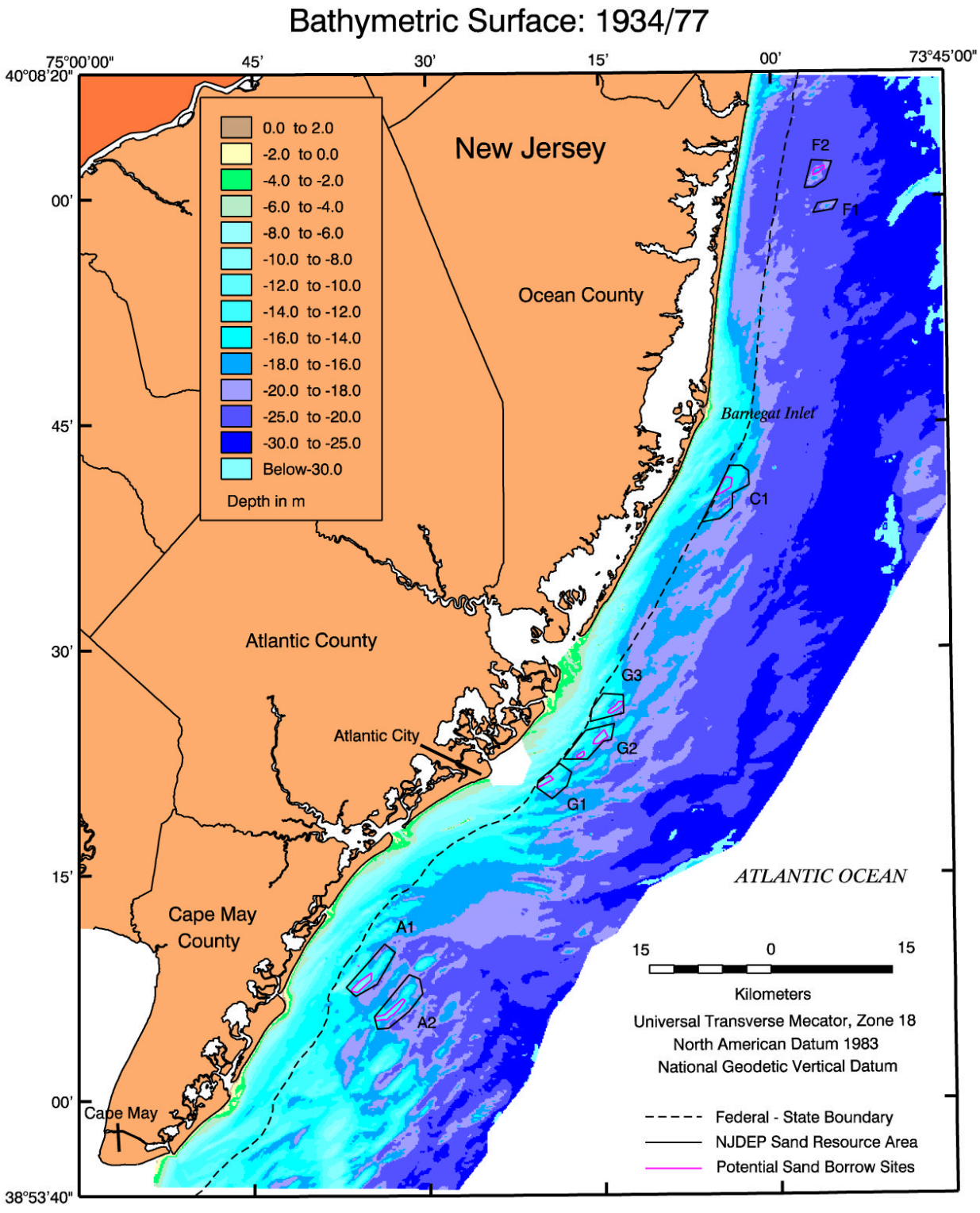

Figure 3-16. Nearshore bathymetry (1934/77) for offshore New Jersey.

an absence of linear sand ridges north of Barnegat Inlet and an abundance of sand ridges seaward of the southern barrier island chain (steep shelf gradient, small horizontal displacement of water surface during sea level rise, greater reworking of shelf surface, straight and parallel contours; low shelf gradient, large horizontal displacement of water surface during sea level rise, reworking of shelf surface over larger area, contours reflect ancient beach deposits).

The shelf surface seaward of Barnegat Inlet illustrates the influence of tidal inlet sedimentation processes on shelf morphology. The delta-shaped bulge in contours, marked by the 12-m depth contour, documents the longshore extent (about 20 km) of inlet-influenced sedimentation on shelf morphology. The 12-m depth contour again bulges seaward of the Little Egg-Brigantine-Absecon Inlets area, backed by an estuary with a substantial tidal prism. South of this region, the 12-m depth contour exists landward of the Federal-State boundary, except at offshore shoal deposits. Inlet sedimentation processes in this area are important to coastal evolution, but small bays behind the southern islands result in small tidal prisms that produce greater geomorphic changes on the upper shoreface than on the continental shelf. Offshore linear sand ridges dominate the shelf surface in southern New Jersey, creating ideal locations for potential sand borrow sites for beach nourishment.

3.2.3 Shelf Sediment Transport Dynamics

Although the general characteristics of bathymetric surfaces appear similar for 1843/91 and 1934/77, a digital comparison of these surfaces yields a difference plot that isolates areas of erosion and accretion for documenting sediment transport patterns and quantifying trends (Figure 3-17). The most significant changes occurring during this 50- to 130-yr interval were associated with deposition (and erosion) at and seaward of the inlets along the southern New Jersey barrier islands, and alternating patterns of erosion and deposition across the shelf surface in the northeast-southwest-trending sand ridge field from Little Egg Inlet to Cold Springs (Cape May) Inlet.

Fluid flow and sediment transport at and seaward of the inlets separating barrier islands in southeastern New Jersey produce the most pronounced geomorphic changes throughout the study area. Tidal exchange through these inlets mobilizes substantial quantities of sediment near the coastline and on the upper shoreface, resulting in spit growth along the downdrift margin of islands and shoal migration at and adjacent to entrances, illustrated as areas of erosion (yellow to brown) and deposition (green) on Figure 3-17. Polygons of erosion and deposition generally follow contour shapes defined by shoals and troughs on the continental shelf. Shelf bathymetry seaward of the Federal-State boundary and east-southeast of Great Egg Harbor Inlet illustrates the lowest relief features south of Little Egg Inlet (see Figure 3-16), and bathymetric change is minor. Conversely, offshore areas north and south of this zone illustrate a more active surface (Figure 3-17) where numerous shoreface sand ridges reside. Alternating zones of accretion and erosion reflect the migration of continental shelf sand ridges.

Prominent areas of sediment deposition (green polygons) on the upper shoreface are present along the shoreline south of Townsends and Hereford Inlets, and just south of Little Egg Inlet. This trend likely is present at Absecon and Great Egg Harbor Inlets as well, but lack of data does not allow verification of this deposition pattern. These areas of sediment accretion are associated with ebb-tidal shoal migration and sediment bypassing at entrances in response to southward-directed longshore sediment transport. Other areas of deposition on the continental shelf are recognized as relatively small linear features that reflect the southern movement of sand ridges under the influence of nearshore waves and currents. Often, updrift

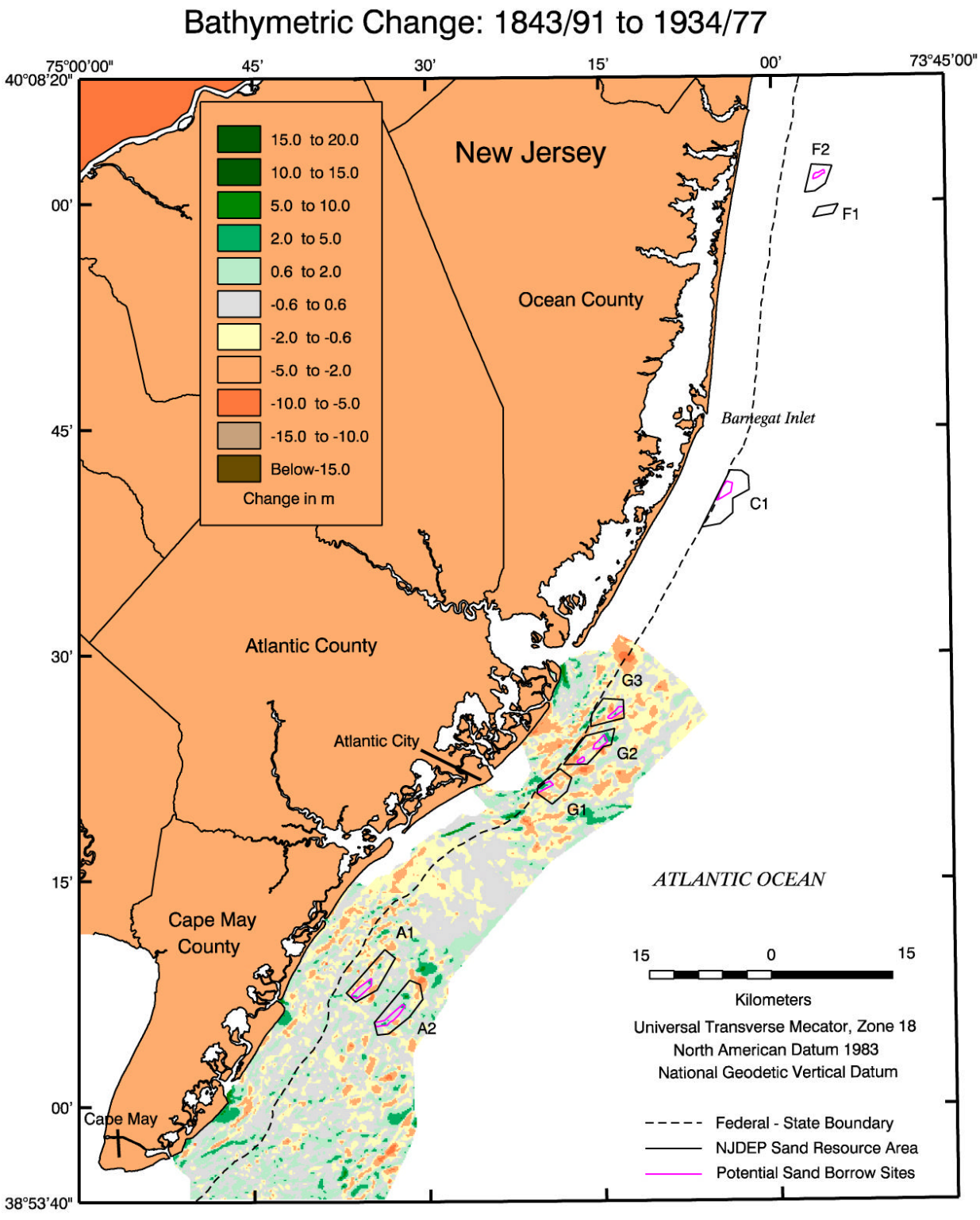

Figure 3-17. Nearshore bathymetry change (1843/91 to 1934/77) for the southeastern New Jersey shoreface.

zones of erosion are associated with downdrift linear deposits, illustrating the historical movement of shoals on the shelf surface. The greatest amount of bathymetric change on the shelf surface exists seaward and between Little Egg and Absecon Inlets.

Sand volume change calculations for zones of accretion and erosion along the shore and on the shelf surface are used to estimate net sand transport rates (see Sections 3.2.4 and 3.2.5). Historical transport rates are used to calibrate simulations of borrow site infilling and nearshore sand transport (Section 5.2).

3.2.4 Magnitude and Direction of Change

Patterns of seafloor erosion and accretion on the continental shelf seaward of the New Jersey coast documented the net direction of sediment transport throughout the study area (Figure 3-17). For the period 1843/91 to 1934/77, net sediment movement is from north to south. This direction of transport is consistent with historical shoreline change trends and channel dredging practice at entrances along the New Jersey coast (any sidecasting, nearshore, or offshore dumping is to the south of inlets). Although overall trends are helpful for assessing potential impacts of sand extraction from the OCS, the specific purpose of the historical bathymetric change assessment is to quantify sediment erosion and accretion and to derive transport rates specifically related to potential sand extraction sites. Of the eight sand resource areas, seven were chosen for evaluating sand extraction scenarios based on minimum beach replenishment requirements and NJDEP geologic data. Area F1 in the northern portion of the study area was not evaluated as a sand borrow area because the volume of sediment available for sand mining was not adequate for potential beach nourishment projects.

For Resource Areas F2 and C1, regional bathymetric change data were not available for quantifying potential sediment transport rates. This is particularly a problem for Area F2 where the sand resource area is in 20 to 25 m of water. Water depths at Resource Area C1 are very similar to those at Areas G1, G2, and G3. For these resource areas, sediment erosion zones parallel to shoreface ridges indicate that potential transport rates available for infilling any proposed borrow sites in the areas would range from about 62,000 to 125,000 m^3/yr (5.6 to 14.0 MCM over about 90 to 120 years; Figure 3-18). This calculation assumes that sediment eroded from areas nearby potential borrow sites reflect the rate at which material would be available for infilling the borrow sites. Because Area C1 is similar in character to Areas G1, G2, and G3, potential transport rates for Areas G1, G2, and G3 are considered representative for assessing infilling at Area C1.

For Resource Areas A1 and A2, sediment erosion zones parallel to shoreface ridges again were used as indicators of potential transport rates available for infilling proposed sand borrow sites in the resource areas (Figure 3-19). Total sediment erosion over a 51-yr period ranged from 8.0 to 10.0 MCM, or about 160,000 to 200,000 m^3/yr. These rates are approximately two times those documented to the north, reflecting a more dynamic offshore environment seaward of the southern barrier island chain. Again, this calculation assumes that sediment eroded from areas nearby potential borrow sites reflects the rate at which material would be available for infilling the borrow sites. The dredging geometry (depth to width to length) for each potential borrow site, as well as the type of sediment available for infilling, are controlling factors for determining sediment infilling (see Section 5.2).

3.2.5 Net Longshore Sand Transport Rates

Well-defined zones of erosion and accretion along the shoreline are documented in Figure 3-17 as regions of littoral sand transport along the barrier island chain of southern New Jersey.

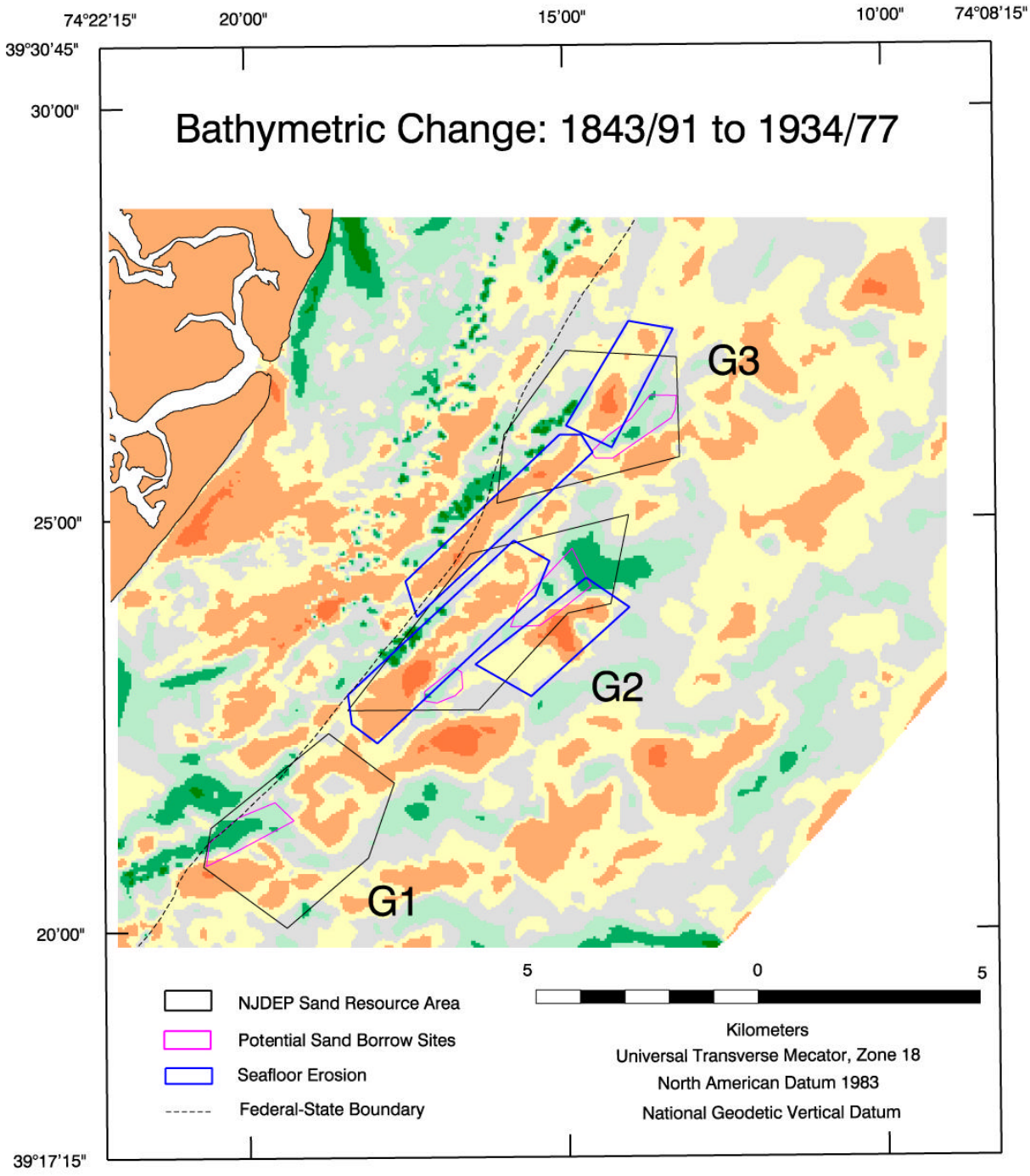

Figure 3-18. Potential borrow site locations relative to sand ridge erosion and deposition in Resource Areas G1, G2, and G3.

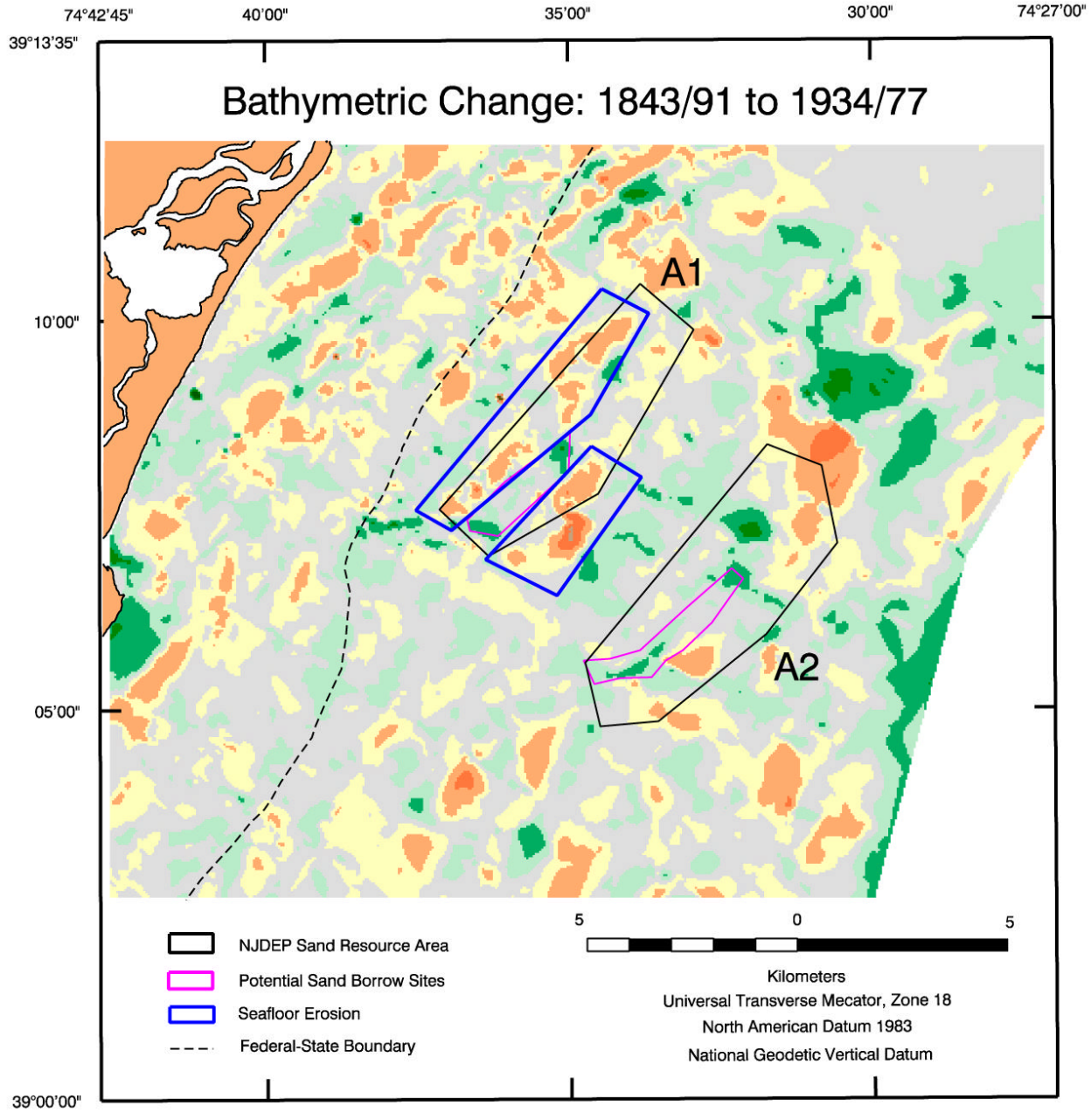

Figure 3-19. Potential borrow site locations relative to sand ridge erosion and deposition in Resource Areas A1 and A2.

The littoral zone extends seaward to about the 7-m (NGVD) depth contour, which represents the approximate depth of closure (based on calculations of d_l from Hallermeier [1981] using USACE Wave Information Study [WIS] data statistics). Along the southeastern coast of New Jersey, alternating zones of erosion and accretion, as determined from historical bathymetry comparisons, were evaluated with respect to the net sediment budget to determine net longshore sand transport rates. For the area south of Little Egg Inlet, net longshore transport rates were determined to be on the order of 70,000 m^3/yr. South of Great Egg Harbor Inlet, data become available again for quantifying net transport rates. As illustrated in Figure 3-17, the quantity of material deposited along the beaches south of Townsends and Hereford Inlets is significantly greater than deposition or erosion trends to the north. As such, net transport rates along the shoreline landward and south of Resource Areas A1 and A2 were determined to be on the order of 190,000 to 230,000 m^3/yr. These results are consistent with published estimates of net longshore sediment transport rates by the USACE (1996, 1997).

3.3 SUMMARY

Shoreline position and nearshore bathymetry change document four important trends relative to study objectives. First, the predominant direction of sediment transport throughout the study area is north to south. Southern Long Beach Island (north of Little Egg Inlet) and southern Island Beach (north of Barnegat Inlet) have migrated at a rate of about 14 m/yr to the south since 1839/42. The ebb-tidal shoals at all inlets in the study area are skewed to the south, and the channels are aligned in a northwest-southeast direction.

Second, the most dynamic features within the study area, in terms of nearshore sediment transport, are the ebb-tidal shoals associated with inlets along the southeastern barrier island chain. Areas of significant erosion and accretion are documented for the period 1843/91 to 1934/77, reflecting wave and current dynamics at entrances, the influence of engineering structures on morphologic change, and the contribution of littoral sand transport from the north to sediment bypassing and shoal migration.

Third, alternating bands of erosion and accretion on the continental shelf east of the Federal-State boundary illustrate relatively slow but steady reworking of the upper shelf surface as sand ridges migrate from north to south. The process by which this is occurring at Resource Areas G1, G2, and G3 suggests that a borrow site in this region would fill with sand transported from an adjacent site at a rate of about 62,000 to 125,000 m^3/yr. At Sand Resource Areas A1 and A2, the potential sand transport rate increases to 160,000 to 200,000 m^3/yr. This increase in potential transport rate reflects a more dynamic offshore environment seaward of the southern barrier island chain. Historical bathymetry change data were not available for quantifying sediment transport trends at Resource Areas C1, F1, and F2.

Finally, net longshore transport rates determined from seafloor changes in the littoral zone between Little Egg Inlet and the beach south of Hereford Inlet indicate an increasing transport rate to the south from about 70,000 m^3/yr south of Little Egg Inlet to 190,000 to 230,000 m^3/yr at Townsends and Hereford Inlets. Variations in transport rate are evident in the patterns of change recorded on Figure 3-17. It appears that areas of largest net transport exist just south of these entrances as a result of natural sediment bypassing from updrift to downdrift barrier beaches.

4.0 WAVE TRANSFORMATION NUMERICAL MODELING

4.1 ANALYSIS APPROACH

A quantitative understanding of wave characteristics, storm surge, sediment transport, and other natural processes is key to implementing an effective borrow site management plan. Computer models provide predictive tools for evaluating various forces governing wave climate, sediment transport processes, and the performance of beach fill extraction from offshore borrow sites. Quantitative information produced from numerical models can be used to maximize the design life of beach replenishment projects and examine the effects of dredging at offshore borrow sites. As a result, management strategies can be developed to explain the physical processes that dominate a region and to furnish appropriate recommendations/solutions for each stretch of coast.

An assessment of potential impacts caused by dredging offshore borrow sites can be determined using wave modeling to estimate refraction, diffraction, shoaling, and wave breaking. Refraction and diffraction may have a significant effect on the impacts waves have on a shoreline. Wave refraction and diffraction generally result in an uneven distribution of wave energy along the coast that affects sediment transport in the region. Wave modeling results provide information on wave propagation across the continental shelf and to the shoreline, revealing areas of increased erosion (“hot spots”) or areas of increased wave energy. These data then provide the basis for nearshore circulation and sediment transport models. In addition, one of the primary advantages of wave modeling is its ability to simulate multiple scenarios. The model domain can be modified (e.g., comparison of existing and post-dredging scenarios, different structural configurations, evaluation of varying beach nourishment templates, etc.) to determine the effect various changes have on the wave climate. Wave input also can be modified to simulate a wide range of wave conditions (e.g., storm events, seasonal variations) to determine changing impacts on shoreline response.

This section focuses on the application and results of wave transformation numerical modeling for offshore New Jersey. A combined refraction and diffraction spectral wave model was used to propagate random waves from offshore to the nearshore region and investigate potential changes in the wave field caused by dredging of offshore borrow areas. The purpose of this section is to describe the framework and capabilities of the wave model, explain its application to the New Jersey coastline, and provide analysis of the modeling results used as input to the numerical circulation and sediment transport models.

4.1.1 Wave Model Description

The spectral wave refraction/diffraction model REF/DIF S (Kirby and Özkan, 1994) was employed to evaluate changes in wave propagation across the New Jersey continental shelf relative to potential sand mining scenarios. REF/DIF S is a combined refraction and diffraction spectral wave model, which can simulate the behavior of a random sea state and incorporates the effects of shoaling, wave breaking, refraction, diffraction, and energy dissipation. Using wave data collected in the New Jersey coastal region, appropriate offshore wave conditions were approximated and used as input data to specify offshore wave boundary conditions. Then, using local bathymetry to create an accurate grid, the model is able to propagate waves to an area of interest along the New Jersey coastline. The following discussion provides a brief description of REF/DIF S.

Understanding water wave propagation over irregular bathymetry can be improved greatly through the implementation of a spectral wave model rather than a monochromatic wave model. The use of a spectral wave model provides the capability to propagate numerous components

of a natural sea state simultaneously through the model domain. The spectral approach makes it possible to calculate nearshore statistical wave parameters and represent the actual sea surface more accurately. Typically, ocean wave energy is composed of a large variety of waves moving in different directions and with different frequencies, phases, and heights. By simulating numerous wave components that propagate toward the New Jersey shoreline, a spectral wave model is superior to a monochromatic wave model, which would include only one specific wave.

To illustrate the increased accuracy gained by using a spectral wave model, a comparison was made between spectral model results (REF/DIF S), monochromatic results (REF/DIF 1), and experimental data collected by Vincent and Briggs (1989) for waves propagating over a submerged shoal. The upper left-hand panel of Figure 4-1 illustrates bathymetry used in the experiments conducted by Vincent and Briggs (1989). The bottom panels present normalized wave height results for two (monochromatic and spectral) model simulations. The dashed black lines on the bottom two plots show contours of the submerged shoal, while the solid white lines are contours of normalized wave height (also presented as a color map). Both monochromatic (REF/DIF 1, lower left-hand panel) and spectral (REF/DIF S, lower right-hand panel) results illustrate wave focusing behind the submerged shoal; however, the monochromatic wave model tends to focus wave energy to a much greater degree than the spectral wave model. In addition, monochromatic wave model results show more “jagged” and unrealistic wave height patterns induced by the presence of the shoal.

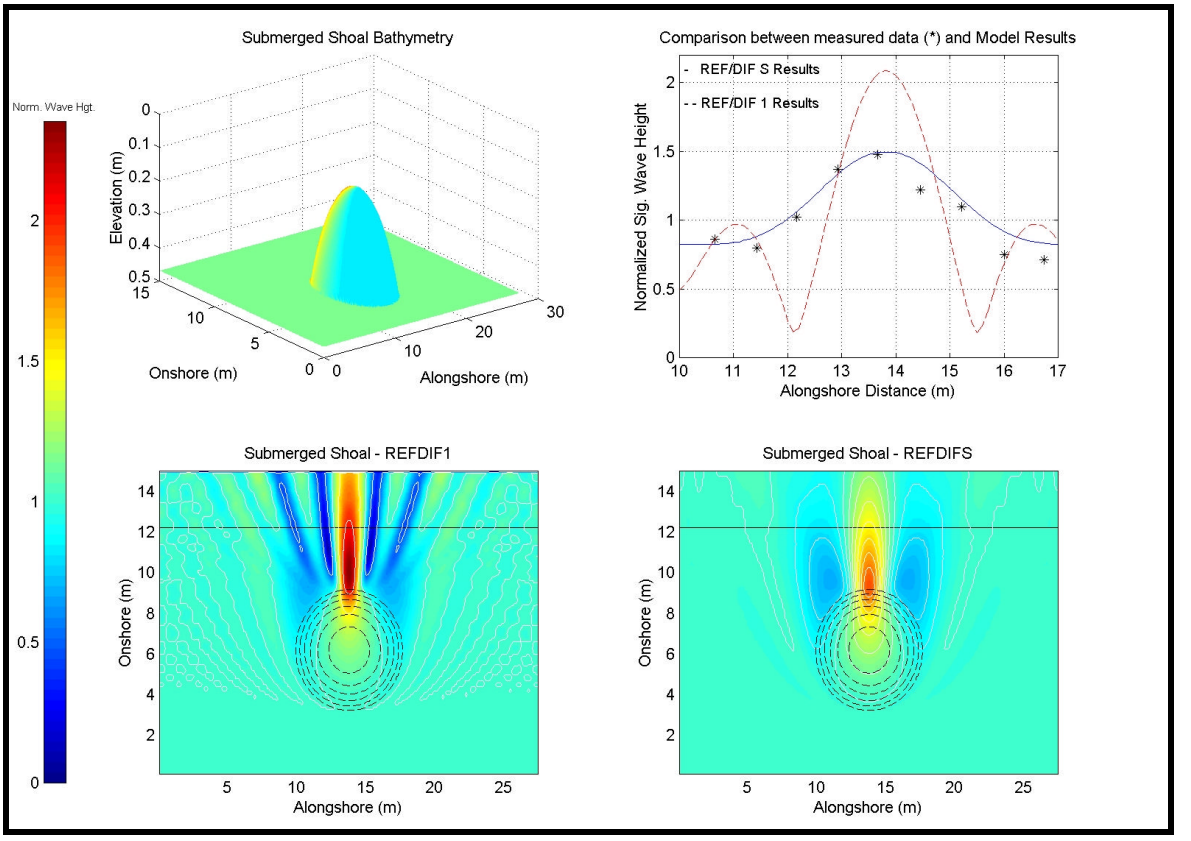

Figure 4-1. Comparison between spectral (REF/DIF S) and monochromatic (REF/DIF 1) wave models. Wave height results are compared to measured data (*) collected by Vincent and Briggs (1989).

The upper-right hand plot shows a comparison between spectral model results (-), monochromatic model results (- -), and measured data (*) for a transect taken 12.2 m from the offshore boundary (indicated by the solid black line in the lower panel plots). Spectral wave model results compare well with the general shape of the curve depicted by the measured data, while monochromatic wave model results over-predict wave focusing and under-predict wave height on either side of the focusing.

REF/DIF S simulates the behavior of a random sea surface by describing wave energy density as a function of direction (directional spectrum) and frequency (frequency spectrum). The two-dimensional wave spectrum is discretized into separate wave components, which constitute an essential part of the input for REF/DIF S. Through a combination of the various wave directions and frequencies, REF/DIF S is able to simulate the behavior of a natural, random sea. In addition, detailed analysis and selection of input spectrum allows the model to assess the impact of different seasonal conditions, varying wave approach pathways, and storms. A detailed description of the theoretical capabilities of REF/DIF S is presented in Appendix B1.

4.1.2 Required Input Conditions

Wave modeling requires specification of offshore wave conditions and a bathymetric grid. By analyzing collected offshore wave data (NOAA wave buoys as well as other sources) or USACE WIS hindcast wave data, the appropriate wave input (spectra) can be developed and used to specify the offshore forcing boundary condition. By using local bathymetry to create an accurate grid, determine lateral boundary conditions, and select appropriate dissipation parameters, the model is capable of propagating waves to the area of interest. A comprehensive description of wave characteristics and spectral input determination can be found in Section 4.2, while development of site-specific reference grids (both existing and post-dredging) for the New Jersey wave transformation numerical modeling can be found in Section 4.3.

4.2 WAVE CHARACTERISTICS AND INPUT SPECTRA

A key component of accurate wave modeling is the analysis and selection of input wave data. The results derived from numerical wave transformation modeling are controlled by the quality of selected input data and parameters. This section describes the analysis and selection of input wave parameters for the modeling effort and focuses specifically on the development of seasonal and extremal spectra.

4.2.1 Wave Data Analysis and Sources

4.2.1.1 Wave Information Study and Additional Data Sources

WIS has met a critical need for wave information in coastal engineering studies since the 1980s. WIS contains time series information of spectrally-based, significant wave height, peak period, peak direction, and wind speed and direction produced from a computer hindcast (prediction) model. The hindcast wave model, WISWAVE (Resio and Tracy, 1983), is run using wind information (speed and direction) at selected coastal locations around the United States. The model predicts wave climate based on local/regional wind conditions. Because the data are numerically generated, consistent and long-term wave data are available at most coastal locations. WIS information originally was calculated by hindcasting deepwater waves from historical surface pressure and wind data (Brooks and Corson, 1984). This Phase I-type model used large-scale atmospheric conditions, a large grid size (hundreds of kilometers), and only one type of wave process, air-sea interaction. Phase I results do not include such effects as

shoaling, bottom friction, or long waves. Although simplifications are present in Phase I-type modeling, it still provides adequate approximations of time-series results.

Wave measurements made by the NOAA during the 1980s made verification of WIS results possible by comparing the statistics and the distributions of wave heights and periods from different time periods (Hubertz et al., 1993). Improvements have been made through subsequent modeling efforts to increase the accuracy of WIS relative to NOAA measurements. Phase II-type WIS data, which include the effects of shoaling, refraction, diffraction, and bottom friction, were used in the present study. The Phase II WIS data provide wave parameter results every three hours, for a twenty-year time period.

The availability and long-term records make WIS information attractive when considering average or seasonal wave conditions. Since the data are widespread and continuous, adoption of the WIS data for development of spectral wave conditions is applicable. WIS stations used are located at or near the offshore boundary of the wave transformation model grid (and shown on Figure 4-2). The closest available WIS station near the offshore boundary was used at each modeling reference grid. Table 4-1 provides a summary of the three WIS stations used in the present spectral wave modeling effort along the New Jersey coast.

Table 4-1. Summary of relevant WIS stations in the modeling domain.

WIS Station	Au2067	Au2069	Au2070
Reference Grid	A	B2	B1 & C
UTM Northing (m)	4,316,895	4,372,742	4,400,488
UTM Easting (m)	543,296	585,980	585,671
Depth (m)	18	22	18
Time Period (yrs)	1976 to 1995	1976 to 1995	1976 to 1995

Each station is located seaward of sand resource areas in 18 to 22-m water depth. Input data (energy and directional spectra) for reference grids were developed from simulated wave data for these three stations. Due to the large modeling domain and the distance between each of the four modeling grids, input spectra were generated for each grid separately. Previous studies and design projects have used WIS data as an accurate measure of wave climate and as input to nearshore wave transformation models for the New Jersey area (Kraus et al., 1988) and in general (Byrnes et al., 1999). There was a noticeable difference in wave characteristics between each of the WIS stations, specifically when partitioning the data by direction of approach. For example, waves arriving from the southwest tended to be slightly larger and longer at station Au2069 than at station Au2070.

Another source of wave data readily available offshore New Jersey is the Long-term Ecosystem Observatory (LEO-15) data, collected by the Mid-Atlantic Bight National Undersea Research Center (MAB-NURC), Institute of Marine and Coastal Sciences (IMCS) at Rutgers University. The LEO-15 data consist of non-directional wave information and numerous other parameters (e.g., salinity, current, temperature, dissolved oxygen, etc.). The National Data Buoy Center (NDBC) also was explored for data observations; however, no NOAA buoys have been deployed offshore New Jersey.

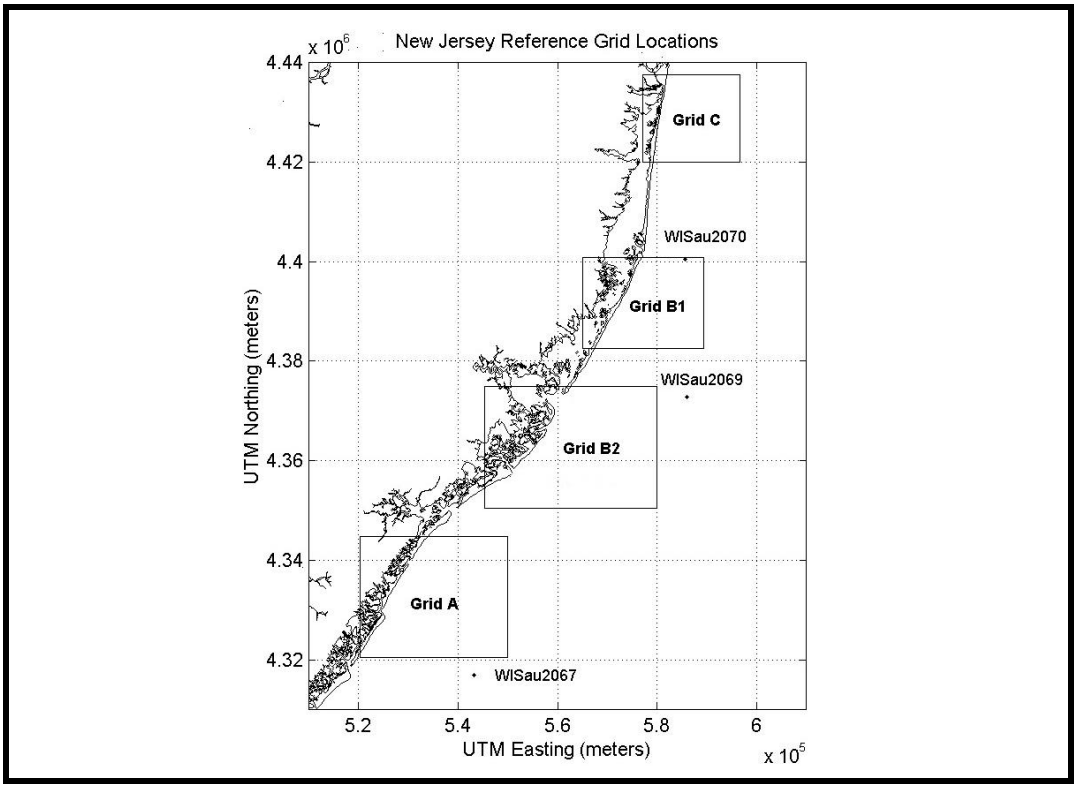

Figure 4-2. Relative location of WIS stations and Reference Grids.

The benefit of using the LEO-15 or other observed data is that it is measured rather than predicted (hindcasted). However, because buoys and/or pressure sensors are collecting actual observations, the instruments are subject to severe weather and mechanical problems, and therefore, a consistent long-term wave record is more difficult to attain. Table 4-2 presents the locations and availability of observed data offshore New Jersey. The observed data consist of numerous gaps and limited deployment times. These variables resulted in an incomplete and unfavorable wave data set. In addition, all wave stations were deployed landward of sand resource areas (Table 4-2), making the observed data ineffective for wave modeling boundary conditions. The spatial and temporal data limitations made it difficult to use these observations for anything more than ancillary data.

Table 4-2. Inventory of relevant observation stations.

Station ID	Location (UTM)	Deployment Time	Wave Data	Wind Data	Wave Direction
LEO-15A	4,367,752 N 564,877 E	5/93 to 10/95	X	O	O
LEO-15B	4,368,251 N 563,488 E	5/93 to 10/95	X	O	O
X = data collected; O = no data collected					

4.2.1.2 Data Comparison

Since no observed data were collected in the vicinity of the WIS stations used in this study, it was difficult to verify their accuracy. General trends in the data can be investigated by comparing WIS data with LEO-15 data for the same time periods; however, the number of data gaps in the LEO-15 data, coupled with the large difference in site location, made verification difficult. Over time periods when data were available at both locations, general trends in wave height and period could be documented. The validity of the WIS data, as well as the overall performance of the wave model, were examined by propagating individual waves from the WIS station to the location of the observed wave data. Wave model simulations were established using discrete WIS spectral data (from selected 3-hour periods at WIS Station Au2069) as input conditions. The derived wave spectrum was propagated from the WIS station to the location of the observed LEO-15 data, which is closer to the coast and lying within the model grid (Grid B2). As waves propagate from offshore to onshore (i.e., from the seaward grid boundary to the LEO-15 measurement location), wave transformations occur in response to bathymetry and wave-wave interactions. By comparing model results with observed LEO-15 data measured at approximately the same time, an estimate of the quality of WIS data could be made. In addition, the relative accuracy of REF/DIF S could be assessed. Three (3) discrete wave spectra were used to develop spectral input for the test simulations. The spectra were selected to represent a variety of wave heights and wave parameters. Table 4-3 presents the input wave spectra used for the comparison runs.

Table 4-3. Input conditions used for comparison of WIS and LEO-15 data.

Test Simulation	Input Wave Height (m)	Input Wave Period (sec)	Approach Direction (grid relative)
Mild	0.9	5.0	-4.0
Normal	1.8	7.0	7.0
Significant	3.1	9.0	-11.0
Large	4.6	12.0	-22.0

Wave heights were extracted from test simulation results at the closest available grid cell to the LEO-15 location within the model domain. Modeled heights were then compared to the LEO-15 data observed at approximately the same time. Table 4-4 presents the results of the comparison. Direction of approach could not be compared, since the LEO-15 data did not record this parameter. Results of the comparison indicate that WIS data and observed LEO-15 data compare reasonably well. The larger the wave height, the larger the percent difference between modeled results and observations. It is unclear if differences are due to the accuracy of WIS data, the accuracy of observed data, the prediction capability of the spectral wave model, variations in direction of wave approach, or some combination of all factors. However, test simulations do show that WIS data provides an adequate measure of wave climate for the region.

Table 4-4. Test simulation results for comparison of WIS and LEO-15 data.

Test Simulation	Modeled Wave Height (m)	LEO-15 Wave Height (m)	Percent Difference
Mild	0.7	0.7	0 %
Normal	1.3	1.2	+8.3%
Significant	2.4	2.1	+14.3%
Large	2.3	2.9	-20.7%

4.2.1.3 Wave Direction Characteristics

A detailed understanding of the local wave climate is required to produce representative wave modeling simulations. The 20-yr (1976 to 1995) WIS data set offers a synopsis of the wave climate offshore New Jersey. An examination of local WIS stations (Au2067, Au2069, and Au2070) provides a detailed description of the wave climate and leads to the development of appropriate input spectra.

Rather than selecting the most common wave heights and directions, a detailed analysis was conducted to summarize existing WIS data into average seasonal and directional wave conditions and spectra. Each season and/or directional bin may contain distinct differences in energy and/or directional spectra, and consequently produce varying impacts at borrow locations. Simulation of these wave characteristics (averaged over 20 years) provides a method of identifying these changes.

Spectral WIS waves were segregated into distinct directional bins for analysis and modeling. The directional bin approach sorts and separates wave data by direction of approach relative to the coastline, independent of when they occur. Discrete directional bins were established to best represent the local directional spectra. For example, waves approaching from between -11.25 to +11.25 were combined to define the shore-normal (0 degree) approach bin. In this manner, the impacts caused by dredging offshore borrow sites were determined for a wide range of directional approaches occurring throughout the year. The directional bin approach identifies all potential effects caused by borrow site excavation, including those directional approaches that occur only small percentages of the time throughout a typical season. Typical wave conditions offshore New Jersey were calculated by averaging 20 years of wave data. Directional spectra developed for New Jersey were presented by percent occurrence.

To allocate historical data into appropriate directional bins, overall wave conditions were examined for each WIS station. Figures 4-3 through 4-5 present the distribution of significant wave height (illustrated using a wave rose plot) for each of the WIS stations used for generation of input wave conditions. The color scale indicates the magnitude of wave height, the circular axis represents the direction of wave approach (coming from) relative to North (0 degrees), and the extending radial lines indicate percent occurrence within each magnitude and directional band. The direction of wave approach at WIS station Au2067 (Figure 4-3) is slightly stronger from the southwest than for the other two stations, which corresponds to the orientation of the shoreline. At station Au2070 (Figure 4-5), wave directions are more concentrated around an easterly approach with a smaller directional spread. As expected, the primary clustering of wave directions tends to be aligned relative to the shoreline orientation. Significant wave heights are relatively similar for each of the WIS stations. Although a smaller percentage of the whole, larger wave heights approach from the northeast as winter storms.

Figure 4-6 shows histograms of peak wave period and direction for WIS station Au2069, averaged over 20 years (1976 to 1995). Figures 4-7 and 4-8 present similar plots for WIS stations Au2069 and Au2070. All three WIS stations experience waves of similar periods over the 20 years. Differences in the wave period distribution do become evident as more detailed directional analysis is performed (section 4.2.2).

WIS wave data was separated into discrete directional approach bins as presented in Tables 4-5 through 4-7. The bold value presented in the first two columns of the tables represents the center of each directional bin, while the italicized values define the extent of the directional bins. The total percent occurrence is the percent of waves falling within each directional bin relative to all the waves hindcast at the WIS station.

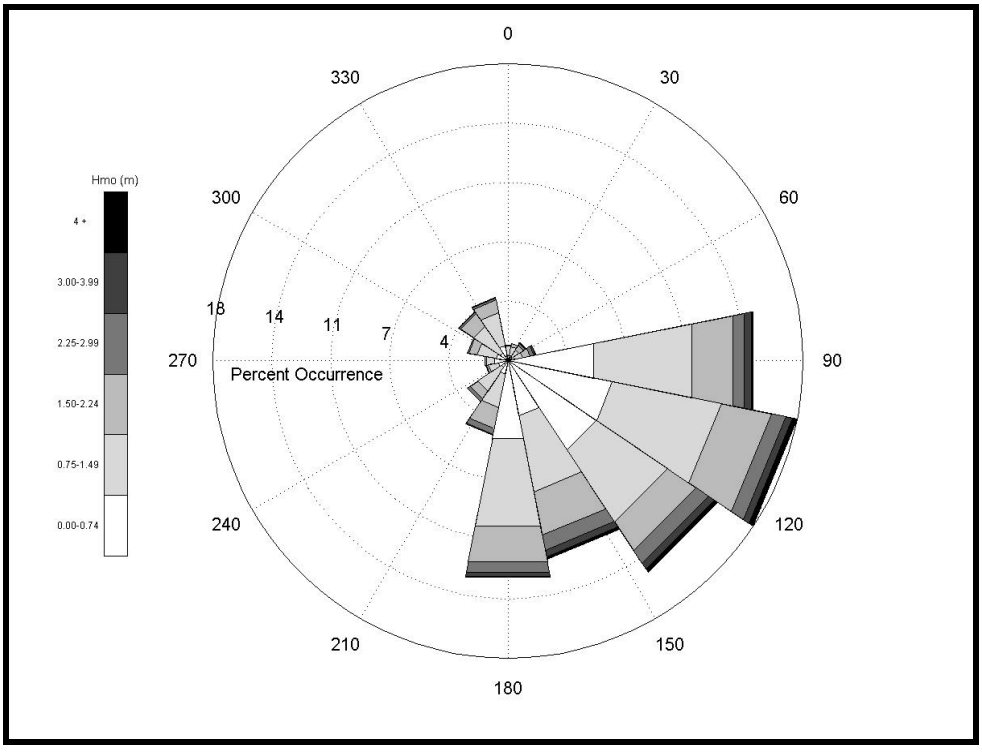

Figure 4-3. Twenty-year averaged wave rose for WIS Station Au2067.

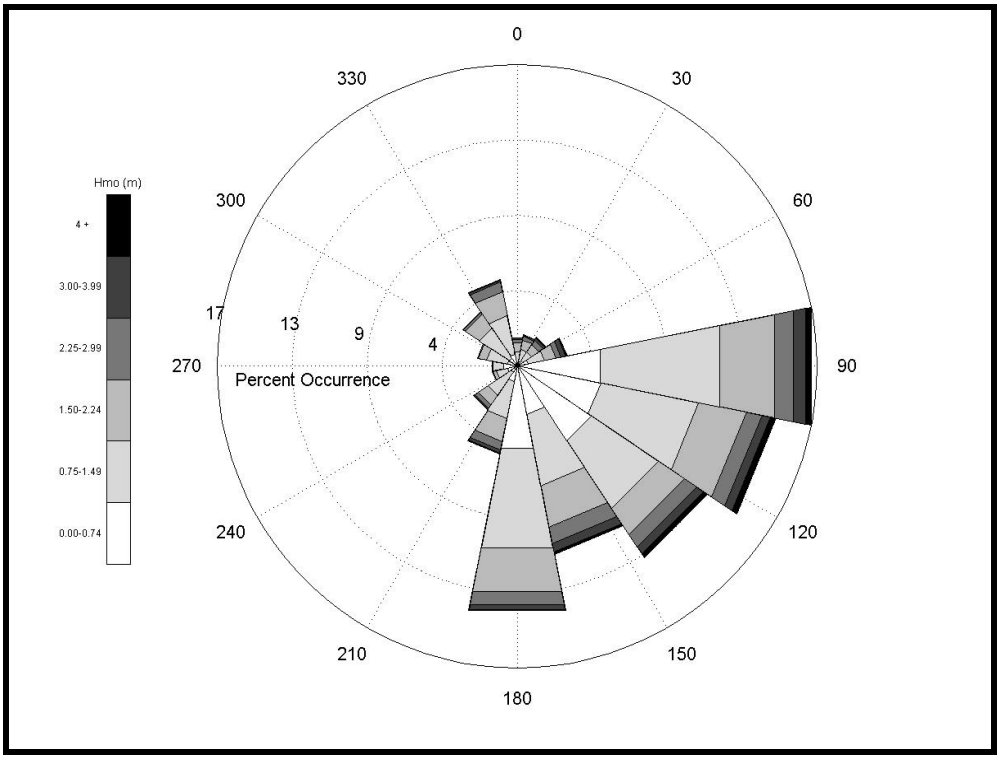

Figure 4-4. Twenty-year averaged wave rose for WIS Station Au2069.

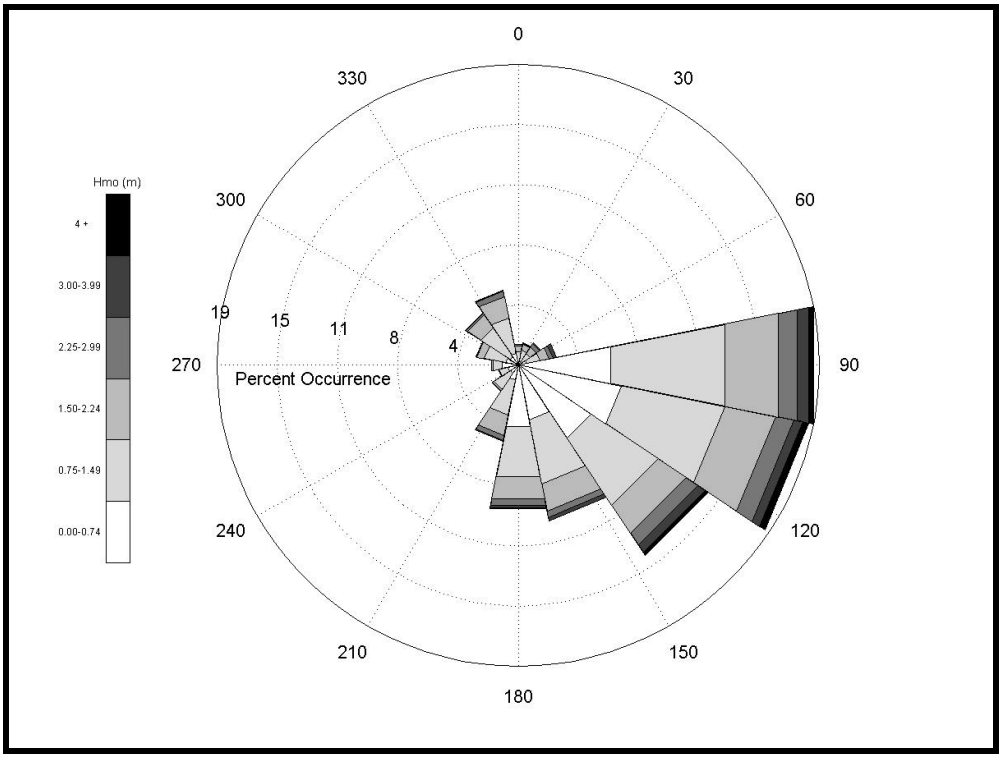

Figure 4-5. Twenty-year averaged wave rose for WIS Station Au2070.

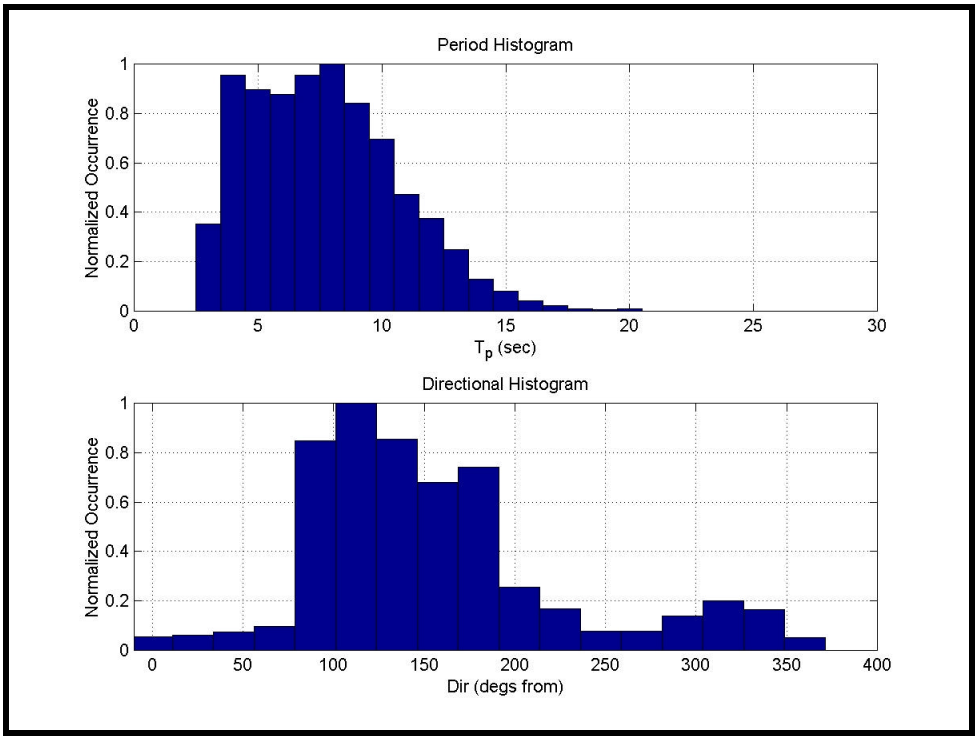

Figure 4-6. Histogram plots of 20-year averaged peak periods and associated wave directions at WIS Station Au2067. The vertical bars are normalized by the greatest occurrence bin.

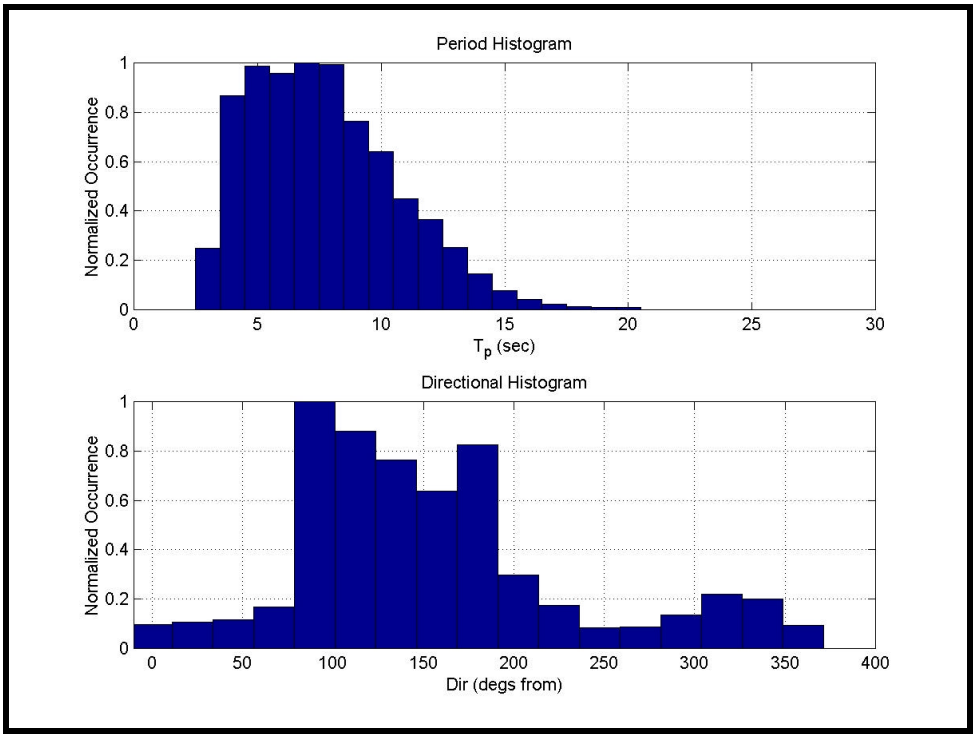

Figure 4-7. Histogram plots of 20-year averaged peak periods and associated wave directions at WIS Station Au2069. The vertical bars are normalized by the greatest occurrence bin.

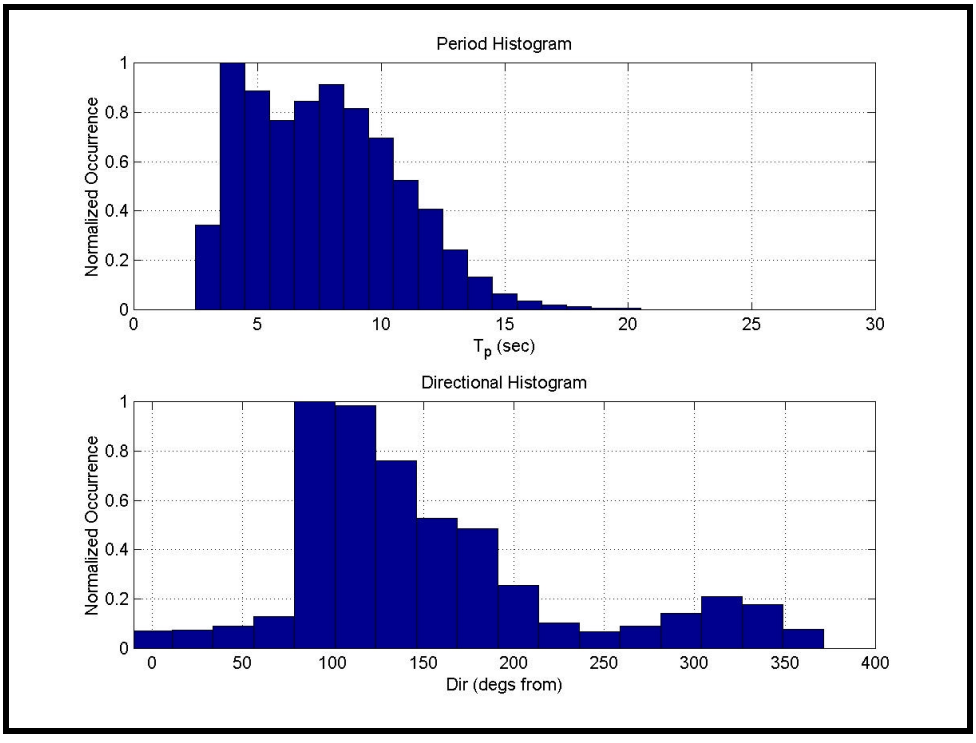

Figure 4-8. Histogram plots of 20-year averaged peak periods and associated wave directions at WIS Station Au2070. The vertical bars are normalized by the greatest occurrence bin.

Table 4-5. Summary of the directional bin breakdown of the Au2067 WIS station data.

Map Relative Direction (coming from, 0E = N)	Grid Relative Direction (coming from, 0E = E)	Total Percent Occurrence
0.0 *(-11.25 to 11.25)*	**90.0** *(78.75 to 101.25)*	0.98
22.5 *(11.26 to 33.75)*	**67.5** *(56.26 to 78.75)*	1.10
45.0 *(33.76 to 56.25)*	**45.0** *(33.76 to 56.25)*	1.33
67.5 *(56.26 to 78.75)*	**22.5** *(11.26 to 33.75)*	1.76
90.0 *(78.75 to 101.25)*	**0.0** *(-11.25 to 11.25)*	15.26
112.5 *(101.26 to 123.75)*	**-22.5** *(-33.75 to -11.24)*	18.03
135.0 *(123.76 to 146.25)*	**-45.0** *(-56.25 to -33.74)*	15.41
157.5 *(146.26 to 168.75)*	**-67.5** *(-78.75 to -56.24)*	12.26
180.0 *(168.76 to 191.25)*	**-90.0** *(-101.25 to -78.74)*	8.24
Waves heading offshore	Waves heading offshore	25.63

Table 4-6. Summary of the directional bin breakdown of the Au2069 WIS station data.

Map Relative Direction (coming from, 0E = N)	Grid Relative Direction (coming from, 0E = E)	Total Percent Occurrence
0.0 *(-11.25 to 11.25)*	**90.0** *(78.75 to 101.25)*	1.89
22.5 *(11.26 to 33.75)*	**67.5** *(56.26 to 78.75)*	2.06
45.0 *(33.76 to 56.25)*	**45.0** *(33.76 to 56.25)*	2.21
67.5 *(56.26 to 78.75)*	**22.5** *(11.26 to 33.75)*	3.14
90.0 *(78.75 to 101.25)*	**0.0** *(-11.25 to 11.25)*	17.26
112.5 *(101.26 to 123.75)*	**-22.5** *(-33.75 to -11.24)*	15.21
135.0 *(123.76 to 146.25)*	**-45.0** *(-56.25 to -33.74)*	13.22
157.5 *(146.26 to 168.75)*	**-67.5** *(-78.75 to -56.24)*	11.08
180.0 *(168.76 to 191.25)*	**-90.0** *(-101.25 to -78.74)*	7.98
Waves heading offshore	Waves heading offshore	28.24

Table 4-7. Summary of the directional bin breakdown of the Au2070 WIS station data.

Map Relative Direction (coming from, 0E = N)	Grid Relative Direction (coming from, 0E = E)	Total Percent Occurrence
0.0 *(-11.25 to 11.25)*	**90.0** *(78.75 to 101.25)*	1.52
22.5 *(11.26 to 33.75)*	**67.5** *(56.26 to 78.75)*	1.58
45.0 *(33.76 to 56.25)*	**45.0** *(33.76 to 56.25)*	1.88
67.5 *(56.26 to 78.75)*	**22.5** *(11.26 to 33.75)*	2.62
90.0 *(78.75 to 101.25)*	**0.0** *(-11.25 to 11.25)*	19.18
112.5 *(101.26 to 123.75)*	**-22.5** *(-33.75 to -11.24)*	18.89
135.0 *(123.76 to 146.25)*	**-45.0** *(-56.25 to -33.74)*	14.62
157.5 *(146.26 to 168.75)*	-67.5 *(-78.75 to -56.24)*	10.20
180.0 *(168.76 to 191.25)*	**-90.0** *(-101.25 to -78.74)*	4.67
Waves heading offshore	Waves heading offshore	24.83

After directional bins were established, frequency and directional histograms were developed for each directional bin. The directional WIS wave conditions were used to develop the energy and directional input spectra for REF/DIF S. A more detailed discussion on the development of individual spectra can be found in Section 4.2.2.

4.2.1.4 High Energy Events

Since high energy events have a significant impact on many physical processes (and in most cases, dominate sediment transport), it is crucial to include storm simulations in wave modeling to assess the potential impact of potential borrow sites. WIS data used in this study include the effects of hurricanes and storms; however, the individual effect of an extreme event is represented as a separate model run. Simulation of a high energy event for the study area is incorporated using extremal analysis. Therefore, high energy events are simulated using wave transformation modeling, in addition to evaluating average directional approaches.

High energy events were evaluated by reviewing existing literature on hurricanes and northeast storms (USACE, 1997) that passed through the New Jersey region, investigating the storm tracks, and using an extremal-value approach to analyze historical data sets. Results of the analysis, coupled with historical storm tracks and wave directions, were used to determine wave heights, directions, and frequencies for simulating a high-energy wave event.

Table 4-8 presents return periods calculated by the United States Army Corps of Engineers, Philadelphia District (1997) based on maximum wave heights hindcasted for thirty recent storms (hurricanes since 1890 and northeasters since 1950). Generally, return values are presented for 10 years, 25 years, 50 years, and 100 years, although any arbitrary return period can be calculated. The return periods calculated here are 20, 50, 100, 200, and 500 years. For instance, a 20-yr return value for a wave height of 4.7 m means that for any given year, there is a 1/20 chance that waves of 4.7 m will be reached. However, the return period is not the same as the probability that an event of a specific size will occur within an interval of time. Nor is the return period the frequency of occurrence of events of a given intensity. The specific selection of parameters representing the high energy (or extreme) wave event can be found in Section 4.2.3.

Table 4-8. Return periods from results of Gumbel Distribution Hindcast (USACE, 1997).

Return Period (yr)	Significant Wave Height (m)		
	Hurricanes only	Northeasters only	All Storms
2	--	--	3.70
5	--	--	4.33
10	--	--	5.07
20	4.75	5.52	5.77
50	5.61	6.42	6.64
100	6.28	7.09	7.28
200	6.92	7.75	7.92
500	7.76	8.61	8.76

4.2.2 Input Condition Parameters

4.2.2.1 Spectra Development

REF/DIF S requires input of a directional wave spectrum, which represents the distribution of wave energy in the frequency and direction domains. The two-dimensional wave spectrum is given as the product of the energy and directional spectra as:

$$S(f,q) = E(f)D(q) \tag{4.1}$$

where *S(f,q)* is the directional wave spectral density function, *D(q)* is the directional spreading function, and *E(f)* is the frequency spectra. The directional spreading function provides the relative magnitude of directional spreading of wave energy, while the frequency spectrum provides the absolute value of wave energy density. Numerous empirical approximations have been developed to represent frequency and directional distributions. A detailed discussion of the methods used in this study are presented in Appendix B2.

4.2.2.2 Selection of Wave Conditions

Using the frequency distribution and directional distribution from WIS data, directional spectra were generated to represent several directional bins. WIS data were segregated by direction of approach and an energy distribution was generated from all waves within each directional bin. WIS energy and directional distributions were matched with TMA frequency and directional spreading functions to obtain a best-fit of the data. The matching procedure involves adjustment and optimization of the peak enhancement factor and directional spreading parameter, as well as appropriate bin selection and energy conservation. After approximating the data with continuous spectra, representative discrete components (in frequency and directional domains) were selected by discretizing the continuous spectra into energy conserving bins. Each component is representative of an energy conserving bin (equal area under the continuous curve).

After separating the WIS data by direction, the energy associated with each WIS measurement is calculated as a function of frequency:

$$E(f) = \frac{1}{8} rgH^2 \tag{4.2}$$

where H represents the associated wave height. The energy associated with each frequency is then summed to create an energy distribution for each approach direction. The total energy at each frequency is normalized by the highest energy. The peak of each energy distribution represents the peak frequency used for generating a TMA spectrum, while peak energy is used to determine significant wave height. A high-frequency cutoff was imposed on the derived spectra at 0.2 Hertz (5 sec) to eliminate short period, low energy waves from the modeling effort. Modeling waves with periods of less than 5 seconds would require a higher resolution model grid, which would substantially increase model simulation time.

Following generation of the directional spectra, values were coupled to produce discrete wave components forming a comprehensive directional bin wave group. For example, ten frequency bins and ten directional bins produced a wave field consisting of 100 individual waves. Tables 4-9 through 4-12 present a summary of the spectral parameters used to develop input conditions corresponding to Grids A, B2, B1, and C, respectively. The parameters were used to develop input wave conditions at the offshore boundaries. The gray rows in Tables 4-9 through 4-12 represent directional bins that were not simulated. Due to the small percentage of wave occurrences, as well as wave model restrictions relative to the angle of approach, certain directional bins were not modeled in this study. In all grids, the simulated model runs represented the vast majority of the wave energy.

4.2.3 High Energy Event Parameters

Two distinct types of storms, northeasters and hurricanes, affect the study area. Northeasters, named after the predominant direction of the associated winds, are large-scale, low pressure disturbances. Wind speeds associated with a northeast storm are generally less than those of a hurricane, although wind gusts can reach hurricane strength in under severe conditions. In addition, northeast storms are typically longer duration than hurricanes and can result in significant damage to the coastline. Hurricanes are a relatively rare occurrence along the New Jersey coastline. By the time a hurricane reaches the latitudes of the New Jersey coast, they are typically either far out to sea or in a state of rapid decay. Despite their infrequent occurrence, hurricanes have the potential to produce devastating impacts along the coastline.

To represent extreme conditions, a 50-yr hurricane and northeast storm event were modeled using the analysis presented in Section 4.2.1.4. Extremal wave heights were determined from return period calculations performed by the U. S. Army Corps of Engineers, Philadelphia District. These calculations were based on historical storms from approximately 1890 to 1997. The corresponding 50-yr hurricane wave period (peak frequency) was determined using the following equation:

$$T = 12.1\sqrt{\frac{H_o}{g}} \tag{4.3}$$

as presented in the Shore Protection Manual (US Army Corps of Engineers, 1984). The corresponding 50-yr Northeast storm wave period (peak frequency) was determined through correlation with historical northeast storm occurrences in the WIS data. The wave period was taken as the average wave period occurring during a Northeast storm. The same correlation method was applied to determine the primary approach direction for both hurricane and Northeast storms by averaging the approach directions of historical storm occurrences.

Since there is a lack of spectral information in the region related to the passing of hurricanes and northeast storm events, directional and energy spectra were estimated for the 50-yr event through utilization of the standard TMA and directional spreading functions. Tables 4-9 through 4-12 present the spectral parameters used to develop the 50-yr storm input conditions corresponding to Grids A, B2, B1, and C, respectively.

A storm surge value was also included in the wave modeling simulation to represent the increased water level experienced during the passage of a large storm event. Surge values reported by Kraus et al. (1988) at Monmouth Beach, New Jersey, were used to determine the storm surge levels associated with a 50-yr hurricane and northeast storm. Storm surge heights of 2.71 m and 2.32 m were determined from the stage frequencies presented by Kraus et al. (1988) for a 50-yr hurricane and 50-yr northeast storm, respectively.

Table 4-9. Wave transformation numerical modeling input conditions and scenarios for Grid A

Scenario (grid relative)	Y-Sub	Spectra Type	# of E Bins	# of θ Bins	T_p (sec)	f_p (Hz)	f_{max} (Hz)	σ_m (+)	σ_m (-)	γ	H_s (m)	θ_{mean} (grid relative)
67.5E	10	TMA	10	5	4.0	0.250	--	--	--	--	1.1	66.8E
45E	10	TMA	10	5	6.0	0.167	--	--	--	--	1.6	44.7E
22.5E	10	TMA	10	5	7.0	0.130	0.3	5.0	5.0	1.3	1.8	22.5E
0E	10	TMA	10	5	10.0	0.090	0.2	5.0	5.0	1.1	1.4	-6.0E
-22.5E	10	TMA	10	5	11.0	0.085	0.2	5.0	5.0	1.2	1.4	-24.0E
-45E	10	TMA	10	5	9.0	0.085	0.2	5.0	5.0	1.0	1.4	-43.9E
-67.5E	10	TMA	10	5	10.0	0.090	0.2	5.0	5.0	1.0	1.5	-66.6E
Northeast storm	10	TMA	10	5	13.0	0.076	0.2	5.0	5.0	1.6	6.4	0.0E
Hurricane	10	TMA	10	5	9.0	0.111	0.2	5.0	5.0	1.6	5.7	-45.0E

Table 4-10. Wave transformation numerical modeling input conditions and scenarios for Grid B2

Scenario (grid relative)	Y-Sub	Spectra Type	# of E Bins	# of θ Bins	T_p (sec)	f_p (Hz)	f_{max} (Hz)	σ_m (+)	σ_m (-)	γ	H_s (m)	θ_{mean} (grid relative)
67.5E	10	TMA	10	5	6.0	0.167	--	--	--	--	1.7	67.4E
45E	10	TMA	10	5	7.0	0.143	--	--	--	--	1.9	44.8E
22.5E	10	TMA	10	5	8.0	0.130	0.2	5.0	5.0	1.0	1.9	22.3E
0E	10	TMA	10	5	12.0	0.078	0.2	5.0	5.0	1.0	1.6	-2.9E
-22.5E	10	TMA	10	5	11.0	0.085	0.2	5.0	5.0	1.0	1.6	-23.8E
-45E	10	TMA	10	5	9.0	0.092	0.2	5.0	5.0	1.0	1.5	-44.0E
-67.5E	10	TMA	10	5	10.0	0.105	0.2	5.0	5.0	1.0	1.6	-66.6E
Northeast storm	10	TMA	10	5	13.0	0.077	0.2	5.0	5.0	1.6	6.4	0.0E
Hurricane	10	TMA	10	5	9.0	0.111	0.2	5.0	5.0	1.6	5.6	-45.0E

Table 4-11. Wave transformation numerical modeling input conditions and scenarios for Grid B1

Scenario (grid relative)	Y-Sub	Spectra Type	# of E Bins	# of θ Bins	T_p (sec)	f_p (Hz)	f_{max} (Hz)	σ_m (+)	σ_m (-)	γ	H_s (m)	θ_{mean} (grid relative)
67.5E	10	TMA	10	5	5.0	0.200	--	--	--	--	1.5	66.9E
45E	10	TMA	10	5	7.0	0.143	--	--	--	--	1.7	44.4E
22.5E	10	TMA	10	5	7.0	0.143	0.2	5.0	5.0	2.0	1.8	22.5E
0E	10	TMA	10	5	10.0	0.092	0.2	5.0	5.0	1.2	1.5	-3.4E
-22.5E	10	TMA	10	5	11.0	0.095	0.2	5.0	5.0	1.3	1.5	-23.4E
-45E	10	TMA	10	5	10.0	0.100	0.2	5.0	5.0	1.0	1.5	-44.0E
-67.5E	10	TMA	10	5	8.0	0.111	0.2	5.0	5.0	1.0	1.3	-65.7E
Northeast storm	10	TMA	10	7	13.0	0.076	0.2	5.0	5.0	1.6	6.4	0.0E
Hurricane	10	TMA	10	7	9.0	0.111	0.2	5.0	5.0	1.6	5.6	-45.0E

Table 4-12. Wave transformation numerical modeling input conditions and scenarios for Grid C

Scenario (grid relative)	Y-Sub	Spectra Type	# of E Bins	# of θ Bins	$T_{1/3}$ (sec)	f_p (Hz)	f_{max} (Hz)	σ_m (+)	σ_m (-)	γ	H_s (m)	θ_{mean} (grid relative)
67.5E	10	TMA	10	5	5.0	0.200	--	--	--	--	1.5	66.9E
45E	10	TMA	10	5	7.0	0.143	0.2	5.0	5.0	1.0	1.7	44.4E
22.5E	10	TMA	10	5	7.0	0.143	0.2	5.0	5.0	2.0	1.8	22.5E
0E	10	TMA	10	5	10.0	0.092	0.2	5.0	5.0	1.2	1.5	-3.4E
-22.5E	10	TMA	10	5	11.0	0.095	0.2	5.0	5.0	1.3	1.5	-23.4E
-45E	10	TMA	10	5	10.0	0.100	0.2	5.0	5.0	1.0	1.5	-44.0E
-67.5E	10	TMA	10	5	8.0	0.111	0.2	5.0	5.0	1.0	1.3	-65.7E
Northeast storm	10	TMA	10	7	13.0	0.076	0.2	5.0	5.0	1.6	6.4	0.0E
Hurricane	10	TMA	10	7	9.0	0.111	0.2	5.0	5.0	1.6	5.6	-45.0E

4.3 GRID GENERATION

4.3.1 Existing Conditions

In REF/DIF S, the reference grid consists of a mesh of points with dimensions IR and JR, as shown in Figure 4-9. At each point within the domain, water depth and ambient current data can be specified. Reference points are separated by spacing DXR (x-direction) and DYR (y-direction). Because REF/DIF S uses at least 5 points per wavelength of the shortest modeled wave, reference grid selection is not trivial. In addition, boundaries of the model domain should be outside of the study area of interest so boundary constraints do not affect modeling results.

The model domain for the present study is divided into four reference grids due to the large region that is required for wave transformation numerical modeling. Figure 4-10 shows the location of each of the four reference grids (A, B1, B2, and C) along the New Jersey coastline. Grids B1 and C are characterized by relatively smooth bathymetry and a uniform shoreline without inlets. However, Grids A and B2 contain complex bathymetry and irregular coastlines with numerous inlets. Local bathymetry in these areas consists of many shoreface sand ridges, extending to depths of 10- to 15-m along a northeasterly trend. These features have a significant impact on incoming wave spectra.

Grids A, B1, B2, and C were created from the most recent bathymetry for the study area (see Section 3). The orientation of the reference grid, especially the offshore boundary, was selected to closely correspond to the location of WIS stations used to develop spectral input, as well as manage the broad directional wave spread. Since REF/DIF S is constrained by the directional spread of input waves, reference grids were rotated for selected directional bins to alleviate this constraint. For example, for waves approaching from the southeast, the grid was rotated toward the southeast, while still preserving the areas of interest (i.e., the beach region and borrow sites). By customizing the rotation of each grid, a full range of directional approaches were simulated. Table 4-13 presents the UTM coordinates for the corners of each of the unrotated and rotated reference grids.

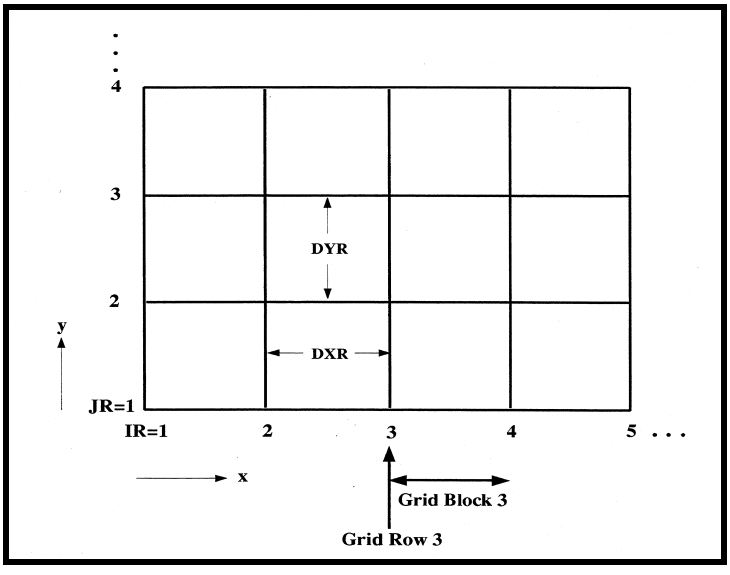

Figure 4-9. Illustration of reference grid notation (Kirby and Özkan, 1994).

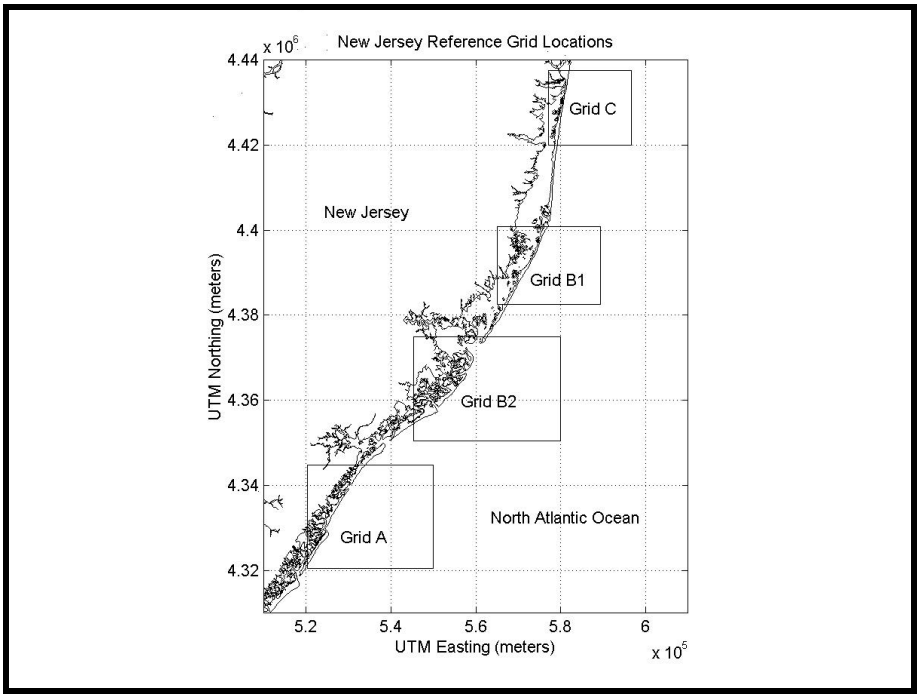

Figure 4-10. Location of the four modeled reference grids along the New Jersey coastline.

Table 4-13. Reference grid dimensions.

Reference Grid	UTM Easting extents (m)	UTM Northing extends (m)
A (unrotated)	519,500 – 549,900	4,308,900 – 4,344,700
A (rotated -45E)	509,780 – 562,240	4,303,300 – 4,355,700
B1 (unrotated)	564,700 – 589,900	4,385,000 – 4,404,200
B1 (rotated -27E)	564,700 – 595,870	4,376,600 – 4,405,100
B2 (unrotated)	553,600 – 579,800	4,341,400 – 4,376,800
B2 (rotated -45E)	549,600 – 582,130	4,347,500 – 4,380,000
C (unrotated)	577,000 – 596,600	4,420,000 – 4,439,600
C (rotated -45E)	570,500 – 599,800	4,415,000 – 4,442,100
C (rotated 45E)	574,000 – 603,300	4,417,000 – 4,444,100

The reference grids cell size is 200 m (DXR) by 200 m (DYR) with interpolated depths obtained from the bathymetric data at each grid intersection point. Interpolated depths were smoothed using a 2-point alongshore zero-phase filtering routine. Figures 4-11 to 4-14 illustrate unrotated bathymetric grids, sand resource areas, and subgrids for each reference grid (A, B1, B2, and C, respectively). In addition, 4-15 presents an example of the rotated reference grid used for simulating certain model runs for Grid A. The reference grid is rotated 45E (clockwise sense).

Although the reference grid spacing was fixed at 200 m by 200 m, subgrids and other input parameters allow REF/DIF S to calculate information at intermediate points within the reference grid. Depths at intermediate points are computed by REF/DIF S by fitting a twisted surface to the reference grid through linear interpolation. In the alongshore direction, each grid

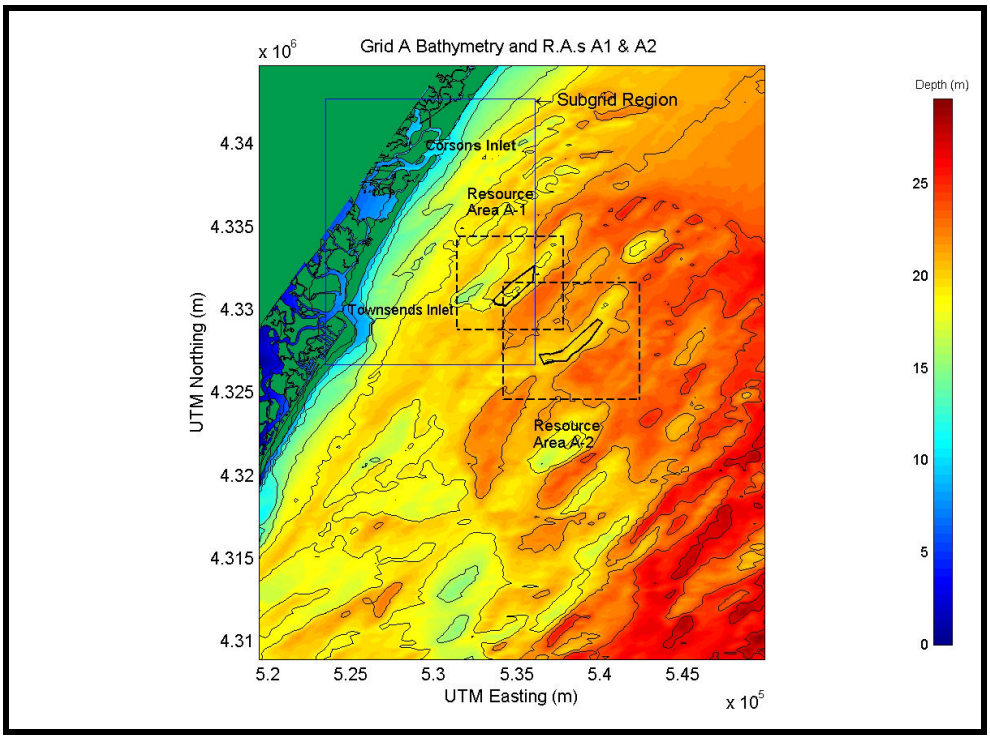

Figure 4-11. Bathymetry for Reference Grid A, the defined sand resource areas, and the nearshore subgrid.

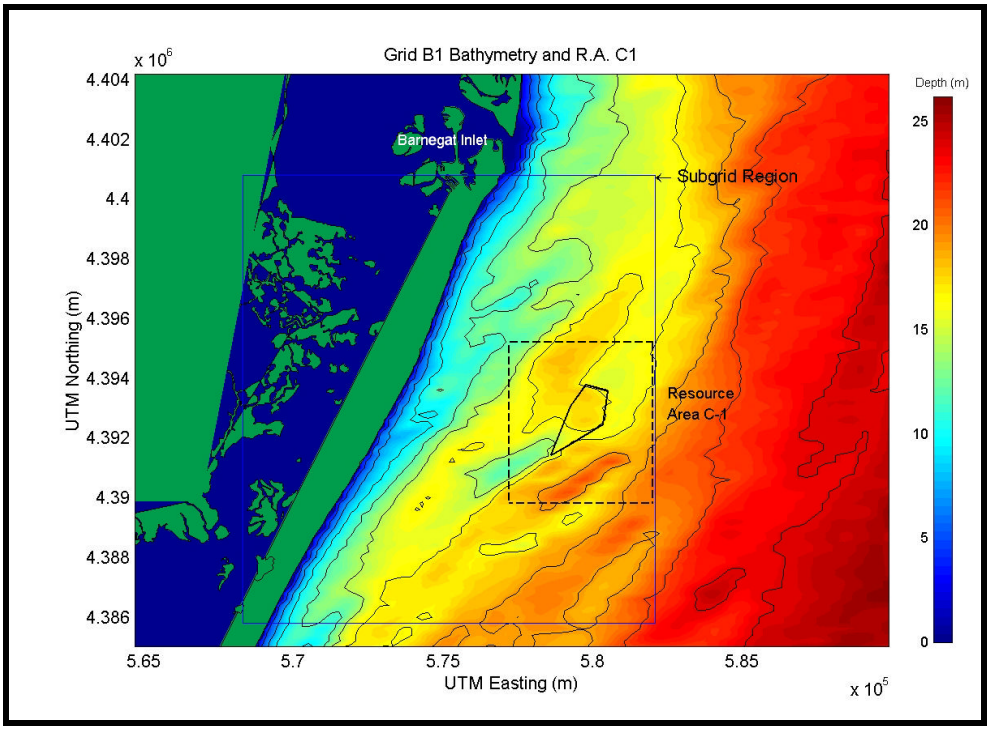

Figure 4-12. Bathymetry for Reference Grid B1, the defined sand resource areas, and the nearshore subgrid.

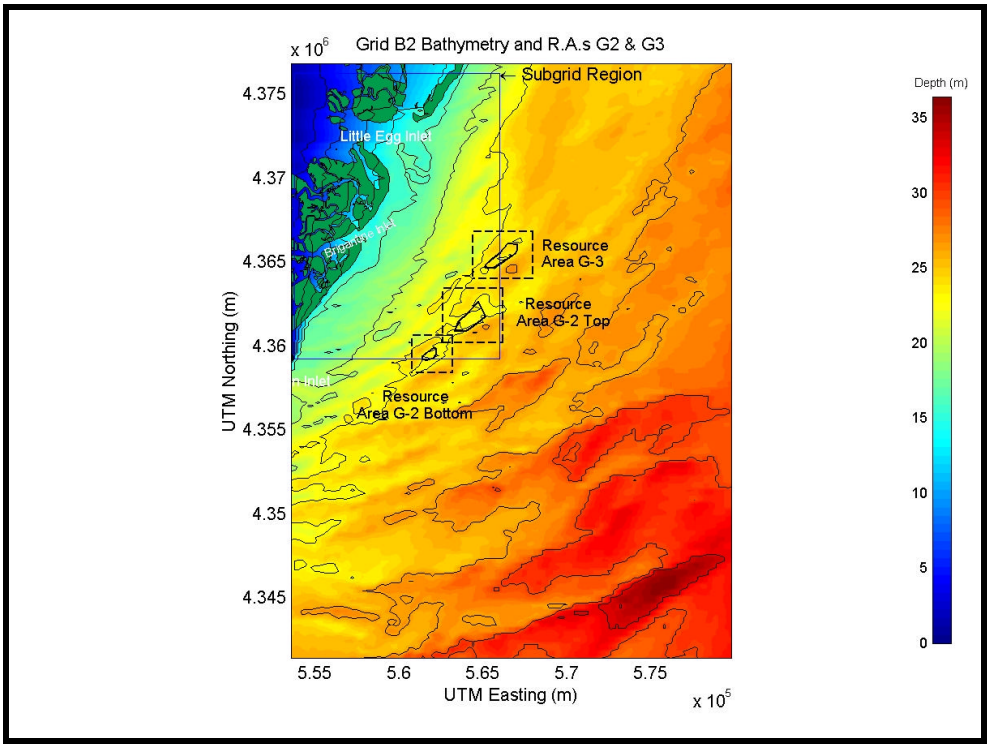

Figure 4-13. Bathymetry for Reference Grid B2, the defined sand resource areas, and the nearshore subgrid.

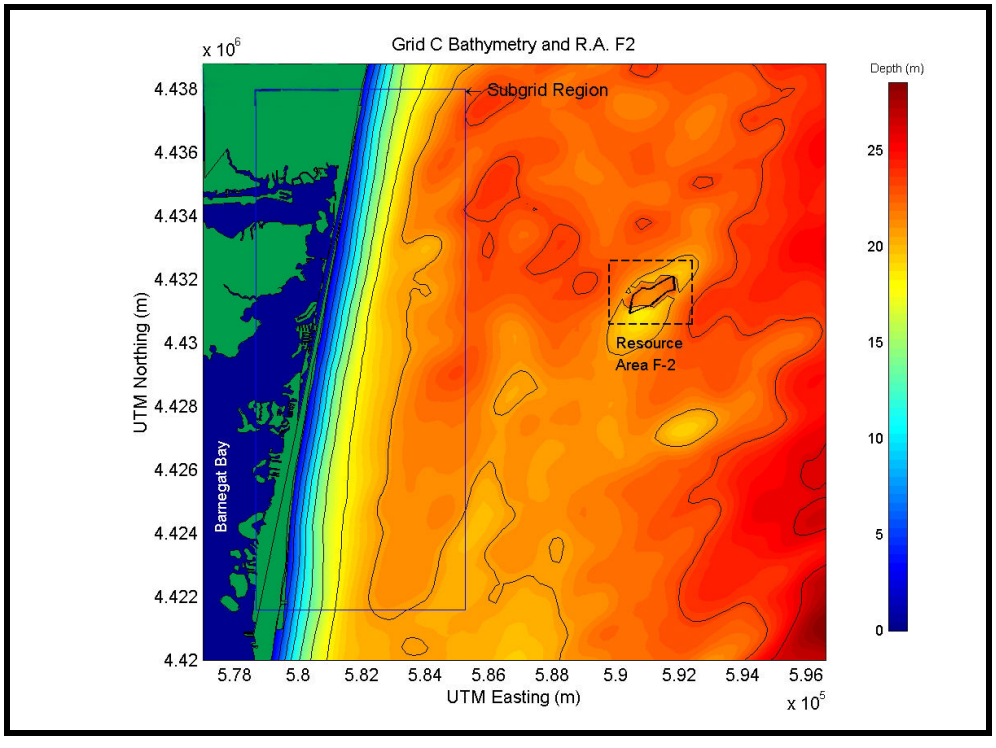

Figure 4-14. Bathymetry for Reference Grid C, the defined sand resource areas, and the nearshore subgrid.

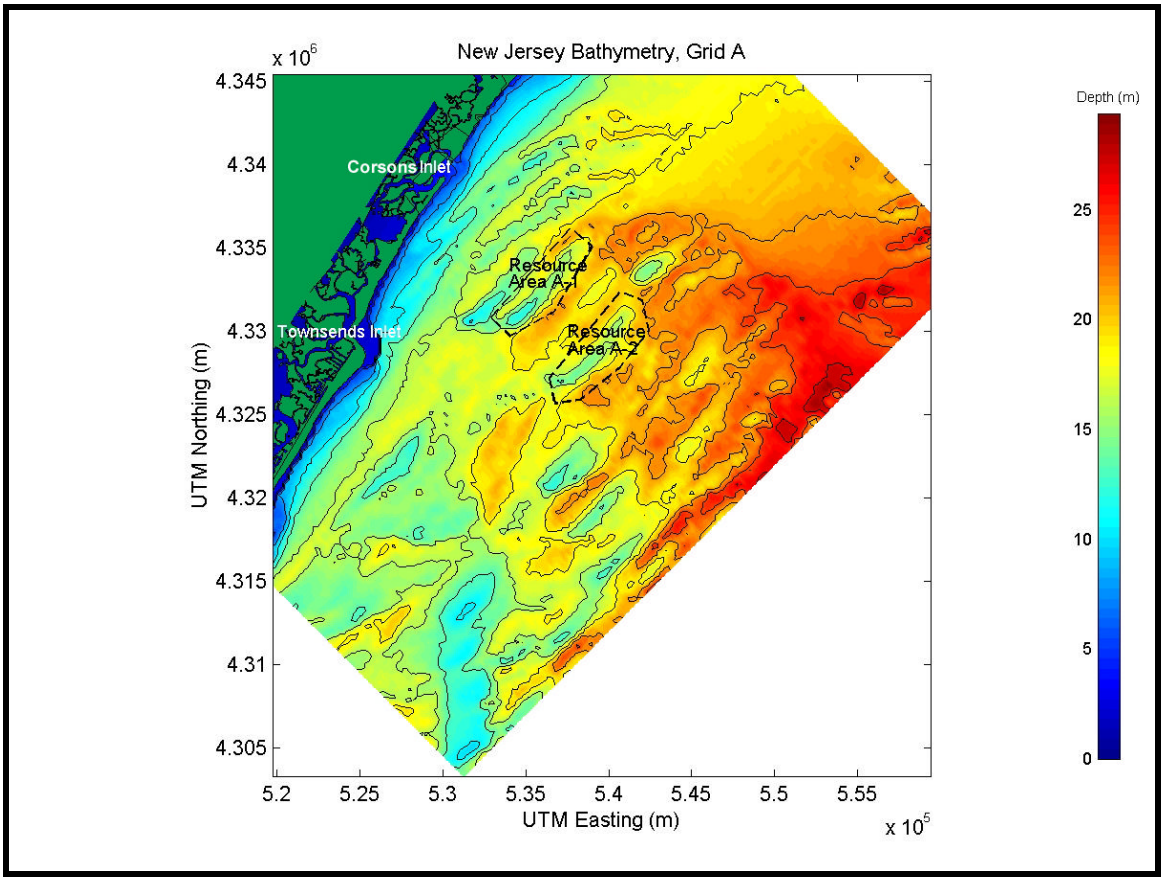

Figure 4-15. Example of a rotated grid (Reference Grid A) to facilitate wave input.

cell was subdivided by ten to yield a grid spacing of 20 m. This subdivision spacing was chosen to optimize computational time versus spatial resolution in the longshore direction, as well as to provide adequate information for nearshore sediment transport modeling. In the onshore direction, REF/DIF S automatically subdivides each reference grid step by the smallest calculated wavelength in the spectrum. Therefore, the onshore spacing varies throughout the domain as a function of the propagating wave field, unless the model is in a subgrid region. In areas where a subgrid is specified, the onshore subdivision must be fixed to correspond to the pre-defined subgrid spacing (i.e., locations where depths and currents are specified).

Nearshore subgrids were created in the reference domains for all shoreline regions, some of which include inlets. For the cases when the reference grids were rotated, the subgrids were also rotated to insure they remained orthogonal to the reference grid. Table 4-14 presents the dimensions and extents of each of the unrotated and rotated subgrids, as shown in Figures 4-11 and 4-15. Wave heights, water depth, and radiation stress results were output from each grid node in the subgrid domain.

Table 4-14. Subgrid dimensions.				
Reference Grid	Onshore Spacing (m)	Alongshore Spacing (m)	Subgrid UTM Easting extents (m)	Subgrid UTM Northing extents (m)
A (unrotated)	5	20	523,500 – 536,100	4,326,700 – 4,342,700
A (rotated -45E)	5	20	519,530 – 544,710	4,326,300 – 4,351,500
B1 (unrotated)	5	20	568,300 – 582,100	4,385,800 – 4,400,800
B1 (rotated -27E)	5	20	568,070 – 584,200	4,372,800 – 4,387,600
B2 (unrotated)	5	20	553,800 – 566,000	4,359,200 – 4,376,200
B2 (rotated -45E)	5	20	551,160 – 571,660	4,357,800 – 4,378,300
C (unrotated)	5	20	578,650 – 582,245	4,421,600 – 4,438,000
C (rotated -45E)	5	20	576,330 – 594,620	4,418,640 – 4,438,800
C (rotated 45E)	5	20	579,830 – 592,580	4,422,600 – 4,440,500

4.3.2 Post-Dredging Scenarios

4.3.2.1 Sand Borrow Site Selection

Offshore borrow sites were identified as potential sources of beach quality sediment (see Section 1.0 for details); these data were used to numerically excavate wave modeling grids to simulate the impacts dredging may have on physical processes in the region (e.g., wave transformation and sediment transport). Refer to Figures 4-11 through 4-14 for the location of borrow areas. Each of the borrow sites were numerically dredged to simulate post-extraction scenarios. When multiple resource areas were present in a single grid, they were dredged simultaneously to simulate the combined impact from all borrow sites and limit the number of model simulations per grid.

4.3.2.2 Numerical Excavation of Gridded Surfaces

Following the selection of potential dredging locations, seven sand resource areas were numerically excavated to evaluate the impact of bathymetry changes on wave transformation, nearshore circulation, and beach and borrow location sediment transport. Depths at sand borrow sites were increased to reflect the effects of potential dredging scenarios. Table 4-15 lists the sand resource areas (as identified in Figures 4-11 through 4-15) where each numerical excavation was performed, as well as the excavation depth and resulting dredged sand volume. For example, if the pre-dredging depth at a grid point within Sand Resource Area A1 is 16 m, the post-dredging depth is increased to 20 m.

Table 4-15. Dredged depth and resulting sand volume within respective sand resource area.		
Sand Resource Area	Depth to be Dredged (m)	Resulting Sand Volume(x 10^6 m^3)
A1	4	8.8
A2	3	7.8
G2 Top	3	4.3
G2 Bottom	3	
G3	3	3.3
F2	3	2.1

4.4 PRE-DREDGING RESULTS

4.4.1 Grid A Simulations

4.4.1.1 Directional Approach Simulations

This section discusses results for simulations of existing (pre-dredging) conditions. Model simulations were performed for typical wave conditions represented by directional bin spectra and extreme wave conditions represented with 50-yr storm spectra (estimated hurricane and Northeaster).

Wave focusing, divergence, and shadowing occur at several locations throughout the Grid A modeling domain, which results in variations of wave energy propagation toward the shoreline. A significant amount of variation exists in wave heights along the nearshore region of Grid A, which is a result of a variety of bathymetric features impacting the transformation of waves within the model domain. Figure 4-16 identifies some of the major features offshore of Townsends and Corsons Inlets, specifically near the proposed borrow sites (A1 and A2).

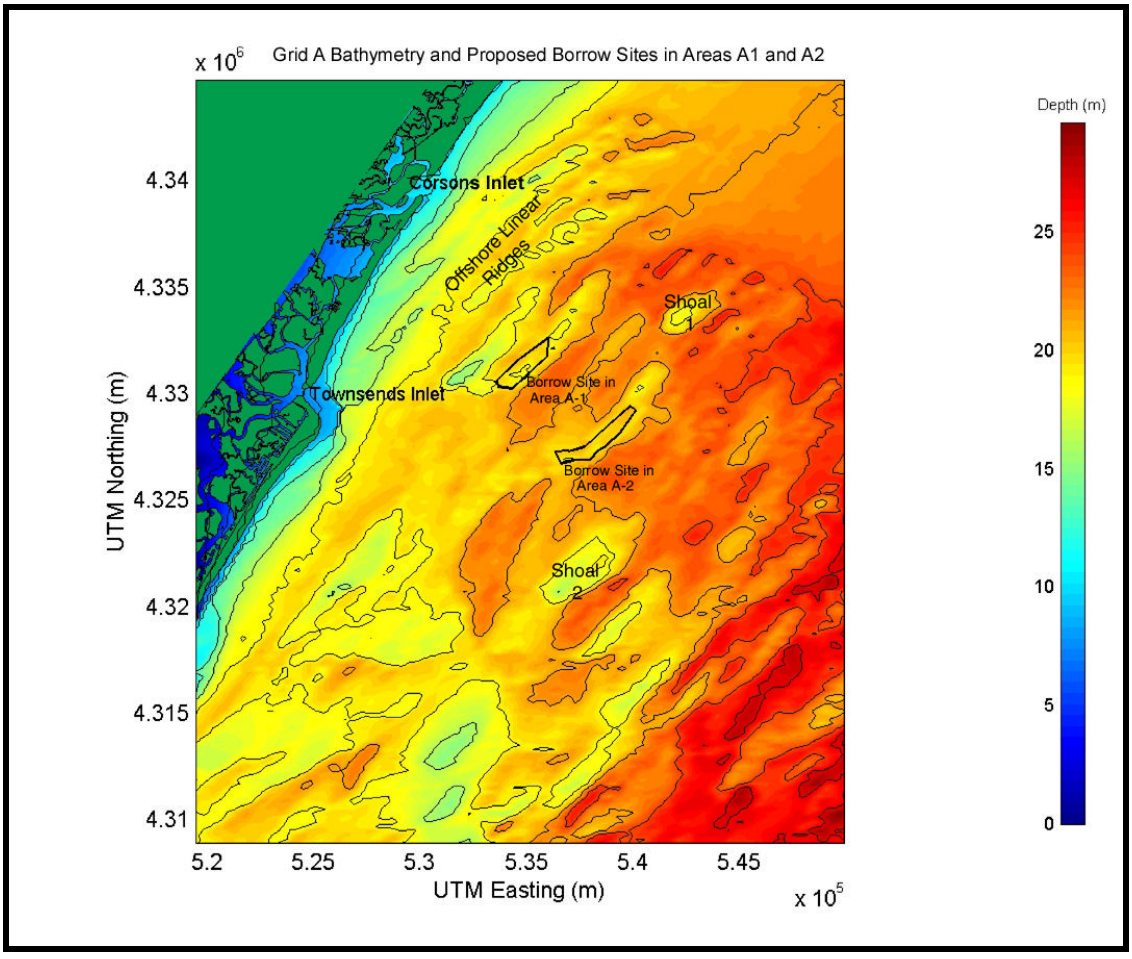

Figure 4-16. Location of key bathymetric features within Grid A and location of proposed borrow site in Resource Areas A1 and A2.

Eastern Wave Approach

Figure 4-17 illustrates REF/DIF S results for Grid A for waves approaching from the east (0 degree directional bin simulation). The color map corresponds to the distribution of significant wave height (m) throughout the modeling domain. Solid black lines represent bathymetric contours. Land masses are shown in solid green. The shoreline presented in the figures is a high water shoreline and is used here for presentation purposes only. The model runs were conducted at depths and shoreline positions relative to NGVD. Arrows on the figure represent the modeled wave angle.

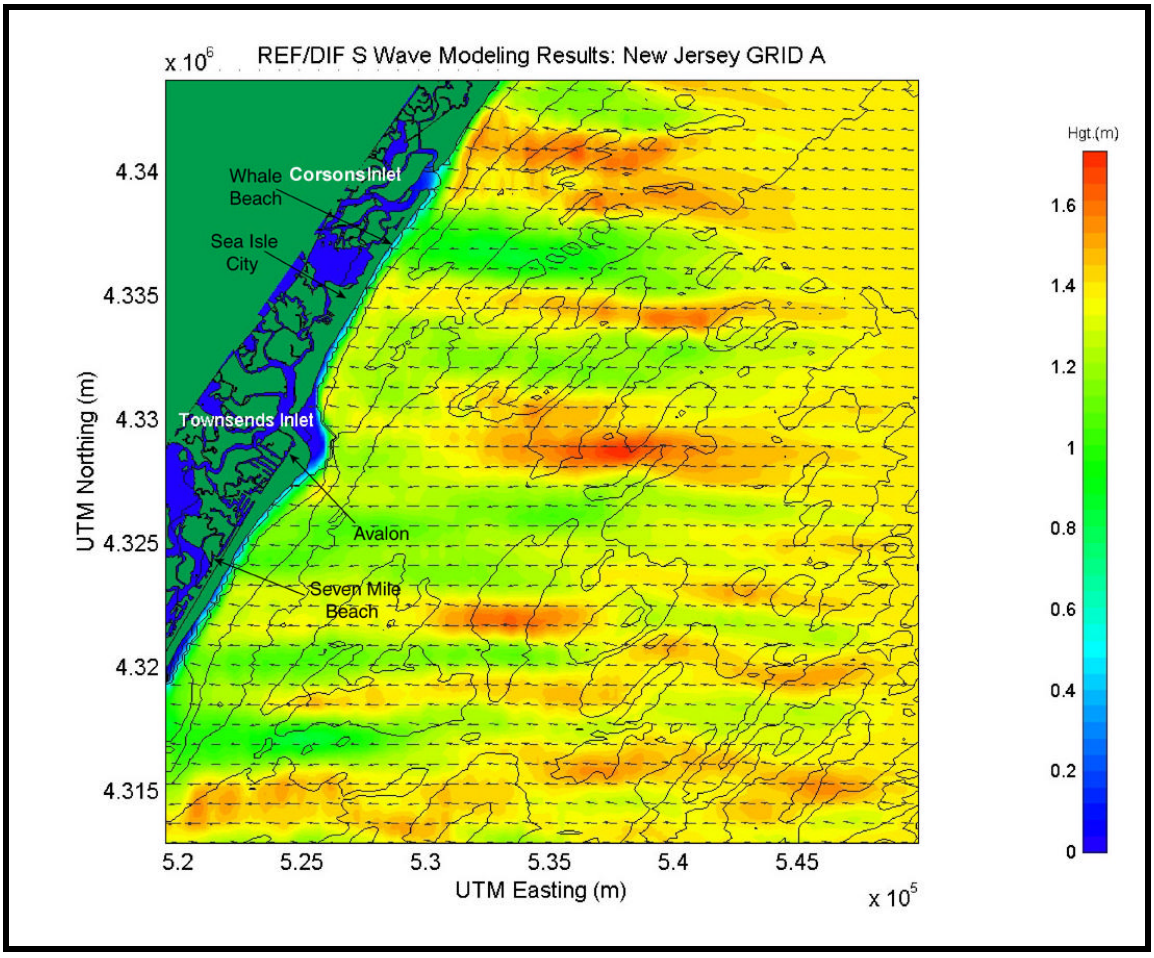

Figure 4-17. Spectral wave modeling results for existing conditions using an eastern approach direction (0 degree bin) at reference Grid A.

The east (0 degree) approach bin consists of an input wave height of 1.4 m, which is the most common significant wave height modeled at Grid A. Waves approach from this directional bin 15.3% of the time, and it is one of the most common approach directions. Changes in wave height and direction begin to occur at approximately the 20-m depth contour. Most of the spectral wave components do not interact with the seafloor at depths greater than 20 m.

The shoal labeled Shoal 1 on Figure 4-16 focuses wave heights to approximately 1.7 m (an increase of approximately 18%). The shoal also produces an increase in wave energy experienced at the coast near Sea Isle City. Waves in this region are approximately 0.2 to 0.3 m larger than neighboring wave heights. Coupled with the convergence caused by the shoal, a

series of smaller depressions in the bathymetric surface located to the north cause a divergence of wave energy, as well as a modest reduction in wave height at the shoreline south of Corsons Inlet (near Whale Beach). A similar increase in wave energy also occurs as waves pass over the oval shoal in the southern portion of the grid (Shoal 2 on Figure 4-16). A portion of the focused wave energy does advance to the coast near Seven Mile Beach, south of Avalon. Waves approximately 1.3 m high are evident at this location.

The linear ridges directly offshore of Corsons Inlet are another source of wave focusing and create an increased wave height observed north of Corsons Inlet. The increase in wave energy does not fully dissipate by the time it reaches the coast and is the most energetic area along the shoreline when waves approach from the east. Wave heights reaching 1.6 m are evident in the nearshore zone. In addition, the oblong trough located northwest of the linear ridges causes a divergence in wave energy, which results in a shadow zone and contributes to the wave focusing caused by the linear ridges.

A significant increase in wave height also is apparent in the region comprising Resource Area A2. The large linear ridge extending from the southwest corner to the northeast corner of the Resource Area, heightens wave energy landward of the feature. Although there is a significant increase in height (approximately 20%) directly behind the ridge, a majority of the energy dissipates before propagating to Townsends Inlet. For this directional approach, minor perturbations to waves occur over shoals located within Resource Area A1. A small increase in wave height is evident, and a slight change in wave direction is exhibited as waves are directed towards the northwest.

For an eastern wave directional approach, there are four regions of increased wave heights along the coast (Table 4-16). Other areas experience reduced wave energy (i.e., the region just south of Corsons Inlet). Wave directions, illustrated by arrows presented in Figure 4-17, are difficult to represent visually. Directions remain relatively constant throughout the modeling domain, although areas of significant convergence or divergence are illustrated. There is also a slight orientation of the waves perpendicular to the coastline (e.g., the region north of Corsons Inlet).

Table 4-16. Coastline areas experiencing increased wave heights during eastern wave approach.

Approximate Location	Approximate Wave Height at Coast (m)
North of Corsons Inlet	1.5 to 1.6
Near Whale Beach	1.3 to 1.4
North of Townsends Inlet	1.2 to 1.3
Seven Mile Beach, South of Avalon	1.3

East-Southeast Wave Approach

Figure 4-18 illustrates REF/DIF S results for Grid A for the east-southeast (-22.5 degree) wave approach. Input wave height for the east-southeast approach direction is 1.4 m, the same as the east approach simulation. The east-southeast approach simulation contains 18.0% of the total waves, thereby making it the most common approach direction. The east-southeast approach direction is almost perpendicular to the orientation of the coastline. Wave-induced transport is directed slightly from the north to south for most areas along the coast. The results from the east-southeast approach simulation exhibit similar wave patterns as the eastern wave approach, with distinctive areas of wave convergence and divergence occurring throughout the domain.

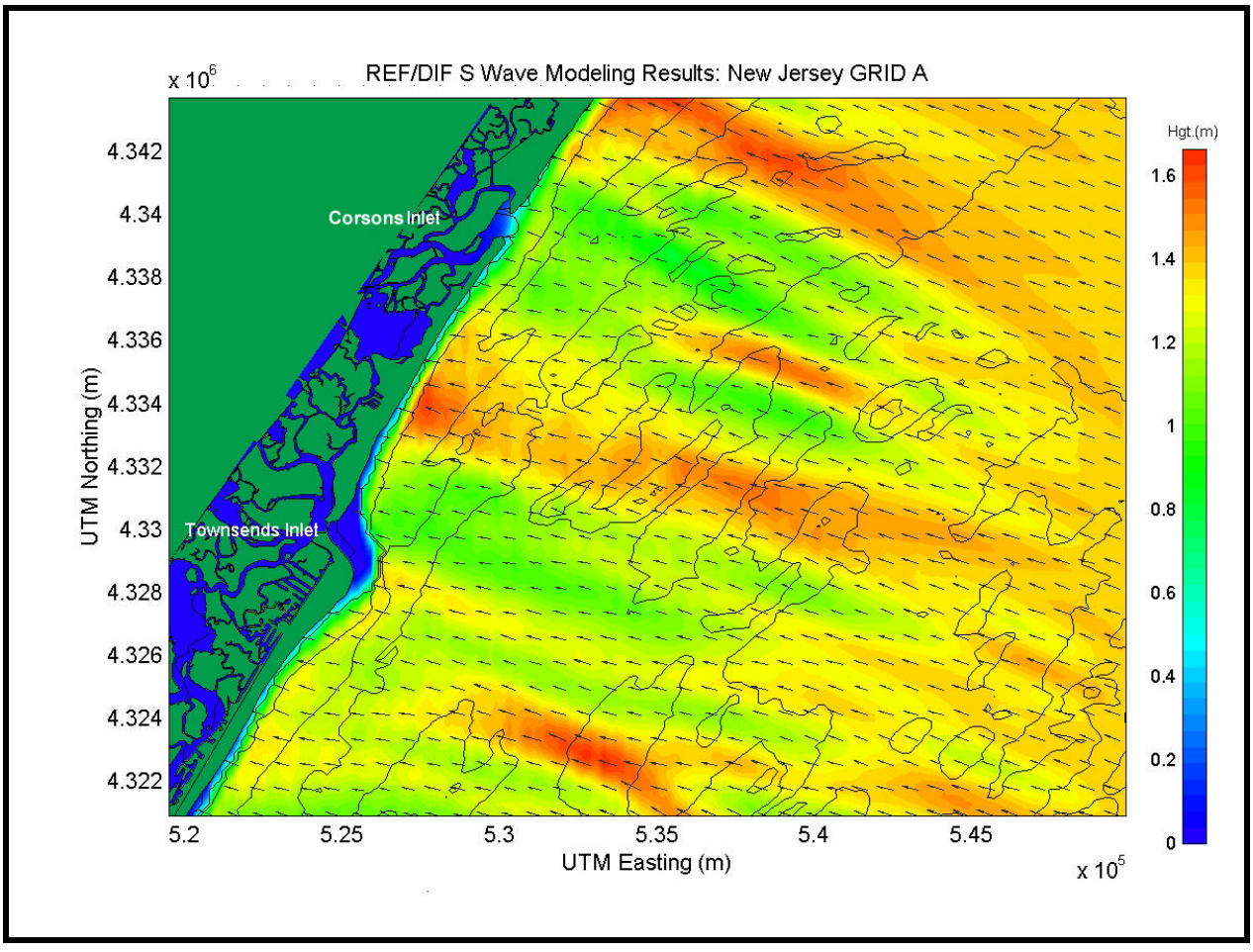

Figure 4-18. Spectral wave modeling results for existing conditions using an east-southeast (-22.5 degree) approach direction at reference Grid A.

Shoals 1 and 2 again focus wave energy to approximately 1.5 to 1.6 m (increase of approximately 14%). Unlike the eastern approach, most of the focused wave energy exhibited behind both shoals dissipates before it reaches the coast. Only a small amount of energy focused by Shoal 2 reaches the coast. In addition, linear ridges in the northern portion of the modeling domain cause a wave height increase to approximately 1.6 m along the coast north of the modeled domain. The oblong trough to the north of the ridges creates an area of wave height reduction to the east-northeast, while directing additional energy to the south over the linear ridges.

Wave focusing also is evident at the upper section of Resource Area A2 near the northern tip of the linear shoal. This energy does not completely dissipate and a significant increase in wave height is visible near Sea Isle City (approximately 1.5 to 1.6 m). The shoals in Resource Area A1 maintain the increased wave energy and allow wave energy originally focused by A2 to continue to propagate toward the coastline. An area of decreased wave energy is evident between shoals in Resource Area A2 and Shoal 1 to the north. As expected, wave focusing caused by these two features results in a deficit of wave energy in the area. Table 4-17 presents a summary of the areas experiencing increased wave heights along the coast due to waves approaching from the east-southeast.

Table 4-17. Coastline areas experiencing increased wave heights during east-southeast wave approach.	
Approximate Location	Approximate Wave Height at Coast (m)
Northern boundary of modeling domain	1.6
Sea Isle City	1.5 to 1.6
Seven Mile Beach, South of Avalon	1.3

East-Northeast Wave Approach

Figure 4-19 illustrates REF/DIF S results for Grid A for the east-northeast (22.5 degree) wave approach. The scale of the colorbar is different than the previous two cases so larger wave heights can be presented for this simulation. The east-northeast approach is highlighted by significantly larger wave heights (1.8 m, and exceeding 2.0 m in areas within the grid) and rare occurrence levels (1.8% of the time). The larger waves and low occurrence level is expected, because wave approach from this direction is dominated by the passage of northeast storms. Wave-induced transport is directed from north to south for this approach, and during most storm events, sediment transport is directed north to south as well. Similar wave pattern features as those found in the eastern approach simulation were identified; however, less variation in wave height appears along the shoreline. Overall wave height arriving at the coast is generally larger, but shows little variation.

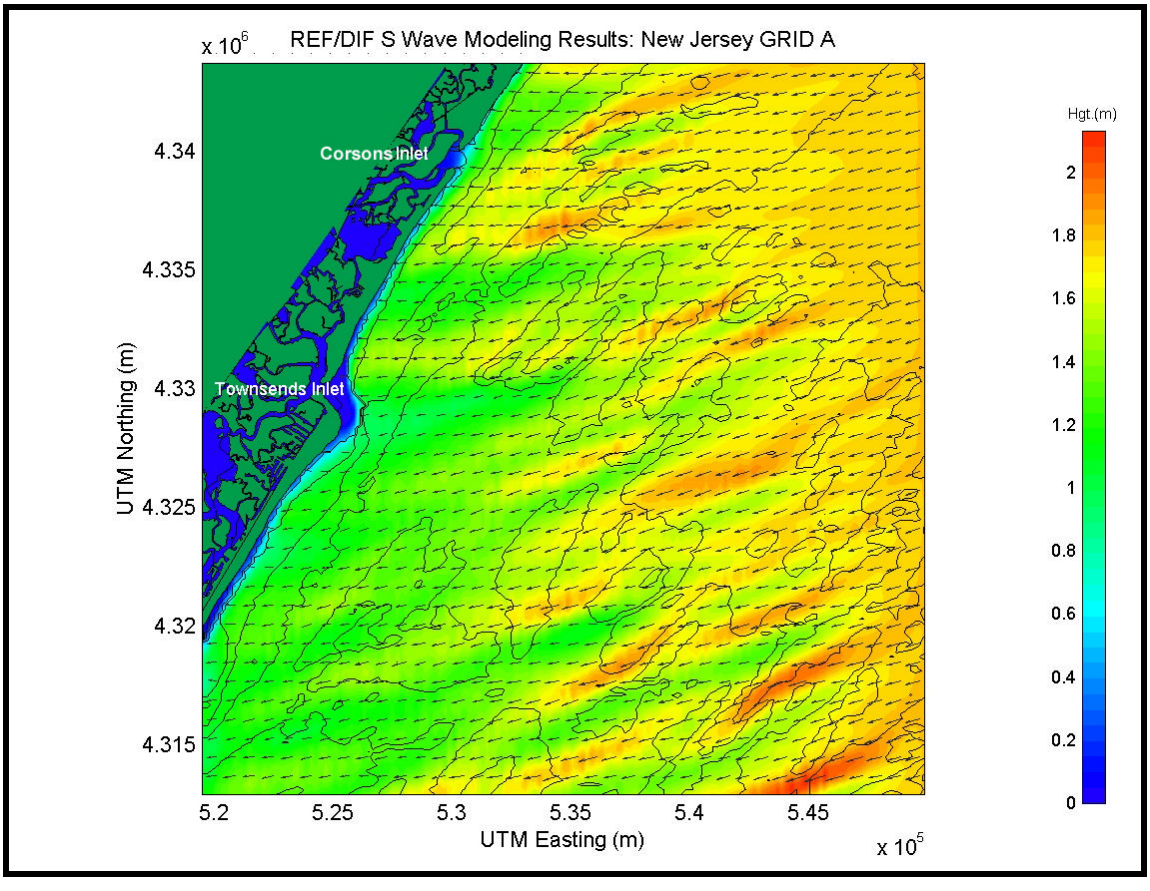

Figure 4-19. Spectral wave modeling results for existing conditions using an east-northeast (22.5 degree) approach direction at reference Grid A.

Shoal 1 produces a wave height increase to approximately 1.9 to 2.0 m for a short stretch behind the shoal. Waves also is refracted towards the shoreline as the waves orient themselves perpendicular to the coast. A mild impact can be identified just north of Townsends Inlet caused by wave focusing from the shoal (wave heights are approximately 1.5 to 1.6 m). Shoal 2 again causes wave-energy focusing in the simulation; however, due to the approach direction, the effect is much less severe than in previously examined cases. The direction of wave approach produces a longer propagation distance for wave travel before reaching the coast. The increase in distance gives the increased wave energy a greater time to disperse. Although Shoal 2 produces an increase in wave energy, modification to the wave field dissipates before reaching the coast.

Linear ridges in the northern portion of the grid are another source of wave-energy focusing for this approach direction. Waves increase to approximately 1.9 m in the lee of these features. The increase in wave energy is refracted perpendicular to the coast over the nearshore bathymetric contours and impacts the shoreline south of Corsons Inlet, near Whale Beach at an approximate height of 1.7 m. The impact area is different than in previously examined cases due to the approach direction. Coupled with these linear ridges, a slight decrease in wave energy is evident behind the shore-oblique trough. This wave energy reduction fades as the waves approach the coast, combining with wave energy increases caused by linear ridges.

In the east-northeast approach simulation, a limited amount of wave focusing is exhibited behind the linear sand/ridge in Resource Area A2 than in previously examined simulations (east and east-southeast approaches). However, the increased magnitude is still significant as wave heights approach 1.8 m (approximately a 0.5 m increase). Despite this increase, the energy increase dissipates quickly and does not impact the coast. Shoals located in Resource Area A1 focus wave energy originally concentrated by Shoal 1, thereby sustaining the wave energy. A similar phenomena occurs in the east-southeast directional approach simulation as wave energy originally focused by Resource Area A2 was maintained through this region. Table 4-18 presents a summary of the areas experiencing increased wave heights along the coast from waves approaching from the east-northeast.

Table 4-18. Coastline areas experiencing increased wave heights during east-northeast wave approach.

Approximate Location	Approximate Wave Height at Coast (m)
South of Corsons Inlet, near Whale Beach	1.6
North of Townsends Inlet	1.5

Southeast Wave Approach

Figure 4-20 illustrates REF/DIF S results for a southeast (-45 degree) wave approach. The southeast directional approach simulation has an input wave height of 1.4 m, which is the same as the east and east-southeast cases. The southeastern approach direction contains 15.4% of the waves, and it is as common as the east approach direction. In general, the areas of convergence and divergence match those of the east-southeast approach. However, due to the change in primary approach direction and peak spectral period, as well as visual differences in the colorbar scale and grid rotation within the geographic coordinates, some differences do exist between the two simulations. The southeast directional approach represents a very direct approach to the coast. Wave-induced transport is slightly south to north for this approach direction, and a potential reverse in the primary direction of sediment transport is likely. Only subtle changes in wave direction near regions of convergence and divergence can be seen at the resolution of Figure 4-20.

Shoal 1 causes an increase in wave energy to approximately 1.8 m, although in this scenario, heightened waves do not reach the shore. The northern linear ridges appear to have a lesser impact in this scenario, most likely due to the primary direction of wave propagation, which advances over the shortest dimension of the northeast extending ridges. Shoals in Resource Area A2 also focus wave energy, although at a reduced amount compared with prior directional approach simulations. The larger wave focusing in the region (approximate increase of 0.4 m) occurs over the peaks of the shoal located within Resource Area A2.

The largest wave focusing occurs in the southern portion of the modeling domain effecting the Stone Harbor area, although this is out of the primary region of interest. Shoal 2 is the most obvious region of wave heightening for the southeast approach simulation, as waves reach approximately 2.0 to 2.1 m for stretches behind the shoal area. The wave energy increase is sustained to the coast and impacts a region just north of Townsends Inlet. This is a subtle difference from the east-southeast approach case, where wave energy increases by this shoal dissipated before reaching the coast. Table 4-19 presents a summary of the areas experiencing increased wave heights along the coast from waves approaching from the southeast.

Table 4-19. Coastline areas experiencing increased wave heights during southeastern wave approach.

Approximate Location	Approximate Wave Height at Coast (m)
North of Townsends Inlet	1.8 to 1.9
Stone Harbor, Seven Mile Beach area	1.7

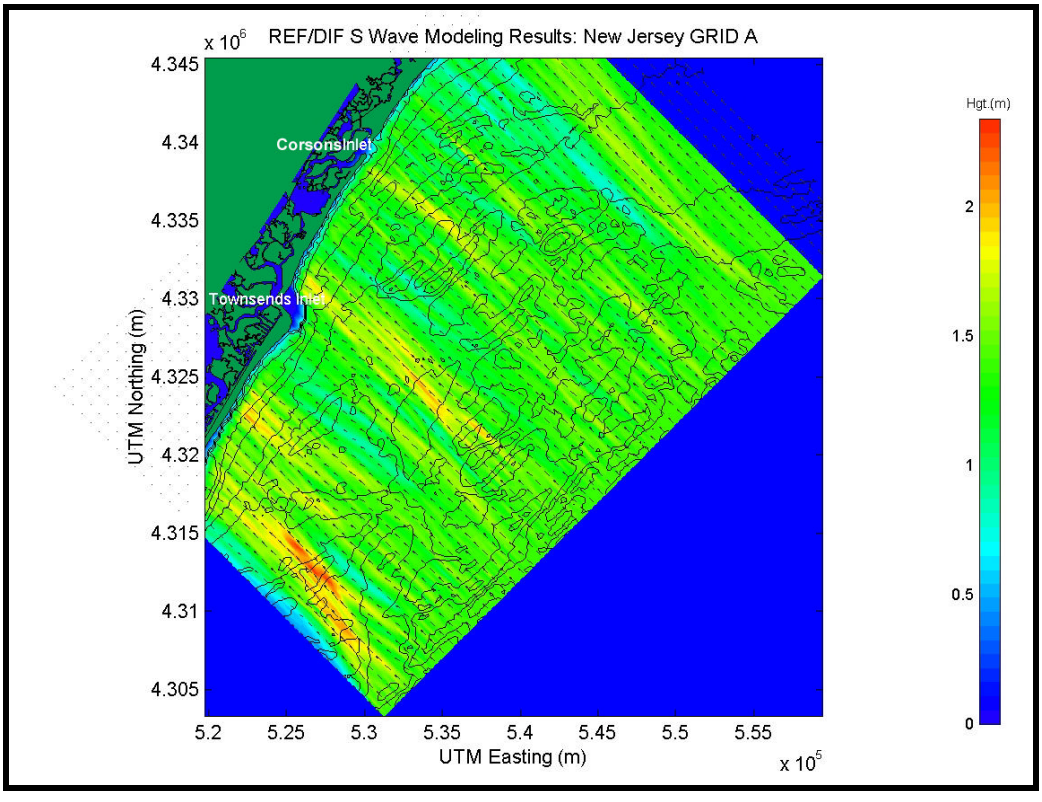

Figure 4-20. Spectral wave modeling results for existing conditions using a southeast (-45 degree) approach direction at reference Grid A.

South-Southeast Wave Approach

Figure 4-21 illustrates REF/DIF S results for Grid A for a south-southeast (-67.5 degree) wave approach simulation. The input wave height was 1.5 m, which is larger than the other east-southeast directional bins (-22.5 and -45 degree cases), and it represents the second highest simulated wave height. Despite the wide angle of approach, the south-southeastern approach direction still contains a major portion of the wave energy (12.3% of the waves). In general, the areas of convergence and divergence are similar to the other southeast approach directions; however, the areas of focusing are more distinctive due to the slightly larger wave height. In addition, the results appear to include more caustics due to the larger approach angle. Sediment transport, as with fluid transport, is expected to be directed from south to north for this directional approach.

Shoal 1 results in wave focusing to approximately 1.7 m. The increased energy is dissipated before it reaches the coast, which is consistent with wave propagation in all the east-southeast approach simulations (-22.5, -45, and -67.5 degrees). Linear ridges to the north of the shoal indicate a smaller impact when compared with wave approaches from the east or northeast. The northeast-southwest orientation of these features coupled with the southeast approach direction, allow waves to cross the shortest dimension of these features, thereby producing a reduced effect on the wave field. In addition, the shoal contained in Resource Area A2 exhibits only minor effects for this approach direction (smaller than any directional scenario). It appears that a higher concentration of waves approaching from the south results in a diminished wave focusing caused by these features. The alterations of the wave field caused by these features dissipate before reaching the coast for the south-southeast approach simulation.

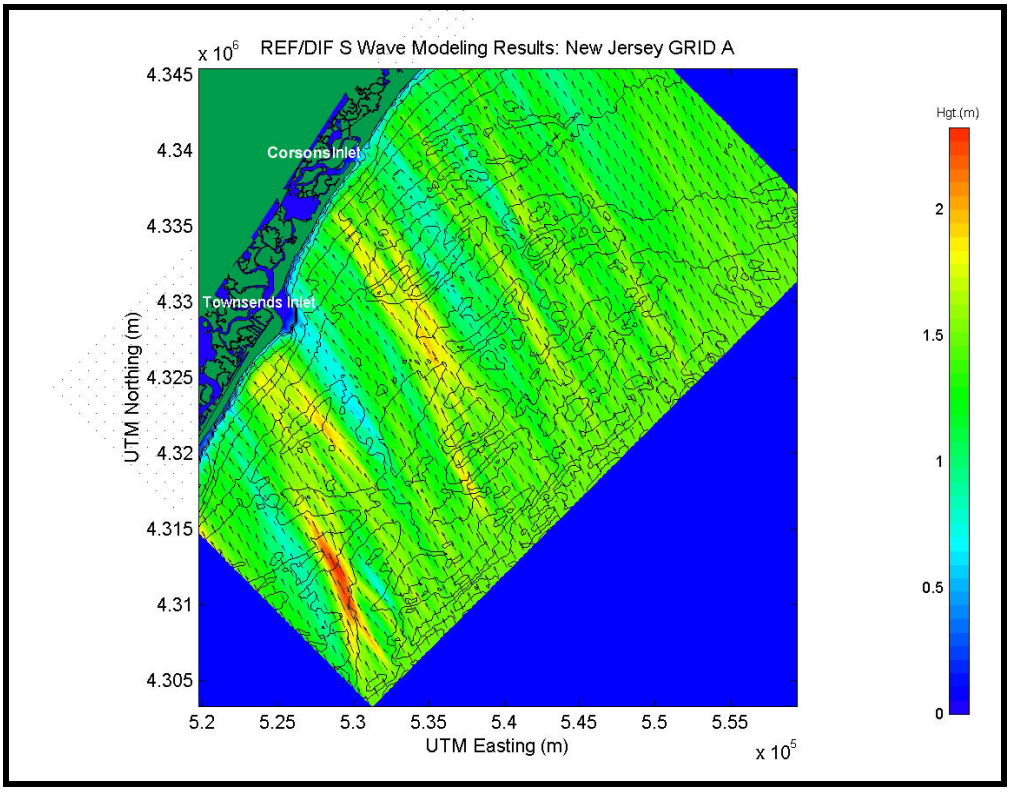

Figure 4-21. Spectral wave modeling results for existing conditions using a south-southeastern (-67.5 degree) approach direction at reference Grid A.

As in other southeast approach simulations, Shoal 2 produces the most evident region of wave convergence (increases wave height to almost 2.0 m), while for approach directions from the east-northeast, Shoal 2 has a greatly reduced impact. The increased wave energy produced in the south-southeast approach simulation propagates to the coast and impacts a region directly south of Corsons Inlet (Whale Beach). Shoals located in Resource Area A1 converge and modify the waves initially focused by the shoal. This phenomena produces some unique wave approach patterns in the region. The series of shoals and depressions in the southern portion of the modeling domain produce the greatest wave focusing in this simulation (waves exceed 2.1 m). Wave energy impacts the coast south of Townsends Inlet, near the city of Avalon. Table 4-20 presents a summary of the areas experiencing increased wave heights along the coast for waves approaching from the south-southeast.

Table 4-20. Coastline areas experiencing increased wave heights during south-southeastern wave approach.

Approximate Location	Approximate Wave Height at Coast (m)
Whale Beach	1.7
South of Townsends Inlet, near Avalon	1.7 to 1.8

4.4.1.2 High Energy Wave Events Simulations

Figure 4-22 illustrates wave transformation results for an estimated 50-yr northeast storm passing over Grid A. The northeast storm simulation represents a rare occurrence as waves approach from the east-northeast with a wave height of 6.4 m. Waves respond to seafloor topography of greater depths than for directional simulations, and energy begins to dissipate near the offshore boundary of the grid. This also causes wave approach directions to be modified farther offshore. As a result, waves orient themselves perpendicular to bathymetric contours throughout the model domain. Wave-induced transport is directed from north to south during a typical northeast storm.

The northeast storm simulation illustrates increased wave heights throughout the model domain. Storm wave propagation patterns are similar to those documented for similar directional approach simulations. For example, the northeast storm simulation includes many comparable results to the east and east-northeast approach cases. However, wave convergence and divergence patterns caused by many of the features are less pronounced for these large storm waves because changes caused by bathymetric features are small when compared to the large wave height. Due to the magnitude of the 50-yr storm simulations, existing modeling techniques may be limited for simulation of these long-period, high-energy wave events, and the accuracy of the results for these simulations is limited by the capabilities of the model.

Figure 4-23 illustrates wave transformation results for a simulated 50-yr hurricane event passing over Grid A. Hurricane waves approach from the southeast with a wave height of 5.6 m. As with the northeast storms, waves respond to the seafloor in deeper water than directional simulations, and they begin to refract and dissipate energy farther offshore. Wave directions are oriented nearly perpendicular to the coast throughout the model domain. Most of the coastal region illustrates increased wave heights during storm passage. Wave heights exceed 3.0 to 4.0 m for most areas along the coast.

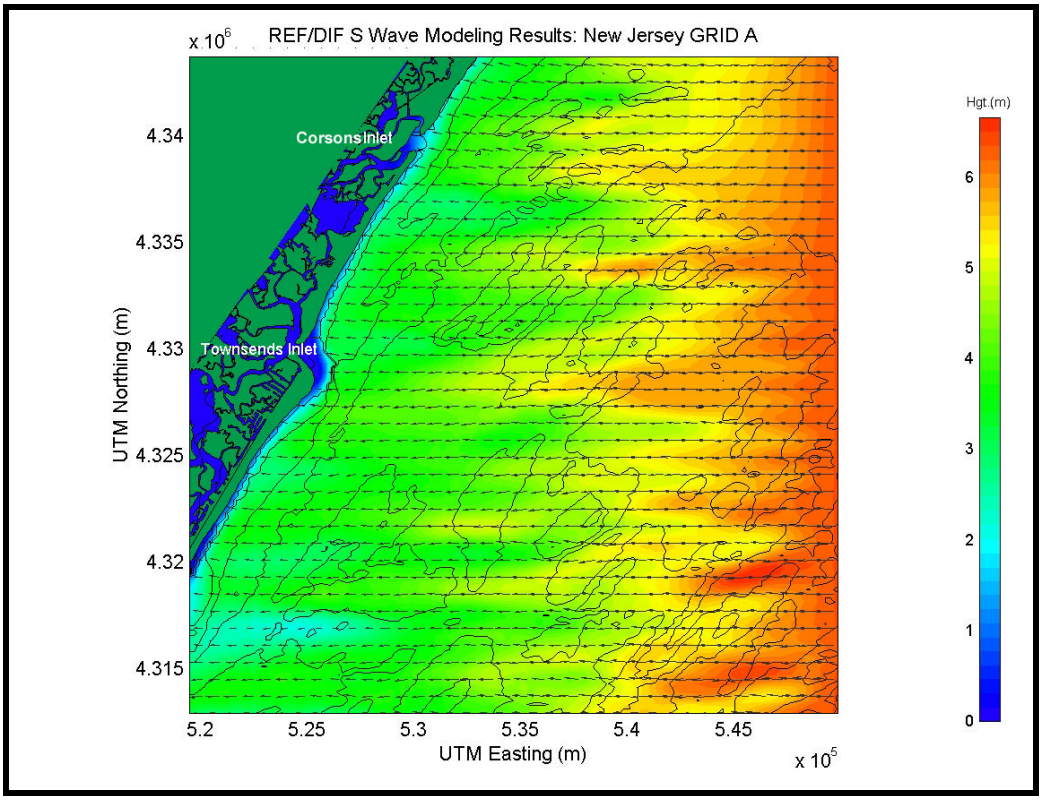

Figure 4-22. Spectral wave modeling results for existing conditions simulating an estimated 50-yr northeast storm event for reference Grid A.

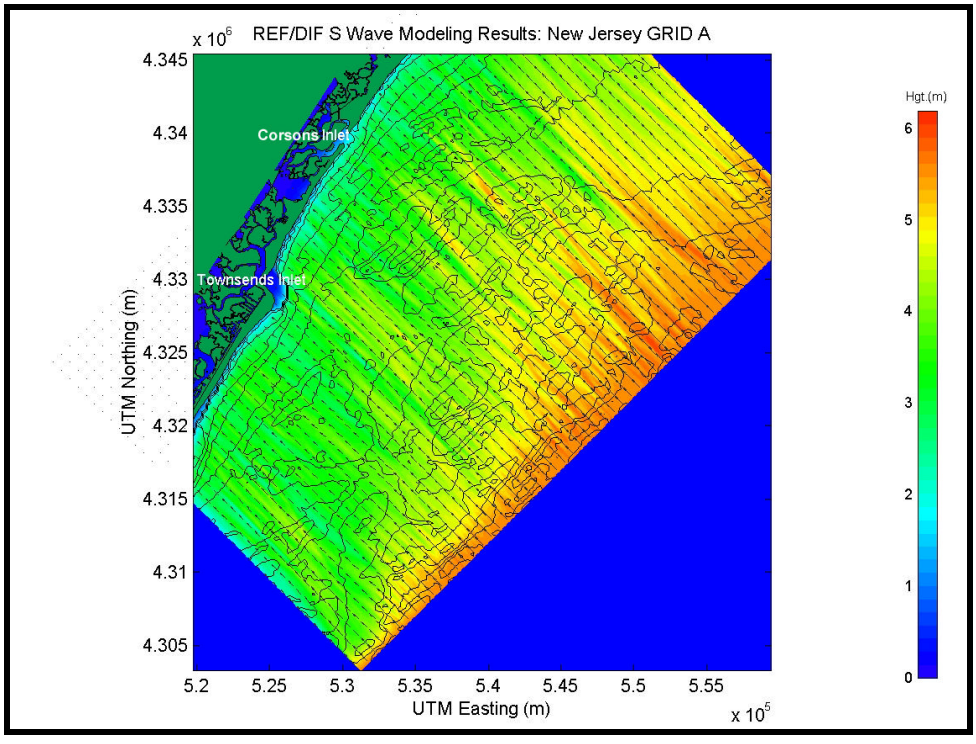

Figure 4-23. Spectral wave modeling results for existing conditions simulating an estimated 50-yr hurricane event for reference Grid A.

4.4.1.3 Model Results Relative to Historical Shoreline Change

The following is a comparison of wave modeling results at wave breaking to historical shoreline change results. Such comparisons may provide insight regarding the potential causes of shoreline change. For example, historical areas of exaggerated shoreline retreat may correlate to areas of focused wave energy. Additionally, wave conditions that correlate with historical shoreline change rates are likely the most influential conditions on nearshore transport processes.

Figure 4-24 illustrates significant wave heights extracted from approximately the line of wave breaking for the east (0 degree) approach simulation compared with historical shoreline change results. The left-hand panel illustrates the nearshore wave transformation results for the east approach simulation, where the colormap represents wave height in meters. The solid black line on the left-hand panel represents the approximate breaker line from which significant wave heights were extracted. The breaker line is very difficult to determine when using spectral wave models since there are a variety of waves, composed of different frequencies and directions, breaking at different times and locations throughout the domain. In addition, the orientation and irregularity of the coastline add difficulty to determining an exact breaker line at the grid resolution provided in the model. Therefore, the breaker line presented is intended only to provide a relative wave height distribution along the coast, rather than the exact region of wave breaking. The right-hand panel presents historical shoreline change rates (1864/86 to 1977) for this stretch of the New Jersey coast, and it is represented by a black line scaled by the bottom axis (m/yr). Significant wave height at breaking is added to the plot and represented by a green line, scaled by the upper axis (m).

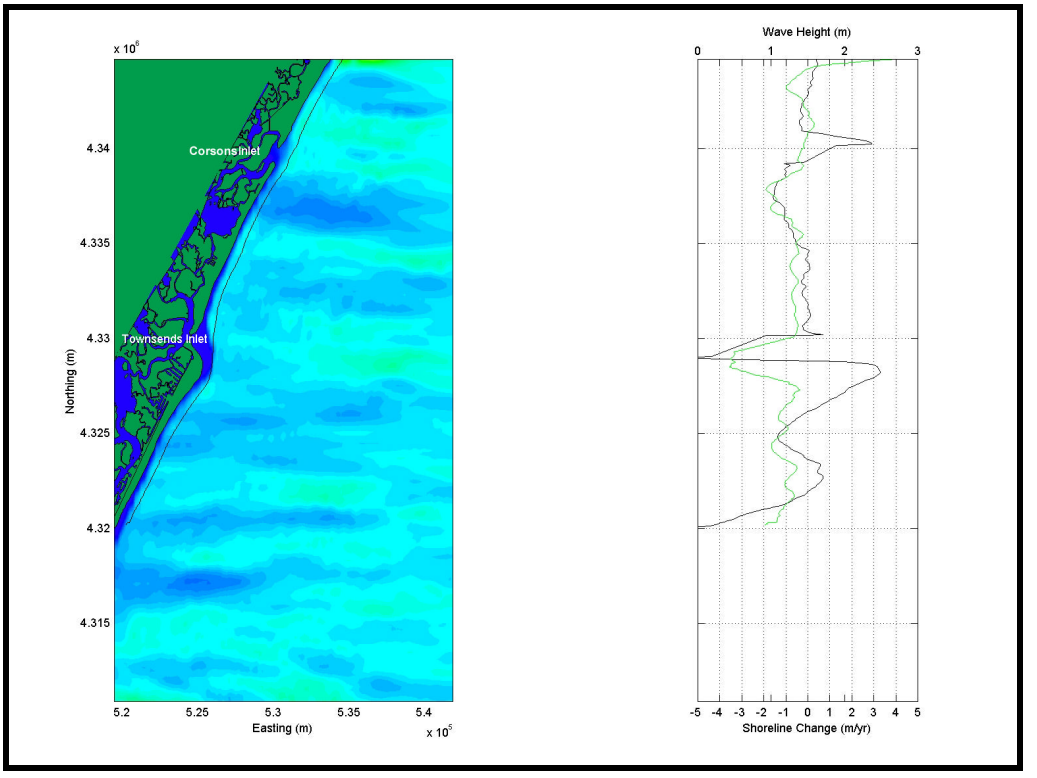

Figure 4-24. Wave height (green line, right-hand panel) taken from approximate breaker line (black line, left-hand panel) for the east (0 degree) approach simulation compared with historical shoreline change rates (black line, right-hand panel; 1864/86 to 1977).

Historical shoreline changes at the two existing inlets (Corsons and Townsends Inlet) dominate change over this stretch of the New Jersey coast, while the rest of the shoreline exhibits slight retreat. Chapter 3 contains a detailed discussion of historical shoreline change rates for this section of the New Jersey coast. For the eastern approach simulation, wave height distribution along the coast is not always consistent with the historical shoreline change rates. For example, shoreline retreat south of Corsons Inlet has associated smaller wave heights where larger waves would be predicted. However, in other areas, the eastern approach wave heights do correlate reasonably with historical shoreline change rates. The eroding region north of Corsons Inlet corresponds to slightly larger wave heights, while shoreline advance just north of Corsons Inlet corresponds to smaller wave heights.

It was anticipated that the wave height distribution and shoreline change rates may not correlate, because Figure 4-24 represents only a percentage (approximately 15%) of the annual average wave energy impacting the coast (i.e., only energy associated with the eastern approach bin). Nonetheless, evaluation of each simulation can provide insight into potential areas of shoreline retreat and advance that are caused by specific directional approaches. Comparisons of the remaining directional simulations with shoreline change rates can be found in Appendix B4.

Directional simulations can be combined to offer a summary of the annual wave climate. Because each directional approach simulation represents a percentage of the total waves impacting the coast over an average year, results of each simulation were superimposed to create an approximate representation of an annual wave climate. The combination of modeling simulations does not represent a complete year because not all the directional approaches are modeled (e.g., waves heading offshore, waves approach the coast at wide angles). By weighting each simulation using the total modeled percentage, each directional approach can be combined to create the best estimate of the annual wave climate. Table 4-21 presents the allotment of percentages for each directional approach simulation.

Table 4-21. Percent occurrence weighting for simulated directional approach bins to reconstruct an approximate annual average for Grid A.

Map Relative Direction (coming from)	Grid Relative Direction (coming from, 0E = E)	Modeled Percent Occurrence	Weighted Percent Occurrence
East-Northeast	22.5 *(11.26 to 33.75)*	1.8	2.9
East	0.0 *(-11.25 to 11.25)*	15.3	24.4
East-Southeast	-22.5 *(-33.75 to -11.24)*	18.0	28.7
Southeast	-45.0 *(-56.25 to -33.74)*	15.4	24.5
South-Southeast	-67.5 *(-78.75 to -56.24)*	12.3	19.6

Figure 4-25 shows the combined wave height distribution extracted along the approximate breaker line compared with shoreline change. In a regional context, shoreline change and wave height distribution correlate moderately well along this portion of the New Jersey coast. The differences that exist likely are caused by the significant influence inlets have on sediment transport along the shoreline (in this case Corsons and Townsends Inlet). In addition, slight changes in the orientation and location of offshore shoals result in a shift in the location of areas of energy convergence and divergence. Therefore, any historical movement of offshore shoals or bathymetric depressions changes the location of increased wave energy along the coast. Because shoreline change information dates back to the 1800s, significant changes in offshore

bathymetry over the time period 1864/86 to 1977 may account for the inconsistent correlation of wave height and shoreline retreat/advance. In addition, storm events may dominate the shaping of the shoreline along this portion of the coast, explaining the inconsistent correlation of the directional wave height distribution with shoreline change rates. The directional approach combination applied does not identify the processes occurring during a specific storm event. However, the northeast storm model simulation revealed a significant increase of wave energy focused near Seven Mile Beach, an area that has experienced net shoreline retreat. Finally, human interference, such as engineering structures, inlet stabilization, and beach nourishment, may also contribute to the inconsistent correlation.

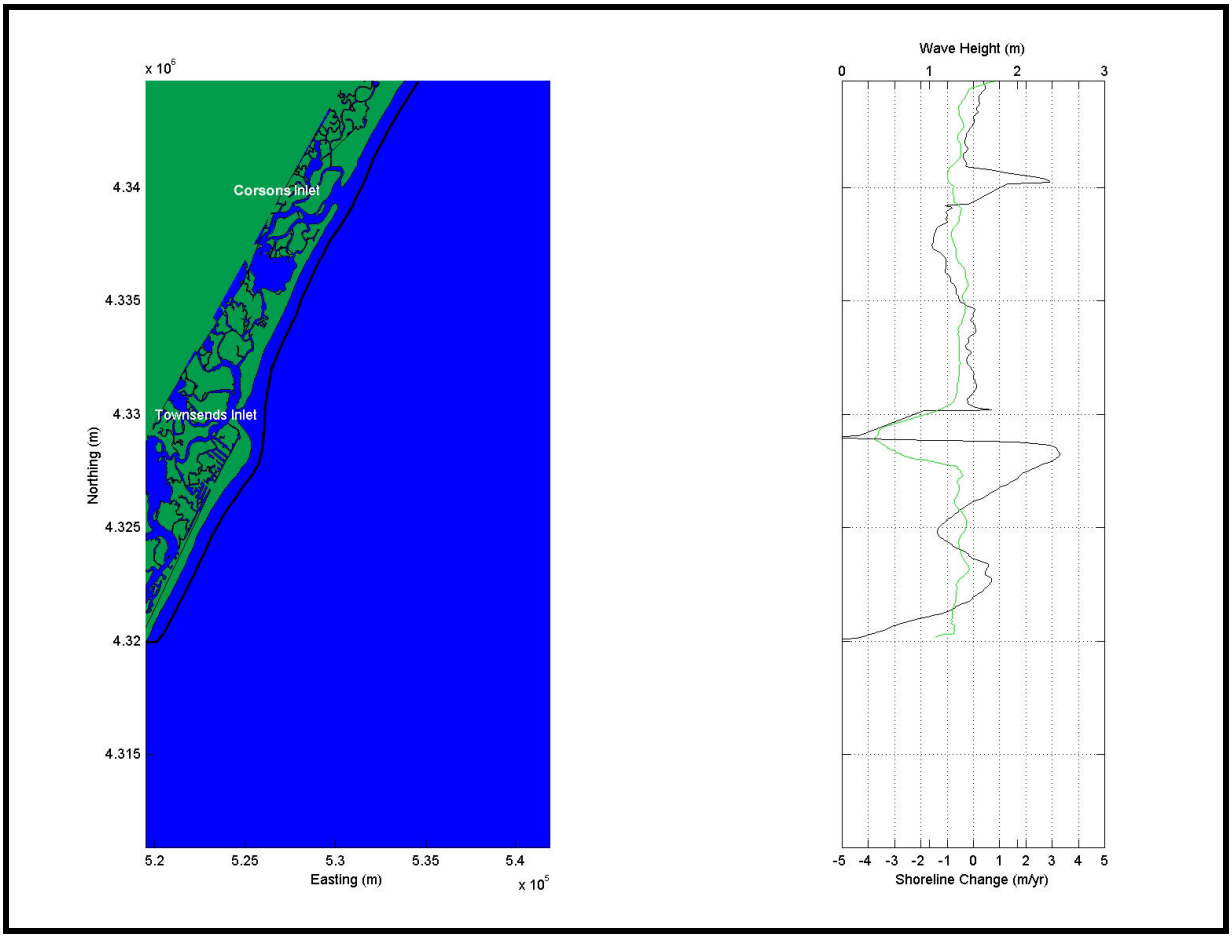

Figure 4-25. Wave height (green line, right-hand panel) taken from the approximate breaker line (black line, left-hand panel) for combined directional approach simulations compared with shoreline change rates (black line, right-hand panel; 1864/86 to 1977).

4.4.2 Grid B1 Simulations

4.4.2.1 Directional Approach Simulations

This section discusses results for simulations of existing (pre-dredging) conditions. Model simulations were performed for typical wave conditions represented by directional bin spectra and extreme wave conditions represented with 50-yr storm spectra (estimated hurricane and northeast storm).

Wave focusing, divergence, and shadowing occur at several locations throughout the Grid B1 model domain, which results in a variation of wave energy propagating towards the shoreline. As in Grid A, a significant amount of variation exists in the wave heights along the nearshore region of Grid B1, which is a result of a variety of bathymetric features impacting the wave transformation within the domain. However, there are fewer significant features within Grid B1 than there were in Grid A. Figure 4-26 identifies some of the major features in the offshore region, specifically near the proposed borrow site (C1).

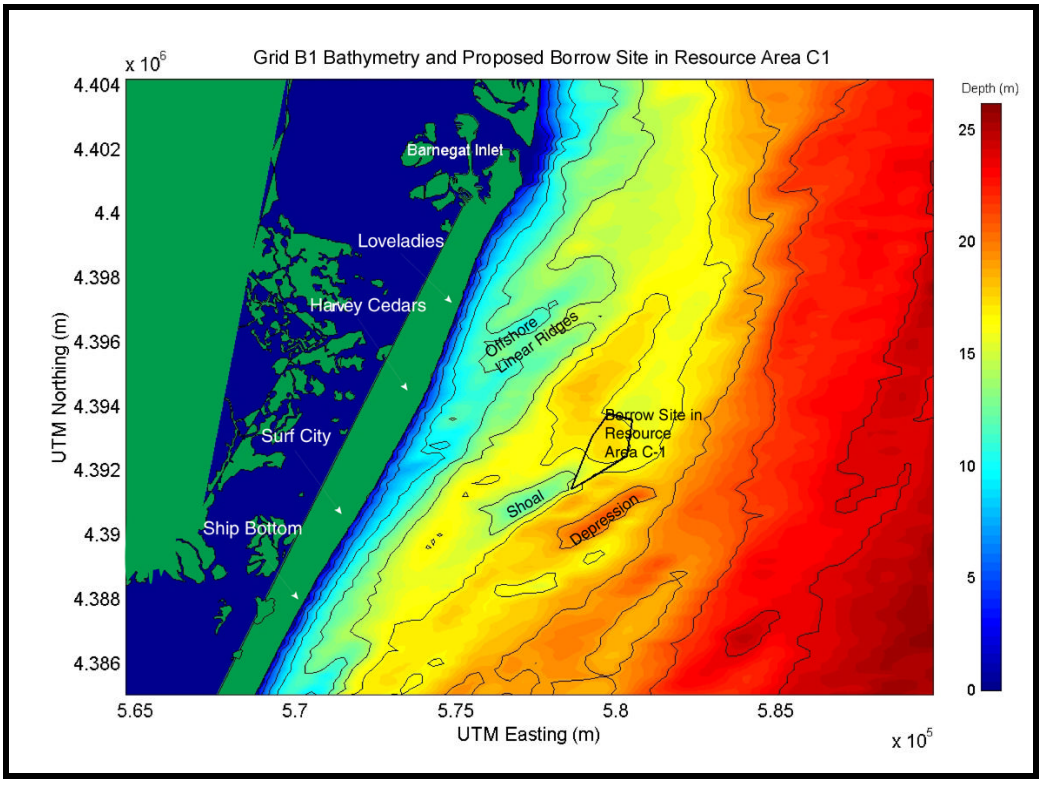

Figure 4-26. Location of key bathymetric features within Grid B1 and location of proposed borrow site in Resource Area C1.

Eastern Wave Approach

Figure 4-27 illustrates wave results for Grid B1 for waves approaching from the east (0 degree directional bin simulation). For this case and all wave modeling results in this section, the color map corresponds to the distribution of significant wave height (m) throughout the modeling domain. Solid black lines represent bathymetric contours, and land masses are shown in solid green. The shoreline presented in the figures is a high water shoreline and is used here for presentation purposes only. The model runs were conducted at depths and shoreline positions corresponding to mean water. Arrows on the figure represent the modeled wave angles as they approach the shoreline.

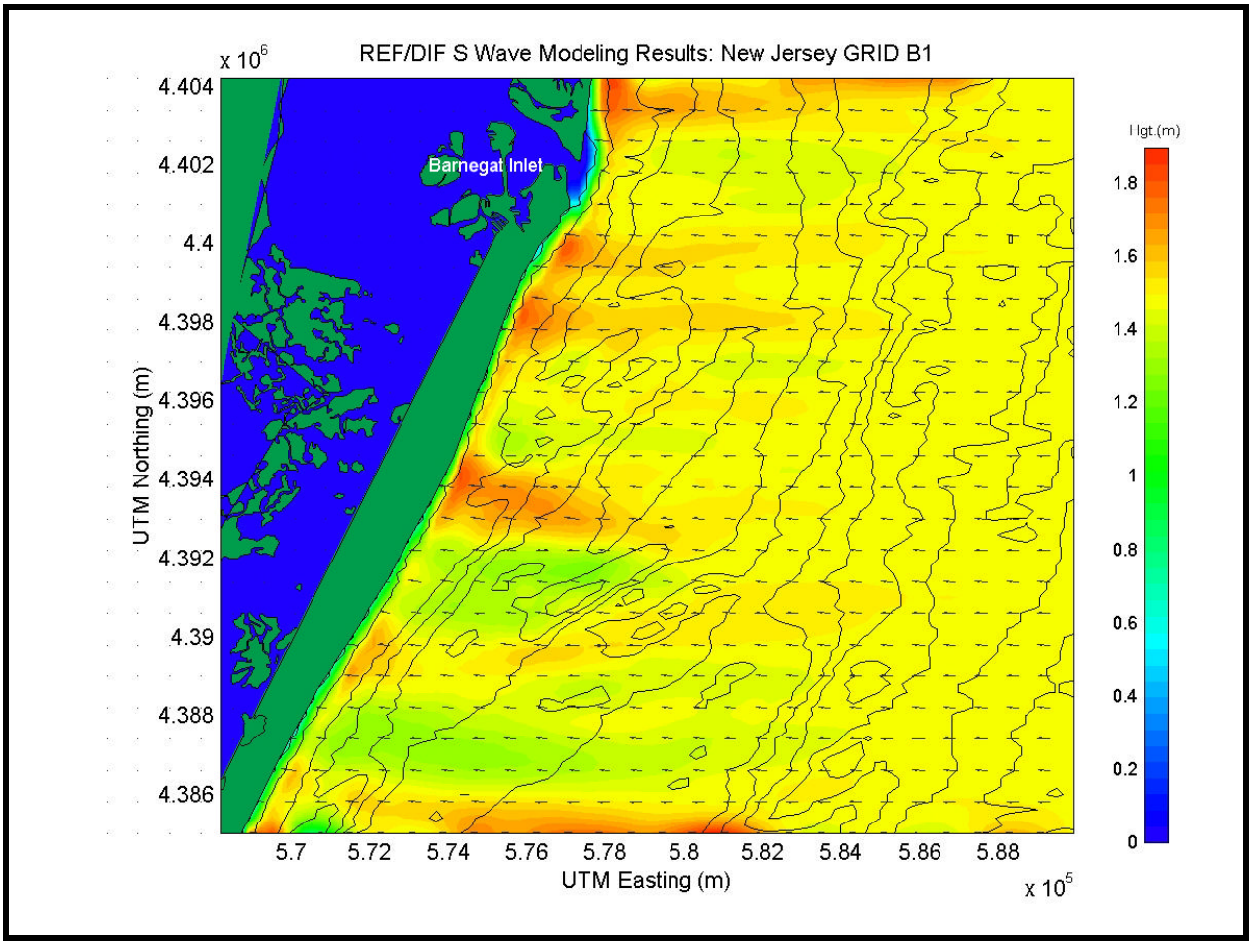

Figure 4-27. Spectral wave modeling results for existing conditions using an eastern approach direction (0 degree bin) at Grid B1.

The east (0 degree) approach bin consists of an input wave height of 1.5 m. Waves approach from this directional bin 19.2% of the time, and this represents the most common approach direction for this grid. Therefore, waves approaching from the east are an essential component of the wave and sediment transport modeling. As with Grid A, fluid and sediment transport would be directed from north to south in the nearshore region. Changes in wave height and direction begin to occur at approximately the 20 m depth contour.

The large depression located due south of the borrow site in Resource Area C1 is a key feature that diverts wave energy to the north and south creating a reduction in wave height (green region) landward of the depression. The reduction in wave height (to approximately 1.1 m) reaches the coast between Harvey Cedars and Surf City. The wave height reduction is slightly larger to the north, as the crest of the shoal located directly landward of the depression causes a focusing of some of the wave energy. The wave energy diverted to the south propagates to the coast, and an increase to approximately 1.6 m is evident near Surf City. The wave energy diverted to the north interacts with the shoal partially comprising Resource Area C1 and focuses waves towards Harvey Cedars. Linear ridges similar to those found in Grid A are also encountered within Grid B1. These linear ridges offshore of Loveladies are another source of wave focusing and cause the increase in wave height observed near the coast. Two distinct bands of wave energy impact the coast as waves reach 1.7 to 1.8 m in height.

For this directional approach, there are three important regions of increased wave heights along the coast. Other areas experience reduced wave energy (e.g., the region between Harvey Cedars and Surf City). Table 4-22 presents a summary of the areas experiencing increased wave heights along the coast from waves approaching from the east.

Table 4-22. Coastline areas experiencing increased wave heights during eastern wave approach at Grid B1.

Approximate Location	Approximate Wave Height at Coast (m)
Harvey Cedars	1.7 to 1.8
Surf City	1.6
Loveladies	1.6 to 1.8

The wave directions, illustrated by the arrows presented in Figure 4-27, are difficult to represent visually. For the eastern directional approach, wave directions remain relatively constant throughout the modeling domain, although areas of significant convergence or divergence do exhibit a visual change. There is also a slight orientation of the waves perpendicular to the coastline.

East-Southeast Wave Approach

Figure 4-28 illustrates wave modeling results for Grid B1 for the east-southeast (-22.5 degree) directional approach. The input wave height for the east-southeast approach direction is 1.5 m, the same as the east approach simulation. The east-southeast approach simulation contains 18.9% of the total waves, thereby making this approach direction the second most common. This approach direction is almost perpendicular to the orientation of the coastline. Fluid transport is directed from the north to south for most areas along the coast. The results from the east-southeast approach simulation exhibit similar wave patterns as the eastern wave approach, with distinctive areas of wave convergence and divergence occurring throughout the domain.

Similar to the eastern approach simulation, the large shoal that contains the proposed borrow site in Resource Area C1 produces the most prominent region of wave convergence. Wave heights increase to approximately 1.8 m and do not significantly dissipate before reaching the coast between Loveladies and Harvey Cedars. The northern edge of the large shoal also creates a small band of wave energy (increase of wave height to 1.7 m) that impacts the coast south of Barnegat Inlet. There is also a region of wave focusing in the southern portion of the grid caused by linear ridges near the southern boundary of the modeling domain. A wave height increase of approximately 0.2 m impacts the coast near Ship Bottom.

The depression south of the proposed borrow site at Resource Area C1 again produces a region of wave divergence and a reduced wave height at the coast (approximately at Harvey Cedars). Most of the remaining region experiences normal wave heights during the east-southeastern approach. Table 4-23 presents a summary of the areas experiencing increased wave heights along the coast from waves approaching from the east-southeast.

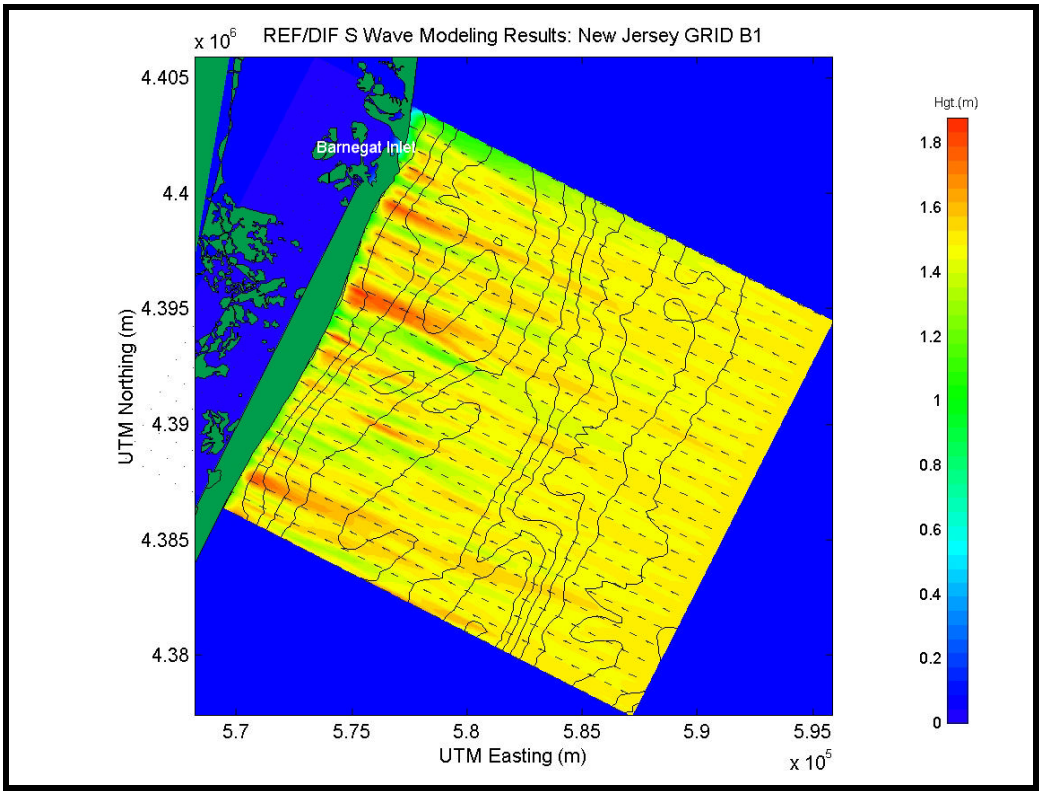

Figure 4-28. Spectral wave modeling results for existing conditions using an east-southeast (-22.5 degree) approach direction at Grid B1.

Table 4-23. Coastline areas experiencing increased wave heights during east-southeast wave approach at Grid B1.

Approximate Location	Approximate Wave Height at Coast (m)
South of Barnegat Inlet	1.7
Between Loveladies and Harvey Cedars	1.8
Ship Bottom	1.7

East-Northeast Wave Approach

Figure 4-29 illustrates REF/DIF S results for Grid B1 for the east-northeast (22.5 degree) directional bin simulation. The east-northeast approach is highlighted by significantly larger wave heights (1.8 m) and rare occurrences (2.6% of the time). The larger waves and low occurrence level is expected because waves from this direction are dominated by the passage of northeast storms. Fluid transport is directed from north to south for this approach, and during most storm events, sediment transport is from north to south as well. Distinct regions of wave focusing and divergence can be identified in this directional approach. The overall wave height arriving at the coast is significantly larger in general than the previously examined cases.

The depression located south of Resource Area C1 produces a significant divergence zone where wave heights are reduced to under 1.0 m. The divergence continues to spread as the waves approach the coast and a reduction in wave height is experienced extending from Ship Bottom north to Surf City. Similarly, the large shoal contained within Resource Area C1 produces a significant region of wave focusing, increasing wave height to 1.8 m. As waves propagate towards the coast, a significant amount of this energy is dissipated. Wave heights of 1.4 to 1.5 m are evident at the coastline north of Surf City. The linear ridges to the north are another source of wave focusing for this approach direction. Waves increase to approximately 1.6 to 1.8 m in the lee of these features. The increase in wave energy is refracted perpendicular to the coast over the nearshore bathymetric contours and impacts the shoreline between Loveladies and Harvey Cedars at a height of 1.7 m. An additional region of increased wave heights also is produced near the Barnegat Inlet area for this directional approach. The convex form of the contours offshore of Barnegat Inlet produce a moderate focusing of wave energy near the inlet entrance. Wave heights in this region reach 1.5 to 1.6 m near the entrance. Table 4-24 presents a summary of the areas experiencing increased wave heights along the coast from waves approaching from the east-northeast.

Table 4-24. Coastline areas experiencing increased wave heights during east-northeast wave approach at Grid B1.

Approximate Location	Approximate Wave Height at Coast (m)
North of Surf City	1.4 to 1.5
Between Loveladies and Harvey Cedars	1.7 to 1.8
Barnegat Inlet Area	1.6 to 1.7

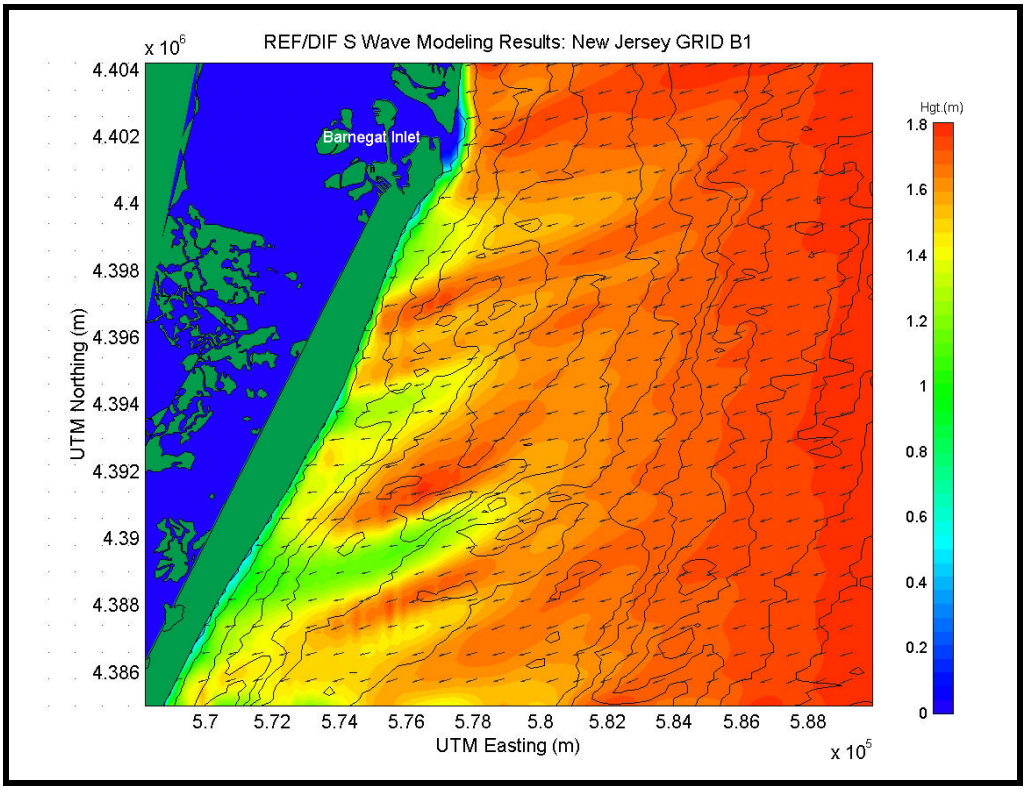

Figure 4-29. Spectral wave modeling results for existing conditions using an east-northeast (22.5 degree) approach direction at Grid B1.

Southeast Wave Approach

Figure 4-30 illustrates wave modeling results for Grid B1 for the southeast (-45 degree) directional bin simulation. The southeast directional approach simulation has an input wave height of 1.5 m, which is the same as the east and east-southeast cases. The southeast approach direction contains 14.6% of the waves, the third highest occurrence level. In general, the areas of convergence and divergence match the east-southeast approach direction. However, due to the change in primary approach direction and peak spectral period, some differences do exist between the two simulations. The southeast wave direction has less variation in wave height along the coastline compared with previously examined cases. Wave heights along the coast remain relatively consistent between 1.4 and 1.6 m. The southeast directional approach represents a slightly southern approach to the coast. Therefore, fluid transport is from south to north, and a potential reverse in the primary direction of sediment transport occurs. Only subtle changes in wave direction near regions of convergence and divergence can be seen at the resolution of Figure 4-30.

The shoals in Resource Area C1 again cause an increase in wave energy in this simulation; although the focusing is not nearly as distinct. Coupled with the linear ridges, which lie landward of Resource Area C1, a patchy band of increased wave height (varying between 1.4 to 1.7 m) impacts the coast at Loveladies north to Barnegat Inlet. As in Grid A, the northern linear ridges appear to have a lesser impact in this scenario, most likely due to the primary direction of wave propagation, which advances over the shortest dimension of the northeast-oriented ridges. The shoal to the southeast of Resource Area C1 causes wave focusing that heightens wave energy to 1.5 to 1.6 m. The higher wave heights appear to be caused by the margins of the shoal. This increase in wave energy impacts the coast in the vicinity of Harvey Cedars. Finally, a moderate area of wave convergence can be identified to the south of Ship Bottom. Table 4-25 presents a summary of the areas experiencing increased wave heights along the coast from waves approaching for the southeast.

Table 4-25. Coastline areas experiencing increased wave heights during southeast wave approach at Grid B1.

Approximate Location	Approximate Wave Height at Coast (m)
Harvey Cedars	1.4 to 1.6
Ship Bottom to Surf City	1.5
Loveladies to Barnegat Inlet	1.5 to 1.6

South-Southeast Wave Approach

Figure 4-31 illustrates wave modeling results for Grid B1 for the south-southeast (-67.5 degree) directional bin simulation. The south-southeast directional approach simulation has an input wave height of 1.3 m, which is the smallest modeled wave height for this grid. Despite the wide angle of approach, the south-southeast approach direction still contains a major portion of the wave energy (10.2% of the waves), although not as much as for Grid A. In general, the areas of convergence and divergence are similar to other southeast approach directions; however, the areas of focusing are less distinctive due to smaller wave heights. In addition, little variation in wave height is evident along the coastline. The wave height only reaches 0.7 to 0.9 m along the entire coast. Sediment and fluid transport are directed from south to north for this directional approach, opposite the primary direction of sediment movement.

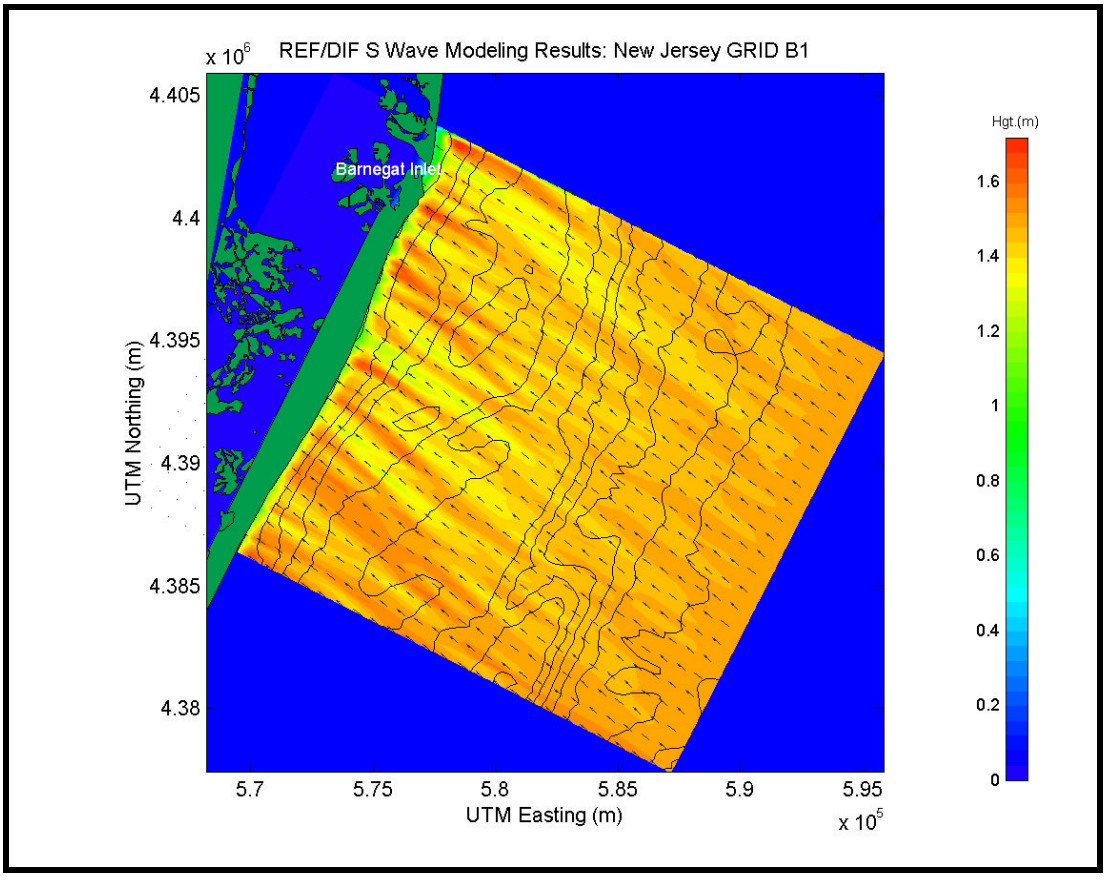

Figure 4-30. Spectral wave modeling results for existing conditions using a southeast (-45 degree) approach direction at Grid B1.

Only minor modifications to the wave field are visible throughout the modeling domain for this simulation. The shoals in Resource Area C1 produce slight wave focusing as waves nearing 0.9 m in height advance to the coast south of Barnegat Inlet. In addition, the shoal located southeast of Resource Area C1 causes mild wave height increases near Harvey Cedars. In both cases, wave energy focusing appears as irregular bands rather than uniform area of wave energy and does not exceed the offshore wave height. Linear ridges to the north of Resource Area C1 indicate a smaller impact when compared with wave approaches from the east or northeast. Similar to Grid A, the elongate dimensions of these features coupled with the southeast approach direction, allow the waves to cross the shortest dimension of these features, thereby producing a reduced effect on the wave field. Some erratic wave convergence patterns appear in the southern portion of the modeling domain caused by the irregular bathymetric contours in the offshore region. Although the increases in wave height are not significant for this simulation, Table 4-26 presents a summary of areas experiencing slightly larger wave heights along the coast than other areas in the model domain.

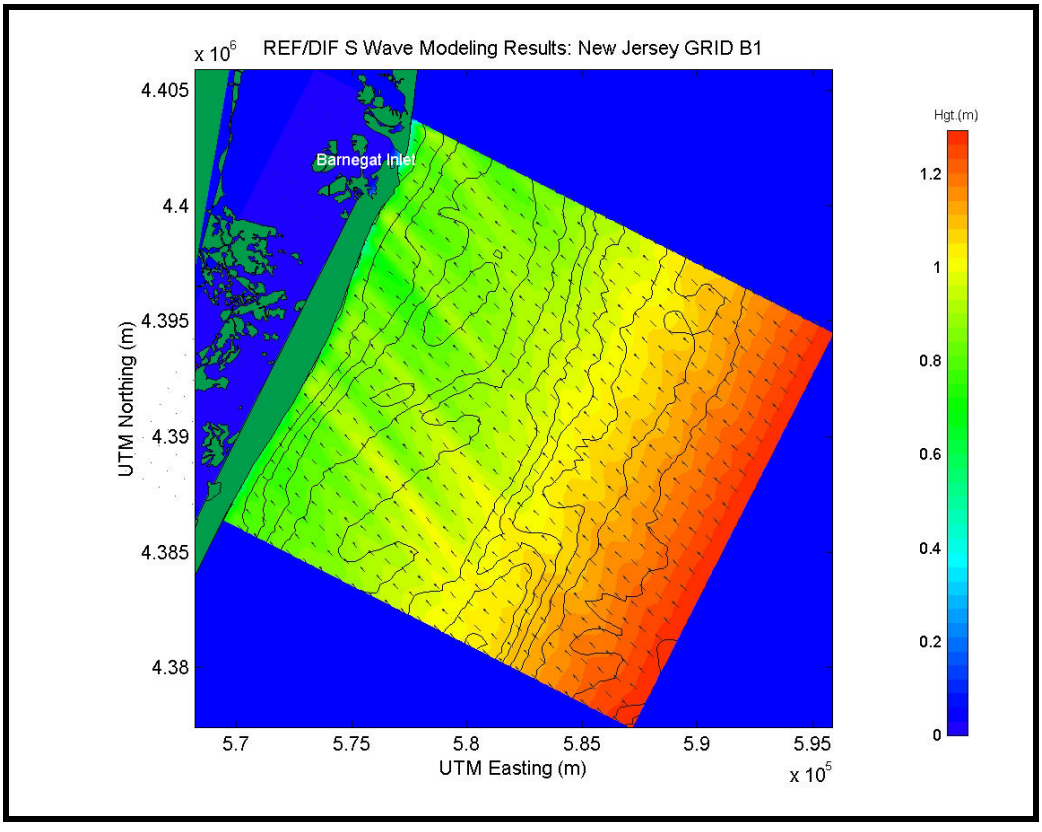

Figure 4-31. Spectral wave modeling results for existing conditions using a south-southeast (-67.5 degree) approach direction at Grid B1.

Table 4-26. Coastline areas experiencing increased wave heights during south-southeastern wave approach at Grid B1.

Approximate Location	Approximate Wave Height at Coast (m)
Harvey Cedars	0.9
South of Barnegat Inlet	0.7 to 0.9

4.4.2.2 High Energy Wave Events Simulations

Figure 4-32 illustrates wave transformation results for an estimated 50-yr northeast storm propagating over Grid B1. The northeast storm simulation represents a rare occurrence as waves approach from the east and/or northeast with a wave height of 6.4 m. The waves respond to the seafloor much sooner than in the directional simulations, and begin to dissipate energy near the offshore boundary of the grid. This also causes the wave approach directions to be modified farther offshore. As a result of the more pronounced wave refraction, the directions orient themselves perpendicular to the coast throughout the model domain. Fluid transport, as well as sediment transport, is directed from north to south during a typical northeast storm.

As in Grid A, the northeast storm simulation is highlighted by an increased wave height throughout the region. The wave convergence and divergence patterns caused by many of the bathymetric features are less pronounced with large storm waves because changes caused by the features are small when compared with the large input wave height. Due to the magnitude of the 50-yr storm simulations, existing modeling techniques may be limited for simulation of these long-period, high-energy wave events and the accuracy of the results for these simulations is limited by the capabilities of the model (see Section 4.2.1.2).

Figure 4-33 illustrates wave transformation results for an estimated 50-yr hurricane propagating over Grid B1. The hurricane simulation also represents a rare but energetic occurrence as waves approach from the southeast with a wave height of 5.6 m. Similar to the northeast storm case, waves respond to the seafloor in deeper water than in the more commonly occurring directional simulations, and begin to refract and dissipate energy greater distances offshore. Wave directions are oriented nearly perpendicular to the coast throughout the model domain. Wave heights exceeds 3.0 to 4.0 m for most areas along the coast.

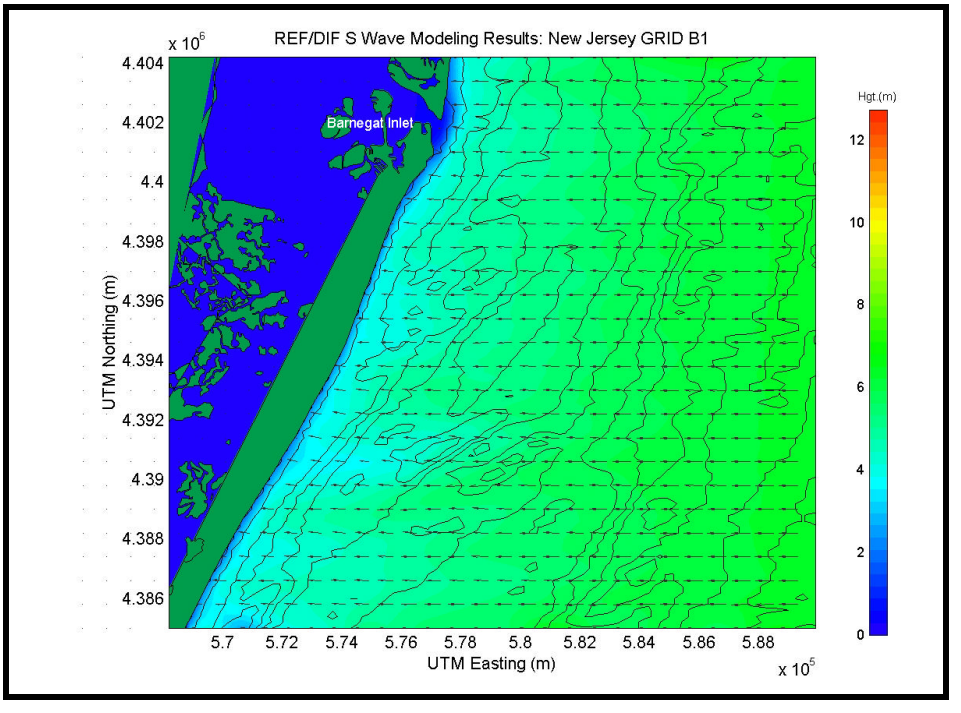

Figure 4-32. Spectral wave modeling results for existing conditions simulating an estimated 50-yr northeast storm event at reference Grid B1.

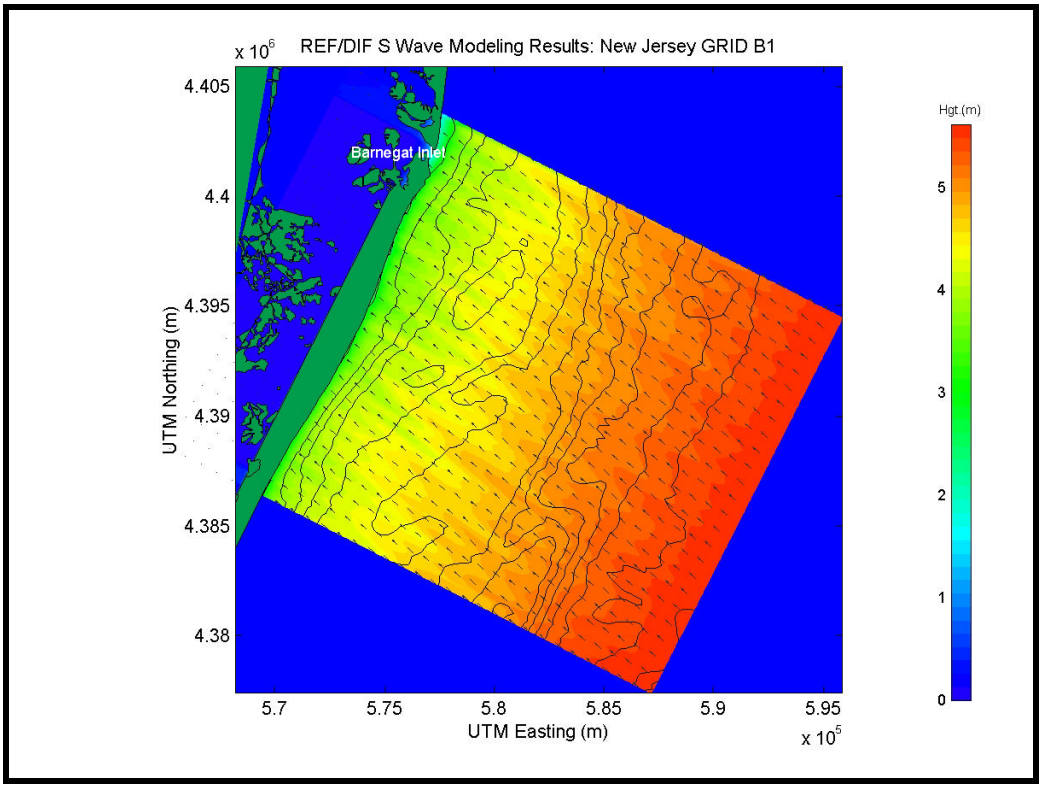

Figure 4-33. Spectral wave modeling results for existing conditions simulating an estimated 50-yr hurricane event at reference Grid B1.

4.4.2.3 Model Results Relative to Historical Shoreline Change

Figure 4-34 illustrates significant wave heights extracted along a transect line for the east (0 degree) approach simulation compared with historical shoreline change results. The left-hand panel illustrates the nearshore wave transformation results for the east approach simulation, where the colormap represents wave height in meters. The solid black line in the left-hand panel represents the approximate breaker transect from which significant wave heights were extracted. The breaker transect line is very difficult to determine when using spectral wave models since there are a variety of waves, composed of different frequencies and directions, breaking at different times and locations throughout the domain. In addition, the orientation and irregularity of the coastline add difficulty to determining an exact breaker line at the grid resolution provided in the model. Therefore, the breaker line presented is intended only to provide a relative height distribution along the coast, rather than the exact region of wave breaking. The right-hand panel presents historical shoreline change rates for this stretch of the New Jersey coast and is represented by a black line scaled by the bottom axis (m/yr). The significant wave height is added to the plot and represented by a green line and scaled by the upper axis (m).

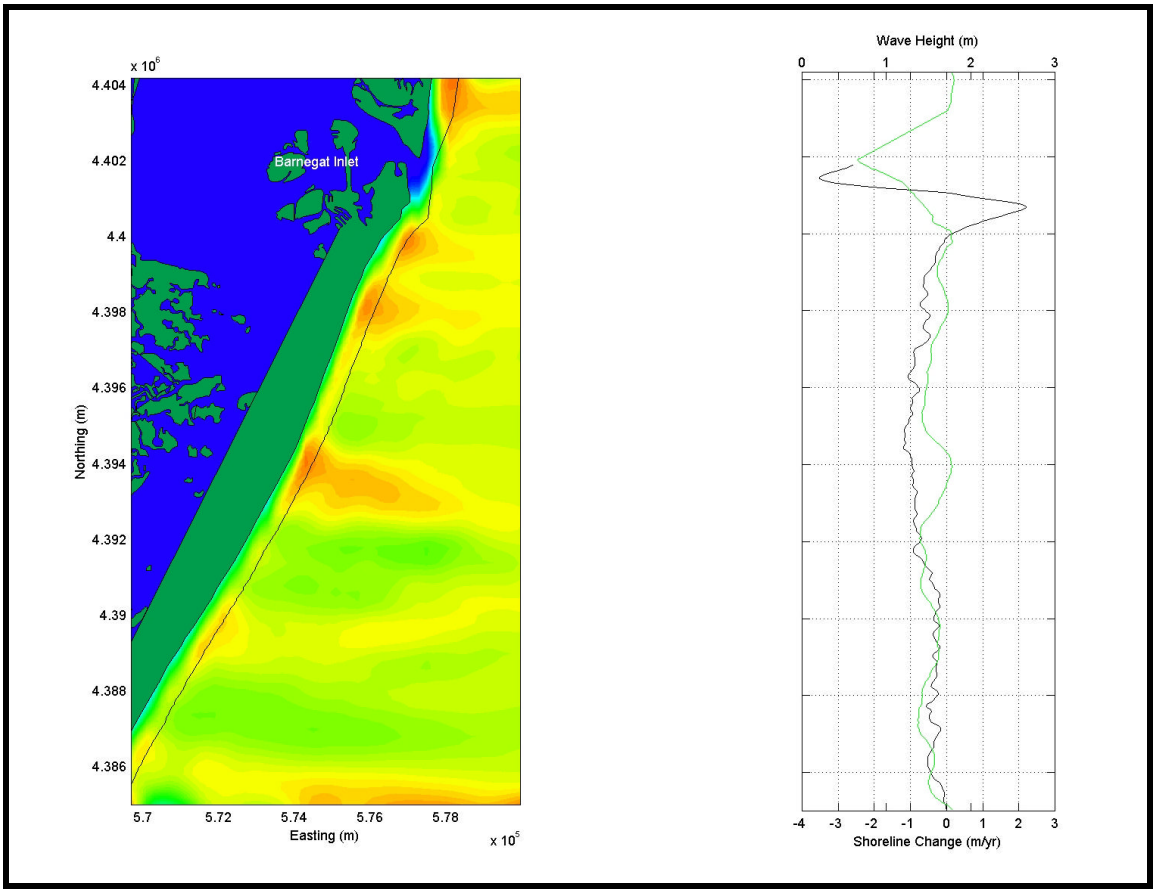

Figure 4-34. Wave height (green line, right-hand panel) taken from approximate breaker line (black line, left-hand panel) for the east (0 degree) approach simulation compared with historical shoreline change rates (black line, right-hand panel; 1864/68 to 1977).

It is evident from the distribution of shoreline change rates that Barnegat Inlet significantly impacts this stretch of the New Jersey coast, while the rest of the shoreline exhibits slight retreat or is relatively stable. Chapter 3 contains a detailed discussion of the historical shoreline change rates for this section of the New Jersey coast. For the eastern approach simulation, the wave height distribution along the coast is consistent with the historical shoreline change rates for most of the coastline. For example, an historical shoreline retreat area near Harvey Cedars (exceeding -1.0 m/yr) is associated with a significant increase in predicted wave height. This is a contrast with Grid A, where the correlation between historical shoreline change rates and wave heights was inconsistent. For Grid B1, the eastern approach direction represents a higher percentage of wave occurrence (19.2%, compared to only 15% for Grid A), and may explain the greater correlation. However, due to the relative stability of the coastline, it is difficult to identify a conclusive correlation.

It was anticipated that the wave height distribution and historical shoreline change rates may not correlate, because Figure 4-34 represents only a percentage (approximately 19%) of the annual average wave energy impacting the coast (i.e., only energy associated with the eastern approach bin). Nonetheless, evaluation of each simulation can provide insight regarding potential areas of shoreline retreat and/or advance that are caused by specific directional approaches. Comparisons of the remaining directional simulations to historical shoreline change rates can be found in Appendix B4.

As with Grid A, the directional simulations can be combined to offer a summary of the annual wave climate, although a portion of the wave energy will be ignored when using the directional approach method. Because each directional approach simulation represents a percentage of the total waves impacting the coast over an average year, the results of each simulation were superimposed to create an approximate representation of an annual wave climate. The combination of modeling simulations does not represent a complete year because not all the directional approaches are modeled (e.g., waves heading offshore, waves approach the coast at wide angles). By weighting each simulation using the total modeled percentage, each directional approach can be combined to create the best estimate of the annual wave climate. Table 4-27 presents the allotment of percentages for each directional approach simulation.

Table 4-27. Percent occurrence weighting for simulated directional approach bins to reconstruct an approximate annual average wave climate for Grid B1.

Map Relative Direction (coming from)	Grid Relative Direction (coming from, 0E = E)	Modeled Percent Occurrence	Weighted Percent Occurrence
East-Northeast	22.5 *(11.26 to 33.75)*	2.6	4.0
East	0.0 *(-11.25 to 11.25)*	19.2	29.3
East-Southeast	-22.5 *(-33.75 to -11.24)*	18.9	28.9
Southeast	-45.0 *(-56.25 to -33.74)*	14.6	22.3
South-Southeast	-67.5 *(-78.75 to -56.24)*	10.2	15.6

Figure 4-35 shows the combined wave height distribution extracted along the approximate breaker line compared with historical shoreline change. The left-hand panel illustrates the transect (black line) from which significant wave heights were extracted. The right-hand panel presents the historical shoreline change rates for this stretch of the New Jersey coast and is represented by a black line scaled by the bottom axis (m/yr). The combined wave height distribution for the directional approach simulations is represented by a green line and scaled by the upper axis (m).

Figure 4-35 illustrates a consistent correlation between historical shoreline change and the distribution of wave heights along the coast. Most of the region exhibits wave heights ranging from 1.0 to 1.4 m, and mild shoreline retreat is indicated. A significant increase in shoreline retreat is visible from approximately 4,392,000 Northing and extends north to approximately Loveladies. The wave height exhibits a similar trend, as larger waves occur over this stretch of coast.

In a regional context, shoreline change and wave height distribution correlate well along this portion of the New Jersey coast. The differences that do exist in the northern portion of the domain likely are caused by the influence Barnegat Inlet has on sediment transport along the shoreline. In addition, slight changes in the orientation and location of offshore shoals result in a shift in the location of areas of energy convergence and divergence. Therefore, any historical movement of the offshore shoals and or bathymetric depressions changes the location of increased wave energy along the coast. Because shoreline change information dates back to the 1800s, significant changes in the offshore bathymetry over the time period (1864/68 to 1977) may account for any inconsistent correlation of wave height and shoreline retreat/advance. In addition, storm events may dominate shoreline response along this portion of coast. The directional approach combination applied does not identify the processes occurring during a specific storm event. Finally, human interference, such as engineering structures, inlet stabilization, and beach nourishment, may contribute to areas of inconsistent correlation.

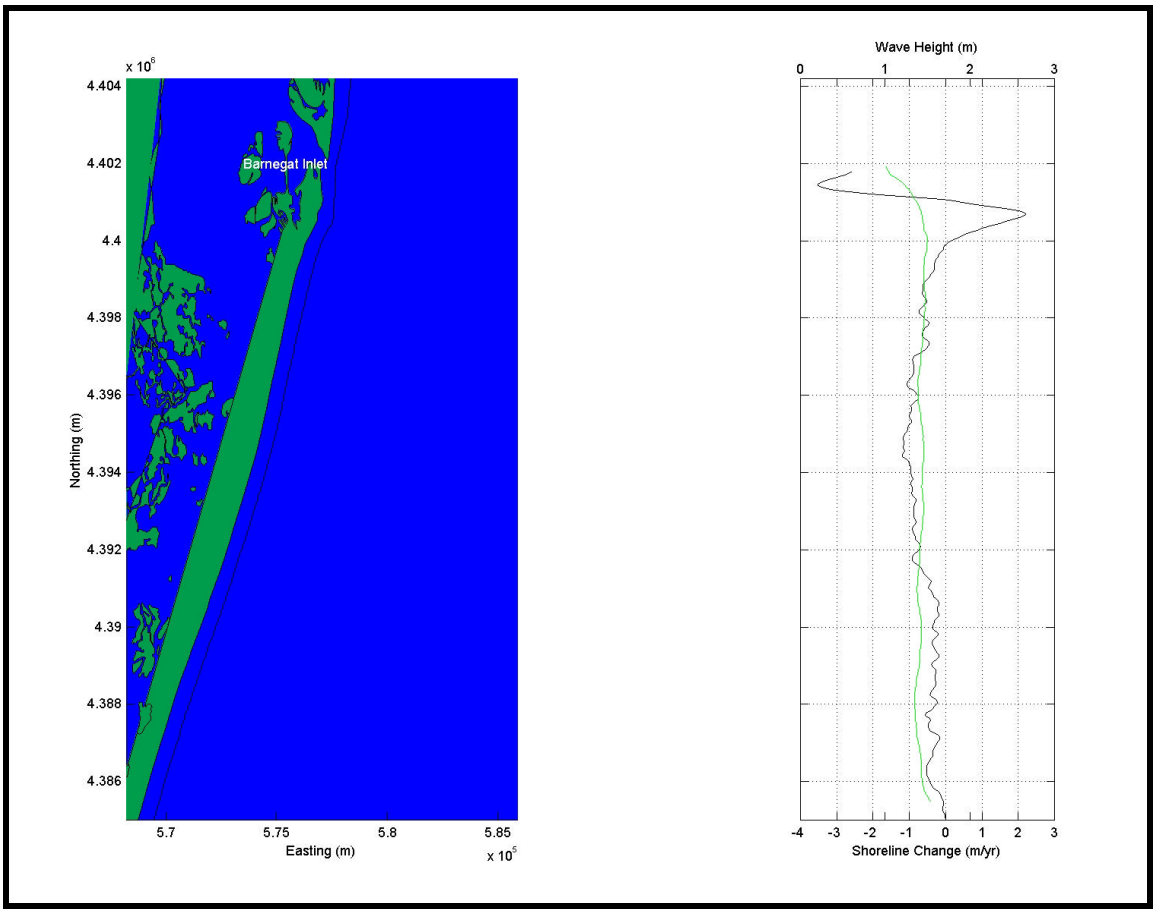

Figure 4-35. Wave height (green line, right-hand panel) taken from approximate breaker line (black line, left-hand panel) for combined directional approach simulations compared with historic shoreline change rates (black line, right-hand panel; 1864/68 to 1977).

4.4.3 Grid B2 Simulations

4.4.3.1 Directional Approach Simulations

Wave focusing, divergence, and shadowing occur at several locations throughout the Grid B2 modeling domain, which results in a variation of wave energy propagating toward the shoreline. A significant amount of variation exists in the wave heights along the nearshore region of Grid B2, resulting from a variety of bathymetric features impacting wave transformation within the domain. Proposed borrow sites are located in the primary array of offshore, northeast trending, shoreface-attached linear ridges. Figure 4-36 identifies some of the major features in the offshore region, specifically near the proposed borrow sites (G2 and G3). A gap in bathymetric information was located offshore of Absecon Inlet. Therefore, the proposed borrow site G1 was not considered in this study and the domain of the modeling grid was adjusted to reflect available information.

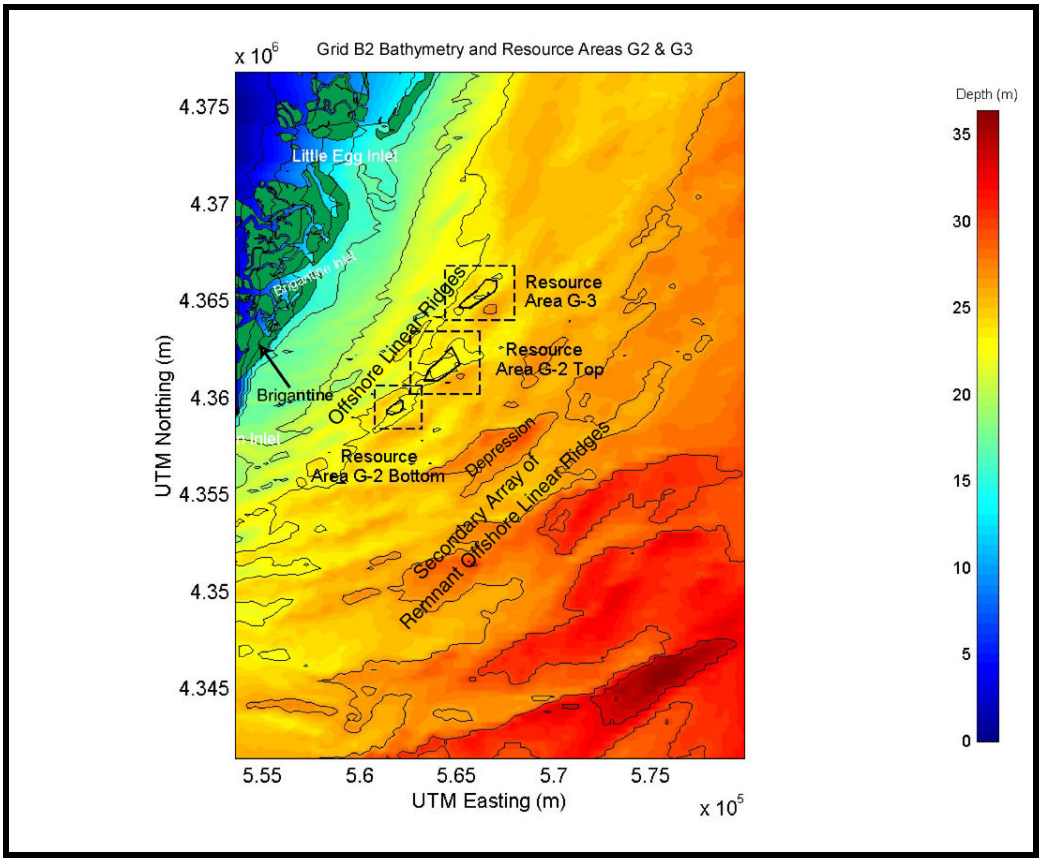

Figure 4-36. Location of key bathymetric features within Grid B2 and location of proposed dredge area G2 and G3.

Eastern Wave Approach

Figure 4-37 illustrates wave modeling results for Grid B2 for waves approaching from the east (0 degree directional bin simulation). For this case and all wave modeling result figures in this section, the color map corresponds to the distribution of significant wave height (m) throughout the modeling domain. Solid black lines represent bathymetric contours, and land masses are shown in green. The shoreline presented in the figures is a high water shoreline and is used here for presentation purposes only. The model runs were conducted at depths and shoreline positions corresponding to mean water. Arrows on the figure represent the modeled wave angle as they approach the shoreline.

The east (0 degree) approach bin consists of an input wave height of 1.6 m. Waves approach from this directional bin 17.3% of the time, and this represents the most common approach direction for this grid. Fluid and sediment transport would be directed from north to south in the nearshore region during an eastern wave approach. Changes in wave height and direction begin to occur at approximately the 20 m depth contour. Most of the spectral wave components do not interact with the seafloor at depths greater than 20 m, similar to the results shown for Grid A and B1. In general wave heights in the northern portion of the modeling domain tend to be larger than in the south. This is due to the increase of irregular bathymetric features located in the northern part of the grid as well as the truncation of the modeling grid in the southern portion.

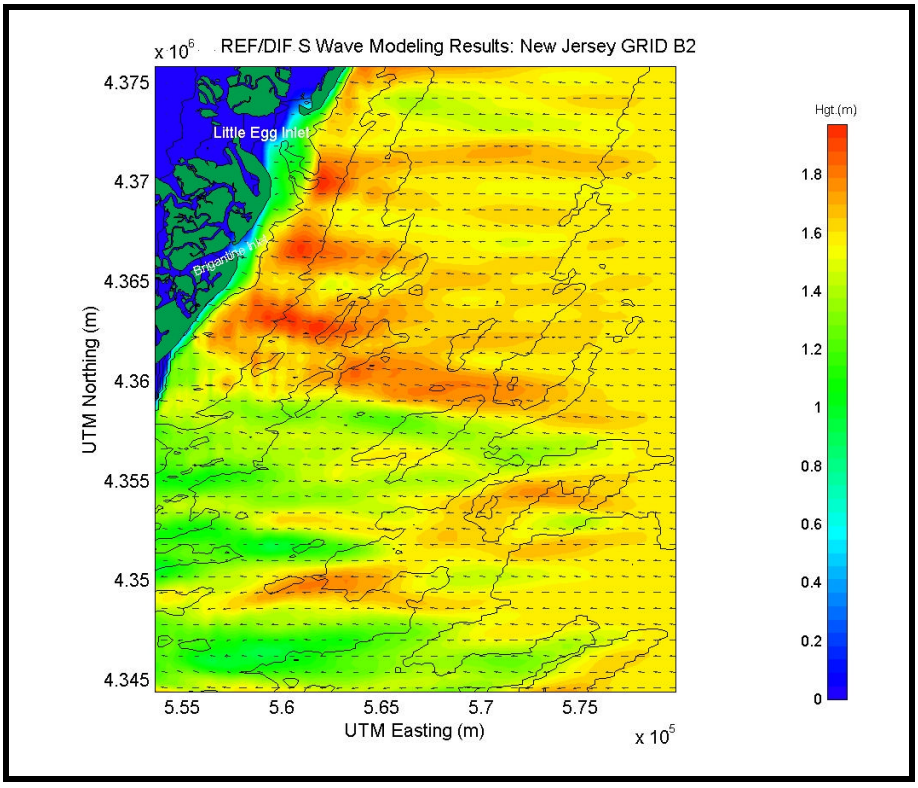

Figure 4-37. Spectral wave modeling results for existing conditions using an eastern approach direction (0 degree bin) at reference Grid B2.

The sand resource areas, as well as the potential borrow sites, are situated on the first array of offshore linear ridges. The shore-attached northeast extending shoals that comprise the ridge have a significant impact on wave magnitudes and approach directions. Specifically, the shoals contained in Resource Areas G2 and G3 produce areas of wave convergence. The shoal located within Resource Area G3, which also represents the potential borrow site, produces wave focusing that reaches 1.9 m at the entrance to Brigantine Inlet. This represents an increase in wave height of approximately 19%. The shoals within Resource Area G2 result in a similar wave convergence, producing a region of heightened wave energy near the city of Brigantine and extending northward to the entrance of Brigantine Inlet. Wave heights approach 1.7 to 1.9 m throughout this region. North of the resource areas, a ridge offshore Little Egg Inlet causes wave focusing to approximately 1.9 m near the entrance to the inlet.

The group of remnant offshore linear ridges also impacts wave transformation in this region. The northeast extending shoal located at approximately 4,360,000 Northing, 574,000 Easting focuses wave energy that is subsequently focused by the shoals within Resource Area G2. Minor bathymetric features within this shoal field also produce smaller wave heights. In addition to increased wave heights, a divergence in wave energy is caused by the bathymetric depression to the southwest of the resource areas where wave height is reduced to less than 1.2 m.

As discussed above, there are three distinct regions of increased wave heights along the coast. Table 4-28 presents a summary of the areas experiencing increased wave heights along the coast from waves approaching from the east.

Table 4-28. Coastline areas experiencing increased wave heights during eastern wave approach at Grid B2.	
Approximate Location	Approximate Wave Height at Coast (m)
Brigantine	1.8 to 1.9
Entrance to Brigantine Inlet	1.9
Entrance to Little Egg Inlet	1.9

For the eastern directional approach, wave directions remain relatively constant throughout the modeling domain, although areas of significant convergence or divergence are illustrated in Figure 4-37. There also is a slight orientation of the waves perpendicular to the coastline.

East-Southeast Wave Approach

Figure 4-38 illustrates wave modeling results for Grid B2 for the east-southeast (-22.5 degree) directional bin simulation. The input wave height for the east-southeast approach direction is 1.6 m. This approach simulation contains 15.2% of the total waves, thereby making it the second most common. The east-southeast approach direction is almost perpendicular to the orientation of the coastline. Based on the orientation of waves over the nearshore rows of the model domain, fluid transport is directed from the north to south for most areas. Wave modeling results from the east-southeast approach exhibit similar wave transformation patterns as the eastern wave approach, with distinctive areas of wave convergence and divergence occurring throughout the domain. Again, wave heights in the northern portion of the modeling domain tend to be larger than in the southern part of the domain.

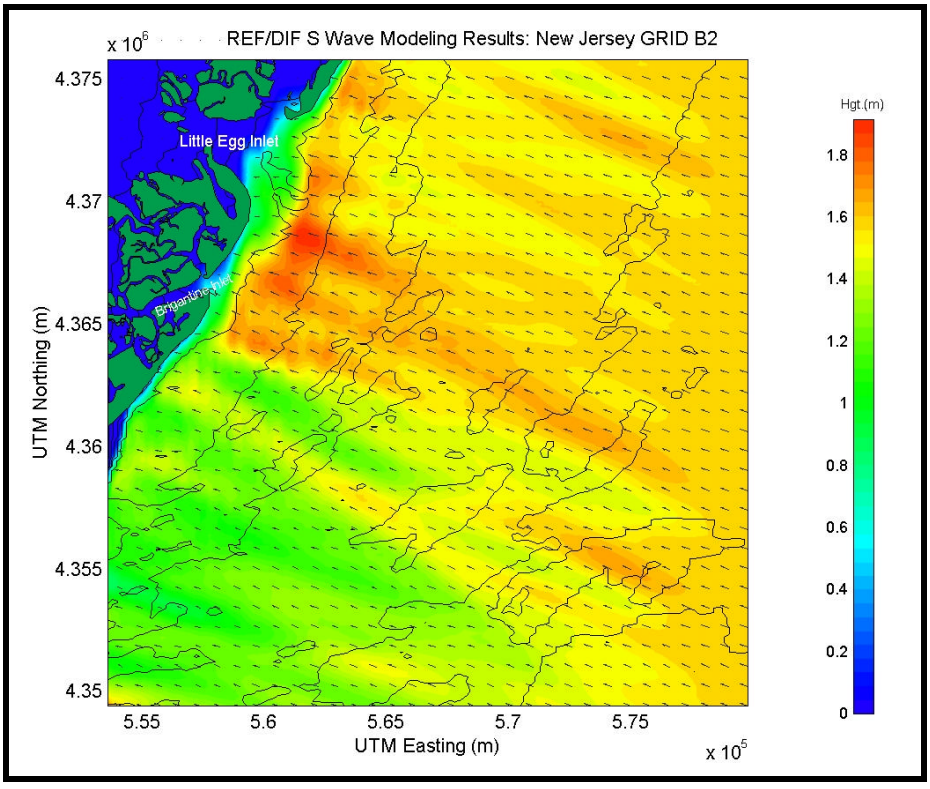

Figure 4-38. Spectral wave modeling results for existing conditions using an east-southeast (-22.5 degree) approach direction for reference Grid B2.

The shoals in Resource Area G2 produce an increase in wave height to approximately 1.7 m that impacts the nearshore seaward of Brigantine Inlet and directly to the south. Shoals within Resource Area G3 produce wave heights that increase to approximately 1.9 m and do not significantly dissipate before reaching the coast between the entrances to Brigantine and Little Egg Inlets. Wave height increases to the north of this region are evident as well. Smaller fluctuations along the primary linear ridge cause modifications to the wave field and focusing in areas seaward of Little Egg Inlet.

As with the eastern wave approach, offshore linear ridges also impact wave transformation in this region. Specifically, the northeast extending shoal located at approximately 4,360,000 Northing, 574,000 Easting focuses wave energy that is subsequently focused by the shoals within Resource Area G3. In addition to wave heightening, wave energy divergence is caused by the bathymetric depression to the southwest of the resource areas, where wave height is reduced to approximately 1.0 m. Table 4-29 presents a summary of the areas experiencing increased wave heights along the coast for waves approaching from the east-southeast.

Table 4-29. Coastline areas experiencing increased wave heights during east-southeastern wave approach at Grid B2.

Approximate Location	Approximate Wave Height at Coast (m)
Between Brigantine Inlet and Little Egg Inlet	1.8 to 1.9
Brigantine Inlet and adjacent area to the south	1.6 to 1.7
North of Little Egg Inlet	1.6

East-Northeast Wave Approach

Figure 4-39 illustrates wave modeling results for Grid B2 for the east-northeast (22.5 degree) directional bin simulation. The east-northeast approach is highlighted by significantly larger wave heights (1.9 m) and rare occurrence levels (3.1% of the time). The large waves and low occurrence level is expected, because waves from this direction are dominated by the passing of northeast storms. Fluid transport is directed from north to south for this approach, as is sediment transport. Distinct areas of wave focusing and divergence are present for this directional approach; however, in many cases these areas of increased energy dissipate before arriving at the coast. The east-northeast approach direction appears to minimize the impact of the northeast extending offshore linear ridges. Yet, the overall wave height arriving at the coast is generally larger than the previously examined cases.

The shoals located along the primary linear ridge, and contained in the resource areas, generate small regions of wave convergence. For example, the shoal within Resource Area G2 top (at approximately 4,361,500 Northing; 564,000 Easting) produces waves up to 2.0 m high. Similar occurrences appear along the primary linear ridge. Most of the wave energy focused by shoals along the primary ridge dissipates before reaching the coast. A slight increase in wave energy was identified for the region just south of Brigantine Inlet caused by the convergence of wave energy over Resource Area G3. Wave heights in the region exceed 1.5 m.

The secondary array of remnant offshore linear ridges has a greater influence on wave transformation for the east-northeast wave approach than in previously examined cases. The shoal located at approximately 4,360,000 Northing, 574,000 Easting again focuses wave energy to over 2.1 m. This increase in wave energy, coupled with the depression to the southwest, produces a distinct band of wave convergence and wave divergence. Additional features along the southern portion of the offshore linear ridges produce supplementary variations in the wave

field. However, most of these transformations occur out of the area of interest or propagate into the region of unavailable bathymetric information. Table 4-30 presents a summary of the areas experiencing increased wave heights along the coast from waves approaching from the east-northeast.

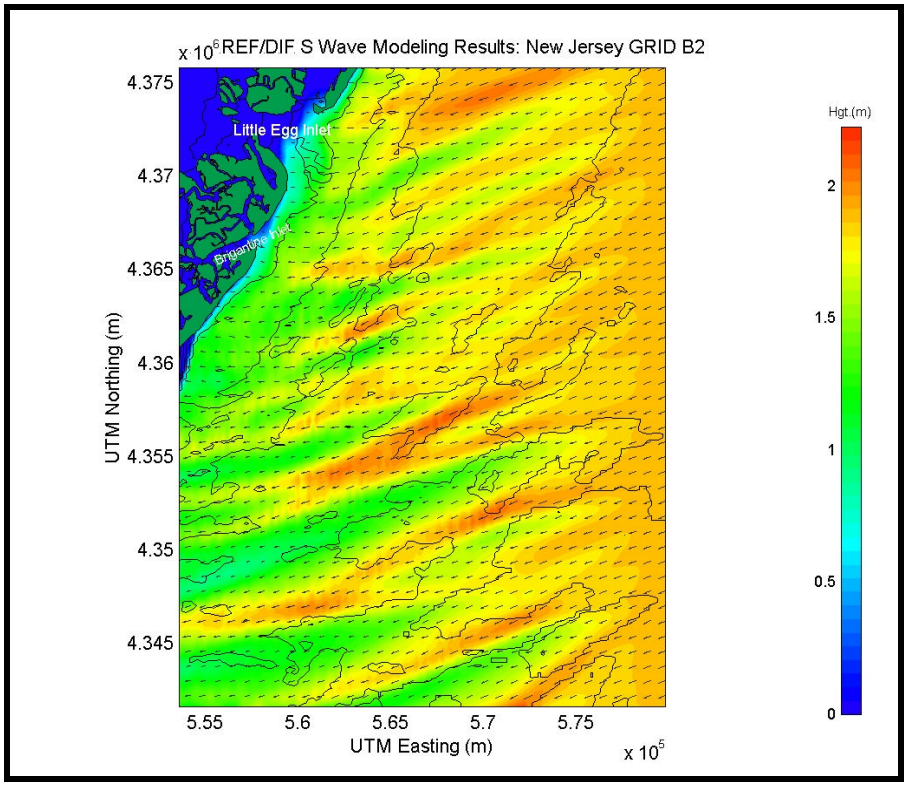

Figure 4-39. Spectral wave modeling results for existing conditions using an east-northeast (22.5 degree) approach direction for reference Grid B2.

Table 4-30. Coastline areas experiencing increased wave heights during east-northeast wave approach at Grid B2.

Approximate Location	Approximate Wave Height at Coast (m)
South of Brigantine Inlet	1.5 to 1.6

Southeast Wave Approach

Figure 4-40 illustrates wave modeling results for Grid B2 for the southeast (-45 degree) directional bin simulation. The southeast approach simulation has an input wave height of 1.5 m, the smallest significant wave height of the modeled approach simulations. The southeast approach direction contains 13.2% of the waves. In general, the areas of convergence and divergence are similar to the east-southeast approach direction. The southeast wave direction has less distinct regions of variation compared with previously examined cases. However, wave heights along the coast do fluctuate between approximately 1.1 and 1.7 m. Fluid transport is slightly south to north for this approach direction. Only subtle changes in wave direction near regions of convergence and divergence can be seen at the resolution of Figure 4-40.

Shoals extending along the primary linear ridge again play a major role in wave transformation patterns. The shoals of Resource Areas G2 and G3 focus wave energy on a region south of Little Egg Inlet and along the northern portion of the entrance to Little Egg Inlet, respectively. Wave heights range from approximately 1.7 to 1.8 m in these regions. Shoal features existing along the southern portion of the primary ridge cause wave height increases in the southern section of the modeling domain. Specifically, the shoal located at approximately 4,360,000 Northing, 561,000 Easting produces wave heights of 2.0 m and higher seaward of the town of Brigantine. Table 4-31 presents a summary of the areas experiencing increased wave heights along the coast from waves approaching from the southeast.

Table 4-31. Coastline areas experiencing increased wave heights during southeastern wave approach at Grid B2.

Approximate Location	Approximate Wave Height at Coast (m)
Entrance to Little Egg Inlet	1.7 to 1.8
South of Little Egg Inlet	1.7
Brigantine	1.8 to 1.9

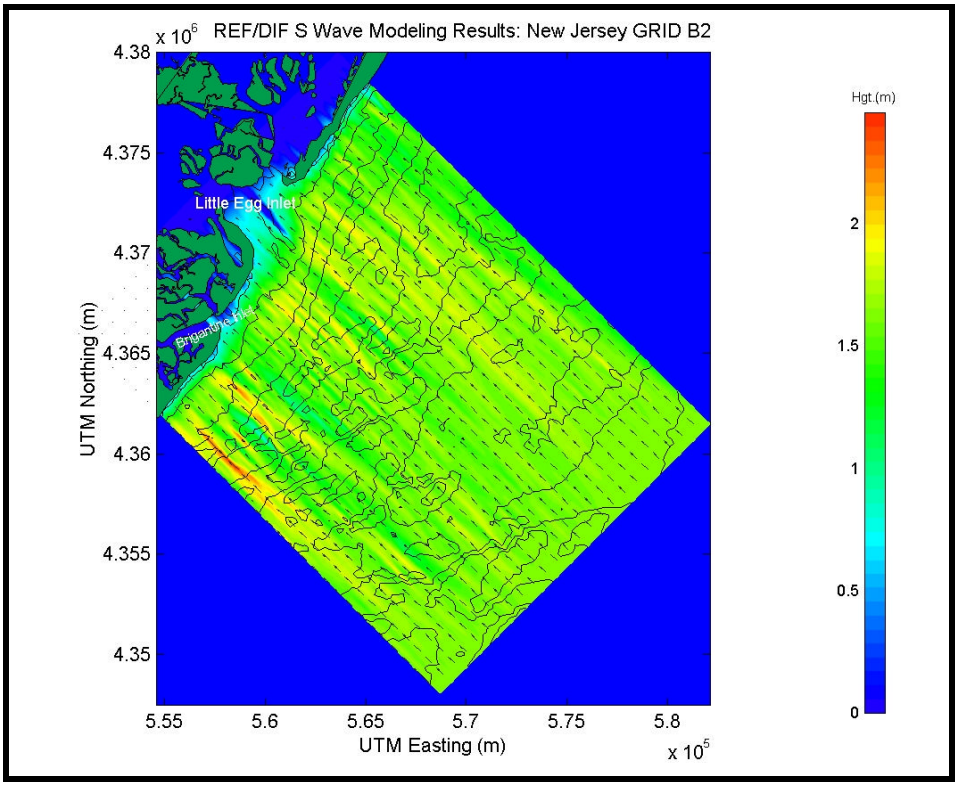

Figure 4-40. Spectral wave modeling results for existing conditions using a southeast (-45 degree) approach direction for reference Grid B2.

South-Southeast Wave Approach

Figure 4-41 illustrates wave modeling results for Grid B2 for the south-southeast (-67.5 degree) directional bin simulation. The south-southeast directional approach simulation has an input wave height of 1.6 m. Despite the wide angle of approach, the south-southeast approach direction still contains a major portion of the wave energy, 11.1% of the waves. In general, the

areas of convergence and divergence are similar to other southeast approach directions; however, the areas of wave energy focusing are less pronounced and more banded possibly due to the wide approach angle. Sediment and fluid transport is directed from south to north for this directional approach.

Irregular bathymetric features associated with the northeast extending offshore linear ridges create an area of increased wave energy in the southern portion of the modeling domain. The area from Brigantine Inlet north to a Little Egg Inlet experience wave heights ranging from 1.3 to 1.7 m. This region is south of the potential borrow sites and will not be affected by dredging within the Resource Areas. The shoals located within Resource Area G3 also produce a region of wave convergence, although it is less distinct than for other directional approaches. The convergence produces an increase in wave energy that impacts the coast north of Little Egg Inlet. Wave heights in this region are approximately 1.5 m. Although the increases in wave height are smaller than for other approach directions, Table 4-32 indicates areas experiencing slightly larger wave heights along the coast than other areas from waves approaching from the south-southeast.

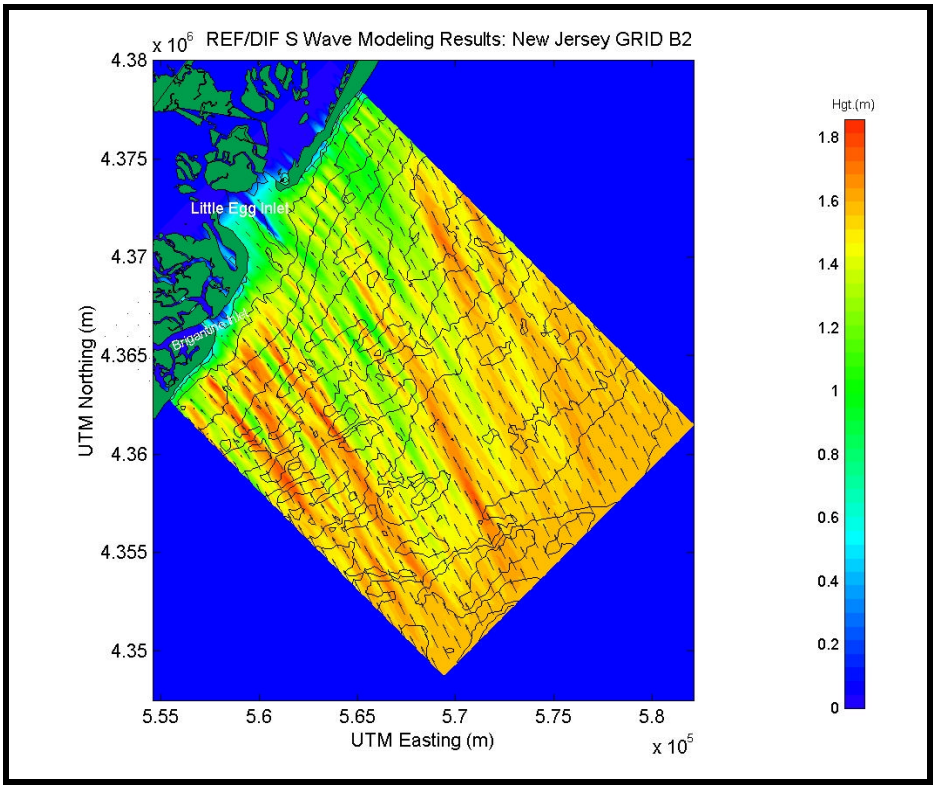

Figure 4-41. Spectral wave modeling results for existing conditions using a south-southeast (-67.5 degree) approach direction for reference Grid B2.

Table 4-32. Coastline areas experiencing increased wave heights during south-southeast wave approach at Grid B2.

Approximate Location	Approximate Wave Height at Coast (m)
North of Little Egg Inlet	1.5
Brigantine to South of Little Egg Inlet	1.4 to 1.7

4.4.3.2 High Energy Wave Events Simulations

Figure 4-42 illustrates wave transformation results for an estimated 50-yr northeast storm. The northeast storm simulation represents a rare occurrence as waves approach from the east and/or northeast with a wave height of 6.4 m. Waves respond to the seafloor much sooner than in the directional simulations, and they begin to dissipate energy near the offshore boundary of the grid. This also causes wave approach directions to be modified farther offshore. As a result, wave directions orient themselves perpendicular to the coast throughout the model domain. Fluid transport, as well as sediment transport, is directed from north to south during a typical northeast storm.

Wave transformation results for Grid B2 are comparable with results for Grids A and B1. The magnitude of waves, as well as the directional and frequency spectrum, remain the same. The northeast storm simulation is highlighted by increased wave height throughout the region. Wave convergence and divergence patterns caused by bathymetric features are less pronounced for large storm waves because wave height changes are small relative to the large initial wave height. In addition, the inclusion of storm surge reduces the impact of bathymetric features by deepening the water. Due to the magnitude of the 50-yr storm simulations, existing modeling techniques may be limited for simulation of long-period, high-energy wave events and the accuracy of results for these simulations is limited by the capabilities of the model (Section 4.2.1.2).

Figure 4-43 illustrates wave transformation results for an estimated 50-yr hurricane propagating over Grid B2. The hurricane simulation represents another rare occurrence as waves approach from the southeast with a wave height of 5.6 m. Similar to the northeast storm case, hurricane waves respond to the seafloor in deeper water than in the more commonly occurring directional simulations, and they begin to refract and dissipate energy at greater distances offshore. Waves are oriented nearly perpendicular to the coast throughout the model domain. Wave heights exceed 3.0 to 4.0 m for most areas along the coast.

4.4.3.3 Model Results Relative to Historical Shoreline Change

Figure 4-44 shows significant wave heights extracted along a transect line for the east (0 degree) approach simulation compared with historical shoreline change for the same region. The left-hand panel illustrates the nearshore wave transformation results for the east approach simulation, where the colormap represents wave height in meters. The solid black line in the left-hand panel represents the approximate breaker transect from which significant wave heights were extracted. The breaker transect line is very difficult to determine when using spectral wave models since there are a variety of waves, composed of different frequencies and directions, breaking at different times and locations throughout the domain. In addition, the orientation and irregularity of the coastline add difficulty to determining an exact breaker line at the grid resolution provided in the model. Therefore, the breaker line presented is intended only to provide a relative height distribution along the coast, rather than the exact region of wave breaking. The right-hand panel presents the historical shoreline change rates for this stretch of the New Jersey coast and is represented by a black line scaled by the bottom axis (m/yr). The significant wave height is added to the plot and represented by a green line and scaled by the upper axis (m).

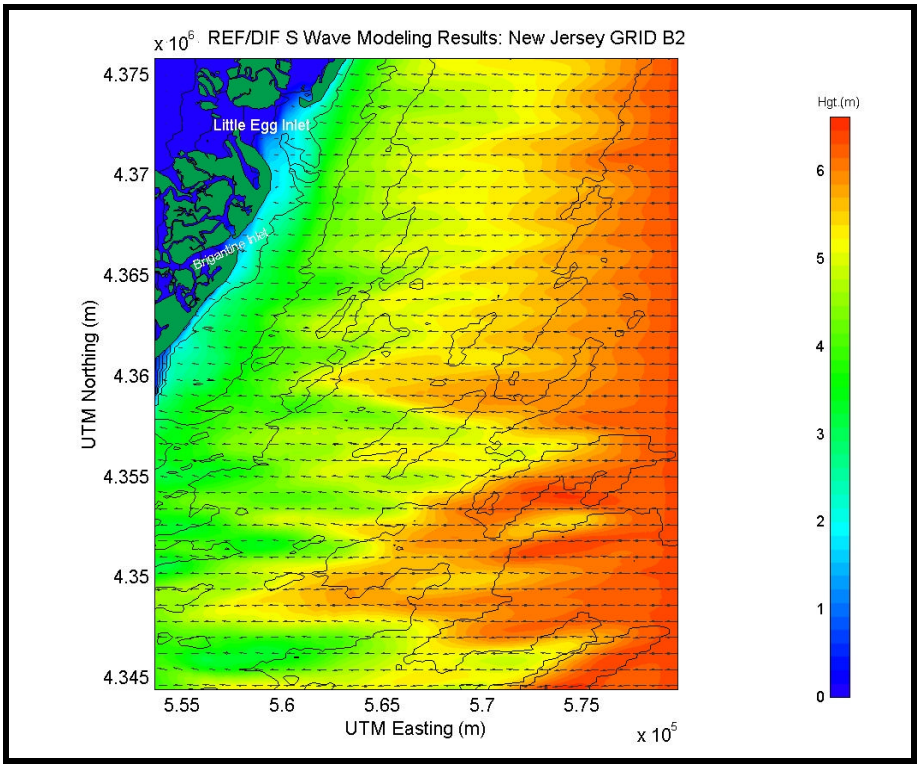

Figure 4-42. Spectral wave modeling results for existing conditions simulating an estimated 50-yr northeast storm event at reference Grid B2.

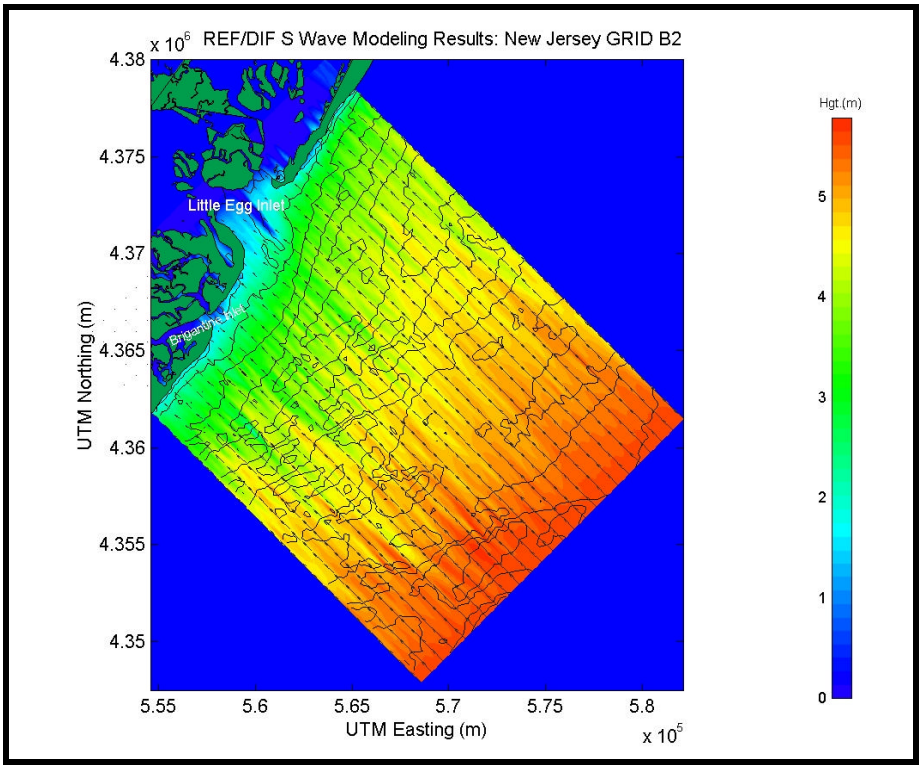

Figure 4-43. Spectral wave modeling results for existing conditions simulating an estimated 50-yr hurricane event at reference Grid B2.

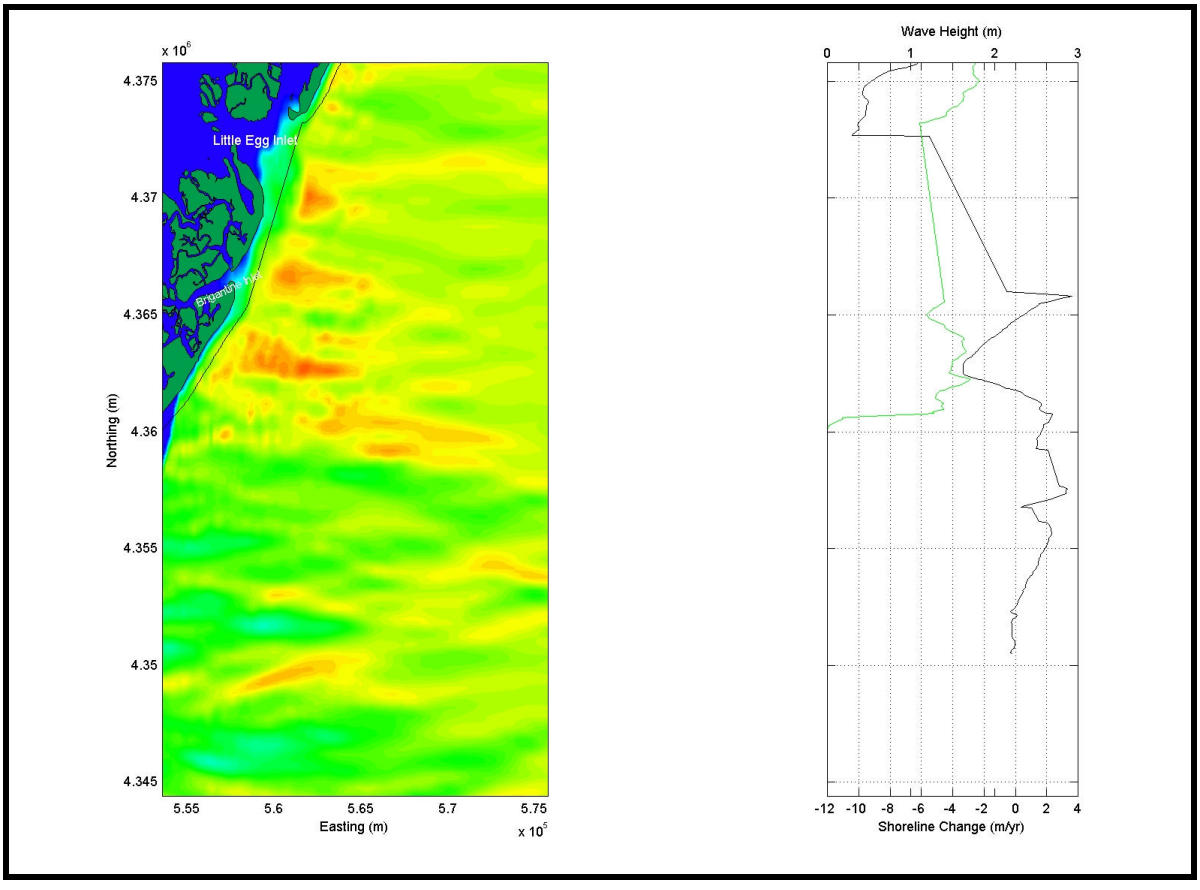

Figure 4-44. Wave height (green line, right-hand panel) taken from the approximate breaker line location (black line, left-hand panel) for the east (0 degree) approach simulation compared with historic shoreline change (black line, right-hand panel; 1864/68 to 1977).

For the region surrounding Little Egg Inlet, no historical shoreline change rates were computed due to lack of historical data. Therefore, wave heights in this region were not presented in Figure 4-44. Chapter 3 contains a detailed discussion of the historical shoreline change rates for this section of the New Jersey coast. For Grid B2, it is difficult to draw any concrete conclusions due to limited spatial data. However, in the eastern approach simulation, the wave height distribution along the coast is consistent with the historical shoreline change rates. For example, the historical shoreline retreat area near Brigantine Inlet (exceeding -2.0 m/yr) is an area highlighted by significantly higher wave heights, as denoted in Table 4-33.

Because Figure 4-44 represents only a percentage (approximately 15%) of the annual average wave energy impacting the coast (i.e., only energy associated with the eastern approach bin), it was anticipated that the wave height distribution and historic shoreline change rates may not correlate. Nonetheless, evaluation of each simulation can provide insight into potential areas of shoreline retreat and/or advance that may be caused by specific directional approaches. Comparisons of the remaining directional simulations with historical shoreline change rates can be found in Appendix B4.

Directional simulations can be combined to offer an idea of the annual wave climate, although a portion of the wave energy will be ignored when using the directional approach

method. Because each directional approach simulation represents a percentage of the total waves impacting the coast over an average year, the results of each simulation were superimposed to create an approximate representation of an annual wave climate. The combination of modeling simulations does not represent a complete year because not all the directional approaches are modeled (e.g., waves heading offshore, waves approaching the coast at wide angles). By weighting each simulation using the total modeled percentage, each directional approach can be combined to create the best estimate of the annual wave climate. Table 4-33 presents the allotment of percentages for each directional approach simulation.

Table 4-33. Percent occurrence weighting for simulated directional approach bins to reconstruct an approximate annual average wave climate for Grid B2.

Map Relative Direction (coming from)	Grid Relative Direction (coming from, 0E = E)	Modeled Percent Occurrence	Weighted Percent Occurrence
East-Northeast	22.5 *(11.26 to 33.75)*	3.1	5.2
East	0.0 *(-11.25 to 11.25)*	17.3	28.8
East-Southeast	-22.5 *(-33.75 to -11.24)*	15.2	25.4
Southeast	-45.0 *(-56.25 to -33.74)*	13.2	22.1
South-Southeast	-67.5 *(-78.75 to -56.24)*	11.1	18.5

Figure 4-45 shows the combined wave height distribution extracted along the approximate breaker line compared with historical shoreline change for the same region. The left-hand panel illustrates the transect (black line) from which significant wave heights were extracted. The right-hand panel presents historical shoreline change for this stretch of the New Jersey coast, as illustrated by a black line scaled by the bottom axis (m/yr). The combined wave height distribution for the directional approach simulations is represented by a green line and scaled by the upper axis (m).

Figure 4-45 illustrates a consistent correlation between historical shoreline change and the distribution of wave heights along the coast. Most of the region exhibits a wave ranging between 1.0 and 1.6 m, while shoreline change rates illustrate significant fluctuations, especially in regions adjacent to Little Egg Inlet. In areas where data are complete, the wave height distribution and historical shoreline change rates correlate relatively well. For example, the large erosional area (exceeding -3.0 m/yr) to the south of Little Egg Inlet is identified in most of the directional approach simulations as an area that experiences increased wave energy. As with other grids, numerous factors could explain the apparent lack of correlation along certain stretches of coast. Slight changes in the orientation and location of offshore shoals result in a shift in the location of areas of energy convergence and divergence. Therefore, any historical movement of the offshore shoals and or bathymetric depressions changes the location of increased wave energy along the coast. Because shoreline change information dates back to the mid-1800s, changes in the offshore bathymetry between 1864/68 and 1977 may account for the inconsistent correlation in wave height and shoreline retreat/advance. In addition, storm events may dominate shoreline response along this portion of coast, explaining the inconsistent correlation of directional wave height distribution and historical shoreline change rates. The directional approach combination applied does not identify the processes occurring during a specific storm event. Finally, human interference, such as engineering structures, inlet stabilization, and beach nourishment episodes, may also contribute to the areas of inconsistent correlation.

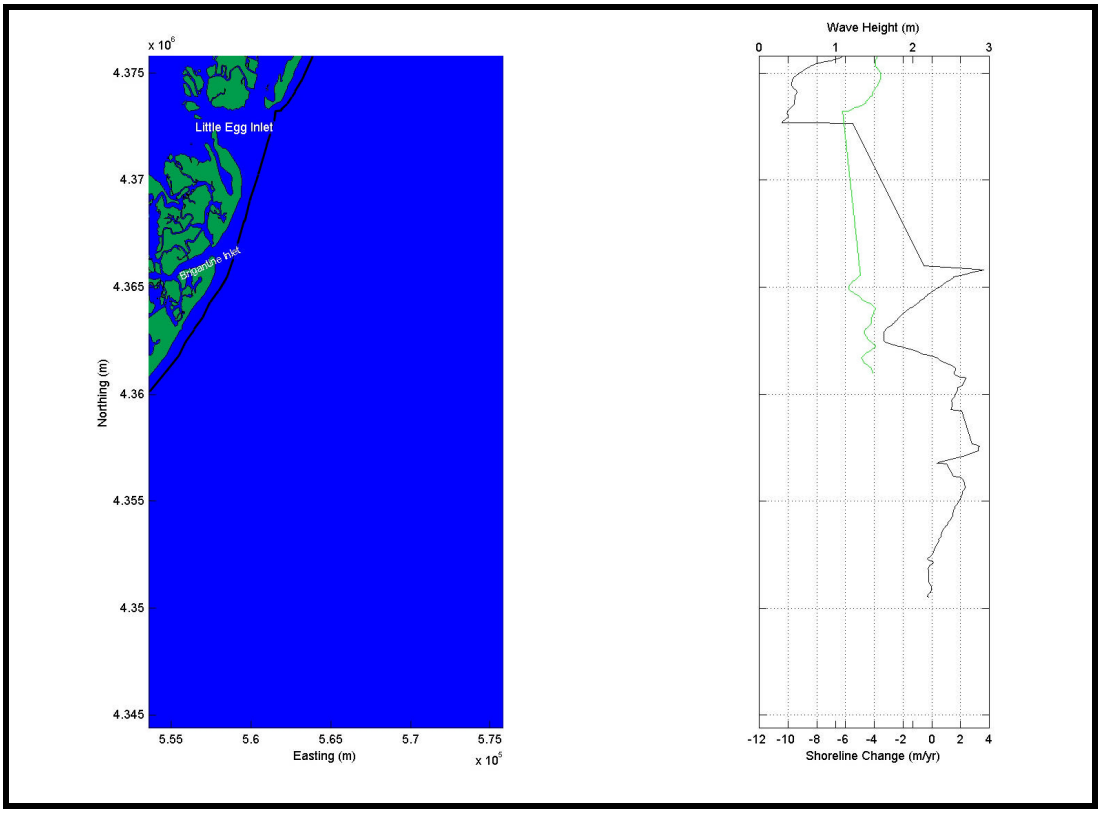

Figure 4-45. Wave height (green line, right-hand panel) taken from the approximate breaker line location(black line, left-hand panel) for combined directional approach simulations compared with historic shoreline change (black line, right-hand panel; 1864/68 to 1977).

4.4.4 Grid C Simulations

4.4.4.1 Directional Approach Simulations

Model simulations (for Grid C) were performed for typical wave conditions represented by directional spectra and extreme wave conditions represented with 50-yr storm spectra (estimated hurricane and Northeast storm) for existing (pre-dredging) conditions. Wave focusing, divergence, and shadowing occur at several locations throughout the Grid C modeling domain, which results in variable wave energy propagating towards the shoreline. Due to a general lack of irregular bathymetric features, the amount of variation is less than that exhibited in previously examined grids; however, there are specific bathymetric changes that produce significant variations in the wave heights along the nearshore region of Grid C. The single potential borrow site is located within a large offshore shoal (approximately 4,431,000 Northing; 591,000 Easting). Grid C consists of shore parallel contours in the nearshore region and sporadic shoals and depressions in the offshore region. Figure 4-46 identifies some of the major features in the offshore region, specifically near the proposed borrow site (F2).

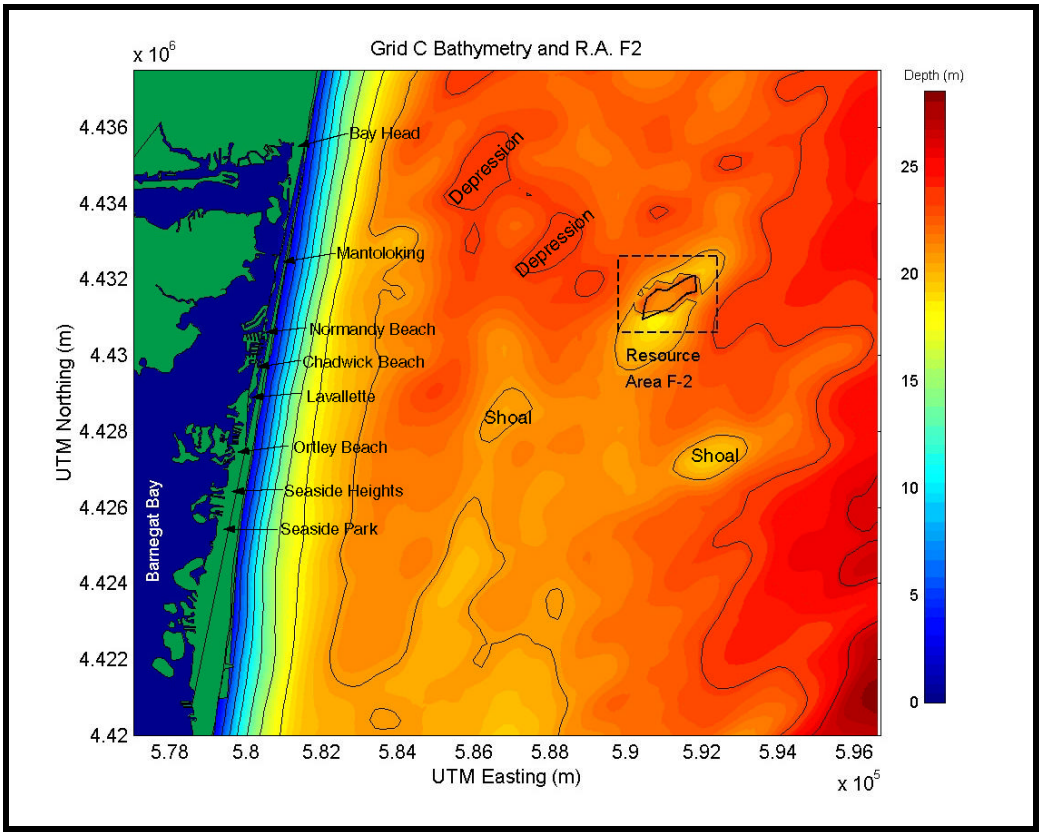

Figure 4-46. Location of key bathymetric features within Grid C and location of the proposed borrow site in Resource Ares F2.

East Wave Approach

Figure 4-47 illustrates wave model results for waves approaching from the east (0 degree directional bin simulation). For this case and all wave modeling result figures in this section, the color map corresponds to the distribution of significant wave height (m) throughout the modeling domain. Solid black lines represent bathymetric contours, and land masses are shown in green. The shoreline presented in the figures is a high water shoreline and is used here for presentation purposes only. The model runs were conducted at depths and shoreline positions corresponding to mean water. Arrows on the figure represent the modeled wave angle as they approach the shoreline.

The east (0 degree) approach bin consists of an input wave height of 1.5 m. Waves approach from this directional bin 19.2% of the time, which represents the most common approach direction for this grid. Fluid and sediment transport is directed from north to south in the nearshore region during an eastern wave approach. Changes in wave height and direction begin to occur at approximately the 20- to 23 m depth contour. Most of the spectral wave components do not interact with the seafloor at depths greater than 20 m. In general, zone of wave convergence and divergence are created from large shoals and depressions that dominate the offshore domain of the modeling grid.

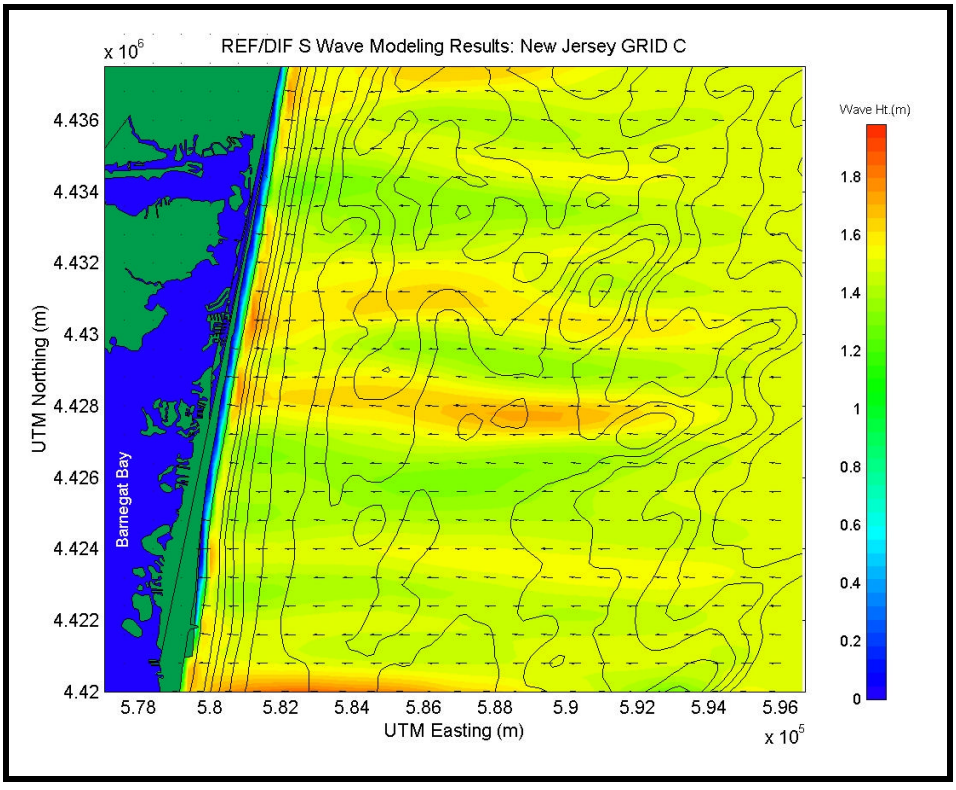

Figure 4-47. Spectral wave modeling results for existing conditions using an eastern approach direction (0 degree bin) for reference Grid C.

Resource Area F2, as well as the proposed borrow site, encompasses a large offshore shoal. This shoal, along with two secondary shoals to the south and southwest, appears to be a part of a remnant northeast extending offshore ridge. These shoals cause a majority of the wave modifications throughout Grid C. Specifically, the shoal in Resource Area F2 focuses wave heights to 1.7 to 1.8 m (an increase of 0.2 to 0.3 m). The increase in wave energy propagates to the coast and reaches a wave height of over 1.8 m prior to breaking. This area of increase extends from Chadwick Beach northward to Normandy Beach. The shoal located to the southwest of Resource Area F2, which influences the wave energy originally focused by the resource area, maintains wave convergence while directing it slightly to the south. The shoal located to the south of Resource Area F2 also produces a region of wave focusing, the most significant wave convergence in the domain. A wide band of wave energy propagates behind the shoal with wave heights reaching 1.7 to 1.8 m. This wave energy is maintained until it impacts the coast near Lavallette. The depressions to the northwest of Resource Area F2 produce a region of wave divergence, and therefore, lower wave heights. This reduction in wave energy is also evident at the coast, near Bay Head, where wave heights are approximately 1.2 m.

For this directional approach, there are two significant regions of increased wave heights along the coast. Table 4-34 presents a summary of the areas experiencing increased wave heights along the coast from waves approaching from the east. For the eastern directional approach, wave directions remain relatively constant throughout the modeling domain, although areas of significant convergence or divergence do exhibit a visual change.

Table 4-34. Coastline areas experiencing increased wave heights during eastern wave approach at Grid C.	
Approximate Location	Approximate Wave Height at Coast (m)
Lavallette	1.7 to 1.8
Chadwick Beach to Normandy Beach	1.7 to 1.8

East-Southeast Wave Approach

Figure 4-48 illustrates REF/DIF S results for Grid C for the east-southeast (-22.5 degree) directional bin simulation. The input wave height for the east-southeast approach direction is also 1.5 m. The east-southeast approach simulation contains 18.9% of the total waves, making this approach direction the second most common. The east-southeast approach direction is almost perpendicular to the orientation of the coastline, and fluid transport is directed slightly from the south to north. The results from the east-southeast approach simulation exhibit similar wave patterns as the eastern wave approach, with distinctive areas of wave convergence and divergence occurring primarily behind the shoals highlighted earlier. These two zones of wave energy are a consistent characteristic in the Grid C modeling domain.

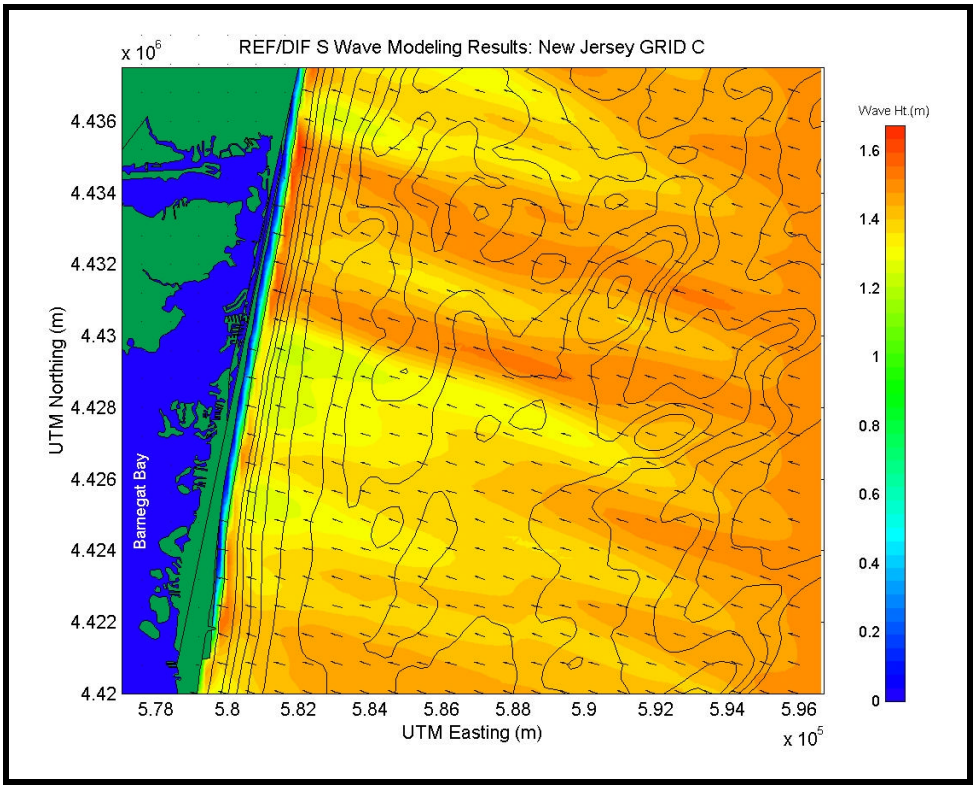

Figure 4-48. Spectral wave modeling results for existing conditions using an east-southeast (-22.5 degree) approach direction for reference Grid C.

Shoals in the offshore region of the domain produce the most significant zones of wave convergence. The shoal in Resource Area F2 produces an increase in wave height to approximately 1.6 m that impacts the coast near Bay Head. The shoal located to the south of Resource Area F2 also produces wave heights that increase to approximately 1.6 m and they do not significantly dissipate before reaching the coast between Normandy Beach and Mantoloking.

Overall, wave transformation patterns for the east-southeast approach are similar to the eastern approach simulation. However, differences do exist in the location of convergence zones along the coast. Table 4-35 presents a summary of areas experiencing increased wave heights along the coast from waves approaching from the east-southeast.

Table 4-35. Coastline areas experiencing increased wave heights during east-southeast wave approach at Grid C.

Approximate Location	Approximate Wave Height at Coast (m)
Between Normandy Beach and Mantoloking	1.6
Bay Head	1.6

East-Northeast Wave Approach

Figure 4-49 illustrates REF/DIF S results for the east-northeast (22.5 degree) directional bin simulation. As in all examined areas, the east-northeast approach is highlighted by significantly larger wave heights (1.8 m) and rare occurrence levels (2.6% of the time). Large waves and low percent occurrence is expected, because waves out of this direction most likely are dominated by northeast storms. Fluid and sediment transport are directed from north to south for this approach. As in the east and east-southeast approach simulations, two distinct zones of wave focusing are caused by the presence of offshore shoals.

The shoal located within Resource Area F2 produces a zone of wave energy that produces wave heights in excess of 1.8 m. The increase in wave energy dissipates to approximately 1.7 m before impacting the coast near Chadwick Beach and Lavallette. The shoal located to the south of Resource Area F2 also produces a zone of increased wave energy with wave heights over 1.8 m. This increased wave energy impacts the coastline south of Seaside Park. An area in the northern portion of the modeling domain also experiences larger wave heights. However, because features along the northern boundary of the modeling domain shape this wave focusing, the confidence level in this energy zone is limited. Table 4-36 presents a summary of the areas experiencing increased wave heights along the coast.

Table 4-36. Coastline areas experiencing increased wave heights during east-northeastern wave approach at Grid C.

Approximate Location	Approximate Wave Height at Coast (m)
South of Seaside Park	1.7 to 1.8
Mantoloking	1.6 to 1.7
Lavallette north to Chadwick Beach	1.6 to 1.8

Northeast Wave Approach

Figure 4-50 illustrates wave modeling results for the northeast (45 degree) directional bin simulation. The northeast wave approach direction was added to the simulations due to the orientation of the northern New Jersey shoreline, as well as the potential influence on sediment transport. The northeast simulation consists of large wave heights (1.7 m) and low occurrence (1.9%). Like the east-northeast approach, the northeast simulation represents a strong northerly approach to the coast. Fluid and sediment transport is north to south for this approach direction. Only subtle changes in wave direction near regions of convergence and divergence can be seen at the resolution of Figure 4-50.

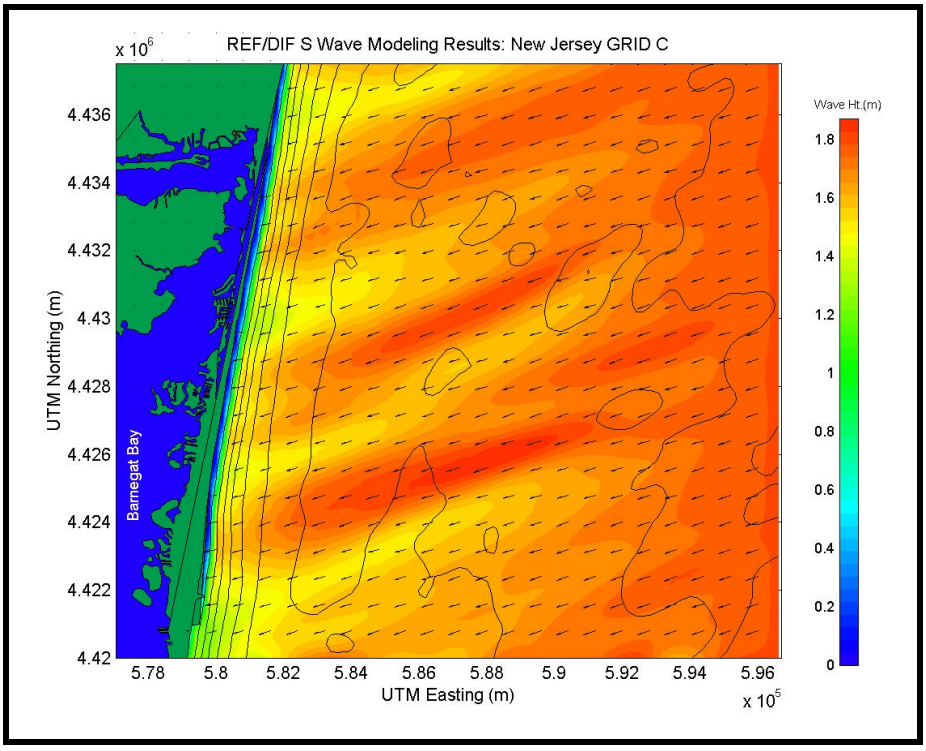

Figure 4-49. Spectral wave modeling results for existing conditions using an east-northeast (22.5 degree) approach direction for reference Grid C.

Two distinct zones of increased wave energy appear within the model domain. Specifically, the shoal in Resource Area F2 focuses wave energy impacting the coast near Seaside Heights. Wave heights range from approximately 1.7 to 1.8 m in these regions. The shoal to the south of Resource Area F2 also produces a zone of increased wave energy that impacts the coast south of Seaside Park. Table 4-37 presents a summary of the areas experiencing increased wave heights along the coast from waves approaching from the northeast.

Table 4-37. Coastline areas experiencing increased wave heights during northeast wave approach at Grid C.

Approximate Location	Approximate Wave Height at Coast (m)
Seaside Heights	1.7 to 1.8
South of Seaside Park	1.7 to 1.8

Southeast Wave Approach

Figure 4-51 illustrates wave modeling results for the southeast (-45 degree) directional bin simulation. This simulation has an input wave height of 1.5 m, which is the same as the east and east-southeast approach simulations. The southeast approach direction contains 14.6% of the waves. In general, the areas of convergence and divergence match the east-southeast approach direction, especially the two zones of increased wave energy produced by the shoals surrounding Resource Area F2. The southeast directional approach represents a slightly southern approach to the coast. Fluid and sediment transport is slightly south to north for this approach direction. Only subtle changes in wave direction near regions of convergence and divergence can be seen at the resolution of Figure 4-51.

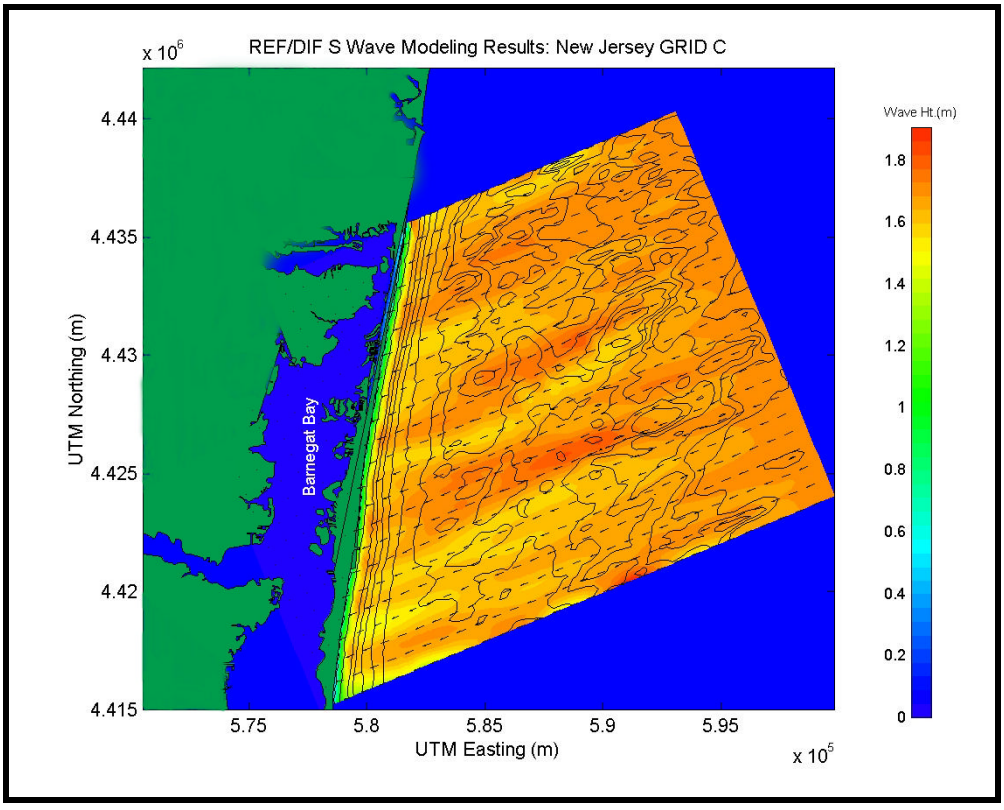

Figure 4-50. Spectral wave modeling results for existing conditions using a northeastern (45 degree) approach direction for reference Grid C.

For the southeast approach direction, shoals located within and surrounding Resource Area F2 produce wave convergence and divergence in the modeling domain. Specifically, the shoal within Resource Area F2 produces an increase in wave height to approximately 1.6 m. The focused wave energy advances to the coast and impacts the Bay Head region. The shoal to the south of Resource Area F2 also focuses wave energy, which is recast in form by the shoal to the southwest of Resource Area F2. The wave height in this energy zone approaches approximately 1.6 m, and it impacts the coast near Mantoloking. To the north, an offshore shoal appears due to the rotation of the modeling domain and causes an additional increase in wave energy, as wave heights exceed 1.7 m. This wave focusing is out of the primary area of interest and impacts the coast near Sea Girt. Table 4-38 presents a summary of the areas experiencing increased wave heights along the coast from waves approaching from the southeast.

Table 4-38. Coastline areas experiencing increased wave heights during southeast wave approach at Grid C.

Approximate Location	Approximate Wave Height at Coast (m)
Sea Girt	1.7 to 1.8
Mantoloking	1.5 to 1.6
Bay Head	1.5 to 1.6

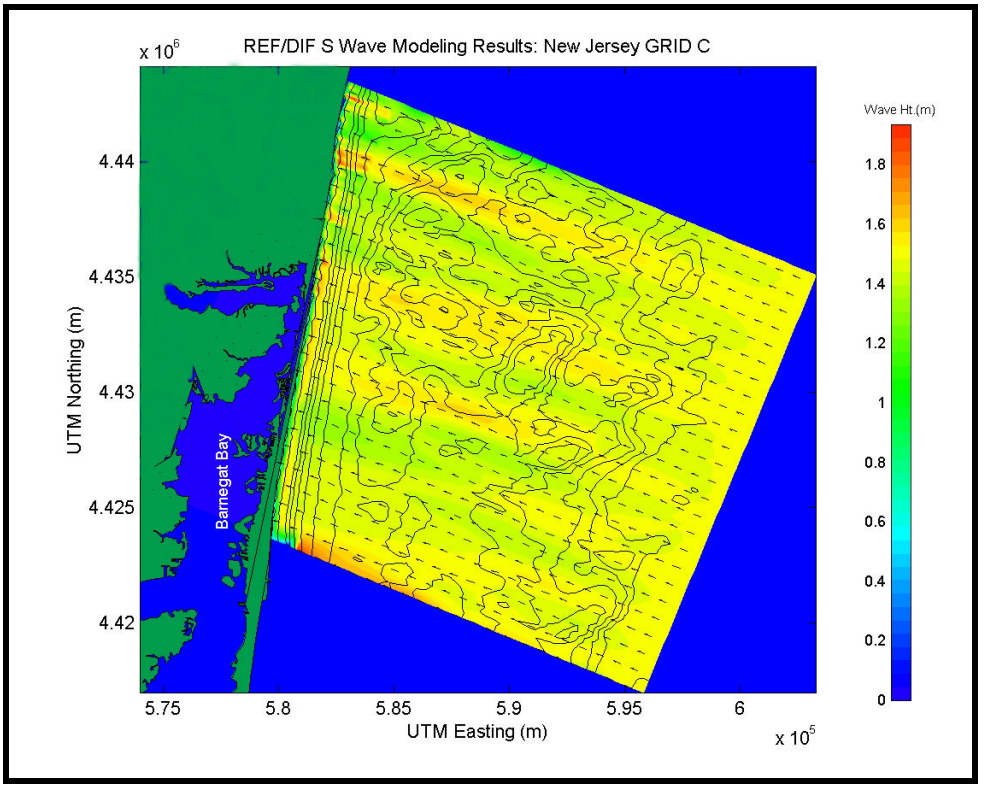

Figure 4-51. Spectral wave modeling results for existing conditions using a southeastern (-45 degree) approach direction for reference Grid C.

South-Southeastern Wave Approach

Figure 4-52 illustrates wave modeling results for the south-southeast (-67.5 degree) directional bin simulation. This approach simulation has an input wave height of 1.3 m, the smallest of the simulated directional approaches. Despite the wide angle of approach, the south-southeast approach direction still contains a major portion of the wave energy, 10.2% of the waves. In general, the areas of wave convergence and divergence are similar to other southeast approach directions; however, the areas of focusing are less distinct possibly due to the wide approach angle and smaller incoming waves. Sediment and fluid transport is directed from south to north for this directional approach, and is opposite the primary direction of sediment movement.

Although wave convergence caused by the shoals in and around Resource Area F2 is less evident (most likely due to both the smaller wave heights and wide approach angle), the effects of these bathymetric features can be documented. The wave energy focused throughout the domain is able to dissipate significantly before propagating to the coast. Specifically, shoals within and surrounding Resource Area F2 result in increased wave heights to approximately 1.4 m, but in each case, the focused wave energy dissipates before reaching the coast. Most of the coast experiences wave heights less than or equal to 1.0 m in the south-southeastern simulation. A region of increased wave energy (1.4 to 1.5 m) is visible along the southern edge of the modeling domain; however this is likely due to waves entering the domain through the lateral boundary. Although the increases in wave height are smaller than other approach directions, Table 4-39 presents a summary of the areas experiencing slightly larger wave heights along the coast.

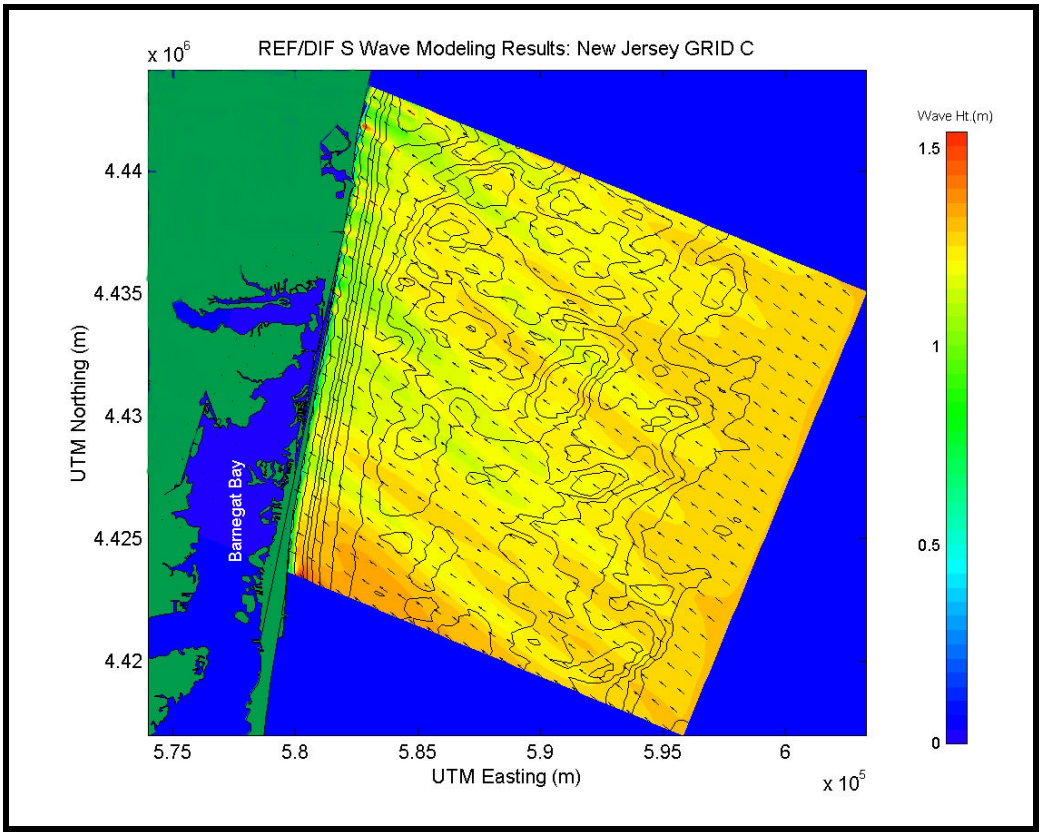

Figure 4-52. Spectral wave modeling results for existing conditions using a south-southeastern (-67.5 degree) approach direction for reference Grid C.

Table 4-39. Coastline areas experiencing increased wave heights during south-southeast wave approach at Grid C.

Approximate Location	Approximate Wave Height at Coast (m)
Between Ortley Beach and Lavallette	1.3
South of Seaside Park	1.5

4.4.4.2 High Energy Wave Events Simulations

Figure 4-53 illustrates wave transformation results for an estimated 50-yr northeast storm. As with the other grids, the northeast storm simulation represents a rare occurrence as waves approach from the east and/or northeast with a wave height of 6.4 m. The magnitude of the northeast storm, as well as the directional and frequency spectrum, remains the same as simulated in earlier grids. The northeast storm simulation is highlighted by an increased wave height throughout the region. Wave convergence and divergence patterns caused by bathymetric features are less pronounced for these large storm waves because changes caused by bathymetry are small when compared with the large wave height. In addition, the inclusion of storm surge in the model simulation reduces the impact of the bathymetric features by deepening the water. The results of the simulation are similar to those presented for other grids. However, wave convergence caused by the shoal within Resource Area F2, as well as the shoal to the south, are visibly evident in the Grid C results. Wave heights in the lee of seafloor features exceed 6.0 m and impact the coast between Ortley and Normandy Beaches.

Due to the magnitude of the 50-yr storm simulations, existing modeling techniques may be limited for simulation of long-period, high-energy wave events and the accuracy of results for these simulations is limited by the capabilities of the model (section 4.2.1.2).

Figure 4-54 illustrates wave transformation results for an estimated 50-yr hurricane propagating over Grid C. The hurricane simulation represents a rare occurrence as waves approach from the southeast with a wave height of 5.6 m. Similar to the northeast storm case, waves respond to the seafloor in deeper water than for directional simulations, and they begin to refract and dissipate energy a greater distance offshore. Waves are oriented nearly perpendicular to the coast throughout the model domain. The influence of shoals in and south of Resource Area F2 produces an increase in wave height. In addition, the offshore shoal to the north creates a zone of increased wave energy, most of which dissipates before propagating to the coast. Wave heights exceed 3.0 to 4.0 m for most areas along the coast, except for the regions landward of shoals (near Bay Head and Mantoloking), where wave heights reach 5.0 m.

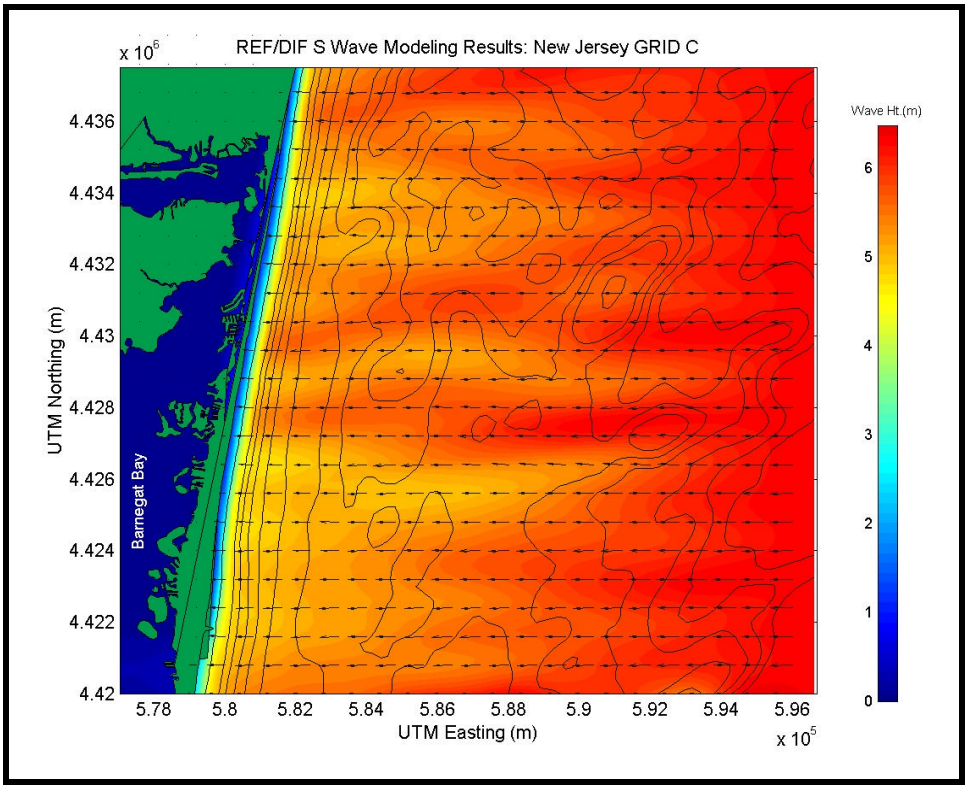

Figure 4-53. Spectral wave modeling results for existing conditions simulating an estimated 50-yr northeast storm event at reference Grid C.

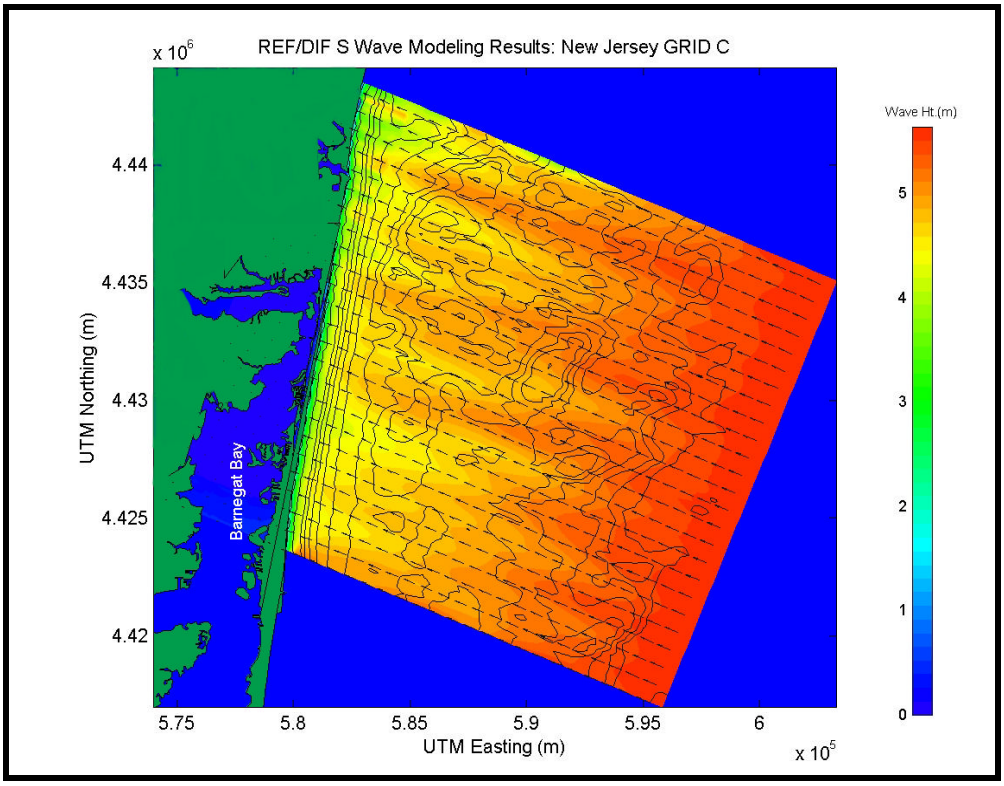

Figure 4-54. Spectral wave modeling results for existing conditions simulating an estimated 50-yr hurricane event at reference Grid C.

4.4.4.3 Model Results Relative to Historical Shoreline Change

Figure 4-55 shows significant wave heights extracted along a transect line for the east (0 degree) and east-southeast (-22.5 degree) approach simulations compared with historical shoreline change. The solid black line on the colormaps represents the approximate breaker transect from which significant wave heights were extracted. The breaker transect line is very difficult to determine when using spectral wave models because there are a variety of waves, composed of different frequencies and directions, breaking at different times and locations throughout the domain. Therefore, the breaker line presented is intended to provide a relative breaker location along the coast, rather than the exact region of wave breaking. The plots associated with each colormap present historical shoreline change rates for this stretch of the New Jersey coast and are represented by a black line scaled by the bottom axis (m/yr). Significant wave height is added to the plot and represented by a green line and scaled by the upper axis (m).

Overall, historical shoreline change rates for the region are relatively consistent, with a majority of the shoreline experiencing shoreline advance. Significant shoreline advance is indicated at the southern boundary of the modeling domain, where the influence of Barnegat Inlet begins to appear. Chapter 3 contains a detailed discussion of historical shoreline change rates for this section of the New Jersey coast. The area of increased wave heights caused by the offshore shoals near Resource Area F2 shifts to the north in the east-southeast approach. For both the east and east-southeast approach simulations, the wave height distributions along the coast do not correlate well with the historical shoreline change rates. Comparisons of the remaining directional simulations to historical shoreline change rates can be found in Appendix B4.

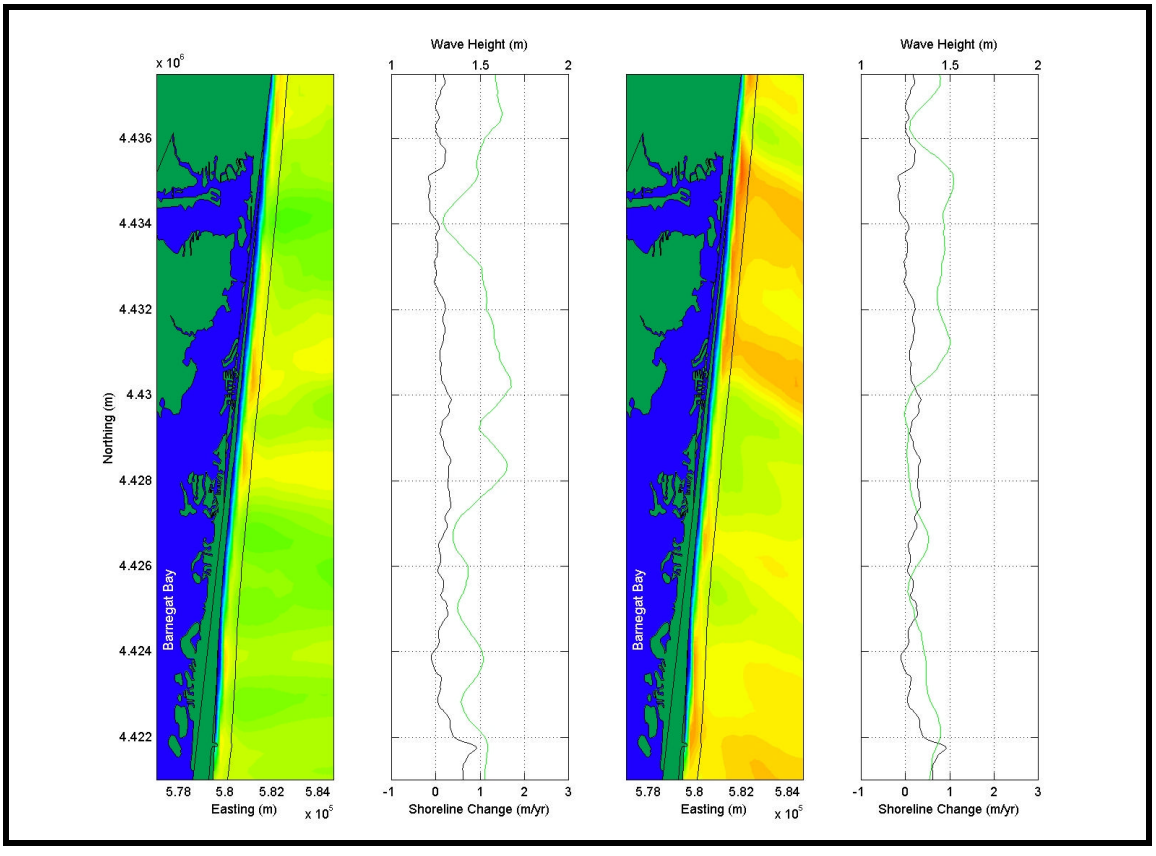

Figure 4-55. Wave height (green line, left-hand center and right-hand panels) taken from approximate breaker line (black line, left-hand and right-hand center panels) for the east (0 degree) and east-southeast (-22.5 degree) approach simulations, compared with historical shoreline change rates (black line, left-hand center and right-hand panels; 1864/68 to 1977).

Similar to other grids, the directional simulations can be combined to estimate the annual wave climate, although a portion of the wave energy will be ignored when using the directional approach method. Because each directional approach simulation represents a percentage of the total waves impacting the coast over an average year, the results of each simulation were superimposed to create an approximate representation of the annual wave climate. The combination of modeling simulations does not represent a complete year because not all the directional approaches are modeled (e.g., waves heading offshore, waves approaching the coast at wide angles). By weighting each simulation using the total modeled percentage, each directional approach can be combined to create an estimate of the annual wave climate. Table 4-40 presents the allotment of percentages for each directional approach simulation.

Figure 4-56 shows the combined wave height distribution extracted along the approximate breaker line position compared with historical shoreline change for the same region. The left-hand panel illustrates the transect (black line) from which significant wave heights were extracted. The right-hand panel presents historical shoreline change rates as a black line scaled by the bottom axis (m/yr). The combined wave height distribution for the directional approach simulations is represented by a green line, scaled by the upper axis (m).

Table 4-40. Percent occurrence weighting for simulated directional approach bins to reconstruct an approximate annual average for Grid C.

Map Relative Direction (coming from)	Grid Relative Direction (coming from, 0E = E)	Modeled Percent Occurrence	Weighted Percent Occurrence
Northeast	45.0 *(33.76 to 56.25)*	1.9	2.8
East-Northeast	22.5 *(11.26 to 33.75)*	2.6	3.9
East	0.0 *(-11.25 to 11.25)*	19.2	28.5
East-Southeast	-22.5 *(-33.75 to -11.24)*	18.9	28.0
Southeast	-45.0 *(-56.25 to -33.74)*	14.6	21.7
South-Southeast	-67.5 *(-78.75 to -56.24)*	10.2	15.1

Most of the region exhibits consistent wave heights of approximately 1.3 to 1.4 m, and shoreline change rates illustrate predominantly advance with minor fluctuations. Numerous factors could explain the discrepancies in correlation between wave height and shoreline change throughout Grid C. Slight changes in the orientation and location of offshore shoals result in shifts in the location of areas of energy convergence and divergence. Therefore, any historical movement of the offshore shoals and or bathymetric depressions may change the location of increased wave energy along the coast. In addition, storm events may dominate shoreline change along this portion of the coast, explaining the inconsistent correlation between wave height distribution and historical shoreline change rates.

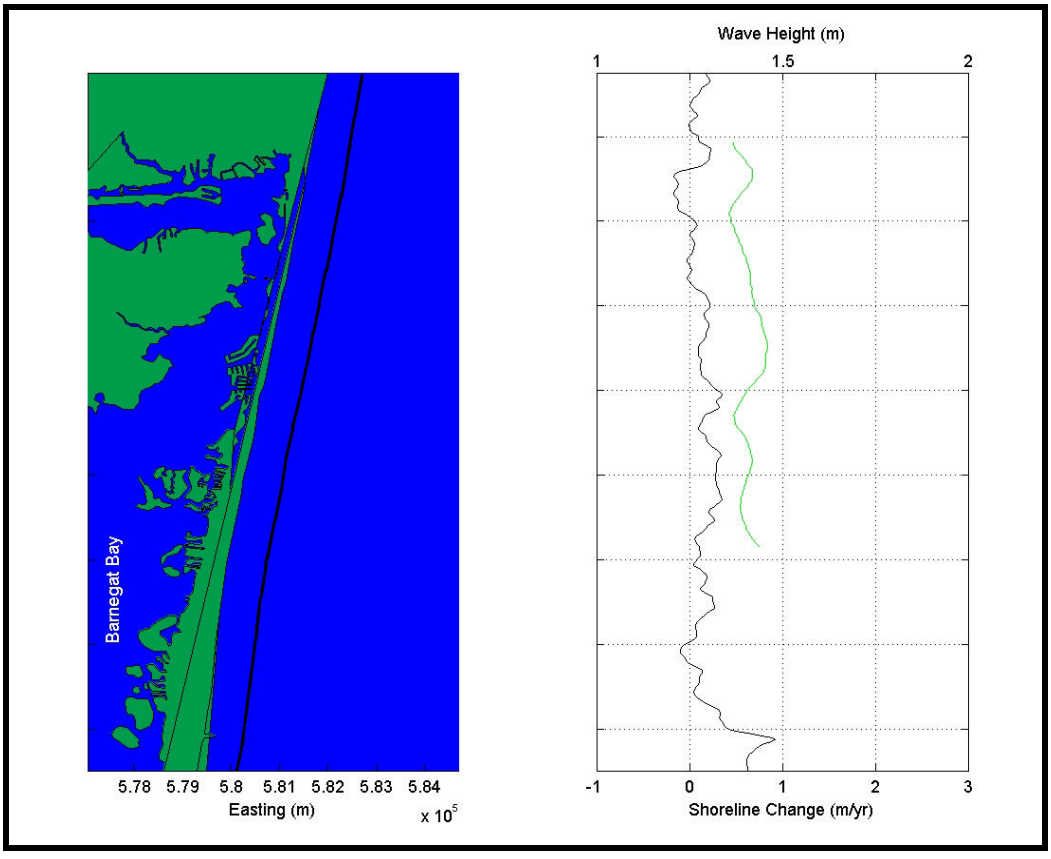

Figure 4-56. Wave height (green line, right-hand panel) taken from the approximate breaker line (black line, left-hand panel) for combined directional approach simulations compared with historical shoreline change rates (black line, right-hand panel; 1864/68 to 1977).

4.5 COMPARISON OF PRE- AND POST-DREDGING RESULTS

4.5.1 Grid A Simulations

4.5.1.1 Post-Dredging Results

Following wave modeling runs for existing conditions, simulations were performed for post-dredging scenarios. Results were produced for each of the directional bin spectra and the 50-yr storm events to evaluate potential physical impacts of offshore sand mining. Figure 4-57 presents the results for the eastern approach bin (Grid A) for the post-dredging scenario. The color map corresponds to the distribution of significant wave height (m) throughout the model domain. The solid black lines represent bathymetric contours. Other than the differences in bathymetry, the same boundary conditions were used in the simulation to produce results shown in Figure 4-57.

The same general wave patterns described in Section 4.4.1 are evident in the post-dredging model results (e.g., wave focusing behind Shoals 1 and 2). It is difficult to visually identify any significant differences between pre- and post-dredging results. This is true for all directional and 50-yr storm simulations. Because modifications to the wave field are not very evident after initial inspection of results, evaluation is that the impact of potential sand mining operations on the wave field can be considered small compared with natural changes occurring throughout the model domain. The remaining simulated post-dredging model results for Grid A can be found in Appendix B5.

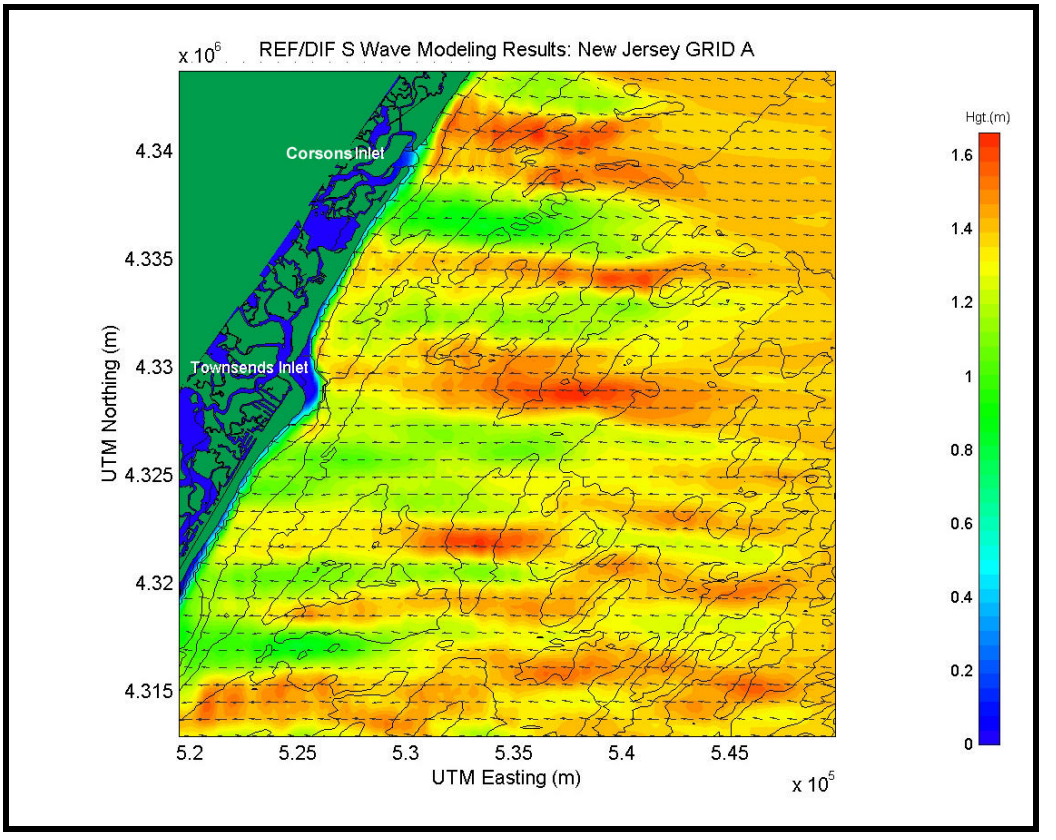

Figure 4-57. Spectral wave modeling results for post-dredging scenario using an eastern (0 degree) approach direction for reference Grid A.

4.5.1.2 Existing Conditions Versus Post-Dredging Seasonal Results

Differences in wave heights (between pre- and post-dredging results) were computed at each grid point within the model domain to document potential impacts caused by specific sand mining scenarios. Pre-dredging wave simulations were subtracted from the post-dredging wave results so that positive (negative) differences indicate an increase (decrease) in wave height related to sand mining at potential borrow sites. In all directional cases, maximum increases/decreases in wave height range from ±0.3 to 0.6 m. In most cases, a significant amount of the modification caused by the sand mining dissipates before reaching the coast.

Figure 4-58 is a difference plot for the eastern (0 degree) approach simulation presented in Figures 4-18 (pre) and 4-57 (post). A different color map is applied to illustrate the difference plots. The white polygons on each figure represent the proposed sand borrow sites. Dark blue colors indicate a decrease in wave height, while green shades indicate an increase in wave height. As expected, sand mining creates a zone of decreased wave energy behind the sand borrow site and increased energy adjacent to the borrow site. Comparison of pre- and post-dredging scenarios represents a unique case for Grid A because the two borrow sites in Resource Areas A1 and A2 can have a cumulative effect on the waves from certain approach directions. For example, waves passing over Resource Area A2 may propagate and be effected by sand dredging in Resource Area A1.

A maximum increase of approximately 0.15 m (11% increase relative to offshore significant wave height) and a maximum decrease of 0.4 m result from the sand extraction scenario for Resource Areas A1 and A2 for the eastern wave approach simulation. The oblong shape of the borrow site in Resource Area A2 produces some interesting effects when approached directly from the east. The bend in the borrow site causes the area to behave like two distinct borrow sites. There is a significant amount of mixing of the decrease/increase regions. In addition, some waves that propagate over Resource Area A2 are then deflected again by Resource Area A1, an interaction that hinders the natural dissipation process.

Difference plots for the remaining directional simulations for Grid A are presented in Appendix B6. During the other directional approach simulations, patterns of wave modifications are comparable. The areas of divergence and convergence occur in a similar manner for all cases. Wave height decreases directly behind the borrow sites and increases in adjacent areas. Maximum increases/decreases in wave height are similar (± 0.2 to 0.6 m) to those for the eastern approach.

During the east-northeast (22.5 degree) approach, wave changes have a greater distance to propagate before reaching the coast. Therefore, although the input wave is greater, the changes caused by sand dredging have less of an impact during the east-northeast approach than the other cases. The east-southeast (-22.5 degree) approach simulation exhibits maximum changes of ±0.2 m. Modifications to the wave field are very distinct for this approach (east-southeast) and the interaction between the two potential borrow sites is more evident. The southeast (-45 degree) and south-southeast (-67.5 degree) approach directions are similar, with maximum differences approaching 0.6 m. Changes in these two cases are more consolidated compared to the other simulations due to the direction of approach. As in the other cases, a majority of the wave energy dissipates before it reaches the coast.

Table 4-41 presents the areas along the coast that are impacted by the potential offshore dredging at Resource Areas A1 and A2 for each directional approach simulation. The table presents the approximate location of each impact area, as well as the magnitude of the increase or decrease and the percent change relative to the offshore wave height. In all cases, the percent change is small, with a maximum increase of +15.0%. Gray rows indicate increases in wave height experienced at the coast caused by the potential dredging, while white rows

indicate decreases caused by the potential dredging. In certain areas, potential offshore dredging may be beneficial by reducing the height in an area that experienced greater wave energy under existing conditions. Overall, the impact caused by potential offshore dredging at sand borrow sites during normal conditions is relatively small. At most, only minor changes are expected in the wave field and nearshore sediment transport potential.

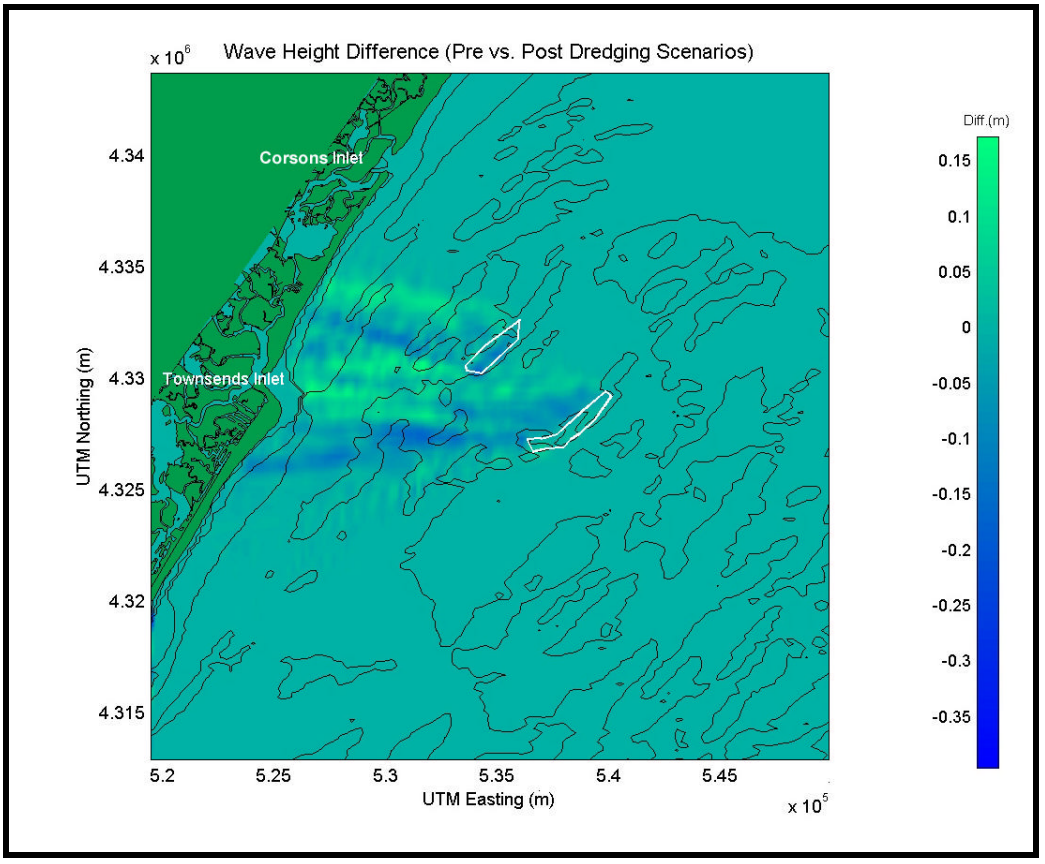

Figure 4-58. Wave height modifications resulting from potential offshore mining at Sand Resource Areas A1 and A2 for the eastern (0 degree) approach simulation. Green shades identify areas of increased wave height, while blue shades identify areas of decreased wave height.

Table 4-41. Coastline regions impacted by potential offshore dredging in Resource Areas A1 and A2.

Approach Direction	Approximate Shoreline Location	Approximate UTM Northing (m)	Wave Height Change (m) at Coast	Percent Change
East (0E)	Sea Isle City	4,334,000	+0.11	+8.4
East (0E)	North of Townsends Inlet	4,330,500	+0.04	+2.9
East (0E)	Seven Mile Beach / South Avalon	4,326,000	-0.10	-8.3
East (0E)	South of Sea Isle City	4,332,700	-0.05	-3.6
E-SE (-22.5E)	Sea Isle City	4,334,000	-0.20	-12.5
E-SE (-22.5E)	Whale Beach	4,335,700	+0.21	+15.0
E-SE (-22.5E)	South of Sea Isle City	4,331,000	+0.15	+12.0
SE (-45E)	Northern Sea Isle City / Whale Beach	4,335,000	-0.19	-12.7
SE (-45E)	Sea Isle City	4,334,000	+0.09	+5.6
SE (-45E)	Entrance to Corsons Inlet	4,339,500	+0.09	+6.0
S-SE (-67.5E)	Northern Sea Isle City / Whale Beach	4,335,000	+0.15	+9.4
S-SE (-67.5E)	South of Corsons Inlet	4,339,000	-0.20	-12.5
E-NE (22.5E)	North of Townsends Inlet	4,330,500	-0.09	-5.6
E-NE (22.5E)	Avalon / South Avalon	4,326,000	+0.09	+6.4

4.5.1.3 High Energy Wave Event Results

Differences in wave heights were also computed for 50-yr storm simulations to identify potential impacts of offshore sand mining. Figures 4-59 and 4-60 show results for the 50-yr hurricane and 50-yr northeast storm, respectively. A similar distribution of wave energy change as indicated in the directional results is illustrated (i.e., wave energy reduction directly behind the borrow site and an adjacent increase in energy). The change plots for the hurricane and northeast storm simulations indicate a maximum increase in wave height of approximately 1.4 m (24.5% increase over offshore wave heights) and 0.8 m (12.5% increase), respectively. A wave reduction of 0.6 m is observed in the shadow zones of borrow sites.

In Grid A, a significant amount of wave energy is dissipated before the waves reach the shore as modifications to wave heights are less than 0.4 m along a majority of the coast. Shoreline areas from Corsons Inlet south to Sea Isle City may experience minor changes in wave energy and sediment transport during a typical hurricane and northeast storm event. However, relative to the magnitude of the incoming waves, a change of 0.4 m is not expected to have a significant effect during a large storm event that has impacted the coast.

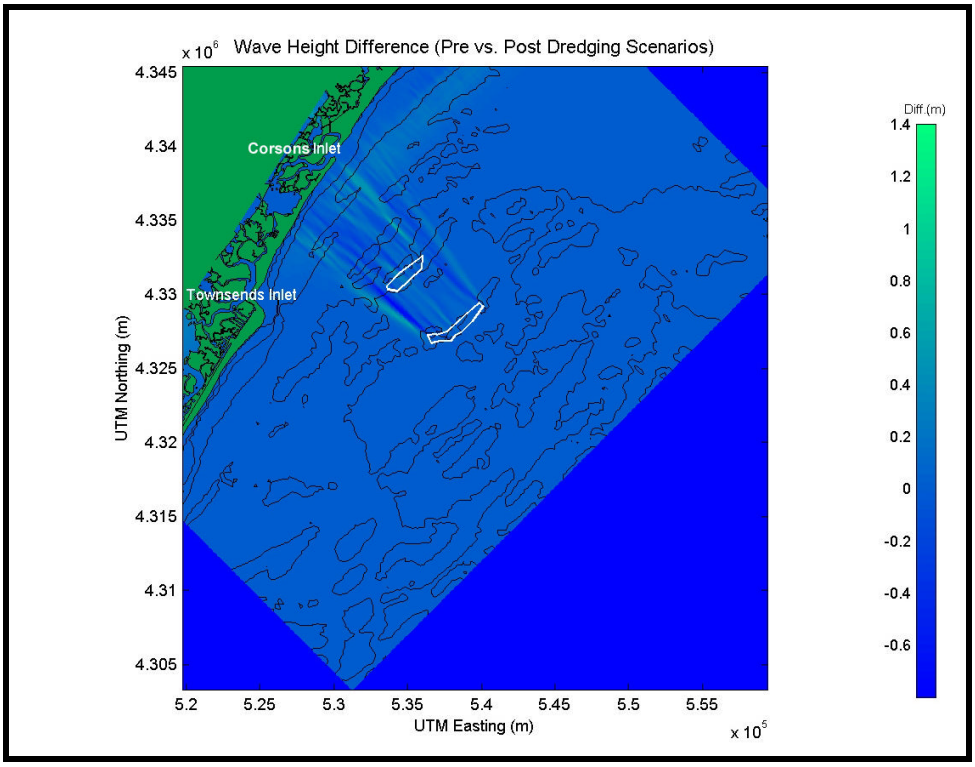

Figure 4-59. Wave height modifications resulting from potential offshore mining in Sand Resource Areas A1 and A2 for a 50-yr hurricane event. Green shades identify areas of increased wave height, while blue shades identify areas of decreased wave height.

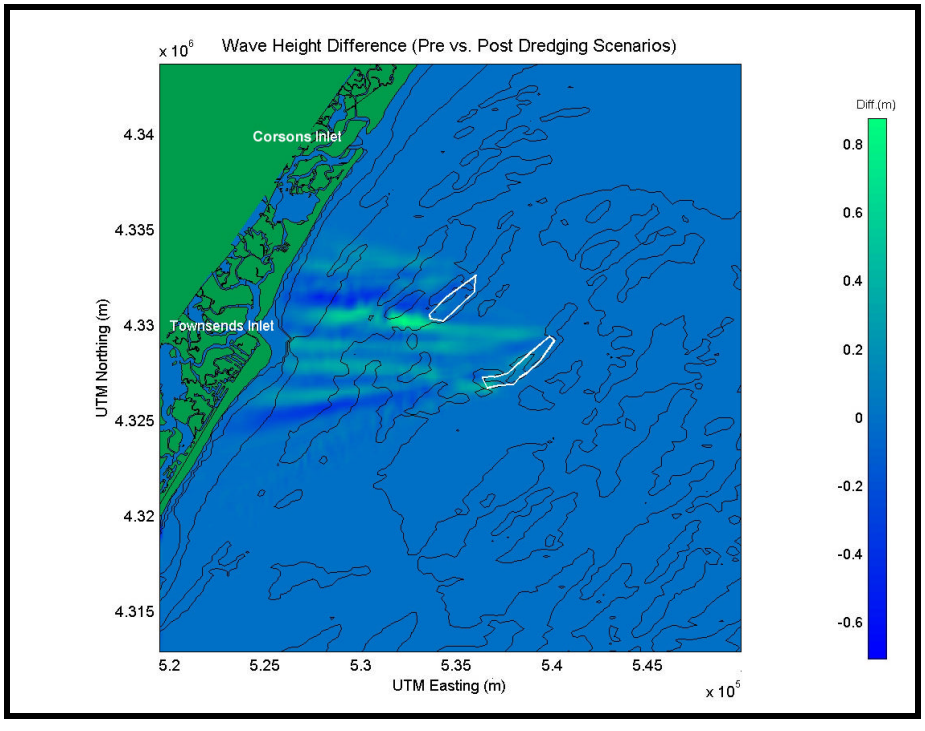

Figure 4-60. Wave height modifications resulting from potential offshore sand borrow sites in Resource Areas A1 and A2 for a 50-yr northeast storm event. Green shades identify areas of increased wave height, while blue shades identify areas of decreased wave height.

4.5.2 Grid B1 Simulations

4.5.2.1 Post-Dredging Results

Following wave modeling runs for existing conditions, simulations were performed for post-dredging scenarios. Results were produced for each of the directional bin spectra and the 50-yr storm events to evaluate potential physical impacts of offshore sand mining. Figure 4-61 presents wave transformation results for the eastern wave approach bin (Grid B1) for the post-dredging scenario. The color map corresponds to the distribution of significant wave height (m) throughout the model domain. The solid black lines represent bathymetric contours. Other than the differences in bathymetry, the same boundary conditions were used in the simulation to produce pre-dredging results (see Figure 4-28.)

Post-dredging model results illustrate the same wave patterns as those described for pre-dredging model runs (e.g., impact of the offshore northeast extending linear ridges). It is difficult to visually identify any significant differences between the pre- and post-dredging results. This is true for all directional and 50-yr storm simulations. Because the modifications to the wave field are not evident, the impact of the potential sand mining operations on the wave field can be considered small compared with natural changes occurring throughout the model domain. Due to the visual similarity in wave propagation patterns, the remaining simulated post-dredging model results can be found in Appendix B5.

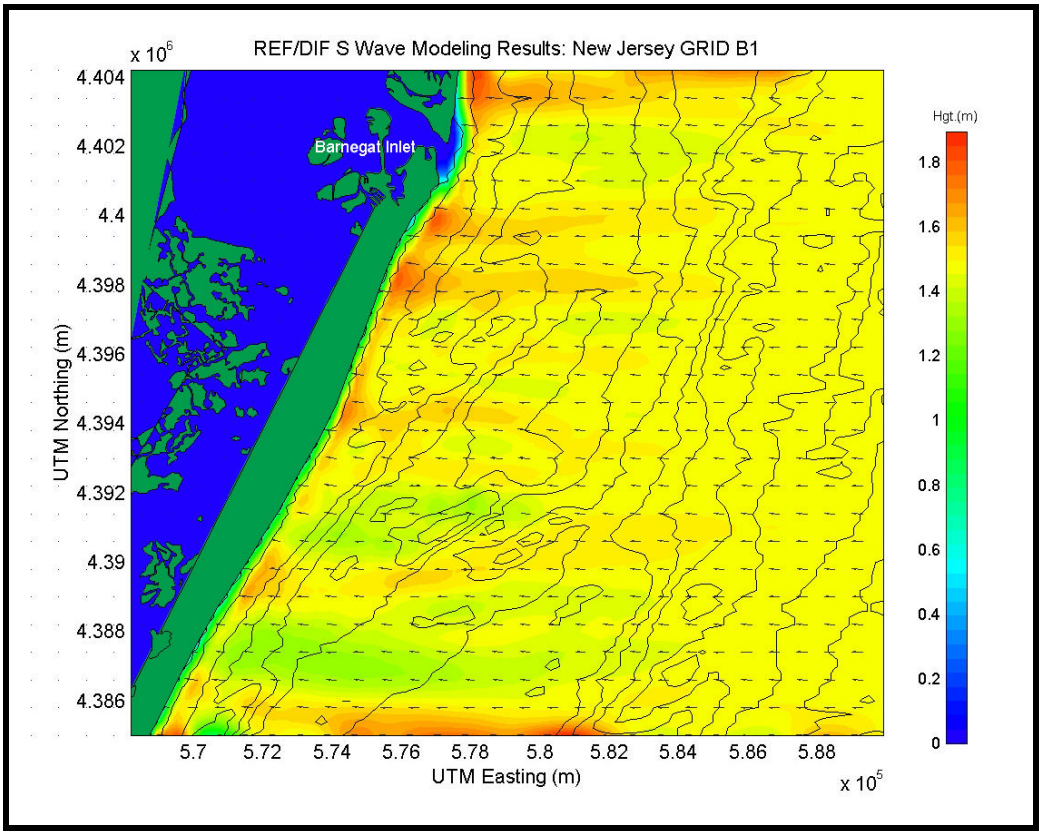

Figure 4-61. Spectral wave modeling results for post-dredging scenario using an the eastern (0 degree) approach direction for reference Grid B1.

4.5.2.2 Existing Conditions Versus Post-Dredging Seasonal Results

Differences in wave heights between pre- and post-dredging model runs were computed at each grid point within the model domain to document potential impacts caused by specific sand mining scenarios. Pre-dredging wave simulations were subtracted from the post-dredging wave results so that positive (negative) differences indicate an increase (decrease) in wave height related to sand mining at potential borrow sites. In all directional cases, maximum changes in wave height ranged from ±0.07 to 0.12 m, significantly smaller than those experienced at Grid A. However, unlike Grid A, a significant amount of the modification caused by potential sand mining does not dissipate before reaching the coast. In addition, because there is only one proposed borrow site in Grid B1, the difference results appear much smoother than those for Grid A.

Figure 4-62 is a difference plot for the eastern (0 degree) approach simulation presented in Figures 4-28 and 4-61. The white polygon in Figure 4-62 shows the location of the proposed sand borrow site. Dark blue colors indicate a decrease in wave height, while green shades represent an increase in wave height. As expected, sand mining creates a zone of decreased wave energy behind the sand borrow site and increased energy adjacent to the borrow site. Waves propagating over the sand borrow site are deflected outward, while a zone of reduced wave height is created directly behind the borrow site. A maximum increase of approximately 0.12 m and a maximum decrease of about 0.2 m result from the sediment extraction scenario for Resource Area C1 for the eastern approach simulation.

Difference plots for the remaining directional simulations for Grid B1 are presented in Appendix B6. For the other directional approach simulations, wave modification patterns are comparable. Areas of divergence and convergence occur in a similar manner for all cases. Wave height decreases directly behind the borrow site and increases in adjacent areas. Maximum changes are similar to the eastern approach (± 0.1 to 0.2 m), except during a south-southeast wave approach, where changes are smaller (± 0.07 to 0.15 m) due to the smaller incoming wave heights. As expected, wave modification impact zones along the coast vary based on direction of wave approach.

The primary dissimilarity among the various difference plots is the areas along the coast affected by potential offshore dredging. Table 4-42 presents the areas impacted by potential offshore dredging at Resource Area C1 for each directional approach simulation. The table presents the approximate location of each impact area, as well as the magnitude of change and percent change relative to existing wave heights. In all cases, the percent change is small, with a maximum increase of +14.0%. Gray rows indicate increases in wave height predicted at the coast and caused by potential dredging activities, whereas white rows indicate decreases caused by potential dredging operations. In certain areas, proposed offshore dredging may be beneficial to the physical environment by reducing wave heights in an area that experienced increased wave energy under existing conditions. For example, during the east-southeast approach, wave height reduction of approximately 0.15 m occurs between Loveladies and Harvey Cedars, an area that under existing conditions experiences an increase in wave energy. However, in other areas, potential offshore dredging causes an increase in wave height that experienced heightened wave energy under existing conditions.

Overall, the impact caused by potential offshore dredging at sand borrow sites during normal conditions is relatively small. At most, only minor changes are expected in the wave field and nearshore sediment transport patterns.

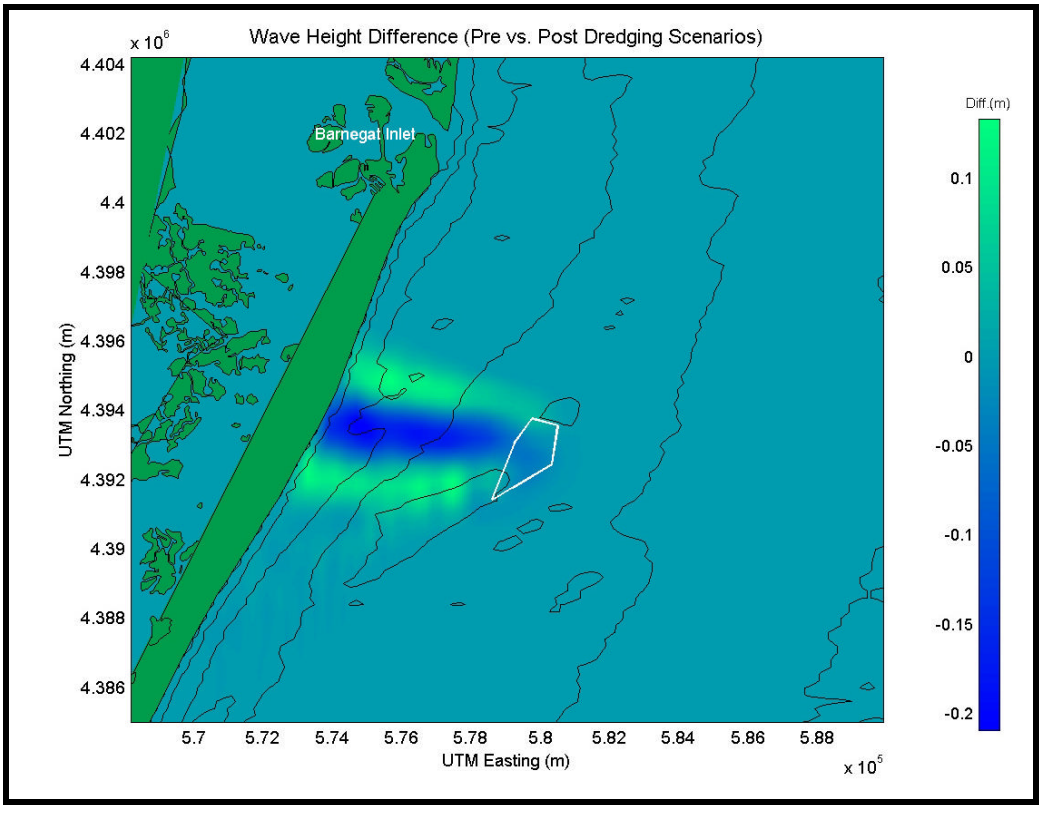

Figure 4-62. Wave height modifications resulting from potential offshore mining at the proposed sand borrow site in Resource Area C1 for the eastern (0 degree) approach simulation. Green shades identify areas of increased wave height, while blue shades identify areas of decreased wave height.

Table 4-42. Coastline regions impacted by the potential offshore dredging of Resource Area C1.

Approach Direction	Approximate Shoreline Location	Approximate UTM Northing (m)	Wave Height Change (m) at Coast	Percent Change
East (0E)	Harvey Cedars	4,394,000	+0.10	+6.7
East (0E)	South of Harvey Cedars / North of Surf City	4,392,000	+0.10	+7.7
East (0E)	North of Harvey Cedars / South of Loveladies	4,396,000	-0.17	-9.4
E-SE (-22.5E)	Between Harvey Cedars and Loveladies	4,395,250	-0.15	-6.3
E-SE (-22.5E)	Loveladies	4,396,250	+0.10	+6.3
E-SE (-22.5E)	Harvey Cedars	4,394,000	+0.10	+6.5
SE (-45E)	Loveladies	4,396,250	-0.16	-10.0
SE (-45E)	North of Harvey Cedars	4,395,000	+0.10	+8.3
SE (-45E)	Between Loveladies and Barnegat Inlet	4,400,000	+0.12	+7.5
S-SE (-67.5E)	South of Barnegat Inlet	4,401,000	+0.07	+8.2
S-SE (-67.5E)	Between Loveladies and Barnegat Inlet	4,400,000	-0.14	-14.0
S-SE (-67.5E)	Loveladies	4,396,250	+0.04	+4.6
E-NE (22.5E)	Ship Bottom	4,388,750	+0.05	+4.2
E-NE (22.5E)	Surf City	4,390,750	-0.15	-10.7
E-NE (22.5E)	South of Harvey Cedars	4,392,500	+0.10	+5.5

4.5.2.3 High Energy Wave Event Results

Differences in wave heights were also computed for 50-yr storm simulations to identify potential impacts of offshore sand mining. Figures 4-63 and 4-64 show results for the 50-yr hurricane and 50-yr northeast storm, respectively. A similar distribution of wave energy change as is illustrated relative to directional results (i.e., wave energy reduction directly behind the dredged area and an adjacent increase in energy). The difference plots for the hurricane and northeast storm simulations indicate a maximum increase in wave height of approximately 0.16 m (3.4% increase) and 0.4 m (5.7% increase), respectively. Wave height reduction of 0.2 to 0.5 m is observed in the shadow zones of borrow sites. The changes are significantly less than those observed at Grid A.

Unlike Grid A, a significant amount of wave energy does not dissipate before reaching the shore. Shoreline areas from Harvey Cedars north to Barnegat Inlet may experience a change in wave height and sediment transport during a typical hurricane event. During a typical northeast storm, shoreline areas from Surf City north to Harvey Cedars may experience a change in wave height and sediment transport patterns. However, relative to the magnitude of incoming waves, the changes exhibited at this grid are not expected to have a significant effect during a large storm event.

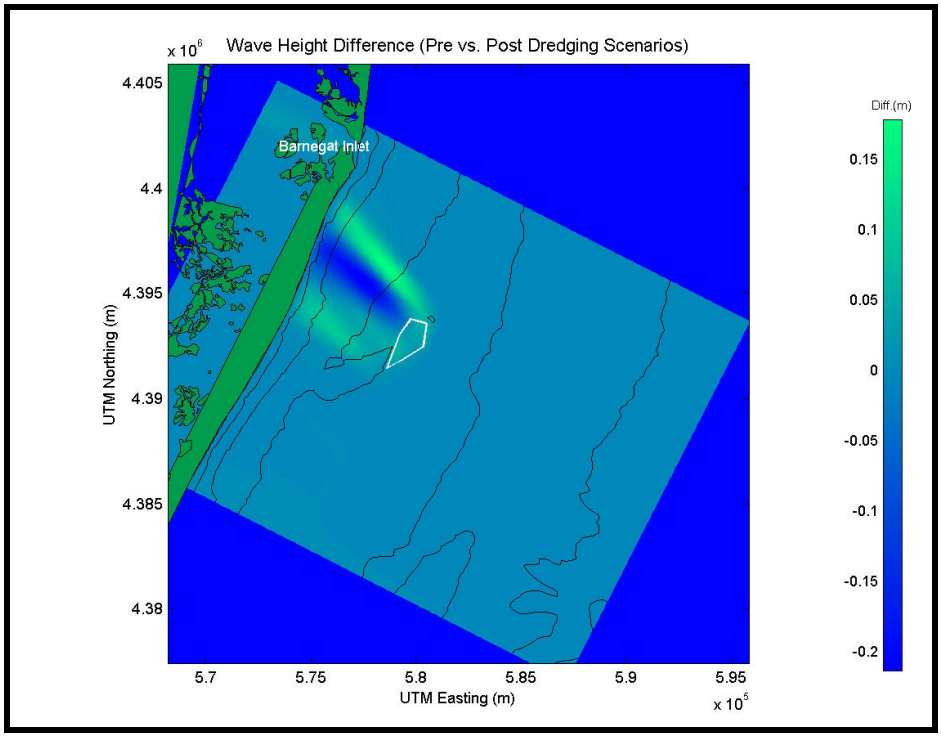

Figure 4-63. Wave height modifications resulting from potential offshore mining at the proposed borrow site in Resource Area C1 for a 50-yr hurricane event. Green shades identify areas of increased wave height, while blue shades identify areas of decreased wave height.

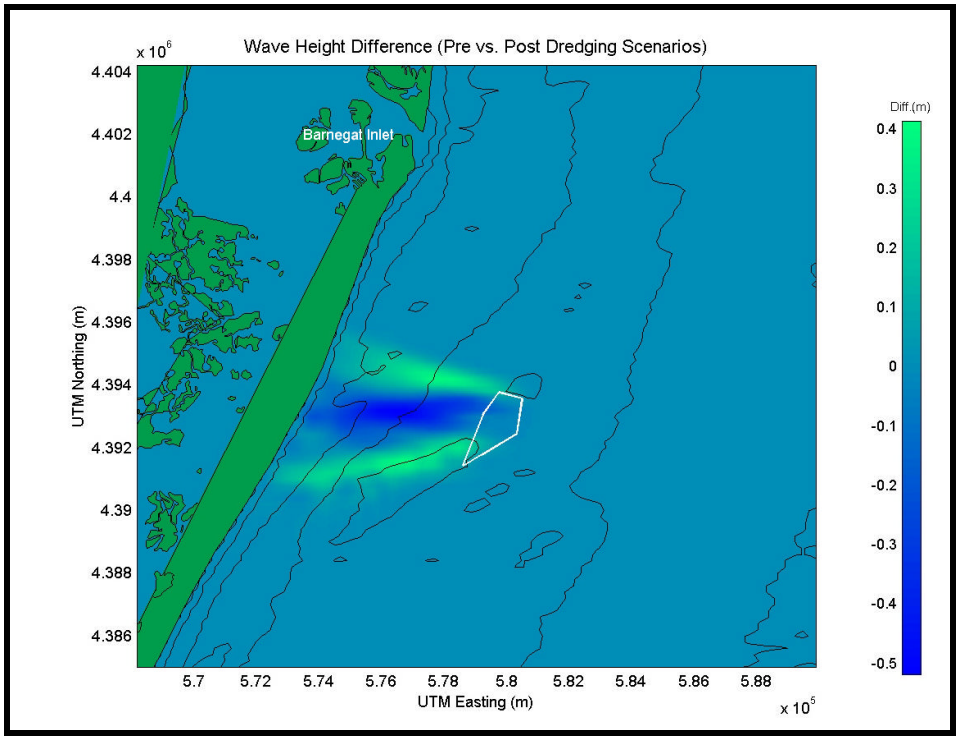

Figure 4-64. Wave height modifications resulting from potential offshore mining at the proposed borrow site in Resource Area C1 for the 50-yr northeast storm event. Green shades identify areas of increased wave height, while blue shades identify areas of decreased wave height.

4.5.3 Grid B2 Simulations

4.5.3.1 Post-Dredging Results

Results were produced for each of the directional bin spectra and the 50-yr storm events to evaluate potential physical impacts of offshore sand mining in Grid B2. Figure 4-65 presents results for the eastern approach bin. As with pre0dredging model runs, the color map corresponds to the distribution of significant wave height (m) throughout the model domain. The solid black lines represent bathymetric contours. Other than the differences in bathymetry, the same boundary conditions were used in pre- and post-dredging simulations.

Similar wave refraction patterns are evident in the post-dredging model results relative to pre-dredging model runs (e.g., impact of the offshore northeast extending linear ridges, etc.). It is difficult to visually identify any significant differences between the pre- and post-dredging results. This is true for all directional and 50-yr storm simulations. Because modifications to the wave field are not obvious after initial inspection, the impact of the potential sand mining operations on the wave field can be considered small compared with natural changes occurring throughout the model domain. The remaining simulated post-dredging model results can be found in Appendix B5.

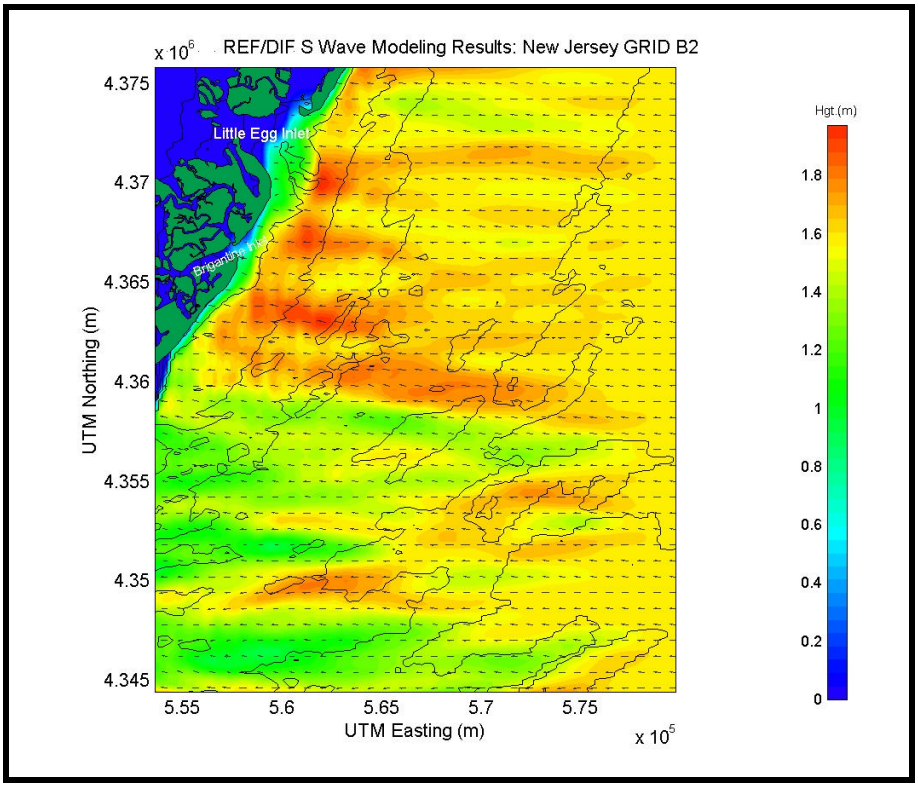

Figure 4-65. Spectral wave modeling results for post-dredging scenario using an eastern (0 degree) approach direction for reference Grid B2.

4.5.3.2 Existing Conditions Versus Post-Dredging Seasonal Results

Differences in wave heights (between pre- and post-dredging model runs) were computed at each grid point within the model domain to document potential impacts caused by proposed sand mining scenarios. Pre-dredging wave simulations were subtracted from the post-dredging wave results so that positive (negative) differences indicate an increase (decrease) in wave

height related to sand mining at potential borrow sites. In all directional bin cases, maximum change in wave height ranges from ±0.16 to 0.6 m, similar to the results illustrated for Grid A. Similar to Grid A, a significant amount of wave modification caused by the sand mining dissipates before reaching the coast. Four potential borrow sites are contained within Grid B2; G1, G2 bottom, G2 top, and G3. The proposed borrow site G1 is not considered in some of the difference plots, due to the lack of bathymetric information located offshore of Absecon Inlet. Interaction among waves modified by potential borrow site excavation is examined by numerically dredging all potential borrow sites simultaneously. This examines the worst case impact on the wave field.

Figure 4-66 is a difference plot for the pre- and post-dredging simulations for the eastern (0 degree) wave approach. The white polygons represent the potential sand borrow site locations. Dark blue colors illustrate a decrease in wave height, while green shades indicate an increase in wave height. As expected, sand mining at the proposed borrow sites creates a zone of decreased wave energy behind the borrow site and increased energy adjacent to the borrow site. Waves propagating over the sand borrow site are deflected outward, while a zone of reduced wave height is created directly behind the site. A maximum wave height increase of approximately 0.16 m and a maximum decrease of 0.2 m result from the sediment extraction scenarios for Resource Areas G1 through G3 in the eastern approach simulation. Interaction between areas of increased wave energy may result in a slightly greater increase in wave height. However, the bands of increased and decreased wave heights are relatively distinct.

Difference plots for the remaining directional simulations at Grid B2 are presented in Appendix B6. For the other directional approach simulations, patterns of wave modifications are comparable. The areas of divergence and convergence occur in similar locations for all cases. Wave height decreases directly behind the dredged region and increases in adjacent areas. Maximum changes are slightly larger for the other approach directions (ranging from ±0.16 to 0.6 m). Wave heights are able to dissipate more rapidly when waves approach from the east-northeast. The orientation of the coast, coupled with the direction of wave approach, produces a longer distance over which waves may propagate. In most cases, potential borrow sites G2 top and G2 bottom create regions where wave modifications interact with each other. As expected, the wave modification impact zones along the coast vary based on direction of wave approach.

The primary distinction among the various difference plots is the areas along the coast that are affected by potential offshore dredging. Table 4-43 presents the areas along the coast impacted by potential offshore dredging at Resource Areas G2 top, G2 bottom, and G3 for each directional approach simulation. The table presents the approximate location of each impact area, as well as the magnitude of wave height increase or decrease and the percent change relative to existing conditions. In all cases, the percent change is small, with a maximum increase of +15.6%. Gray rows indicate increases in wave height experienced at the coast caused by potential dredging activities, while white rows indicate decreases. In certain areas, the dredging at offshore borrow sites may be beneficial by reducing the height in an area that experienced increased wave energy under existing conditions. For example, during the east approach, wave height reduction of approximately 0.15 m occurs near Brigantine, an area that under existing conditions experiences an increase in wave energy. In these cases, potential offshore dredging helps reduce wave energy. However, in other areas, potential offshore dredging causes an increase in wave height in areas that already experience increased wave energy under existing conditions.

As for previously examined grids, the impact caused by potential offshore dredging at sand borrow sites during normal conditions is relatively small. At most, only minor changes are expected in the wave field and nearshore sediment transport patterns.

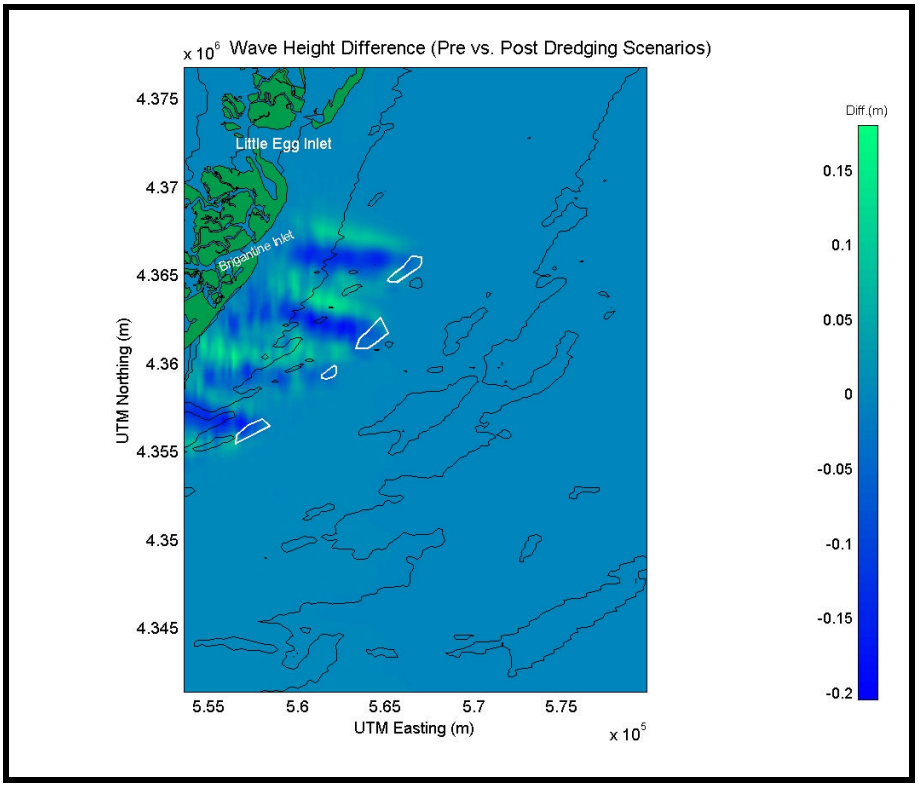

Figure 4-66. Wave height modifications resulting from potential offshore mining at sand borrow sites in Resource Areas G1 through G3 for the eastern (0 degree) approach simulation. Green shades identify areas of increased wave height, while blue shades identify areas of decreased wave height.

4.5.3.3 High Energy Wave Event Results

Differences in wave height also were computed for 50-yr storm simulations to identify potential impacts of offshore sand mining. Figures 4-67 and 4-68 show results for the 50-yr hurricane and 50-yr northeast storm, respectively. A similar distribution of wave energy change as indicated in the directional results is illustrated (i.e., wave energy reduction directly behind the dredged area and an adjacent increase in energy). The change plots for the hurricane and northeast storm simulations indicate a maximum increase in wave height of approximately 0.6 m (13.3% increase) and 0.4 m (8.0% increase), respectively. A wave reduction of 0.4 to 0.5 m is observed in the shadow zones of borrow sites. The changes are significantly more than those observed at Grid B1.

However, unlike Grid B1, a significant amount of wave energy does dissipate before reaching the shore, especially during a hurricane simulation. Shoreline areas from Brigantine north to Little Egg Inlet may experience a change in wave heights and sediment transport during a typical hurricane or northeast storm. However, relative to the magnitude of the incoming waves, the changes exhibited at this grid are not expected to have a significant effect during a large storm event.

Table 4-43. Coastal regions impacted by the potential offshore dredging in Resource Areas G2 top, G2 bottom, and G3.

Approach Direction	Approximate Shoreline Location	Approximate UTM Northing (m)	Wave Height Change (m) at Coast	Percent Change
East (0E)	South of Brigantine	4,361,000	+0.15	+11.5
East (0E)	South of Brigantine Inlet	4,365,000	+0.09	+5.6
East (0E)	North of Brigantine Inlet	4,367,500	+0.09	+6.0
East (0E)	Brigantine	4,362,500	-0.15	-8.8
East (0E)	Brigantine Inlet	4,366,500	-0.10	-5.7
E-SE (-22.5E)	Northern Brigantine	4,364,000	-0.15	-9.4
E-SE (-22.5E)	South of Brigantine Inlet	4,365,000	-0.16	-9.2
E-SE (-22.5E)	North of Brigantine Inlet	4,367,500	-0.18	-12.0
E-SE (-22.5E)	Brigantine Inlet	4,366,500	+0.14	+8.2
E-SE (-22.5E)	Just north of Brigantine	4,363,000	+0.16	+12.3
E-SE (-22.5E)	Brigantine	4,362,500	+0.15	+13.0
E-SE (-22.5E)	South of Little Egg Inlet	4,370,000	+0.08	+6.2
SE (-45E)	North of Brigantine Inlet	4,367,500	-0.30	-16.7
SE (-45E)	Brigantine	4,362,500	-0.25	-14.3
SE (-45E)	South of Brigantine	4,362,000	+0.05	+2.9
SE (-45E)	South of Brigantine Inlet	4,365,000	+0.25	+15.6
SE (-45E)	South of Little Egg Inlet	4,370,000	+0.10	+9.6
S-SE (-67.5E)	North of Little Egg Inlet	4,375,000	+0.05	+3.8
S-SE (-67.5E)	Entrance to Little Egg Inlet	4,372,000	+0.13	+10.4
S-SE (-67.5E)	South of Little Egg Inlet	4,369,000	-0.25	-17.2
S-SE (-67.5E)	South of Brigantine Inlet	4,365,000	-0.20	-11.4
S-SE (-67.5E)	North of Brigantine Inlet	4,367,500	+0.20	+12.1
S-SE (-67.5E)	North of Brigantine	4,364,000	+0.12	+6.7
E-NE (22.5E)	South of Brigantine	4,361,000	+0.15	+10.7
E-NE (22.5E)	North of Brigantine	4,364,000	+0.16	+11.4

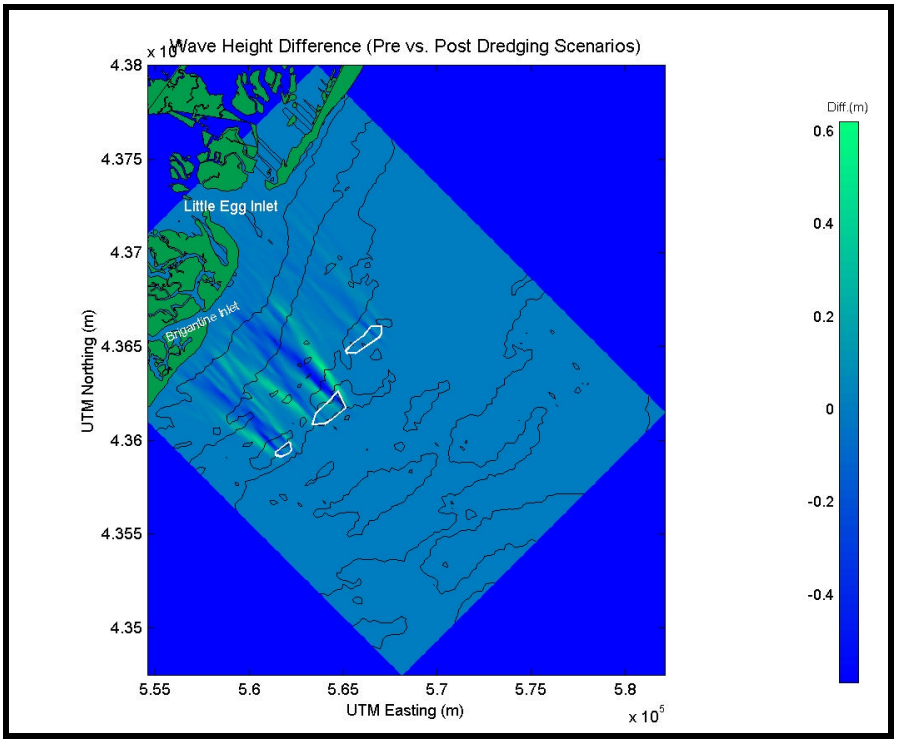

Figure 4-67. Wave height modifications resulting from potential offshore sand mining in Resource Areas G2 top, G2 bottom, and G3 during a 50-yr hurricane event. Green shades identify areas of increased wave height, while blue shades identify areas of decreased wave height.

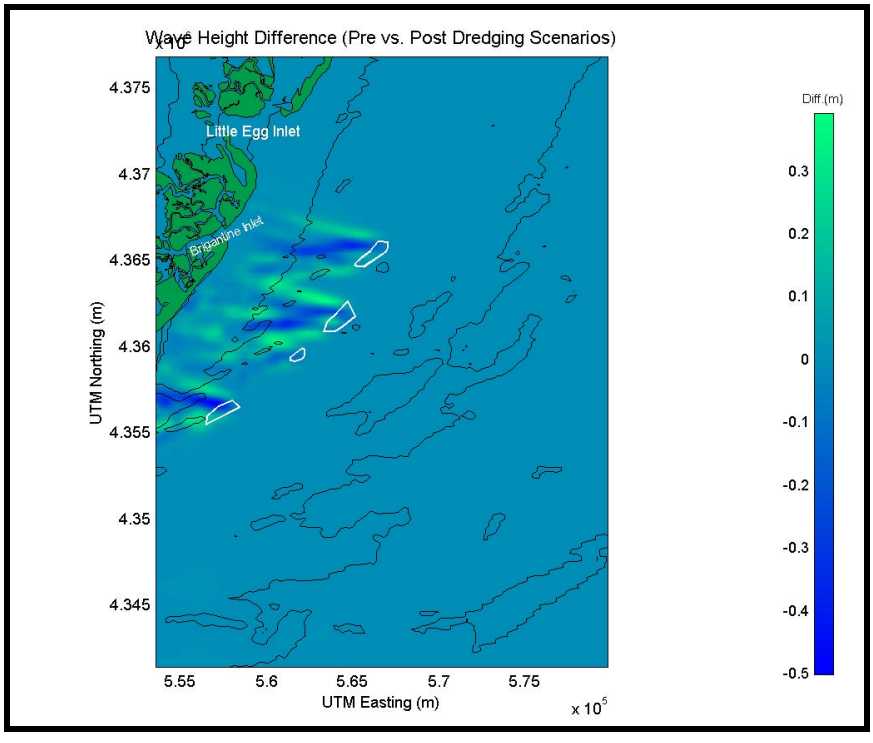

Figure 4-68. Wave height modifications resulting from potential offshore mining in Sand Resource Areas G1, G2 top, G2 bottom, and G3 for the 50-yr northeast storm event. Green shades identify areas of increased wave height, while blue shades identify areas of decreased wave height.

4.5.4 Grid C Simulations

4.5.4.1 Post-Dredging Results

Following wave modeling runs for existing conditions in Grid C, simulations were performed for post-dredging scenarios. Results were produced for each of the directional bin spectra and the 50-yr storm events to evaluate potential physical impacts of offshore sand mining. Figure 4-69 illustrates results for the eastern approach bin for the post-dredging scenario. Other than differences in bathymetry, the same boundary conditions were used in pre- and post-dredging simulations.

The same wave patterns described for pre-dredging simulations are evident in the post-dredging model results (e.g., impact of the shoals south and southeast of Resource Area F2, etc.). Because modifications to the wave field are not obvious after initial inspection, the impact of potential sand mining operations on the wave field can be considered small compared with natural changes occurring throughout the model domain. The remaining simulated post-dredging model results can be found in Appendix B5.

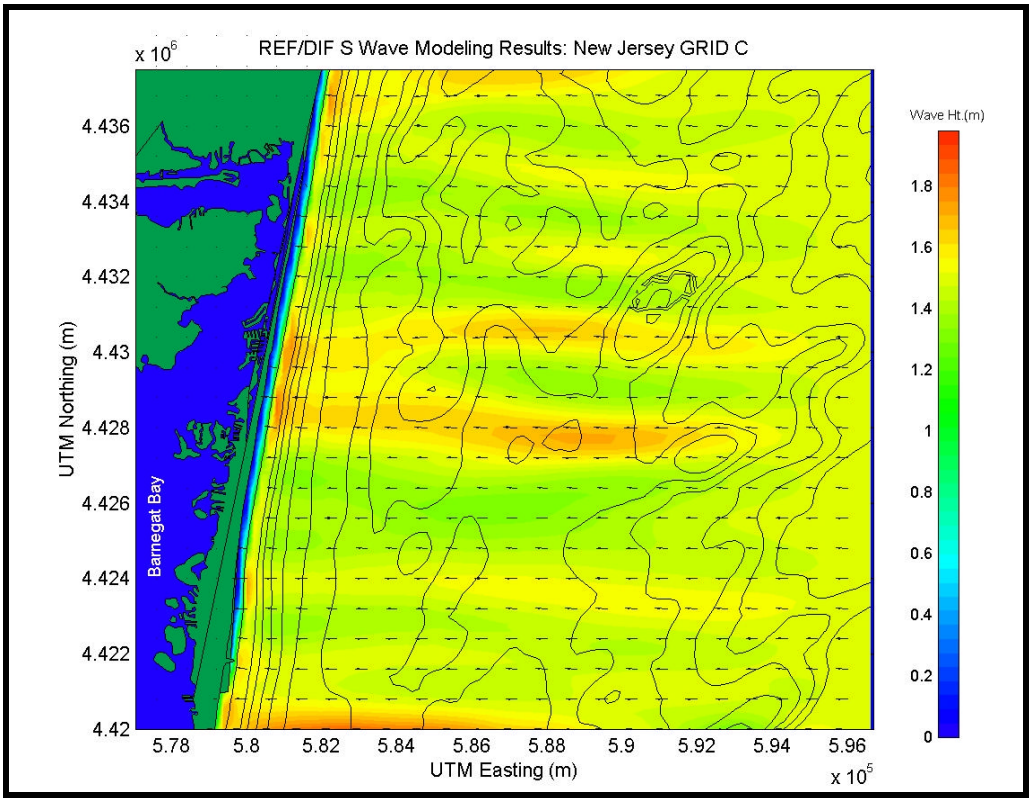

Figure 4-69. Spectral wave modeling results for post-dredging scenario using an eastern (0 degree) approach direction for reference Grid C.

4.5.4.2 Existing Conditions Versus Post-Dredging Seasonal Results

Differences in wave height between pre- and post-dredging simulation for Grid C were computed at each grid point within the model domain to document potential impacts caused by specific sand mining scenarios. Pre-dredging wave simulations were subtracted from the post-dredging wave results so that positive (negative) differences indicate an increase (decrease) in wave height related to sand mining at potential borrow sites. In all directional bin cases, maximum changes in wave height ranged from ±0.06 to 0.2 m. However, unlike Grids A and B2, a significant amount of the modification caused by sand mining does not dissipate before reaching the coast.

Figure 4-70 shows the difference plot for the eastern (0 degree) approach simulation presented in Figures 4-48 (pre) and 4-69 (post). Dark blue colors indicate a decrease in wave height, while green shades indicate an increase in wave height. As expected, sand mining creates a zone of decreased wave energy behind the sand borrow site and increased energy adjacent to the borrow site. Waves propagating over the sand borrow site are deflected outward, while a zone of reduced wave height is created directly behind the site. A maximum increase of approximately 0.1 m and a maximum decrease of 0.2 m result from the sediment extraction scenario for Resource Areas F2. Because there is only one potential borrow site within Grid C, the difference plots are relatively easy to interpret compared with results observed for Grid A or B2, which had multiple borrow locations.

Difference plots for the remaining directional simulations at Grid C are presented in Appendix B6. For the other directional approach simulations, patterns of wave modifications are comparable. Areas of divergence and convergence occur in similar locations for all cases. Wave height decreases directly behind the dredged region, and it increases in adjacent areas. Maximum changes for the other directional approaches (±0.05 to 0.07 m) are smaller than the eastern approach, except during a northeast wave approach, where larger waves result in more significant changes (±0.2 to 0.25 m). The northeast approach also exhibits a more scattered wave modification zone. Overall, the wave modification impact zones along the coast vary based on direction of wave approach.

The primary distinction among the various difference plots is the areas along the coast that are affected by potential offshore dredging. Table 4-44 presents the areas along the coast impacted by potential offshore dredging at Resource Area C1 for each directional approach simulation. The table presents the approximate location of each impact area, as well as the magnitude of wave height increase or decrease and the percent change relative to existing conditions. In all cases, the percent change is small, with a maximum increase of +9.0%. Furthermore, wave modifications at grid C are smaller than other grids. In Table 4-44, gray rows indicate increases in wave height experienced at the coast caused by potential dredging activities, while white rows indicate decreases in wave height. In certain areas, the dredging at offshore borrow sites may be beneficial by reducing the height in an area that experienced increased wave energy under existing conditions. For example, during an east-southeast approach, wave height reduction of approximately 0.16 m occurs near Bay Head, an area that under existing conditions experiences an increase in wave energy. In these cases, potential offshore dredging helps reduce wave energy. However, in other areas, the potential offshore dredging causes an increase in wave height in areas that already experience increased wave energy under existing conditions.

Overall, the impact caused by potential offshore dredging at sand borrow sites during normal conditions is relatively small, especially at grid C. At most, only minor changes are expected in the wave field and nearshore sediment transport patterns.

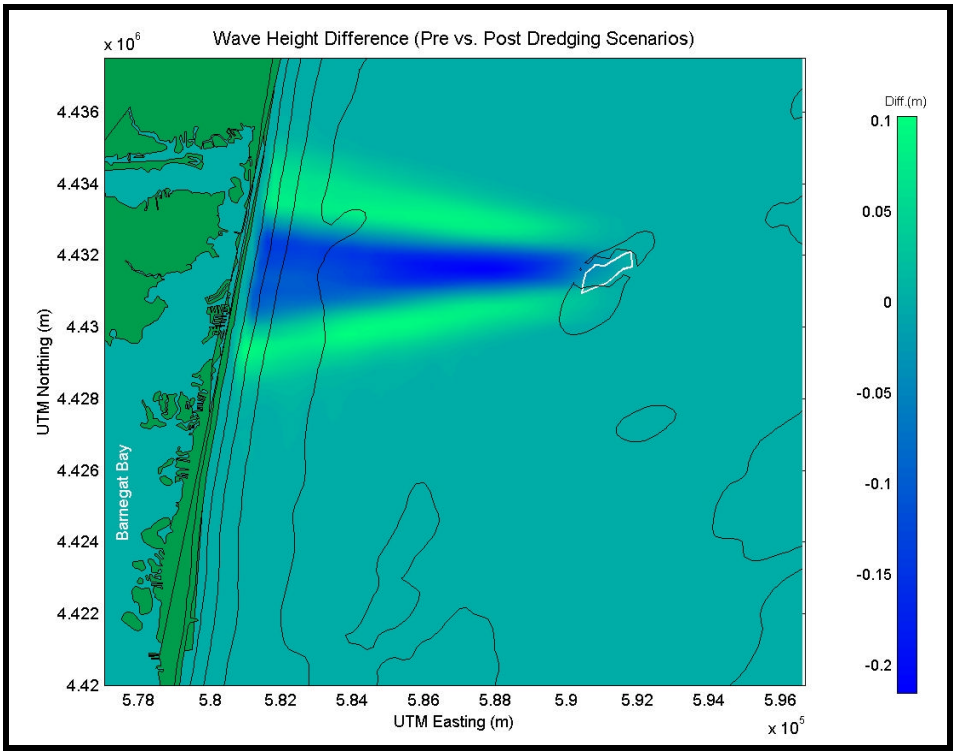

Figure 4-70. Wave height modifications resulting from potential offshore sand mining at Resource Area F2 for the eastern (0 degree) approach simulation. Green shades identify areas of increased wave height, while blue shades identify areas of decreased wave height.

4.5.4.3 High Energy Wave Event Results

Differences in wave heights were also computed for 50-yr storm simulations to identify potential impacts of offshore sand mining. Figures 4-71 and 4-72 show results for the 50-yr hurricane and 50-yr northeast storm, respectively. A similar distribution of wave energy change as indicated in the directional results is illustrated (i.e., wave energy reduction directly behind the dredged area and an adjacent increase in energy). The change plots for the hurricane and northeast storm simulations indicate a maximum increase in wave height of approximately 0.25 m (5.0% increase) and 0.4 m (6.8% increase), respectively. A wave reduction of 0.2 to 0.9 m is observed in the shadow zones of borrow sites.

At Grid C, a significant amount of wave energy does not dissipate before reaching the shore. Shoreline areas from Bay Head northward may experience a change in wave heights and sediment transport during a typical hurricane event. During a typical northeast storm, shoreline areas from Lavallette north to south of Bay Head may experience a change in wave heights and sediment transport patterns. However, relative to the magnitude of the incoming waves, the changes exhibited at this grid are not expected to have a significant effect during a large storm event.

Table 4-44. Coastal regions impacted by the potential offshore dredging of Resource Area F2.

Approach Direction	Approximate Shoreline Location	Approximate UTM Northing (m)	Wave Height Change (m) at Coast	Percent Change
East (0E)	Lavallette	4,428,250	+0.10	+5.9
East (0E)	North of Mantoloking	4,433,500	+0.10	+7.1
East (0E)	Chadwick Beach north to Mantoloking	4,431,000	-0.20	-11.4
E-SE (-22.5E)	Bay Head	4,434,900	-0.16	-9.9
E-SE (-22.5E)	North of Bay Head	4,436,500	+0.08	+5.9
E-SE (-22.5E)	Mantoloking	4,432,100	+0.10	+6.3
SE (-45E)	North of Bay Head	4,439,000	-0.10	-6.1
SE (-45E)	North of Bay Head	4,437,500	+0.10	+6.3
SE (-45E)	North of Bay Head	4,441,000	+0.07	+4.7
S-SE (-67.5E)	North of Bay Head	4,443,000	+0.09	+7.5
S-SE (-67.5E)	North of Bay Head	4,446,000	-0.03	-3.0
S-SE (-67.5E)	North of Bay Head	4,444,500	-0.08	-6.7
S-SE (-67.5E)	North of Bay Head	4,445,000	+0.07	+5.8
E-NE (22.5E)	Chadwick Beach	4,429,750	+0.06	+4.3
E-NE (22.5E)	Ortley Beach	4,428,000	-0.12	-7.5
E-NE (22.5E)	Seaside Heights	4,426,000	+0.04	+2.6
NE (45E)	South of Seaside Park	4,423,000	+0.15	+9.0
NE (45E)	South of Seaside Park	4,422,500	-0.15	-9.3
NE (45E)	South of Seaside Park	4,421,500	+0.10	+6.1
NE (45E)	South of Seaside Park	4,420,000	-0.09	-5.0
NE (45E)	South of Seaside Park	4,419,250	+0.08	+4.7

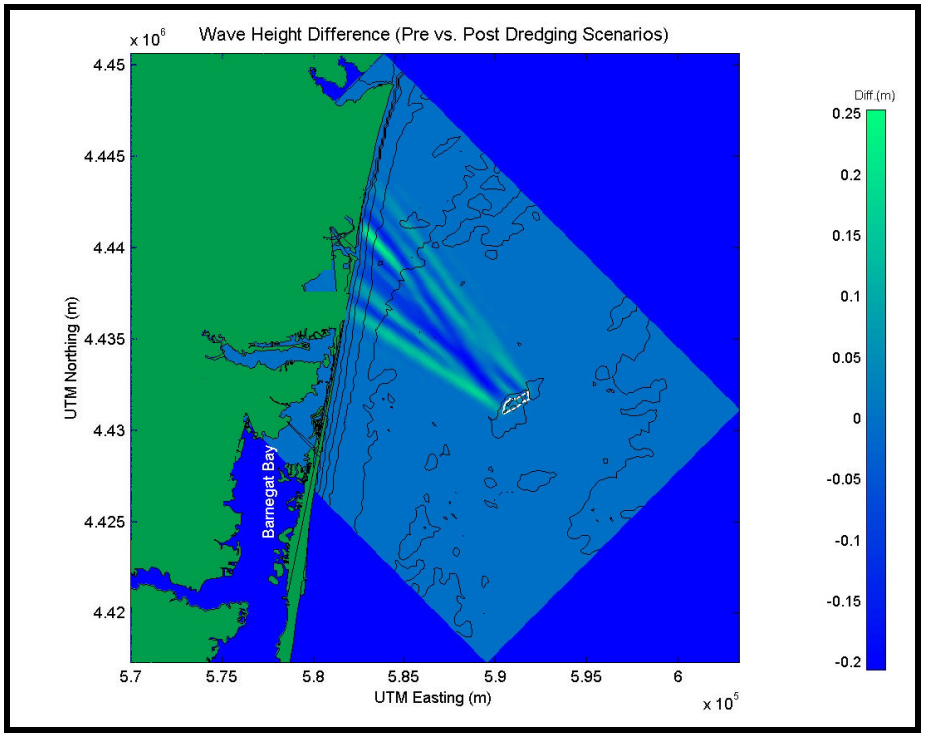

Figure 4-71. Wave height modifications resulting from potential offshore sand mining in Resource Area F2 a 50-yr hurricane event. Green shades identify areas of increased wave height, while blue shades identify areas of decreased wave height.

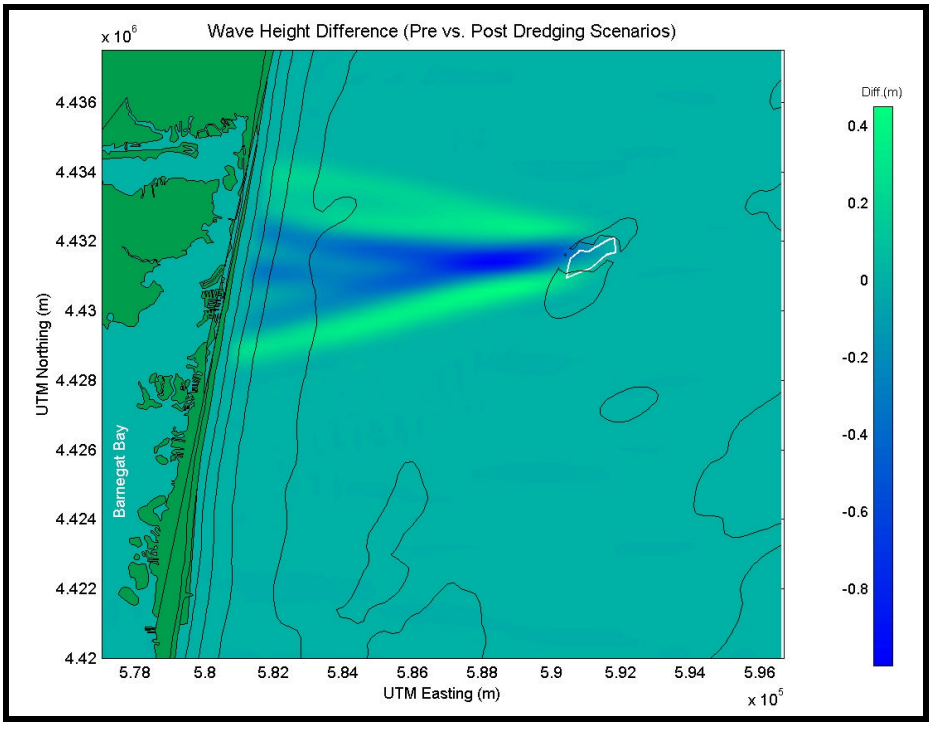

Figure 4-72. Wave height modifications resulting from potential offshore sand mining in Resource Area F2 for the 50-yr northeast storm event. Green shades identify areas of increased wave height, while blue shades identify areas of decreased wave height.

4.6 DISCUSSION

This following discussion summarizes an analysis of possible impacts to the nearshore wave climate caused by potential sand mining offshore New Jersey. The analysis approach relied upon the spectral wave model REF/DIF S to simulate the behavior of a random sea, incorporating the effects of shoaling, wave breaking, refraction, diffraction, and energy dissipation. Historical hindcast wave information was allocated into directional bins, and an energy distribution was developed for all waves contained in each approach bin. Energy and directional distributions were then used to generate representative energy and directional spectra. The study region was divided into four distinct modeling grids to evaluate the potential impact of the sand mining on wave transformation.

Wave transformation modeling was performed for existing conditions with directional and 50-yr storm spectra. Model results identify key areas of wave convergence, divergence, and shadow zones offshore New Jersey. In the directional approach simulations, significant wave heights experience little variation up to the 20 m depth contour where waves begin to feel the influence of bathymetry. Significant bathymetric features (e.g., shore-attached, northeast extending linear ridges; offshore shoals; bathymetric depression;) within each modeling domain are the primary cause of wave transformation patterns. The influence of bathymetry on the wave field and impact zones along the coast change as waves approach from various directions.

The region offshore of Townsends and Corsons Inlets (Grid A) has a relatively consistent longshore wave height distribution. Several areas of wave convergence and/or divergence were identified within the domain caused by the shoals surrounding Resource Areas A1 and A2. These features focus wave energy at various locations along the coast depending on the wave approach direction. The area to the south of Barnegat Inlet (Grid B1) experiences mild shoreline retreat and a consistent wave height distribution along the shoreline. Shoals and depressions south of Resource Area C1, as well as offshore linear ridges to the north, produce significant wave transformation within the modeling domain. Wave energy focused by these features most often impact the Harvey Cedars and Loveladies regions. Offshore Little Egg and Brigantine Inlets (Grid B2), wave transformation again is produced by numerous linear ridges. Increased wave heights appear most frequently near Brigantine Inlet. The area seaward of northern Barnegat Bay (Grid C) also experiences wave height changes produced by offshore shoals and depressions within the modeling domain. Consistent wave focusing is observed by the shoal within Resource Area F2, as well as the shoals to the south and southeast of F2. Wave energy focused by these features impacts regions from Seaside Park north to Bay Head, depending on approach direction.

For the 50-yr hurricane and northeast storm, wave patterns are similar to the directional approach results. An increase in wave height is documented in many areas where wave convergence occurs. For example, the shoal present in Resource Area F2 produces wave convergence that result in 6.0 m wave heights during a typical 50-yr northeast storm. The 50-yr hurricane and northeast storm simulated in the present study represents a major storm that could have impact on the approaching wave field and sediment transport patterns.

Post-dredging model simulations were performed by numerically excavating the proposed borrow sites for each of the four grids. Differences in wave height between pre- and post-dredging scenarios offshore New Jersey indicate maximum wave height increases for directional approach simulations ranging from 0.1 to 0.25 m (7 to 16% of the initial wave height). The magnitude of modifications increase as the magnitude of the waves increase or when the orientation of potential borrow sites align with waves to produce maximum impact (e.g., southeast approach at Grid A). In Grids A and B2, which are the southernmost grids, these

maximum changes dissipate relatively quickly as waves advance towards the coast and break. In Grids B1 and C, maximum changes do not dissipate as readily. At potential impact areas along the coast, wave height changes average ±0.13 m, ±0.11 m, ±0.15 m, and ±0.10 m for Grids A, B1, B2, and C, respectively. These modifications represent changes of approximately ±3 to 15% when compared with wave heights for existing conditions. Overall, the impact caused by potential offshore dredging during normal conditions is minimal, if at all.

During extreme wave conditions (e.g., a 50-yr storm), wave heights are increased from 0.4 to 1.4 m, suggesting a rather significant change. However, as a result of the increased magnitude of the incoming waves, this represents a change of less than 10%. Due to the orientation of the shoreline and the proposed borrow sites, a hurricane has more significant impacts on Grids A and B2 (Resource Areas A1, A2, G1, G2, and G3), while a northeast storm more significantly impacts Grids B1 and C (Resource Areas C1 and F2). For most of the sand borrow sites, a significant amount of wave energy is dissipated before the waves reach the coast, especially for Grids A and B2. As such, wave height increases are less than 0.4 m along a majority of the coast. A maximum change of 0.4 m in wave height is not expected to increase nearshore erosion above existing conditions during a storm event.

Borrow sites within Sand Resource Areas A1 and A2, which are located offshore of Townsends Inlet, have a greater impact on the wave field due to the larger extraction volumes (8,800,000 and 8,600,000 m^3, respectively). In addition, regions with multiple borrow sites (Grids A and B2), indicate a greater potential for wave modifications with simultaneous dredging. Overall, wave transformation impacted by potential borrow sites is minimal during normal and storm sea conditions.

5.0 CIRCULATION AND SEDIMENT TRANSPORT DYNAMICS

This section analyzes the physical processes regime of the New Jersey continental shelf and discusses circulation, wave, and sediment transport processes to evaluate the potential environmental impact of offshore sand mining. Current and wave processes provide physical mechanisms for moving sediment throughout the New Jersey coastal zone. The following discussion documents the physical mechanisms potentially impacted by sand mining within specific offshore locations.

5.1 CURRENTS AND CIRCULATION

Circulation patterns observed at specific areas within the study region were evaluated within the context of potential offshore sand mining operations. The following discussion uses long-term current measurements obtained during previous studies in the region to provide an understanding of temporal variations of inner shelf circulation (time scales of hours to months). The analyses presented in this section describe circulation characteristics within the study region, including major forcing influences, time scales of variability, and the magnitude of resulting currents. The results from this section were used to provide estimates of sediment transport potential at offshore borrow sites.

5.1.1 Historical Data Analysis

Historical current records for data collected at LEO-15 (offshore Barnegat Inlet, New Jersey) were chosen for detailed analysis of current processes. The site is located in about 13 m water depth at 39°27.70' N, 74°15.73' W. The data include measurements obtained from August 1993 through August 1995. All data were recorded by an S-4 current meter mounted approximately 1 m above the seafloor.

The LEO-15 data sets were obtained over an approximate two-year period; however, gaps in the two-year record due to instrument maintenance and data recovery made numerical analysis of the entire record problematic. Therefore, the data were analyzed as a series of 30-to-90 day blocks, with statistics generated for each data block. The procedures used to calculate these statistics and determine relevant physical processes will be discussed in the following sections.

The current data were first rotated from a north/east coordinate system to a cross-shelf/along-shelf coordinate system. This rotation of the coordinate system allowed the currents to be analyzed either normal to or tangential to the shoreline. The sign convention holds that positive across-shelf flow is directed onshore and negative across-shelf flow is directed offshore. Positive along-shelf flow is directed approximately northward and negative along-shelf flow is directed to the south.

5.1.1.1 Description of Observed Currents

Measurement of bottom currents at the LEO-15 location throughout the approximate two-year period (1993 to 1995) revealed considerable variability of flow speeds and directions. The mean flow was to the southwest along the inner shelf bathymetric contours.

Strongest flow was observed in the along-shelf direction, with peak velocities of nearly 50 cm/sec noted on several occasions; these maximum currents were directed down-shelf, or to the south. Maximum northward currents reached 37 cm/sec. Along-shelf bottom currents never exceeded 50 cm/sec (1 knot). Flow reversals, when currents directed to the north reversed to flow in a southerly direction, were noted frequently. Along-shelf standard deviations were of order 9 cm/sec.

In the cross-shelf direction, mean flow was oriented onshore, consistent with upwelling processes that push bottom waters up onto the shelf. Maximum cross-shelf flow was 31 cm/sec (directed onshore); minimum flow was -13 cm/sec (directed offshore). Cross-shelf standard deviations were of order 5 cm/sec.

A more detailed analysis of the current regime at this location was possible following numerical separation of the overall measured currents into known physical processes.

5.1.1.2 Numerical Decomposition of Observed Currents

Currents observed along the continental shelf represent the cumulative effects of many different physical processes, each possessing unique time scales and amplitudes. These processes occur simultaneously; hence, the current observed at any one time can be considered the summation, or superposition, of all these individual processes. This section describes the numerical procedures used to separate the observed currents into individual subsets, each with specific time scales of variability. This procedure allows analysis of each process to determine their relative importance to total circulation in the region.

Separation of the total signal into specific process components was performed using various numerical analysis techniques, such as tidal harmonic decomposition, as well as the application of a series of low-, band-, and high-pass filters. The results of the numerical separation analysis represent subsets of individual time series. Each subset represents a specific physical process, such as:

- high-frequency currents (non-tidal processes with periods less than approximately 33 hours)
- tidal currents (diurnal and semi-diurnal constituents)
- wind-driven currents (1 to 15 day frequency band)
- low frequency or seasonal currents (greater than 15 day periodicity).

The first step in the separation analysis is to remove tidal currents from the raw data using harmonic analysis. Harmonic analysis calculates the amplitude and phase of 21 individual tidal constituents using a least-squares fit of the constituent sinusoid to the raw data signal. The tidal constituents removed included K1, M2, M4, M6, S2, N2, O1, S4, S6, M8, MK3, MN4, MS4, 2N2, OO1, M1, J1, Q1, 2Q1, L2, and 2SM2. A majority of these constituents represent high frequency tides, or tides having periods less than approximately 28 hours (diurnal tides). Low frequency tides, such as Msf or Mm tides that vary on a fortnightly (approximately 13 to 14 days) period, were not removed from the records because of the relatively short length of the time series (roughly thirty days or two fortnightly cycles).

The result of this analysis is a separation of the total observed currents into two time series: one time series is predicted tides, based on a reconstruction of individual tidal components (the summation of 21 sinusoidal functions), and the second time series is non-tidal or residual currents. The residual current was generated by subtracting (point by point) the reconstructed tidal time series from the original signal.

The residual signal became the basis for subsequent analyses. The first step in processing was to remove the remaining high frequency energy. This was accomplished by applying a PL33 low-pass filter over the residual signal. The PL33 is a standard oceanographic filter which uses 1/33 hours as the cutoff frequency, and is used primarily to remove tidal energy (or all signal energy with periodicity less than 33 hours) from oceanographic time series. Some energy leakage can occur near the cutoff frequency using this filtering method; however, this

effect is minimal since the significant diurnal (and higher frequency) tides had been removed prior to this step. The low-passed time series was termed the subtidal signal.

The subtidal signal was subtracted from the previous residual signal, resulting in a high frequency time series containing all non-tidal currents having periods less than approximately 33 hours. This high-frequency signal (typically referred to as noise) contained significant energy, which can be due to several sources, including actual flow field turbulence, wave-induced flow, as well as possible data contamination due to mooring motions. The high frequency signal was saved as a separate time series for later analysis and comparison.

The subtidal signal was then reduced further into distinct frequency bands. The first frequency band was defined as processes with time scales of 1 to 15 days. It was assumed to include wind-driven flows, as well as other processes of similar time scales, such as the southwestward-propagating coastally trapped free waves described by Ou et al. (1981), and observed by Noble et al. (1983). Buoyancy-driven flow may also be included in this frequency band. This wind-driven band was expected to yield significant energy (based on previously-published research). The signal was derived by high-pass filtering the subtidal signal with a 15-day cutoff, and was termed the wind-driven signal, on the assumption most of the energy within this band results from wind forcing.

The second time band defined processes with periodicity greater than 15 days. It was termed the seasonal band, although processes with higher frequencies than seasonal (e.g., 15 to 30 days) are inherently included in this band. This series was derived by subtracting the wind-driven signal from the subtidal signal.

Each time series was extracted in sequential manner from the raw signal to a set of individual process-specific signals, each representing the dominant current occurring at specific time scales. This separation procedure was repeated for every data set. Separating these processes from the whole illustrated the relative contribution of each to the total observed circulation at a selected sand resource area. The signal variance of each resulting time series represents its energy level. Comparing the variance of each process to the total signal variance yields a representation of how much energy the process contributed to the whole.

5.1.1.3 Current Components

Tidal Currents

Cross-shelf tides were predominantly semi-diurnal, specifically the M_2 lunar semi-diurnal tide, with maximum amplitudes of order 7 to 8 cm/sec during spring tides and maximum amplitudes of approximately 4 cm/sec during neap tides. Along-shelf tidal currents were mixed diurnal tides with maximum amplitudes of approximately 5 to 7 cm/sec during spring tide conditions, and maximum amplitudes of 2 to 3 cm/sec during neap conditions.

The analysis revealed that tidal currents affect cross-shelf flow processes more than along-shelf processes. The magnitude of tidal variance was approximately equivalent between cross- and along-shelf component; however, tides possessed a higher fraction of cross shelf flow, containing about 50 to 80% of the total cross-shelf energy. Along-shelf tidal currents, while having equivalent magnitude of variance as the cross-shelf component, contained a smaller fraction of the overall along-shelf flow (approximately 5 to 20% of the total), suggesting that while tides dominated cross-shelf currents, they were less important to the along-shelf flow.

High-Frequency Currents

High frequency currents were defined as all non-tidal oscillations having periods less than approximately 33 hours, and can result from flow turbulence, responses to localized wind stress,

measurement noise, and other random motions of the water column. In shallow water, high-frequency processes tend to contribute a greater fraction to the overall current energy than in deeper water. Inertial currents were also contained within this frequency band, as the inertial frequency at New Jersey latitudes is approximately 19 hours.

The standard deviation of cross-shelf high-frequency currents was about 3 to 4 cm/sec, meaning that at any time, the currents vary typically by 3 to 4 cm/sec. The standard deviation of along-shelf flow was about 1 to 2 cm/sec. High frequency currents contributed approximately 20% of the total cross-shelf variance, and approximately 12% of the total along-shelf variance. The data reveal some correlation between high frequency currents and subtidal wind-driven currents, suggesting that these high frequency currents result from wind stress forcing.

Inertial currents contained small amounts of energy (typically less than 2% of the total), with maximum amplitudes less than 3 cm/sec. These currents were transient, decaying to zero after an initial perturbation (typically wind forces). The initiation of inertial currents appeared correlated to sub-tidal wind-driven currents.

Wind-driven Currents

Wind-driven currents contributed most significantly to the observed currents (Figure 5-1), containing on average over half of the total along-shelf current variance. In winter, the along-shelf current variance was nearly three times that in summer, and accounted for as much as 70% of the total energy. Wind-driven currents accounted for only about 10% of the cross-shelf energy.

Wind-driven energy during the winter of 1994 was nearly twice the energy of the wind-driven currents during the winter of 1995. This increase in wind-driven energy between successive years may be due to singular events (i.e., storms) that influenced currents for brief durations, or could be produced by other non-locally generated oscillations within the Mid-Atlantic Bight (Ou et al., 1981), specifically coastally-trapped waves propagating along the shelf. Noble et al. (1983) analyzed current meter records along the Mid-Atlantic Bight, and suggest that 75 to 90% of the subtidal variance is due to wind-driven currents or free wave events, and that the relative magnitudes of energy from these two processes can vary substantially from year to year. Strong wind-driven flows were observed in late February, 1994 (Figure 5-2); these episodic events, either storm induced or free waves, contributed significantly to the overall current energy estimates.

Wind-driven flows in the along-shelf direction were found to exceed 30 cm/sec, and exceeded 20 cm/sec frequently. Wind-driven flows in the cross-shelf direction were always less than 10 cm/sec (Figure 5-3).

Low-Frequency Currents

Low frequency currents were not well-resolved since the records were relatively short (i.e., only a few low-frequency cycles were included in each record). Low-frequency values included the mean current. Mean flow was southerly in the along-shelf direction, approximately 2 to 3 cm/sec. Mean cross-shelf currents were found to be positive, or directed onshore, during most of the time periods analyzed. Mean cross-shelf flows were approximately 1 to 5 cm/sec, and stronger during winter time periods. Mean along-shelf flows were negative, flowing southerly. The winter of 1994 time period (February to March), the mean along-shelf flow was approximately 7 cm/sec to the south (Figure 5.2).

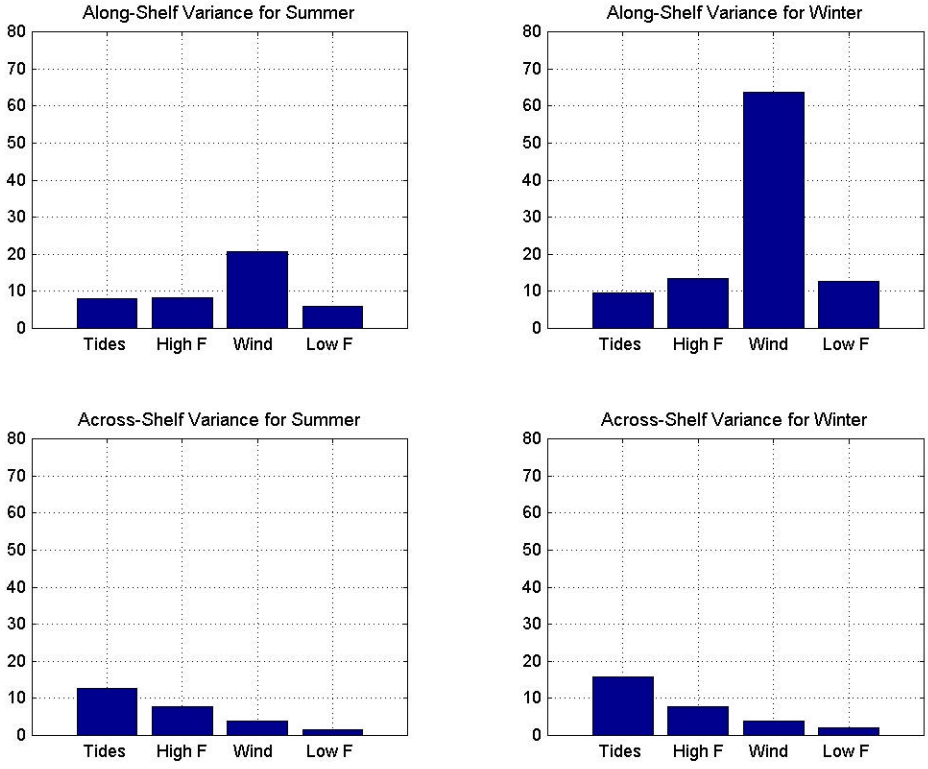

Figure 5-1. Histogram showing the relative energy (variance) of separated current processes: tides, high frequency, wind-driven, and low-frequency flows. Units are $(cm/sec)^2$. Along-shelf wind-driven flows in winter were the most energetic current component.

Low frequency variance ranged from 5 to 22% of the total in the along-shelf direction; low frequency variance ranged from 1 to 13% in the across-shelf direction. The variance magnitudes show that low frequency currents in the along-shelf direction are about four times more energetic than cross-shelf flow.

5.1.1.4 Seasonal Variability

The previous section revealed the dominant circulation processes on the New Jersey shelf were attributed to variability in the 1 to 15 day frequency band, termed the wind-driven band. This result is consistent with previous studies in the region (Noble et al., 1983). Figure 5-1 shows the relative energy of calculated current components as a function of time; wind-driven energy during winter time periods was significantly greater than during summer. Nearly all this winter increase in energy was oriented along the shelf. There was no meaningful seasonal difference in wind-driven energy in the cross-shelf direction. Notably, the wind-driven variance appeared strongly influenced by singular events (i.e., storms or perhaps non-locally generated free waves). Northeast storms are much more likely to occur during the winter (Louis Berger Group, 1999), thus it is not surprising that along-shelf wind-driven currents were stronger during winter time periods. Winter of 1994 (specifically February to March 1994) variance in wind-driven currents was much higher than that for the winter of 1995 (specifically November to April 1995). These 1994 wind-driven currents appeared to have been dominated by a singular event that occurred in late February 1994 (Figure 5-2). Tidal energy was nearly constant throughout the year, with little-to-no seasonal variability.

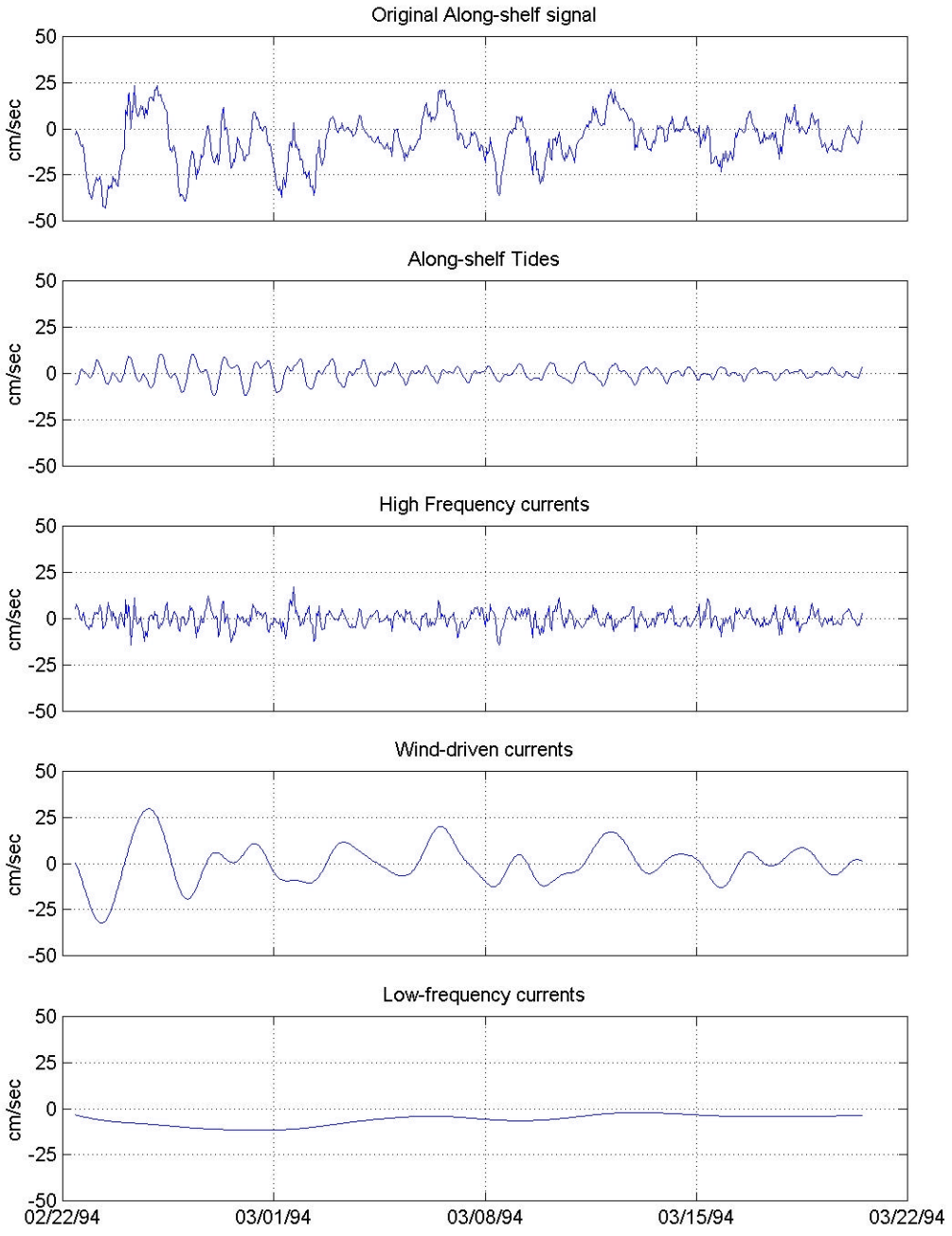

Figure 5-2. Time series of individual along-shelf flow processes for February-March (Winter) 1994. Note the strong wind-driven currents that occurred in late February. These strong currents likely resulted from either a storm (local wind response) or freely-propagating waves. In either case, wind-driven currents account for most of the along-shelf signal.

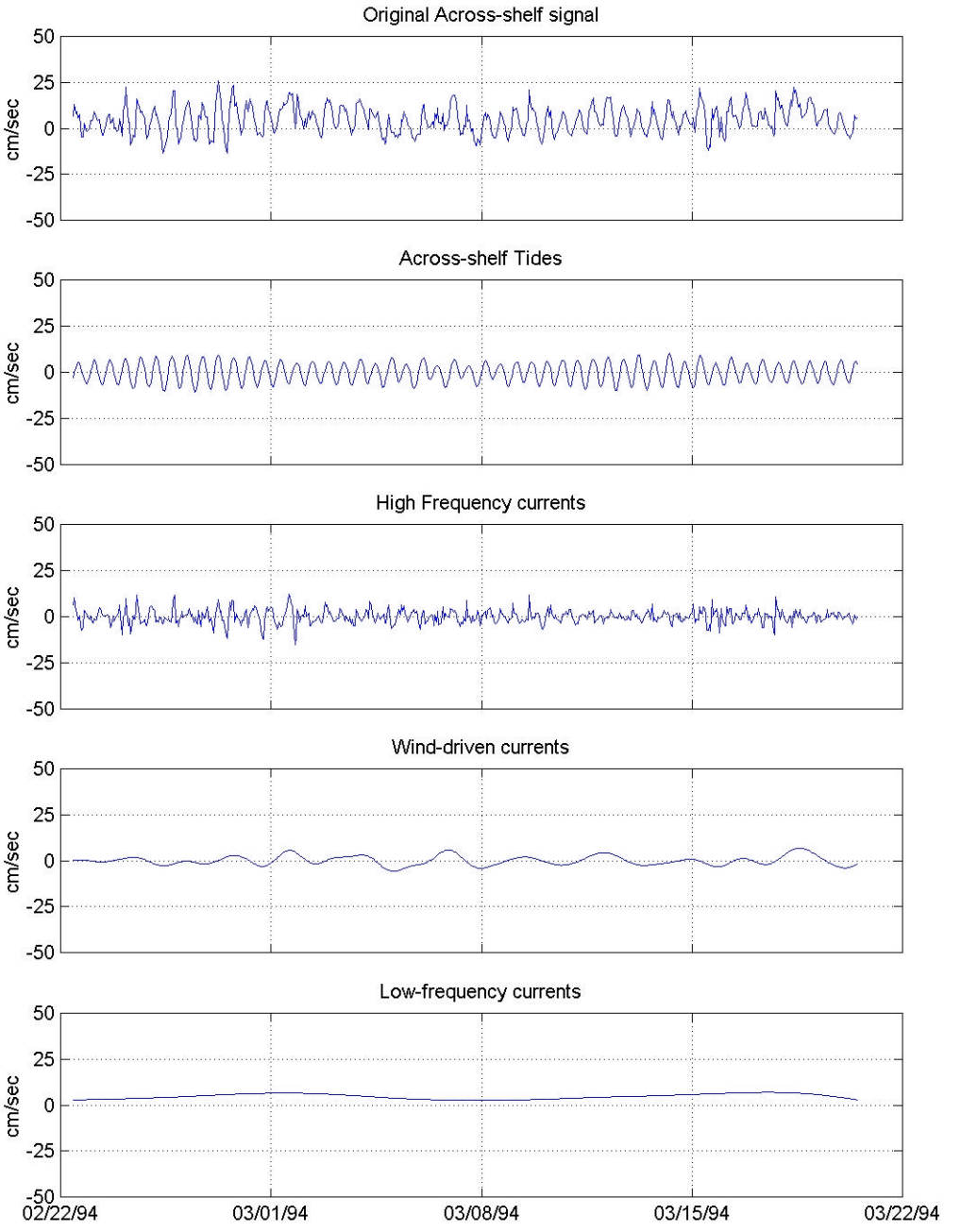

Figure 5-3. Time series of individual cross-shelf flow processes for February-March (Winter) 1994. Note the lack of wind-driven currents in late February, when the along-shelf flow (Figure 5-2) showed noticeable variability. Semi-diurnal tides account for most of the cross-shelf signal.

High-frequency and low-frequency currents were both slightly greater in winter than in summer. These currents were shown to be correlated to wind-driven currents, suggesting atmospheric forcing events may be root cause for variability at these frequencies, thus would also strengthen during time periods of stronger atmospheric forcing. Winter season, with a corresponding weakening of the Bermuda High pressure zone and southern migration of the Icelandic Low pressure zone, brings predominant Arctic winds out of the north and northwest (Louis Berger Group, 1999). These Arctic winter winds are generally stronger than typical summer winds from the south, thus inducing a corresponding increase in shelf current energy.

5.1.2 Summary of Flow Regimes at Offshore Borrow Sites

The analysis presented above suggests along-shelf currents possess greater energy than cross-shelf flows. The mean along-shelf flow was directed southward. Along-shelf currents were found dominated by wind-driven processes, accounting for as much as 70% of the total current energy. Wind-driven processes were greatest in winter; however, wind-driven flows appeared strongly biased by singular events, such as local responses to storm winds or non-locally generated free waves that influenced the magnitude of wind-driven current energy.

Cross-shelf bottom currents were affected most significantly by semi-diurnal tides, with a mean onshore flow. Wind-driven currents were found to be less significant in the cross-shelf direction.

Seasonal variability was most significant for wind-driven currents. Winter and autumn data records were most energetic, with summer and spring data sets possessing smaller energy values. Louis Berger Group (1999) show that extratropical storms (i.e., northeast storms) occur more frequently during fall and winter time periods. Analysis of the wind-driven time series showed current energy values could be biased by singular events, such as storms or non-locally generated free waves. Currents, which appear dominated by wind-driven processes, are stronger during time periods of higher wind activity. In addition to wind-driven currents, high frequency (noise, random motions) and low-frequency currents also appear to be stronger during winter time periods. This suggests these high- and low-frequency flow processes may also be coupled to atmospheric forcing.

The evidence collected in this analysis, and supported by previous studies, suggests that shelf flow is strongest during singular events (i.e., storms or non-locally generated free waves), and that these currents flow primarily along the shelf. This evidence can be extrapolated to suggest that these singular events, with corresponding higher currents, have the greatest potential to transport sand. If so, sediment transport patterns may be predominately in the along-shelf direction, with a net transport oriented in the direction of the mean southerly flow. The data also showed that these same singular events had little impact on cross-shelf currents, suggesting that cross-shelf sediment transport due to currents may be weak.

5.1.3 Wave-Induced Bottom Currents

A propagating wave not only causes a displacement in the water surface, but also displaces water particles beneath the passing wave. This displacement induces local currents, which over the period of the passing wave take on an orbital shape (orbital velocities). In shallow water, the orbits of water particles tend to take on an elliptical shape, while in deeper water the orbits are more circular (Figure 5-4). Associated with these water particle trajectories are the particle horizontal (u_{orbit}) and vertical (w_{orbit}) orbital velocity components. These velocity components contribute to the initiation and transport of sediment at the seabed. Therefore, knowledge of orbital velocities at the seabed is a key parameter for determining sediment

transport characteristics at potential offshore borrow areas. This section describes the method used to calculate wave-induced orbital velocities at the seabed.

Figure 5-4. Shallow water and deep water wave orbits.

The relationship between a progressive wave and the particle motion it generates beneath the surface is well described by linear wave theory. Linear wave theory is used to derive the expression of the velocity potential (f) as:

$$f = -\frac{Hg}{2s}\frac{\cosh k\left(h+z\right)}{\cosh\left(kh\right)}\cos\left(kx\right)\sin\left(s\,t\right) \tag{5.1}$$

where H is the wave height; Φ is the wave frequency; k is the wave number; h is the still water depth; z is the point of interest in the water column (positive upwards from still water); x is the horizontal point of interest along the wave, g is the gravitational constant, and t is the temporal point of interest. The resulting horizontal and vertical velocities under the wave are given by:

$$u_{orbit} = \frac{-\P f}{\P x} = \frac{H}{2}s\,\frac{\cosh k\left(h+z\right)}{\sinh\left(kh\right)}\cos\left(kx - s\,t\right) \tag{5.2}$$

$$w_{orbit} = \frac{-\P f}{\P z} = \frac{H}{2}s\,\frac{\sinh k\left(h+z\right)}{\sinh\left(kh\right)}\sin\left(kx - s\,t\right) \tag{5.3}$$

Equations (5.2) and (5.3) reveal that the velocity at the bottom (z = -h) consists only of the u_{orbit} component, while w_{orbit} is zero. Thus, at the seabed, the motion of water particles is purely horizontal (assuming the water cannot penetrate the seabed). This allows the reduction of the velocity at the bottom to:

$$U_B = \frac{H}{2}\frac{s}{\sinh\left(kh\right)} \tag{5.4}$$

The horizontal motion, as the seabed oscillates positively (under a crest) and negatively (under a trough), depends on the spatial and temporal position of the wave (Figure 5-5). Therefore, the absolute maximum bottom currents induced by the wave occur at the crest and/or the trough of the passing wave.

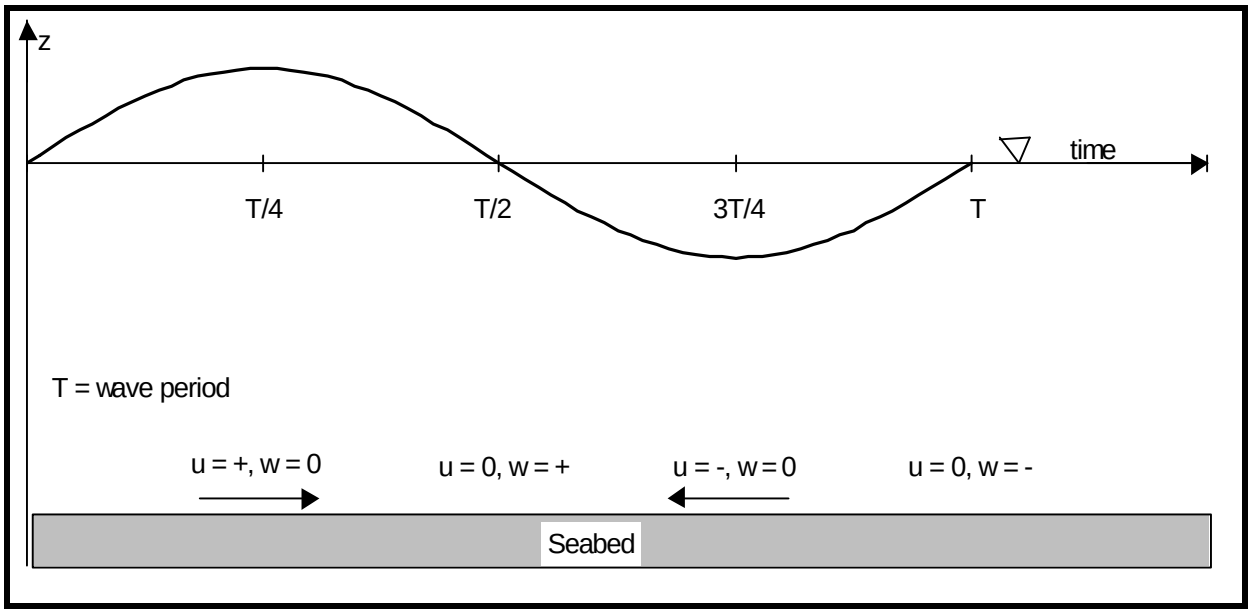

Figure 5-5. Schematic of wave-induced bottom velocities.

Applying linear wave theory, coupled with the wave model results at the dredged borrow areas, wave-generated bottom currents can be determined. Wave height, wave period, wave direction, and water depth are extracted from the wave model at each of the designated borrow areas (and for each season/event scenario) and used to calculate the maximum horizontal orbital velocity at the seafloor for each grid point within the selected domain. Wave-induced bottom velocities can then be combined with ambient currents and utilized to determine sediment initiation and potential transport at the offshore borrow sites.

The wave-induced bottom velocity is a key factor contributing to the initiation and transport of sediment. Although no net sediment transport is caused by the orbital motions for purely sinusoidal waves, shearing velocities created at the seabed by the waves are a primary contributor to the initialization of sediment into the water column (Fredsoe and Deigaard, 1992).

5.1.4 Wave-Induced Longshore Currents

In addition to orbital velocities generated beneath a propagating wave, longshore currents are generated in the nearshore zone (generally landward of the breaker line) by waves approaching obliquely to the coast. This longshore current is the primary advective force generating littoral drift along the beach. Several models have been developed that take simplified information from monochromatic wave models to develop empirical or semi-empirical relationships between calculated wave information and longshore sediment transport rate. However, the use of REF/DIF S output allowed development of a sediment transport model based on spectral wave parameters. As part of the output, REF/DIF S calculates radiation stress values (S_{xx}, S_{xy}, and S_{yy}) at each model grid cell for the entire spectra. Therefore, a single set for radiation stress values at each grid cell provides the basis of sediment transport analyses. The methodology requires a two-part procedure: wave-induced currents were developed following the work of Ebersole and Dalrymple (1980), and the cross-shore distribution of currents was utilized to generate local longshore sediment transport rates based on the work of Bodge (1986).

The governing equations of the wave-induced current model are the depth-averaged continuity equation and the depth-averaged *x* and *y* direction momentum equations. All of these

equations are developed by integrating the standard form of the equations over the depth of the water column and then time-averaging the results. Previous work incorporating this methodology includes Birkemeier and Dalrymple (1976), Ebersole and Dalrymple (1979), Yan (1987), Winer (1988), and Ramsey (1991).

Due to the inherent complexities of wave-induced current formation in the surf zone, certain assumptions are required in the derivation of governing equations for the wave-induced current model. A primary simplification is that the flow field may be represented in two dimensions by depth and time-averaging the equations. Therefore, the vertical variation in the velocity profile is lost. The advantage of depth averaging the equations is to reduce the complicated three-dimensional problem to a more tractable two-dimensional one. However, some details of the flow field may be missed by only considering horizontal flow.

5.1.4.1 Governing Equations

The form of the continuity equation used in this model assumes that the water density is constant and can be represented by:

$$\frac{\partial \bar{h}}{\partial t} + \frac{\partial}{\partial x}(UD) + \frac{\partial}{\partial y}(VD) = 0 \tag{5.5}$$

where

U = the x component of the mean current
V = the y component of the mean current
$\bar{h}$ = the mean water surface elevation
D = the total water depth $(h + \bar{h})$
h = the local still water depth

The continuity equation represents the conservation of mass per unit surface area under the assumption that the water density does not change with depth or time. Although seasonal temperature variations may affect water density, the influence of density variability on wave-induced current velocities within the surf zone can be considered negligible.

The horizontal depth-averaged momentum equations were originally derived by Phillips (1969) and for the purpose of the wave-induced current model take the form:

$$\frac{\partial}{\partial t}(UD) + \frac{\partial}{\partial x}\left(U^2 D\right) + \frac{\partial}{\partial y}(UVD) = -gD\frac{\partial \bar{h}}{\partial x} - \frac{D}{r}\frac{\partial \overline{ti}}{\partial y} - \frac{1}{r}\frac{\partial S_{xy}}{\partial y} - \frac{1}{r}\frac{\partial S_{xx}}{\partial x} + \frac{1}{r}t_{sx} - \frac{1}{r}t_{bx} \tag{5.6}$$

and

$$\frac{\partial}{\partial t}(VD) + \frac{\partial}{\partial x}(UVD) + \frac{\partial}{\partial y}\left(V^2 D\right) = -gD\frac{\partial \bar{h}}{\partial x} - \frac{D}{r}\frac{\partial \overline{ti}}{\partial x} - \frac{1}{r}\frac{\partial S_{xy}}{\partial x} - \frac{1}{r}\frac{\partial S_{yy}}{\partial y} + \frac{1}{r}t_{sy} - \frac{1}{r}t_{by} \tag{5.7}$$

for the x and y direction, respectively, where

U = x component of mean current
V = y component of mean current
$\bar{h}$ = mean water surface elevation
D = total water depth

r = water density
τ_t = lateral stress due to turbulent mixing
τ_{bx} = x component of bottom shear stress
τ_{by} = y component of bottom shear stress
τ_{sx} = x component of surface shear stress
τ_{sy} = y component of surface shear stress.

Many of the terms in the depth-averaged momentum equations require certain empirical guidelines to compute their values. The theory governing bottom friction and lateral mixing are not completely understood and, therefore, need empirical formulations or scaling arguments to estimate their values.

First, the bottom shear stress typically is based on some type of drag coefficient and can be expressed as:

$$t_{bi} = r f \overline{u_{ti} |u_t|} \tag{5.8}$$

where u_t is composed of the mean current and the wave orbital velocity, u_{ti} is its component form (either in the x or y direction), and the overbar indicates time averaging over one wave period. The empirical friction factor is represented by f. The magnitude of the total velocity, expressed as $|u_t|$, is equal to $\sqrt{u^2 + v^2}$ where the u and v velocity components are

$$u = U + u_{xw} = U + u_w \cos q \tag{5.9}$$

$$v = V + u_{yw} = V + u_w \sin q \tag{5.10}$$

U and V are the mean current speeds defined previously. The wave orbital velocities in the x and y direction are u_{xw} and $u_{yw,}$ respectively, where $u_w = \sqrt{u_{xw}^2 + u_{yw}^2}$. The total velocity can then be expressed as

$$|u_t| = \sqrt{U^2 = V^2 = u_w^2 = 2Uu_w \cos q = 2Vu_w \sin q} \tag{5.11}$$

The wave orbital velocity exhibits oscillatory behavior which may be expressed as

$$u_w = u_{\max} \cos s t \tag{5.12}$$

where u_{max} is the maximum orbital velocity at the bottom which can be written as

$$u_{\max} = \frac{s |a|}{\sinh kh} \tag{5.13}$$

For numerical efficiency, a simplified model that includes wave orbital velocities and a strong current assumption may be formulated as

$$t_{bi} = pf |u_t'| U_i \tag{5.14}$$

where

$$|u_t'| = \sqrt{U^2 + V^2} + u_{\max} \tag{5.15}$$

This equation implies that there is no interaction between the wave orbital velocity and the mean current velocity. The equations for x and y components may be expressed as

$$t_{bx} = pf |u_t'| U \tag{5.16}$$

and

$$t_{by} = pf|u_t'|V \tag{5.17}$$

This simplification allows calculation of bottom shear stresses without the computational demands of full integral equations. Increasing the friction factor may offset any differences between this approach and the more complete integral equations. The selection of a proper value for the friction factor is very important in modeling currents and will be discussed in Section 5.1.4.3.

5.1.4.2 Lateral Mixing

Longshore currents vary with distance offshore, where strongest currents typically are found near the wave break point. If the wave-induced current model did not include cross-shore mixing, the predicted longshore velocity profile would change abruptly to zero at the breaker line as shown in Figure 5-6. To simulate the effect of turbulent mixing in the surf zone, some type of cross-shore mixing within the velocity profile is required. In addition, longshore mixing may be required if morphologic controls (e.g. shore perpendicular channels or shoals in the surf zone) or groins create rip currents. Since this application of the wave-induced current model for the New Jersey coast involves a sandy coast with no major shore protection structures, the focus of lateral mixing only involves the cross-shore direction.

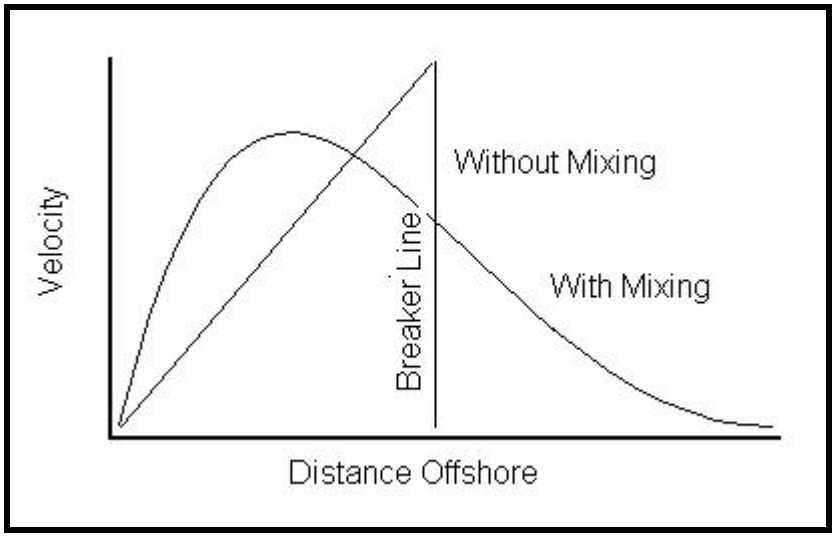

Figure 5-6. Schematic longshore velocity profiles with and without cross-shore mixing (the abrupt reduction in velocity for the without mixing case occurs at the breaker line).

Harris et al. (1963) were the first to conduct field and laboratory studies to measure the intensity of mixing within the surf-zone. Their work involved releasing known amounts of tracer in the nearshore region and calculating the strength of mixing based on measured concentration of the tracer at a later time. Qualitative results indicated that the tracer dispersed rapidly in the on/offshore direction and that, in the absence of rip currents, cross-shore mixing was confined mainly to the surf zone. In addition, they noted that mixing in the longshore direction was largely due to advection of the dye by the longshore current.

Longuet-Higgins (1970) used the two depth-integrated equations of motion which assumed that the turbulent fluctuation term, $-\overline{\rho u'v'}$, is independent of depth to derive a different equation for cross-shore mixing. Another major assumption required in the derivation was that the momentum transfer due to turbulent fluctuations may be represented as a product

of the mixing length coefficients (ε_χ, ε_γ) and derivatives of the mean current. In equation form, this can be expressed as

$$t_i = -r\left(e_y \frac{\partial U}{\partial y} + e_x \frac{\partial V}{\partial x}\right) \tag{5.18}$$

Longuet-Higgins made additional assumptions regarding horizontal mixing in the surf-zone based on the horizontal eddy viscosity coefficient, ε_χ. Since the turbulent eddies responsible for lateral mixing must be smaller than the distance from an arbitrary point to the shoreline, it follows that ε_χ must tend to zero as the shoreline is approached. However, the decrease in ε_χ, between the breakerline and the shoreline is not necessarily linear. The approach adopted by Longuet-Higgins was to assume that ε_χ is proportional to the offshore distance, *x*, multiplied by a typical shallow water wave celerity, $\sqrt{gh}$. When the bottom slope is uniform, a simple equation governs the longshore current profile. Although beach profiles in nature are not uniform, the simplified approach provides a reasonable method for determining an appropriate mixing coefficient. Expressing the cross-shore mixing coefficient as

$$e_x = Nx\sqrt{gh} \tag{5.19}$$

and using a number of scaling arguments for the variables, the probable limits for the constant *N* were found to be $0 < N < 0.016$.

This equation or some slight modification has become the standard formula for calculating mixing in longshore current models. Seaward of the plunge line, ε_χ is kept at the maximum value. Since there is little turbulence seaward of the plunge line, the high value of the mixing coefficient ensures that there is a reasonable amount of lateral mixing in the cross-shore direction. For the spectral wave model, much of the cross-shore mixing is represented by gradual breaking of waves, where longer wave components break farther from shore. This representation of a wave breaking envelope tends to distribute longshore currents in a manner similar to the with mixing case shown in Figure 5-6. Therefore, significant redistribution of longshore currents using the above methodology was not necessary, and values for the cross-shore mixing coefficient were minimized.

5.1.4.3 Model Verification

Because the primary purpose for calculating the cross-shore distribution of the longshore current was to calculate the littoral drift rate, model validation to field experiments was required to gauge computational accuracy. The model was verified using the field data sets of Kraus and Sasaki (1979) and Thornton and Guza (1989). These data represented a broad range of field conditions, with wave periods ranging from 4.1 to 12.8 sec. Kraus and Larson (1991) used both data sets to verify the one-dimensional longshore current model, NMLONG. Unfortunately, these field test cases provide only cross-shore variation in the longshore current. No two-dimensional field data sets were found for model verification. Several laboratory experiments have been performed to evaluate two-dimensional wave-induced current fields, including currents near groins (Winer, 1988) and shore parallel breakwaters (Ramsey, 1991).

For the field cases modeled, radiation stresses were calculated based on the results of a monochromatic wave refraction model designed to estimate wave heights and directions within the nearshore region. Since this wave model over-simplified nearshore wave conditions, limited wave-induced current model verification was anticipated. However, results of the current model compared favorably with both data sets. In addition, the modeled longshore current distribution was similar to those predicted by the NMLONG model.

Kraus and Sasaki (1979) measured the longshore current profile along seven transects on a sandy beach facing the Sea of Japan. Current measurements were made simultaneously along each transect by divers positioned at 5-m intervals. The current was measured by timing the migration of neutrally buoyant floats located at about mid-depth. An average current velocity was computed based on three successive measurements along each transect. Field observations during the field experiment indicated the waves arrived as clean swell, with a significant wave height of 1.0 m, a period of 4.1 sec, and an angle at breaking of 9 degrees relative to the shoreline.

A comparison of field experiment results and wave-induced current model output used in this study is shown in Figure 5-7. Due to the relatively steep waves, two significant peaks of longshore current velocity were computed by the model: one peak just landward of the observed breaker line (about 40 m offshore) and one peak adjacent to the shoreline. This increase in current strength near the swash zone is typical of steep wave conditions (Bodge, 1986). The results from two different model runs are shown, with the friction factor ranging between 0.0025 and 0.0030. Both the magnitude and offshore position of the maximum longshore current compare well with field data. In addition, the modeled prediction of current strengths seaward of the breaker line closely matched the data. However, the modeled current magnitude was under-predicted relative to field measurements.

To further verify the applicability of the wave-induced current model, wave and longshore current data from Thornton and Guza (1989) were utilized. The data were collected at Leadbetter Beach, California at a location where nearshore contours were relatively straight and parallel. Although four cases were presented in the initial work, only the February 5th Case was used for comparison with the wave model. Wave conditions for this case were a root-mean-square wave height of 0.45 m, a wave period of 12.8 sec, and an angle at breaking of 8.4 degrees relative to the shoreline.

A comparison of field data and wave-induced current model output is shown in Figure 5-8. The results from three different model runs are shown, with the friction factor ranging between values of 0.002 and 0.004. This range of friction values is similar to those employed by Kraus and Larson (1991). The magnitude of the maximum longshore current compares well with field data; however, the model predicted the location of the peak current much closer to the shoreline than the data indicated. In this case, use of a monochromatic wave model to generate radiation stresses for the wave-induced current model effectively eliminated cross-shore mixing associated with various spectral components.

5.1.4.4 Wave-Induced Currents Along the New Jersey Coast

Model verification provided confidence that the wave-induced current model could be used to effectively evaluate longshore currents as the basis for littoral drift prediction. A sensitivity analysis was performed to determine appropriate values for the friction coefficient. Based on the verification runs, as well as previous work by Ramsey (1991), the appropriate value of *f* was determined to be 0.003. This value was used for all model runs associated with the New Jersey study.

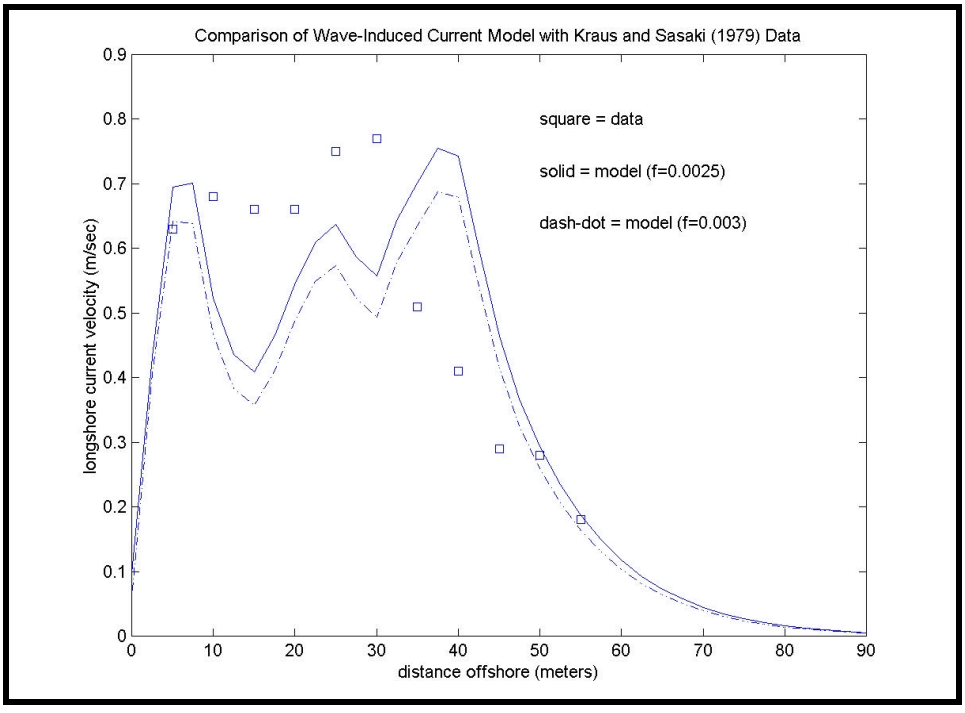

Figure 5-7. Comparison of model and observed longshore current velocities from field measurements taken by Kraus and Sasaki (1979).

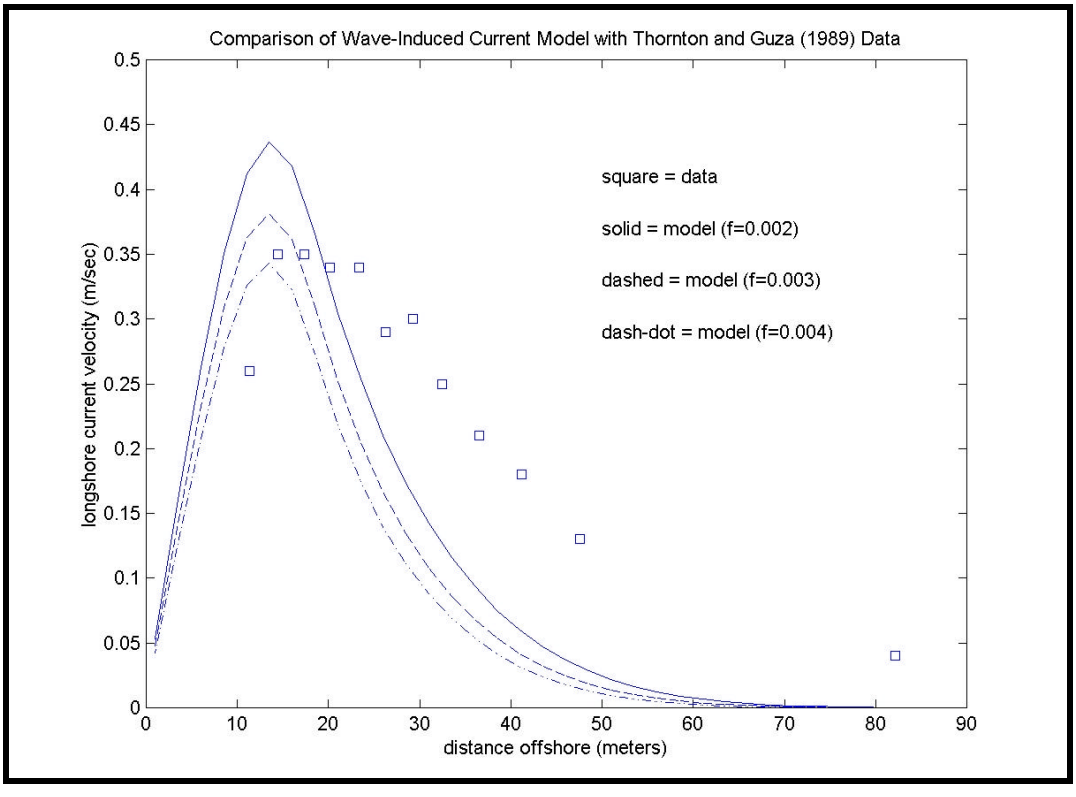

Figure 5-8. Comparison of modeled to observed longshore current velocities from field measurements taken by Thornton and Guza (1989).

Because the results of the wave-induced current model are merely an intermediary step in the calculation of longshore sediment transport, only sample results from the current model are presented in this report. The wave-induced current model was run for the wave modeling sub-grids (A, B1, B2, and C) for each spectral wave condition (either seven or eight depending on the location), and for existing conditions and post-dredging scenarios. Model runs included average annual wave conditions, as well as 50-year extreme wave conditions resulting from hurricanes and northeast storms. A total of 58 model runs were required to simulate these conditions along the New Jersey coast. The results of one run (the existing conditions at Grid A for the -22.5° wave condition) are described in detail below. This example provides an overview of typical wave-induced current predictions associated with the modeling effort.

First, radiation stress in the longshore direction across a shore perpendicular transect is denoted as S_{xy}. Although the combined effects of the other two radiation stress components (S_{xy}, S_{xy}) are important to the two-dimensional current regime, S_{xy} provides the primary driving force for longshore currents. As waves reach the break point, it is the variation in S_{xy} across the surf zone that induces longshore current motion. Figure 5-9 illustrates the longshore and cross-shore distribution of S_{xy}, indicating regions of longshore energy focus. In general, areas of higher S_{xy} values have higher maximum current velocities.

Cross-shore variability of the longshore current also can impact longshore sediment transport. Areas with relatively wide surf zones may exhibit low maximum longshore current velocities; however, currents exist over a larger area on these beaches and if currents are strong enough to mobilize sediment, longshore transport rates can be higher than beaches with higher maximum currents. Along much of the New Jersey shoreline, the beachface can be relatively steep; however, the milder offshore slope generally provides a wide surf zone (often in excess of 150 m). In addition, the energetic wave climate along the Atlantic coast of New Jersey creates significant wave-induced longshore currents. The maximum current strengths shown on Figure 5-9 directly reflect the transport trends along this stretch of beach, where the strongest currents are located to the north of Townsends Inlet. Although the wave condition shown in Figure 5-9 represents waves propagating from the east-southeast, shoreline orientation causes breaking waves to generate southerly-directed currents and longshore sediment transport. This condition is typical along much of the New Jersey shoreline, where predominant wave conditions propagate from the east and southeast; however, the southwest-to-northeast orientation of the shoreline (especially in the southern half of the State) causes these waves to break obliquely to the shoreline and generate southerly-directed currents.

Figure 5-10 provides four longshore current profiles indicating the variability of currents along the shoreline between Townsends Inlet and the beach just north of Corsons Inlet. Although there is some variability in profile shape along this stretch of shoreline, especially in the vicinity of tidal inlets, longshore current velocities become negligible within 200 m of the shoreline at all locations. The surf zone width appears to be slightly wider near the southern end of Grid A, likely due to larger wave heights in this region. For the -22.5° wave condition, maximum longshore current speeds vary by more than 50%, ranging from approximately 0.5 to 1.0 m/s. Although not a direct link, the longshore variation in maximum current is an indication of longshore sediment transport trends. Typically, areas with greater wave-induced current velocities will have a higher longshore sediment transport potential. A detailed analysis of longshore sediment transport potential is provided in Section 5.2.2.

Because the wave-induced current analysis was an intermediary step between wave transformation modeling and longshore sediment transport modeling, detailed results for each seasonal or extremal cases have not been provided. As described above, variations in longshore currents were similar to trends depicted in nearshore sediment transport modeling described in Section 5.2.2.

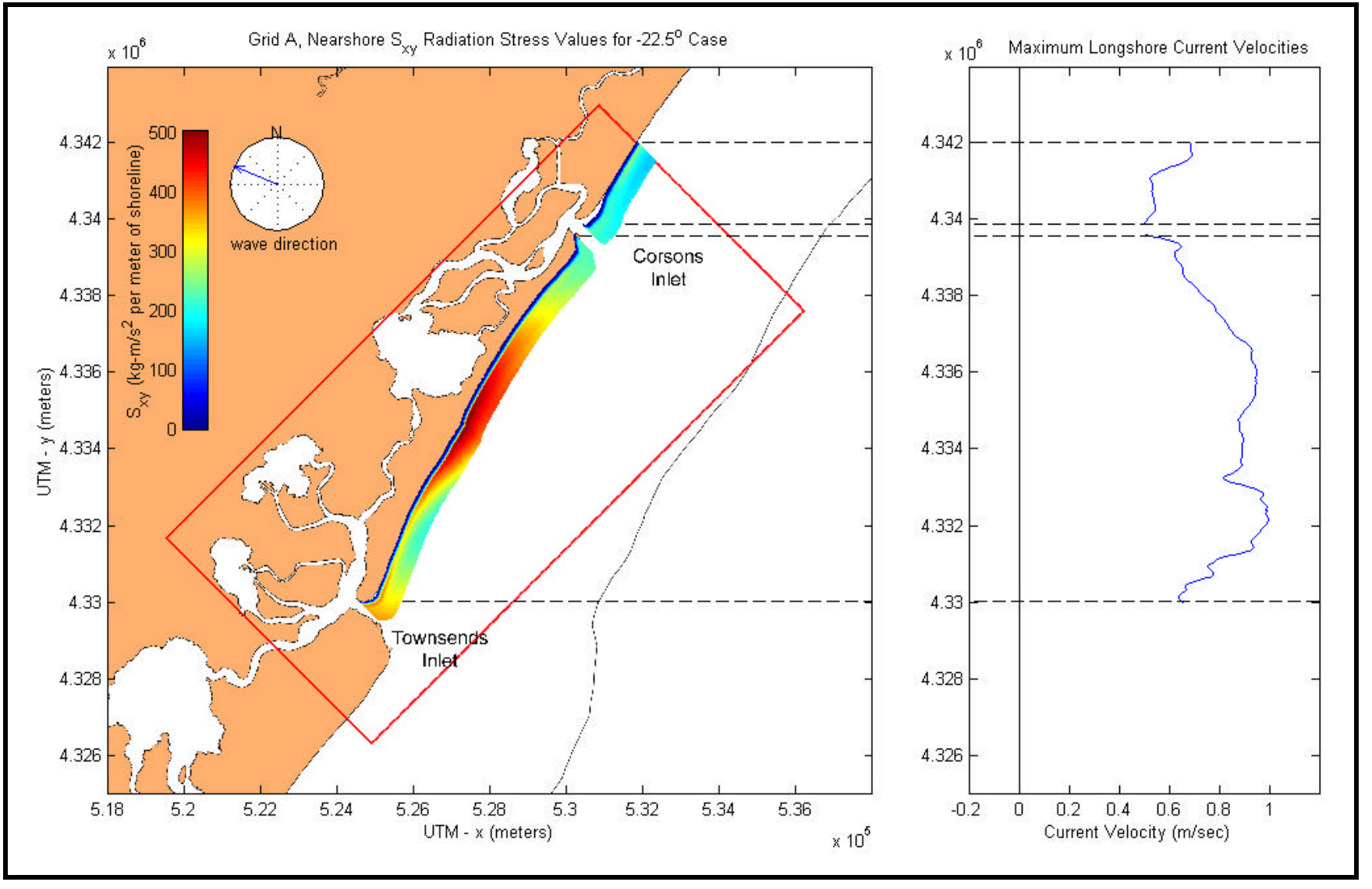

Figure 5-9. S_{xy} radiation stress and maximum longshore current velocities predicted by the wave-induced current model within Grid A for the -22.5° wave condition. Positive velocities are toward the south.

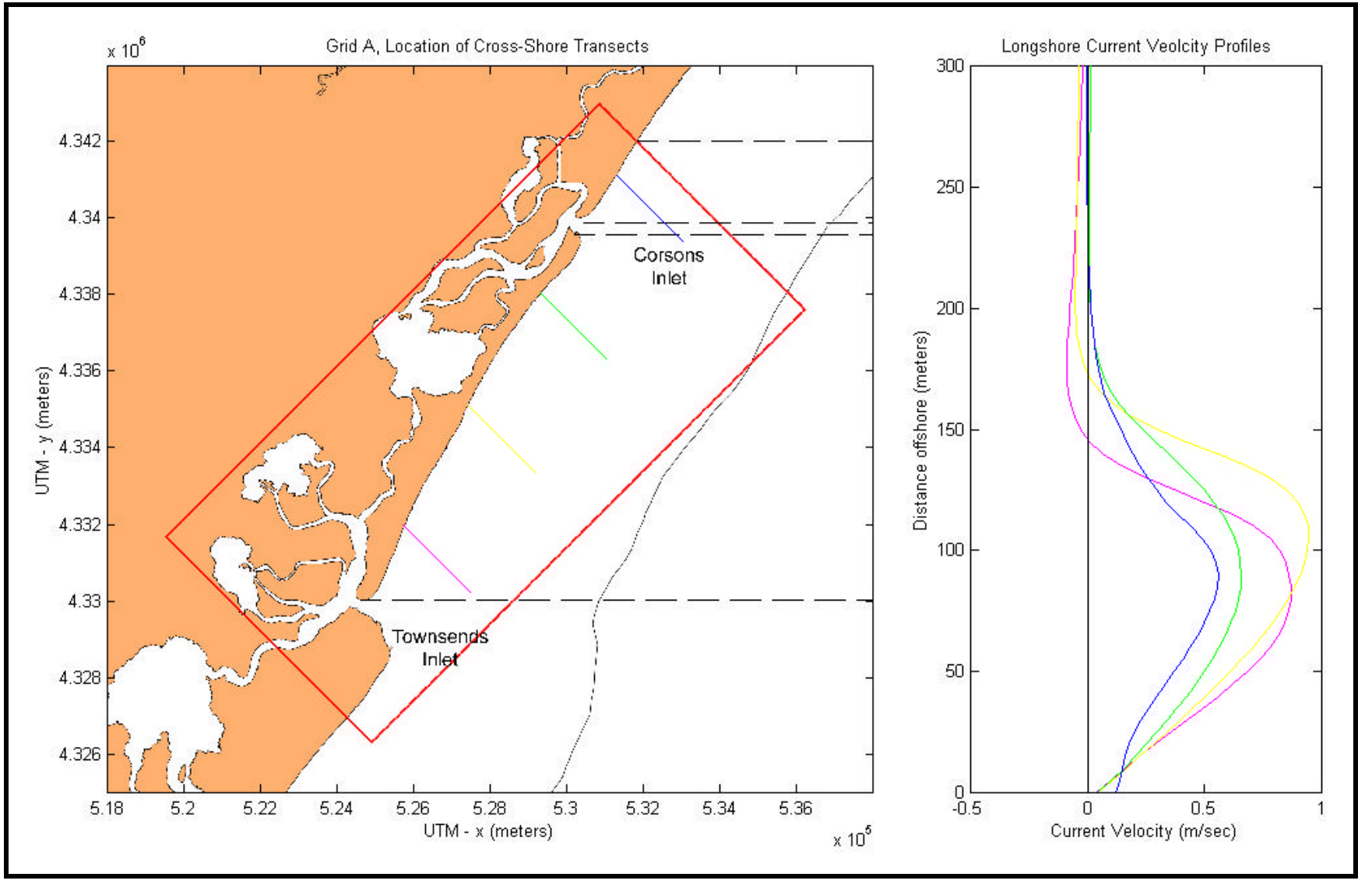

Figure 5-10. Longshore current profiles along selected transects within Grid A for the -22.5° wave condition (colored transects in the left sub-plot correspond to like colored profiles in the right sub-plot).

5.2 SEDIMENT TRANSPORT MODELING

5.2.1 Sediment Transport at Borrow Sites

Potential sand mining activities at offshore borrow areas may lead to changes in sediment transport mechanics occurring at or near proposed offshore dredging locations. The purpose of this section is to identify the approximate quantity and direction of sediment transport at potential borrow sites and estimate the duration for infilling of borrow areas. Spectral wave model results, along with historical and measured current observations, were employed for the analysis of sand transport at borrow sites. This section examines the interaction of wave-induced bottom orbital velocities and ambient currents, the initiation of sediment motion at potential borrow areas, and the relative magnitude and direction of sediment transport.

5.2.1.1 Initiation of Sediment Motion Under Combined Wave and Current Action

Assuming purely oscillatory wave motion (linear theory) without currents results in no net sediment transport at the offshore borrow areas. If sediment is lifted from a non-sloping seafloor into the water column, the amount of sediment transported forward (in the direction of wave propagation) during half of the cycle will equal the amount being transported backwards during the second half of the cycle. In order to produce a net difference in sediment transport, additional physical phenomena are required. These include:

- bottom slopes on the seafloor
- tidal and/or wind-driven currents
- wave asymmetry (non-linearity)
- wave-induced mass transport

In areas outside the surfzone, it is critical to account for wave and current interactions inside the bottom boundary layer when evaluating potential sediment transport. Introducing coastal currents to wave motions adds difficulty in estimating shear, dissipation, and sediment transport dynamics. A number of approaches have been developed by Lundgren (1972), Bakker (1974), Smith (1977), and Bakker and van Doorn (1978) to attempt to solve this problem.

Only Madsen and Grant (1976, 1977), Grant and Madsen (1978, 1979) and Tanaka and Shuto (1981), considered current and wave interaction situations, where the current and wave have an arbitrary angle with each other. Tanaka and Shuto (1981) used a one-layer eddy viscosity approach, which most likely over simplified the problem. Madsen and Grant (1976, 1977), and Grant and Madsen (1978, 1979) derived sediment transport relationships for predicting net sediment transport rates in the presence of second order effects such as bottom slope, wave asymmetry, coastal currents, and mass transport currents. They concluded that only cases involving small amplitude wave theory (i.e., linear) and a steady current are understood to a level that it is reasonable to evaluate resulting sediment transport rates with any degree of confidence. Fortunately, this is the situation for offshore New Jersey, including the potential offshore borrow areas. Appendix C1 provides a comprehensive discussion of the theoretical background of sediment initiation under combined wave and current forces.

5.2.1.2 Relative Magnitude and Direction of Transport

Sediment initiation provides valuable insight regarding sediment movement, but it does not provide information relative to the magnitude or direction of sediment transport. Therefore, sediment transport rates and transport directions need to be calculated in and around the

offshore borrow areas (Figures 5-11 to 5-14) to assess overall sediment transport potential, as well as provide insight into:

- approximate rates of sediment transport,
- estimates on borrow site infilling rates, and
- directional fluctuations in sediment transport patterns

This section presents the results of offshore sediment transport analyses at potential borrow site locations following a proposed dredging episode. Sediment initiation and potential sediment transport rates were estimated in and around the dredged area.

Offshore sediment transport rates are based on analytical expressions developed by Madsen and Grant (1976). Qualitatively they involve:

1. determining the time-varying values of sediment transport in the northing (y) and easting (x) directions,
2. time-averaging these sediment transport component results, and
3. calculating the net sediment transport magnitude and direction.

Appendix C2 provides a theoretical discussion of sediment transport calculations.

To accurately calculate sediment transport rates, as well as initiation of motion, information about sediment size at each of the seven sand resource areas is required. Table 5-1 summarizes various sediment sizes at each of the borrow areas. The values were obtained from grain size analyses performed on samples taken at each of the seven sand resource areas.

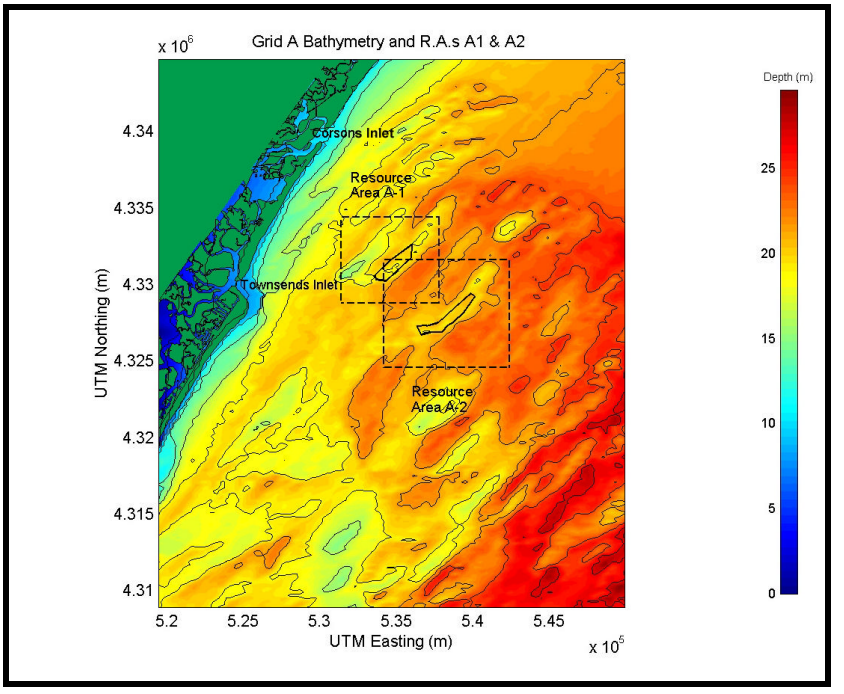

Figure 5-11. Location of the offshore observation regions within Sand Resource Areas A1 and areas A2. These observation areas were used to determine potential sediment transport at borrow sites following numerical dredging.

Table 5-1. Sediment sizes at Sand Resource Areas A1 through G3.			
Resource Area	d_{10} (mm)	d_{50} (mm)	d_{90} (mm)
A1	0.59	0.35	0.21
A2	1.70	0.62	0.30
C1	0.40	0.20	0.14
G2 Top	1.40	0.66	0.30
G2 Bottom	1.40	0.66	0.30
G3	0.90	0.51	0.26
F2	2.40	0.46	0.27

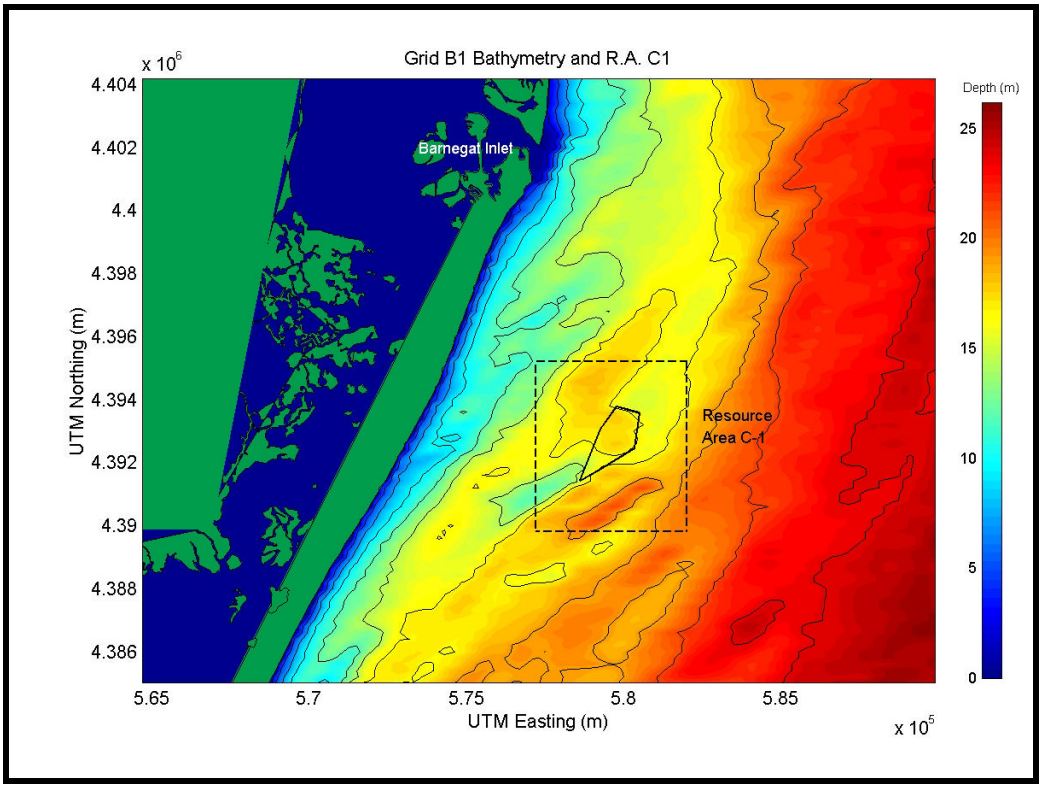

Figure 5-12. Location of the offshore observation regions within Sand Resource Area C1. These observation areas were used to determine potential sediment transport at the borrow sites following numerical dredging.

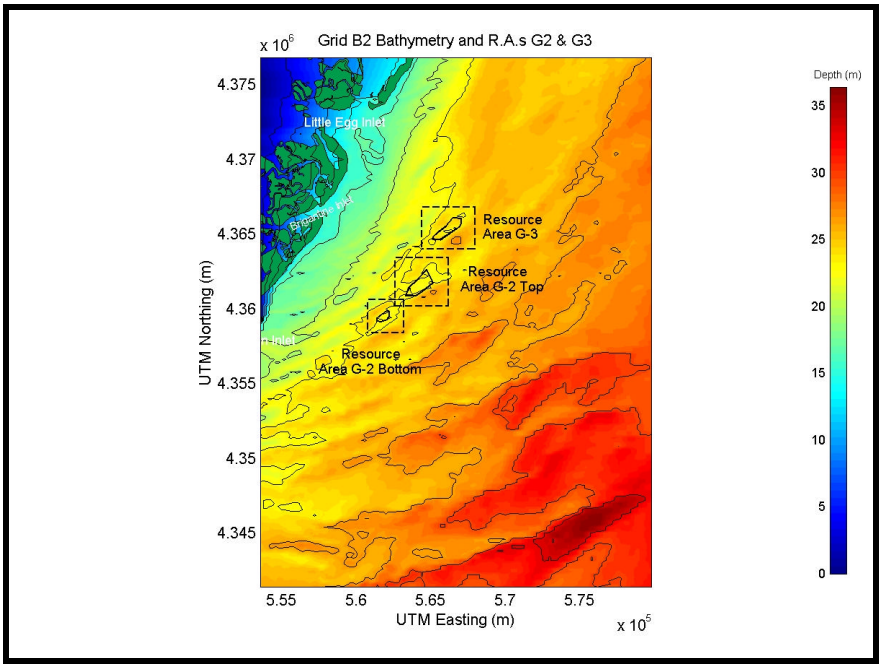

Figure 5-13. Location of the offshore observation regions within Sand Resource Areas G2 Top, G2 Bottom, and G3. These observation areas were used to determine potential sediment transport at the borrow sites following numerical dredging.

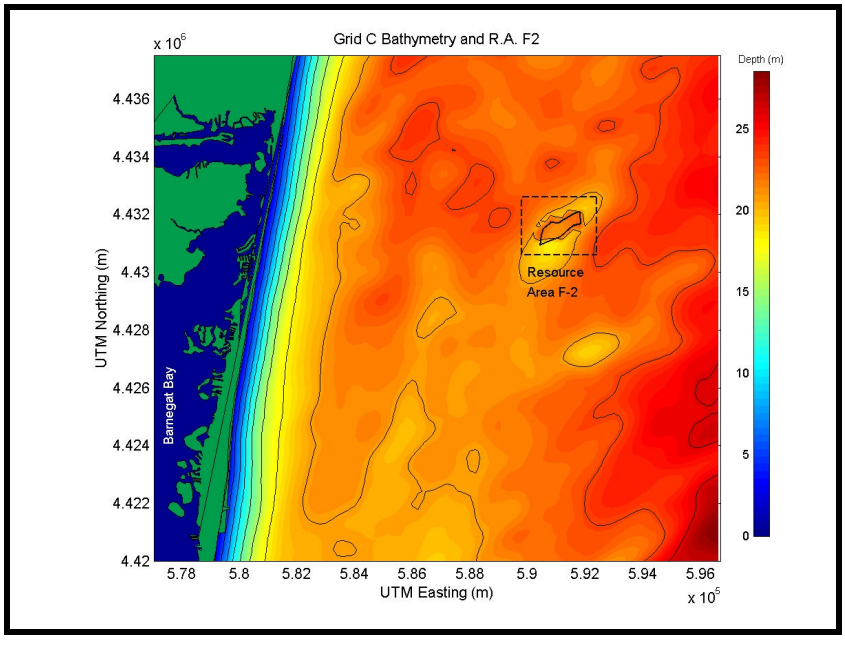

Figure 5-14. Location of the offshore observation regions within Sand Resource Area F2. These observation areas were used to determine potential sediment transport at the borrow sites following numerical dredging.

Seven potential sand borrow sites were investigated to determine: 1) sediment transport rate estimates into and around the dredged areas and 2) approximate infilling rates. Directional results are presented and discussed. In addition, a yearly average is formulated from

directional results, including the influence of calm seas (waves heading offshore). The directional simulations can be combined to reflect the annual wave climate, although a portion of the wave energy will be ignored when using the directional analysis method. Because each directional approach simulation represents a percentage of the total waves impacting the coast over an average year, the results of each simulation were weighted to create an approximate representation of an annual wave climate. Waves propagating offshore were assumed to represent calm conditions. Table 5-2 summarizes the bins and percent contribution of each bin. In general, more energy is associated with waves that travel from the east and southeast.

Table 5-2. Percent contributed based on energy per bin.

Approach Direction	Directional Bin (Grid Relative)	Resource Area by Grid			
		Grid A (A1 & A2)	Grid B1 (C1)	Grid B2 (G2 & G3)	Grid C (F2)
Northeast	45E	--	--	--	2.3%
East-Northeast	22.5E	2.3%	3.4%	3.8%	3.4%
East	0E	19.7%	26.1%	22.2%	26.1%
East-Southeast	-22.5E	23.1%	25.8%	19.6%	25.8%
Southeast	-45E	19.8%	19.9%	17.0%	19.9%
South-Southeast	-67.5E	15.8%	13.9%	14.1%	13.9%
---	Calm	19.3%	10.9%	23.3%	8.6%

5.2.1.3 Hydrodynamics and Sediment Transport for Resource Areas A1 and A2

Figures 5-15 through 5-19 illustrate directional hydrodynamic and sediment transport results at the sand borrow site in Area A1, while the influence of potential sand mining activities at the borrow site in Area A2, relative to hydrodynamics and sediment transport, is documented in Figures 5-20 through 5-24. The figures include maximum wave-induced bottom velocities (upper left panel), steady near-bottom currents (upper right panel), sediment initiation potential (lower left panel), and net sediment transport (lower right panel). For the upper left panel, thin solid lines indicate the depth contour of the numerically-dredged bathymetry, the thick black-lined polygon represents the borrow site in Sand Resource Area A1, and the overlaid color map illustrates the magnitude of wave-induced bottom velocity (m/s). Red areas indicate regions of higher bottom velocity, while blue areas indicate lower velocities. Vectors indicate the direction and magnitude (length) of wave-induced bottom velocity at each grid point. The x-axis (easting) and the y-axis (northing) indicate the exact location on the subgrid within the sand resource area.

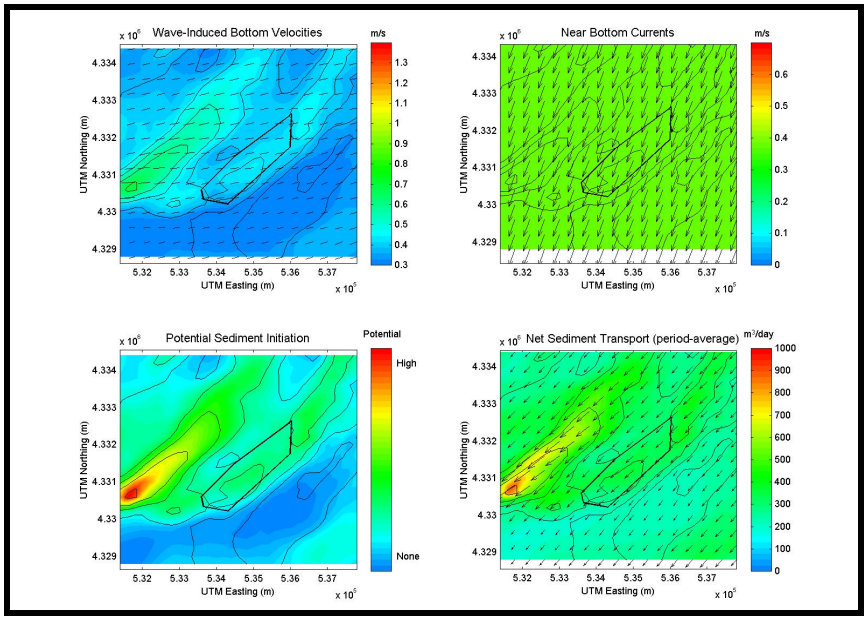

Figure 5-15. East-Northeast (22.5°) influenced hydrodynamic and sediment transport results at Sand Resource Area A1.

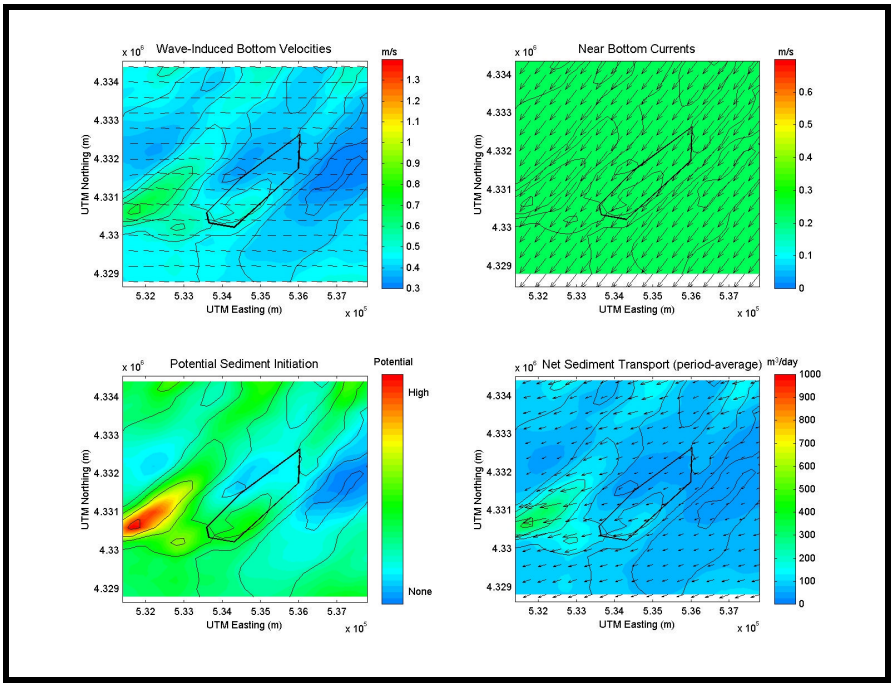

Figure 5-16. East (0°) influenced hydrodynamic and sediment transport results at Sand Resource Area A1.

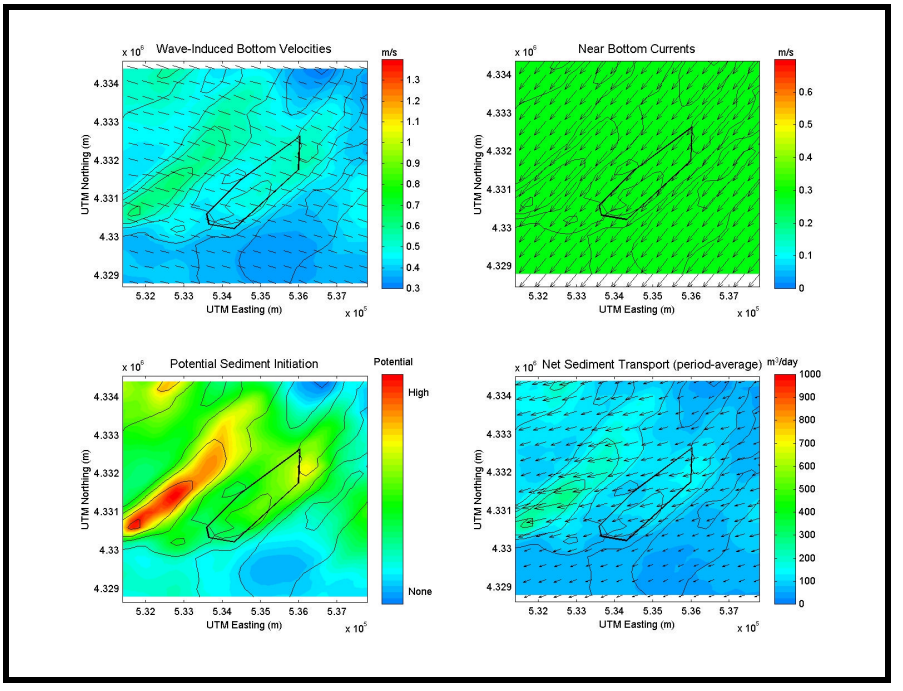

Figure 5-17. East-Southeast (-22.5°) influenced hydrodynamic and sediment transport results at Sand Resource Area A1.

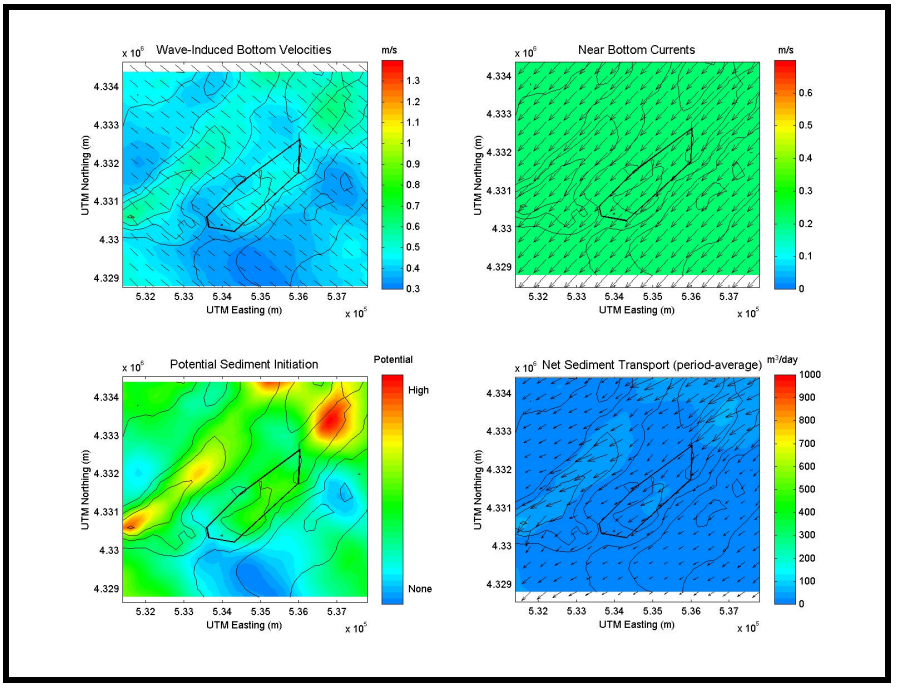

Figure 5-18. Southeast (-45°) influenced hydrodynamic and sediment transport results at Sand Resource Area A1.

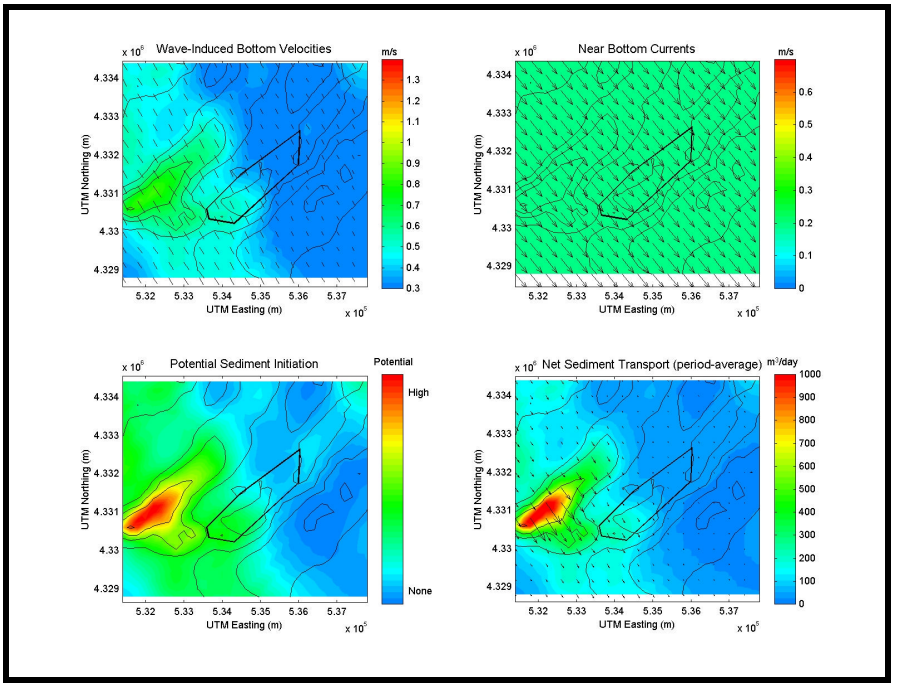

Figure 5-19. South-Southeast (-67.5°) influenced hydrodynamic and sediment transport results at Sand Resource Area A1.

Borrow sites in Areas A1 and A2 experience some of the highest ambient currents of all borrow sites. This results in larger quantities of sediment being transported into and around the numerically-dredged sites. For the east-northeast approach (22.5° case), wave-induced bottom velocities range from 0.3 to 0.7 m/s for borrow sites in Areas A1 (Figure 5-15) and A2 (Figure 5-20). Orbital velocities are greater when the depths are shallower, such as the nearshore shoals to the west of the dredged site in Area A1 and to the north of dredged site in Area A2. Although wave-induced bottom currents do fluctuate, the ambient currents are constant at approximately 0.2 m/s in each case. Wave-induced bottom currents interact with ambient bottom currents throughout the domain. The combination of these processes is used to predict sediment initiation and transport at the borrow location. In general, the shallower the water depth, the greater the sediment initiation and transport. Although sediment initiation is the highest near shoals, sediment movement is being initiated and transported throughout the resource areas. At Area A1, the direction of sediment transport is to the southwest. Although sediment transport is relatively high to the west of the dredged site in Area A1, transport is relatively low in and around the borrow site (approximately 350 m^3/day). Overall, sediment transport at A2 is lesser than A1, at approximately 100 to 300 m^3/day.

When waves approach predominantly from the east (0° bin), sediment transport changes to a west southwest direction (Figure 5-16 and 5-21). Wave-induced bottom velocities fall within the same range as the east-northeast case. When combining these data with steady near bottom currents, a decrease in overall sediment transport is evident. The areas that were relatively high in sediment initiation and transport for the east-northeast case continue to remain relatively high. In general, this is not true for Area A2. Locations of high initiation shift from the shoal and lower portion of the dredged site to the upper portion of the dredged site. This results in an increase of sediment transport in that region.

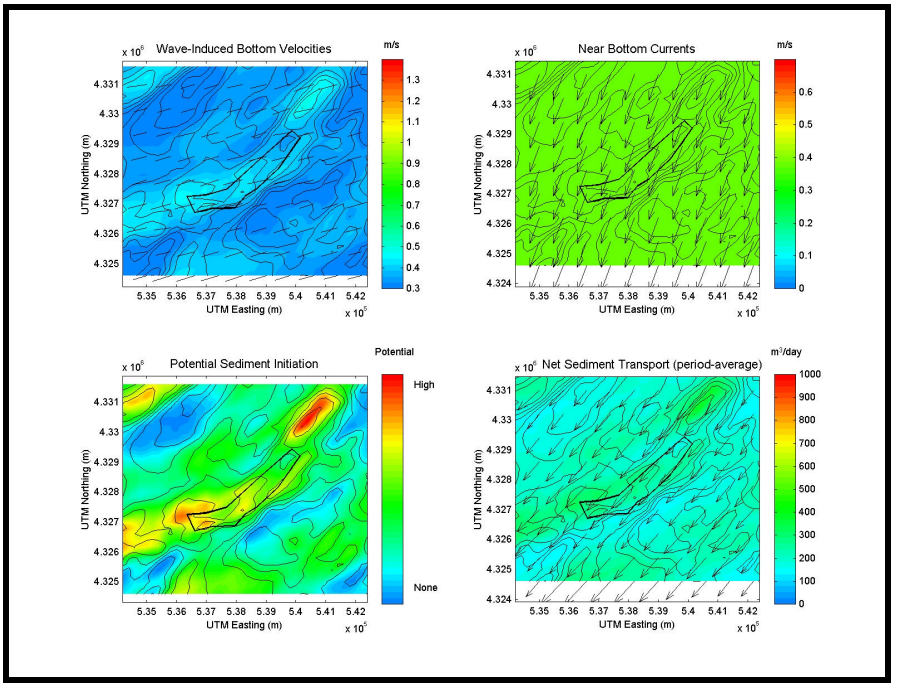

Figure 5-20. East-Northeast (22.5°) influenced hydrodynamic and sediment transport results at Sand Resource Area A2.

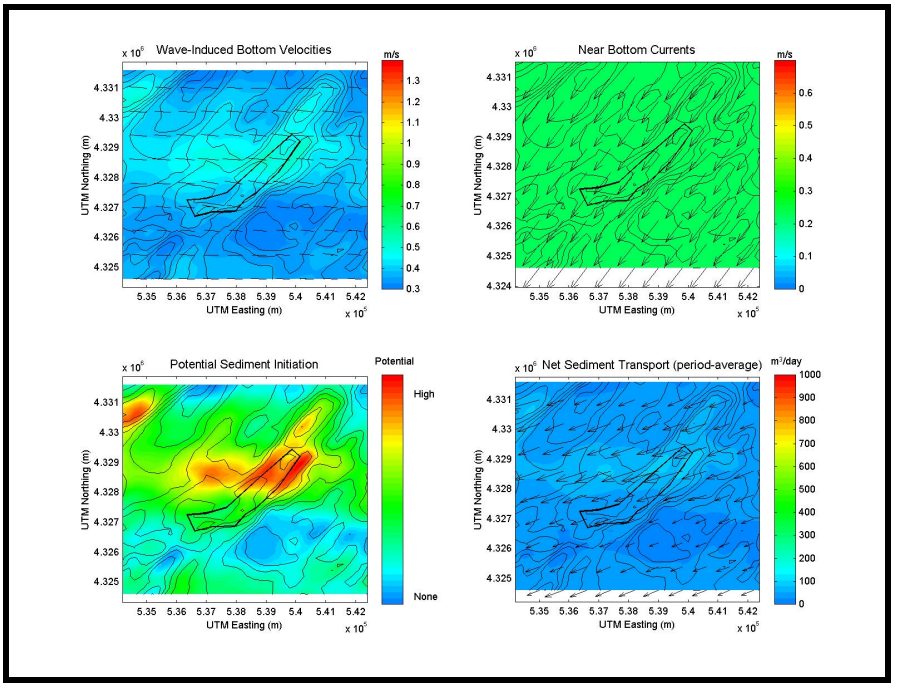

Figure 5-21. East (0°) influenced hydrodynamic and sediment transport results at Sand Resource Area A2.

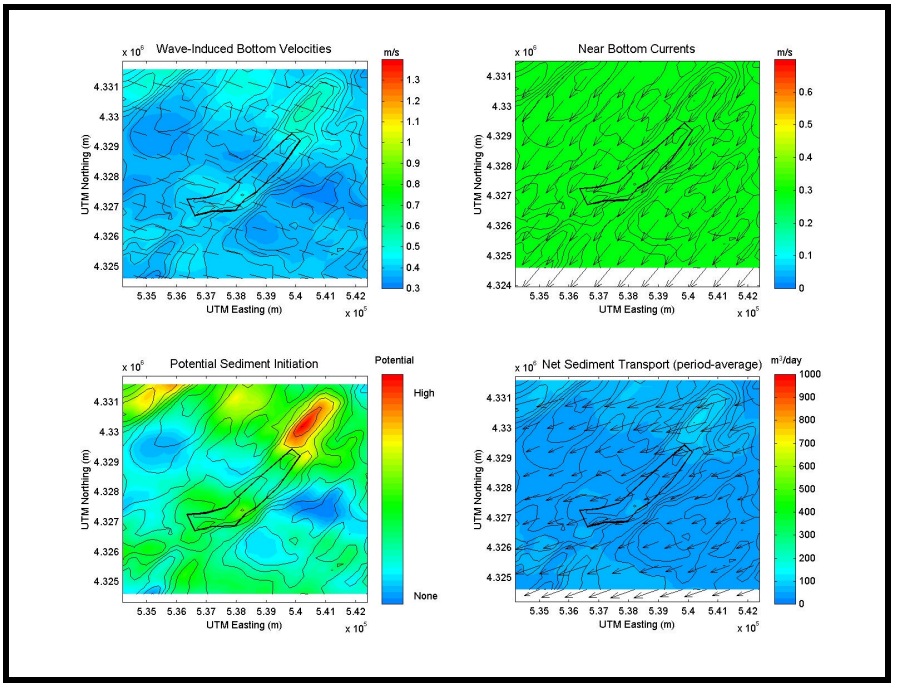

Figure 5-22. East-Southeast (-22.5°) influenced hydrodynamic and sediment transport results at Sand Resource Area A2.

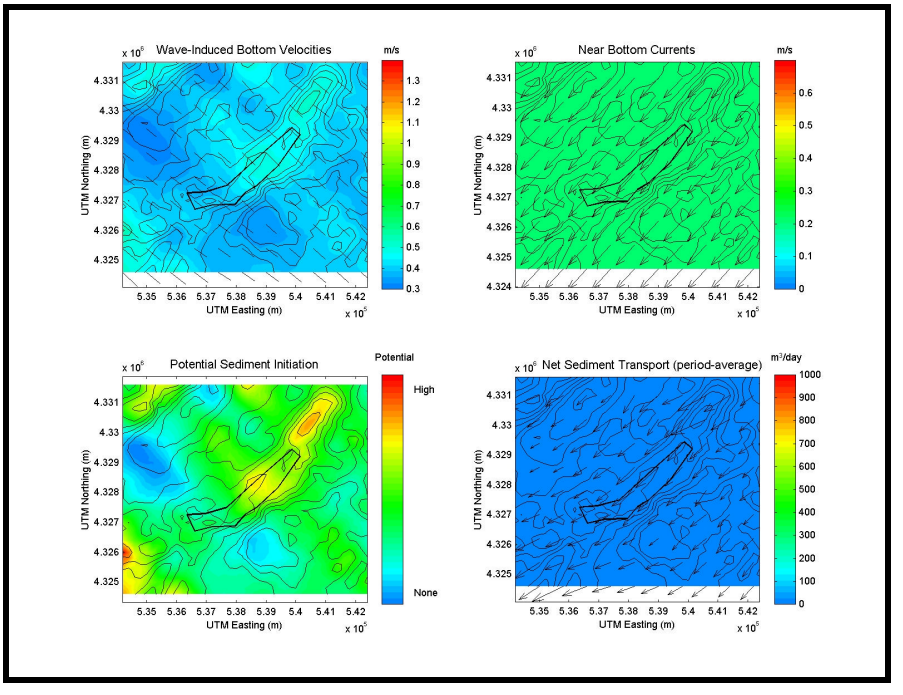

Figure 5-23. Southeast (-45°) influenced hydrodynamic and sediment transport results at Sand Resource Area A2.

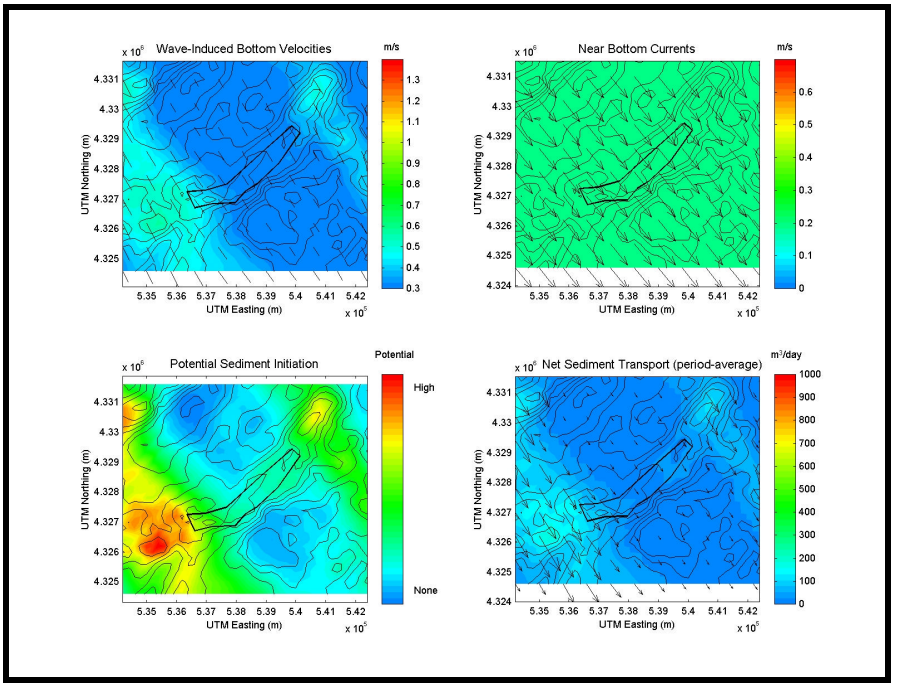

Figure 5-24. South-Southeast (-67.5°) influenced hydrodynamic and sediment transport results at Sand Resource Area A2.

Changing the mean direction of waves to an east-southeast approach (-22.5° bin) yields sediment transport rates that are slightly higher for Area A1 (Figure 5-17), particularly along its western shoal, while sediment transport at Area A2 (Figure 5-22) is reduced to approximately 50 to 100 m^3/day. This likely is caused by the reduction in wave height experienced at A2. The reduction in wave height for this approach direction is due to the difference in wave energy resulting from proposed dredging at the borrow site in Area A1. Waves propagate towards Area A2 directly after passing over Area A1. Transport is in a southwesterly direction at both A1 and A2. Although net sediment transport direction is influenced by wave-induced and steady bottom currents, sediment transport results more closely follow the direction of ambient currents.

Minimal sediment transport occurs when waves approach from the southeast (-45°). Although steady currents are flowing in a similar path to the previous direction of approach and the orbital velocity magnitudes are similar to the previous directional cases, wave angles are more northerly. This results in an ambient current flowing nearly perpendicular to wave-induced bottom currents. Therefore, the processes oppose each other to a greater degree than in previous cases. The southeast approach simulations produce the smallest sediment transport results for Areas A1 (Figure 5-18) and A2 (Figure 5-23). However, this simulation is still important since it represents 15.4% of the total occurrence. Sediment transport rates for Areas A1 and A2 are quite uniform at approximately 50 m^3/day.

The south-southeast approach (-67.5°), illustrates wave-induced bottom currents and steady bottom currents flowing in the same direction, creating an increase in net sediment transport rates, especially over shoals. Transport in and around Areas A1 and A2 are 50 to 400 m^3/day (Figure 5-19) and 50 to 75 m^3/day (Figure 5-24), respectively. This approach occurs 12.3% percent of the time. Table 5-3 provides a summary of sediment transport rates for each of the directional approaches modeled.

Table 5-3. Sediment Transport Summary for Areas A1 and A2

Approach Direction	Approach Bin (Grid relative)	% Contributed	Maximum Transport Rate (m^3/day)*	Peak Transport Rate at A1 (m^3/day)*	Peak Transport Rate at A2 (m^3/day)*
Northeast	45E	--	--	--	--
East-Northeast	22.5E	2.3%	350	300	200
East	0E	19.7%	100	80	50
East-Southeast	-22.5E	23.1%	100	100	50
Southeast	-45E	19.8%	100	50	25
South-Southeast	-67.5E	15.8%	300	75	50
---	calm	19.3%	0	0	0

* within borrow area

5.2.1.4 Hydrodynamics and Sediment Transport for Resource Area C1 (Grid B1)

Sediment transport rates for Resource Area C1 are lower than those calculated at Resource Areas A1 and A2. Although sediment transport was high in a few isolated areas within the observation grid, these areas were not directly adjacent to the dredged borrow site. As expected, wave-induced bottom velocities were lower in the borrow site than in the surrounding domain, while ambient bottom currents were uniform in magnitude throughout the observation domain. The various wave-induced bottom currents and ambient bottom currents for each directional simulation yielded a variety of different scenarios.

The east-northeast case (22.5°) is characterized by fairly uniform wave-induced bottom velocities, and completely uniform ambient bottom currents (Figure 5-25). The highest initiation region is a shoal to the west of the dredged borrow site, although overall sediment transport is quite constant. Sediment transport is slightly reduced within the dredged site, as well as toward the south. Sediment transport magnitude ranges between 18 and 60 m^3/day, and the direction of transport is towards the southeast.

Figure 5-26 shows sediment transport results when waves propagate from the east (0° bin). This directional approach produces the maximum sediment transport potential at Resource Area C1. Overall, wave-induced bottom velocities were relatively high to the northeast, north, west, and southwest of the borrow site, while they were reduced inside and to the southeast of the dredged site. When coupled with steady ambient bottom currents, initiation was moderate to low within the dredged site. However, sediment transport, which was to the west northwest, was constant (60 m^3/day) throughout most of the observation domain, with high transport occurring in the northwest corner.

Sediment transport magnitude for the east-southeast case (-22.5°) is greater than that for the east-northeast case, but sediment transport initiation locations are similar. The east-southeast simulation accounts for over 50% of the sediment transport at Resource Area C1. Figure 5-27 illustrates reduced sediment transport within the dredged site and to the south and southeast of the dredged site. Although wave-induced bottom velocities for this case generally are greater than the east-northeast case, steady ambient current magnitude is reduced. In addition, wave-induced bottom currents and steady ambient bottom currents interact in opposite directions to one another, which further reduces initiation potential and transport. Transport within the dredged site is approximately 17 m^3/day to the east.

With the wave-induced bottom currents and steady ambient bottom currents aligned, sediment transport increases for the southeast case (-45°; Figure 5-28). This results in a fairly uniform sediment transport rate (40 m^3/day), becoming reduced within and to the southeast of the numerically-dredged borrow site. For the -45° directional approach, sediment transport is directed offshore.

Figure 5-29 illustrates sediment transport results for the south-southeast case (-67.5°). This directional approach produces the smallest sediment transport potential at Resource Area C1. The dredged site, and the areas to the northwest and southeast, experienced minimal transport (0 to 5 m^3/day). Although wave-induced velocities and steady bottom currents were aligned, transport was still small. This is due to reduced wave height and wave period. This directional approach had the smallest wave heights, and it is reflected in the wave-induced velocities. The areas with minimal sediment transport correspond to locations with minimal wave-induced bottom velocities. Wave-induced bottom velocities are the smallest of all directional cases simulated.

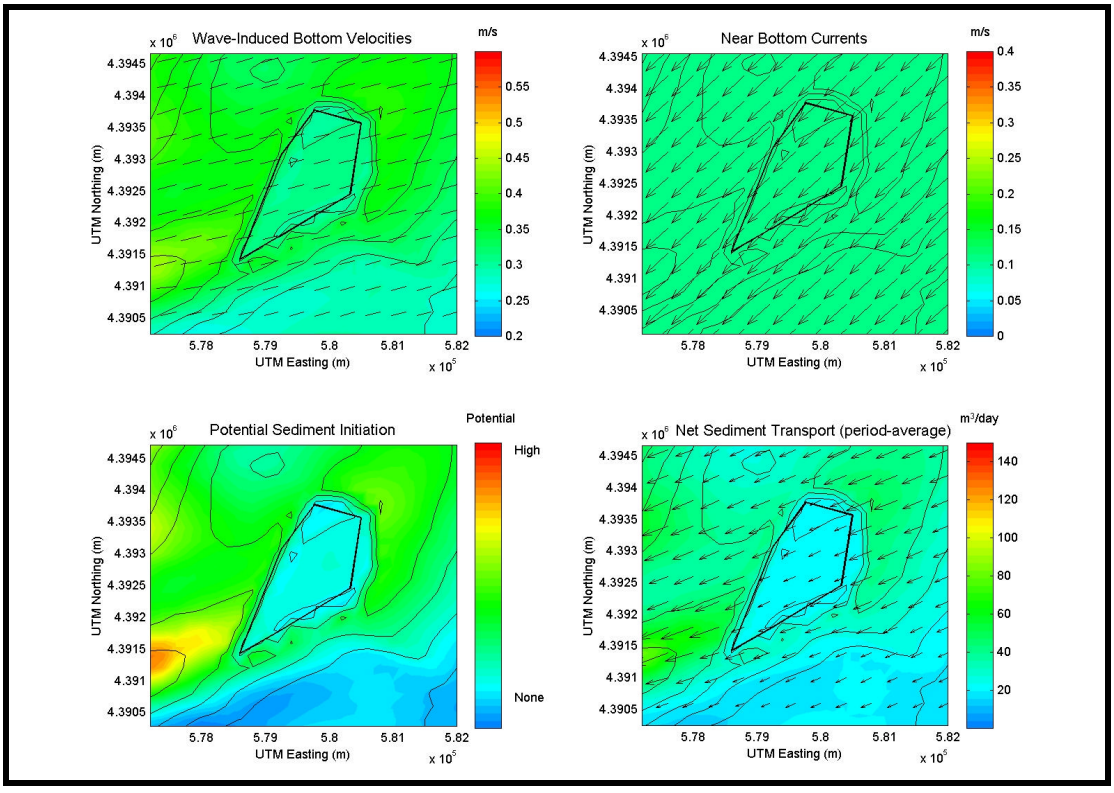

Figure 5-25. East-northeast influenced hydrodynamic and sediment transport results at Sand Resource Area C1.

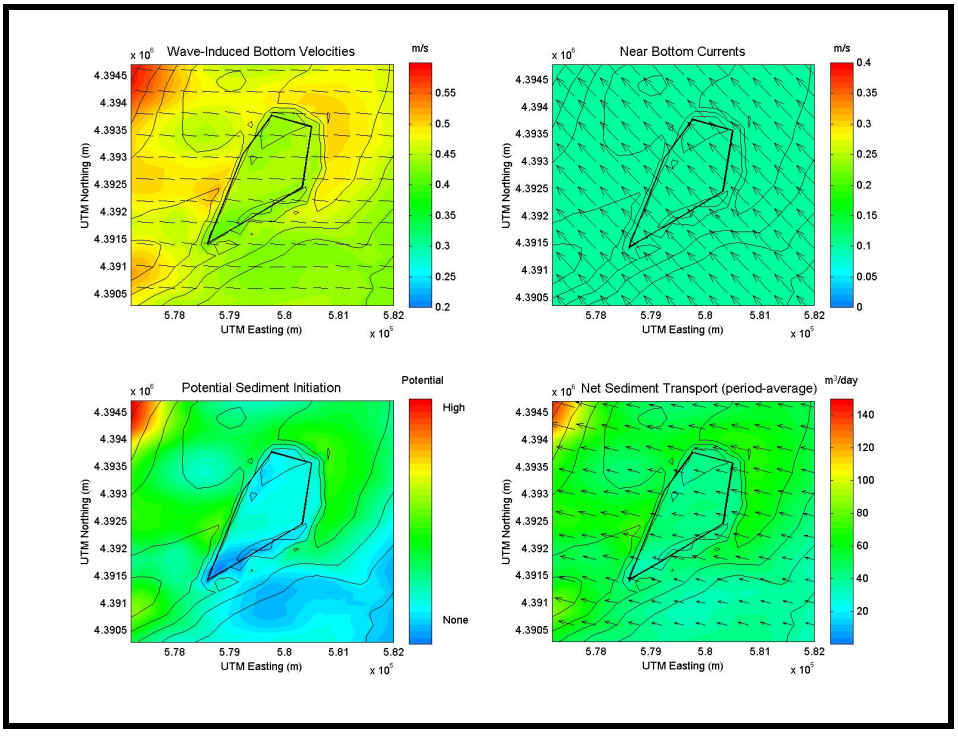

Figure 5-26. East influenced hydrodynamic and sediment transport results at Sand Resource Area C1.

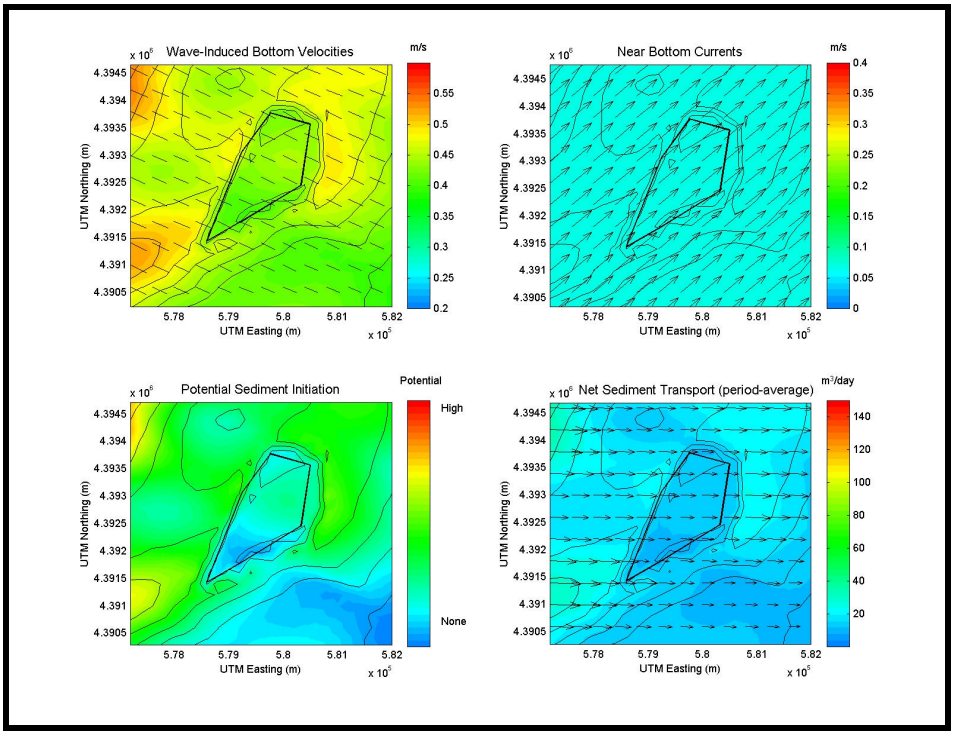

Figure 5-27. East-southeast influenced hydrodynamic and sediment transport results at Sand Resource Area C1.

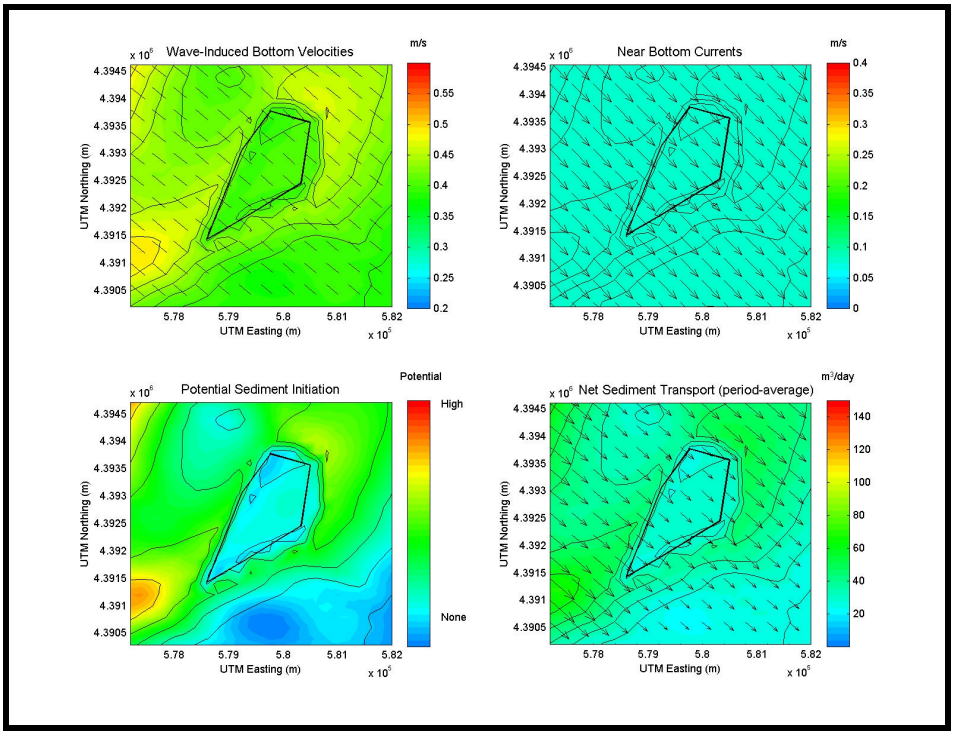

Figure 5-28. Southeast influenced hydrodynamic and sediment transport results at Sand Resource Area C1.

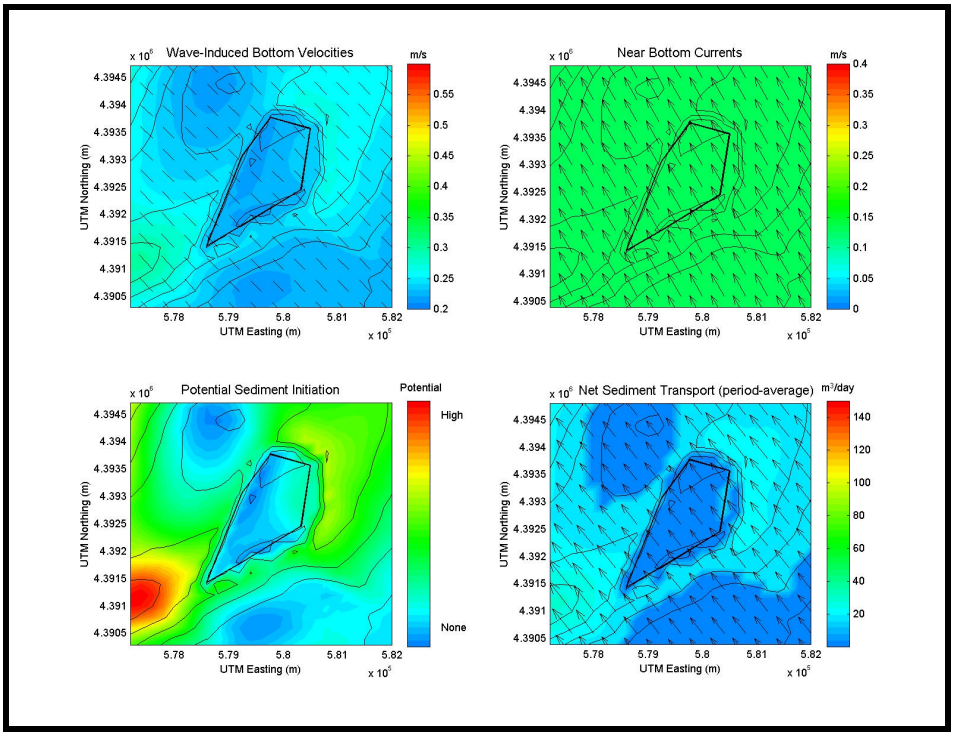

Figure 5-29. South southeast hydrodynamic and sediment transport results at Sand Resource Area C1.

Table 5-4 summarizes sediment transport rates and contributing percentages for each of the directional approaches modeled. Maximum and peak (most frequently occurring) sediment transport rates are presented for each of the directions modeled. Calm time represents a period of time low energy waves are propagating onshore or waves are heading offshore.

Table 5-4. Sediment Transport Summary for Resource Area C1

Approach Direction	Approach Bin	% Contributed	Maximum Transport Rate (m^3/day)*	Peak Transport Rate (m^3/day)*
Northeast	45	--	--	--
East-Northeast	67.5	3.4%	60	20
East	90	26.1%	70	65
East-Southeast	112.5	25.8%	20	17
Southeast	135	19.9%	60	23
South-Southeast	157.5	13.9%	15	0
---	calm	10.9%	0	0

* within borrow area

5.2.1.5 Hydrodynamics and Sediment Transport for Resource Areas G2 and G3 (Grid B2)

Grid B2 comprises three potential borrow sites: G2 Top, G2 Bottom, and G3. For each directional approach simulation, the velocities and transport directions are similar for each of the three borrow sites. The wave-induced bottom currents for all borrow sites range between 0.3 and 0.8 m/s, while near bottom currents remain constant for each resource area with respect to direction. The combined effect of these two hydrodynamic processes is used to predict potential sediment transport at each of the proposed borrow sites.

When waves approach from the east-northeast (22.5°), ambient currents flow from the northwest, and sediment transport at each of the resource areas (G2 Top, G2 Bottom, and G3) is directed toward the southeast (Figures 5-30, 5-31, 5-32, respectively). This direction is influenced by the oscillatory nature of the waves and the steady flow of ambient currents. In areas where wave-induced velocities are low, sediment transport is low. This includes the areas southeast of the dredged borrow site at Resource Areas G2 Top and G3, and the area northwest of the dredged borrow site at G2 Bottom. This process is mirrored in the sediment initiation plots at each of the resource areas. Sediment transport rates within G2 Top and G2 Bottom range between 0 and 30 m^3/day, while the rate ranges between 0 and 85 m^3/day at G3. The east-northeast approach represents the largest waves and occurs approximately 2.9% of time.

Percent occurrence increases for waves propagating from the east (0°) to 14.1%. Figures 5-33, 5-34, and 5-35 illustrate the results of the eastern wave approach (consisting of longer period waves) for proposed borrow sites. Wave-induced bottom velocities have increased when compared with the previous directional case. Specifically, locations to the northwest and north of dredged sites have experienced this increase. Ambient currents remain steady and are directed toward the northeast. The interaction of these two processes produces net sediment transport directed toward the northeast. In general, transport is greater at G2 Top and G3 than at G2 Bottom. G2 Bottom is characterized by a no transport zone south of the resource area, while reduced transport only occurs in a few select locations.

Sediment transport is further reduced at each of the resource areas when waves propagate from the east-southeast (-22.5°). In this directional case, wave-induced currents and

steady ambient currents oppose one another, causing a reduction in overall sediment transport (Figures 5-36, 5-37, and 5-38). Transport at Resource Areas G2 Top and G2 Bottom are fairly uniform, at 5 to 10 m^3/day. Sediment transport at G3 ranges from 10 to 20 m^3/day. These sediment transport results are significant because the eastern wave approach composes 15% of the wave field.

Figures 5-39, 5-40, and 5-41 illustrate results for the southeast (-45°) approach simulation, indicating relatively low sediment transport results due to the interaction of wave-induced and ambient current fields. The opposing nature of the waves and currents, as in the southeast case, reduces overall sediment transport potential. Sediment transport rates, which are relatively low compared with previously examined directional cases, range from 0 to 30 m^3/day for all directional borrow sites.

Relatively high transport rates occur when wave-induced bottom currents and steady near bottom currents are aligned. For example, G2 Top, G2 Bottom, and G3, attain greater sediment transport rates in the south-southeast (-67.5°) case than in cases where the hydrodynamic processes act in opposite directions to one another (i.e., the southeast approach). Figures 5-42, 5-43, 5-44 illustrate the sediment transport results for the south-southeast approach simulation. Sediment transport rates are increased due to positive interaction between waves and currents. At deeper locations, such as the areas southeast of dredged sites in Areas G2 Top and G3, transport is low (0 to 15 m^3/day). In these regions, initiation of sediment movement under waves is difficult due to increased water depth.

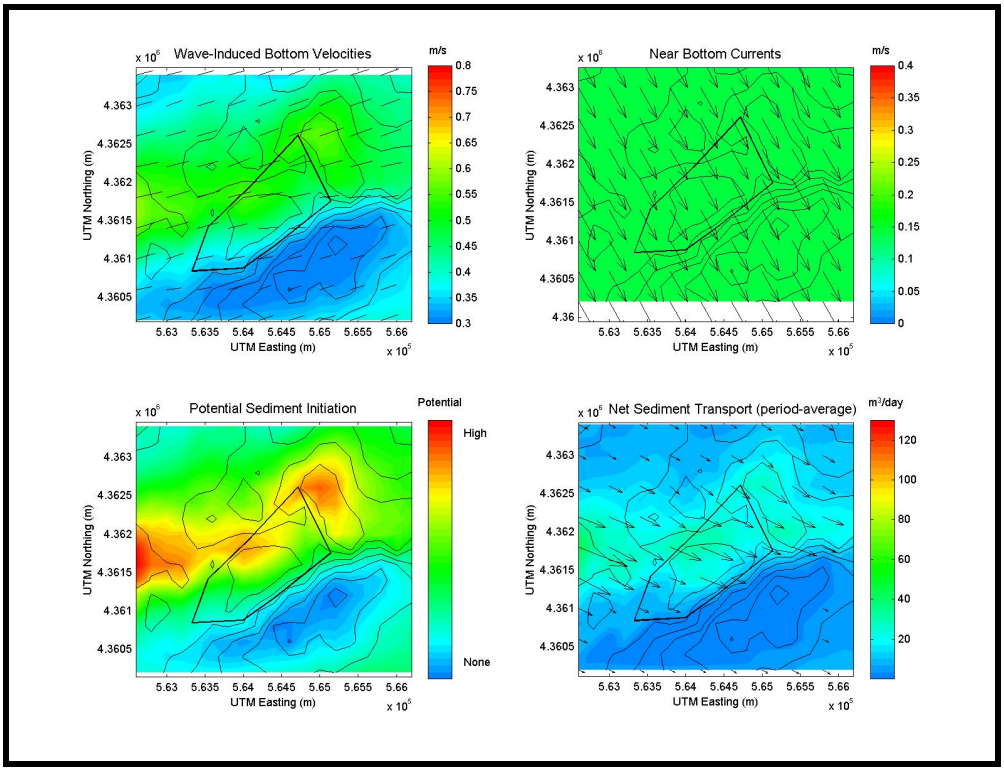

Figure 5-30. East-northeast (22.5°) influenced hydrodynamic and sediment transport results at Sand Resource Area G2 Top.

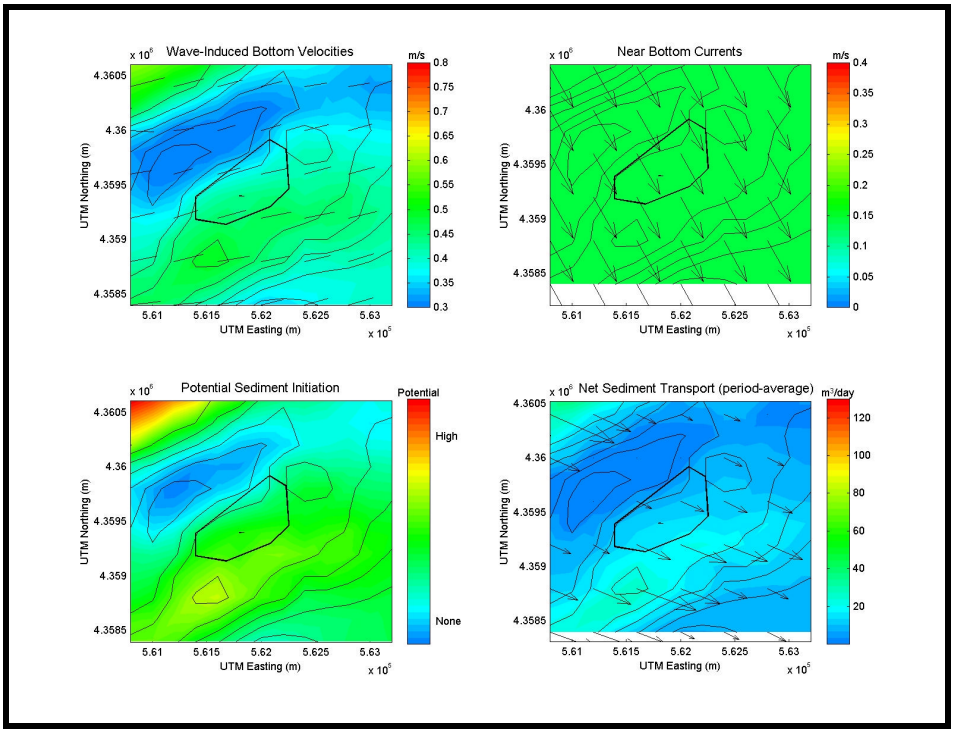

Figure 5-31. East-northeast (22.5°) influenced hydrodynamic and sediment transport results at Sand Resource Area G2 Bottom.

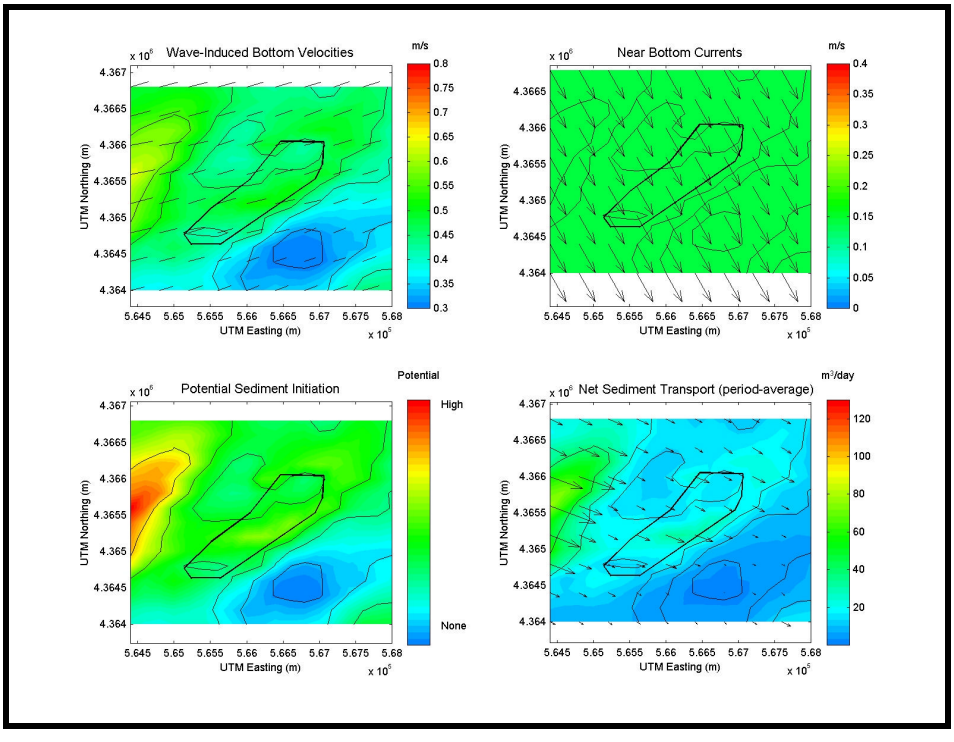

Figure 5-32. East-northeast (22.5°) influenced hydrodynamic and sediment transport results at Sand Resource Area G3.

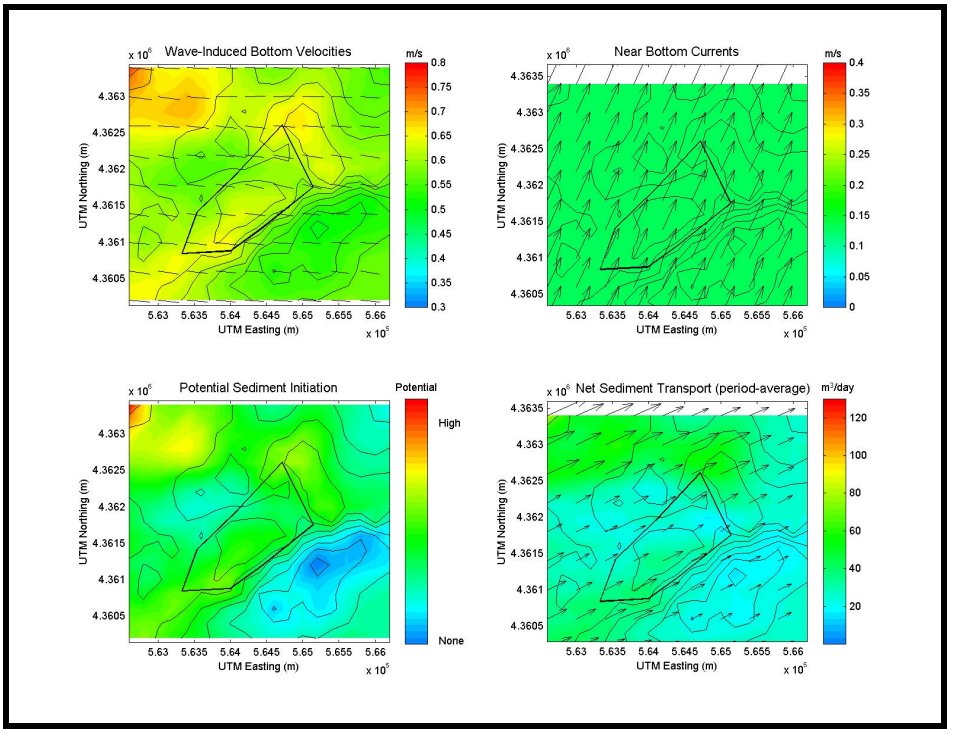

Figure 5-33. East (0°) influenced hydrodynamic and sediment transport results at Sand Resource Area G2 Top.

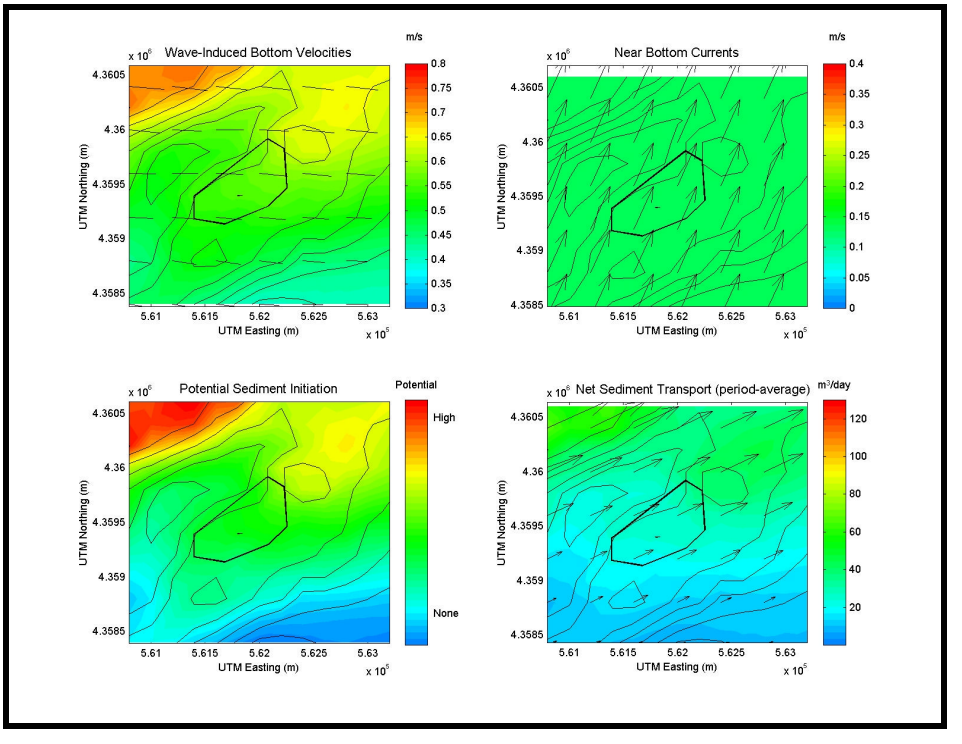

Figure 5-34. East (0°) influenced hydrodynamic and sediment transport results at Sand Resource Area G2 Bottom.

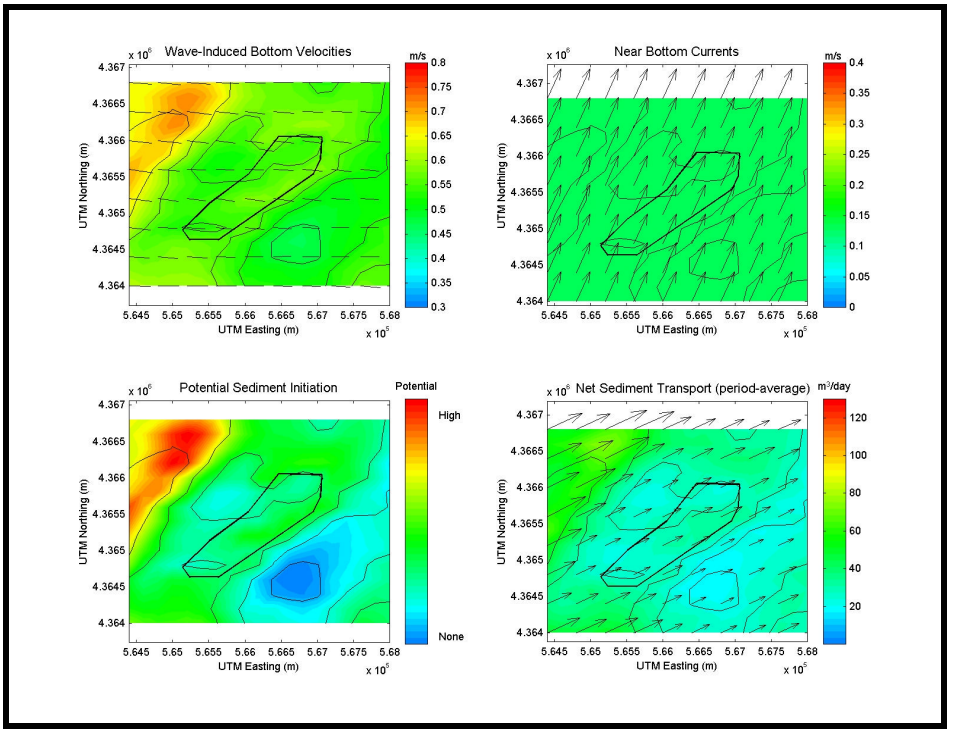

Figure 5-35. East (0°) influenced hydrodynamic and sediment transport results at Sand Resource Area G3.

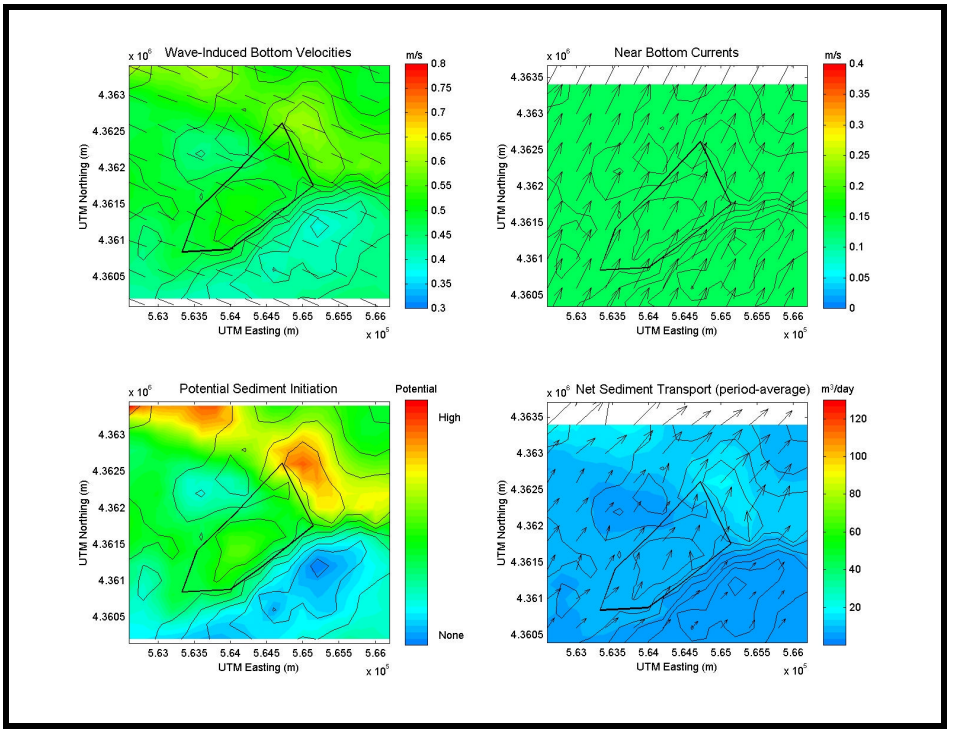

Figure 5-36. East-southeast (-22.5°) influenced hydrodynamic and sediment transport results at Sand Resource Area G2 Top.

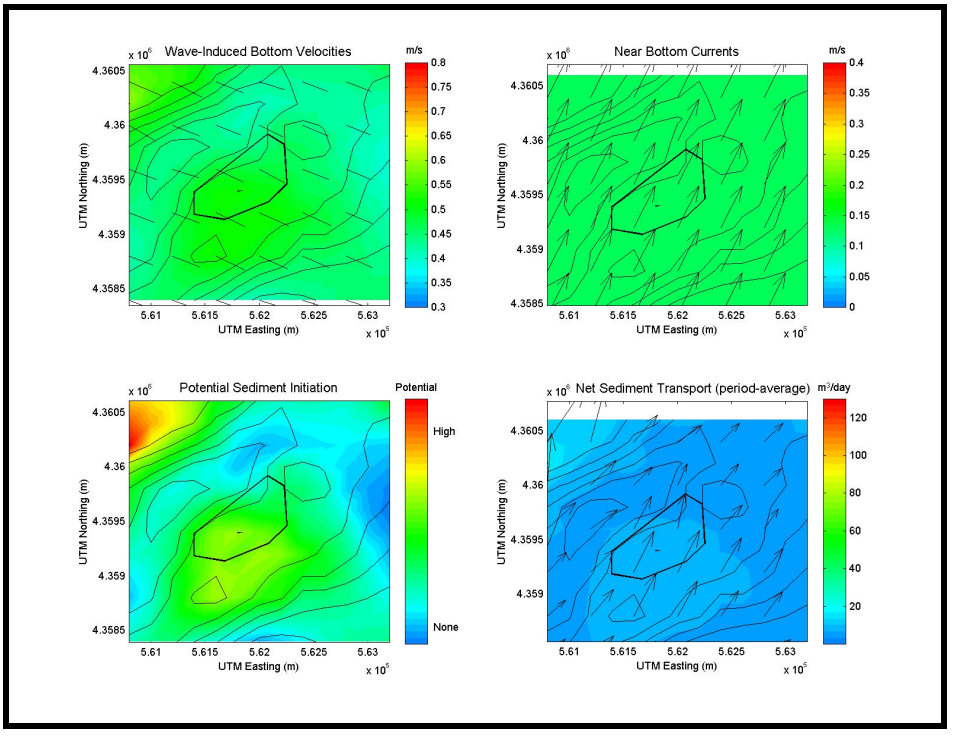

Figure 5-37. East-southeast (-22.5°) influenced hydrodynamic and sediment transport results at Sand Resource Area G2 Bottom.

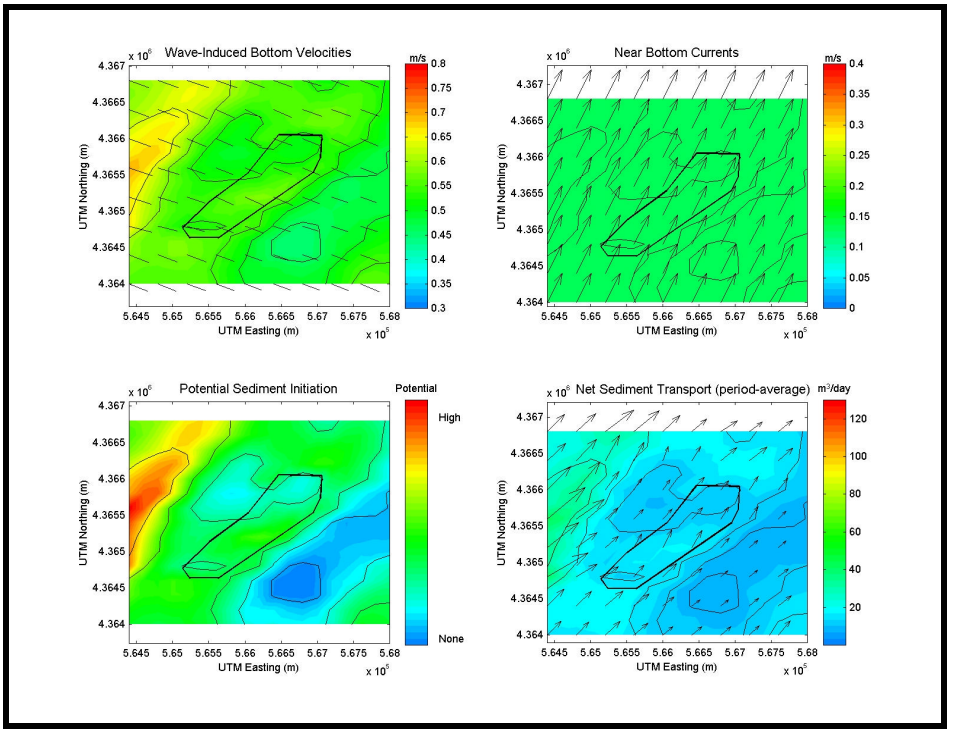

Figure 5-38. East-southeast (-22.5°) influenced hydrodynamic and sediment transport results at Sand Resource Area G3.

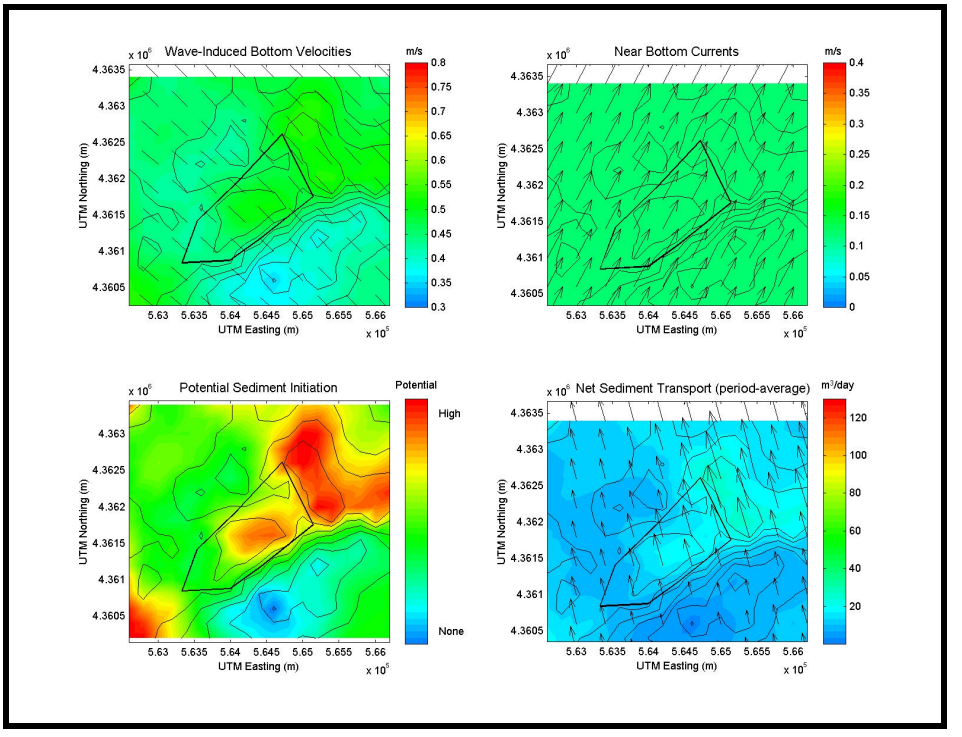

Figure 5-39. Southeast (-45°) influenced hydrodynamic and sediment transport results at Sand Resource Area G2 Top.

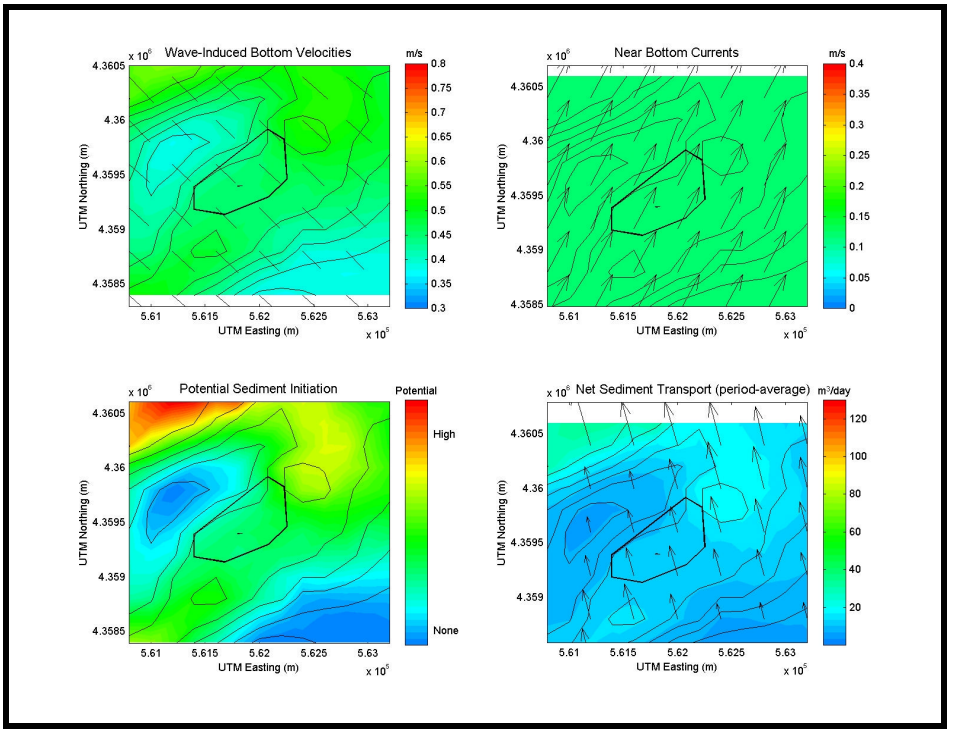

Figure 5-40. Southeast (-45°) influenced hydrodynamic and sediment transport results at Sand Resource Area G2 Bottom.

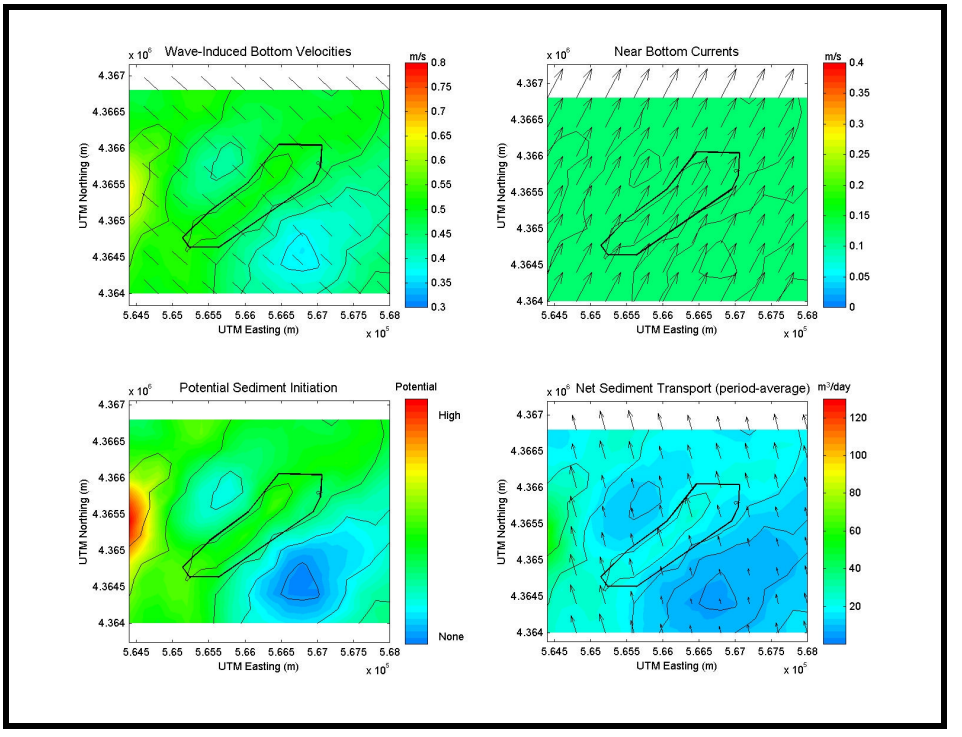

Figure 5-41. Southeast (-45°) influenced hydrodynamic and sediment transport results at Sand Resource Area G3.

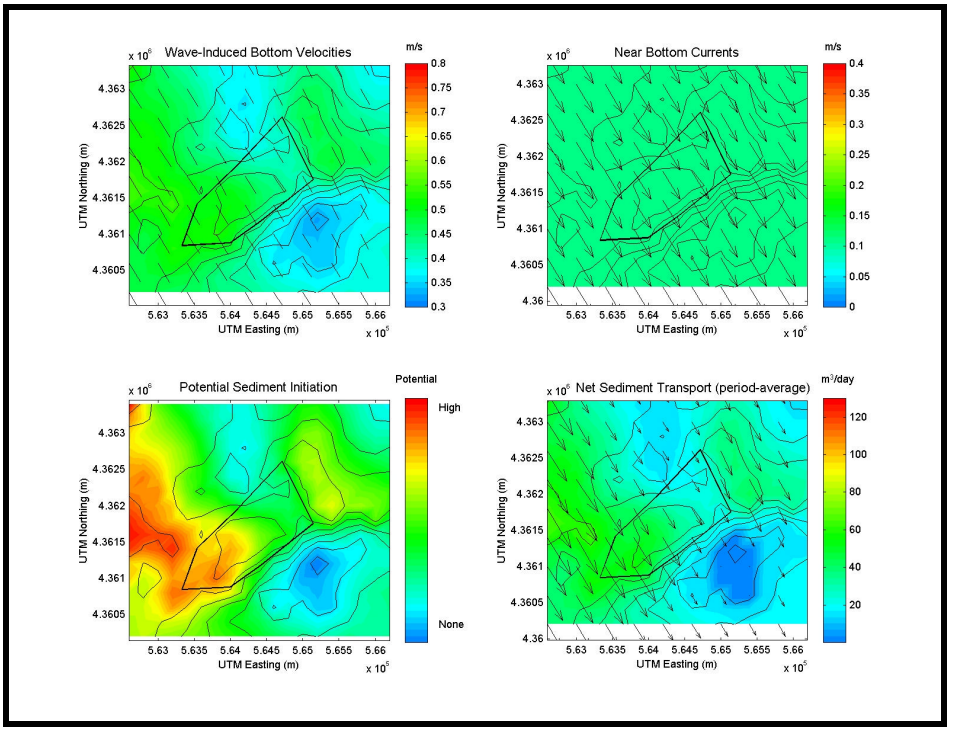

Figure 5-42. South-southeast (-67.5°) influenced hydrodynamic and sediment transport results at Sand Resource Area G2 Top.

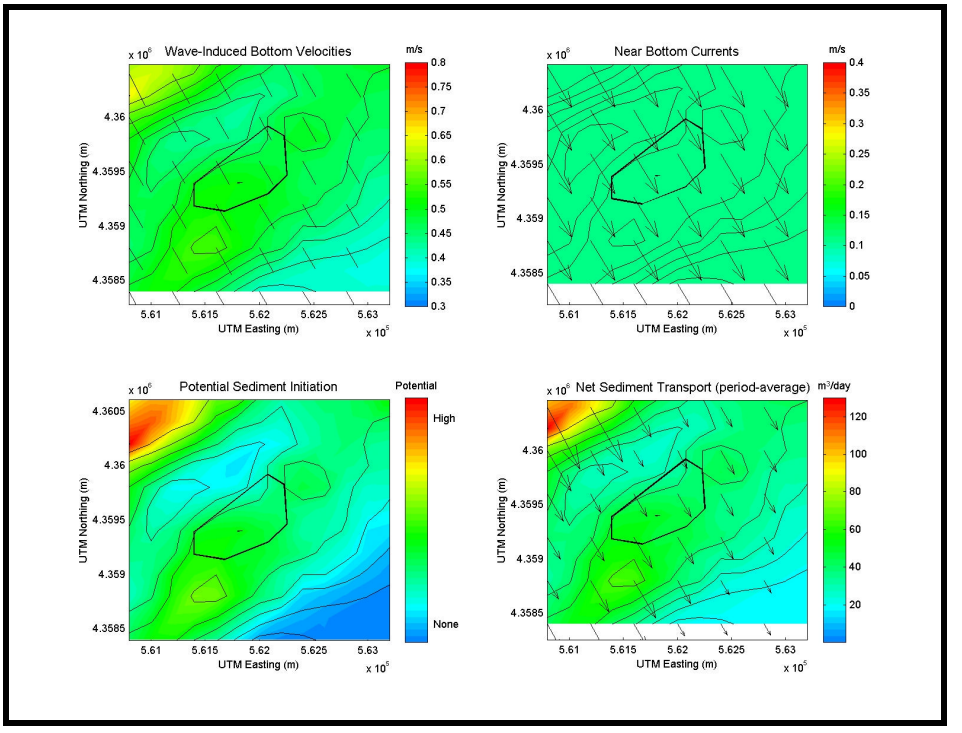

Figure 5-43. South-southeast (-67.5°) influenced hydrodynamic and sediment transport results at Sand Resource Area G2 Bottom.

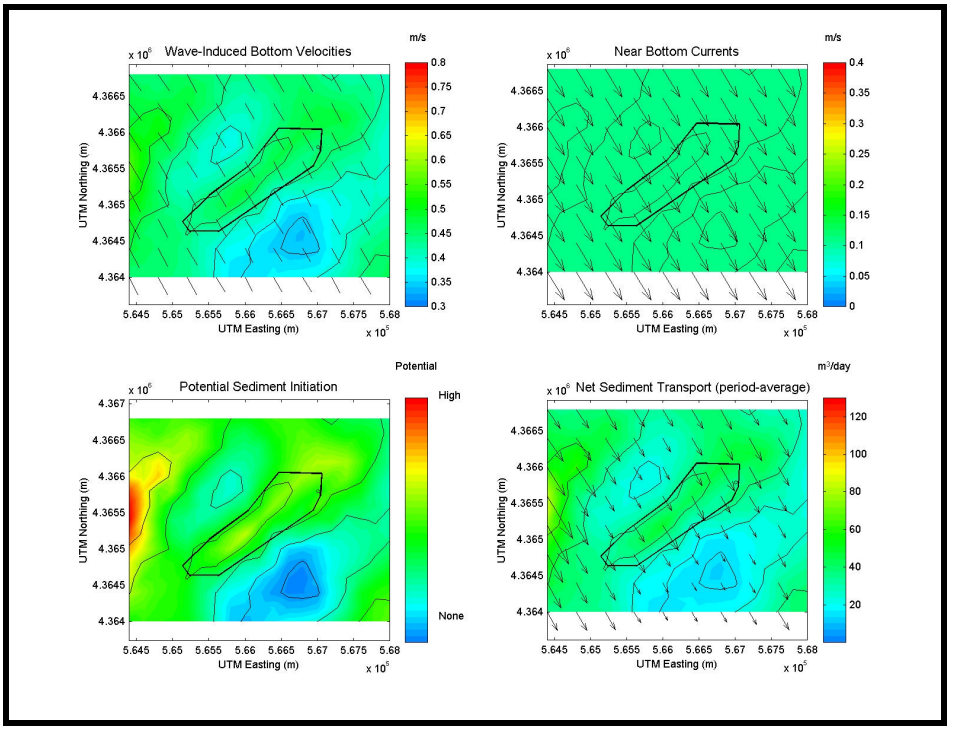

Figure 5-44. South-southeast (-67.5°) case hydrodynamic and sediment transport results at Sand Resource Area G3.

Table 5-5 presents the maximum and peak sediment transport rates for each directional approach simulation. The maximum value represents the greatest sediment transport magnitude from the three borrow locations. Peak sediment transport documents the most dominant transport rate within a particular borrow site. Also listed in the table is the percentage contribution to overall sediment transport, which represents the significance of each directional simulation. For example, borrow sites may experience a large peak sediment transport rate; however, this may be a rare occurrence. Therefore, sediment transport rates and percent contribution need to be weighted accordingly. The yearly sediment transport magnitudes and infilling times for borrow sites G2 Top, G2 Bottom, and G3 can be found in section 5.2.1.7.

5.2.1.6 Hydrodynamics and Sediment Transport for Resource Area F2 (Grid C)

Sand Resource Area F2 is the northern most borrow site in the study, and it is characterized by a variety of transport patterns. For the northeast case (45°), wave-induced bottom currents are generated in an approximate northeast/southwest direction (Figure 5-45). A maximum velocity of approximately 0.25 m/s occurs around the dredged borrow site, while velocities are slightly less within the site. Steady, near-bottom, ambient currents are not significant (approximately 0.01 m/s). Although waves are large for this case, small ambient currents are not competent enough to result in net sediment transport. The combined wave/current processes are not enough to erode sediment from the seafloor. However, this only occurs 1.7% of the time, a relatively small duration.

Table 5-5. Sediment Transport Summary for Grid B2

Approach Direction	Approach Bin	% Contributed	Maximum Transport Rate (m^3/day)*	Peak Transport Rate at G2 Top (m^3/day)*	Peak Transport Rate at G2 Bottom (m^3/day)	Peak Transport Rate at G3 (m^3/day)*
Northeast	45	--	--	--	--	--
East-Northeast	67.5	3.8%	50	30	18	19
East	90	22.2%	50	50	30	35
East Southeast	112.5	19.6%	20	15	15	19
Southeast	135	17.0%	25	18	15	22
South-Southeast	157.5	14.1%	55	30	55	50
---	calm	23.3%	0	0	0	0
* within borrow area						

Figure 5-46 illustrates an increase of sediment transport for the east-northeast case (22.5°) adjacent to, but not within, the dredged borrow site. Based on an overall increase in wave-induced bottom currents and near bottom ambient currents, net sediment transport of approximately 8 m^3/day to the southwest is predicted. The east-northeast case also has a relatively low occurrence of 2.5%.

Contrary to the two previous cases, the east simulation (0°) for Grid C produces high sediment transport rates (Figure 5-47). Although the ambient current magnitude is similar to the previous case, wave-induced bottom velocities are greater due to an increase in wave period and change in approach direction. Maximum wave-induced bottom velocities occur to the south of the dredged borrow site, while velocities with the dredged site are approximately 0.37 m/s. The combination of waves and ambient currents generate sediment transport magnitudes

ranging from 8 to 20 m^3/day directed offshore. The east approach simulation represents 19% of the wave conditions, the greatest percent contribution.

Sediment transport magnitudes for the east-southeast direction (-22.5°) are small (Figure 5-48), but some movement is observed. East-southeast wave-induced bottom currents oppose ambient near bottom currents flowing to the northeast. Uniform sediment transport (approximately 8 m^3/day) directed to the east is observed for this approach simulation. The east-southeast wave approach occurs 18.8% of the time and represents the second highest occurrence percentage.

Figure 5-49 illustrates results for the southeast simulation (-45°). Wave-induced bottom current patterns are similar to previous cases. Although ambient near-bottom velocities are approximately the same as the previous two cases, the direction changes. This results in zero sediment transport along the northeast perimeter of the dredged borrow site, and at the northwest and southeast corners of the resource area. In general, a sediment transport magnitude of 10 m^3/day is directed toward the southeast.

The final directional simulation modeled for Resource Area F2 is for waves propagating from the south-southeast (-67.5°). Although wave-induced bottom velocities and ambient near bottom currents are aligned, sediment transport is small (0 to 7.7 m^3/day). The sediment transport panel in Figure 5-50 illustrates the effects of reduced wave height and wave period for this approach direction. A decrease in both of these variables results in a decrease in wave-induced bottom velocities and potential sediment transport.

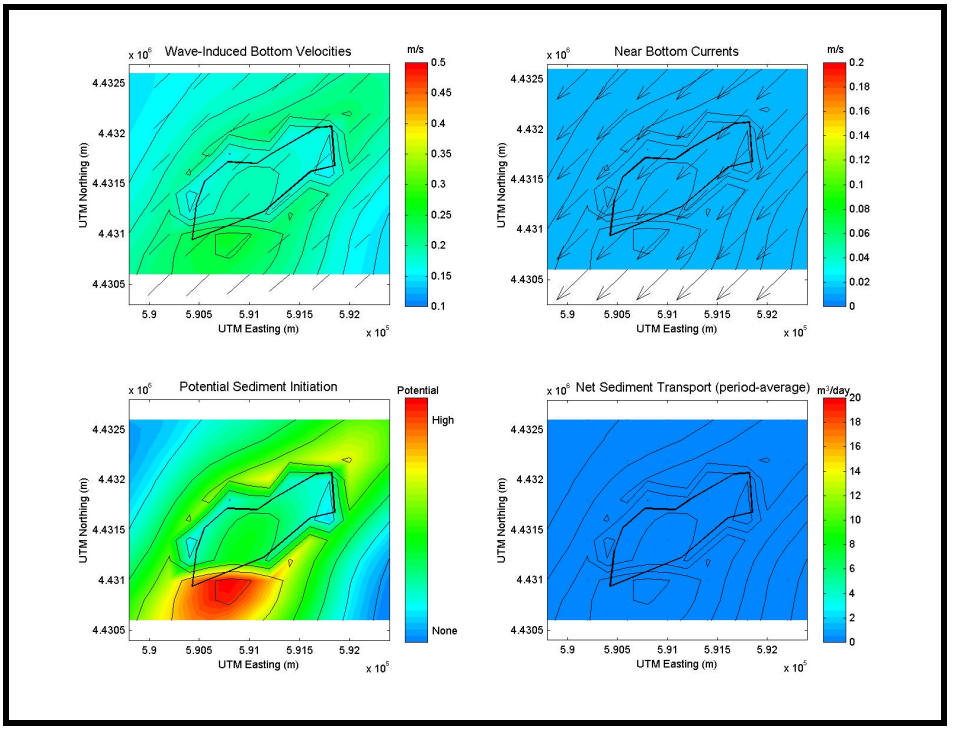

Figure 5-45. Northeast (45°) influenced hydrodynamic and sediment transport results at Sand Resource Area F2.

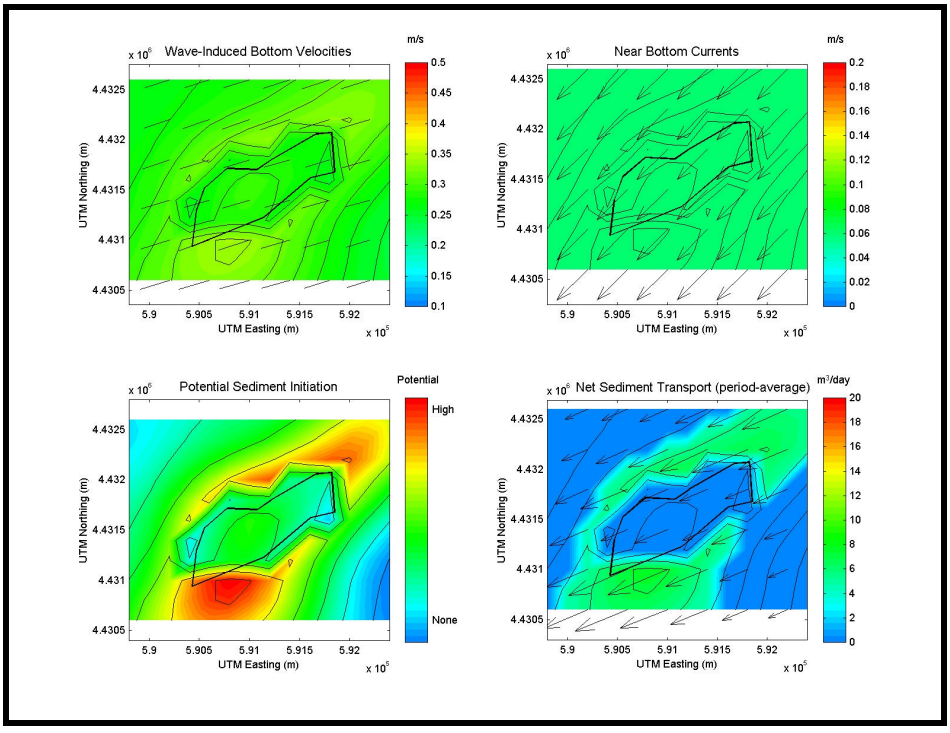

Figure 5-46. East-northeast (22.5°) influenced hydrodynamic and sediment transport results at Sand Resource Area F2.

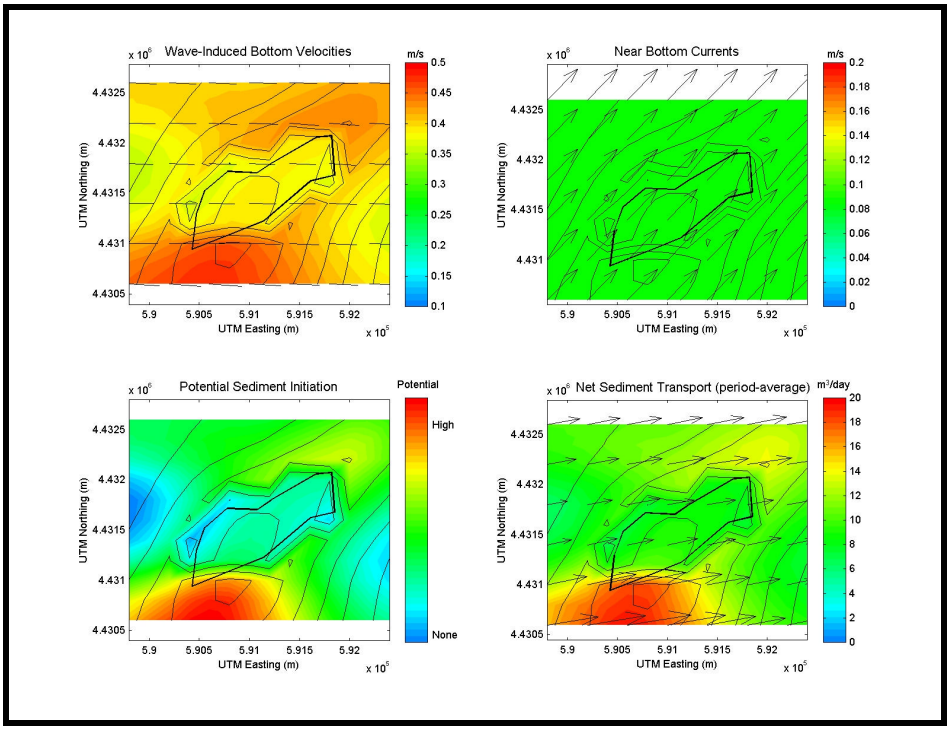

Figure 5-47. East (0°) influenced hydrodynamic and sediment transport results at Sand Resource Area F2.

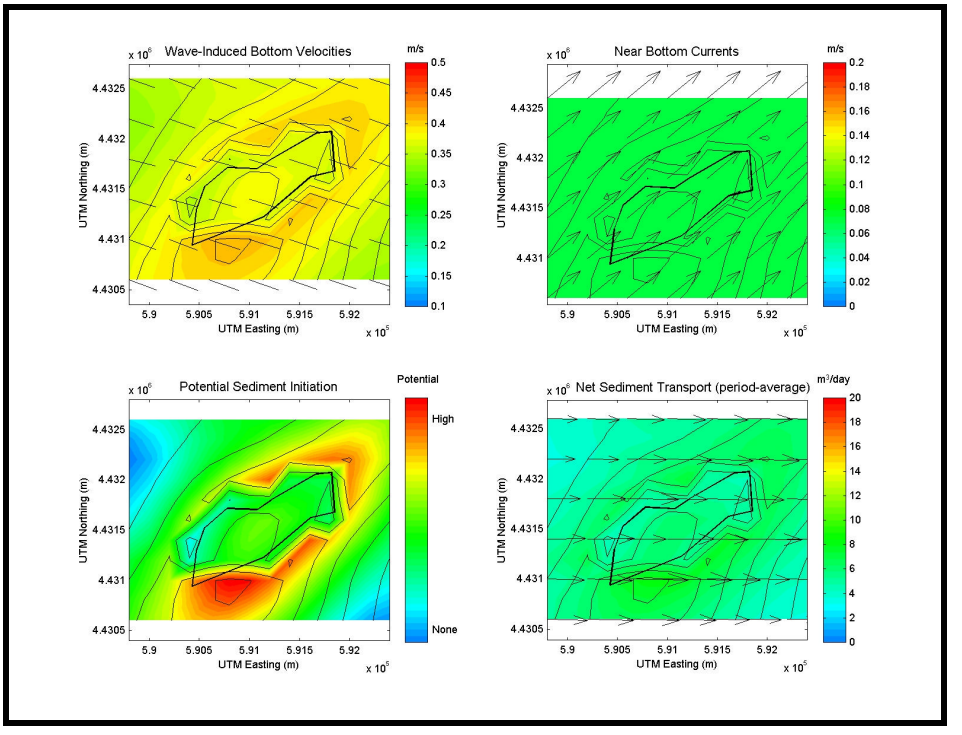

Figure 5-48. East-southeast (-22.5°) influenced hydrodynamic and sediment transport results at Sand Resource Area F2.

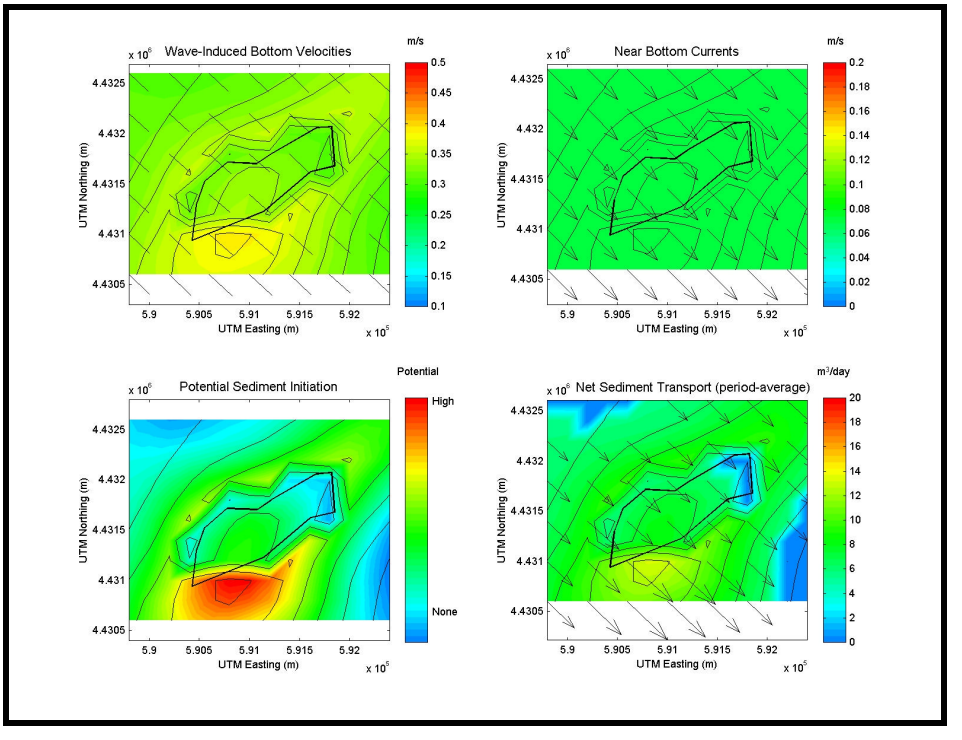

Figure 5-49. Southeast (-45°) influenced hydrodynamic and sediment transport results at Sand Resource Area F2.

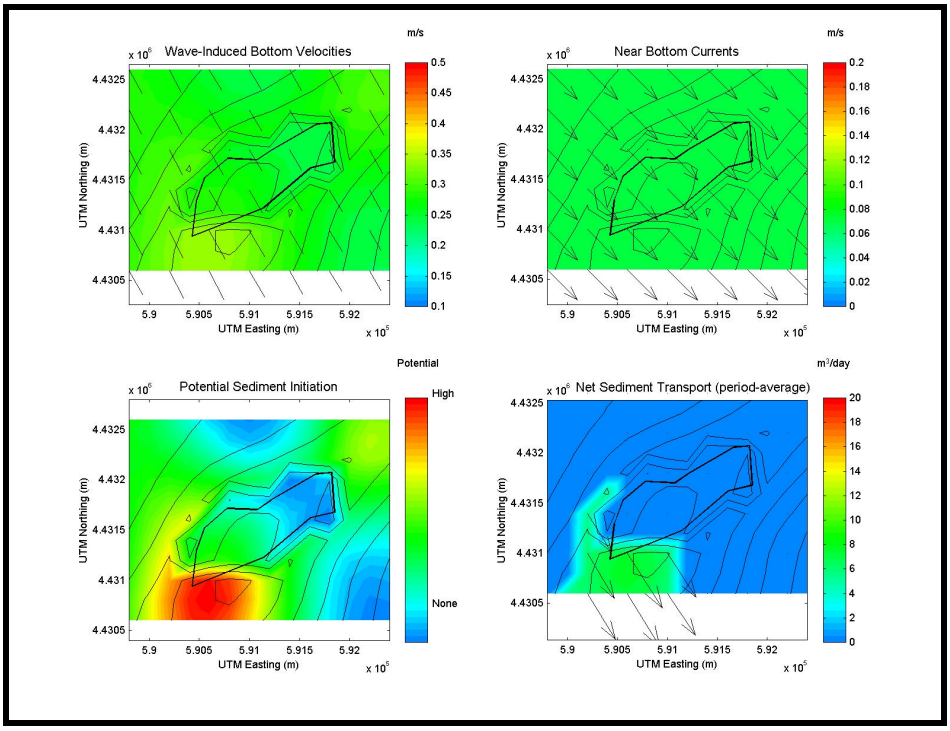

Figure 5-50. South-southeast (-67.5°) influenced hydrodynamic and sediment transport results at Sand Resource Area F2.

Table 5-6 presents maximum and peak (most frequently occurring) sediment transport rates for each of the directions modeled. Included in the table is the contribution of each directional case, as well as the percent of calm time. Calm time represents a period of time when low energy waves are propagating onshore or incident waves are propagating offshore. By representing realistic wave contributions, sediment transport rates and infilling times can be portrayed more accurately (see 5.2.1.7). Overall, this region experiences small sediment transport rates when compared with the magnitudes observed at other potential borrow sites; the magnitude of ambient currents tend to be smaller for this region.

Table 5-6. Sediment Transport Summary for F2

Approach Direction	Approach Bin	% Contributed	Maximum Transport Rate (m^3/day)*	Peak Transport Rate (m^3/day)*
Northeast	45	2.3%	0	0
East-Northeast	67.5	3.4%	1	1
East	90	26.1%	14	8
East-Southeast	112.5	25.8%	6	4
Southeast	135	19.9%	6	0
South-Southeast	157.5	13.9%	10	6
---	calm	8.6%	0	0
* within borrow area				

5.2.1.7 Annual Sediment Transport Magnitude and Direction, and Infilling Times

Table 5-7 presents estimated infilling times for the potential offshore borrow sites along the coast of New Jersey. Volumes were estimated based on quantities required to restore New Jersey beaches after a major storm event (see Section 7.1). The table includes information on the magnitude and direction of sediment transport into the sand borrow sites, dredged sand volume, and the approximate time to fill in the dredged site based on sand transport results presented in the previous sections.

Table 5-7. Summary of directional-averaged (including calm seas) sediment transport results and estimated infilling times.

Resource Area	Magnitude of Sand Transport (m^3/day)	Direction of Net Sand Transport (to)	Dredged Sand Volume (x 10^6 m^3)	Time to Fill Dredged Area (years)
A1	450	SW	8.8	54
A2	327	SW	7.8	65
C1	55	W	6.1	303
G2 Top	100	NE	3.4	93
G2 Bottom	40	E	0.95	65
G3	110	NE	3.3	82
F2	28	E	2.1	205

The magnitude of sediment transport represents the approximate rate during an average day. This rate is determined by weighting each directional approach simulation by the occurrence percentage, including calm time, to generate a representative year. The third column presents the associated average direction, including calm seas. Although the magnitudes and directions of sand transport may fluctuate from day to day, the values presented here are for an average year. Transport rates range from a minimum of 28 m^3/day to a high of 450 m^3/day, while the infilling rate varies between 54 to 303 years. This range of infilling times is based on the volume of sand numerically dredged from the borrow site as well as the sediment transport rate. These infilling times would most likely be reduced if storm events were incorporated into the analysis.

The analysis for infilling time assumes a constant rate of transport through each directional bin and does not include the effects of modified bathymetry. For example, as the dredged region begins to fill, sediment transport dynamics and morphodynamics change. Therefore, sediment transport rates will fluctuate as the borrow site evolves during infilling. This dynamic, time-dependent process is not accounted for in the present analysis. In addition, our analysis does not include suspended sediment entering the local region. For example, sediment may enter the borrow site in Sand Resource Area A1 from Townsends Inlet and Corsons Inlet, reducing the infilling time for that borrow area. Despite these assumptions, the analysis presented provides a reasonable estimate of infilling times.

Resource area C1 has an estimated infilling time on the order of hundreds of years. This is the longest infilling time, and it is a result of reduced sediment transport rates and a large potential borrow volume. Infilling times are reduced to less than a century for the borrow sites G2 Top, G2 Bottom, and G3. Northeast storms and hurricanes may increase sediment initiation and transport, thereby reducing the infilling time for these borrow sites. Borrow site F2 has a sand transport rate of 28 m^3/day and an infilling time of 205 years. Although this duration time is long, sediment transport rates may be increased during storm events, thereby reducing the infilling time.

5.2.2 Nearshore Sediment Transport Modeling

Nearshore sediment transport is a complex process that depends on waves, wind, and tidal action to affect coastal change. Although infrequent storm events represent the most significant erosion process, it is long-term variations in wave climate (combination of storm and normal conditions) that govern beach planform. Wave action constantly moves sand in the longshore direction due to wave-induced currents created by breaking waves. Waves incident from the east will tend to cause littoral drift to be directed to the west. Although wind and tides also govern sediment transport, the quantity of sand moved by these forcing mechanisms is minor compared with wave-induced movement.

To adequately evaluate sediment transport along the New Jersey coastline, a methodology incorporating wave orbital velocities needed to suspend sediment and mean wave-induced currents to advect sediment alongshore was employed. Grant (1943) first investigated the combined effect of orbital velocities and longshore currents on sediment transport processes. Over the past three decades, numerous researchers have developed methodologies for evaluating longshore transport rates based on calculations of the longshore current (e.g., Komar and Inman [1970], Grant and Madsen [1978], Sawaragi and Deguchi [1978], and Bodge [1986]). Due to the inherent complexities of surf zone dynamics caused by turbulent flow and energy dissipation, none of the methods provide perfect agreement with field data. However, utilizing reasonable assumptions, as well as a longshore sediment transport analysis technique based on sound scientific principles, a quantitative estimate of wave-induced transport can be determined.

To date, expressions for evaluating the distribution of longshore sediment transport across the surf zone have assumed that sediment is mobilized by (a) energy dissipation from breaking waves, (b) bottom shear stress induced by the peak horizontal orbital velocities alone, or (c) combined peak orbital velocities and the mean longshore current (Bodge, 1989). Mobilized sediment is then advected by the mean longshore current. Therefore, the distribution of longshore currents across the surf zone provides the driving force needed to predict local longshore transport rates. Based on the review provided by Bodge (1989), most investigators have relied on the expression for longshore current on a planar beach developed by Longuet-Higgins (1970).

The existing models indicate that longshore sediment transport is largest between the breaker line and approximately midway across the surf zone, and that the transport rate trends to zero at the shoreline and outside the breaker line. Most models do not account for the often-significant longshore transport that occurs in the swash zone. Field data have indicated that significant sediment transport may occur in the swash zone; about 10% to 30% of the total transport occurs seaward of the breaker line, and greater transport is often associated with shallower depths such as bars. Overall, there is large variability in the shape of the transport distribution profile (Bodge, 1989). Although existing models have limitations, many of these models have been used successfully to evaluate the general characteristics of the longshore transport distribution.

5.2.2.1 Model Development

Stresses exerted by waves vary in the cross-shore direction, typically decreasing from the breaker line to the shoreline. However, this decrease may not occur in a uniform manner due to the presence of bars and troughs. The longshore current also has a characteristic profile, and because sand transport is the result of combined waves and currents, its distribution will be related to the distribution of waves and currents. Using data from field and laboratory

experiments, Bodge and Dean (1987) tested five existing cross-shore distribution relationships. They provided a rating system for each relationship, ranging from fair to poor based on comparisons with measurements. Bodge and Dean (1987) also proposed a relationship for the cross-shore distribution of longshore sediment transport which assumed that sediment is mobilized in proportion to the local rate of wave energy dissipation per unit volume and transported alongshore by the mean current. In equation form, this expression is

$$q_x(y) = k_q \frac{1}{d} \frac{\partial}{\partial x}\left(EC_g\right) V_\ell \tag{5.20}$$

where $q_x(y)$ is the local longshore transport per unit width offshore, y represents the cross-shore coordinate, k_q is a dimensional normalizing constant, d is the local water depth in the surf zone (including wave-induced setup), E represents the local wave energy density, C_g is the local wave group celerity, and V_i is the local mean longshore current speed. The above expression can be expanded by assuming shallow water wave conditions, small angles of wave incidence, and a nonlinear value for the wave group celerity ($C_g = (g(H+d))^{1/2}$) as:

$$q_x(y) = k_q \frac{1}{8} r g \frac{H}{\sqrt{H+d}} \left[2\frac{dH}{dy} + \frac{H}{2(H+d)} \frac{d}{dy}(H+d) \right] V_\ell \tag{5.21}$$

in which H is the local wave height in the surf zone. This shallow water equation represents conditions landward of the breakpoint. Seaward of the breakpoint, transport is assumed to be negligible since no energy dissipation occurs. This simplification could underestimate the transport rate by between 10% and 30%, because field measurements have indicated that this amount of transport occurs seaward of the breaker line. However, the REF/DIF S wave model employed in this study used a spectral wave breaking model. By employing this type of wave breaking model, no definitive breakpoint exists and a small amount of transport will occur in the region where some of the high period spectral components break. Therefore, sediment transport occurs seaward of the standard definition of the breakpoint. Energy dissipation, as well as the associated transport, within this offshore region was assumed to characterize transport seaward of the breakpoint. The distribution of $q_x(y)$ was integrated across the nearshore zone to compute longshore transport rates for each cross-shore profile.

5.2.2.2 Sediment Transport Along the New Jersey Coast

The REF/DIF S wave and wave-induced current models provided needed information for the littoral drift evaluation. Longshore currents were derived from the wave-induced current model, and wave parameters (wave height and water depth) were derived from wave modeling results. Because the purpose of the sediment transport modeling task was to determine impacts of offshore sand mining on the nearshore region, a sensitivity analysis of the empirical constants utilized in the transport equation was not required. Instead, the k_q value was determined from the bathymetric change analysis. Based on maximum annual transport rates of between 100,000 and 300,000 m^3/yr, the k_q value was set and remained constant for all model runs. By comparing existing sediment transport potential rates to variations in the rates resulting from the various dredging scenarios, the relative impact of dredging on nearshore transport processes were quantitatively evaluated.

The modeling grids used for the longshore sediment transport analysis are shown in Figure 5-51 and are denoted in a similar fashion as the wave modeling grids previously described. For Grids A, B2, and B1, a single model sub-grid was developed using the wave modeling results. In these cases, sediment transport modeling results for each wave condition could be summed to develop annualized longshore sediment transport quantities. Unfortunately, each wave model sub-grid used for Grid C incorporated a different stretch of

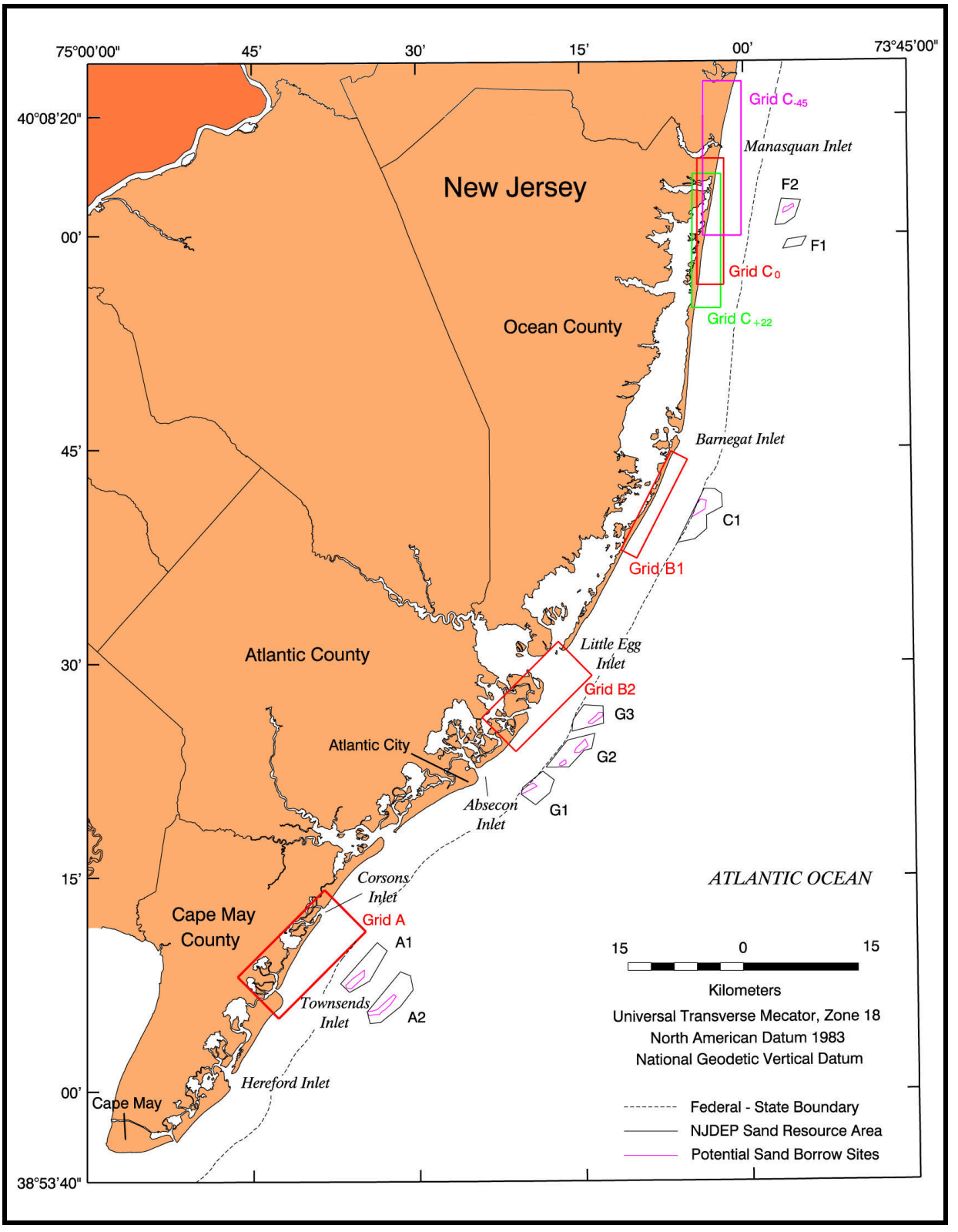

Figure 5-51. Map showing the various Grids used for wave-induced current and longshore sediment transport potential modeling.

shoreline, with a very limited region common to all grids (see Grids C_{+22}, C_0, and C_{-45} on Figure 5-51). Therefore, it was not possible to compute annualized sediment transport for Grid C.

Similar to the wave-induced current model, the longshore sediment transport model was run for the four wave modeling grids (Grids A, B1, B2, and C) and each spectral wave condition under existing conditions and post-dredging scenario. This required a total of 58 model runs. Results from all model runs are included in Appendix C3. As an example, the results of one run (the existing conditions at Grid A for the -22.5° wave condition) are described in more detail below. This example provides an overview of typical wave-induced sediment transport predictions associated with the modeling effort.

The S_{xy} radiation stress component provided the primary driving force for wave-induced currents and longshore sediment transport. Radiation stress values were generated from REF/DIF S modeling; therefore, results of the wave-induced current and longshore sediment transport models were dependent on the numerical evaluation of the nearshore wave climate. Figure 5-52 illustrates the longshore and cross-shore distribution of S_{xy}, indicating regions of wave energy focus. As expected, areas of higher S_{xy} values have higher longshore sediment transport rates. Longshore sediment transport rates for each case were calculated by weighting the potential transport rate by the percent occurrence of the specific wave condition. Because all sediment transport for this case is directed north-to-south, the general increase in sediment transport rate immediately south of Corsons Inlet from UTM Northing coordinate 4,339,500 m to approximately 4,336,000 m would indicate a tendency toward erosion. The opposite is also true, where the decrease in sediment transport rate from UTM Northing coordinate 4,332,000 m to approximately 4,330,000 m would be indicative of a shoreline segment experiencing accretion. For Grid A, the highest southerly-directed sediment transport rates are mid-way between Corsons and Townsends Inlets. Due to specific regions of wave focusing and sheltering associated with this wave condition, some areas of increased or decreased sediment transport potential existed along the shoreline. For example, sediment transport calculations for the –22.5° wave condition indicated a reduction in southerly-directed transport in the vicinity of the tidal inlets. This reduction is likely a result of wave sheltering by offshore shoals associated with each inlet (both Corsons Inlet and Townsends Inlet).

Offshore wave conditions and bathymetry, as well as the orientation of the shoreline, govern the direction of wave-induced sediment transport. For the New Jersey shoreline, wave conditions are dominated by waves propagating from the east and southeast. Due to shoreline orientation, these waves tend to drive sediment strongly toward the south in the southern portion of New Jersey, where the shoreline is oriented northeast-to-southwest. In the northern portion of New Jersey, this trend is reversed, where the combination of sheltering provided by Long Island/New England and the north-to-south orientation of the shoreline allow sediment transport to be more strongly influenced by waves propagating from the southeast.

Each of the regional sediment transport modeling (Grids A, B1, B2, and C) results indicated large variations in transport magnitude. Similar to previous studies (e.g. Buteux, 1982), sediment transport modeling indicated a net longshore sediment transport south of Barnegat Inlet directed toward the south, with the magnitude generally increasing from north-to-south. With the large number of tidal inlets along the New Jersey coast, sediment transport reversals are common; however, the overall tendency is north-to-south littoral drift south of Barnegat Inlet. Between Barnegat and Manasquan Inlets, the net longshore sediment transport direction may be either north or south. North of Manasquan Inlet, the net transport becomes strongly toward the north (Caldwell, 1966).

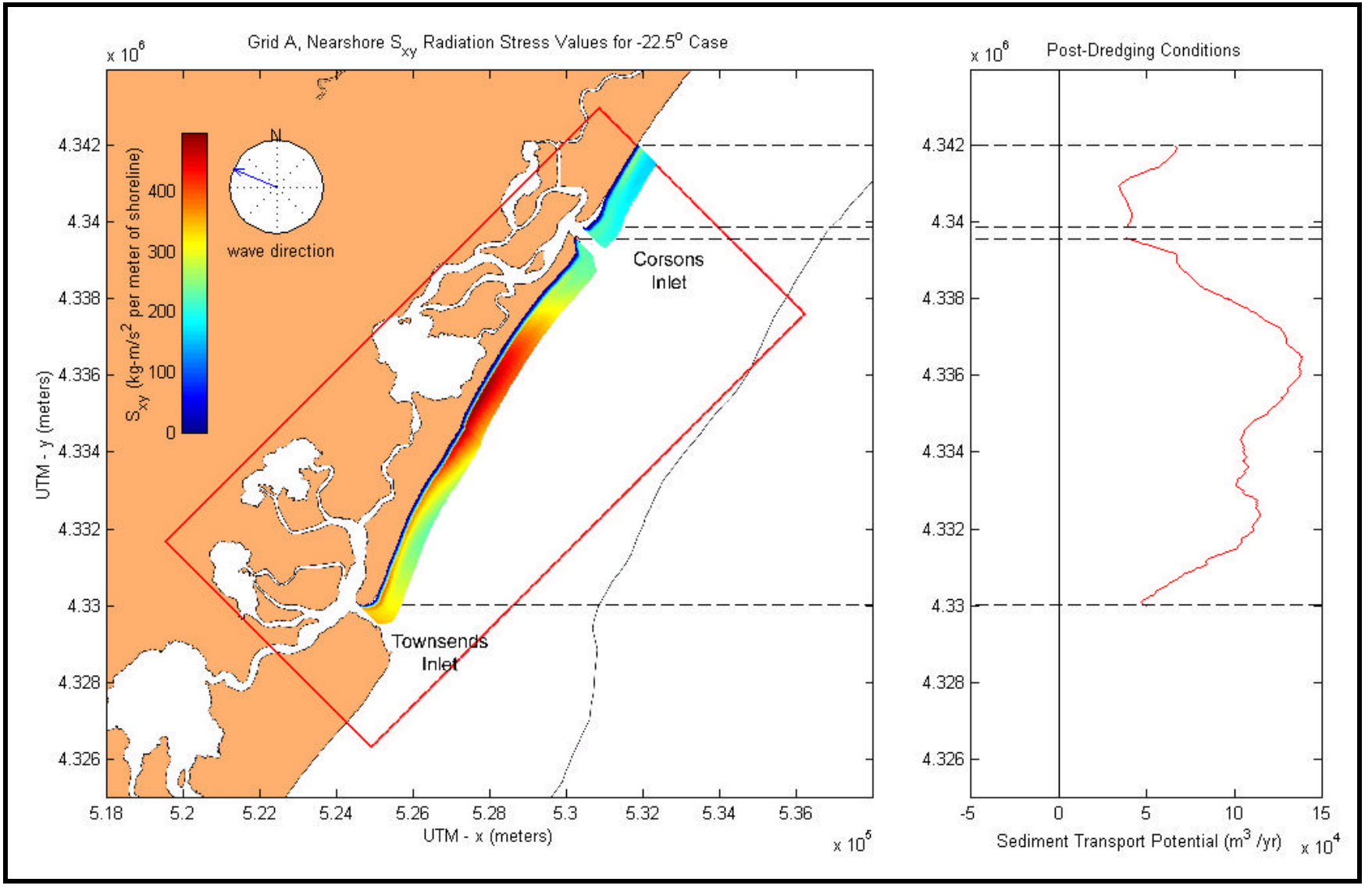

Figure 5-52. S_{xy} radiation stress values and annualized sediment transport potential for the –22.5° wave condition within Grid A.

Figures 5-53 to 5-55 illustrate annual sediment transport for Grids A, B2, ad B1, respectively. Results of gross southerly and northerly transport, as well as net transport were computed for each of these grids. Sediment transport potential within Grid A is nearly uni-directional, with the south-directed transport typically an order of magnitude larger than the north-directed transport (Figure 5-53). The maximum net sediment transport rate is approximately 300,000 m^3/year to the south at UTM Northing coordinate 4,336,000 m. North of Corsons Inlet, only the region immediately updrift (north) of the inlet exhibits some north-directed littoral drift. This area is likely influenced by the redirection of waves by shoals associated with the inlet. In a similar manner, the regions immediately downdrift of Corsons Inlet and immediately updrift of Townsends Inlet also exhibit an increase in gross northerly sediment transport potential.

The sediment transport potential within Grid B2 also is predominantly toward the south (Figure 5-54); however, the net transport magnitude is lower than the transport computed for Grid A. The maximum net sediment transport rate is approximately 200,000 m^3/year to the south in the region south of Little Egg Inlet at UTM Northing coordinate 4,369,000 m. In general, net longshore sediment transport is between 100,000 and 150,000 m^3/year to the south along much of this region; however, the calculations exhibited large variations over the relatively short stretch of shoreline evaluated. Similar to Grid A, the series of shoals associated with tidal inlets within the modeled region caused areas of wave focusing, as well as wave sheltering. In addition, northerly-directed sediment transport becomes significant within the southern portion of Grid B2, where the nearshore region is not influenced by ebb tidal shoals. The maximum northerly transport is approximately 60,000 m^3/year at UTM Northing coordinate 4,364,000 m.

The Grid B1 shoreline represents a relatively straight stretch of the New Jersey shoreline without tidal inlets. Although some researchers have found that a sediment transport "nodal point" exists in this region (Ashley, et al., 1986), sediment transport modeling indicated a net southerly drift along this stretch of shoreline (Figure 5-55). The maximum net sediment transport rate is approximately 100,000 m^3/year to the south, about 4,000 m south of Barnegat Inlet at UTM Northing coordinate 4,398,000 m. The wave energy remains relatively consistent along the Grid B2 shoreline; however, redirection of wave energy due to offshore bathymetry (i.e., wave refraction) causes a reduction in the south-directed transport south of UTM Northing coordinate 4,393,000 m. Because the north-directed littoral drift shows little variation along this stretch of shoreline (between 60,000 and 90,000 m^3/year), the reduction in south-directed transport in the southern half of the grid causes a reduction and/or reversal of the net south-directed transport.

As described previously, each wave model sub-grid used for Grid C incorporated a different stretch of shoreline, with a very limited region common to all grids (see Grids C_{+22}, C_0, and C_{-45} on Figure 5-51). Therefore, it was not possible to compute annualized sediment transport for Grid C. Since the –22.5° wave condition had the greatest influence on sediment transport, sediment transport associated with this wave condition was used to describe the characteristics of littoral drift in this region. Sheltering provided by Long Island prevents south-propagating open ocean waves from affecting longshore sediment transport. Instead, the only waves propagating from the north and northeast are locally generated wind waves that have limited energy to influence local sediment transport processes. As a result, east and southeast wave conditions dominate wave-induced sediment transport. The nearly north-to-south shoreline orientation within Grid C and the energetic east/southeast wave conditions cause a net littoral drift to the north. Although net and gross annual transport was not calculated for Grid C, Figure 5-56 is representative of longshore transport in this region. Within the limits of Grid C, the north-directed transport is relatively consistent, with no obvious areas of wave focusing.

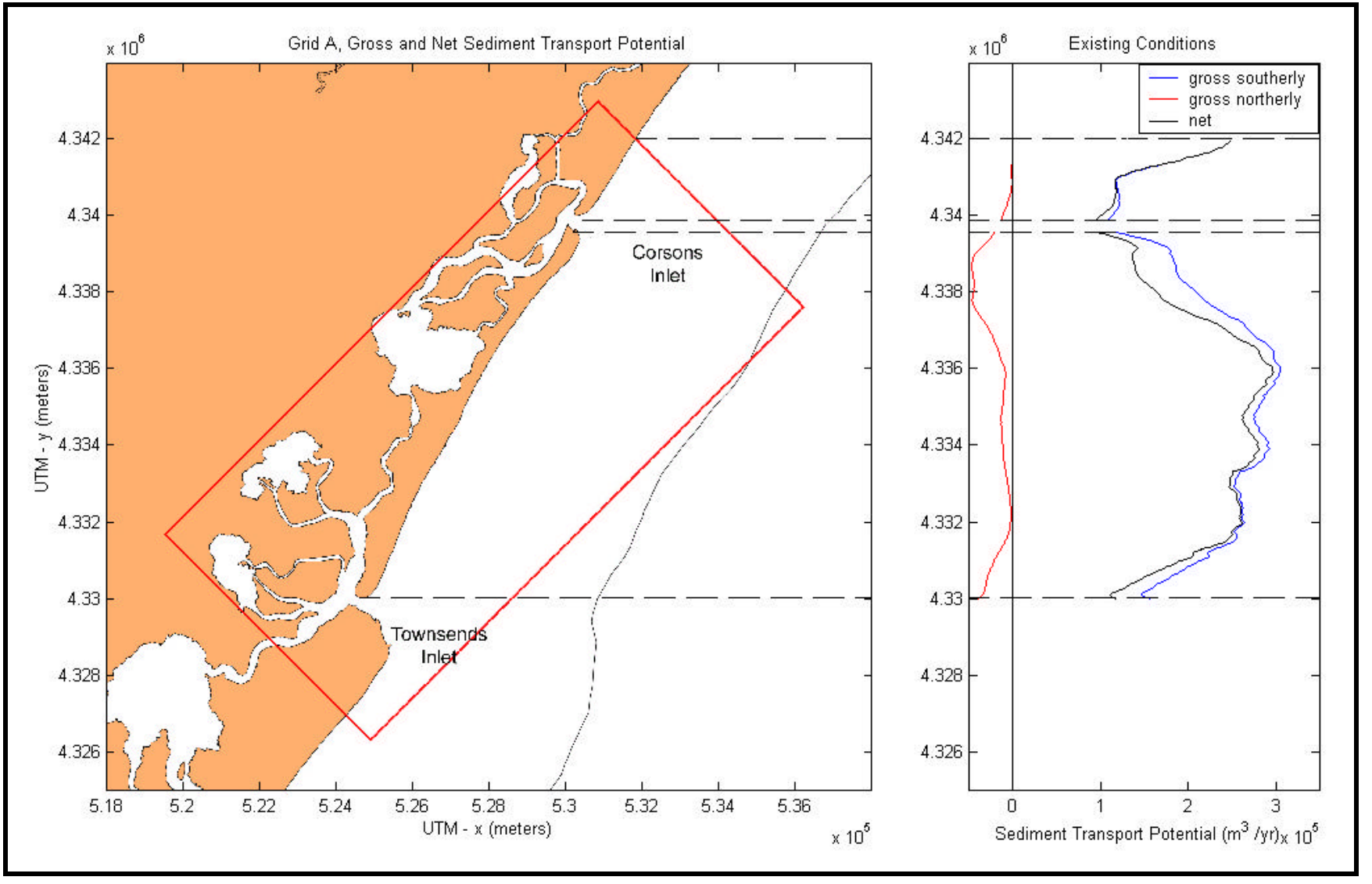

Figure 5-53. Gross and net annual longshore sediment transport potential for Grid A.

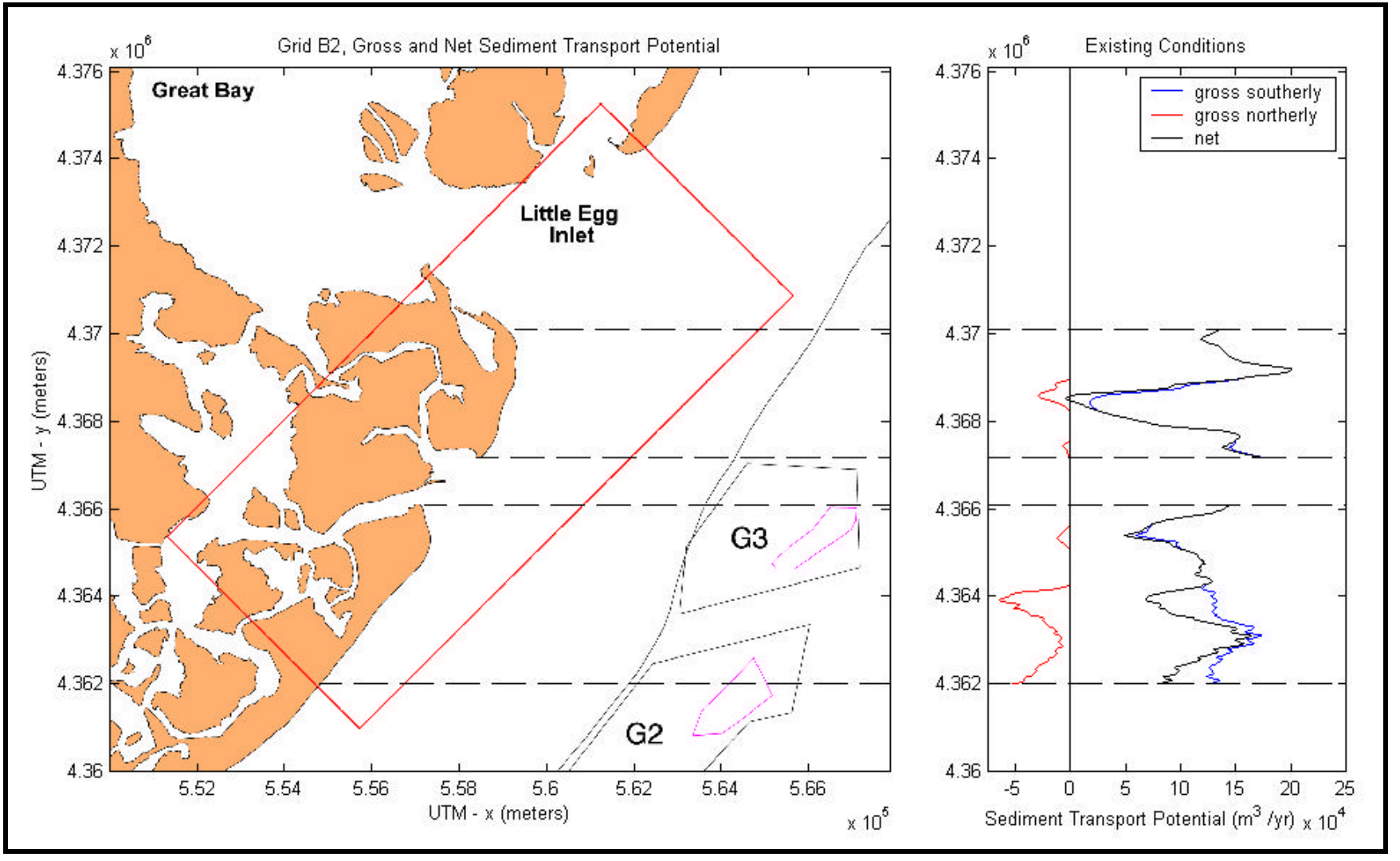

Figure 5-54. Gross and net annual longshore sediment transport potential for Grid B2.

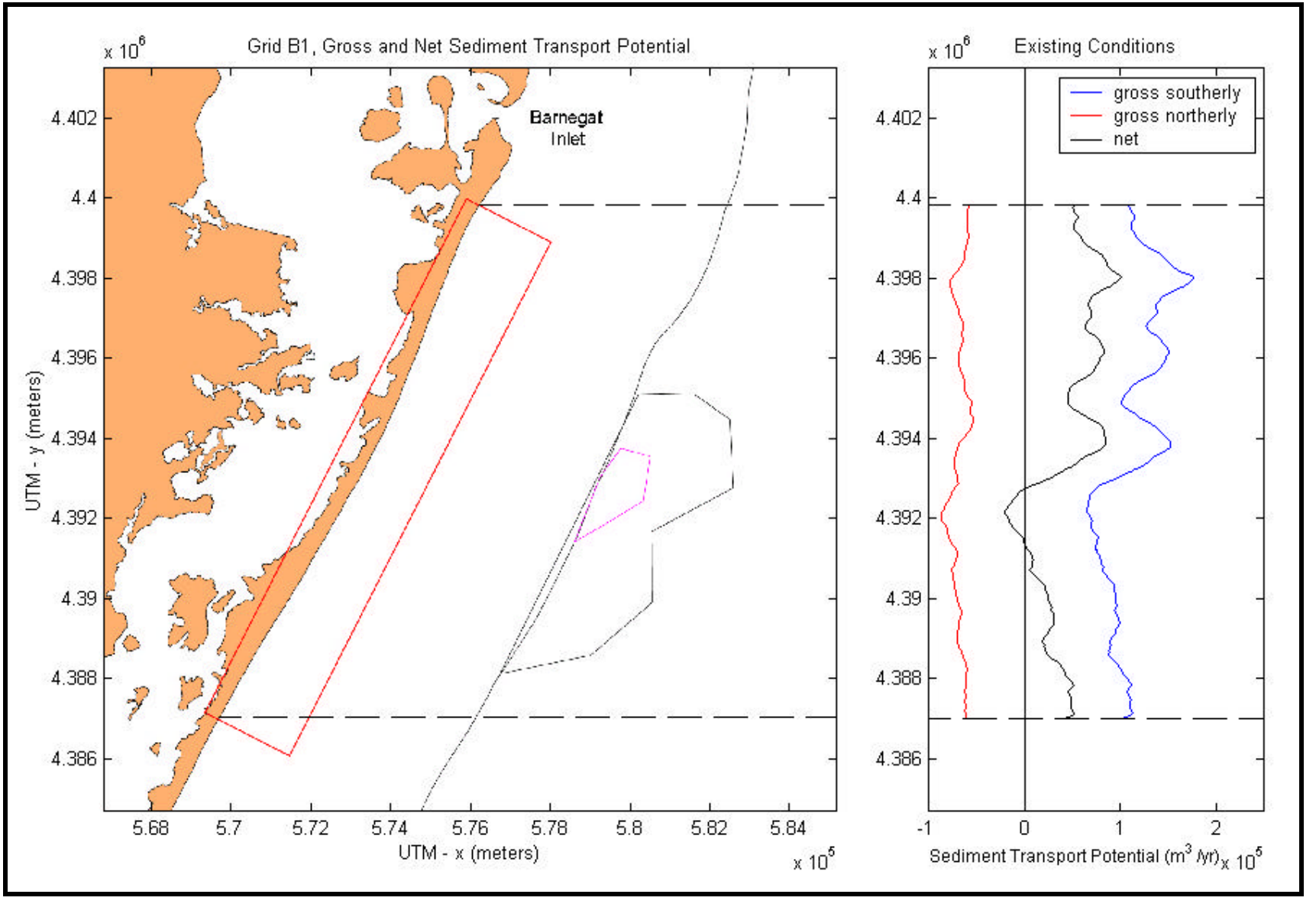

Figure 5-55. Gross and net annual longshore sediment transport potential for Grid B1.

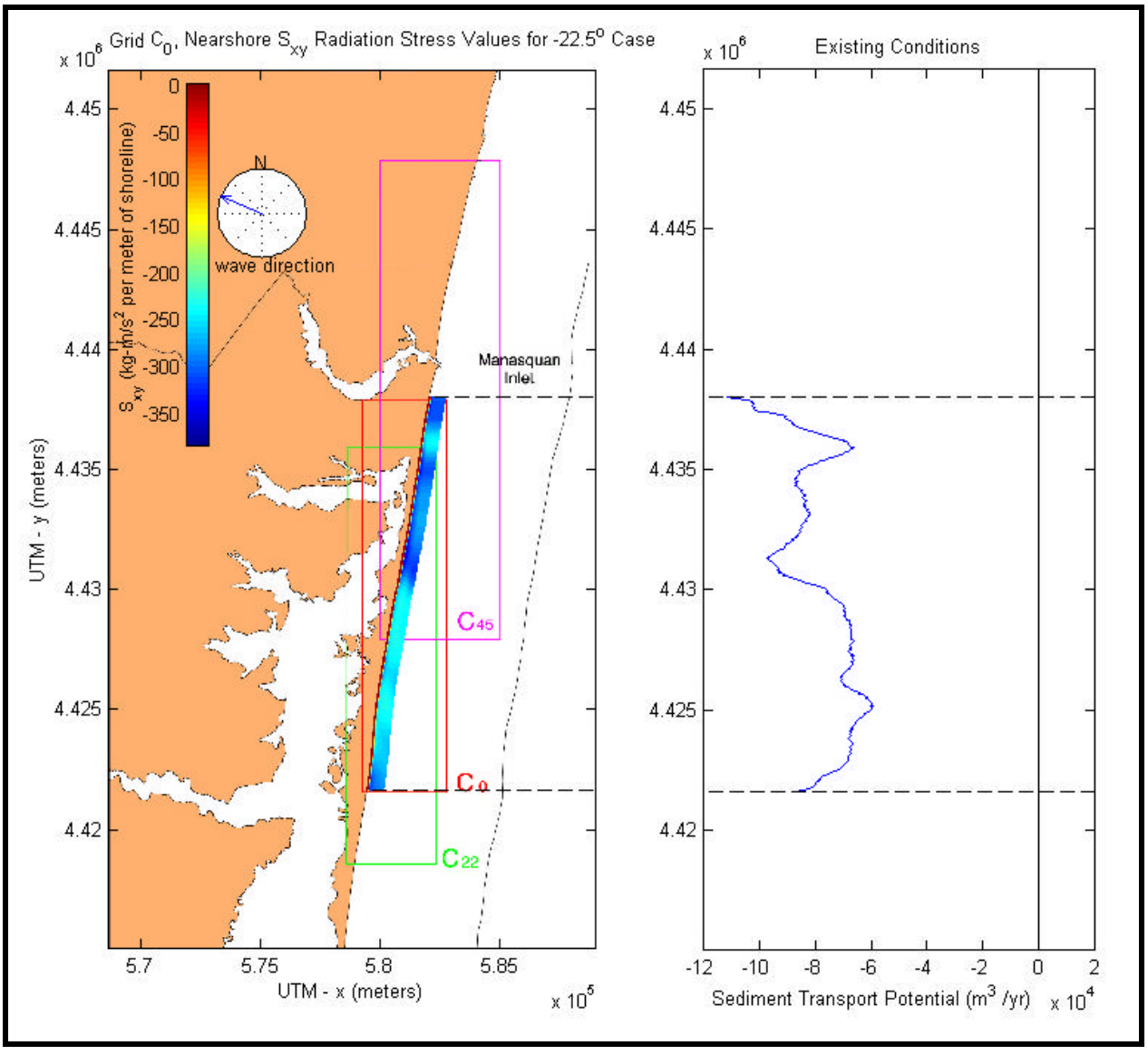

Figure 5-56. S_{xy} radiation stress values and annualized sediment transport potential for the –22.5° wave condition within Grid C.

In addition to average wave conditions, REF/DIF S was used to evaluate nearshore wave transformation associated with northeast storm and hurricane conditions. Unfortunately, limitations of this modeling approach become evident for these extreme wave conditions. Along the coast of New Jersey, wave modeling results for storm conditions (e.g. Figure B5-6) indicate model shortcomings associated with wave breaking and wave energy focusing. For example, the northeast storm wave modeling results for Grid A indicate an immediate reduction in wave height (through wave breaking) as waves propagate across the grid. This indicates that wave breaking is occurring at the seaward limit of the grid, and the offshore extent of the grid likely is inappropriate for modeling these extreme conditions. Figure B5-6 (similar to all storm wave conditions modeled) indicates a gradual reduction in wave height as waves propagate from offshore to the shoreline. In many cases, storm wave heights are less than 1 meter at a distance of 1,000 m from shore. This unrealistic depiction of energy dissipation illustrates the

inability of the wave breaking model used in this version of REF/DIF S to accurately represent storm wave conditions.

Although it may be possible to use a modified version of REF/DIF S to model extreme wave conditions in the future, the limits inherent in the existing model make quantitative analysis of storm modeling results questionable. Similar to the storm wave modeling results, the sediment transport rates calculated for the 50-year northeast storm and hurricane events illustrated significant longshore variability. For example, Figure 5-57 illustrates large changes in sediment transport potential from 600,000 m^3/year toward the north to 450,000 m^3/year toward the south over less than 700 m of shoreline (between UTM Northing coordinates 4,363,900 m and 4,364,600 m). No obvious offshore bathymetric features explain this change in wave direction over the relatively short spatial scale. More realistic wave modeling and associated sediment transport modeling results were produced for the hurricane at Grid B1 (Figure 5-58). In this case, hurricane waves propagating from the southeast generated nearly uniform north-directed currents transporting sediment toward Barnegat Inlet.

In addition to providing net sediment transport rates, the transport model provided the cross-shore distribution of longshore sediment transport across the surf zone. Figure 5-59 illustrates this cross-shore distribution in relation to the cross-shore distribution of the mean longshore current at three selected transects. Based on the results of sediment transport modeling, peak current velocities occur landward of peak sediment transport rates. Because most wave models predict rapid energy dissipation at the breaker line, and the sediment transport equation used strongly depends on the wave energy dissipation rate, the highest sediment transport rate can be expected relatively close to the break point. Field and laboratory data collected by Bodge and Dean (1987) indicate that peak transport rates often occur near the breakpoint. The current distribution predicted by the longshore current model also corresponds to other model approaches, where maximum currents occur in the seaward half of the surf zone.

5.2.2.3 Nearshore Sediment Transport Versus Historical Shoreline Change

As a simplistic measure of the longshore sediment transport model's applicability to the New Jersey shoreline, accretion/erosion potential predicted by the model was compared with shoreline change results. The accretion/erosion potential was determined by calculating sediment transport change normalized to the maximum computed change. In this manner, the relative magnitude of erosion and accretion can be evaluated for the entire shoreline segment. Because the calculation of accretion/erosion potential is dependent on the slope of the net sediment transport curve, smoothing of this curve was performed to determine general transport trends. Shoreline change for the longest time period where data were available for the entire coast (1899 to 1977) was plotted for comparison purposes. The results of this analysis are shown in Figures 5-60, 5-61, and 5-62 for Grids A, B2, and B1, respectively. As described previously, it was not possible to compute annual sediment transport trends for the Grid C shoreline; however, the change in sediment transport associated with the –22.5° wave condition is shown in Figure 5-63. This condition represents the typical wave condition with the greatest sediment transport potential for Grid C.

The purpose of the comparison between *modeled* change in sediment transport potential and *measured* shoreline change is to determine whether the wave, wave-induced current, and sediment transport modeling approaches yield meaningful and useful results. The sediment transport potential analysis assumes that an infinite volume of sediment is available for transport, all sediment has similar grain size characteristics, and tidal inlets and/or coastal structures do not significantly influence transport patterns. In addition, long-term shoreline change

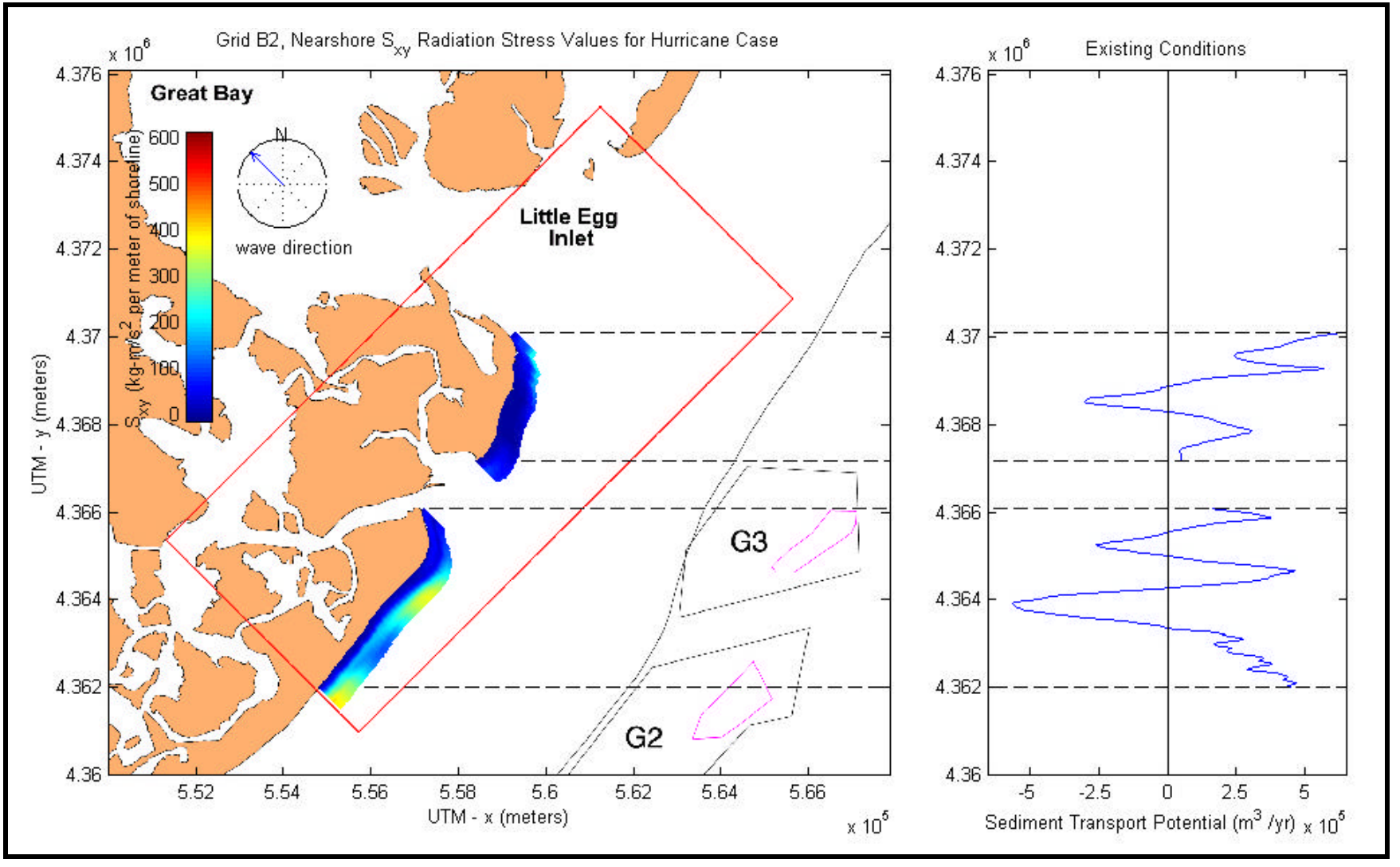

Figure 5-57. Longshore sediment transport potential for 50-year hurricane condition at Grid B2.

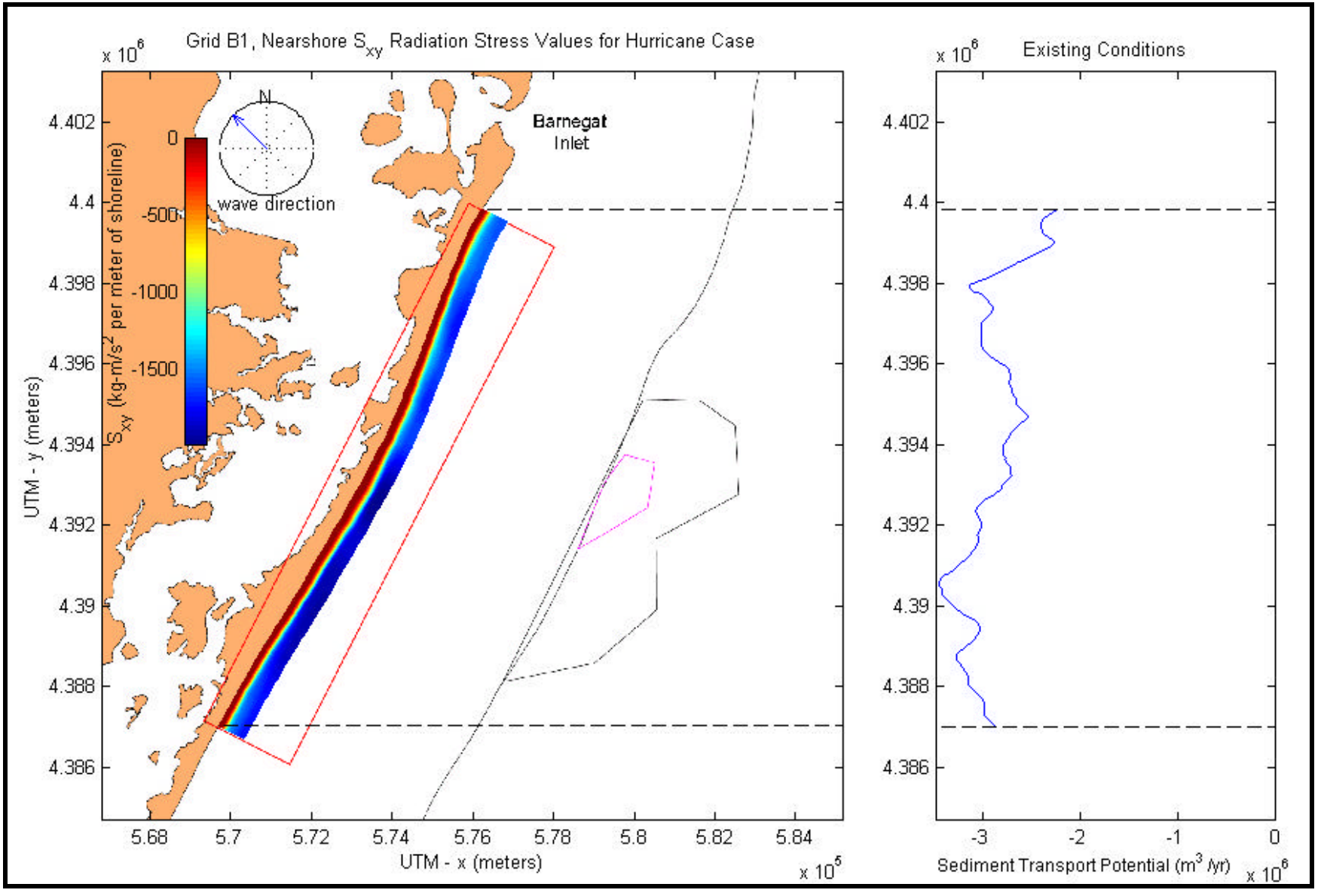

Figure 5-58. Longshore sediment transport potential for 50-year hurricane condition at Grid B1.

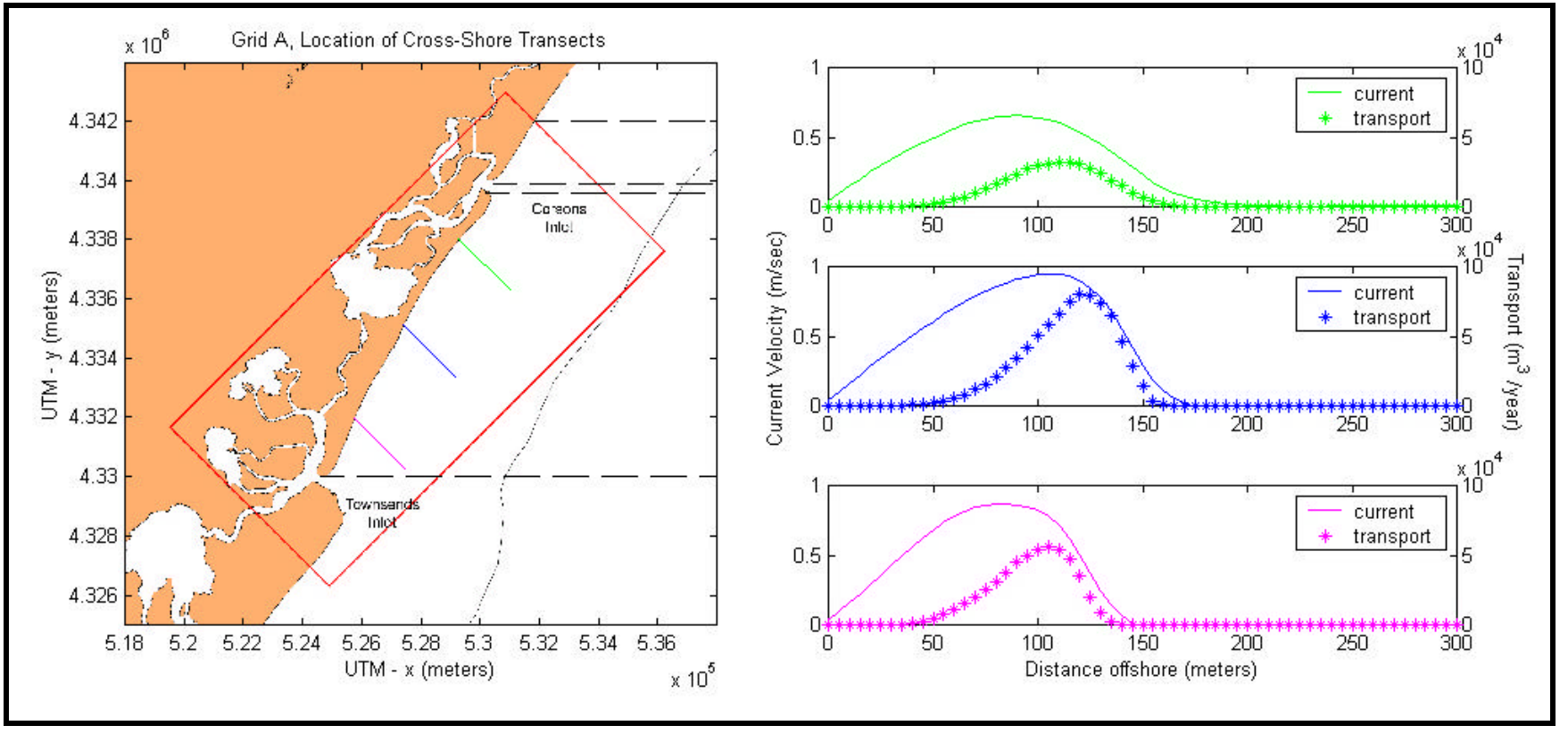

Figure 5-59. Cross-shore distribution of longshore current and sediment transport for three selected transects for the –22.5° wave condition within Grid A.

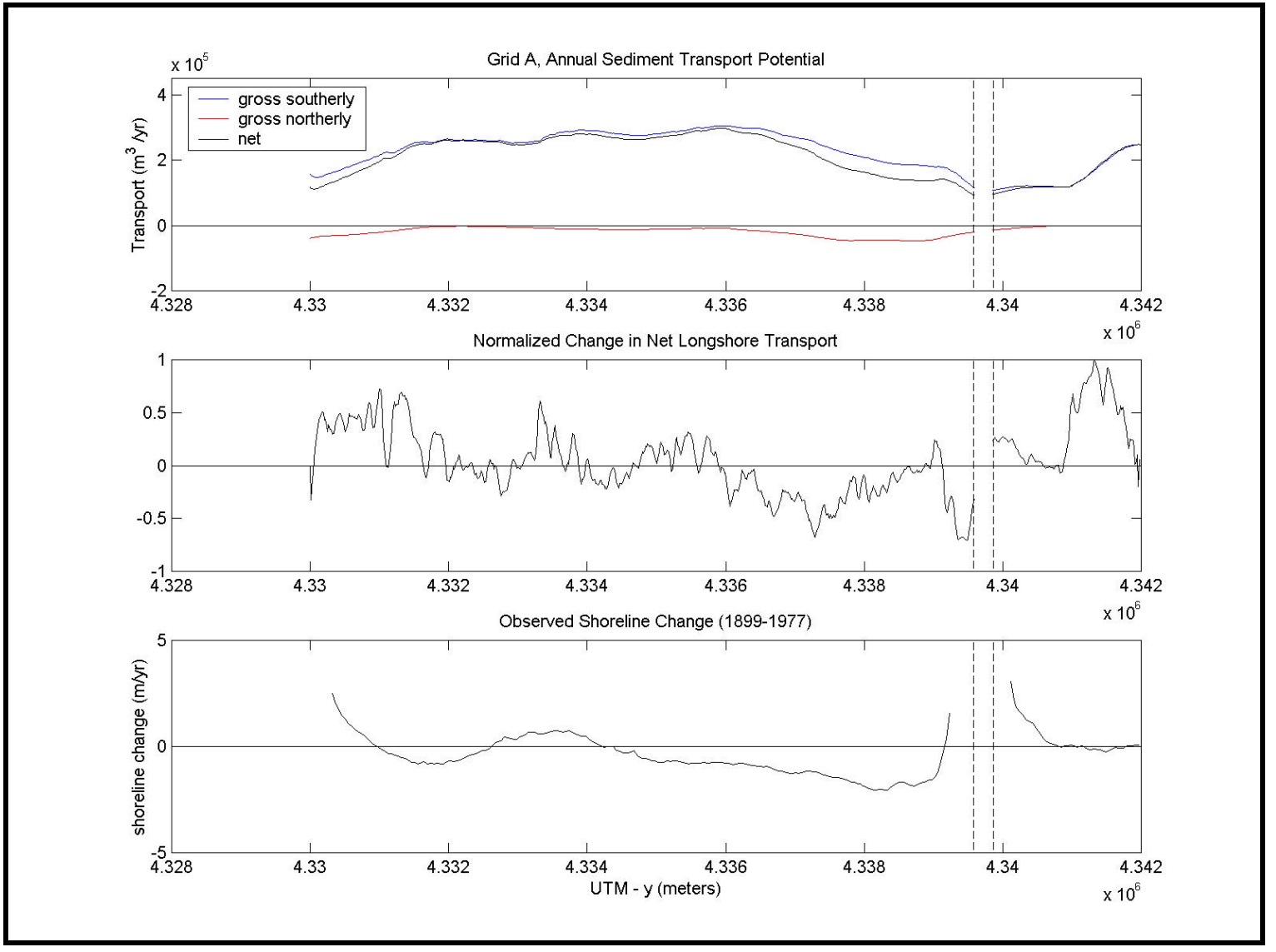

Figure 5-60. Annual longshore sediment transport potential, normalized change in longshore transport (modeled accretion/erosion potential), and observed shoreline change between 1899 and 1977 for Grid A.

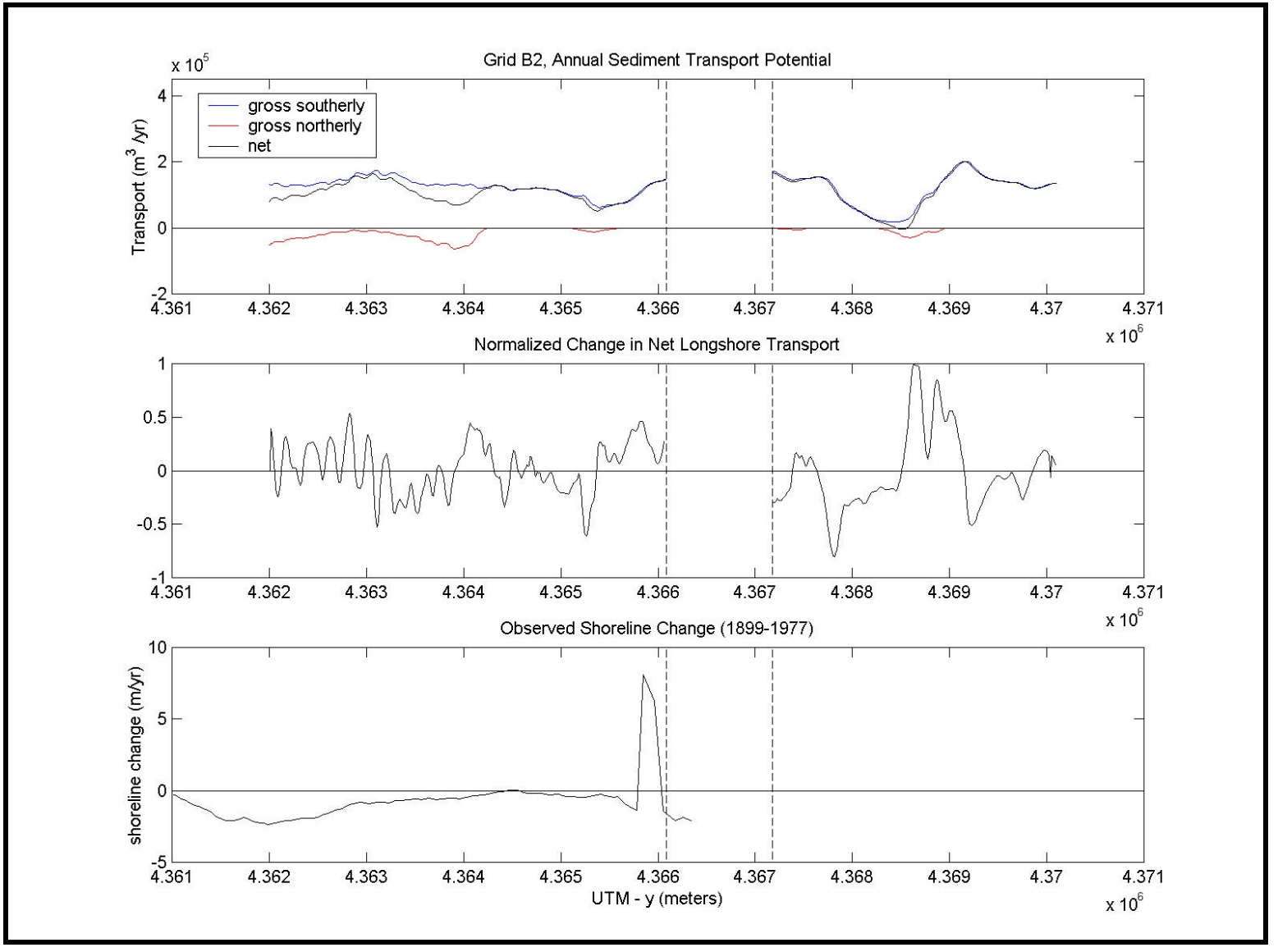

Figure 5-61. Annual longshore sediment transport potential, normalized change in longshore transport (modeled accretion/erosion potential), and observed shoreline change between 1899 and 1977 for Grid B2.

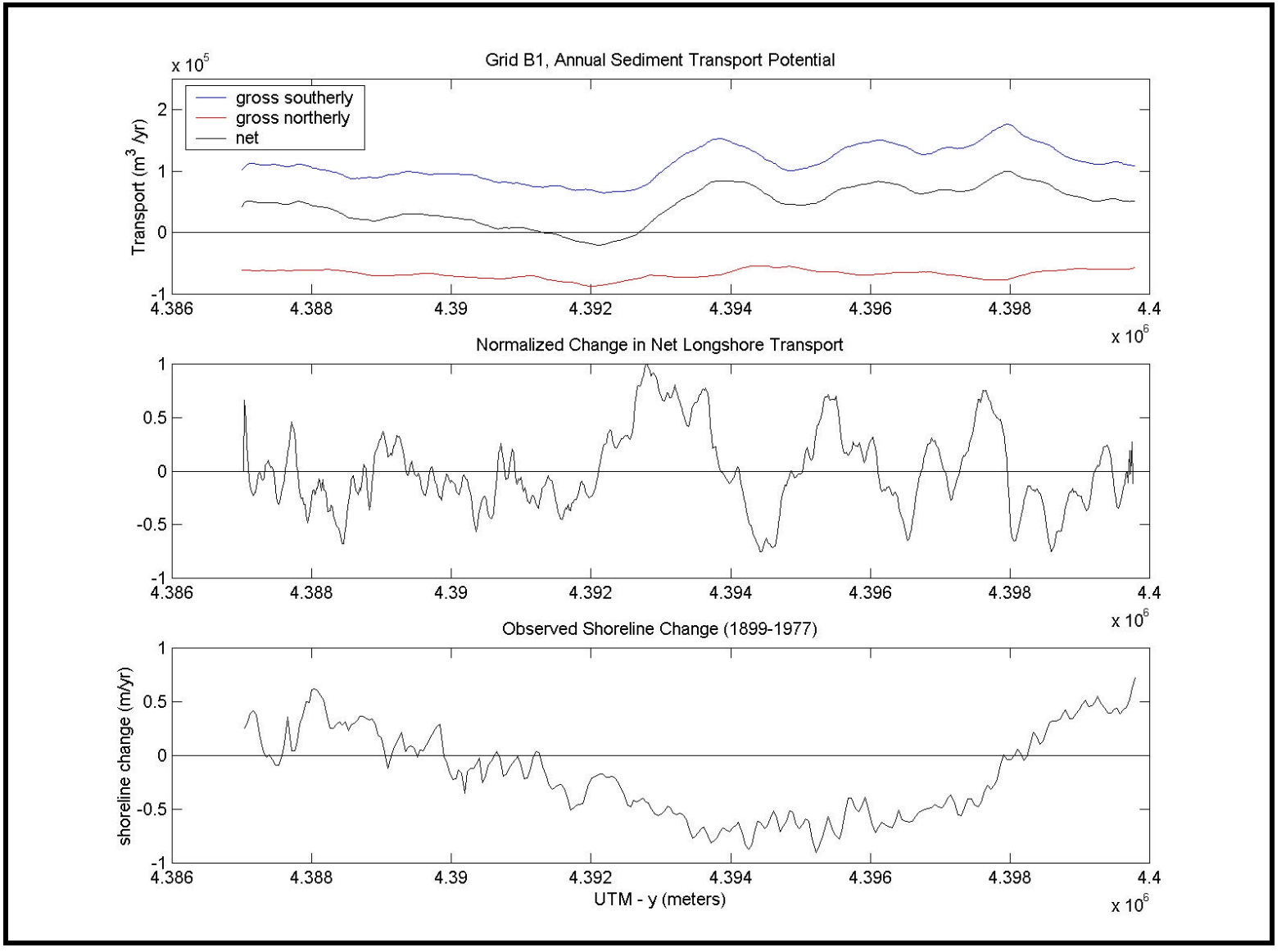

Figure 5-62. Annual longshore sediment transport potential, normalized change in longshore transport (modeled accretion/erosion potential), and observed shoreline change between 1899 and 1977 for Grid B1.

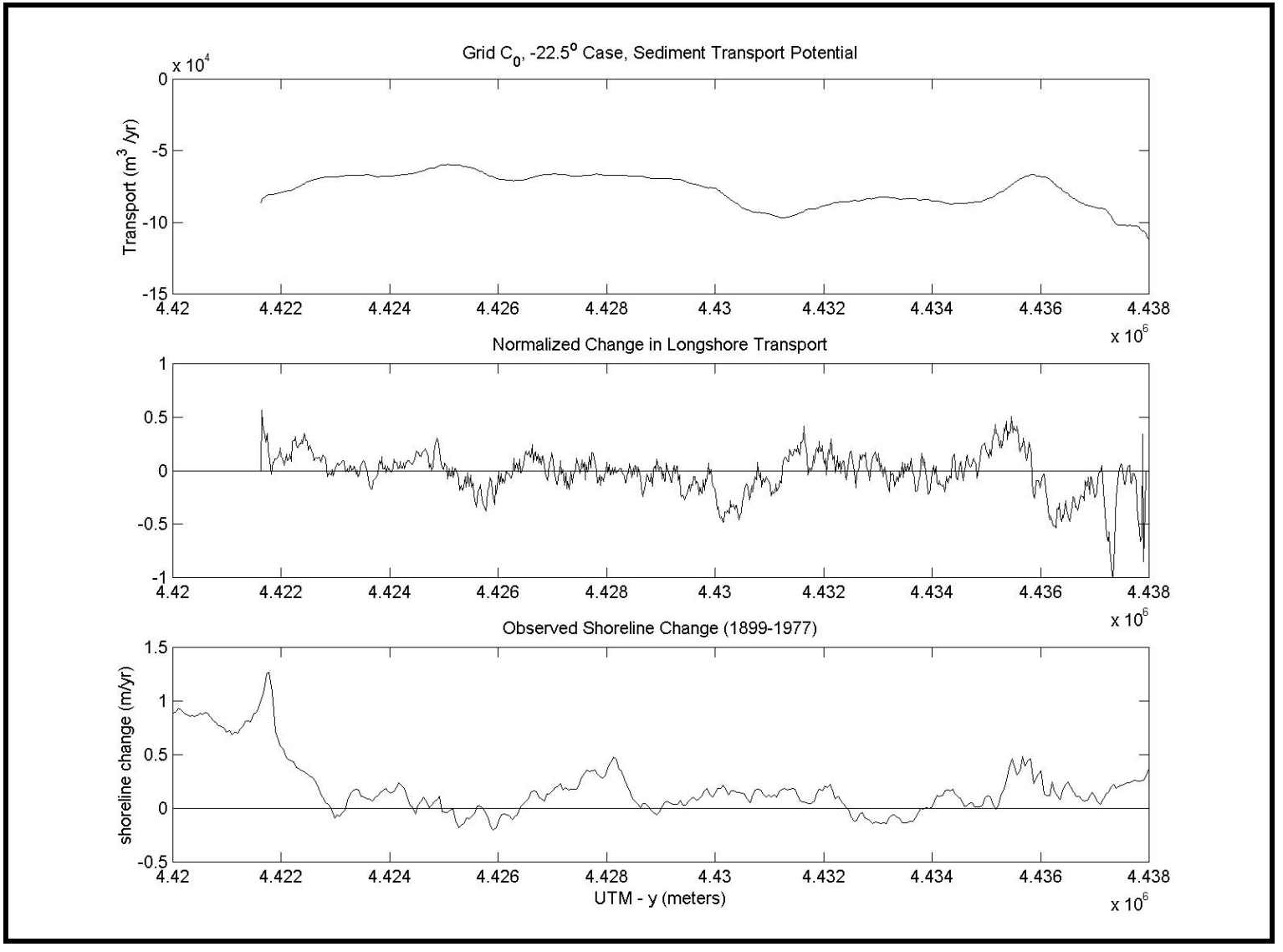

Figure 5-63. Annual longshore sediment transport potential for the –22.5° wave condition, normalized change in longshore transport (modeled accretion/erosion potential), and observed shoreline change between 1899 and 1977 for Grid C.

measurements do not account for beach nourishment projects. Although much of the New Jersey shoreline is influenced by coastal structures, there are several tidal inlets within the study limits, several large-scale beach nourishment projects have been performed along New Jersey's beaches, and grain size can be variable, the model/data comparison can yield useful information. Since the goal of the wave and sediment transport analysis is to determine the potential impacts of offshore sand mining on wave-induced transport, the modeling analyses provides a valuable tool for quantitatively determining the potential magnitude of this impact.

Figure 5-60 illustrates large variability in accretion/erosion trends predicted by the sediment transport model. Due to this high variability, it is difficult to determine obvious trends for the normalized transport change. North of Corsons Inlet (approximate UTM Northing coordinate 4,339,800 m), the model indicates a trend toward accretion, where the south-directed sediment transport decreases in magnitude from north-to-south. Except in the region immediately updrift of the inlet (about 40% of the shoreline length), historical shoreline change data indicates a stable shoreline. It is quite possible that the sediment supply north of Corsons Inlet is limited; therefore, actual shoreline change does not reflect the accretion predicted by the model. South of Corsons Inlet, the trends predicted by the model closely match historical shoreline change. Between UTM Northing coordinate 4,335,000 m and Corsons Inlet (approximately 5,000 m), model predictions and historical data generally indicate erosion. In addition, the model accurately predicted the observed accretion between UTM Northing coordinate 4,332,500 m and 4,334,000 m. South of UTM Northing coordinate 4,332,500 m, the model generally predicts accretion; however, shoreline change data show accretion and erosion. Although modeled change in sediment transport does not match observed shoreline change within Grid A at all locations, overall trends are predicted well for most regions, except immediately north of Corsons and Townsends Inlets.

Similar to Grid A, Figure 5-61 shows large variability in accretion/erosion trends predicted by the sediment transport model for Grid B2. Due to the influence of natural tidal inlets within Grid B2, regional shoreline change likely is dominated by inlet hydrodynamics and barrier beach overwash processes, rather than wave-induced currents. For example, ebb shoal sediments may influence the extension of the spit along the south side of Brigantine Inlet; therefore, wave-induced sediment transport modeling would not predict the substantial accretion observed in this area. Instead, sediment transport modeling results indicate a net southerly drift of approximately 100,000 m^3/year over the modeled shoreline segment of Brigantine Island (a similar quantity was computed by the USACE [1996]). Although the modeled change in sediment transport potential is highly variable in this region, no clear indication of long-term erosion or accretion could be discerned. Because much of the regional sediment transport is influenced by tidal inlets, it is likely that the observed erosion along Brigantine Island may be a result of a net sediment deficit (i.e., sediment is not available to downdrift beaches), rather than an increase of south-directed sediment transport potential.

Grid B1 represents the only stretch of shoreline modeled for the New Jersey study that does not have a tidal inlet; therefore, one of the major complications limiting the sediment transport modeling/observed shoreline change comparison is eliminated. Despite this simplification, Figure 5-62 exhibits large variability in accretion/erosion trends predicted by the sediment transport model. It is difficult to determine obvious trends for the normalized transport change due to this high variability. In contrast, observed shoreline change data show relatively consistent accretion at both the north and south ends of Grid B1, as well as erosion along an approximate 7,000 m shoreline stretch in the middle of the grid. A more appropriate comparison is the general trend between net longshore sediment transport and observed shoreline change. Between UTM Northing coordinate 4,392,500 m and UTM Northing coordinate 4,398,000 m, increased net sediment transport potential (in excess of 50,000 m^3/year toward the south)

corresponds to a region of shoreline retreat. South of UTM Northing coordinate 4,392,000 m, the reduced south-directed transport potential corresponds to observed accretion.

Figure 5-62 illustrates large variability in accretion/erosion trends predicted by the sediment transport model for the -22.5° wave condition and observed shoreline change data. Neither analysis technique indicates a clear trend of erosion or accretion.

Although many of the observed and predicted accretion/erosion trends were predicted well, several shoreline reaches indicated opposite trends, where the observed and computed accretion/erosion contradicted each other. Direct comparison of measured shoreline change and computed sediment transport have several sources of potential error and variability. First, the modeled change in longshore transport represents sediment moving throughout the surf zone and shoreline change merely indicates migration of a single line. Observations of bathymetric change throughout the nearshore would indicate sediment transport trends associated with the shoreline and offshore shoals, which is especially important in the vicinity of tidal inlets. Therefore, shoreline change alone may not be the best indicator of coastal change.

Sediment transport modeling also assumes an infinite sediment source. If erosion potential is high along a certain stretch of shoreline, the model assumes that this volume is available for transport. However, natural beaches typically are in a state of constant adjustment toward equilibrium based on current environmental conditions (waves, tides, winds, etc.). Therefore, the shoreline may not be able to provide the sand volume required by wave conditions, a sediment deficit is created downdrift, and the beach does not behave exactly as the model predicts. Typically, sediment transport models are appropriate for use on sandy coasts because they can accurately predict long-term trends in these areas.

Engineering improvements to the shoreline also are not considered in the analysis of sediment transport potential. Regions that are influenced by coastal structures (e.g. jetties and groins) are not accounted for in the computation of transport rates. In addition, beach nourishment programs that have been placed along the New Jersey coast are not removed from the long-term shoreline change analysis.

Although similar potential errors exist for comparing observed shoreline change with computed accretion/erosion tendency, the trends predicted by the sediment transport modeling compare relatively well with measured long-term shoreline change. In general, the largest discrepancies between predicted and observed shoreline change were associated with regions where tidal inlet processes influenced nearshore sediment transport processes. For regions not influenced by tidal inlets (the central portion of Grid A, Grid B1, and most of Grid C), sediment transport analyses predicted the observed shoreline change patterns relatively well.

6.0 BIOLOGICAL FIELD SURVEYS

6.1 BACKGROUND

Two biological field surveys provided environmental data in and around eight sand resource areas offshore New Jersey. The surveys were conducted in May and September 1998. Infaunal, epifaunal, demersal fish, and sediment grain size samples, sediment profile images, and water column data were collected. The following sections provide the methods, results, and discussion for the biological field surveys; information pertaining to the sediment profiling camera element is provided in Appendix D1.

6.2 METHODS

6.2.1 Survey Design

The primary objective of the New Jersey field surveys in May and September 1998 was to characterize benthic ecological conditions (i.e., infauna, epifauna, demersal fishes, and sediment grain size) in eight sand resource areas (Figure 6-1). Supporting data collected in the areas consisted of water column profiles. A secondary objective was to obtain descriptive data on infauna and sediment grain size at three adjacent stations (Figure 6-1).

For the original proposal in 1997, the NJGS identified six potential sand resource areas. The total numbers of samples by type that were originally proposed for the six sand resource areas during Surveys 1 and 2 were as follows:

Sample Type	Survey 1 (May 1998)	Survey 2 (Sep 1998)
Infauna		
Sediment Profiling Camera	90 stations (2 images/station)	30 stations (2 images/station)
Smith-McIntyre Grab	30 stations (1 grab/station)	60 stations (1 grab/station)
Sediment Grain Size		
Smith-McIntyre Grab	90 stations (1 grab/station)	60 stations (1 grab/station)
Epifauna		
Mongoose Trawl	6 transects	6 transects
Water Column		
Hydrolab Profile	6 stations	6 stations

After the original proposal in 1997, the NJGS changed the number of sand resource areas from six to eight. The change necessitated modifications to the original sampling plan in 1998.

The following sampling rationale pertains to Survey 1 in May 1998 and Survey 2 in September 1998. The sampling plan for Surveys 1 and 2 is summarized in Table 6-1.

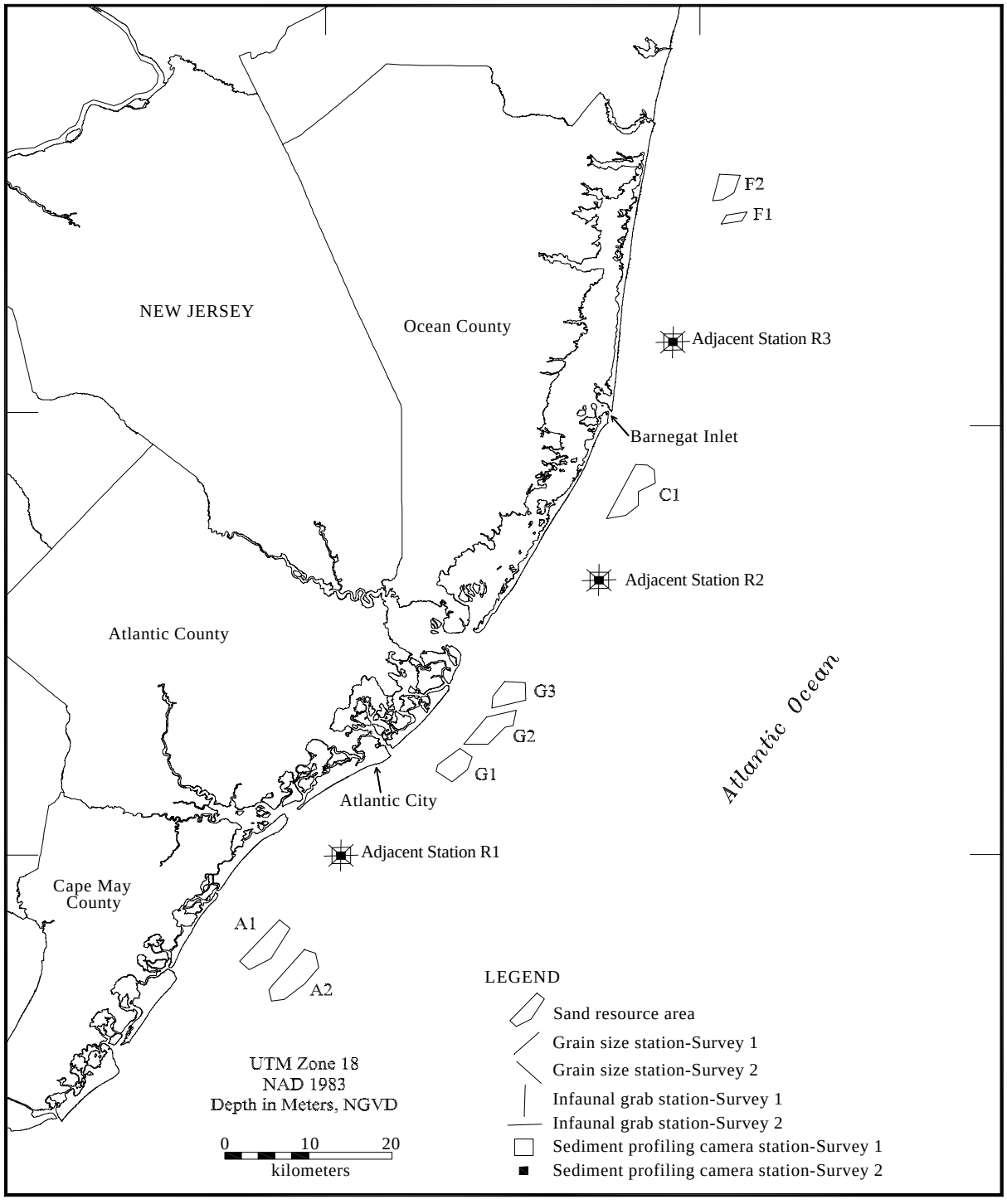

Figure 6-1. Adjacent stations relative to the eight sand resource areas and the New Jersey coast.

Table 6-1. Sampling for the New Jersey May 1998 Survey 1 and September 1998 Survey 2. Where number of samples planned differ from number of samples collected, number of samples collected are given in parentheses.

Area	Surface Area (million sq ft) and Percent of Total	Water Depth (m)	Number of Stations									
			Sediment Profiling Camera		Smith-McIntyre Grab				Epifaunal Trawls		Hydrolab	
					Infauna		Grain Size					
			Survey 1	Survey 2	Survey 1	Survey 2	Survey 1	Survey 2	Survey 1	Survey 2	Survey 1	Survey 2
A1	164 16%	8-20	13	4	4	9	13	9	1	1	1	1
A2	204 20%	8-21	19	4	4	8	19 (18)	8	1	1	1	1
C1	190 18%	12-21	16	5	5	11	16	11	1	1	1	1
F1	29 3%	16-22	4 (2)	2	2	3	4	3	0	0	0	0
F2	79 8%	15-22	6 (2)	2	2	5	6	5	1	1 (2)	1	1 (2)
G1	113 11%	8-20	8	3	3	6	8	6	1 (0)	1	1 (0)	1
G2	142 14%	9-19	12	4	4	8	12	8	0 (1)	0 (1)	0 (1)	0 (1)
G3	107 10%	9-20	9	3	3	7	9	7	1	1	1	1
R1	--	--	1	1	1	1	1	1	0	0	0	0
R2	--	--	1	1	1	1	1	1	0	0	0	0
R3	--	--	1	1	1	1	1	1	0	0	0	0
Total Number of Stations			90 (84)	30	30	60	90 (89)	60	6	6 (8)	6	6 (8)

Table 6-1 lists surface area information, water depth ranges, and number of stations by sample type for each of the eight sand resource areas and three adjacent stations. Sampling locations are shown in Figures 6-2 to 6-9. Sample types, sample codes, coordinates, and water depths are tabulated in Appendix D2**.**

Infauna and Sediment Grain Size

Survey 1 (May 1998)

To determine the number of infaunal and sediment grain size samples to collect at each of the eight sand resource areas during the May 1998 Survey 1, surface area and percent of total surface area for each area were calculated (Table 6-1). The percent of the total surface area for each of the sand resource areas then was multiplied by the total number of stations originally proposed for the project minus three for the adjacent stations, resulting in the number of samples per area.

The next step was to determine the placement of the infaunal (sediment profiling camera and Smith-McIntyre grab) and sediment grain size stations within each area to characterize existing assemblages. The goal in placement of the sediment profiling camera and sediment grain size stations was to provide broad spatial and depth coverage within the sand resource areas and, at the same time, ensure that the samples would be independent of one another to satisfy statistical assumptions. To accomplish this goal, a systematic sampling approach was used to provide broad spatial and depth coverage of the target populations. This approach can, in many cases, yield more accurate estimates of the mean than simple random sampling (Gilbert, 1987). Grids were placed over figures of each sand resource area. The number of grid cells was determined by the number of samples per area. One sampling station then was randomly placed within each grid cell of each sand resource area. Randomizing within grid cells eliminates biases that could be introduced by unknown spatial periodicities in the sampling area.

This systematic sampling approach resulted in designation of 90 locations for the sediment profiling camera and sediment grain size stations. These 90 stations were used for both the sediment profiling camera and sediment grain size sampling to maximize comparisons of grain size data from the two types of sampling equipment. All station locations then were pre-plotted on geodetically corrected maps.

Attention then was directed to selection of areas to be sampled for infauna with a Smith-McIntyre grab. Whereas 90 stations were proposed for sediment profiling camera and sediment grain size sampling, 30 stations were proposed for infaunal sampling using a Smith-McIntyre grab. Because the purpose of the grab samples was to maximize interpretation of the sediment profiling camera and sediment grain size data, it was desirable to collect the grab samples at the sediment profiling camera stations. Maps of the 90 sediment profiling camera and sediment grain size stations were analyzed and 30 stations were selected. Due to the limited number of grabs per area, grab stations were manually selected to maximize spatial, depth, and habitat considerations.

Some samples that were planned for Survey 1 were not collected due to bad weather. Sediment profiling camera images were not collected at Stations 3 and 4 in Area F1 and Stations 1 through 4 in Area F2. In addition, a grain size sample was not taken at Station 15 in Area A2.

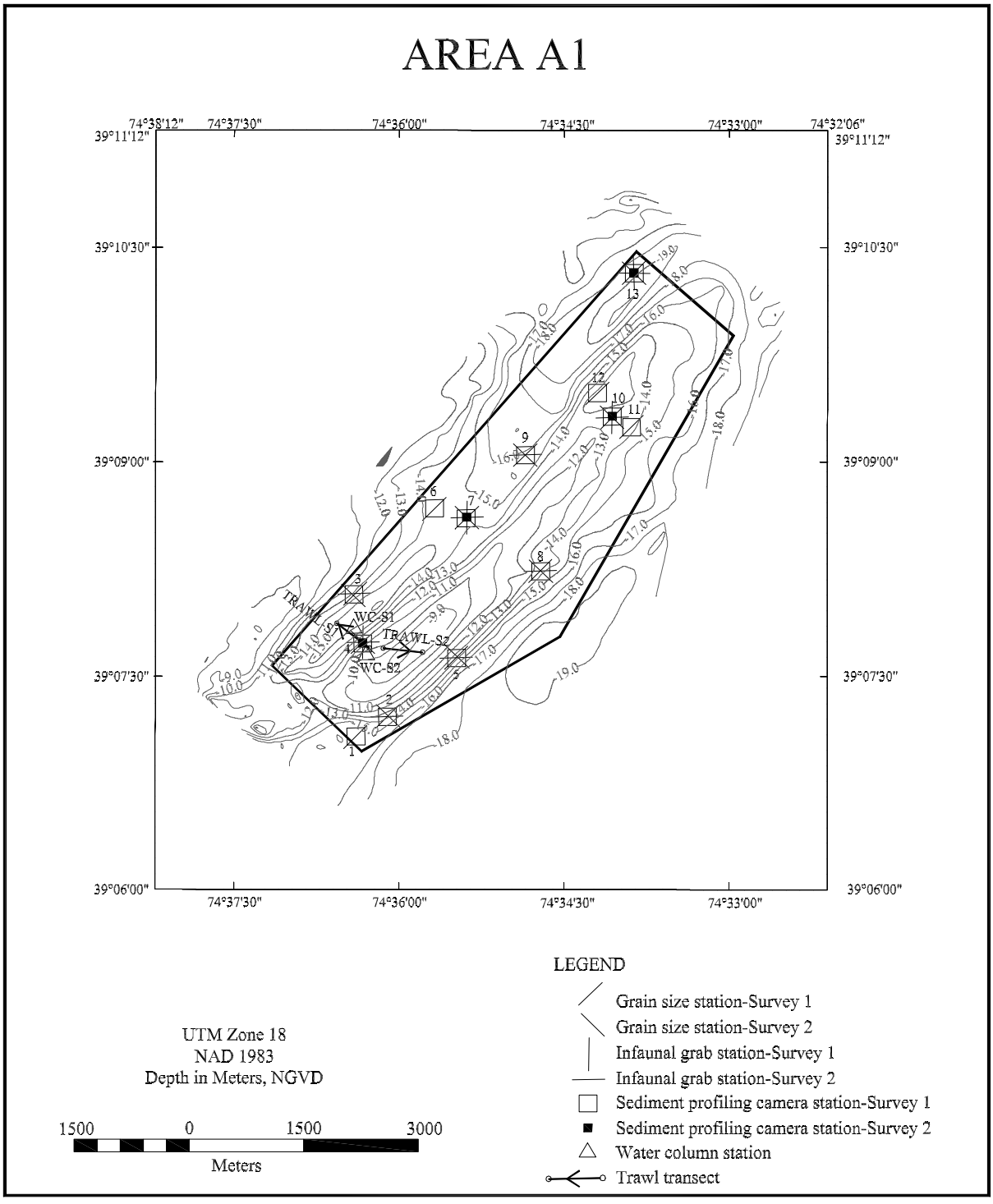

Figure 6-2. Sampling locations for New Jersey Sand Resource Area A1.

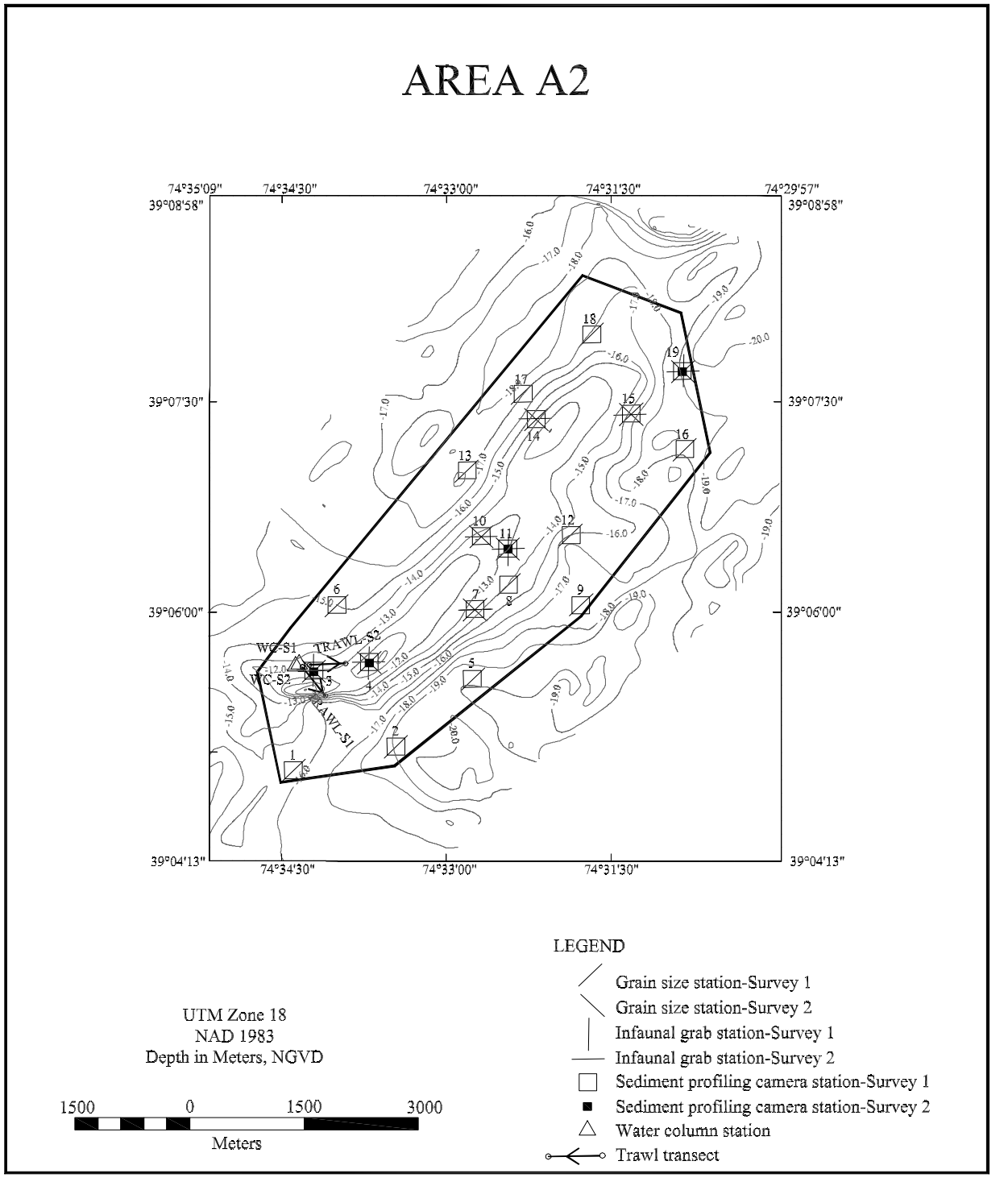

Figure 6-3. Sampling locations for New Jersey Sand Resource Area A2.

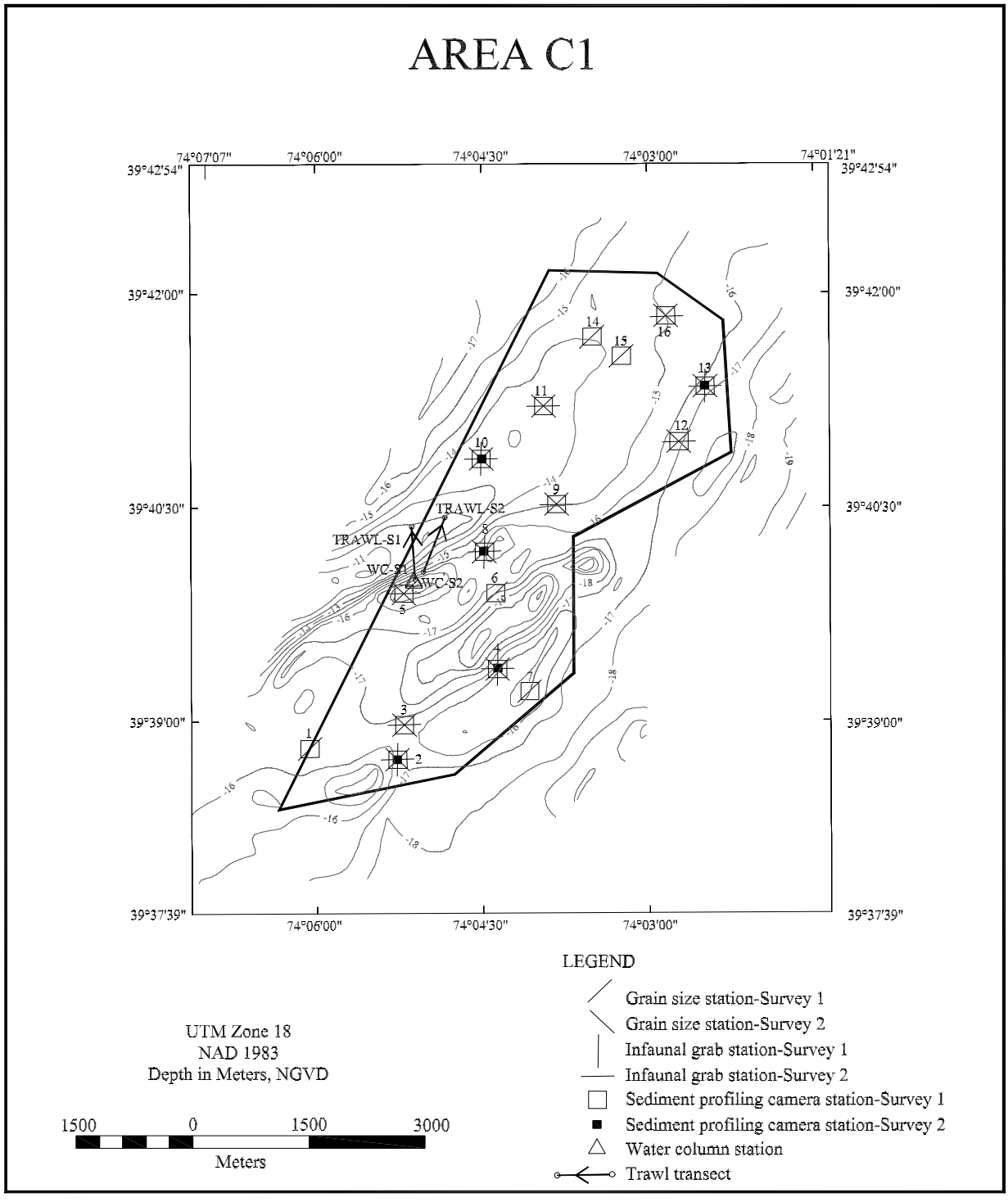

Figure 6-4. Sampling locations for New Jersey Sand Resource Area C1.

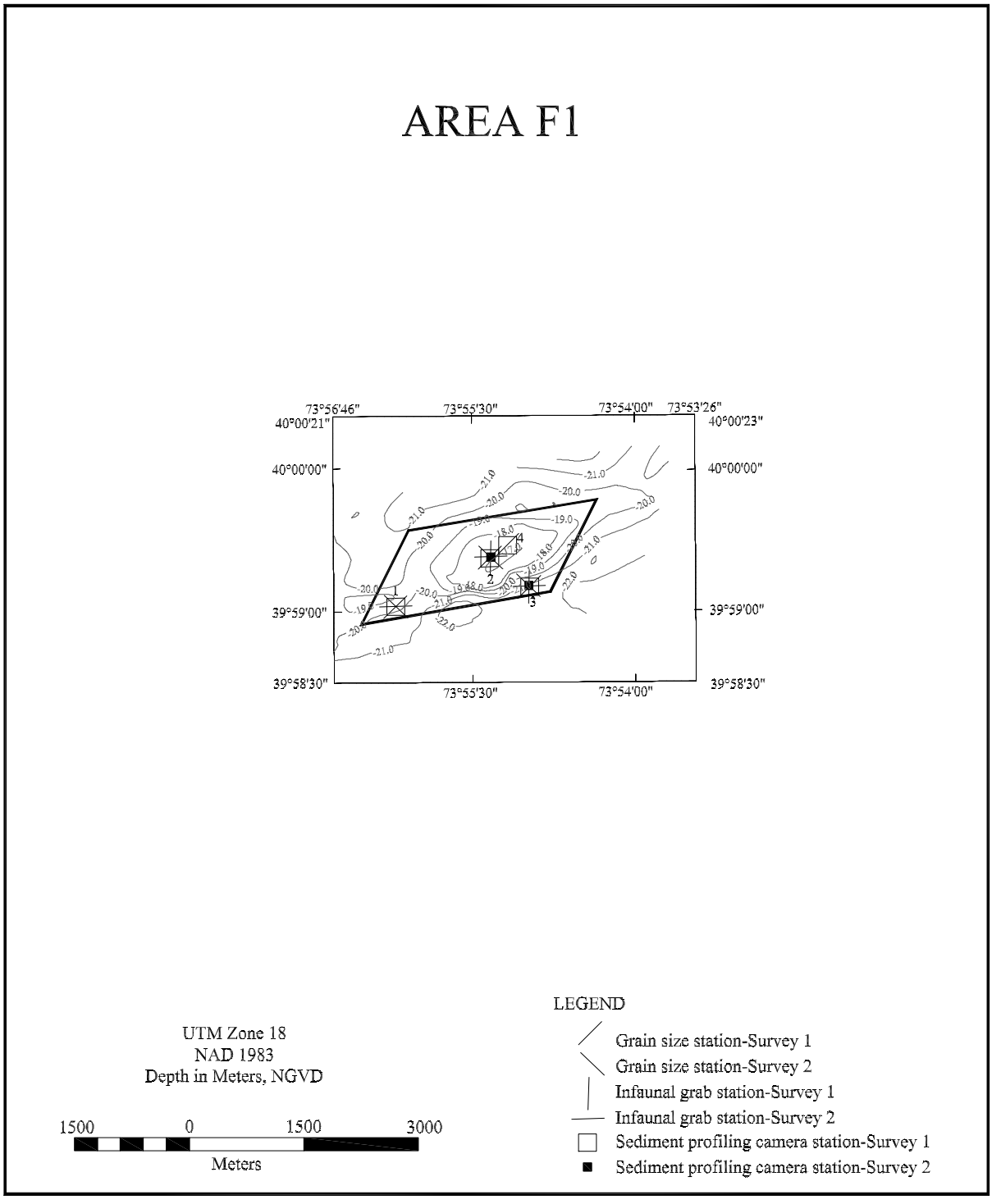

Figure 6-5. Sampling locations for New Jersey Sand Resource Area F1.

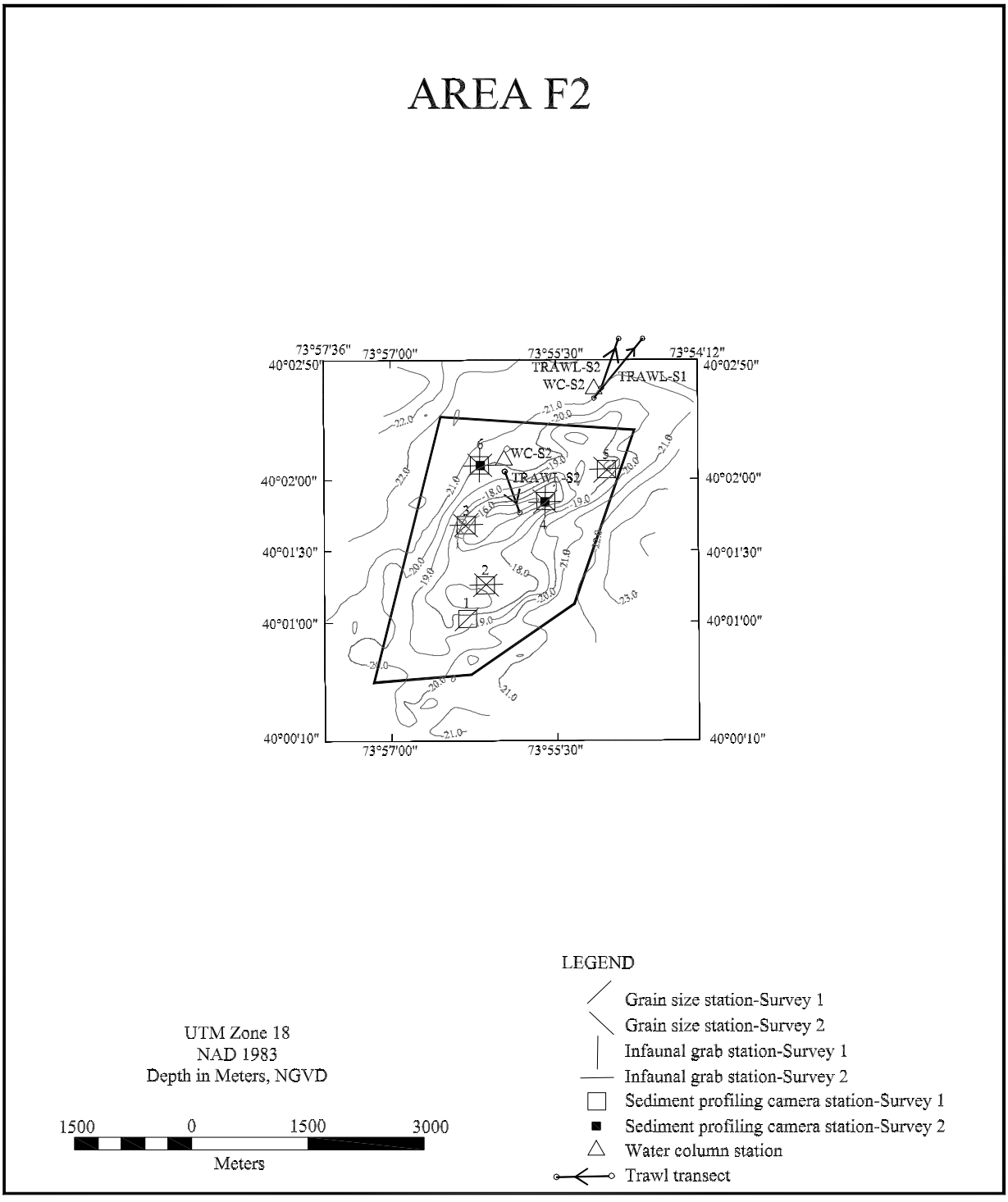

Figure 6-6. Sampling locations for New Jersey Sand Resource Area F2.

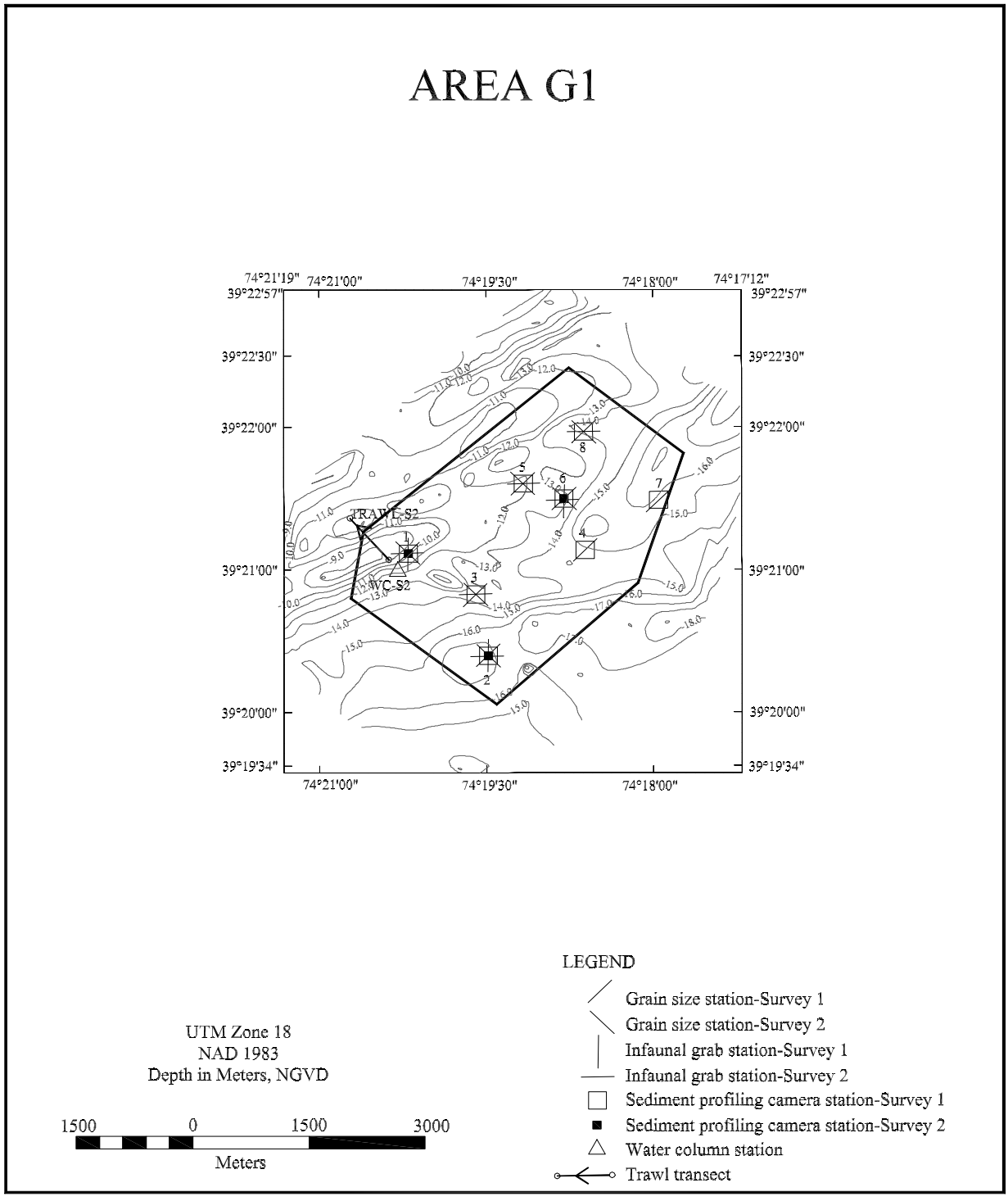

Figure 6-7. Sampling locations for New Jersey Sand Resource Area G1.

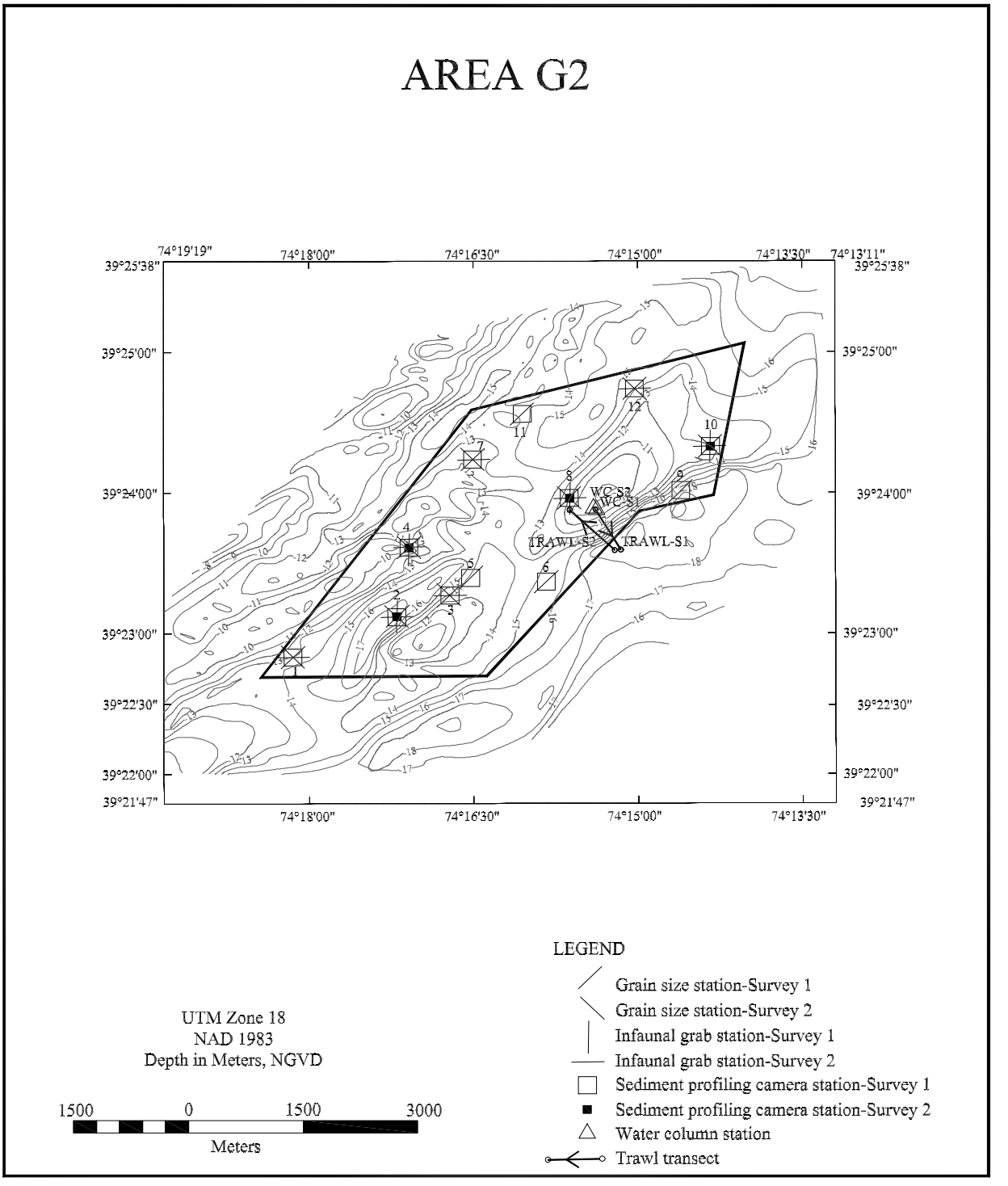

Figure 6-8. Sampling locations for New Jersey Sand Resource Area G2.

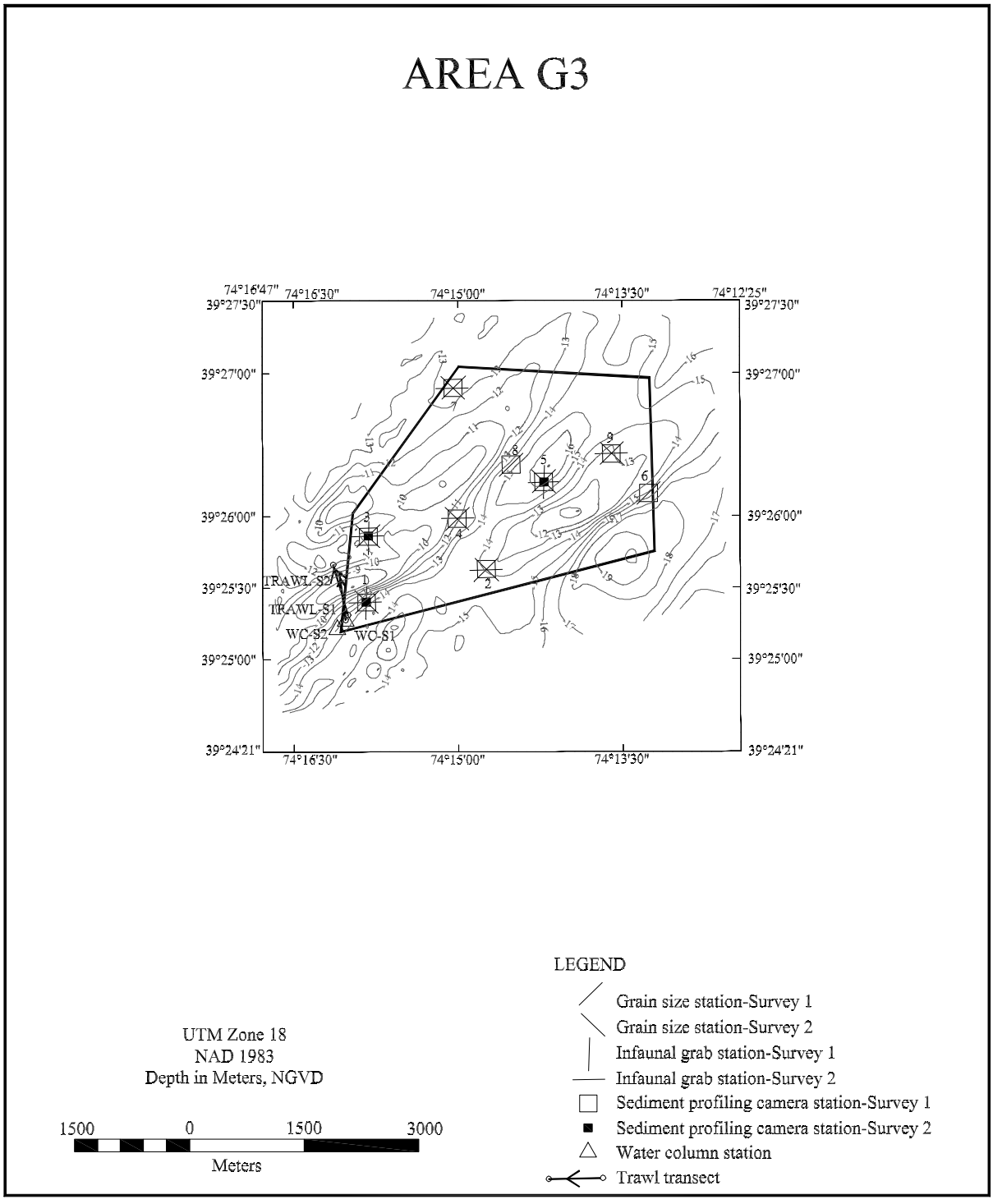

Figure 6-9. Sampling locations for New Jersey Sand Resource Area G3.

Survey 2 (September 1998)

Placement of infaunal and sediment grain size stations for the September 1998 Survey 2 was determined based on post-plots and results of the analyses of samples collected from infaunal and sediment grain size stations during the May 1998 Survey 1. The Survey 2 rationale was to sample previously sampled stations for temporal comparisons and further investigate areas of heterogeneity.

The 30 sediment profiling camera stations for Survey 2 occupied the same locations as the 30 Smith-McIntyre infaunal stations for Survey 1 because these stations were originally selected to maximize spatial, depth, and habitat considerations. This also would enable comparisons of temporal effects because the sediment profiling camera also was used at these 30 stations during Survey 1.

During Survey 2, 60 Smith-McIntyre infaunal stations and 60 Smith-McIntyre sediment grain size stations were sampled. The locations of the 60 Smith-McIntyre infaunal stations and 60 Smith-McIntyre sediment grain size stations were identical to each other so that resulting grain size data could be used to interpret the infaunal data. The first 30 of these 60 stations were in the same locations as the 30 sediment profiling camera stations for Survey 2 and the 30 Smith-McIntyre infaunal stations during Survey 1 which 1) enabled comparison of grain size data from the Smith-McIntyre and sediment profiling camera equipment during Survey 2; 2) maximized interpretation of the sediment profiling camera infaunal images based on Smith-McIntyre infaunal identifications from Survey 2; and 3) allowed comparisons of temporal effects by comparing the Smith-McIntyre data from Surveys 1 and 2.

Based on the results of the Survey 1 sample analyses, there was an interest in furthering the investigation of the abundance and distribution of juvenile Atlantic surfclams and infauna during Survey 2. The remaining 30 of the 60 Smith-McIntyre stations for Survey 2 were located at some stations where Smith-McIntyre sampling for infauna did not occur during Survey 1 to broaden the geographic coverage for juvenile Atlantic surfclams and infauna within the sand resource areas. These other 30 stations where Smith-McIntyre samples were taken for infauna and grain size during Survey 2 were as follows:

Area	Stations
A1	2, 3, 5, 8, 9
A2	7, 10, 14, 15
C1	3, 5, 9, 11, 12, 16
F1	1
F2	2, 3, 5
G1	3, 5, 8
G2	1, 3, 7, 12
G3	2, 4, 7, 9

Epifauna and Demersal Fishes

The original proposal for sampling epifauna and demersal fishes was to tow a trawl along one transect in each sand resource area. The original proposal included six areas and six trawl transects. During the sampling design stage for Survey 1, the six trawl transects were assigned to the eight new areas such that a trawl transect was to be made in all of the potential sand resource areas except Areas F1 and G2. Area F1 was eliminated during the original sampling design stage because it was the smallest of the eight areas and was adjacent to Area F2, which has a similar depth range. Area G2 was eliminated during the sampling design stage because it was located between and had approximately the same depth range as Areas G1 and G3.

Trawls were towed to cover as wide a depth range within a potential sand resource area as possible within the limits of the length of a trawl tow. During Survey 1, Area G2 was trawled inadvertently rather than Area G1 and the trawl for Area F2 was taken outside of the boundary for Area F2. The trawl for Area F2 was designated F2-Out. During Survey 2, trawls were made in Areas G1 and G2, and inside and outside the boundary of Area F2 (designated F2-In and F2-Out, respectively). Trawls also were made inside the boundaries of Areas A1, A2, C1, and G3, as was done during Survey 1. Trawl transects for Survey 2 were made along lines that were close to those used during Survey 1.

Water Column

For Surveys 1 and 2, a water column profile was made at the beginning point of each trawl transect prior to actual trawling. Parameters measured were temperature, salinity, dissolved oxygen, and depth. A water column profile was taken in all of the potential sand resource areas except Area F1 for reasons explained in the previous epifauna and demersal fishes section.

6.2.2 Field Methods

6.2.2.1 Vessel

The May field survey was conducted aboard the R/V LIONEL WALFORD based in Sandy Hook, New Jersey. Field sampling occurred from 3 to 8 May 1998. The September field survey was conducted aboard the R/V WEATHERBIRD based in Beaufort, North Carolina. This survey took place from 18 to 21 September 1998.

6.2.2.2 Navigation

A differential global positioning system (DGPS) was used to navigate the survey vessels to all sampling stations. The DGPS was connected to an on-board computer equipped with Hypack Navigation Software Version 6.4 (Coastal Oceanographics, 1996). With this system, the ship's position was displayed in real-time on a monitor affixed to a counter top in the wheel house. All sampling stations were pre-plotted and stored in the Hypack program. While in the field, the actual positions of all samples collected were recorded and stored by the program.

6.2.2.3 Water Column

Temperature, salinity, dissolved oxygen, and depth were measured with a portable Hydrolab unit. The Hydrolab was calibrated as needed each working day. Hydrolab measurements of temperature (ºC), salinity (ppt), and dissolved oxygen (mg/L) were taken at 1.5-m intervals from the surface to bottom. The Hydrolab was fastened to a weighted line then lowered to depth by hand. All measurements were recorded on standard data sheets.

6.2.2.4 Sediment Grain Size

One grab sample was taken with a Smith-McIntyre grab at each pre-plotted sediment sampling station. Once a sample was deemed acceptable (i.e., adequate penetration and undisturbed surface layer), a subsample of sediment (about 250 g) was removed with a 5-cm diameter acrylic core tube and placed in a labeled plastic bag for grain size analyses. This sample was stored at 4ºC (i.e., on ice).

6.2.2.5 Infauna

The same Smith-McIntyre grab samples collected at each pre-plotted sediment sampling station (see Section 6.2.2.4) were used for infauna. After a subsample of sediment was removed for grain size analyses, the remainder of the grab sample was sieved through 0.5-mm sieve for infaunal analyses. The infaunal sample was placed in a container and preserved in 10% formalin with rose bengal stain.

6.2.2.6 Epifauna and Demersal Fishes

A 25-ft mongoose trawl was towed for 10 min (bottom time) along the pre-plotted transects. The path of each trawl tow was logged into the Hypack navigation system. Once the trawl was on deck, the contents of the catch bag were sorted then identified to the lowest practical taxon. All organisms were identified and returned to the sea. Identifications were recorded on standard trawl data sheets.

6.2.3 Laboratory Methods

6.2.3.1 Sediment Grain Size

Sediment grain size analyses were conducted using combined sieve and hydrometer analyses according to recommended American Society for Testing Materials (ASTM) procedures. Grain-size samples were washed in demineralized water, dried, and weighed. Coarse and fine fractions (sand/silt) were separated by sieving through a U.S. Standard Sieve Mesh No. 230 (62.5 μm). Sediment texture of the coarse fraction was determined at half-phi intervals by passing the sediment through nested sieves. The weight of the materials collected in each particle size class was recorded. Boyocouse hydrometer analyses were used to analyze the fine fraction (<62.5 μm).

6.2.3.2 Infauna

Formalin-preserved infaunal samples were rinsed on a U.S. Standard No. 30 (0.59-mm) sieve and transferred to 70% isopropanol. Before sorting, samples were passed through a series of sieves (0.3, 0.5, 0.6, 1, and 2 mm) to separate the organisms into size classes. Samples were sorted by hand under dissecting microscopes. All sediment in each sample was examined by a technician who removed all infauna observed. Organisms were identified to the lowest practical taxon and counted. A minimum of 10% of all samples were resorted by different technicians as a quality control measure. Voucher specimens of each taxon were archived at the Barry A. Vittor & Associates, Inc. laboratory.

6.2.4 Data Analysis

6.2.4.1 Water Column

Temperature, salinity, dissolved oxygen, and depth values were entered into an electronic spreadsheet and tabulated. Depth profiles were plotted for temperature-salinity and temperature-dissolved oxygen.

6.2.4.2 Sediment Grain Size

A computer algorithm was used to determine size distribution and provide interpolated size information for the fine fraction at 0.25-phi intervals. Percentages of gravel, sand, silt, and clay were calculated and recorded along with a Folk's description for each sample.

6.2.4.3 Infauna

Summary statistics including number of taxa, number of individuals, density, diversity (*H'*), evenness (*J'*), and species richness (*D*) were calculated for each sampling station. Diversity (*H'*), also known as Shannon's Index (Pielou, 1966), was calculated as follows:

$$H' = -\sum_{S}^{i=1} p_i \ln(p_i)$$

where *S* is the number of taxa in the sample, *i* is the *i*th taxa in the sample, and p_i is the number of individuals of the *i*th taxa divided by (N) the total number of individuals in the sample.

Evenness (*J'*) was calculated with Pielou's (1966) index of evenness:

$$J' = \frac{Ç'}{\ln(S)}$$

where *H'* is Shannon's index as calculated above and *S* is the total number of taxa in a sample.

Species richness (D) was calculated by Margalef's index:

$$D = \frac{(S - 1)}{\ln(N)}$$

where *S* is the total number of taxa in the sample, and N is the number of individuals in the sample.

Spatial and temporal patterns in infaunal assemblages were examined with cluster analysis. Cluster analyses were performed on similarity matrices constructed from raw data matrices consisting of taxa and samples (station – survey). Only species-level taxa, with the exception of two species complexes that can be only reliably identified to genus, were included in the analysis. Of these taxa, only those contributing at least 0.1% of the total abundance of species level taxa were included. Raw counts of infaunal taxa were transformed with the $\log_{10}(n+1)$ transformation prior to similarity analysis. Both normal (stations) and inverse (taxa) similarity matrices were generated using the Bray-Curtis index that was calculated using the following formula:

$$B_{jk} = \frac{2\sum_{i} \min(x_{ij}, x_{ik})}{\sum_{i} (x_{ij} + x_{ik})}$$

where B_{jk} (for normal analysis) is the similarity between samples *j* and *k*; x_{ij} and x_{ik} are the abundances of species *i* in samples *j* and *k*. *B* ranges from 0.0 when two samples have no species in common to 1.0 when the distribution of individuals among species is identical between samples. For inverse analysis, the B_{jk} is the similarity between species *j* and *k*; x_{ij} and x_{ik} are the abundances of species *j* and *k* in sample *i*.

Normal similarity matrices were clustered using the group averaging method of clustering, and inverse similarity matrices were clustered using the flexible sorting method of clustering (Boesch, 1973). Flexible sorting was performed with $\beta = -0.25$, a widely accepted value for this analysis (Boesch, 1973).

The extent to which sample groups formed by normal cluster analysis of the entire data set could be explained by environmental variables such as sediment grain size parameters was examined by canonical discriminant analysis (SAS Institute Inc., 1989). Canonical discriminant analysis identifies the degree of separation among predefined groups of variables in multivariate

space. This analysis examined the relationships among the environmental variables and the station groups as indicated by the normal cluster analysis.

6.2.4.4 Epifauna and Demersal Fishes

Data on epifauna and demersal fishes were summarized by numbers of taxa and number of individuals per tow in each sand resource area. Normal and inverse cluster analyses as described previously (Section 6.2.4.3) were used to examine patterns in the epifaunal/demersal fish data set. Both normal and inverse clustering were performed with the group averaging algorithm.

6.3 RESULTS

6.3.1 Water Column

Raw data for water column profiles made during Survey 1 are provided in Appendix D3, Table D3-1**.** Depth profiles of temperature-salinity and temperature-dissolved oxygen for the May 1998 Survey 1 are shown in Figures 6-10 and 6-11. Temperature profiles varied little from surface to bottom in Resource Areas A1, C1, and G3. For Areas F2 and G2, the profiles showed a slight discontinuity at about 5 m below the surface. Surface temperatures ranged from 11.9°C at Area F2 to 12.9°C in Areas A1 and G3. Bottom temperatures ranged from 8.2°C at Area F2 to 11.2°C in Area A1. Salinity profiles were fairly uniform from surface to bottom in Areas A1, A2, C1, and G3. For Areas F2 and G2, the profiles shifted to higher values at about 10 m water depths. Surface salinity values ranged from 26.0 ppt in Area C1 to 31.5 ppt in Areas A1 and A2. Bottom salinity values ranged from 28.5 ppt in Area C1 to 33.8 ppt at Area F2. Figure 6-11 gives the dissolved oxygen profiles recorded during the May 1998 Survey 1. With the exception of Area F2, these profiles did not vary appreciably from surface to bottom. Surface dissolved oxygen values ranged from 6.98 mg/L in Area G3 to 8.70 mg/L at Area F2. Bottom measurements ranged from 6.41 mg/L in Area G2 to 9.60 mg/L at Area F2.

Raw data for water column profiles made during Survey 2 are given in Appendix D3**,** Table D3-2. Temperature, salinity, and dissolved oxygen profiles made during the September 1998 Survey 2 are shown in Figures 6-12 and 6-13. Temperature profiles changed little or just slightly from surface to bottom in Resource Areas A1, A2, G1, G2, and G3. Temperature profiles for Area F2 exhibited a definite discontinuity at about 15 m below the surface. Surface temperatures during Survey 2 ranged from 22.4°C in Area A2 to 23.6°C in Area G2. Bottom temperatures ranged from 12.5°C for Area F2 (F2-Out) to 22.2°C in Area G1. Salinity profiles were uniform from surface to bottom in all resource areas during the September 1998 Survey 2. Surface salinity values ranged from 27.5 ppt in Areas G1, G2, and G3 to 33.1 ppt in Area A1. Bottom salinity values ranged from 27.6 ppt in Areas G1 and G2 to 33.4 in Area A2. Dissolved oxygen profiles were uniform from surface to bottom in Areas A2, G1, and G2, whereas dissolved oxygen profiles from Areas A1, C1, F2, and G3 decreased with depth (Figure 6-13). Surface dissolved oxygen values ranged from 6.96 mg/L in Area F2 (F2-Out) to 8.03 mg/L in Area G1. Bottom dissolved oxygen values ranged from 2.94 mg/L in Area G3 to 6.48 mg/L in Area G2. Hypoxic conditions were not found during either Surveys 1 or 2.

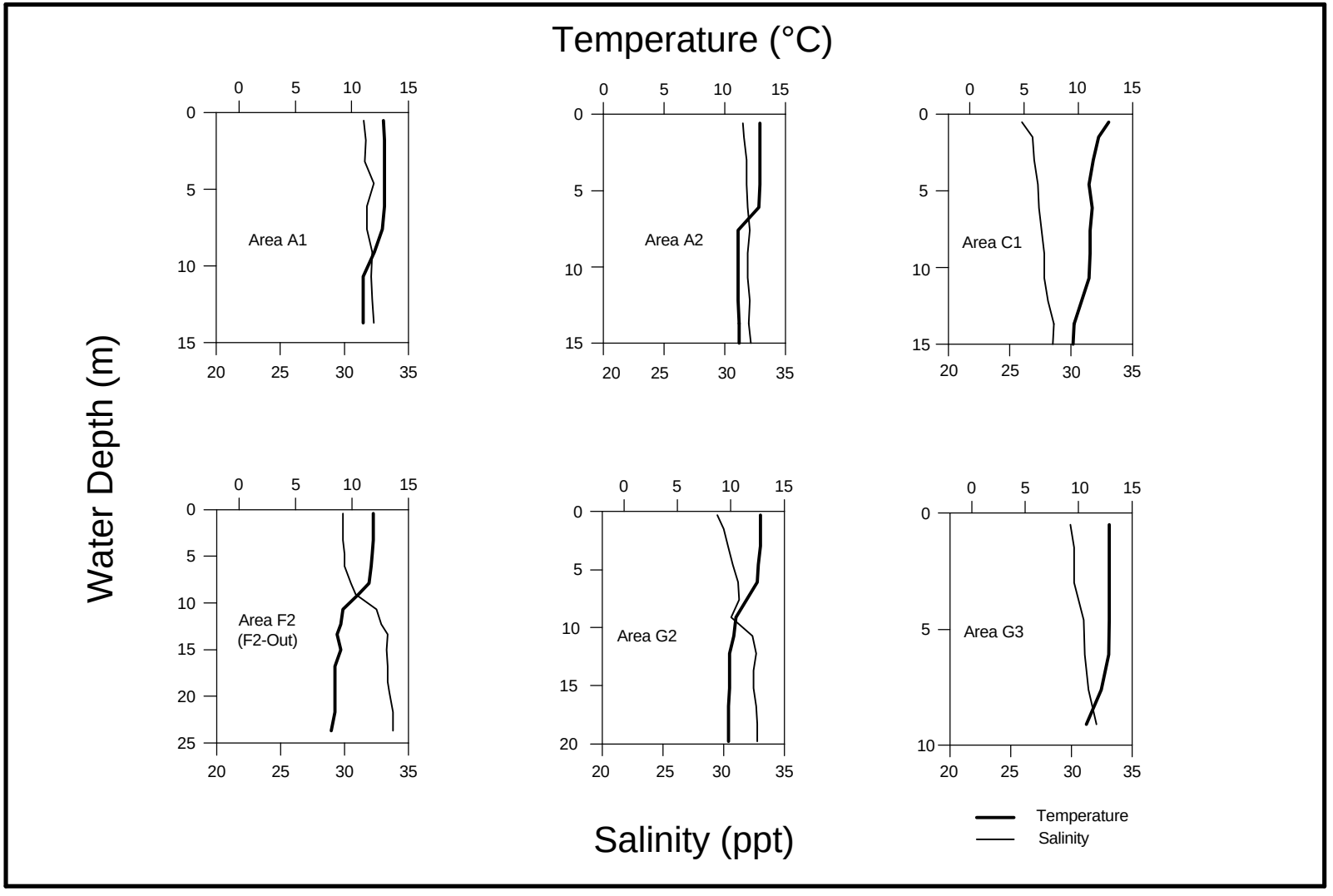

Figure 6-10. Temperature and salinity water column profiles from Resource Areas A1, A2, C1, F2, G2, and G3 during the May 1998 Survey 1 offshore New Jersey.

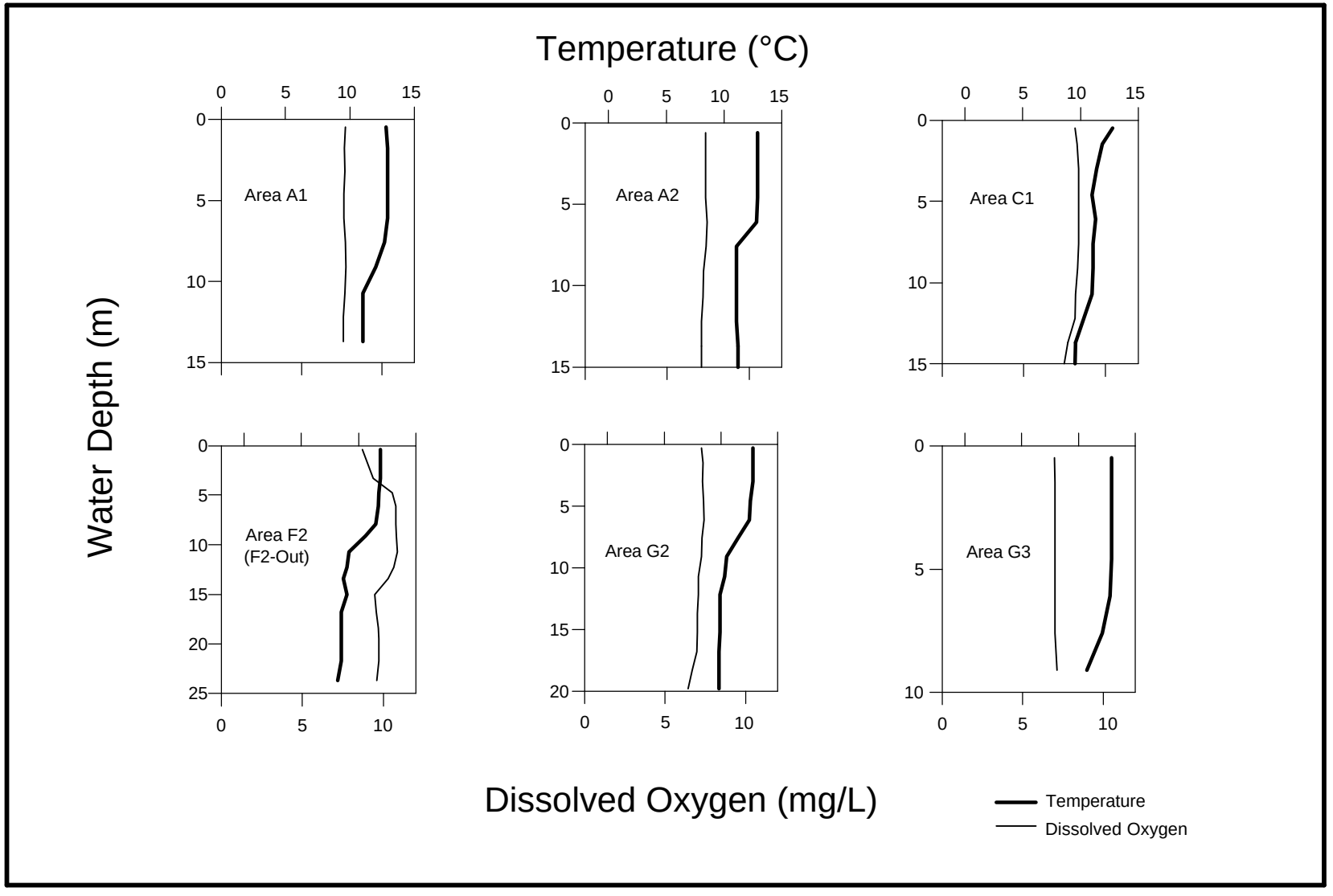

Figure 6-11. Temperature and dissolved oxygen water column profiles from Resource Areas A1, A2, C1, F2, G2, and G3 during the May 1998 Survey 1 offshore New Jersey.

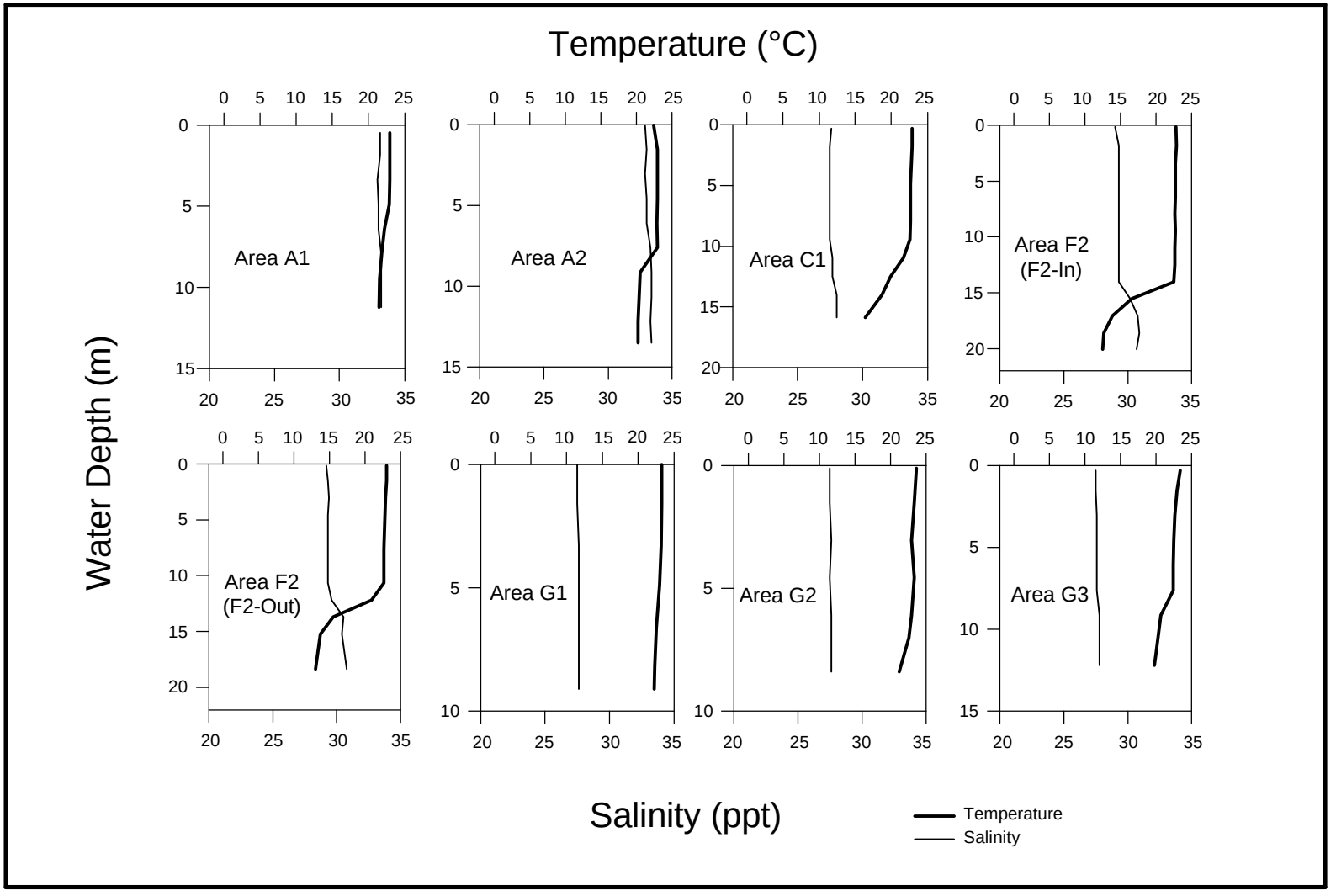

Figure 6-12. Temperature and salinity water column profiles from Resource Areas A1, A2, C1, F2, G1, G2 and G3 during the September 1998 Survey 2 offshore New Jersey.

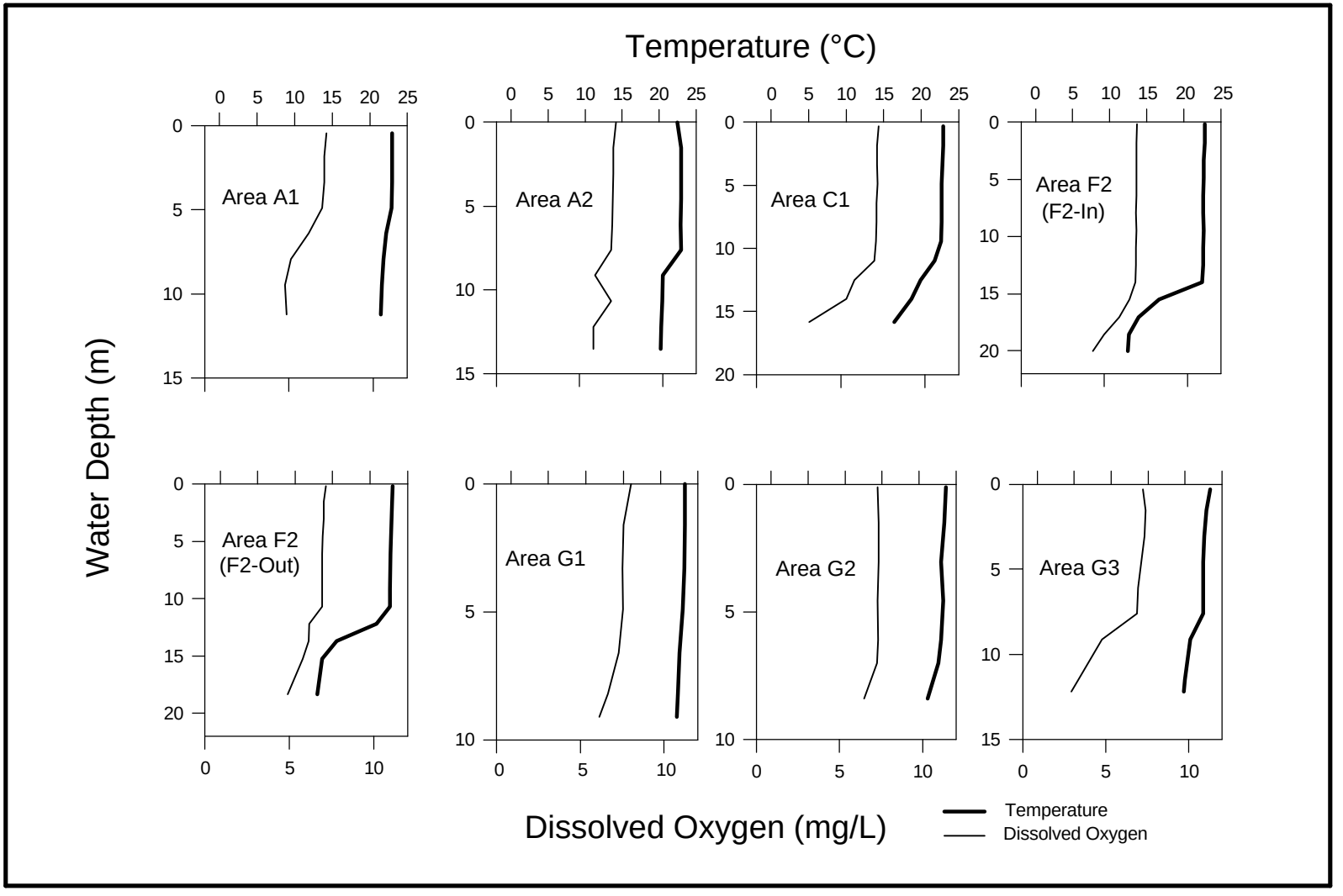

Figure 6-13. Temperature and dissolved oxygen water column profiles from Resource Areas A1, A2, C1, F2, G1, G2, and G3 during the September 1998 Survey 2 offshore New Jersey.

6.3.2 Sediment Grain Size

Sediment grain size composition of Smith-McIntyre grab samples taken in the resource areas during the May 1998 Survey 1 ranged from gravel to sandy mud (Appendix D4, Table D4-1). Proportions of gravel, sand, and fine sediment in the samples varied within and among resource areas. Samples with high sand fractions (>95%) were most common, followed by samples with high gravel fractions (>10%). In Area A1, 9 of 13 grab samples collected during Survey 1 contained >96% sand. The remaining samples were gravelly sand or sandy gravel. Area A2 yielded 8 of 19 samples with >95% sand. The remaining samples contained sandy gravel and gravelly sand. Eight of 16 samples from Area C1 contained >97% sand. The proportion of gravel in the remaining samples ranged from 0 to 81.3%. Area F1 produced two of four samples with >95% sand. The other two samples were distinguished by high gravel fractions with sand. In Area F2, two of six samples had >99% sand; the other four samples contained varying proportions of gravel with sand. In Areas G1, G2, and G3, the samples contained high sand fractions. In Area G1, 5 of 8 samples were >96% sand. In Area G2, 11 of 12 samples were represented by >97% sand. In Area G3, 8 of 9 samples were >98% sand.

General patterns of grain size composition of the grab samples taken during the September 1998 Survey 2 were similar to the patterns seen during the May 1998 Survey 1 (Appendix D4, Table D4-2). Six of nine grab samples collected during the September 1998 Survey 2 from Resource Area A1 contained >98% sand. In Resource Area A2, three of eight samples contained >99% sand, five samples contained gravelly sand, and one sample was sandy gravel. In Resource Area C1, 7 of 11 samples contained >98% sand; the other four samples contained gravel fractions ranging from 19.6 to 79.5%. The three samples from Resource Area F1 were composed of varying fractions of sand and gravel; only one of the three samples exhibited >91% sand. Resource Area F2 yielded two of five samples with >99% sand; the other three samples consisted of gravelly sand and sandy gravel. In Resource Area G1, grab samples yielded mostly sand, with five of six samples containing >98% sand. Resource Area G2 had seven of eight samples with >96% sand. In Resource Area G3, all seven samples contained >98% sand.

6.3.3 Infauna

The phylogenetic list of infauna collected in bottom grabs during the May and September 1998 surveys is presented in Appendix D5 along with other infaunal data from the surveys. For both surveys combined, 57,098 individuals were collected, representing 202 taxa in 10 separate phyla. As a group, infauna were more abundant during the May survey when overall density averaged 772 individuals/grab as compared to 566 individuals/grab during the September survey. Eighty-seven taxa (43% of total) were common to both surveys. Of those taxa found in just one of the two surveys, 68% (78 taxa) were sampled during the September cruise. The archiannelid *Polygordius* (lowest practical identification level [LPIL]) was numerically dominant in the grabs, representing 18% of all infauna censused over both surveys. Other than *Polygordius*, taxa that were among the top 10 numerical dominants during both the May and September surveys included the bivalve *Nucula proxima*, oligochaetous annelids, and rhynchocoels.

Table 6-2 lists the numerically dominant taxa sampled from each of the resource areas and adjacent stations during the May survey. Numerically dominant taxa sampled during the May survey included *Spiophanes bombyx* (polychaete; 16.4% of all collected individuals), Ascidiacea (tunicate; 16.1%), *Polygordius* (archiannelid; 16.1%), *Mytilus edulis* (bivalve; 11.6%),

Table 6-2. Ten most abundant infaunal taxa from samples collected during the May 1998 Survey 1 in the eight resource areas (A1, A2, C1, F1, F2, G1, G2, and G3) and three adjacent stations (R1, R2, and R3) offshore New Jersey.

Area	Taxonomic Name	Count	Area	Taxonomic Name	Count
A1	*Mytilus edulis*	795	G2	*Spiophanes bombyx*	1,732
	Turbonilla interrupta	354		*Polygordius* (LPIL)	367
	Ampelisca macrocephala	288		*Mytilus edulis*	107
	Ascidiacea (LPIL)	247		Oligochaeta (LPIL)	77
	Pisione remota	182		Rhynchocoela (LPIL)	74
	Mercenaria mercenaria	166		*Nucula proxima*	74
	Ampelisca (LPIL)	140		*Tanaissus psammophilus*	63
	Spiophanes bombyx	127		*Spisula solidissima*	53
	Oligochaeta (LPIL)	115		Cirratulidae (LPIL)	49
	Polygordius (LPIL)	104		*Protohaustorius wigleyi*	44
A2	*Polygordius* (LPIL)	232	G3	*Spiophanes bombyx*	1,883
	Oligochaeta (LPIL)	109		*Caulleriella* sp.J	162
	Astarte castanea	59		*Polygordius* (LPIL)	93
	Tanaissus psammophilus	53		*Chiridotea tuftsi*	55
	Chiridotea tuftsi	48		*Spisula solidissima*	52
	Spio setosa	47		Oligochaeta (LPIL)	35
	Rhynchocoela (LPIL)	43		*Echinarachnius parma*	32
	Crenella decussata	25		*Unciola irrorata*	31
	Hesionura elongata	22		Rhynchocoela (LPIL)	22
	Ascidiacea (LPIL)	21		*Protohaustorius wigleyi*	19
C1	*Mytilus edulis*	1,122	R1	*Nucula proxima*	390
	Ascidiacea (LPIL)	480		*Spiophanes bombyx*	45
	Polygordius (LPIL)	438		*Ampelisca macrocephala*	36
	Oligochaeta (LPIL)	141		*Spisula solidissima*	33
	Tanaissus psammophilus	124		*Mytilus edulis*	32
	Rhynchocoela (LPIL)	122		*Ampelisca* (LPIL)	29
	Pisione remota	100		*Nephtys picta*	24
	Echinarachnius parma	97		*Tellina* (LPIL)	22
	Spisula solidissima	83		Cirratulidae (LPIL)	14
	Echinoidea (LPIL)	39		*Caulleriella* sp. J	13
F1	Oligochaeta (LPIL)	694	R2	Ascidiacea (LPIL)	2,816
	Polygordius (LPIL)	156		*Mytilus edulis*	562
	Lumbrinerides acuta	88		Rhynchocoela (LPIL)	248
	Tanaissus psammophilus	54		Oligochaeta (LPIL)	184
	Cirrophorus (LPIL)	27		*Spisula solidissima*	82
	Sigalionidae (LPIL)	26		*Pisione remota*	59
	Rhynchocoela (LPIL)	17		*Astarte castanea*	53
	Pisione remota	15		*Polygordius (LPIL)*	39
	Exogone hebes	15		*Crenella decussata*	30
	Echinoidea (LPIL)	14		Bivalvia (LPIL)	25
F2	Ascidiacea (LPIL)	157	R3	*Polygordius* (LPIL)	1,014
	Polygordius (LPIL)	120		Rhynchocoela (LPIL)	43
	Spisula solidissima	85		*Spisula solidissima*	42
	Rhynchocoela (LPIL)	65		Cirratulidae (LPIL)	19
	Pisione remota	47		*Echinarachnius parma*	18
	Oligochaeta (LPIL)	34		*Hemipodus roseus*	17
	Hemipodus roseus	32		Oligochaeta (LPIL)	16
	Astarte castanea	32		Ascidiacea (LPIL)	14
	Tanaissus psammophilus	26		*Tanaissus psammophilus*	9
	Exogone hebes	22		Sigalionidae (LPIL)	8
G1	*Polygordius* (LPIL)	1,166	MAY TOTAL	*Spiophanes bombyx*	3,806
	Nucula proxima	92		Ascidiacea (LPIL)	3,739
	Capitella capitata	91		*Polygordius* (LPIL)	3,732
	Oligochaeta (LPIL)	68		*Mytilus edulis*	2,696
	Mytilus edulis	51		Oligochaeta (LPIL)	1,475
	Capitellidae (LPIL)	44		Rhynchocoela (LPIL)	749
	Rhynchocoela (LPIL)	38		*Nucula proxima*	623
	Tellina (LPIL)	30		*Spisula solidissima*	507
	Ampharetidae (LPIL)	24		*Pisione remota*	418
	Caulleriella sp.J	10		*Turbonilla interrupta*	354

LPIL = Lowest practical identification level

.

and unidentified oligochaetous annelids (6.4%). Together, these taxa comprised 66% of infaunal individuals collected in May. During the May survey, Atlantic surfclam (*Spisula solidissima*) was among the top 10 numerically dominant taxa in several of the resource areas (C1, F2, G2, G3), each of the adjacent stations (R1, R2, and R3), and in the overall May total (Table 6-2). Juvenile *S. solidissima* represented 2.2% of all censused infauna during the May survey.

Numerically dominant taxa collected during the September survey (Table 6-3) were the archiannelid *Polygordius* (19.5% of all collected individuals), the polychaete *Asabellides oculata* (6.4%), unidentified rhynchocoels (5.9%), the tanaid *Tanaissus psammophilus* (5.9%), and the amphipod *Pseudunciola obliquua* (4.5%). Other than *Polygordius*, numerical dominance during September was more evenly distributed among infaunal taxa than was the case during the first survey, with the remaining numerically dominant taxa comprising between 6.4 and 3.9% of collected individuals from all areas combined. Atlantic surfclam was among the top 10 numerically dominant taxa collected in September grab samples only in Areas F1 and F2 (Table 6-3).

Table 6-4 summarizes the number of taxa, number of individuals, density, species diversity, evenness, and richness for each of the sand resource areas and adjacent stations during the May and September surveys. During the May survey, the mean number of taxa sampled per station was greatest in Area A1 (37 taxa), while Area G1 stations averaged the greatest number of taxa (43) in September (Table 6-4). The highest number of infaunal taxa collected from a single station was collected at Station 1 in Area A1 (67 individuals) during the May survey and at Station 2 in Area G1 (61) during the September survey. During the May survey, the mean number of taxa per station was lowest in Areas A2 and G1 (21 taxa), while Area F2 stations averaged the lowest number of taxa (26) in September (Table 6-4). The fewest number of infaunal taxa collected from a single station was collected at Station 4 in Area A2 (14) during May and at Station 13 in Area C1 (18) in September.

The greatest number of infauna collected in a single grab was at Adjacent Station 2 during the May survey (4,296 individuals), due mostly to a high density of the tunicate Ascidiacea (LPIL) (Table 6-2). Excluding adjacent stations, greatest infaunal abundances were sampled from Area A1 (station average = 898 individuals) during the May survey, while Area G2 yielded the greatest mean abundances (800) in September (Table 6-4). The greatest number of individuals collected from a single station was sampled from Station 3 in Area G3 (2,373 individuals) during the May survey and from Station 2 in Area G2 (3,613) in September. Area A2 yielded the lowest mean abundance during the May survey (217), while Area F2 yielded the lowest mean abundance in September (339) (Table 6-4). The fewest number of individuals sampled from a single station during the May survey was collected at Station 1 in Area G1 (41 individuals), while the September survey yielded its lowest count from Station 16 in Area C1 (42).

Mean values of species diversity (H') and species richness (D) were generally higher in September as compared to May, while species evenness (J') was similar during both surveys, although this index was less variable across the study area during September (Table 6-4). Stations in Area A1 yielded the highest mean values of species diversity (2.37) and richness (5.67) during May. During the May survey, the highest measure of mean species evenness was from Area A2 stations (0.73). The lowest mean values of species diversity and richness (1.64 and 3.71, respectively) during the May survey were from Area G1. Species evenness was lowest in Area F1 (0.51) during the May survey. Highest mean values of species diversity and evenness during September were from Area G2 stations (2.48 and 0.71, respectively), while the

Table 6-3. Ten most abundant infaunal taxa from samples collected during the September 1998 Survey 2 in the eight sand resource areas (A1, A2, C1, F1, F2, G1, G2, and G3) and three adjacent stations (R1, R2, and R3) offshore New Jersey.

Area	Taxonomic Name	Count	Area	Taxonomic Name	Count
A1	*Polygordius* (LPIL)	1,555	G2	*Asabellides oculata*	1,121
	Ampelisca sp.X	818		*Nucula proxima*	1,043
	Pseudunciola obliquua	563		Ampharetidae (LPIL)	1,009
	Oligochaeta (LPIL)	296		*Apoprionospio pygmaea*	526
	Rhepoxynius *hudsoni*	295		*Polygordius* (LPIL)	469
	Protohaustorius wigleyi	268		Oligochaeta (LPIL)	276
	Aricidea catherinae	194		Cirratulidae (LPIL)	225
	Ampelisca abdita	185		*Tanaissus psammophilus*	144
	Spiophanes bombyx	148		*Spiophanes bombyx*	125
	Donax variabilis	119		*Tellina agilis*	115
A2	*Polygordius* (LPIL)	543	G3	*Polygordius* (LPIL)	1,071
	Oligochaeta (LPIL)	393		*Asabellides oculata*	628
	Ampelisca abdita	286		Ampharetidae (LPIL)	416
	Donax variabilis	270		*Tanaissus psammophilus*	200
	Aricidea cerrutii	263		*Tellina agilis*	89
	Tanaissus psammophilus	215		*Pseudunciola obliquua*	87
	Rhepoxynius hudsoni	135		Oligochaeta (LPIL)	84
	Protodorvillea kefersteini	102		*Branchiostoma* (LPIL)	79
	Protohaustorius wigleyi	100		Rhynchocoela (LPIL)	65
	Unciola irrorata	98		*Apoprionospio pygmaea*	60
C1	Rhynchocoela (LPIL)	1,562	R1	*Ampelisca* sp. X	606
	Polygordius (LPIL)	767		*Nucula proxima*	258
	Tanaissus psammophilus	492		*Apoprionospio pygmaea*	126
	Pseudunciola obliquua	218		*Tellina agilis*	67
	Oligochaeta (LPIL)	158		*Polygordius* (LPIL)	38
	Actiniaria (LPIL)	125		*Ilyanassa trivittata*	23
	Exogone hebes	101		*Caulleriella* sp. J	22
	Unciola irrorata	52		*Aricidea wassi*	20
	Parapionosyllis longicirrata	41		*Spiophanes bombyx*	20
	Ampharetidae (LPIL)	37		Oligochaeta (LPIL)	16
F1	*Pseudunciola obliquua*	380	R2	Oligochaeta (LPIL)	153
	Tanaissus psammophilus	377		Rhynochocoela (LPIL)	85
	Polygordius (LPIL)	350		*Cirriformia grandis*	54
	Lumbrinerides acuta	52		*Brania wellfleetensis*	29
	Echinarachnius parma	36		*Polygordius* (LPIL)	22
	Oligochaeta (LPIL)	34		*Pisone remota*	14
	Aricidea (LPIL)	31		Actiniaria (LPIL)	13
	Spisula solidissima	26		*Astarte castanea*	8
	Sigalion arenicola	18		Cirratulidae (LPIL)	8
	Protohaustorius wigleyi	16		*Travisia parva*	8
F2	*Polygordius* (LPIL)	440	R3	*Polygordjius* (LPIL)	295
	Tanaissus psammophilus	397		*Echinarachnius parma*	40
	Pseudunciola obliquua	134		*Tanaissus psammophilus*	25
	Astarte castanea	102		*Pseudunciola obliquua*	19
	Echinarachnius parma	92		*Hemipodus roseus*	13
	Nephtyidae (LPIL)	65		Oligochaeta (LPIL)	13
	Pisione remota	52		Cirratulidae (LPIL)	9
	Rhynchocoela (LPIL)	39		Actiniaria (LPIL)	7
	Spisula solidissima	36		*Sigalion arenicola*	6
	Microphthalmus (LPIL)	31		*Politolana polita*	4
G1	*Polygordius* (LPIL)	1,081	SEPT TOTAL	*Polygordius* (LPIL)	6,631
	Apoprionospio pygmaea	613		*Asabellides oculata*	2,186
	Asabellides oculata	412		Rhynchocoela (LPIL)	2,007
	Spiophanes bombyx	279		*Tanaissus psammophilus*	1,990
	Nucula proxima	119		*Pseudunciola obliquua*	1,536
	Protohaustorius wigleyi	81		Oligochaeta (LPIL)	1,527
	Oligochaeta (LPIL)	77		*Nucula proxima*	1,498
	Glycera dibranchiata	64		Ampharetidae (LPIL)	1,481
	Cirratulidae (LPIL)	62		*Ampelisca* sp.X	1,445
	Spiochaetopterus oculatus	62		*Apoprionospio pygmaea*	1,326

LPIL = Lowest practical identification level.

Table 6-4. Summary of infaunal statistics by survey for sand resource areas (A1, A2, C1, F1, F2, G1, G2, and G3) and adjacent stations (R1, R2, and R3) offshore New Jersey.

May 1998 (Survey 1)

Area	No. of Taxa		No. of Individuals		Density (Individuals/m^2)		H' Diversity		J' Evenness		D Richness	
	Mean Per Station	Standard Deviation	Mean Per Station	Standard Deviation	Mean Per Station	Standard Deviation	Mean Per Station	Standard Deviation	Mean Per Station	Standard Deviation	Mean Per Station	Standard Deviation
A1	37	20	898	846	8,975	8,463	2.37	0.61	0.67	0.16	5.67	2.28
A2	21	7	217	181	2,173	1,814	2.20	0.69	0.73	0.20	3.85	1.01
C1	28	9	625	616	6,254	6,158	2.01	0.52	0.63	0.20	4.49	0.72
F1	31	1	609	441	6,090	4,412	1.74	0.46	0.51	0.14	4.75	0.49
F2	26	13	351	343	3,505	3,429	2.25	0.24	0.72	0.05	4.26	1.50
G1	21	5	565	612	5,647	6,124	1.64	1.10	0.54	0.37	3.71	0.90
G2	27	8	757	866	7,570	8,658	1.91	0.76	0.59	0.26	4.26	0.77
G3	33	18	878	1,296	8,783	12,960	2.10	0.80	0.64	0.30	5.35	1.41
R1	39		748		7,480		2.13		0.58		5.74	
R2	44		4,296		42,960		1.42		0.38		5.14	
R3	34		1,252		12,520		1.01		0.29		4.63	

September 1998 (Survey 2)

Area	No. of Taxa		No. of Individuals		Density (Individuals/m^2)		H' Diversity		J' Evenness		D Richness	
	Mean Per Station	Standard Deviation	Mean Per Station	Standard Deviation	Mean Per Station	Standard Deviation	Mean Per Station	Standard Deviation	Mean Per Station	Standard Deviation	Mean Per Station	Standard Deviation
A1	41	11	734	625	7,339	6,245	2.41	0.37	0.66	0.11	6.24	1.26
A2	33	8	447	366	4,468	3,660	2.40	0.31	0.69	0.08	5.53	1.19
C1	28	6	384	447	3,842	4,473	2.15	0.76	0.65	0.23	5.10	1.15
F1	36	4	507	393	5,073	3,933	2.14	0.39	0.60	0.13	5.85	0.12
F2	26	5	339	109	3,392	1,092	2.08	0.34	0.64	0.11	4.30	0.83
G1	43	10	644	351	6,438	3,512	2.33	0.51	0.62	0.13	6.68	1.52
G2	35	7	800	1,207	8,000	12,067	2.48	0.41	0.71	0.12	5.70	1.14
G3	40	7	547	392	5,470	3,920	2.42	0.52	0.66	0.16	6.44	0.93
R1	40		1,320		13,200		1.98		0.54		5.43	
R2	31		446		4,460		2.26		0.66		4.92	
R3	27		459		4,590		1.56		0.47		4.24	

highest measure of mean species richness was from Area G1 (6.68). During the September survey, the lowest mean values of species diversity and richness were from Area F2 (2.08 and 4.30, respectively). The lowest mean value of species evenness during the September survey was from Area F1 stations (0.60).

Juvenile Atlantic Surfclam

Each of the sand resource areas yielded juvenile Atlantic surfclam (*S. solidissima*) during both surveys**.** Table 6-5 presents mean densities of juvenile *S. solidissima* from each of the eight sand resource areas and three adjacent stations. Juvenile Atlantic surfclam mean densities were much greater during the May survey than in September at all areas except Areas F1 and G1. Greatest surfclam mean densities occurred at adjacent stations during both the May (Station R2) and September (Station R1) surveys. Within sand resource areas, mean densities in May ranged from 425 clams/m^2 at Area F2 stations to 20 clams/m^2 in Area F1. Mean juvenile Atlantic surfclam densities in September ranged from 87 clams/m^2 at Area F1 stations to 8 clams/m^2 in Area A2. The distribution of juvenile Atlantic surfclams during the surveys was very heterogeneous, as indicated by large standard deviations (Table 6-5). Juvenile surfclams were not associated with any single type of sedimentary habitat, although stations with at least some gravel content tended to yield greater numbers than stations with pure sand.

Cluster Analysis

Patterns of infaunal similarity among stations were examined with cluster analysis. The cluster analysis excluded those taxa that were rare in the samples or had an LPIL designation, except for the polychaete *Mediomastus* (LPIL) and the archiannelid *Polygordius*. When examined over both surveys, normal cluster analysis produced six groups (Groups A through F) of stations (samples) that were similar with respect to species composition and relative abundance (Figure 6-14). Several stations that were not included within any of these six station groupings, yet were dissimilar enough not to be grouped together, were placed into outlier groups (X and Y). Station Groups X and Y contained 13 of the 90 stations sampled during the project and included samples collected during both surveys. Station Groups B and E included samples taken only during the September survey, while Group D contained stations sampled in May. Three of the six station groups (Groups A, C, and F) included samples collected during both surveys. Four of the six station groups (Groups A, C, D, and E) each were represented by relatively few stations, while Groups B (21 stations) and F (31 stations) together contained most of the total project samples (Figure 6-14). Group B stations were distinguished from other stations primarily by the presence of relatively high numbers of the polychaetes *Apoprionospio pygmaea*, *Dispio uncinata*, and *Spiochaetopterus oculatus* and amphipods *Protohaustorius wigleyi* and *Rhepoxynius hudsoni*. Group F stations were depauperate with respect to these taxa, and were further distinguished from other station groupings primarily by exhibiting high numbers of the archiannelid *Polygordius*, the amphipod *Pseudunciola obliquua*, and the tanaid *T. psammophilus*.

Figure 6-14 shows the geographic distribution of infaunal stations grouped by normal analysis. Group F stations were distributed across all resource areas and both surveys, and included all stations in Areas F1 and F2, as well as Adjacent Station 3. Group B stations were located in Areas A1, A2, G1, G2, and G3. Station Group A (seven stations) primarily was associated with Area C1 and Adjacent Station 2. Group C (nine stations) included Adjacent Station 1 and stations in Areas A1, G2, and G3. Group D included one station in each of Areas A1, A2, C1, G2, and G3, while Group E was composed of two stations each in Areas A2 and G2.

Table 6-5. Occurrence and density of juvenile Atlantic surfclam, *Spisula solidissima*, in Smith-McIntyre grab samples taken in the eight sand resource areas and three adjacent stations during the May 1998 Survey 1 and September 1998 Survey 2 offshore New Jersey.

May 1998			
Area	Number of Samples	Mean Density (clams/m^2)	Standard Deviation
A1	4	228	151.3
A2	4	43	56.8
C1	5	166	140.1
F1	2	20	14.1
F2	2	425	558.6
G1	3	23	23.1
G2	4	133	63.4
G3	3	173	161.7
R1	1	330	
R2	1	820	
R3	1	0	

September 1998			
Area	Number of Samples	Mean Density (clams/m^2)	Standard Deviation
A1	9	14	21.3
A2	8	8	8.9
C1	11	25	41.3
F1	3	87	106.9
F2	5	72	86.4
G1	6	37	35.0
G2	8	25	27.8
G3	7	11	9.0
R1	1	100	
R2	1	0	
R3	1	0	

Inverse cluster analysis examining both the May and September surveys resulted in five groups of taxa (Groups 1 through 5) that reflected their co-occurrence in sand resource area samples (Table 6-6). Most taxa included in the cluster analysis were polychaetes (32 taxa), followed by crustaceans (18), bivalve (9) and gastropod mollusks (7), and a single echinoid (*Echinarachnius parma*). Species Group 1 included the most homogeneously distributed taxa found during the study, both among the various sand resource areas and among surveys. This group included the polychaetes *Caulleriella* sp. J and *S. bombyx*, the archiannelid *Polygordius*, the bivalves *S. solidissima* and *Tellina agilis*, amphipods *Acanthohaustorius millsi*, *Protohaustorius wigleyi, Pseudunciola obliquua,* and *R. hudsoni*, and tanaid *T. psammophilus*.

Species Group 1 was particularly associated with Station Group B; all stations in this group included a majority of the taxa comprising Group 1. These taxa generally inhabit areas of sandy sediments, especially the polychaete *S. bombyx* and archiannelid *Polygordius*. Station Group B was, in fact, the most homogeneous station group with respect to sediment composition, as 20 of the 21 stations were characterized by a sand substratum (Figure 6-15). Taxa in Species Groups 2, 3, 4, and 5 were heterogeneously distributed.

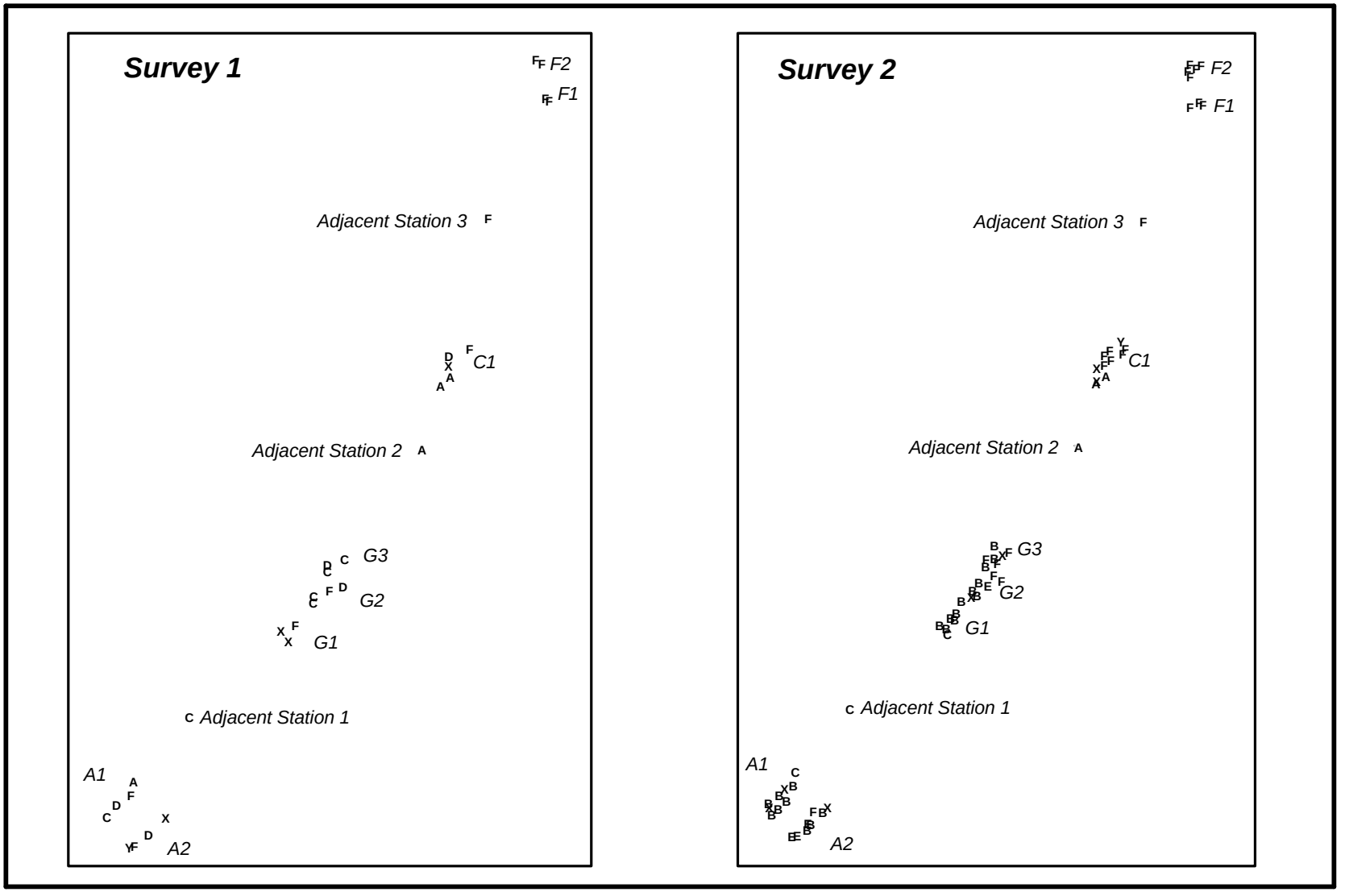

Figure 6-14. Station groups (A to F; X and Y) based on normal cluster analysis of infaunal samples collected during the May 1998 Survey 1 and September 1998 Survey 2 in the eight sand resource areas (A1, A2, C1, F1, F2, G1, G2, and G3) and three adjacent stations offshore New Jersey.

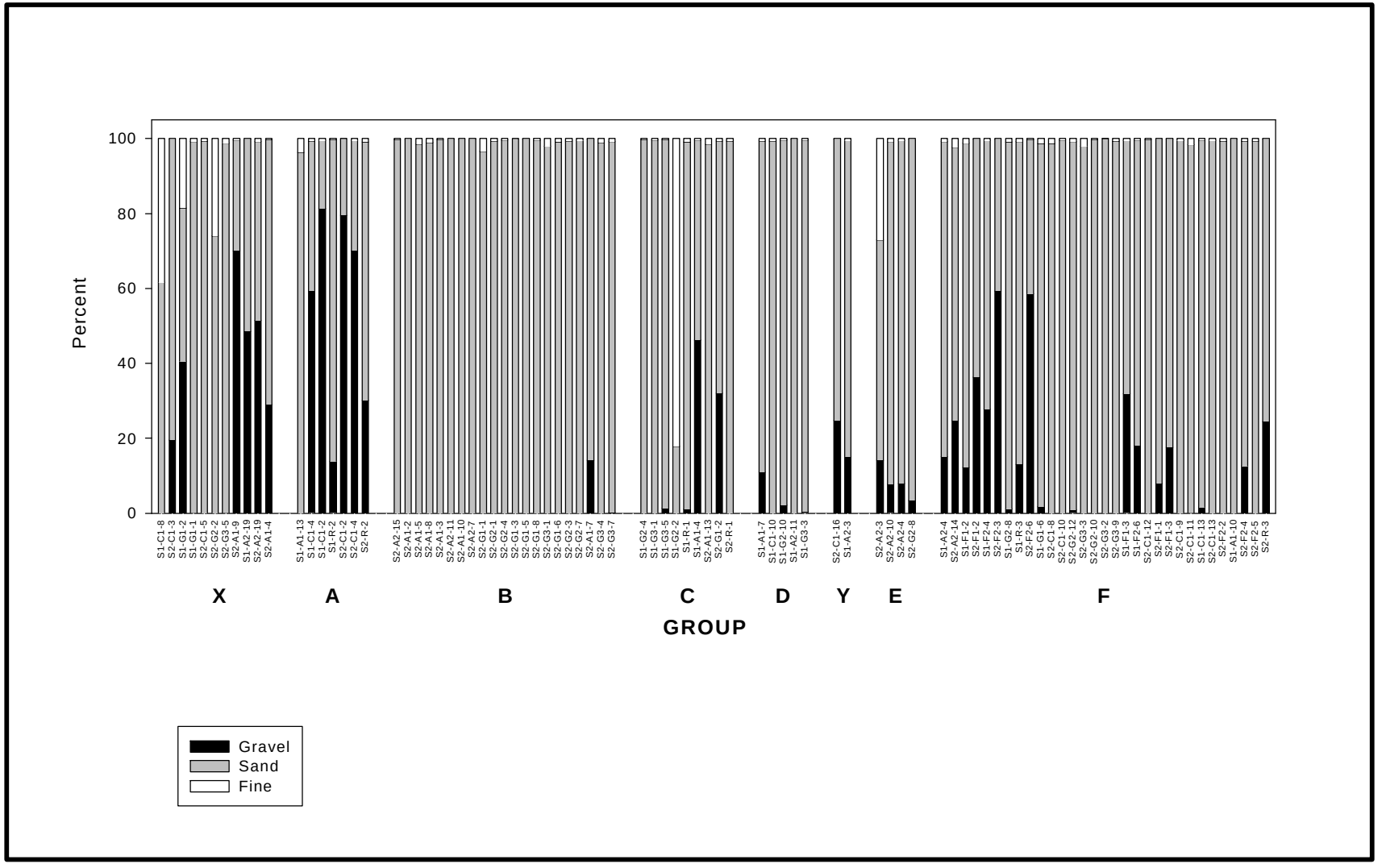

Figure 6-15. Grain size composition of infaunal samples collected during the May 1998 Survey 1 (S1) and September 1998 Survey 2 (S2) in the eight sand resource areas offshore New Jersey. Sample order and groups (A to F; X and Y) are based on normal cluster analysis.

Station Group A was characterized by Group 2 taxa (Table 6-6). Group C was characterized by taxa from Species Groups 1, 3, and 4. Group D was depauperate of common taxa (Table 6-6), while Group E was characterized by taxa from Species Groups 1, 2, and 3.

Table 6-6. Infaunal species groups resolved from inverse cluster analysis of all samples collected during the May 1998 Survey 1 and September 1998 Survey 2 in the eight sand resource areas and three adjacent stations offshore New Jersey.

GROUP 1

Polygordius (LPIL*)*
Tanaissus psammophilus
Pseudunciola obliquua
Spiophanes bombyx
Spisula solidissima
Tellina agilis
Caulleriella sp. J
Protohaustorius wigleyi
Rhepoxynius hudsoni
Acanthohaustorius millsi

GROUP 2

Pisione remota
Astarte castanea
Hemipodus roseus
Mytilus edulis
Crenella decussata
Lumbrinerides acuta
Aricidea cerrutii
Hesionura elongata
Protodorvillea kefersteini
Parougia caeca
Spio setosa

GROUP 3

Petricola pholadiformis
Nereis succinea
Anachis lafresnayi
Brania wellfleetensis
Cirriformia grandis
Chiridotea tuftsi
Sigalion arenicola
Politolana polita
Donax variabilis
Bathyporeia parkeri
Oxyurostylis smithi
Tectonatica pusilla
Echinarachnius parma
Exogone hebes
Parapionosyllis longicirrata
Streptosyllis arenae
Capitella capitata
Diastylis polita
Ampelisca abdita
Unciola irrorata
Aricidea catherinae
Ampelisca sp. X
Apoprionospio dayi
Mediomastus (LPIL)
Ampelisca macrocephala
Mercenaria mercenaria
Odostomia gibbosa

GROUP 4

Tharyx acutus
Asabellides oculata
Nucula proxima
Edotia triloba
Nephtys picta
Phyllodoce arenae
Ilyanassa trivittata
Apoprionospio pygmaea
Dispio uncinata
Spiochaetopterus oculatus
Magelna papillicornis
Euspira heros
Acanthohaustorius shoemakeri
Microprotopus raneyi
Turbonilla interrupta
Americamysis bigelowi

GROUP 5

Glycera dibranchiata
Mitrella lunata
Harmothoe imbricata

LPIL = Lowest practical identification level.

Canonical Discriminant Analysis

Data collected during the two surveys were analyzed using canonical discriminant analysis to determine which environmental factors most affected the distribution of infaunal assemblages. The first two canonical discriminant variates were used to analyze variability among those station groups identified by normal cluster analysis as being similar with respect to species composition and relative abundance. The first canonical variate correlated best with percent gravel (0.6978) and percent sand (-0.6814), and to a lesser degree with survey (-0.5489) and station water depth (0.4859). The second canonical variate best correlated with latitude (Northing [0.8371]) and longitude (Easting [0.7659]).

Patterns of infaunal similarity among stations (normal cluster analysis) and the co-occurrence of taxa within samples (inverse cluster analysis) were examined for each sand resource area. The following describes the results of this area-by-area analysis for each survey, as well as the affinities of the station groups and species groups identified by cluster analyses. Due to the heterogeneity of most taxa distributions, generally low abundances, and relatively limited sampling, only well-defined species groups generated from the inverse analyses are included in the discussion.

AREA A1

Normal cluster analysis resulted in four station groups in Area A1 (Station Groups A through D) that were similar with respect to assemblage composition and abundance of infaunal taxa (Table 6-7). Group A consisted of two stations that were characterized by the polychaetes *Hemipodus roseus*, *Hesionura elongata,* and *Parougia caeca* and bivalves *Crenella decussata* and *M. edulis*. Station Group B included eight stations sampled primarily during the September survey that were distinguished from other groups by yielding high numbers of the amphipods *A. millsi*, *Protohaustorius wigleyi*, and *Pseudunciola obliquua* and tanaid *T. psammophilus*. Juvenile Atlantic surfclam (*S. solidissima*) was associated primarily with Group B stations. Group C consisted of two stations that were characterized by the exclusive or near exclusive presence of the polychaete *Mediomastus*, bivalve *N. proxima*, gastropod *Turbonilla interrupta*, and amphipod *Unciola irrorata*. Group D was represented by a single station from the September survey that was generally depauperate but did yield taxa that were rare at other stations, including the polychaete *Harmothoe imbricata* and gastropods *Crepidula fornicata* and *M. lunata* (Table 6-7).

Inverse cluster analysis resulted in three groups of taxa (Species Groups 1 through 3) that reflected their co-occurrence in samples collected in Area A1 (Table 6-7). Species Group 1 had the most homogeneously distributed taxa in Area A1 and included the polychaetes *Caulleriella* sp. J and *S. bombyx*, archiannelid *Polygordius*, bivalve *Donax variabilis*, gastropod *Tectonatica pusilla,* amphipods *A. millsi*, *Bathyporeia parkeri*, *Protohaustorius wigleyi*, *Pseudunciola obliquua*, and *R. hudsoni,* cumacean *Oxyurostylis smithi*, and tanaid *T. psammophilus.* Group 2 consisted of taxa collected primarily from two stations, including the polychaetes *Hemipodus roseus*, *Hesionura elongata*, *Parougia caeca*, and *Pisione remota,* bivalves *C. decussata* and *M. edulis*, and isopod *Chiridotea tuftsi*. Species Group 3 also contained taxa collected primarily from two stations. Group 3 taxa included the polychaetes *Aricidea catherinae*, *Asabellides oculata*, *Mediomastus*, *Nephtys picta*, *Phyllodoce arenae*, and *Tharyx acutus,* bivalve *N. proxima*, gastropods *Ilyanassa trivittata* and *T. interrupta*, and amphipods *Ampelisca abdita* and *U. irrorata* (Table 6-7).

Sediments in Area A1 were fairly homogeneous, as all but two sampled stations were characterized by sand substrata. Those stations that had high gravel content yielded taxa that were rare or absent at other stations, including the polychaete *H. imbricata*, bivalves *Astarte castanea* and *Mercenaria mercenaria*, gastropods *C. fornicata, Mitrella lunata,* and *Odostomia gibbosa*, and amphipod *Ampelisca macrocephala*. Species Group 1 was primarily associated with Station Group B, Species Group 2 was associated with Station Group A, and Species Group 3 was associated with Station Group C. Station 13 yielded high abundances of certain taxa and supported distinct assemblages during both the May (e.g., polychaete *P. remota* and bivalve *M. edulis*) and September (e.g., polychaete *Apoprionospio dayi* and amphipod *Ampelisca* sp. X) surveys, despite having sediments similar to other stations in Area A1. Station 13 was situated in a trough feature and was the deepest (20 m) station in Area A1.

Table 6-7. Two-way table from normal (Station Groups A-D) and inverse (Species Groups 1-3[a]) cluster analysis of infaunal samples collected during the May 1998 Survey 1 (S1) and September 1998 Survey 2 (S2) in Sand Resource Area A1 offshore New Jersey. Data are presented as total counts for individual taxa.

Taxon	A		B								C		D	
	S1-A1-13	S2-A1-4	S1-A1-7	S1-A1-10	S2-A1-7	S2-A1-10	S2-A1-3	S2-A1-2	S2-A1-5	S2-A1-8	S1-A1-4	S2-A1-13	S2-A1-9	
Polygordius (LPIL[b])	75	561	6	17	530	1	5	97	13	32	6	20	170	1
Protohaustorius wigleyi		1	21	11	5	37	78	51	62	33		1		
Rhepoxynius hudsoni		85	4	1	19	47	32	55	28	28			1	
Spiophanes bombyx				80	15	14	23	26	26	17	47	22	5	
Pseudunciola obliquua		1		7	525	1	11	9	16					
Tanaissus psammophilus	1			5	25	4	12	7	35	2				
Caulleriella sp.J		4	3	6	17	3	7	1	17	5	2		2	
Donax variabilis		8			1	52	33		25					
Bathyporeia parkeri		2				6	21	46	20	5				
Acanthohaustorius millsi			1		1	12		36	11	1				
Tectonatica pusilla		4	2	1	2	5	13	18	6	8		4		
Oxyurostylis smithi		3			12	7	7	5	2	8		7		
Bathyporeia quoddyensis				17										
Spisula solidissima	5		22	22	6	1	1		4			1		
Exogone hebes			2	4	6		1			1				
Sigalion arenicola				3	3		6							
Dissodactylus mellitae					8				13					
Magelona papillicornis					2			6	3					
Mytilus edulis	791	48									4			2
Pisione remota	182	47						1						
Parougia caeca	28	32												
Hesionura elongata	7	36												
Crenella decussata	17	5												
Hemipodus roseus	9	11												
Chiridotea tuftsi	2	3				1	2	3						
Ampelisca macrocephala											288			
Mercenaria mercenaria											166			
Odostomia gibbosa											37			
Astarte castanea											10			
Glycera dibranchiata				2								3	7	
Mitrella lunata							1					1	35	
Crepidula fornicata		1											22	
Harmothoe imbricata										1			8	
Aricidea cerrutii		13												
Brania wellfleetensis		10												
Paraeupolymnia sp.A		9												
Lumbrinerides acuta		9												
Ampelisca sp.X												816	2	
Apoprionospio dayi												115		
Ampelisca abdita		19				11	1		2	1	69	125	26	3
Aricidea catherinae		57									54	137		
Unciola irrorata		6				1		1		1	52	85	2	
Tellina agilis			5	5				18		42	51	49		
Turbonilla interrupta											354	82		
Nucula proxima				1							44	50	2	
Mediomastus (LPIL)			1								36	9		
Phyllodoce arenae					1	1	6				4	9	1	
Asabellides oculata					5						3	6	5	
Nephtys picta		8			5	3	1			1	21	8		
Ilyanassa trivittata		4				1	2			1	10	2		
Tharyx acutus		3									5	1		

[a] Due to the heterogeneity of most taxa distributions, generally low abundances, and relatively limited sampling, only well-defined species groups generated from the inverse analyses are numbered.

[b] LPIL = Lowest practical identification level.

Area A2

Normal cluster analysis resulted in three station groups in Area A2 (Groups A through C). Group A included the same station (Station 19) sampled during both the May and September surveys and was depauperate with respect to most of the numerically dominant taxa found in Area A2 (Table 6-8). Group A did yield taxa that were absent at all other stations in Area A2 (the polychaete *Spio setosa* and amphipod *U. irrorata*). Group A also yielded high numbers of the archiannelid *Polygordius* and amphipod *A. abdita*. Station Group B included six stations, two of which (Stations 3 and 4) were sampled during both surveys. Group B was distinguished from other station groups primarily by the presence of the polychaetes *Aricidea cerutii*, *H. elongata*, *Pisione remota*, and *Protodorvillea kefersteini* and bivalves *A. castanea* and *C. decussata*. The archiannelid *Polygordius*, isopod *C. tuftsi*, and tanaid *T. psammophilus* were found at all Group B stations. Station Group C consisted of four stations and yielded an abundance of the amphipods *A. millsi*, *P. wigleyi*, and *R. hudsoni*. The echinoid *E. parma* was found only at Group C stations.

Inverse cluster analysis resulted in four groups of co-occurring taxa (Groups 1 through 4) in Area A2 (Table 6-8). Group 1 included the polychaetes *Aricidea cerutii*, *H. elongata, Pisione remota,* and *Protodorvillea kefersteini* and bivalves *Astarte castanea* and *C. decussata*. Taxa in Species Group 2 were collected mostly from a single station (Station 19) during both the May and September surveys, and included the polychaete *S. setosa* and amphipods *A. abdita* and *U. irrorata*. Group 3 contained the most homogeneously distributed taxa in Area A2 and included the polychaete *Sigalion arenicola*, archiannelid *Polygordius*, bivalve *D. variabilis*, isopods *C. tuftsi* and *Politolana polita*, amphipod *R. hudsoni,* and tanaid *T. psammophilus*. Species Group 4 included the polychaetes *Phyllodoce arenae* and *S. bombyx,* amphipods *A. millsi* and *P. wigleyi*, cumacean *O. smithi*, and echinoid *E. parma.*

Station groupings in Area A2 were separated by sediment type. Station Group A was represented by Station 19 during both surveys and was characterized by a sandy gravel substratum. Group B stations all were characterized by gravelly sand, while Group C stations were characterized by a sand substratum. Species Group 1 was associated with Station Group B, Group 2 taxa were associated with Group A stations, Group 3 taxa were associated with stations in Groups B and C, and Group 4 taxa were associated primarily with Station Group C.

Area C1

Normal cluster analysis resulted in five station groups in Area C1 (Groups A through E). Three station groups (Groups A, B, and D) each included a single station that was generally depauperate (Table 6-9). Groups A and D consisted of stations sampled during September, while the Group B station was sampled during the May survey. Group A did yield polychaete taxa (*Cirriformia grandis* and *Glycera dibranchiata*) that were rare at other stations. Station Group C included two stations (2 and 4) that were sampled during both the May and September surveys and were distinguished from other station groups by yielding high numbers of the polychaete *P. remota* and bivalves *C. decussata* and *M. edulis*. Group E was represented by five stations sampled primarily during the September survey, and yielded high abundances of the archiannelid *Polygordius*, amphipod *Pseudunciola obliquua*, tanaid *T. psammophilus,* and echinoid *E. parma*.

Inverse cluster analysis resulted in two groups of co-occurring taxa (Groups 1 and 2) in Area C1 (Table 6-9). Species Group 1 included several polychaetes, including *Caulleriella* sp. J, *E. hebes*, *N. picta*, *Parapionosyllis longicirrata*, *Sigalion arenicola*, *and Streptosyllis arenae*. Group 1 also included the archiannelid *Polygordius*, bivalve *S. solidissima*, amphipod

Table 6-8. Two-way table from normal (Station Groups A-C) and inverse (Species Groups 1-4[a]) cluster analysis of infaunal samples collected during the May 1998 Survey 1 (S1) and September 1998 Survey 2 (S2) in Sand Resource Area A2 offshore New Jersey. Data are presented as total counts for individual taxa.

Taxon	A		B						C				
	S1-A2-19	S2-A2-19	S1-A2-3	S1-A2-4	S2-A2-14	S2-A2-3	S2-A2-10	S2-A2-4	S1-A2-11	S2-A2-15	S2-A2-11	S2-A2-7	
Protodorvillea kefersteini					102								1
Aricidea cerrutii				7	258		2	3					
Astarte castanea			2	57	78			15					
Crenella decussata				25	51	1	1	38					
Hesionura elongata			12	10	54		2						
Pisione remota			1	9	27	1							
Ampelisca abdita	4	283			1				4	1		1	2
Unciola irrorata	16	98											
Spio setosa	47	11											
Hemipodus roseus		18					2	3					
Brania wellfleetensis		3			2	2	6	7					
Bathyporeia parkeri							15				6	5	
Ampelisca sp.X		5					14				2		
Tectonatica pusilla							3	4			3	1	
Acanthohaustorius shoemakeri							3				2	1	
Polygordius (LPIL[b])	147	311	16	63	143	7	37	18	6			27	3
Tanaissus psammophilus		1	6	47	40	9	8	149		1	2	5	
Chiridotea tuftsi			1	45	8	16	48	9	2		1	6	
Donax variabilis					9	56	49	31		4	54	67	
Rhepoxynius hudsoni					2		11	2		56	22	42	
Politolana polita					2	5	13	15			2	2	
Sigalion arenicola				1	2	7	2	10		3	4	2	
Protohaustorius wigleyi	1		1	2			2	2	13	5	49	42	4
Acanthohaustorius millsi	1							1	10		27	22	
Echinarachnius parma									2	13	2	2	
Spiophanes bombyx						4	1	2		5	2	27	
Oxyurostylis smithi		1			1			2		6	5	6	
Phyllodoce arenae		1						1		3	1	3	
Synchelidium americanum						1	1		3	1			
Nephtys picta		2								1	1		
Ilyanassa trivittata		1	1							1		1	
Mytilus edulis				5		2		10	2				
Lumbrinerides acuta				1				9					
Caecum johnsoni				4				2					
Streptosyllis arenae				3				1			1		
Spisula solidissima				5	2		1	1	12			2	
Tellina agilis			6	3					10			1	
Dispio uncinata			1	2								6	
Parapionosyllis longicirrata			1	3									

[a] Due to the heterogeneity of most taxa distributions, generally low abundances, and relatively limited sampling, only well-defined species groups generated from the inverse analyses are numbered.

[b] LPIL = Lowest practical identification level.

Table 6-9. Two-way table from normal (Station Groups A-E) and inverse (Species Groups 1 and 2[a]) cluster analysis of infaunal samples collected during the May 1998 Survey 1 (S1) and September 1998 Survey 2 (S2) in Sand Resource Area C1 offshore New Jersey. Data are presented as total counts for individual taxa

Taxon	A	B	C				D	E					
	S2-C1-3	S1-C1-8	S1-C1-4	S1-C1-2	S2-C1-2	S2-C1-4	S2-C1-5	S1-C1-10	S2-C1-16	S2-C1-8	S2-C1-10	S2-C1-11	
Microphthalmus similis			8	1									
Glycera americana			8										
Glycera dibranchiata	10												
Cirriformia grandis	10												
Chiridotea tuftsi	7		1								1		
Scoletoma acicularum	3					2							
Polygordius (LPIL[b])			10	43	2	33	1	6	2	44	24	172	
Tanaissus psammophilus	1				1			2		2	17	16	
Pseudunciola obliquua							1		1	27	22	44	
Echinarachnius parma								14	4		3	7	
Spisula solidissima			33	13		1		8	1	9		3	
Parapionosyllis longicirrata			2	8	8				2		1		1
Exogone hebes											1	4	
Streptosyllis arenae								1	1		3	1	
Caulleriella sp.J								2	2	7	1	5	
Nephtys picta	1						4			2	1	4	
Sigalion arenicola								2	6	2			
Spiophanes bombyx		1		2	1	1	4	1					
Nucula proxima			2	3			8			1			
Harmothoe imbricata			1	22									
Asabellides oculata		6	2	5									
Hemipodus roseus				7	8	4			1	3			
Astarte castanea		1		8	6							2	
Mytilus edulis	1	6	10	65	4	5							2
Pisione remota		1	81	18	16	19							
Unciola irrorata	3		2	25	31	7	1						
Crenella decussata	2		12	5	2	1							
Ophelia denticulata	2		2	1	1	3			2				
Ampharete acutifrons					6					1			
Phyllodoce arenae										1			
Brania wellfleetensis									1				
Edotia triloba					1		1			3			
Tellina agilis							1		1	4			
Politolana polita									1		4		
Rhepoxynius hudsoni								5		1	13	10	
Protohaustorius wigleyi								9	2			9	
Dispio uncinata											1	2	

[a] Due to the heterogeneity of most taxa distributions, generally low abundances, and relatively limited sampling, only well-defined species groups generated from the inverse analyses are numbered.

[b] LPIL = Lowest practical identification level.

Pseudunciola obliquua, tanaid *T. psammophilus,* and echinoid *E. parma*. Group 2 included the polychaetes *A. oculata*, *H. imbricata*, *H. roseus*, *Ophelia denticulata*, and *P. remota,* bivalves *A. castanea*, *C. decussata*, and *M. edulis*, and amphipod *U. irrorata*.

The two primary station groups in Area C1 (Groups C and E) were characterized by different substratum types. Group C stations had gravel bottoms and Group E stations had sand bottoms. Species Group 1 was associated primarily with Station Group E, and Species Group 2 was associated primarily with Station Group C (Table 6-9).

Area F1

Normal cluster analysis resulted in two station groups in Area F1 (Groups A and B). Station Group A consisted of three stations that yielded relatively high numbers of the polychaetes *Goniadella gracilis*, *H. roseus*, and *P. remota* (Table 6-10). Group B included two stations during the September survey that yielded relatively high numbers of the polychaetes *N. picta* and *S. bombyx*, amphipods *Protohaustorius wigleyi* and *Pseudunciola obliquua*, tanaid *T. psammophilus,* and echinoid *E. parma*. Juvenile Atlantic surfclams were collected at all Area F1 stations.

Inverse cluster analysis resulted in two groups of co-occurring taxa (Groups 1 and 2) (Table 6-10). Species Group 1 included mostly polychaetes (*E. hebes*, *Lumbrinerides acuta*, *N. picta*, *Sigalion arenicola*, and *Spiophanes bombyx*) and crustaceans (*C. tuftsi*, *Protohaustorius wigleyi*, *Pseudunciola obliquua*, and *T. psammophilus*), and also included the archiannelid *Polygordius*, bivalve *S. solidissima,* and echinoid *E. parma*. Group 2 consisted entirely of polychaetes, including *Aricidea cerrutii*, *G. gracilis*, *H. roseus*, *Parapionosyllis longicirrata*, *Pisione remota*, and *Scolelepis squamata*.

Area F1 is characterized by a centrally located, elevated ridge feature and assemblage composition was different across station locations. Station 2 was situated on top of the ridge, while Stations 1 and 3 were located in deeper water adjacent to the ridge. Species Group 1 was associated with both station groups and Species Group 2 was associated primarily with Station Group A, which included stations that had gravelly substrata.

Area F2

Normal cluster analysis resulted in two station groups in Area F2 (Groups A and B). Station Group A consisted of two stations that yielded high numbers of the polychaetes *Asabellides oculata*, *Capitella jonesi*, *Notomastus hemipodus*, and *T. acutus* (Table 6-11). Group B consisted of five stations sampled primarily during the September survey. Group B stations were characterized by the exclusive or near exclusive presence of the polychaetes *Ampharete finmarchica*, *Aphelochaeta marioni*, and *Mediomastus*.

Inverse cluster analysis resulted in two groups of co-occurring taxa (Groups 1 and 2), with both groups represented entirely by polychaetes (Table 6-11). Species Group 1 contained the most homogeneously distributed taxa, including *Ampharete acutifrons*, *A. americana*, *A. finmarchica*, *Aphelochaeta marioni*, *C. capitata*, *Mediomastus*, and *S. oculatus*. Group 2 contained co-occurring taxa primarily from two stations, and included *Asabellides oculata*, *C. jonesi*, *N. hemipodus*, *P. kefersteini*, and *T. acutus*.

Species Group 1 was distributed across both station groups, while Species Group 2 was associated primarily with Station Group A. Group A stations were situated on top of a ridge feature at depths of 18 m, while some of the Group B stations were located in deeper water (19 to 22 m) at the base of the ridge. Sediments at Group A stations were sandy gravel or gravelly sand, while Group B stations mostly had sand or gravelly sand.

Table 6-10. Two-way table from normal (Station Groups A and B) and inverse (Species Groups 1 and 2[a]) cluster analysis of infaunal samples collected during the May 1998 Survey 1 (S1) and September 1998 Survey 2 (S2) in Sand Resource Area F1 offshore New Jersey. Data are presented as total counts for individual taxa.

Taxon	A			B		
	S1-F1-3	S1-F1-2	S2-F1-2	S2-F1-1	S2-F1-3	
Polygordius (LPIL[b])	126	30	77	271	2	1
Tanaissus psammophilus	37	17	45	210	122	
Lumbrinerides acuta	1	87	43	8	1	
Spisula solidissima	3	1	21	3	2	
Chiridotea tuftsi			13	2		
Pseudunciola obliquua			2	340	38	
Echinarachnius parma	2	1	2	12	22	
Sigalion arenicola	1	1	4	5	9	
Exogone hebes	10	5		11	2	
Protohaustorius wigleyi		1		15	1	
Spiophanes bombyx				6	8	
Nephtys picta			1	10	3	
Unciola irrorata			1	1	3	
Aricidea catherinae				2	3	
Dipolydora socialis					3	
Edotia triloba	2			1	1	
Politolana polita	1			1	1	
Dispio uncinata				1	1	
Ilyanassa trivittata	1				1	
Parapionosyllis longicirrata		9	1	3		2
Hemipodus roseus	1	10	14	1		
Goniadella gracilis	2	5	3			
Pisione remota		15	6			
Aricidea cerrutii		3	6			
Scolelepis squamata		4				
Astarte castanea	3	3	1	1	1	
Caulleriella sp.J	3	1	2		1	
Cirrophorus ilvana	8	1				
Mytilus edulis	2					
Cancer irroratus			2		2	
Harmothoe imbricata			2			
Pseudoleptocuma minor			1	3		
Hippomedon serratus			1	1		
Asabellides oculata				3		
Aricidea wassi				2		

[a] Due to the heterogeneity of most taxa distributions, generally low abundances, and relatively limited sampling, only well-defined species groups generated from the inverse analyses are numbered.

[b] LPIL = Lowest practical identification level.

Table 6-11. Two-way table from normal (Station Groups A and B) and inverse (Species Groups 1 and 2[a]) cluster analysis of infaunal samples collected during the May 1998 Survey 1 (S1) and September 1998 Survey 2 (S2) in Sand Resource Area F2 offshore New Jersey. Data are presented as total counts for individual taxa.

Taxon	A		B					
	S1-F2-4	S2-F2-3	S1-F2-6	S2-F2-2	S2-F2-4	S2-F2-5	S2-F2-6	
Ampharete americana	86	69	34	75	18	41	237	1
Ampharete acutifrons	20	7	6	145	47	134	64	
Capitella capitata	82		3		15	18	3	
Ampharete finmarchica		1	1	94	4	32	3	
Mediomastus (LPIL[b])			5	61	3	24	4	
Spiochaetopterus oculatus	1	1			4	20	4	
Aphelochaeta marioni			1	2	3	9	4	
Asabellides oculata	32	100				1	1	2
Capitella jonesi	47	49					3	
Notomastus hemipodus	32	11		1	4			
Tharyx acutus	7	11					2	
Protodorvillea kefersteini	3	4	1				3	
Schistomeringos pectinata				9	2	4		
Glycera capitata					2	3		
Hemipodus roseus						5		
Glycera dibranchiata				1	1	2	1	
Nephtys incisa				1		2		
Cirriformia grandis			22	2		1		
Nephtys picta				3				
Travisia parva				2				
Owenia fusiformis					2			
Caulleriella sp.J		19						
Glycera americana		5	1					
Microphthalmus similis		4						
Nereis succinea		2						
Onuphis eremita		2						
Leitoscoloplos robustus		2						
Goniadella gracilis			1				4	
Pherusa plumosa							8	
Microphthalmus hartmanae							5	
Magelona papillicornis							3	
Nephtys bucera							3	
Leitoscoloplos fragilis							2	
Orbinia americana							2	
Aricidea catherinae							2	
Nereis acuminata	1						1	
Ophelia denticulata		1					1	
Axiothella mucosa	2	1						
Diopatra cuprea	1	1						
Parougia caeca	9							
Lumbrinerides acuta	4							
Scoletoma acicularum	3							
Scoletoma fragilis	3							
Scoletoma verrilli	3							
Aricidea wassi	2							

[a] Due to the heterogeneity of most taxa distributions, generally low abundances, and relatively limited sampling, only well-defined species groups generated from the inverse analyses are numbered.

[b] LPIL = Lowest practical identification level.

Area G1

Normal cluster analysis resulted in five station groups in Area G1 (Groups A through E). Four of the five station groups in Area G1 each contained a single station (Table 6-12). Station Group A was depauperate with respect to the numerically dominant taxa sampled from Area G1. Group B yielded high numbers of the polychaete *C*. *capitata* and bivalve *M*. *edulis*. Group C yielded high numbers of the archiannelid *Polygordius* but was otherwise depauperate. Group D was distinguished from other station groups by yielding high numbers of the polychaete *A*. *oculata* and by the near exclusive presence of the polychaetes *G*. *dibranchiata* and *Pectinaria gouldii,* bivalve *Petricola pholadiformis*, and gastropod *M*. *lunulata*. Station Group E included five stations sampled during the September survey. Several taxa were found only in this group, including the polychaete *S*. *oculatus*, gastropod *T*. *interrupta*, amphipod *P. obliquua,* and mysid *Americamysis bigelowi*. Station Group E also yielded high numbers of the polychaetes *A*. *pygmaea* and *S*. *bombyx* and tanaid *T*. *psammophilus*. All station groups in Area G1 yielded juveniles of the bivalve *S*. *solidissima*.

Inverse cluster analysis resulted in four groups of co-occurring taxa (Groups 1 through 4) in Area G1 (Table 6-12). A pair of taxa sampled mostly from a single station (polychaete *C*. *capitata* and bivalve *M*. *edulis*) represented Group 1. Species Group 2 included primarily polychaetes (*Asabellides oculata*, *Apoprionospio pygmaea*, *D*. *uncinata*, *Magelona papillicornis*, *N*. *picta*, *Owenia fusiformis*, *P*. *arenae*, *Spiochaetopterus oculatus*, *Sphiophanes bombyx*, and *T*. *acutus*), the gastropod *T*. *interrupta*, and crustaceans (*Acanthohaustorius shoemakeri*, *Americamysis bigelowi*, *Pseudunciola obliquua*, *Protohaustorius wigleyi*, *R*. *hudsoni*, and *T*. *psammophilus*). Group 3 contained sparsely distributed taxa that were sampled primarily from a single station during the September survey, and included polychaetes (*Caulleriella* sp. J, *G*. *dibranchiata*, *Nereis succinea*, and *P*. *gouldii*), bivalves (*N*. *proxima*, *P*. *pholadiformis*, and *T. agilis*), the gastropod *M*. *lunulata*, and cumacean *Diastylis polita*. Species Group 4 included bivalve (*D*. *variabilis* and *S*. *solidissima*) and gastropod (*E. heros* and *I*. *trivittata*) mollusks, as well as crustaceans (*A*. *millsi*, *C*. *tuftsi*, *O*. *smithi*, and *Parahaustorius attenuatus*).

Species Group 1 (polychaete *C*. *capitata* and bivalve *M*. *edulis*) was associated with Station Group B (muddy sandy gravel), Species Group 2 was associated with Station Group E (sand), and Group 3 taxa were associated primarily with Station Group D (sandy gravel). Species Group 4 was distributed across station groups. Station 2 was isolated as a station group during both surveys (Groups B and D) and, in addition to having a distinct sedimentary regime relative to other stations, was the deepest infaunal station in Area G1.

Area G2

Normal cluster analysis resulted in three station groups in Area G2 (Groups A through C). Station Group A included a single station sampled during the September survey that yielded high numbers of the polychaete *A. oculata* and bivalve *N*. *proxima* (Table 6-13). The presence of the polychaete *N*. *succinea*, bivalve *P*. *pholadiformis*, and gastropod *Anachis lafresnayi* also characterized Group A stations. Group B consisted of four stations from both surveys that yielded high numbers of the polychaetes *A*. *pygmaea* and *S*. *bombyx*. The bivalve *M. edulis* was collected only from Group B stations. Group C consisted of seven stations that yielded taxa not found in Station Groups A or B, primarily during the September survey, including the isopod *Politolana polita*, amphipod *P*. *obliquua*, and tanaid *T*. *psammophilus*.

Inverse cluster analysis resulted in three groups of co-occurring taxa (Groups 1 through 3) (Table 6-13). Species Group 1 contained primarily polychaetes, including *Asabellides oculata*, *Apoprionospio pygmaea*, *Loimia medusa*, *N*. *picta*, *P*. *arenae*, and *T*. *acutus*, and also included

Table 6-12. Two-way table from normal (Station Groups A-E) and inverse (Species Groups 1-4[a]) cluster analysis of infaunal samples collected during the May 1998 Survey 1 (S1) and September 1998 Survey 2 (S2) in Resource Area G1 offshore New Jersey. Data are presented as total counts for individual taxa.

Taxon	A	B	C	D	E					
	S1-G1-1	S1-G1-2	S1-G1-6	S2-G1-2	S2-G1-1	S2-G1-6	S2-G1-3	S2-G1-5	S2-G1-8	
Capitella capitata		91								1
Mytilus edulis	2	48	1							
Polygordius (LPIL[b])		7	1,159	96	45	4	100	282	554	2
Apoprionospio pygmaea				7		7	341	213	45	
Spiophanes bombyx	1	1	3	2	49	45	30	79	74	
Protohaustorius wigleyi	3	1	2	1	6	5	58	3	8	
Asabellides oculata				393	3	3	1	7	5	
Phyllodoce arenae				7		6	2	3	5	
Nephtys picta				5	1	6	3	5	3	
Tanaissus psammophilus		1	1	1	1	24	10	17	2	
Pseudunciola obliquua						30	3	4	2	
Americamysis bigelowi						18	9	3	8	
Spiochaetopterus oculatus					4	6	9	30	13	
Dispio uncinata				1	15	4	5	14	13	
Magelona papillicornis						1	8	4	11	
Rhepoxynius hudsoni			1	1	1	2	3	3	9	
Turbonilla interrupta							34	8	3	
Acanthohaustorius shoemakeri								7	1	
Owenia fusiformis						5	2	2	1	
Tharyx acutus						1	2	4		
Glycera dibranchiata				64						3
Mitrella lunata				34		1				
Pectinaria gouldii				14						
Nereis succinea				11				1		
Petricola pholadiformis				9					1	
Nucula proxima	2	89	1	114		1	1	3		
Tellina agilis	2	1	4	40			9			
Caulleriella sp.J		2	8	14		2			1	
Unciola irrorata				5		5	1			
Diastylis polita		4		1		4				
Acanthohaustorius millsi	2			3	1		30	1		4
Euspira heros	2			9	3	1	5	1	2	
Ilyanassa trivittata	1			11	3		1			
Parahaustorius attenuatus		1			6	1				
Spisula solidissima	1	5	1	1	4		3	10	4	
Donax variabilis					6			4	4	
Chiridotea tuftsi	2				6	1			4	
Oxyurostylis smithi				1	1			1	2	

[a] Due to the heterogeneity of most taxa distributions, generally low abundances, and relatively limited sampling, only well-defined species groups generated from the inverse analyses are numbered.

[b] LPIL = Lowest practical identification level.

Table 6-13. Two-way table from normal (Station Groups A-C) and inverse (Species Groups 1-3[a]) cluster analysis of infaunal samples collected during the May 1998 Survey 1 (S1) and September 1998 Survey 2 (S2) in Sand Resource Area G2 offshore New Jersey. Data are presented as total counts for individual taxa.

Taxon	A	B				C							
	S2-G2-2	S1-G2-2	S1-G2-4	S2-G2-1	S2-G2-4	S1-G2-10	S2-G2-10	S2-G2-12	S2-G2-3	S2-G2-7	S1-G2-8	S2-G2-8	
Mytilus edulis		39	67								1		
Diastylis polita		38			1								
Nereis succinea	73				1								
Petricola pholadiformis	54				1								
Anachis lafresnayi	33												
Brania wellfleetensis												22	
Asabellides oculata	1,045	4	8	72	2				1	1			
Nucula proxima	1,026	74		14	1				1	1			
Edotia triloba	28	19	2	5				3					
Nephtys picta	3	4	3	13	7			1	1	1			
Ilyanassa trivittata		9		8	4			1	1				
Spiochaetopterus oculatus		1		12	1		1	1	4	6			1
Phyllodoce arenae	1			7	2		2	1	4	4			
Euspira heros	5		2	4	4		1		1	4			
Apoprionospio pygmaea				359	163				2			2	
Tharyx acutus	7			65			1						
Loimia medusa				13									
Spiophanes bombyx		1,652	75	32	18	2	2		37	32	3	4	
Polygordius (LPIL[b])		20	44	358	13	8	30	7	4	8	295	49	
Tellina agilis	4	12	27	38	5		42	7	2	13	2	4	
Protohaustorius wigleyi	2		36	5	16	7	12		5	9	1		
Spisula solidissima		11	7	5	8	22	3		1	2	13	1	2
Chiridotea tuftsi			27	1					1	2	1	4	
Acanthohaustorius millsi			26		7				15	1	2		
Magelona papillicornis			6	3	1				11	4			
Unciola irrorata			12	6	1		2						
Sigalion arenicola			1	3			2	2	1			2	
Dispio uncinata					6				7	29			
Parahaustorius attenuatus						1			1	8			
Pseudunciola obliquua							8	25	46	12			
Rhepoxynius hudsoni			3		2	7	7	12	23	7			
Oxyurostylis smithi				1			4	18	6	2		1	3
Tanaissus psammophilus						2	42	15	1	7	61	79	
Politolana polita							10	2	1	6		11	
Caulleriella sp.J		1	1	2		2	6		4	1	1	1	
Echinarachnius parma		4				6	6		2				
Exogone hebes						2	5			1			
Aricidea cerrutii											21	1	
Hemipodus roseus								4			5		
Streptosyllis arenae						1	1	1			4	1	

[a] Due to the heterogeneity of most taxa distributions, generally low abundances, and relatively limited sampling, only well-defined species groups generated from the inverse analyses are numbered.

[b] LPIL = Lowest practical identification level.

bivalve (*N. proxima*) and gastropod (*E. heros* and *I. Trivittata*) mollusks and the isopod *Edotia triloba*. Species Group 2 included the most homogeneously distributed taxa in Area G2. Numerically dominant taxa in Group 2 included the polychaete *S. bombyx*, archiannelid *Polygordius*, and bivalve *T. agilis*. Other Group 2 taxa included the polychaetes *M. papillicornis* and *Sigalion arenicola*, bivalve *Spisula solidissima*, isopod *C. tuftsi*, and amphipods *A. millsi, P. wigleyi,* and *U. irrorata.* Species Group 3 contained mostly crustaceans, including *O. smithi*, *Parahaustorius attenuatus*, *Politolana polita*, *Pseudunciola obliquua*, *R. hudsoni*, and *T. psammophilus*. Other Group 3 taxa included the polychaetes *Caulleriella* sp. J and *E. hebes* and echinoid *E. parma*.

Species Group 1 was associated primarily with Station Groups A and B, Species Group 2 was associated with stations in Groups B and C, and Group 3 taxa were associated primarily with Station Group C (Table 6-13). Group B stations were located in the southwestern corner of Area G2, while Group C stations were located primarily in the northeastern corner of this sand resource area. Station 2 was located in a trough feature that apparently is an area of fine sediment deposition; sediments at this station were classified as sandy mud (May) or silty sand (September). Station 2 yielded very high abundances of the polychaetes *A. oculata* and *S. bombyx* and bivalve *N. proxima.*

Area G3

Normal cluster analysis resulted in three station groups in Area G3 (Groups A through C) that were separated by survey (Table 6-14). Group A contained a single station sampled during the September survey that yielded high numbers of the polychaetes *A. oculata* and *N. succinea*, bivalve *P. pholadiformis*, and gastropod *Anachis lafresnayi*. Station Group B consisted of three stations from the May survey that yielded high numbers of the polychaete *S. bombyx*, bivalve *S. solidissima,* isopod *C. tuftsi*, and echinoid *E. parma*. The bivalve *M. edulis* and amphipod *Americhelidium americanum* were found only at Group B stations. Group C included six stations from the September survey that yielded high numbers of the polychaete *Spiochaetopterus oculatus,* archiannelid *Polygordius*, amphipods *Pseudunciola obliquua* and *R. hudsoni*, and tanaid *T. psammophilus*. Several taxa were found only at Group C stations, including the polychaetes *D. uncinata* and *Nephtys bucera*, isopod *Ancinus depressus,* and amphipod *Acanthohaustorius shoemakeri*.

Inverse cluster analysis resulted in four groups of co-occurring taxa (Groups 1 through 4) (Table 6-14). Species Groups 1 and 2 contained heterogeneously distributed taxa, while Groups 3 and 4 were distributed more evenly across Area G3 stations. Group 1 included the bivalve *M. edulis*, gastropod *Odostomia gibbosa*, the crustaceans *A. americanum* and *U. irrorata* (amphipoda), *C. tuftsi* (isopoda), and *Pseudoleptocuma minor* (cumacea), and echinoid *E. parma*. Group 2 included the polychaetes *Apoprionospio pygmaea*, *D. uncinata*, and *S. oculatus*, gastropod *T. interrupta,* and crustaceans *Ancinus depressus* (isopod), *Acanthohaustorius shoemakeri* and *Microprotopus raneyi* (amphipods), and *Americamysis bigelowi* (mysid). Species Group 3 was the most homogeneously distributed group, and included polychaetes (*Caulleriella* sp. J and *S. bombyx*), the archiannelid *Polygordius*, bivalves (*S. solidissima* and *T. agilis*), amphipods (*Protohaustorius wigleyi*, *Pseudunciola obliquua*, and *R. hudsoni*), and the tanaid *T. psammophilus*. Group 4 contained mostly polychaetes, including *A. oculata*, *Diopatra cuprea*, *Nephtys picta*, *Nereis succinea*, and *P. arenae*, and also included the bivalves *N. proxima* and *P. pholadiformis,* gastropod *Anachis lafresnayi*, and isopod *E. triloba*.

Species Group 1 was associated with Station Group B, while Species Group 2 was associated with Station Group C. Species Groups 3 and 4 were distributed across all station

Table 6-14. Two-way table from normal (Station Groups A-C) and inverse (Species Groups 1-4[a]) cluster analysis of infaunal samples collected during the May 1998 Survey 1 (S1) and September 1998 Survey 2 (S2) in Sand Resource Area G3 offshore New Jersey. Data are presented as total counts for individual taxa.

Taxon	A	B			C						
	S2-G3-5	S1-G3-3	S1-G3-1	S1-G3-5	S2-G3-1	S2-G3-4	S2-G3-7	S2-G3-3	S2-G3-2	S2-G3-9	
Odostomia gibbosa				17							1
Chiridotea tuftsi		1	16	38	2			1		1	
Echinarachnius parma			12	20					3	4	
Unciola irrorata			5	26			2				
Pseudoleptocuma minor			8	4					1		
Mytilus edulis		1	3	9							
Amerinchelidium americanum		1	6	2							
Apoprionospio pygmaea	1				55		4				2
Microprotopus raneyi	14				16		4	1			
Spiochaetopterus oculatus	1				17	4	1	6	2		
Ancinus depressus					11	1	6	4			
Dispio uncinata					11	7	3				
Acanthohaustorius shoemakeri					27				1	1	
Turbonilla interrupta					11						
Americamysis bigelowi					7						
Spiophanes bombyx	1	8	42	1,833	6	6		2	5		3
Spisula solidissima	2	8	8	36	2	1	1		2		
Caulleriella sp.J	12		2	160		21	6		8	5	
Polygordius (LPIL[b])	1	18	37	38	263	600	93	64	34	16	
Pseudunciola obliquua				3	20	26	12	3	12	14	
Rhepoxynius hudsoni			3	2	16	21	5	4	10	2	
Tellina agilis	17	1	3	11	8	8	4	22	18	12	
Tanaissus psammophilus		4	2	4	4	44	11	8	50	83	
Protohaustorius wigleyi		8	7	4	3	8	6	4	10	8	
Asabellides oculata	553		3	2	37	3	31	4			4
Nephtys picta	20	1	3	12	7	1	9				
Nucula proxima	11		1	10	1	1					
Petricola pholadiformis	48				2	1			1		
Anachis lafresnayi	25			1	1						
Edotia triloba	12			2	1		12			1	
Phyllodoce arenae	7				2	2	6	1	1	1	
Nereis succinea	11					1	2				
Diopatra cuprea	6						1			1	
Acanthohaustorius millsi		3	6			2	4	3			
Magelona papillicornis				5	1	3	2				
Ilyanassa trivittata			1			2	6				
Euspira heros	1		1	1		2	2				
Hesionura elongata			1							20	
Aricidea cerrutii									1	9	
Tectonatica pusilla	4				2	1		5	2	4	
Politolana polita		2						11	9	7	
Streptosyllis arenae		2						2	2	4	
Nephtys bucera						2	1	2		1	
Oxyurostylis smithi	1						7	2		4	
Hemipodus roseus							1	1		4	
Brania wellfleetensis									11		
Diastylis polita						2			4		

[a] Due to the heterogeneity of most taxa distributions, generally low abundances, and relatively limited sampling, only well-defined species groups generated from the inverse analyses are numbered.

[b] LPIL = Lowest practical identification level.

groups, although Group 4 taxa were most abundant in Station Group A (Table 6-14). Sediments were homogeneous in Area G3, consisting primarily of sand. Station groups were separated by survey, and water depth also may have been a factor influencing assemblage composition. Station 5 was situated in a trough feature, was the deepest station in Area G3, and yielded relatively high abundances of certain taxa, including polychaetes *A*. *oculata*, *Caulleriella* sp. J, and *S*. *bombyx*.

6.3.4 Epifauna and Demersal Fishes

During the May 1998 Survey 1, a total of 17,474 individuals in 29 taxa was collected by trawl at six of the eight sand resource areas (Table 6-15). An extremely large catch of the sand dollar *E. parma* at Area F2 contributed 17,005 individuals to this total. In addition to the sand dollar, 469 specimens of epifauna and demersal fishes were collected in 28 taxa. Trawls yielded 107 individuals in 15 fish taxa and were numerically dominated by hakes (*Urophycis* spp.), clearnose skate (*Raja eglanteria*), windowpane (*Scophthalmus aquosus*), scup (*Stenotomus chrysops*), and summer flounder (*Paralichthys dentatus*). Invertebrates excluding the sand dollar contributed 13 taxa and 362 specimens to the trawl catches. The sea star *Asterias forbesi*, hermit crab *Pagurus* sp., sand shrimp *Crangon septemspinosa*, and rock crab *Cancer irroratus* were the top ranking species in terms of abundance. A single adult Atlantic surfclam (*S. solidissima*) specimen was collected in Area A1 and two adult specimens were collected at Area F2 during the May survey.

The highest number (19) of taxa (fishes and invertebrates combined) was recorded for Area C1 during May 1998; the lowest number (5) of fish and invertebrate taxa was recorded for Area A1. The number of invertebrate and fish taxa collected per haul averaged 12.3. Area G2 yielded the most fish taxa (10), followed by Areas C1 and G3 (8 taxa each). The number of fish taxa per haul ranged from 1 to 10 and averaged 5.8. Area C1 produced the highest number (11) of invertebrate taxa, followed by Area F2 (9). The number of invertebrate taxa per haul ranged from 4 to 11 and averaged 6.5.

The most specimens of fishes and invertebrates combined were recorded from Areas F2 (17,095) and C1 (169) during the May 1998 survey. The numbers of fish and invertebrate individuals collected per haul ranged from 14 to 17,095 and averaged 2,912.3. Fishes were not abundant; highest catches came from Areas G2 (36) and C1 (34). The number of fish individuals collected per haul ranged from 1 to 36 and averaged 17.8. A huge catch of sand dollars in Area F2 overwhelmed invertebrate abundance estimates. Without considering Area F2, Area C1 yielded the highest number of invertebrate specimens (135) and Area A2 the lowest (12). The number of invertebrate individuals collected per haul ranged from 12 to 17,084 and averaged 2,894 (including sand dollars). Excluding sand dollars, the numbers of invertebrate individuals ranged from 10 to 132 and averaged 60.3.

During the September 1998 Survey 2, eight trawl samples at seven of the eight sand resource areas produced 31 taxa (19 fishes and 12 invertebrates) represented by 2,541 individuals (761 fishes and 1,780 invertebrates) (Table 6-16). As with Survey 1, the most abundant species was the sand dollar represented by 864 individuals. This was followed by squid (*Loligo* sp.) and bay anchovy (*Anchoa mitchilli*) contributing 637 and 630 individuals, respectively. Other abundant fish species in the catches included clearnose skate, northern searobin (*Prionotus carolinus*), and scup. Other numerically important invertebtrates caught during Survey 2 were sea star, hermit crab (*Pagurus longicarpus*), common northern moon-shell (*Euspira* [*Lunatia*] *heros*), and squid (*Loligo pealei*).

Table 6-15. Epifauna and demersal fishes collected by mongoose trawl and ranked by numerical abundance from the May 1998 Survey 1 at six potential sand resource areas offshore New Jersey.

Species	Area						Total
	A1	A2	C1	F2 (F2-Out)	G2	G3	
FISHES							
Urophycis sp.			11	4	8	3	26
Raja eglanteria			5	2	13	5	25
Scophthalmus aquosus	1	2	5	1		7	16
Paralichthys dentatus				1	7		8
Stenotomus chrysops			6		1	1	8
Pleuronectes americanus			1	1	1	3	6
Raja egg case			4	1		1	6
Merluccius bilinearis			1		1		2
Prionotus carolinus				1	1		2
Prionotus evolans					2		2
Syacium sp.						2	2
Ammodytes americanus					1		1
Anchoa mitchilli						1	1
Lophius americanus			1				1
Peprilus triacanthus					1		1
INVERTEBRATES							
Echinarachnius parma		2	3	17,000			17,005
Asterias forbesi		1	88	33			122
Pagurus sp.	1	5	22	5	20	6	59
Crangon septemspinosa		2	4	11	29	7	53
Cancer irroratus			9	13	26		48
Loligo pealei	28	2	2	6	2	1	41
Euspira heros	2			13	6	4	25
Ilyanassa trivittata				1		3	4
Spisula solidissima	1			2			3
Ensis directus			2				2
Pagurus pollicarus			2				2
Libinia dubia			1				1
Nudibranch sp.			1				1
Pandalus sp.			1				1
FISH TOTALS							
Total Individuals	1	2	34	11	36	23	107
Total Taxa	1	1	8	7	10	8	15
INVERTEBRATE TOTALS							
Total Individuals	32	12	135	17,084	83	21	17,367
Total Taxa	4	5	11	9	5	5	14
FISH AND INVERTEBRATE TOTALS COMBINED							
Total Individuals	33	14	169	17,095	119	44	17,474
Total Taxa	5	6	19	16	15	13	29

Table 6-16. Epifauna and demersal fishes collected by mongoose trawl and ranked by numerical abundance form the September 1998 Survey 2 at seven potential sand resource areas offshore New Jersey

Species	Area								Total
	A1	A2	C1	F2 (F2-In)	F2 (F2-Out)	G1	G2	G3	
FISHES									
Anchoa mitchilli						630			630
Raja eglanteria	8	32						1	41
Prionotus carolinus	4	4	3		2	1		7	21
Stenotomus chrysops			1			13		1	15
Paralichthys sp.		9							9
Peprilus triacanthus			2			1	5		8
Raja egg case			1		7				8
Raja ocellata				2	6				8
Paralichthys dentatus		1	2		2				5
Centropristis striata	2	1							3
Trachinocephalus myops		2	1						3
Cynoscion regalis								2	2
Micropogonias undulatus						1		1	2
Chilomycterus schoepfi						1			1
Fistualria tabacaria						1			1
Pleuronectes ferrugineus					1				1
Raja sp.				1					1
Scophthalmus aquosus			1						1
Sphoeroides dorsalis								1	1
INVERTEBRATES									
Echinarachnius parma	3	11	8	707	135				864
Loligo sp.		22	80	157	84	120	144	30	637
Asterias forbesi	8	27	97	1		3	4	2	142
Pagurus longicarpus	6	16	10	4	8	8	7	2	61
Euspira heros				2	27				29
Loligo pealei	16								16
Cancer irroratus		1	1	3	5				10
Ilyanassa trivittata				2	6		1		9
Pagurus pollicarus	2	3						2	7
Libinia dubia			2		1				3
Astarte castenea					1				1
Homarus americanus					1				1
FISH TOTALS									
Total Individuals	14	49	11	3	18	648	5	13	761
Total Taxa	3	6	7	2	5	7	1	6	19
INVERTEBRATE TOTALS									
Total Individuals	35	80	198	876	268	131	156	36	1,780
Total Taxa	5	6	6	7	9	3	4	4	12
FISH AND INVERTEBRATE TOTALS COMBINED									
Total Individuals	49	129	209	879	286	779	161	49	2,541
Total Taxa	8	12	13	9	14	10	5	10	31

A trawl haul (F2-Out) at Area F2 produced the highest number (14) of total taxa during September 1998, followed by the haul in Area C1 which produced 13 taxa. The fewest total taxa (5) were collected in Area G2. On average, the total number of combined taxa per haul was 10.1. The greatest number of fish taxa (7) was collected in Areas C1 and G1. The number of fish taxa per haul ranged from 1 to 7 and averaged 4.6. The number of invertebrate taxa per haul ranged from 3 in Sand Resource Area G1 to 9 at Sand Resource Area F2 (F2-Out). The average number of invertebrate taxa per trawl haul was 5.5.

Total catches during September 1998 varied among sand resource areas, ranging from 49 individuals in Areas A1 and G3 to 879 individuals in Area F2 (F2-In). The average catch was 317.6 individuals per haul for all eight areas. Fish catches ranged from 3 individuals in Area F2 (F2-In) to 648 individuals in Area G1 and averaged 95.1 individuals per haul. Invertebrate catches ranged from 35 in Area A1 to 876 individuals per haul in Area F2 (F2-In). The average invertebrate catch per haul was 222.5 individuals per haul.

Normal cluster analysis of the trawl samples revealed two major station groups, A and B, that separated the samples by survey (Table 6-17). The first, Group A, consisted of all samples from the May 1998 Survey 1, whereas Group B included the eight samples from September 1998 Survey 2. Within Group B, the samples were arranged in a north-south fashion suggesting a gradient of species composition.

The inverse analysis formed six species groups (Table 6-17). Two of these groups consisted of single species. Group 1 was composed of taxa collected frequently during both surveys. Group 2 consisted of taxa collected mostly during the May 1998 Survey 1.

6.4 DISCUSSION

Benthic assemblages surveyed from the sand resource areas offshore New Jersey consisted of members of the major invertebrate and vertebrate groups commonly found in the study area. Numerically dominant infaunal groups included numerous crustaceans, echinoderms, molluscans, and polychaetes, while epifaunal taxa consisted primarily of decapods, sand dollars, gastropods, and squids. The numerically dominant infaunal and epifaunal groups collected during the 1998 sand resource areas surveys are typical components of benthic assemblages in the study area. Similarly, the numerically dominant demersal fishes collected in trawls within the resource areas revealed consistency with previous surveys. Fishes such as bay anchovy (*Anchoa mitchilli*), clearnose skate (*Raja eglanteria*), northern searobin (*Prionotus carolinus*), scup (*Stenotomus chrysops*), and windowpane (*Scophthalmus aquosus*) were numerical dominants during the surveys and these species consistently are among the most ubiquitous and abundant demersal taxa in the region (Able and Hagen, 1995; Barry A. Vittor & Associates, Inc., 1999a).

Results of the 1998 sand resource area surveys support the findings of other investigations that have found strong associations of infaunal taxa with particular sedimentary habitats (Pearce et al., 1981; Chang et al., 1992; Theroux and Wigley, 1998). Canonical correlation analysis indicated that the composition of benthic assemblages inhabiting New Jersey resource areas was affected primarily by relative percentages of gravel and sand comprising surficial sediments at area stations. Surficial sediments were mixtures of sand and gravel at most stations in the northernmost resource areas (Areas F1 and F2), as compared to more varied habitat types in the other more southern resource areas (Areas A1, A2, C1, G1, G2, and G3). The southernmost resource areas included several stations with relatively high gravel content, but most other stations in these areas were characterized by sand bottoms (Figure 6-15). Infaunal assemblage distributions reflected these sediment type distributions. Station groupings based on normal cluster analysis of infaunal samples from the resource area

Table 6-17. Two-way table from normal (Station Groups A and B) and inverse (Species Groups 1-4) cluster analysis of trawl samples collected during the May 1998 Survey 1 (S1) and September 1998 Survey 2 (S2) from sand resource areas (A1, A2, C1, F2, G1, G2, and G3) offshore New Jersey. Data are presented as total counts for individual taxa.

Taxa	A						B								
	S1-A1	S1-A2	S1-C1	S1-G2	S1-F2 (Out)	S1-G3	S2-A1	S2-A2	S2-C1	S2-G1	S2-G2	S2-G3	S2-F2 (In)	S2-F2 (Out)	
Echinarachnius parma		2	3		17,000		3	11	8				707	135	1
Loligo sp.								22	80	120	144	30	157	84	
Pagurus longicarpus							6	16	10	8	7	2	4	8	
Asterias forbesi		1	88		33		8	27	97	3	4	2	1		
Prionotus carolinus				1	1		4	4	3	1		7		2	
Paralichthys dentatus				7	1			1	2					2	
Libinia dubia			1						2					1	
Peprilus triacanthus				1					2	1	5				
Ilyanassa trivittata					1	3					1		2	6	
Raja ocellata													2	6	2
Anchoa mitchilli						1				630					
Stenotomus chrysops			6	1		1			1	13		1			
Raja eglanteria			5	13	2	5	8	32				1			
Pagurus sp.	1	5	22	20	5	6									
Crangon septemspinosa		2	4	29	11	7									
Urophycis sp.			11	8	4	3									
Scophthalmus aquosus	1	2	5		1	7			1						
Loligo pealei	28	2	2	2	6	1	16								
Cancer irroratus			9	26	13			1	1				3	5	
Euspira heros	2			6	13	4							2	27	
Pleuronectes americanus			1	1	1	3									
Merluccius bilinearis			1	1											
Ensis directus			2												
Prionotus evolans				2											
Spisula solidissima	1				2										3
Pagurus pollicaris			2				2	3				2			4
Centropristis striata							2	1							
Paralichthys sp.								9							
Trachinocephalus myops								2	1						
Syacium sp.						2									5
Cynoscion regalis												2			6
Micropogonias undulatus										1		1			

surveys indicated homogeneity of infaunal assemblage types in the northern resource areas and varied assemblage types in the southernmost resource areas (Figure 6-14). Each of the adjacent stations (R1, R2, and R3) were included in the same Station Group (Group C, A, and F, respectively) for both the May and September surveys. The latitudinal difference in infaunal assemblage and sediment-type distributions was reflected by the second canonical variate, which correlated best with relative geographic location (northing and easting) of resource areas and adjacent stations.

Resource area stations with surficial sediments containing a relatively high percentage of gravel supported a number of taxa that were rare at stations characterized by a sand substratum. These gravel-inhabiting taxa included bivalves, such as *Astarte castanea*, *Crenella decussata* and *Mytilus edulis*, suspension-feeding invertebrates that feed efficiently when buried in coarse sediments. The gastropods *Crepidula fornicata* and *Mitrella lunata* and the polychaetes *Harmothoe imbricata*, *Hemipodus roseus*, and *Pisione remota* also were positively associated with gravel-sized sediments, habitat which provides interstitial space for these types of foraging carnivores (Pettibone, 1963; Young and Rhoads, 1971).

The most ubiquitous infauna collected during the surveys tended to exhibit greatest population densities at stations characterized by sand. Infaunal taxa that were abundant in sand included the polychaetes *Caulleriella* sp. J (= *C*. cf. *killariensis*) and *Spiophanes bombyx*, archiannelid *Polygordius*, bivalve *Tellina agilis*, amphipods *Acanthohaustorius millsi*, *Pseudunciola obliquua*, *Protohaustorius wigleyi,* and *Rhepoxynius hudsoni*, and tanaid *Tanaissus psammophilus*. Numerical dominance by these taxa in sand habitats reaffirms results from previous investigations in the study area (Pearce et al., 1981; Chang et al., 1992). Certain of the numerically dominant infaunal taxa were distributed across a range of sedimentary habitats (i.e., sand and gravel), especially the annelids *Polygordius* and *S. bombyx*. The free-living, burrowing amphipods *A. millsi*, *Pseudunciola obliquua*, *Protohaustorius wigleyi,* and *R. hudsoni* comprised a group that were positively associated with sand and negatively associated with gravel during the resource areas surveys, the only example of such an association clearly defined from the 1998 data.

Juvenile surf clam (*Spisula solidissima*) distribution in relation to sedimentary habitat agreed with previous investigations of Mid-Atlantic shelf waters (Parker, 1967; Parker and Fahlen, 1968). Stations with substantial gravel content tended to yield greater abundance than areas with high percentages of sand. Juvenile surf clam abundance was greatest in Areas F1 (September 1998 Survey 2) and F2 (May 1998 Survey 1), where gravel content of surficial sediments was consistently higher than in other resource areas. Juvenile surf clams also were common in sand bottom habitats, as has been observed by other investigations (Pearce et al., 1981), indicating no selective settlement of surf clam spat. Reasons for higher surf clam abundance in areas with measurable gravel, therefore, likely are post-settlement ecological factors, such as possibly higher rates of clam survivorship in gravel habitats relative to sand.

Stations that had a relatively high percentage of mud or silt yielded high numbers of deposit feeding taxa such as the polychaetes *Asabellides oculata* and *Capitella capitata* and the nut clam *Nucula proxima*. These species typically are strongly associated with fine sediments (Pearce et al., 1981; Chang et al., 1992).

In addition to sedimentary habitat, canonical discriminant analysis indicated that the composition of benthic assemblages inhabiting New Jersey sand resource area stations was somewhat affected by water depth. Within areas, station water depths varied primarily due to patchy bathymetric features (i.e., ridges and troughs). Depths of shallower stations in most areas generally ranged between 10 and 12 m, while the deepest stations had depths of 17 to 19 m; however, depth-related variability in benthic assemblage composition likely is due more to

environmental parameters that are correlated with water depth. In other words, absolute water depth may be an ultimate factor influencing benthic assemblages, but hydrology and sedimentary regime are proximate factors that are influenced to some degree by water depth.

Bathymetric features can affect environmental variables that determine the suitability of infaunal habitats. Trough features, especially those that are spatially abrupt, tend to dissipate current flow and promote deposition of fine materials that are suspended in the water column. An example of this was evident in Area G2, where Station 2 was located in a trough feature that apparently is an area of fine sediment deposition; sediments at this station were classified as sandy mud (May) and silty sand (September). This station yielded very high abundances of the polychaetes *A. oculata* and *S. bombyx* and the nut clam *N. proxima*. These organisms, along with spionid polychaetes (*Apoprionospio dayi* and *Spio setosa*) and certain amphipods (*Ampelisca* spp. and *Unciola irrorata*), are trough-inhabiting taxa and deposit feeders that are adapted to living in fine sediments. Some stations located in trough features adjacent to ridges supported relatively high numbers of the polychaete *A. oculata* during the September survey. In Area A2, Station 19 was the deepest infaunal station and supported an assemblage distinct from other Area A2 stations during both the May and September surveys, including an abundance of the polychaete *S. setosa* and amphipods *Ampelisca abdita* and *U. irrorata*.

Depth-related variability in benthic assemblage composition during the surveys may be discerned by comparing stations that were in proximity to one another, yet supported different infaunal assemblages even if they were characterized by a similar sedimentary regime. In Area A1, for example, Station 13 was situated in a trough feature (20 m depth), while other A1 stations had an average depth of about 14 m. Despite having sediments similar to other stations in Area A1, this station supported distinct assemblages during both the May (e.g., polychaete *Pisione remota* and bivalve *M. edulis*) and September (e.g., polychaete *A. dayi* and amphipod *Ampelisca* sp. X) surveys.

In addition to sediment-based and bathymetry-based spatial variability in the southern resource areas, there were temporal differences in the composition of infaunal assemblages. Canonical discriminant analysis indicated that the composition of benthic assemblages inhabiting stations was affected to a substantial degree by survey. In the southern resource areas, Station Groups B and E included samples collected during the September survey, while Group D contained stations sampled in May. Temporal changes in infaunal assemblages were not observed among northern resource areas (F1 and F2). In the northern areas, temporal effects on the composition of infaunal assemblages may have been overridden by local sedimentary habitats.

Temporal variability in infaunal assemblage composition was evidenced by both qualitative and quantitative community measures. Nearly half of the infaunal taxa sampled over the entire project were included in both the May and September surveys; however, most (68%) of the remainder of censused taxa were collected only during the September cruise, resulting in higher mean values of species richness compared to the May survey (Table 6-4). It is unknown whether higher measurements of infaunal taxa richness in September were due primarily to temporal recruitment patterns or were an artifact of an expanded September sampling effort, when twice the number of samples were collected as were collected during the May survey. Also, overall infaunal abundance was greater during the May survey than was observed during September. Temporal variation of infaunal density is typical of the study area, although consistent patterns of variability are difficult to identify (Pearce et al., 1976), and may not exist for many infaunal taxa. Both the number of epifaunal taxa and overall epifaunal abundance were greater in September as compared to the May survey, as well, and this temporal abundance pattern also is characteristic of the study area (Hales et al., 1995; Viscidio et al., 1997).

Offshore New Jersey, there is considerable variation in the abundance and distribution of demersal taxa, both spatially and seasonally (Able and Hagen, 1995; Barry A. Vittor & Associates, Inc., 1999a), and this dynamic may have been manifest in the results of the sand resource area surveys. Ultimately, low fish densities and relatively limited sampling preclude any definitive statements about causes of variability in fish abundance and distribution, based on the results of the surveys. However, some variability between areas was apparent in the composition of trawls. In particular, during the May survey, both overall fish abundance and the number of fish taxa were markedly lower in Areas A1 and A2 compared to other resource areas. Reasons for this distributional variability are not apparent; hydrological parameters measured concurrently with trawls did not differ between Areas A1 and A2 and the more northern areas. Neither was infaunal and epifaunal (potential prey) abundance lower in Areas A1 and A2 than in the more northerly stations. Given that there were no apparent habitat differences between areas, low fish abundance in Areas A1 and A2 simply may have been a matter of natural variability, perhaps due to seasonality. The various areas yielded comparable fish abundance and species richness measurements during the September survey.

Some patterns of fish distribution and abundance that are comparable to historic data were found during the surveys. Overall, fish abundance was higher in September than in May, due primarily to a large number of bay anchovy sampled from Area G1. This abundance pattern agrees with the results of previous long-term sampling efforts that found peak fish abundance occurs in offshore New Jersey waters during the months September through November, largely due to an abundance of bay anchovy (Able and Hagen, 1995). Windowpane was much more common in September trawls than those taken during the May survey, a temporal abundance pattern observed previously for this species (Able and Hagen, 1995; Barry A. Vittor & Associates, Inc., 1999a).

The results of the sand resource area surveys agree well with previous descriptions of benthic assemblages residing in shallow shelf waters offshore New Jersey. Overall, canonical discriminant analysis indicated that sedimentary regime most affected the composition of infaunal assemblages. Trough and sand ridge features further contributed to the prominent spatial variability exhibited by infaunal assemblages. Bathymetric features contribute to a multi-dimensional heterogeneity of benthic habitats that vary temporally as well as spatially. Despite inherent spatial and temporal heterogeneity in the distribution and abundance of demersal taxa, results of the 1998 surveys of the sand resource areas generally are consistent with historical demersal survey results in the region.

7.0 POTENTIAL EFFECTS

One of the primary purposes of this project is to provide site-specific information for decisions on requests for non-competitive leases from local, State, and Federal agencies. The information may be used to determine whether or not stipulations need to be applied to a lease. The information also may be incorporated into an Environmental Assessment (EA) or Environmental Impact Statement (EIS), if so required.

Environmental impact analyses of mining operations should be based on commodity-specific, technology-specific, and site-specific information, whenever possible (Hammer et al., 1993). First, the specific mineral of interest and the technological operations for a specific mining operation need to be defined because these two parameters determine the impact producing factors that need to be considered. Once the impact producing factors are known, this information can be translated into statements concerning the impacts that might occur to the full suite of potentially affected environmental resources that may need to be addressed, including geology, chemical and physical oceanography, air quality, biology, and socioeconomics. Then, decisions can be made regarding the type of mitigation necessary to determine the preferred alternative for a specific marine mining operation to acquire project approval.

This section focuses on providing information on potential impacts related to physical processes and biological considerations of sand mining for beach nourishment from seven of the eight sand resource areas offshore New Jersey. Sand for beach replenishment is the commodity of interest. Two primary dredging technologies are available for offshore sand mining operations, depending on distance from source to project site, the quantity of sand being dredged, and the depth to which sand is extracted at a site (Herbich, 1992). They are: 1) cutterhead suction dredge, where excavated sand is transported through a direct pipeline to shore, and 2) hopper dredge, where sand is pumped to the hopper, transported close to the replenishment site, and pumped to the site through a pipeline from the hopper or from a temporary offshore disposal area close to the beach fill site. As a general rule, cutterhead suction dredging is most effective for projects where the sand resource is close to shore (within 8 km), the dredging volumes are large (>8 MCM), and the excavation depth is on the order of 2.5 to 4 m (Taylor, 1999). Hopper dredging becomes a more efficient procedure when sand resource areas are greater than 8 km from shore, dredging volumes are relatively small (<2 MCM), and the excavation depth at the sand resource area is less than 2 m (Taylor, 1999). Ultimately, a combination of these factors will be evaluated by dredgers to determine the most cost effective method of sand extraction and beach replenishment for a given project. Availability of dredging equipment also may be a factor for determining the technique to be used; however, the number of cutterhead suction and hopper dredges in operation is about equal in the industry today (Taylor, 1999). As such, both technologies will be evaluated for potential biological effects.

7.1 OFFSHORE SAND RESOURCE AREAS

Eight potential sand resource areas were identified offshore New Jersey in Federal waters by the NJGS and the U.S. Minerals Management Service, INTERMAR. All sand resource areas are very similar geologically (coarse-to-fine sand-ridge deposits with relief of 3 m or greater and resource volumes of at least 2 MCM). However, sand from the borrow site in Sand Resource Area C1 has a median grain size of 0.2 mm (fine sand), the smallest grain size for any of the potential resource areas. Regardless, all identified potential sand borrow sites are of great interest to the State, primarily due to their proximity to eroding beaches critical for storm protection and recreation. Physical processes (waves and currents) and biological habitat at

borrow sites on the sand ridges illustrate minor variability offshore New Jersey. However, habitat variability within resource areas varies widely depending on surface area boundaries and geographic position. Although these eight potential sand resource areas were designated as ones with greatest potential, it is possible that sand could be dredged from intervening offshore areas because consistency of shoal deposits is widespread seaward of the New Jersey coast.

The amount of dredging that occurs at any given site is a function of Federal, State, and local needs for beach replenishment. There is no way of predicting the exact sand quantities needed in the foreseeable future, so an upper value for any given project was estimated based on discussions with State personnel and the MMS. Preliminary analysis of short-term impacts (storm and normal conditions) at specific sites along New Jersey beaches indicates that about 2 MCM of sand could be needed for a given beach replenishment event. Long-term shoreline change data sets suggest that a replenishment interval of about 5 to 10 years would be expected to maintain beaches. This does not consider the potential for multiple storm events impacting the coast over a short time interval, nor does it consider longer time intervals absent of destructive storm events. Instead, the estimate represents average change over decades that is a reasonable measure for coastal management applications.

Given the quantity of 2 MCM of sand per beach replenishment event, the surface area covered for evaluating potential environmental impacts is a function of the average dredging depth. Two factors should be considered when establishing dredging practice and depth limits for proposed extraction scenarios. First, regional shelf sediment transport patterns should be evaluated to determine net transport directions and rates. It is more effective to dredge the leading edge of a migrating shoal, and infilling of dredged areas occurs more rapidly at these sites (Byrnes and Groat, 1991; Van Dolah et al., 1998). Second, shoal relief above the ambient shelf surface should be a determining factor controlling depth of dredging. Geologically, shoals form and migrate on top of the ambient shelf surface, indicating a link between fluid dynamics, sedimentology, and environmental evolution (Swift, 1976). As such, average shoal relief is a reasonable depth threshold for maintaining environmentally-consistent sand extraction procedures.

A primary question addressed by the modeling efforts relates to sediment transport and infilling estimates at potential borrow sites and the impact of dredging operations on these estimates. Combined wave-current interaction (waves mobilize the seabed and currents transport the sediment) at the borrow sites results in a net direction of transport into and out of potential sand resource areas. Historical sediment transport dynamics suggest that the net direction of sediment movement is from north to south, and the rate at which sand moves along the shelf varies.

7.2 WAVE TRANSFORMATION

Extraction of sediment from potential borrow sites may result in modifications to physical processes at local borrow sites and in the nearshore zone of New Jersey. The region offshore Townsends and Corsons Inlets (Grid A) has a relatively consistent longshore wave height distribution. Several areas of wave convergence and divergence were caused by the shoals surrounding Areas A1 and A2. These features focus wave energy at various locations along the coast depending on the wave approach direction. The area to the south of Barnegat Inlet (Grid B1) experiences mild shoreline retreat and a consistent wave height distribution along the shoreline. Shoals and depressions south of Area C1, as well as offshore linear ridges to the north, can produce significant wave transformation within the modeling domain. Wave energy focused by these features most often impacts the Harvey Cedars and Loveladies regions. Offshore Little Egg and Brigantine Inlets (Grid B2), wave transformation again is influenced by

numerous linear ridges. Increased wave heights appear most frequently near Brigantine Inlet. The area seaward of northern Barnegat Bay (Grid C) also experiences wave height changes produced by offshore shoals and depressions within the modeling domain. Consistent wave focusing is observed by the shoal within Resource Area F2, as well as the shoals to the south and southeast of F2. Wave energy focused by these features impacts regions from Seaside Park north to Bay Head, depending on approach direction.

For the 50-yr hurricane and northeast storm, wave patterns are similar to the directional approach results. An increase in wave height is documented in many areas where wave convergence occurs. For example, the shoal present in Resource Area F2 produces wave convergence that results in 6.0 m wave heights during a typical 50-yr northeast storm. The 50-yr hurricane and northeast storm simulated in the present study represents a major storm that could have impact on the approaching wave field and sediment transport patterns.

Differences in wave height between pre- and post-dredging scenarios offshore New Jersey indicate maximum wave height changes for directional approach simulations ranging from 0.1 to 0.25 m (7 to 16% of the initial wave height). The magnitude of modifications increase as the magnitude of waves increase or when the orientation of potential borrow sites aligns with waves to produce maximum impact (e.g., southeast approach at Grid A). In Grids A and B2, which are the southernmost grids, maximum wave height changes dissipate relatively quickly as waves advance towards the coast and break. In Grids B1 and C, maximum changes do not dissipate as readily. At potential impact areas along the coast, wave height changes average ±0.13, ±0.11, ±0.15, and ±0.10 m for Grids A, B1, B2, and C, respectively. These modifications represent changes of approximately ±3 to 15% when compared with wave heights for existing conditions. Overall, the impact caused by potential offshore dredging during normal conditions is minimal, if at all.

During extreme wave conditions (e.g., a 50-yr storm), wave heights are increased from 0.4 to 1.4 m, suggesting a rather significant change. However, as a result of the increased magnitude of the incoming waves, this generally represents a change of less than 10%. Due to the orientation of the shoreline and the proposed borrow sites, a hurricane has more significant impacts on Grids A and B2 (Resource Areas A1, A2, G1, G2, and G3), while a northeast storm more significantly impacts Grids B1 and C (Resource Areas C1 and F2). For most of the sand borrow sites, a significant amount of wave energy is dissipated before waves reach the coast, especially for Grids A and B2. As such, wave height increases are less than 0.4 m along a majority of the coast. A maximum change of 0.4 m in wave height is not expected to increase nearshore erosion above existing conditions during a storm event.

Borrow sites within Sand Resource Areas A1 and A2, located offshore of Townsends Inlet, have a greater impact on the wave field due to the larger extraction volumes (8.8 and 8.6 MCM, respectively). In addition, regions with multiple borrow sites (Grids A and B2), indicate a greater potential for wave modifications with simultaneous dredging. Overall, wave transformation impacted by potential borrow sites is minimal during normal and storm conditions.

7.3 CURRENTS AND CIRCULATION

While no large-scale predictive circulation models were developed to quantify the effects of dredging in sand resource areas, the analysis of current patterns resulting from this study suggests proposed sand mining will have negligible impact on large-scale shelf circulation. The proposed sand mining locations are small relative to the entire shelf area, and it is anticipated that resulting dredging will not remove enough material to significantly alter major bathymetric

features in the region. Therefore, the forces and geometric features that principally affect circulation patterns will remain relatively unchanged.

Measurement of bottom currents offshore New Jersey at the LEO-15 stations (seaward of Little Egg Inlet) throughout an approximate two-year period (1993 to 1995) revealed considerable variability in flow speed and direction. The mean flow was to the southwest along the inner shelf bathymetric contours. Strongest flow was observed in the along-shelf direction, with peak velocities of nearly 50 cm/sec noted on several occasions; these maximum currents were directed down-shelf or to the south. Maximum northward currents reached 37 cm/sec, and along-shelf bottom currents never exceeded 50 cm/sec (1 knot). Flow reversals, when currents directed to the north (south) reversed to flow in a southerly (northerly) direction, were noted frequently. Along-shelf standard deviations were of order 9 cm/sec.

In the cross-shelf direction, mean flow was oriented onshore, consistent with upwelling processes that push bottom waters up onto the shelf. Maximum cross-shelf flow was 31 cm/sec (directed onshore); minimum flow was -13 cm/sec (directed offshore). Cross-shelf standard deviations were of order 5 cm/sec. Cross-shelf bottom currents were affected most significantly by semi-diurnal tides, with a mean onshore flow. Wind-driven currents were found to be less significant in the cross-shelf direction. Seasonal variability was most significant for wind-driven currents. Winter and autumn data records were most energetic, with summer and spring data sets possessing smaller energy values. Previous studies (Louis Berger Group, 1999) show that extratropical storms (i.e., northeast storms) occur more frequently during fall and winter. Analysis of the wind-driven time series showed current energy values could be biased by singular events, such as storms or non-locally generated free waves. Currents, which appear dominated by wind-driven processes, are stronger during time periods of higher wind activity. In addition to wind-driven currents, high frequency (noise, random motions) and low-frequency currents also appear to be stronger during winter. This suggests these high- and low-frequency flow processes may also be coupled to atmospheric forcing.

These data suggest that along-shelf currents possess higher energy than cross-shelf flows. Along-shelf currents were dominated by wind-driven processes, accounting for as much as 70% of the total current energy. Wind-driven processes were greatest in winter; however, wind-driven flows appeared strongly biased by singular events, such as local responses to storm winds or non-locally generated free waves that influenced the magnitude of wind-driven current energy.

Information generated from this analysis, and supported by previous studies, suggests that shelf flow, primarily along the shelf, is strongest during singular events (i.e., storms or non-locally generated free waves). This evidence can be extrapolated to suggest that these singular events, with corresponding higher currents, have the greatest potential to transport sand. If so, sediment transport patterns may be predominately in the along-shelf direction, with a net transport oriented in the direction of the mean southerly flow. The data also show that these same singular events had little impact on cross-shelf currents, indicating that cross-shelf sediment transport due to currents is weak.

7.4 SEDIMENT TRANSPORT

Current measurements and analyses, and wave transformation modeling, provide baseline information on incident processes impacting coastal environments under existing conditions and with respect to proposed sand mining activities for beach replenishment. Ultimately, the most important information for understanding physical processes impacts from offshore sand extraction is changes in sediment transport dynamics resulting from potential sand extraction scenarios relative to existing conditions.

Three independent sediment transport analyses were completed to evaluate physical environmental impacts due to sand mining. First, historical sediment transport trends were quantified to document regional, long-term sediment movement throughout the study area using historical bathymetry data sets. Erosion and accretion patterns were documented, and sediment transport rates in the littoral zone and at offshore borrow sites were evaluated to assess potential changes due to offshore sand dredging activities. Second, sediment transport patterns at proposed offshore borrow sites were evaluated using wave modeling results and current measurements. Post-dredging wave model results were integrated with regional current measurements to estimate sediment transport trends for predicting borrow site infilling rates. Third, nearshore currents and sediment transport were modeled using wave transformation modeling output to estimate potential impacts to the longshore sand transport system (beach erosion and accretion). All three methods were compared for documenting consistency of measurements relative to predictions, and potential physical environmental impacts were identified.

7.4.1 Historical Sediment Transport Patterns

Regional geomorphic changes between 1843/91 and 1934/77 were analyzed for assessing long-term, net coastal sediment transport dynamics. Although these data do not provide information on the potential impacts of sand dredging from proposed borrow sites, they do provide a means of calibrating predictive sediment transport models relative to infilling rates at borrow sites and longshore sand transport.

Shoreline position and nearshore bathymetry change document four important trends. First, the predominant direction of sediment transport throughout the study area is north to south. Southern Long Beach Island (north of Little Egg Inlet) and southern Island Beach (north of Barnegat Inlet) have migrated at a rate of about 14 m/yr to the south since 1839/42. The ebb-tidal shoals at all inlets in the study area are skewed to the south, and the channels are aligned in a northwest-southeast direction.

Second, the most dynamic features within the study area, in terms of nearshore sediment transport, are the ebb-tidal shoals associated with inlets along the southeastern barrier island chain. Areas of significant erosion and accretion are documented for the period 1843/91 to 1934/77, reflecting wave and current dynamics at entrances, the influence of engineering structures on morphologic change, and the contribution of littoral sand transport from the north to sediment bypassing and shoal migration.

Third, alternating bands of erosion and accretion on the continental shelf east of the Federal-State boundary illustrate relatively slow but steady reworking of the upper shelf surface as sand ridges migrate from north to south. The process by which this is occurring at Areas G1, G2, and G3 suggests that a borrow site in this region would fill with sand transported from an adjacent site at a rate of about 62,000 to 125,000 m^3/yr. At Areas A1 and A2, the potential sand transport rate increases to 160,000 to 200,000 m^3/yr. This increase in potential transport rate reflects a more dynamic offshore environment seaward of the southern barrier island chain.

Finally, net longshore transport rates determined from seafloor changes in the littoral zone between Little Egg Inlet and the beach south of Hereford Inlet indicate an increasing transport rate to the south from about 70,000 m^3/yr south of Little Egg Inlet to 190,000 to 230,000 m^3/yr at Townsends and Hereford Inlets. Variations in transport rate are evident in the patterns of change recorded on Figure 3-17. It appears that areas of largest net transport exist just south of entrances as a result of natural sediment bypassing from updrift to downdrift barrier beaches. These rates compare well and provide a measured level of confidence in wave and sediment

transport modeling predictions relative to impacts associated with sand dredging from proposed borrow sites.

7.4.2 Sediment Transport at Potential Borrow Sites

In addition to predicted modifications to the wave field, potential sand mining at offshore borrow sites results in minor changes in sediment transport pathways in and around the dredged regions. The modifications to bathymetry caused by sand mining only influence local hydrodynamic and sediment transport processes in the offshore area. Although wave heights may change at the dredged borrow sites, areas adjacent to the sites do not experience dramatic changes in wave or sediment transport characteristics.

Initially, sediment transport at borrow sites will experience rapid changes after sand dredging is complete. Given the water depths at the proposed borrow sites, it is expected that minimal impacts to waves and regional sediment transport will occur during infilling. Sediment that replaces the dredged material will fluctuate based on location, time of dredging, and storm characteristics following dredging episodes. Average transport rates range from a minimum of 28 m^3/day Area F2) to a high of 450 m^3/day (Area A1), while the infilling rate varies between 54 (Area A1) to 303 years (Area C1). This range of infilling times is based on the volume of sand numerically dredged from a borrow site as well as the sediment transport rate. These infilling times would be reduced if storm events were incorporated into the analysis.

The analysis of borrow site infilling time assumes a constant rate of transport from each direction and does not include the effects of modified bathymetry. For example, as a dredged site begins to fill, sediment transport dynamics change. As such, sediment transport rates will fluctuate as a borrow site evolves during infilling. This dynamic process is not simulated in the present analysis. However, the analysis performed provides a reasonable estimate of infilling times for resource management purposes.

Although most borrow sites have infilling times of less than 100 years, Areas C1 and F2 have estimated infilling times on the order of 200 to 300 years. These long infilling times are the result of reduced sediment transport rates and a large potential sand borrow volume. Northeast storms and hurricanes may increase sediment initiation and transport, thereby reducing infilling times at all borrow sites.

7.4.3 Nearshore Sediment Transport Trends

Application of the REF/DIF S wave model, the wave-induced current model, and the longshore sediment transport model provided a basis for comparing existing conditions with post-dredging coastal processes conditions. Dredging at major offshore borrow sites can have a significant effect on coastal erosion/accretion, because changes to the offshore bathymetry can focus wave energy by altering nearshore wave characteristics.

Excavation of a borrow site in the nearshore region can affect both wave heights and the direction of wave propagation. The existence of an offshore swale or trough can cause waves to refract toward the shallower edges of a borrow site. This alteration to the wave field by a borrow site may change local sediment transport rates, where some areas may experience a reduction in longshore transport, and other areas may show an increase. To determine the potential physical impacts associated with dredging of borrow sites located off the New Jersey coast, sediment transport potential modeling based on results of the REF/DIF S modeling, was performed for existing and post-dredging bathymetric conditions. Comparison of computations for existing and post-dredging conditions illustrated the relative impact of borrow site excavation on wave-induced coastal processes.

Comparisons of average annual sediment transport potential were performed for existing and post-dredging conditions to indicate the relative impact of dredging to longshore sediment transport process at Grids A, B2, and B1. Because it was not possible to compute a net transport rate for Grid C (See Section 5.2.2 for details), a comparison of existing and post-dredging conditions was performed for the wave condition responsible for the greatest sediment transport potential (e.g., the -22.5º case).

Understanding modifications to local waves and related sediment transport patterns forms the basis for evaluating the impacts of dredging to wave-induced transport. Due to predominant east and southeast wave conditions along the New Jersey shoreline, annual net longshore sediment transport rates are generally governed by these frequently occurring and relatively long-period waves. In addition, local shoreline orientation also influences the net and gross sediment transport potential.

A plot of existing and post-dredging sediment transport potential, as well as the difference for the –22.5º wave condition at Grid B1 is shown in Figure 7-1. This plot clearly indicates the sheltering and wave focusing effects on transport potential along the coastal region south of Barnegat Inlet. Two distinct bumps in sediment transport potential are indicated on the change plot. The northern (largest) bump primarily is associated with the shadow region directly landward of the borrow site. Because the regional wave climate is dominated by east and southeast wave conditions, this sediment transport potential peak is located approximately 3,000 m north of the offshore location of the borrow site. The peak in sediment transport potential to the south of the shadow region is a result of wave energy focusing resulting from wave refraction processes across the borrow site. Waves propagating across the southern half of the borrow site will be deflected toward the south and *vice versa*. This refraction (or wave deflection) tends to cause an increase in south-directed transport south of the borrow site and a reduction of south-directed transport north of the borrow site. Therefore, a portion of the northern bump also is due to wave refraction across the northern half of the borrow site. The maximum decrease in annual transport rates is approximately 14,000 m^3/yr for this case.

Average annual sediment transport patterns for existing conditions, as well as post-dredging scenarios, were documented for the A, B2, B1, and C sub-grids to determine whether dredging would cause a significant effect above normal conditions. In addition, sediment transport effects were evaluated for both 50-year northeast storm and hurricane storm event. The location of grids utilized for the sediment transport analysis is shown in Figure 5-51.

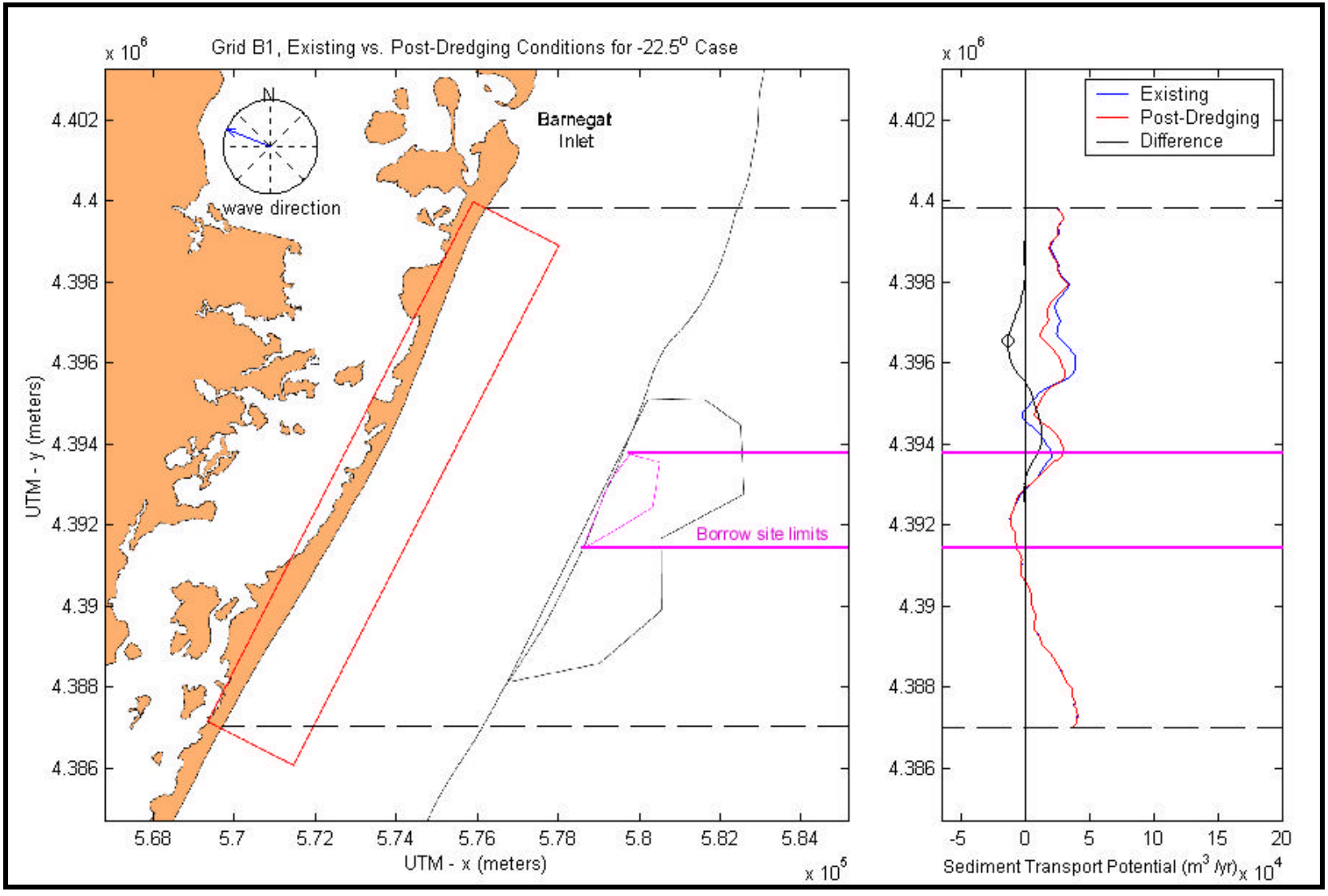

Figure 7-1. Difference in annual transport rates associated with dredging sand borrow sites for the –22.5º wave condition at Grid B1. The UTM Northing coordinate limits of the potential borrow site are shown with thick lines.

7.4.3.1 Grid A

Figure 7-2 illustrates that there is a defined, but somewhat minor impact from dredging in Areas A1 and A2. Due to the offshore distance of Area A2 (approximately 12 km offshore), the region of potential impacts is relatively large. Figure 7-2 indicates that impacts associated with dredging span the entire region modeled for Grid A; however, the offshore distance also serves to reduce the magnitude of these impacts. For the borrow sites in Areas A1 and A2, the maximum variation in annual longshore sand transport rate is approximately 7% of the existing value. In general, the increase or decrease in longshore sediment transport rates associated with the potential borrow sites is distributed over the entire 12 km stretch of shoreline represented by the sediment transport model, with the most significant impacts centered at about UTM Northing coordinate 4,333,000 m (3,000 m north of Townsends Inlet).

The predominant wave direction from the east and southeast shifts the wave-induced impacts of dredging towards the north. As described above, a shadow zone typically is created immediately shoreward of a borrow site, as wave energy is directed away from the shoreline immediately landward of the borrow site. Based on Figure 7-2, the shadow zones landward of Areas A1 and A2 are located approximately 5 km and 1 km north of Townsends Inlet, respectively. These shadow zones are indicated by a significant reduction in south-directed wave energy. Likewise, the largest increase in south-directed transport occurs between the shadow zones (3 km north of Townsends Inlet), where both borrow sites in Areas A1 and A2 have wave energy refracted to the south and north, respectively. This increase in wave energy at the shoreline is responsible for the increased south-directed transport between the shadow zones.

7.4.3.2 Grid B2

Figure 7-3 illustrates the impacts associated with dredging borrow sites between Absecon and Little Egg Inlets (Areas G1, G2, and G3). Due to the limited extent of the wave modeling grid, the impacts illustrated on Figure 7-3 only represent borrow sites in Areas G2 and G3 (Area G1 is located beyond the southern boundary of the model grid). Because the offshore distance of both Areas G2 and G3 is relatively low (approximately 5 km offshore), the region of potential impacts is more confined than the area defined for Area A2, above. Figure 7-3 indicates that impacts associated with dredging primarily include the region south of Brigantine Inlet for Grid B2. In addition, the series of offshore shoals associated with Brigantine and Little Egg Inlets tend to reduce the magnitude of these impacts. For the borrow sites in Areas G2 and G3, the maximum variation in annual longshore sand transport rate is approximately 9% of the existing value. Based on Figure 7-3, only a single shadow zone landward of Resource Areas G2 and G3 exists, approximately 1 km south of Brigantine Inlet. This shadow zone is indicated by a significant reduction in south-directed wave energy. The largest increase in south-directed transport occurs south of the shadow zone (approximately 2 km south of Brigantine Inlet). However, it is unclear whether the shadow zone or the region of increased south-directed wave energy are a result of dredging in Area G2 (one potential borrow site), G3 (two potential borrow sites), or a combination of the three potential borrow sites.

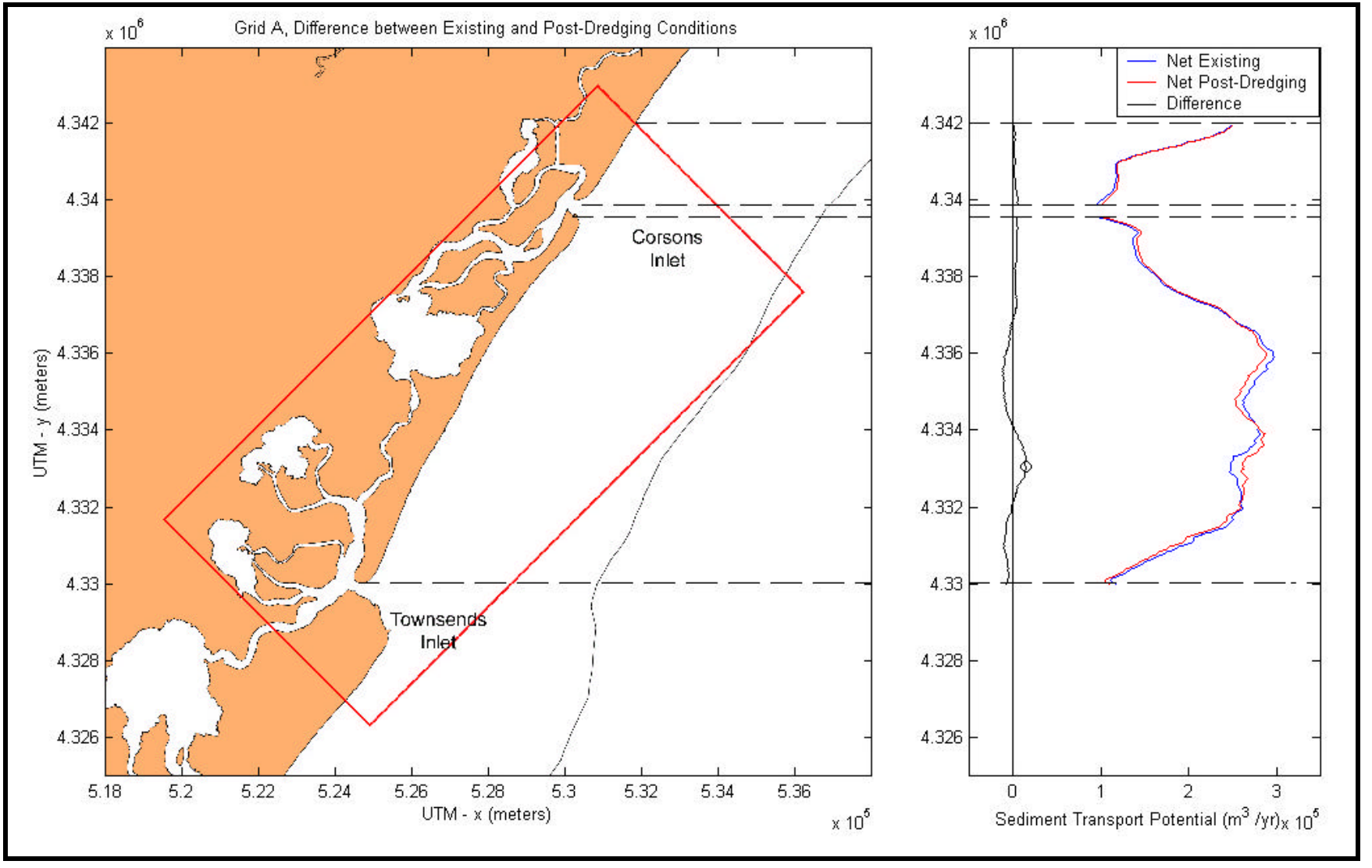

Figure 7-2. Difference in average annual transport rates associated with dredging sand borrow sites for Grid A.

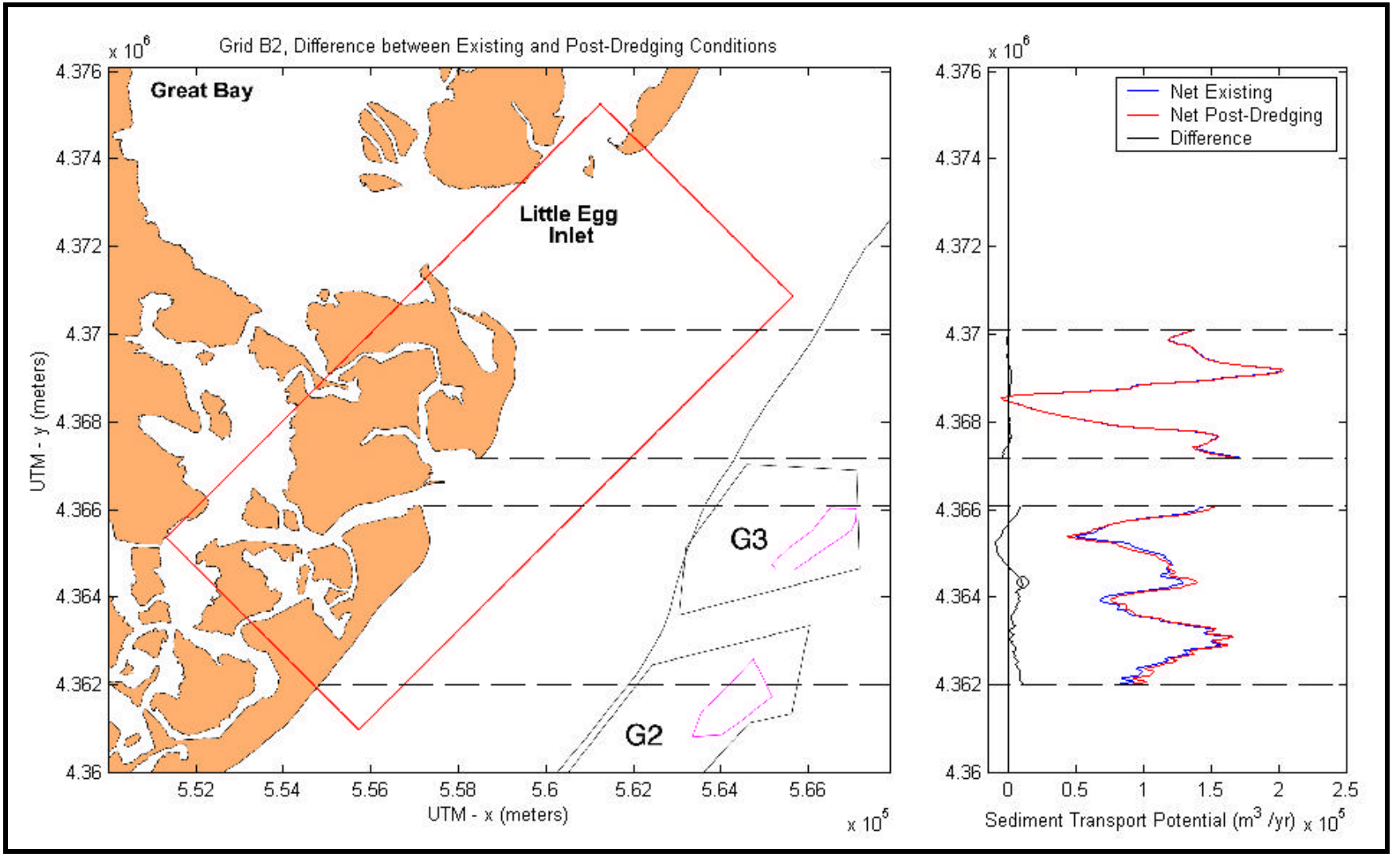

Figure 7-3. Difference in average annual transport rates associated with dredging sand borrow sites for Grid B2.

7.4.3.3 Grid B1

Because a single borrow site exists in Area C1, and no tidal inlets are present within the limits of Grid B1, the effects of dredging are more easily discerned than for the other modeled regions. Figure 7-4 illustrates the impacts associated with dredging the borrow site approximately 9 km south of Barnegat Inlet. Again, southeast and east wave conditions appear to dominate the wave record; therefore, the impacts associated with dredging a borrow site within Area C1 extend north from a region directly west of the proposed borrow site. As described previously, a shadow zone typically is created immediately shoreward of a borrow site, as wave energy is directed away from the shoreline immediately landward of the borrow site. Based on Figure 7-4, a series of shadow zones landward of Area C1 occurs as a result of wave refraction generated by the various wave conditions. The largest shadow zone exists at approximately UTM Northing coordinate 4,394,000 m due to waves propagating from the east. In addition to this shadow zone, waves propagating from the east-southeast cause a reduction in the south-directed transport at UTM Northing coordinate 4,396,000 m, and waves propagating from the southeast cause a shadow zone at UTM Northing coordinate 4,398,500 m. For Area C1, the combined effect of various wave conditions tends to mute the increase in south-directed sediment transport, where the largest increase is approximately 3,000 m^3/yr. Although the maximum variation in annual longshore sand transport rate is approximately 20% of the existing average value, the relatively high percentage of the 45,000 m^3/yr net transport indicates similar impacts as those predicted for Grids A and B2. For example, the maximum change in sediment transport for Grids A and B2 are 14,900 and 10,200 m^3/yr, where the maximum change in sediment transport for Grid B1 is only 9,000 m^3/yr.

7.4.3.4 Grid C

As discussed in Section 5.0, the various wave modeling grids used for Grid C did not incorporate the same stretch of shoreline; therefore, it was not possible to develop annual sediment transport potential along this region. Instead, impacts associated with dredging a borrow site within Area F2 were evaluated using the wave condition generating the largest sediment transport potential (the –22.5º wave condition). Figure 7-5 illustrates the impacts associated with dredging the borrow site south of Manasquan Inlet (Area F2). Due to the offshore distance of this resource area (approximately 9 km offshore), the region of potential impacts is relatively large. Figure 7-5 indicates that impacts associated with dredging include an approximate 8 km segment of shoreline in the northern portion of Grid C; however, the offshore distance also serves to reduce the magnitude of these impacts. For the borrow site in Area F2, the maximum variation in annual longshore sand transport rate is approximately 17% of the existing value. Similar to Grid B1, the relatively low net sediment transport indicates a high percentage of impact to the transport rate; however, the maximum change of approximately 12,700 m^3/yr is similar to the modeled change for Grids A, B2, and B1.

The predominant wave direction from the east and southeast shifts the wave-induced impacts of dredging towards the north. A shadow zone typically is created immediately shoreward of a borrow site as wave energy is directed away from the shoreline immediately landward of the borrow site. Based on Figure 7-5, the shadow zone landward of Area F2 is located approximately 6 km south of Manasquan Inlet. Likewise, the largest increase in north-directed transport occurs on either side of the shadow zone (approximately 4 and 8 km south of Manasquan Inlet, respectively). This increase in wave energy at the shoreline is responsible for the increased north-directed transport both north and south of the primary shadow zone.

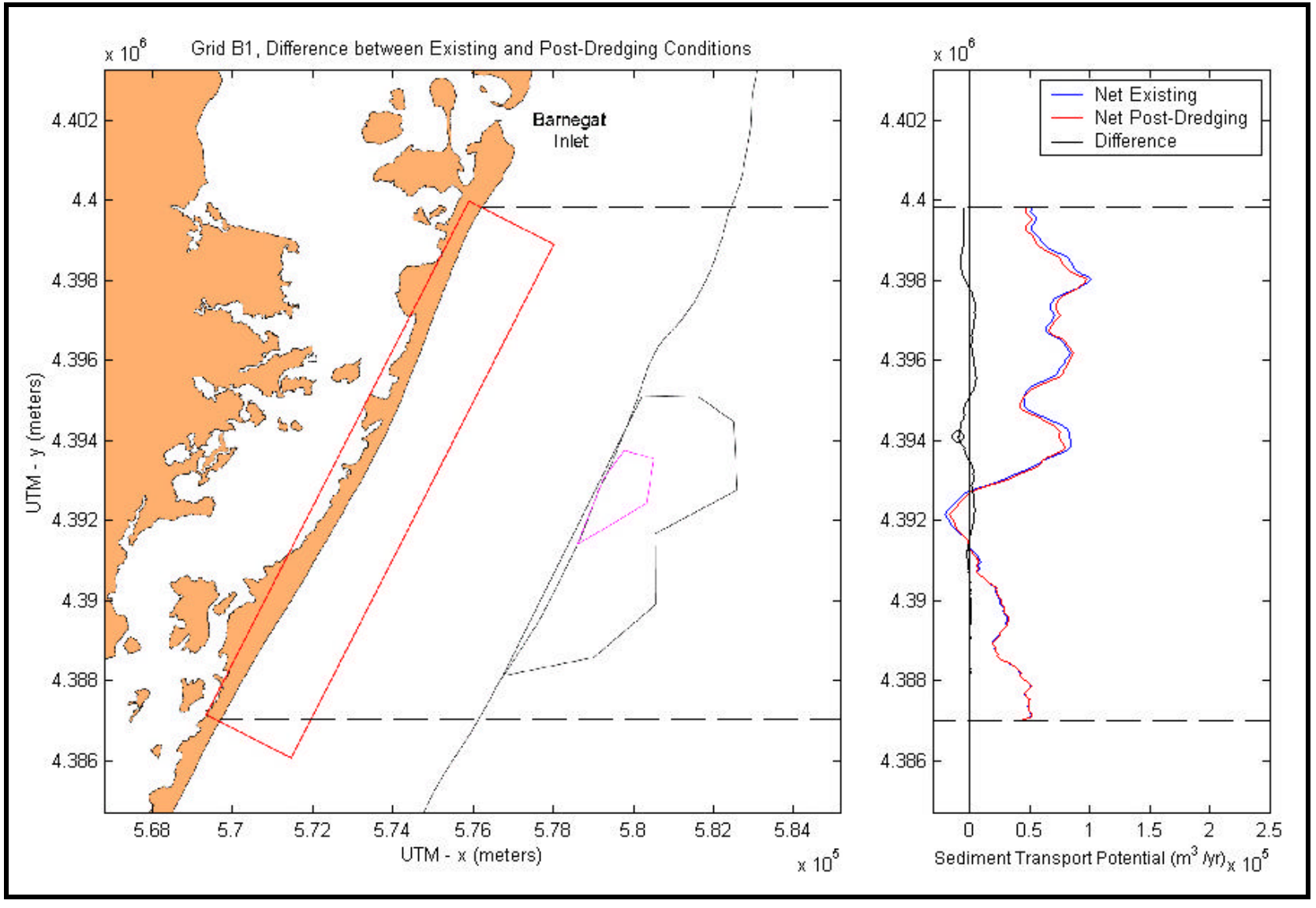

Figure 7-4. Difference in average annual transport rates associated with dredging sand borrow site for Grid B1.

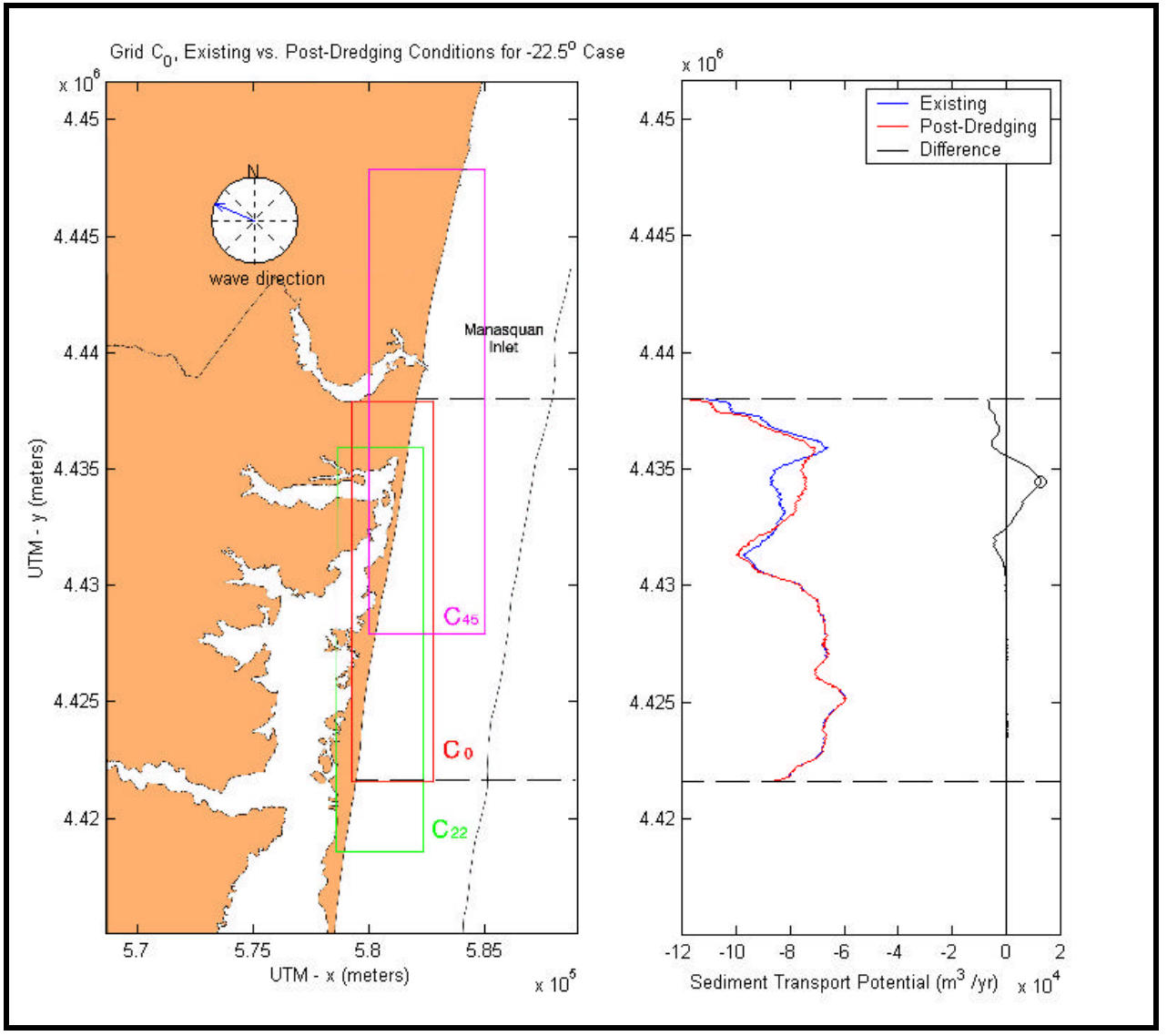

Figure 7-5. Difference in average transport rate for the –22.5º wave condition associated with dredging sand borrow site for Grid C.

7.4.3.5 50-Year Storm Conditions

Although many of the storm conditions modeled yielded results consistent with known shadowing and wave focusing (e.g., the northeast storm condition for Grid A), wave energy dissipation in the existing version of REF/DIF S does not accurately depict wave breaking associated with large long-period waves. For this reason, it was not possible to develop impacts of borrow site dredging for each of the grids modeled. Results for Grids A and B1 were consistent with known coastal processes; however, the series of inlets and shoals within Grid B2, and issues with nearshore wave breaking in Grid C, indicated problems inherent in the wave modeling effort. Therefore, the results of 50-year storm wave modeling only were evaluated for Grids A and B1.

Figures 7-6 and 7-7 illustrate impacts associated with dredging within Grid A for northeast and hurricane storm conditions, respectively. For northeast storm conditions, the borrow sites in Areas A1 and A2 cause a maximum variation in annualized longshore sand transport rate of approximately 10% over the existing value. Due to the direction of wave approach, the increase or decrease in longshore sediment transport rates associated with dredging at potential borrow sites is distributed over a region extending from UTM Northing coordinate 4,338,000 m to Townsends Inlet. For the hurricane condition, waves propagating from the southeast approach nearly shore-normal; therefore, sediment transport associated with hurricane wave conditions is relatively low compared with the northeast storm conditions. Because the annualized transport is low for the hurricane case (a mean transport value of 728,000 m^3/yr), the maximum percentage change resulting from storm conditions is relatively high (about 36%). However, the actual magnitude of the transport difference for the northeast storm and the hurricane was similar, where the difference was 405,000 and 265,000 m^3/yr, respectively.

Similar to annual average conditions, the absence of tidal inlets and the presence of a single potential borrow site within Grid B1 allowed more simplified determination of impacts associated with offshore dredging. Figure 7-8 and 7-9 illustrate the impacts associated with dredging within Grid B1 for northeast and hurricane storm conditions, respectively. For northeast storm conditions, dredging at the borrow site in Area C1 causes a maximum variation in annualized longshore sand transport rate of approximately 18% over the existing value. Due to the direction of wave approach, the increase or decrease in longshore sediment transport rates associated with potential borrow sites is distributed over a region extending from UTM Northing coordinate 4,390,000 m to 4,394,700 m. For the hurricane condition, waves propagating from the southeast cause the impact area to shift farther north when compared with the northeast storm results. Unlike the other storm conditions, the hurricane condition within Grid B1 causes northerly littoral transport; therefore, the positive side of the difference curve indicates wave sheltering. In this case, the shadow region extends from approximately UTM Northing coordinate 4,395,000 m to 4,397,000 m. The borrow site in Area C1 causes a maximum variation in annualized longshore sand transport rate of approximately 15% over the existing value for hurricane waves.

7.4.3.6 Significance of Transport Trends

Quantitative evaluation of potential effects to nearshore sediment transport rates associated with proposed dredging scenarios was performed using a statistical analysis of predicted rates for annual average conditions (Table 7-1). The region of influence for each borrow site was characterized using three calculated parameters, in addition to a visual comparison of existing and post-dredging sediment transport rates.

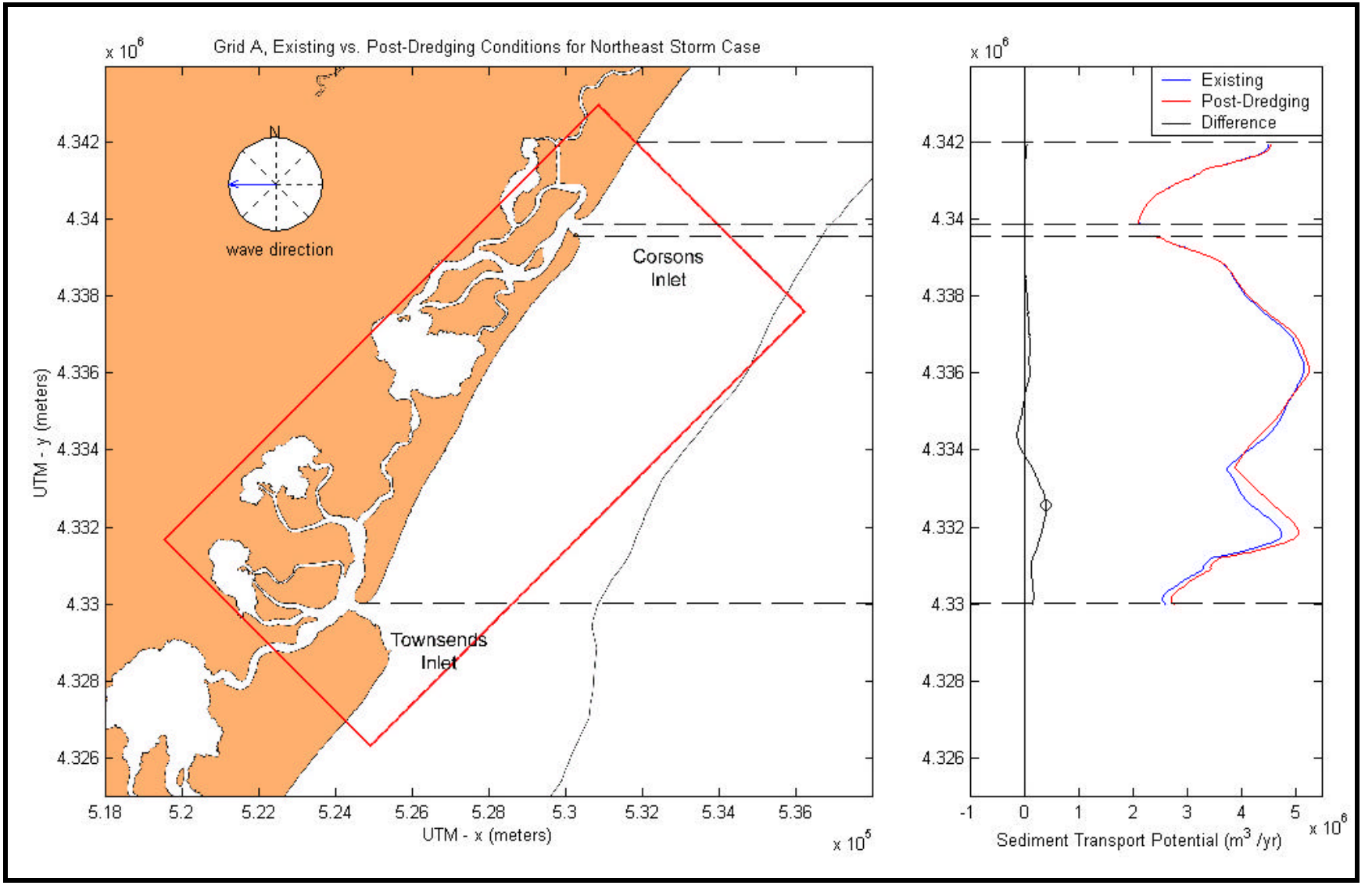

Figure 7-6. Difference in annualized transport rate for northeast storm wave condition associated with dredging sand borrow sites for Grid A.

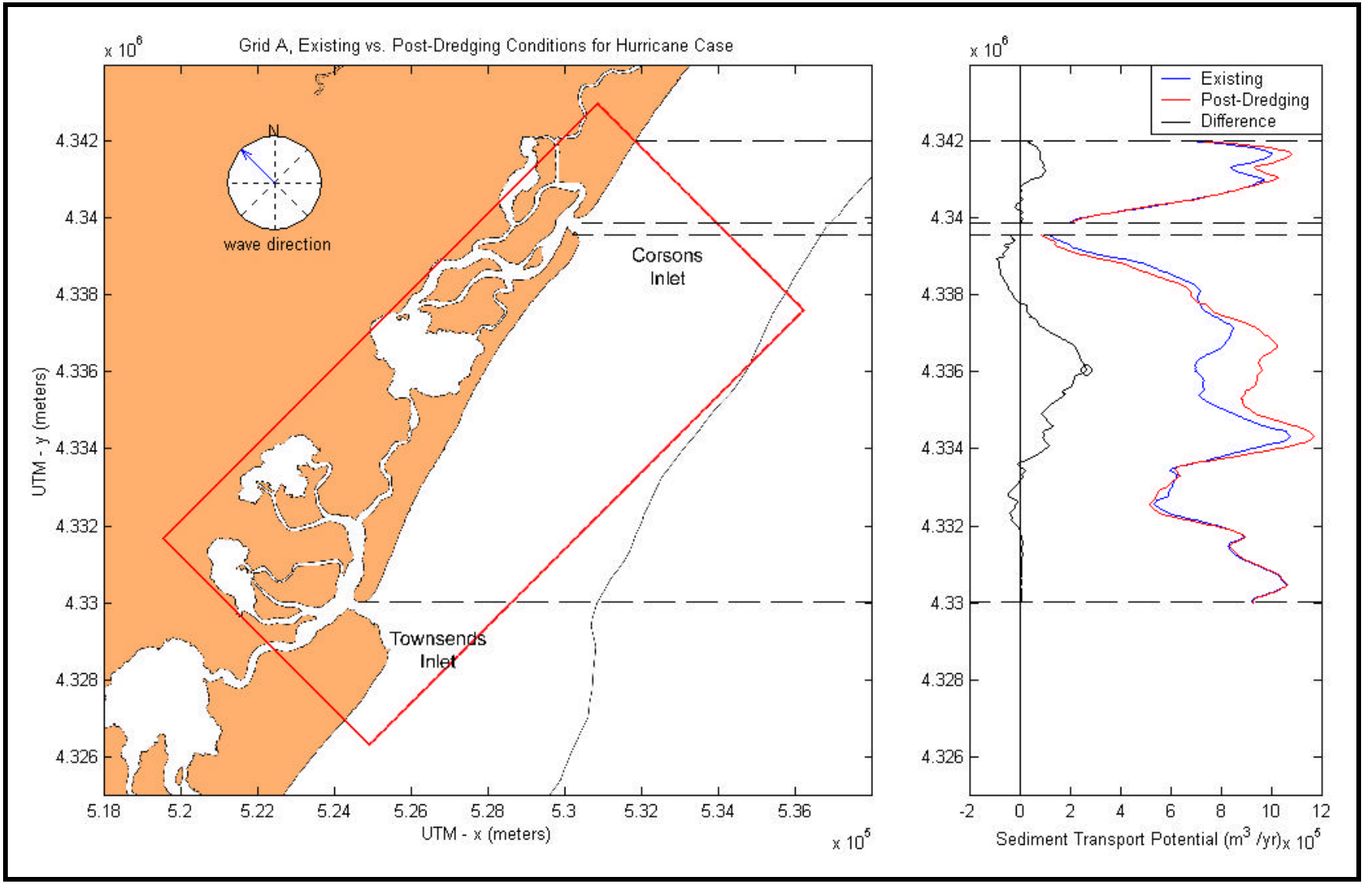

Figure 7-7. Difference in annualized transport rate for the hurricane wave condition associated with dredging sand borrow sites for Grid A.

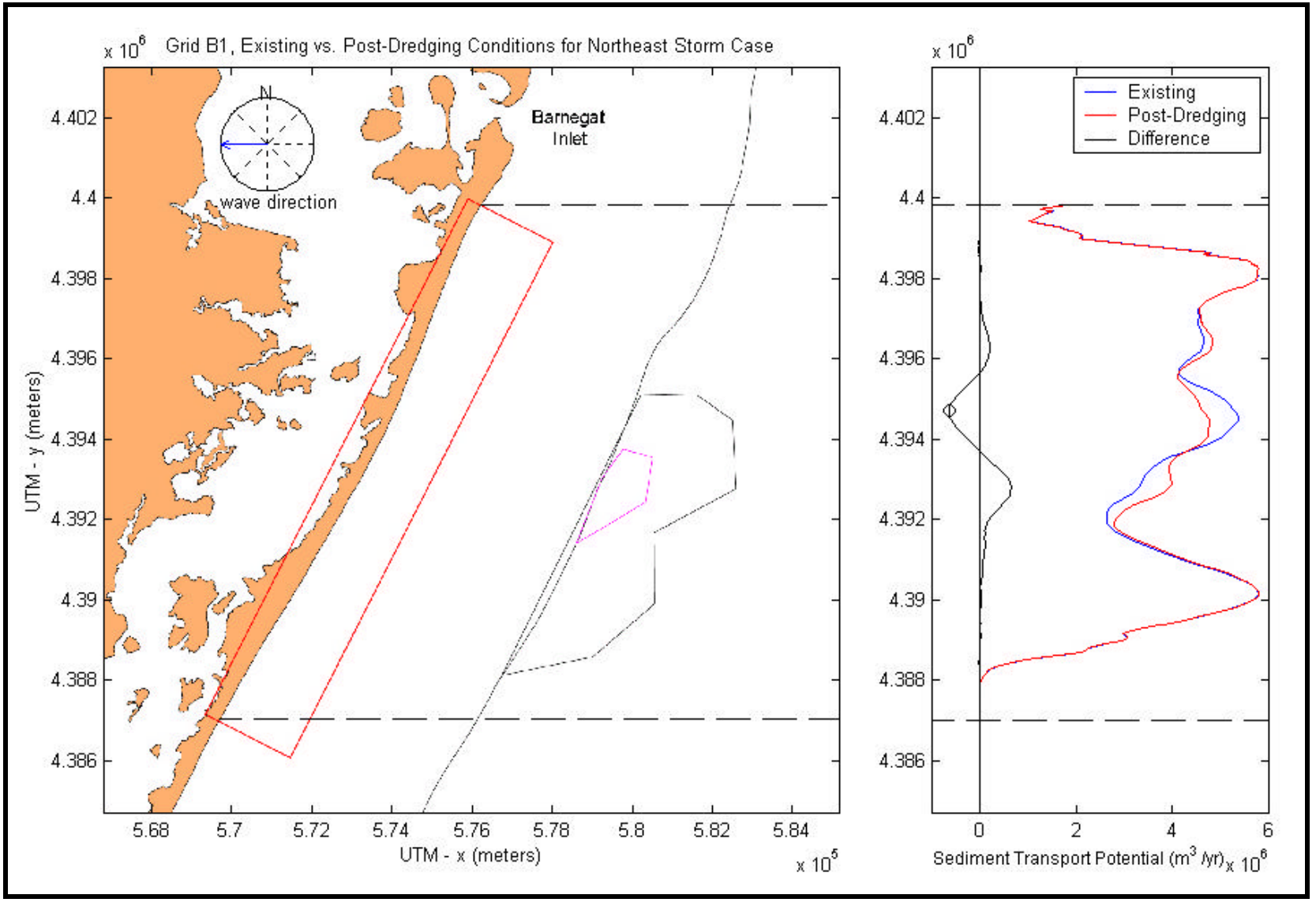

Figure 7-8. Difference in annualized transport rate for northeast storm condition associated with dredging the sand borrow site for Grid B1.

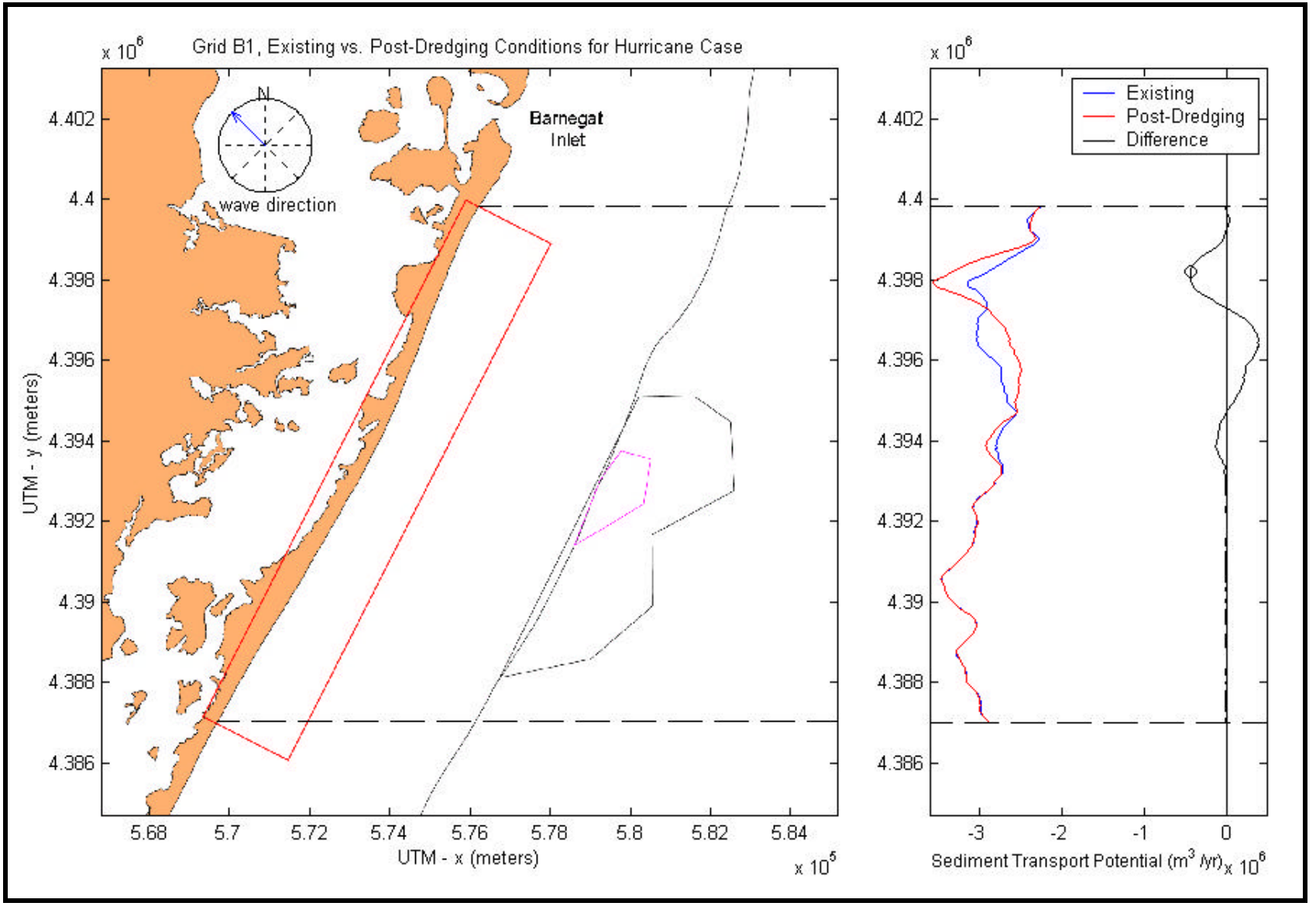

Figure 7-9. Difference in annualized transport rate for the hurricane wave condition associated with dredging the sand borrow site for Grid B1.

Table 7-1. Statistical parameters for annual average sediment transport conditions associated with Sub-Grids A, B2, B1, and C.

	Sub-Grid			
	A	B2	B1	C*
Mean Transport (m^3/yr)	208,000	117,000	45,000	-77,000
Absolute Value of the Maximum Difference in Transport (m^3/yr))	14,900	10,200	9,000	12,700
Percentage Difference	7.2	8.7	20.0	16.5
* For sub-grid C, the difference calculations only represent the –22.5º wave condition				

For average annual conditions, mean longshore sand transport rates were approximately equal landward of borrow sites in resource areas along the New Jersey coast. The absolute value of the mean difference between existing and post-dredging conditions was relatively consistent, ranging between 9,000 (20.0%) and 14,900 m^3/yr (7.2%) along the New Jersey shoreline. Although the percent difference computed for the northern two grids (Grids B1 and C) was larger than that calculated farther south, this trend is a result of the relatively low net transport rates along the northern beaches rather than an increase in impacts associated with dredging.

Upon initial evaluation, the differences between existing and post-dredging transport rates appear to be significant. To determine the relative significance of this difference, a simple analysis of uncertainties associated with nearshore sediment transport calculations was performed. An estimate of uncertainties was based on procedures described by Rosati and Kraus (1991). Although the sediment transport calculation technique used in this study was slightly different than the method employed by Rosati and Kraus (1991), both procedures were based on wave height and direction. Using conservative estimates for error associated with wave height and wave direction of 10%, sediment transport rates can be predicted to within ±35%. These errors can be attributed to the inherent uncertainties in the WIS data set (wave height and directional accuracy) used to develop offshore wave conditions. The ±35% value is significantly higher than the impacts associated with any of the borrow sites evaluated along the New Jersey coast.

Analysis of uncertainties related to longshore sediment transport estimates indicates that variations in transport associated with potential dredging scenarios are an order of magnitude lower than the uncertainty associated with sediment transport calculations. Therefore, the potential effects of offshore sand mining seaward of the New Jersey coast on longshore sand transport rates are insignificant for the scenarios tested in this study. Alternative scenarios are not expected to pose any greater effects unless the quantity of sand dredged from a site is substantially larger than potential dredged volumes selected for this study.

7.5 BENTHIC ENVIRONMENT

The purpose of this section is to address potential effects of offshore dredging activity on benthic organisms, including analyses of the potential rate and success of recolonization following cessation of dredging activities. This section is divided into four parts. The first two parts summarize information from the existing literature on effects and recolonization. The first part (Section 7.5.1) describes potential impacts to benthic organisms from the physical disturbance of dredging, which causes removal, suspension/dispersion, and deposition of sediments. The second part (Section 7.5.2) discusses the potential rate and success of

recolonization. The third part (Section 7.5.3) provides predictions of impacts and recolonization relative to the eight sand resource areas off New Jersey. Finally, the fourth part (Section 7.5.4) of this benthic section discusses potential effects to the Atlantic surfclam.

Ecological effects of marine mining and beach nourishment operations have been reviewed by numerous authors (Thompson, 1973; Naqvi and Pullen, 1982; Nelson, 1985; Cruickshank et al., 1987; Goldberg, 1989; Grober, 1992; Hammer et al., 1993; National Research Council, 1995). Effects vary from detrimental to beneficial, short to long term, and direct to indirect (National Research Council, 1995).

Most reviews on the effects of beach nourishment operations have focused on potential impacts at the beach. Comprehensive assessments of the effects on biological resources at open ocean sand borrow sites have been limited (National Research Council, 1995). Alterations to biological resources in offshore sand borrow sites are generally of longer duration, and the consequences of those changes have not been well-defined (National Research Council, 1995). The remainder of this section focuses on potential impacts of dredging operations at offshore areas.

7.5.1 Effects of Offshore Dredging on Benthic Fauna

The primary impact producing factor relative to dredging offshore borrow sites is mechanical disturbance of the seabed. This physical disruption includes removal, suspension/dispersion, and deposition of dredged material. This section focuses on the potential biological effects of these physical processes on benthic fauna.

7.5.1.1 Sediment Removal

Physical removal of sediments from a borrow site removes benthic habitat along with infaunal and epifaunal organisms that are incapable of avoiding the dredge, resulting in drastic reductions in the number of individuals, number of species, and biomass. Extraction of habitat and biological resources may in turn disrupt the functioning of existing communities. Removal of benthic resources is of concern because they are important in the food web for commercially and recreationally important fishes and invertebrates, and contribute to the biodiversity of the pelagic environment through benthic-pelagic coupling mechanisms. These mechanisms include larval transport and diurnal migrations of organisms, which may have substantial impact on food availability, feeding strategies, and behavioral patterns of other members of the assemblage (Hammer and Zimmerman, 1979; Hammer, 1981).

Removal of sand resources can expose underlying sediments and change the sediment structure and composition of a borrow site, consequently altering its suitability for burrowing, feeding, or larval settlement of some benthic organisms. Many studies show decreases in mean grain size, and in some cases, increases in silt and clay in borrow sites following dredging (National Research Council, 1995). Changes in sediment composition could potentially prevent recovery to an assemblage similar to that which occurred in the borrow site prior to dredging and could by implication affect the nature and abundance of food organisms for commercial and recreational fishery stocks (Coastline Surveys Limited, 1998; Newell et al., 1998). In some cases, dredging borrow sites may create new and different habitat from surrounding substrates, which could result in increased habitat complexity and biodiversity of an area.

The influence of sediment composition on benthic community composition has been recognized since the pioneer studies of Peterson (1913), Thorson (1957), and Sanders (1958). However, more recent reviews suggest that precise relationships between benthic assemblages and specific sediment characteristics are poorly understood (Gray, 1974; Snelgrove and Butman, 1994; Newell et al., 1998). Sediment grain size, chemistry, and organic content may

influence recolonization of benthic organisms (McNulty et al., 1962; Thorson, 1966; Snelgrove and Butman, 1994), although the effects of sediment composition on recolonization patterns of various species are not always significant (Zajac and Whitlatch, 1982). Because the complexity of soft-sediment communities may defy any simple paradigm relating to any single factor, Hall (1994) and Snelgrove and Butman (1994) proposed a shift in focus towards understanding relationships between organism distributions and the dynamic sedimentary and hydrodynamic environments. It is likely that the composition of benthic assemblages is controlled by a wide array of physical, chemical, and biological factors that interact in complex ways and are variable with time.

Removal of sediments from borrow sites can alter seabed topography, creating pits that may refill rapidly or cause detrimental impacts for extended periods of time. Borrow sites have been known to remain well-defined 8 years after dredging (Marsh and Turbeville ,1981; Turbeville and Marsh, 1982). Although nearly 12 years may be required for some offshore borrow sites to refill to pre-dredge profiles, intentionally locating borrow sites in highly depositional areas may dramatically reduce the time for refilling (Van Dolah et al., 1998). In general, shallow dredging over large areas causes less harm than small but deep pits, particularly pits opening into a different substrate surface (Thompson, 1973; Applied Biology, Inc., 1979). Deep pits also can hamper commercial trawling activities and harm level-bottom communities (Thompson, 1973). If borrow pits are deep, current velocity is reduced at the bottom, which can lead to deposition of fine particulate matter and in turn a biological assemblage much different in composition than the original. Deep holes may decrease dissolved oxygen to hypoxic or anoxic levels and increase hydrogen sulfide levels (Murawski, 1969; Saloman, 1974; National Research Council, 1995).

7.5.1.2 Sediment Suspension/Dispersion

Dredging causes suspension of sediments, which increases turbidity over the bottom. This turbidity undergoes dispersion in a plume that drifts with the water currents. The extent of suspension/dispersion depends on the type of dredging equipment, techniques for operating the equipment, amount of dredging, thickness of the dredged layer, sediment composition, sediment transport processes, etc.

Herbich and Brahme (1991) and Herbich (1992) reviewed sediment suspension caused by existing dredging equipment, and discussed potential technologies and techniques to reduce suspension and the associated environmental impacts. In general, cutterhead suction dredges produce less turbidity than hopper dredges. A cutterhead suction dredge consists of a rotating cutterhead, positioned at the end of a ladder, that excavates the bottom sediment. The cutterhead is swung in a wide arc from side to side as the dredge is stepped forward on pivoting spuds, and the excavated material is lifted from the bottom by a suction pipe and transferred by pipeline as a slurry (Hrabovsky, 1990; LaSalle et al., 1991). Sediment suspension is caused by the rotating action of the cutterhead and the swinging action of the ladder (Herbich, 1992). A properly operated cutterhead dredge can limit sediment suspension to the lower portion of the water column (Herbich and Brahme, 1991; Herbich, 1992). A well-designed cutterhead, selection of an appropriate cutterhead for a given sediment, the correct relationship between rotational speed of the cutterhead and the magnitude of hydraulic suction, and suitable swing rate of the cutterhead, along with hooded intakes, may reduce turbidity at the cutterhead, although these conditions are rarely achieved (Herbich, 1992). Measurements around properly operated cutterhead dredges show that elevated levels of suspended sediments can be confined to the immediate vicinity of the cutterhead and dissipate rapidly with little turbidity reaching surface waters (Herbich and Brahme, 1991; LaSalle et al., 1991; Herbich, 1992). Maximum suspended sediment concentrations typically occur within 3 m above the cutterhead

and decline exponentially to the sea surface (LaSalle et al., 1991). Suspended sediment concentrations in near-bottom waters may be elevated up to several hundred meters laterally from the cutterhead location (LaSalle et al., 1991).

A hopper dredge consists of one, two, or more dragarms and attached dragheads mounted on a ship-type hull or barge with hoppers to hold the material dredged from the bottom (Herbich and Brahme, 1991). As the hopper dredge moves forward, sediments are hydraulically lifted through the dragarm and stored in hopper bins on the dredge (Taylor, 1990; LaSalle et al., 1991). Hopper dredging operations produce turbidity as the dragheads are pulled through bottom sediments. However, the main source of turbidity during hopper dredging operations is sediment release during hopper overflow (Herbich and Brahme, 1991; LaSalle et al., 1991; Herbich, 1992). A plume may occasionally be visible at distances of 1,200 m or more (LaSalle et al., 1991).

Much attention has been given to turbidity effects from dredging, although most reviews have concerned estuaries, embayments, and enclosed waters (e.g., Sherk and Cronin, 1970; Sherk, 1971; Sherk et al., 1975; Moore, 1977; Peddicord and McFarland, 1978; Stern and Stickle, 1978; Herbich and Brahme, 1991; LaSalle et al., 1991; Kerr, 1995). Turbidity effects should be less important in unprotected offshore areas for several reasons. Offshore sands tend to be coarser with less clay and silt than inshore areas. The open ocean environment also provides more dynamic physical oceanographic conditions, which minimize settling effects. In addition, offshore organisms are adapted to sediment transport processes, which create scouring, natural turbidity, and sedimentation effects under normal conditions. Impacts should be evaluated in light of natural variability as well as high level disturbances associated with such events as storms, trawling, floods, hypoxia/anoxia, etc. (Herbich, 1992). Physical disturbance of the bottom and resulting biological impacts from dredging are similar to those of storms and trawling but at a much smaller spatial scale.

Turbidity interferes with the food gathering process of filter feeders and organisms that feed by sight by inundation with nonnutritive particles. Large quantities of bottom material placed in suspension decrease light penetration and change the proportion of wavelengths of light reaching the bottom, leading to decreases in photosynthetic activity. Suspension and dispersion of sediments may cause changes in sediment and water chemistry as nutrients and other substances are released from the substratum and dissolved during the dredging process. Coastline Surveys Limited (1998) proposed that for aggregate mining operations using hopper dredges, the far-field visible plume contains an organic mixture of fats, lipids, and carbohydrates from organisms entrained and fragmented during the dredging process and discharged with the overflow. Dredging may produce localized hypoxia or anoxia in the water column due to oxygen consumption of the suspended sediments (LaSalle et al., 1991). Suspension and dispersion processes also uncover and displace benthic organisms, temporarily providing extra food for bottom feeding species (Centre for Cold Ocean Resources Engineering, 1995).

7.5.1.3 Sediment Deposition

Suspended sediments settle and are deposited nearby or some distance from dredged sites. The extent of deposition and the boundaries of biological impact are dependent on the type and amount of suspended sediments and physical oceanographic characteristics of the area.

Dredging effects are not necessarily limited to the borrow site alone. The types of far-field impacts from suspension and deposition of sediments can be detrimental or beneficial. Deposition of sediments can suffocate and bury benthic fauna, although some organisms are able to migrate vertically to the new surface (Maurer et al., 1986). Johnson and Nelson (1985)

found decreases in abundances and numbers of taxa at nondredged stations, although these decreases were not as extreme as those observed in the borrow site. McCaully et al. (1977; as cited by Johnson and Nelson, 1985) also observed that dredging effects can extend to other nearby areas, and noted decreases in abundance ranging from 34 to 70% at undredged stations within 100 m of a dredged area. Conversely, benthos may show an increase in biodiversity downstream from dredged sites (Centre for Cold Ocean Resources Engineering, 1995). In some areas, population density and species composition of benthic invertebrates increased rapidly outside dredged sites, with the level of enhancement decreasing with increasing distance from the dredged area up to a distance of 2 km (Stephenson et al., 1978; Jones and Candy, 1981; Poiner and Kennedy, 1984). The enhancement was ascribed to the release of organic nutrients from the dredge plume, a process known from other studies (Ingle, 1952; Biggs, 1968; Sherk, 1972; Oviatt et al., 1982; Coastline Surveys Limited, 1998; Newell et al., 1998). This suggestion was supported by records of nutrient releases from benthic areas during intermittent, wind-driven bottom resuspension events (Walker and O'Donnell, 1981), significant increases in nutrients in the water column from simulated storm events in the laboratory (Oviatt et al., 1982), and review of the literature indicating a major restructuring force in infaunal communities is the response of species to resources released from the sediments by periodic disturbance (Thistle, 1981). Fishing also may improve temporarily down current of the dredging area and continue for some months (Centre for Cold Ocean Resources Engineering, 1995).

7.5.2 Recolonization Rate and Success

7.5.2.1 Adaptations for Recolonization and Succession

In dynamic areas that undergo frequent perturbations, benthic invertebrates tend to be small bodied, short lived, and adapted for maximum rate of population increase with high fecundity, efficient dispersal mechanisms, dense settlement, and rapid growth rates (MacArthur, 1960; MacArthur and Wilson, 1967; Odum, 1969; Pianka, 1970; Grassle and Grassle, 1974). In contrast, organisms in stable areas tend to be relatively larger and longer lived with low fecundity, poor dispersal mechanisms, slow growth rates, and adaptations for non-reproductive processes such as competition and predator avoidance. Recolonization of a disturbed area often is initiated by organisms that have the adaptive characteristics for rapid invasion and colonization of habitats where space is available due to some natural or man-induced disturbance. These early colonizers frequently are replaced during the course of succession through competition by other organisms, unless the habitat is unstable or frequently perturbed.

Although the distinction between the adaptive strategies is somewhat arbitrary and is blurred in habitats that are subject to only mild disturbance, the lifestyle differences are fundamentally important because they help explain variations in succession and recolonization rate and success following disturbance (Coastline Surveys Limited, 1998; Newell et al., 1998). Knowledge of faunal component lifestyles allows some predictions of dredging impacts and subsequent recolonization and recovery of community composition (Coastline Surveys Limited, 1998; Newell et al., 1998).

7.5.2.2 Successional Stages

Successional theory states that organism-sediment interactions result in a predictable sequence of benthic invertebrates belonging to specific functional types following a major seafloor disturbance (Rhoads and Germano, 1982, 1986). Because functional types are the biological units of interest, the succession definition does not rely on the sequential appearance of particular species or genera (Rhoads and Boyer, 1982). This continuum of change in benthic

communities has been divided arbitrarily into three stages (Rhoads et al., 1978; Rhoads and Boyer, 1982; Rhoads and Germano, 1982):

Stage I is the initial pioneering community of tiny, densely populated organisms that appears within days of a natural or anthropogenic disturbance. Stage I communities are composed of opportunistic species that have high tolerance for and can indicate disturbance by physical disruption, organic enrichment, and chemical contamination of sediments. The organisms have high rates of recruitment and ontogenetic growth. Stage I communities tend to physically bind sediments, making them less susceptible to resuspension and transport. For example, Stage I communities often include tube-dwelling polychaetes or oligochaetes that produce mucous to build their tubes, which stabilizes the sediment surface. Stage I communities include suspension or surface deposit-feeding animals that feed at or near the sediment-water interface. The Stage I initial community may reach population densities of 10^4 to 10^6 individuals per m^2;

Stage II is the beginning of the transition to burrowing, head-down deposit feeders that rework the sediment deeper with time and mix oxygen from the overlying water into the sediment. Stage II animals may include tubiculous amphipods, polychaetes, and mollusks. These animals are larger and have very low population densities compared to Stage I animals; and

Stage III is the mature and stable community of deep-dwelling, head-down deposit feeders. In contrast to Stage I organisms, these animals rework the sediments to depths of 3 to 20 cm or more, loosening the sedimentary fabric and increasing the water content of the sediment. They also actively recycle nutrients because of the high exchange rate with the overlying water resulting from their burrowing and feeding activities. The presence of Stage III taxa can be a good indication that the sediment surrounding these organisms has not been severely disturbed recently, resulting in high benthic stability and health. Loss of Stage III species results in the loss of sediment stirring and aeration and may be followed by a build-up of organic matter (eutrophication) of the sediment. Because Stage III species tend to have relatively low rates of recruitment and ontogenetic growth, they may not reappear for several years once they are excluded from an area. These inferences are based on past work, primarily in temperate latitudes, showing that Stage III species are relatively intolerant to physical disturbance, organic enrichment, and chemical contamination of sediments. Population densities are low (10 to 10^2 individuals per m^2) compared to Stage I.

The general pattern of succession of benthic species in a marine sediment following cessation of dredging or other environmental disturbance begins with initial recolonization. Initial recolonization occurs relatively rapidly by small opportunistic species that may reach peak population densities within months of a new habitat becoming available after catastrophic mortality of the previous assemblage. As the disturbed area is invaded by additional larger species, the population density of initial colonizers declines. This transitional period and assemblage with higher species diversity and a wide range of functional types may last for years, depending on numerous environmental factors. Provided environmental conditions remain stable, some members of the transitional assemblage are eliminated by competition, and

the species assemblage forms a recovered community composed of larger, long-lived, and slow growing species with complex biological interactions with one another.

7.5.2.3 Recolonization Rates

The rate of recolonization is dependent upon numerous physical and biological factors and their interactions. Physical factors include the time of year, depth of the borrow site, water currents and water quality, sediment composition, bedload transport, temperature and salinity, natural energy levels in the area, frequency of disturbance, latitude, etc. Recovery times may be shorter in warmer waters at lower latitudes as compared to colder waters at higher latitudes (Coastline Surveys Limited, 1998; Newell et al., 1998).

Recolonization of borrow sites may occur by transport of larvae from neighboring populations by currents and subsequent growth to adults, immigration of motile species from adjacent areas, organisms contained in sediment slumping from the sides of pits, or return of undamaged organisms from the dredge plume. The rate of recolonization depends on the size of the pool of available colonists (Bonsdorff, 1983; Hall, 1994). Other biological factors such as competition and predation also determine the rate of recolonization and the composition of resulting benthic communities. Timing of dredging is important because many benthic species have distinct peak periods of reproduction and recruitment. Because larval recruitment and adult migration are the primary recolonization mechanisms, biological recovery from physical impacts generally should be most rapid if dredging is completed before seasonal increases in larval abundance and adult activity (Herbich, 1992). Recovery of a community disturbed after peak recruitment, therefore, will be slower than one disturbed prior to peak recruitment (LaSalle et al., 1991).

Benthic recolonization and succession have been reviewed to varying extents for a wide variety of habitats throughout the world (e.g., Thistle, 1981; Thayer, 1983; Hall, 1994; Coastline Surveys Limited, 1998; Newell et al., 1998). Recolonization is highly variable and ranges from within months (e.g., Saloman et al., 1982) to more than 12 years (e.g., Wright, 1977), depending on the habitat type and other physical and biological factors. Focusing on dredging, Coastline Surveys Limited (1998) and Newell et al. (1998) suggested that, in general, recovery times of 6 to 8 months are characteristic for many estuarine muds, 2 to 3 years for sand and gravel, and 5 to 10 years as the deposits become coarser.

The Centre for Cold Ocean Resources Engineering (1995) estimated times for recovery of a reasonable biodiversity (number of species and number of individuals) based on sediment type. In this study, recovery was defined as attaining a successional community of opportunistic species providing evidence of progression towards a community equivalent to that previously present or at non-impacted sites. Fine-grained sediments may need only 1 year before achieving a recovery level biodiversity, medium-grained deposits 1 to 3 years, and coarse-grained deposits 5 or more years. For a hypothetical borrow site dredging scenario off Ocean City, Maryland, the Centre for Cold Ocean Resources Engineering (1995) stated that virtually all benthic species would be lost, but there may be temporary improvement of fishing due to release of nutrients. Recolonization would start within weeks of closure and moderate biodiversity would occur within 1 year. The borrow site would be colonized initially by a very different species complex than originally present. An estimate of 2 to 3 years was given for the community to begin to show succession to pre-impact sand habitat species.

Recolonization of a borrow site was studied 3 km offshore of Great Egg Harbor Inlet near Ocean City, New Jersey (Scott and Kelly, 1998). Macrobenthic organisms were able to colonize the borrow site rapidly. Approximately 2 years after the last dredging, the number of taxa, diversity, and abundance in the borrow site recovered to conditions that existed in other borrow

sites and undisturbed areas before dredging. The community composition within the borrow site may have changed, although the community change was described as not significant and not a result of dredging because the community composition of the borrow site was similar to the composition observed at the adjacent stations. Good juvenile surf clam recruitment occurred in the borrow site, but the population may not have reached size levels in nearby undisturbed sites 2 years after the last dredging. Although biomass and size of surf clams appeared diminished, there was no indication that the population would not stabilize given additional time. As dredging events were conducted in all seasons and no apparent effect was detected, no changes in the timing of dredging appeared to be necessary (Scott and Kelly, 1998).

Studies of recolonization listed and discussed by Grober (1992) and the National Research Council (1995) indicate that recolonization of offshore borrow sites is highly variable. This variability is not surprising considering the differences between studies in geographic locations, oceanographic conditions, sampling methods and times, etc. Part of the problem in determining recolonization patterns is seasonal and year to year fluctuations in benthic community characteristics and composition. Without adequate seasonal and yearly data prior to dredging, it is difficult to determine whether differences in community characteristics and composition are due to temporal changes or dredging disturbance.

Results and conclusions from these offshore borrow site studies indicate that recolonization usually begins soon after dredging ends. Recolonization periods range in duration from a few months to several years. Although abundance and diversity of benthic fauna within the borrow sites often returned to levels comparable to predredging or reference conditions within less than 1 year, several studies documented changes in benthic species composition that lasted much longer, particularly where sediment composition was altered (e.g., Johnson and Nelson, 1985; Bowen and Marsh, 1988; Van Dolah et al., 1992, 1993; Wilber and Stern, 1992).

Most recolonization studies of borrow sites concentrated on three main features of infaunal communities, namely the number of individuals (population density), number of species (diversity), and weight (biomass as an index of growth). Dredging is usually accompanied by an immediate and significant decrease in the number of individuals, species, and biomass of benthic infauna. Using biological community parameters (e.g., total taxa, total number of individuals, species diversity, evenness, richness, etc.), previous studies tend to indicate that recovery of borrow sites occurs in approximately 1 year after dredging. However, these parameters do not necessarily reflect the complex changes in community structure and composition that occur during the recovery process. Major changes in species assemblages and community composition usually occur shortly after dredging such that a different type of community exists. Although the number of individuals, species, and biomass of benthic infauna may approach pre-dredging levels within a relatively short time after dredging, recovery of community composition may take longer.

7.5.2.4 Recolonization Success and Recovery

Assessing impacts of dredging and recolonization and recovery of borrow sites is difficult because most biological communities are complex associations of species that often undergo major changes in population densities and community composition, even in areas that are far removed and unaffected by dredging and other disturbances. Recolonization success and recovery do not necessarily mean that communities should be expected to return to the pre-dredged species composition. To gauge recovery, it is important to compare the community composition of dredged areas with control areas during the same seasons because community composition changes with time.

When long-term alterations in sediment structure and composition occur as a result of dredging, long-term differences in the composition of benthic assemblages inhabiting those sites may occur as well. The recovery time of benthic assemblages after dredging can depend in large measure on the degree and duration of sediment alteration from sand borrowing (Van Dolah, 1996). Recolonization success and recovery also are controlled by compaction and stabilization processes involving complex interactions between particle size, water currents, waves, and biological activities of the benthos following sediment deposition (Oakwood Environmental Ltd., 1999). While the abundance and diversity of infaunal assemblages may recover relatively rapidly in dredged areas, it may take years to recover in terms of sediment and species composition.

One conclusion commonly held is that perturbations to infaunal communities in borrow sites are negligible because organisms recolonize rapidly (Wilber and Stern, 1992). This conclusion often is based on measures including densities, species diversity/evenness indices, relative distribution of classes or phyla, and species-level dendrograms. For example, many researchers have recognized that borrow and reference area infaunal communities can differ considerably at the species level, although these differences usually are considered insignificant because species diversity is high. According to Wilber and Stern (1992), reliance upon these studies may lead to a premature conclusion that impacts to borrow site infauna are minimal because these measures are relatively superficial and ambiguous characteristics of infaunal communities. Wilber and Stern (1992) reexamined infaunal data from four borrow site projects by grouping species into functional groups called ecological guilds based on similarities in feeding mode, locomotory ability, and sediment depth occurrence. Their analyses showed that infaunal communities in borrow and control areas can differ in several ways and that these differences can last several years. Polychaetes and amphipods that recolonize borrow sites are small-bodied and confine their movement and feeding to the surface sediment or the interface between the sediment and water column. In contrast, control areas have well-developed infaunal communities commonly consisting of large-bodied organisms that move and feed deep in the sediment (Wilber and Stern, 1992). They concluded that the infaunal communities recolonizing borrow sites may remain in an early successional stage for 2 to 3 years or longer as opposed to being completely recovered in shorter time frames.

The conclusions of Wilber and Stern (1992) coincide with the model of succession discussed previously. The model states pioneering or opportunistic species are the first to colonize an area after a physical disturbance to the bottom (e.g., dredging borrow sites). Pioneering species tend to share several ecological traits, including a tendency to confine activities to the sediment-water interface, possibly because subsurface conditions cannot support a significant number of organisms. The subsurface environment changes with time after the disturbance, possibly by actions of early colonizers, and becomes suitable for deposit feeders and mid-depth burrowers. The relative absence of deposit feeders and mid-depth burrowers is interpreted to mean an area is still in the state of recovery.

Although most of the literature on recolonization rate and success in borrow sites concerns infauna, some information exists for epifauna. The numbers of taxa and individuals collected by trawls in a borrow site off Duval County, Florida greatly exceeded the control area numbers 4 months after dredging and were generally higher 7 and 13 months after dredging (Applied Biology, Inc., 1979). There were no detectable differences between pre-dredging and post-dredging (8 and 16 months) epifaunal communities in a borrow site surveyed by otter trawl and video camera off Egmont Key, Florida (Blake et al., 1995).

7.5.3 Predictions Relative to the Sand Resource Areas

Based upon the commodity-specific, technology-specific, and site-specific information provided in Sections 1.0 and 7.0, the following predictions can be made regarding the potential effects of offshore dredging on benthic organisms (Section 7.5.3.1) and the recolonization rate and success (Section 7.5.3.2) relative to the eight sand resource areas off New Jersey.

7.5.3.1 Potential Benthic Effects

Sediment Removal

The immediate impact of excavating upper sediments of a sand resource area would be removal of portions of the benthic invertebrate populations that inhabit surficial shelf sediments. Lost individuals would be those with slow-moving or sessile lifestyles, primarily those comprising infaunal populations. Surveys within and adjacent to each of the candidate borrow sites, as well as benthic investigations of nearby waters, reveal that infaunal assemblages of inner shelf waters of the study area predominantly are invertebrates, including crustaceans, echinoderms, mollusks, and polychaetous annelids.

The expected loss of benthic fauna due to sediment excavation from the sand resource areas could be considered to represent a negligible impact on the ecosystem when evaluating the impact on a spatial scale. Use of any of the sand resource areas does not entail complete excavation of those areas. Impacts most likely would be localized and short-term. Specific locations within resource areas that are to be dredged will be selected based on particular sedimentary and bathymetric characteristics, leaving a significant extent of non-dredged areas surrounding and interspersed throughout the impacted areas. These undisturbed areas would be a primary source of colonizing fauna for the excavated sites (Van Dolah et al., 1984), and would complement colonization of altered substrata via larval recruitment. The great densities and fecundity of invertebrate populations, along with the relatively small areas of impact proposed, likely would preclude significant long-term negative effects on benthic populations.

Correlation between sediment composition and the composition of infaunal assemblages has been demonstrated in numerous environmental surveys, including the 1998 surveys of the New Jersey sand resource areas. Invertebrate populations inhabiting marine soft bottoms offshore New Jersey exhibit heterogeneous distributions that largely are the result of local sedimentary regime. Modification of surficial sediments and local bathymetry could result in an alteration of the areal extent and relative distribution of assemblage types, by altering the distribution of sediment types capable of supporting those assemblages.

It is possible that a change in the composition of surficial sediments within excavated areas could become a long-term result of dredging. Several factors could contribute to such an outcome, primarily the type of sediments exposed by dredging and the degree of fine sediment deposition into dredged areas. These factors would depend primarily on the depth of excavation, which would be determined by the vertical relief of the sand shoal to be excavated, the vertical extent of those sediments suitable for coastal nourishment projects, and the volume of sand required.

Because the inner shelf ecosystem of the Middle Atlantic Bight exhibits some heterogeneity in sediment types and their associated assemblages, those transitional infaunal assemblages that initially colonize dredged areas likely would be similar to some naturally occurring assemblages that inhabit nearby non-dredged areas, especially fine sediment areas within inter-ridge troughs. When viewed within a context of scale, removal of sediments from portions of the New Jersey inner continental shelf would at most minimally alter the existing spatial balance of habitat (sediment) types. Moreover, those habitats that have relatively high levels of finer sediments are not uninhabitable, or necessarily less functional in an ecological

sense, when compared to sand or gravel substrata. Various sediment habitat types merely differ in their level of suitability for certain types of infaunal taxa. Localized changes in habitat suitability that result from sand removal likely will be ephemeral and inconsequential in the shelf ecosystem, a system where both infaunal assemblage types and sedimentary parameters are dynamic and spatially variable.

Motile populations, including non-migratory foragers, would be less stressed by sediment removal than infauna or sessile epifauna. Most macroepifaunal and demersal fish populations would have a low probability of being adversely impacted directly by the dredging of surficial sediments. Slow-moving or burrowing sessile epifauna inhabiting the project area include echinoderm and decapod taxa, and local populations of these types of benthic organisms would most likely experience a reduction in density due to sediment removal. Motile epifauna generally are migratory and are not endemic to the sand resource areas. Most demersal populations exhibit naturally dynamic distributions, moving between areas within the Middle Atlantic Bight on a seasonal basis (Able and Hagen, 1995).

Any impacts of sediment removal on epifaunal and demersal taxa likely would be indirect in nature, through habitat alteration. A reduction of infaunal biomass resulting from sediment removal could have an indirect effect upon the distribution of certain demersal fishes and other epibenthic predators by interrupting established energy pathways to the higher trophic levels represented by these foraging taxa. Reductions in densities of the preferred prey of bottom-feeding taxa could induce migration of foragers to unimpacted areas. However, a relatively small percentage of infaunal prey items that typically are consumed by demersal taxa would be rendered unavailable for consumption as a result of prey removal along with surficial sediments. Benthic predators simply would select alternative areas in which to forage. The loss of infaunal biomass due to sediment excavation, therefore, is unlikely to adversely affect normal energy flow through New Jersey inner shelf sand bottoms.

In addition to widely documented spatial variation, the location and extent of inner shelf-inhabiting infaunal and demersal populations vary seasonally in the study area. Seasonal variability should be considered when evaluating potential impacts due to sand removal. The timing of sand removal would seem to be less critical for minimizing the impact upon infauna than for other faunal categories of concern (e.g., key pelagic species), due to the great abundance and reproductive potential of infaunal populations. Many numerically dominant infaunal taxa inhabiting the study area are known to exhibit either year-round or late winter-early spring periods of recruitment. Because of these patterns of recruitment and lower winter densities, removal of sand between late fall and early spring might result in less stress on benthic populations.

Sediment Suspension/Dispersion

Whether cutterhead suction dredging or hopper dredging ultimately is utilized for sand mining, the amount of sediment suspension that results from these excavation methods is not anticipated to be of a scale that would cause significant negative impacts to the benthic community. New Jersey sand resource areas are characterized by a relatively limited volume of fine sediments, indicating that the shelf area encompassing the resource areas currently is not a depositional environment, but is hydrologically dynamic. In general, benthic assemblages of the inner New Jersey shelf probably are adapted to periodic reworking of surficial sediments caused by storm events. Impacts of dredging-induced elevations in turbidity (associated mainly with hopper dredging) would be short-term and localized. Motile taxa could avoid turbid areas.

Sediment Deposition

Of the various faunal categories, infaunal and burrowing epifaunal populations would be most negatively affected by significant deposition of sediments; however, efficient methods of sediment excavation would preclude all but a relatively minor amount of sediment deposition. Suspension and transport of sediments away from dredged sites should be minimal and any subsequent deposition would be insignificant in degree. In the unlikely event that significant dredging-related deposition of fine-grained sediments were to occur, the deposited sediments likely would not persist on the seafloor because of the high-energy inner shelf environment. However, some low or depressional areas of the seafloor could exhibit a substantial deposition of fine sediments under this scenario. Given the relatively small amount of sediment suspension anticipated to occur during dredging, the degree of burial should be substantially less than would be required to impact negatively on the infaunal community.

7.5.3.2 Potential Recolonization Rate and Success

The rate of post-dredging recovery of benthic assemblages within an excavated borrow site will depend primarily on the depth of sand excavation. While surface area of impact could be minimized by excavating a shoal to a greater depth, deep excavation likely would extend the time for complete recovery of infaunal assemblages within the impacted area. The creation of a bathymetrically abrupt pit has potential to inhibit water current flow through such a feature, possibly resulting in a "dead zone" characterized by deposition of fine particles and hypoxia or anoxia. This scenario would extend the duration of ecological impact beyond that which would occur with a more shallow cut over a much larger area.

Recent results of long-term environmental monitoring of a borrow site located 3.6 km offshore Coney Island have demonstrated potential consequences of dredging an abrupt pit feature (Barry A. Vittor & Associates, Inc., 1999b). A nearby reference area also was sampled before (1992) and after dredging (1995 through 1998). Prior to dredging, average water depths were approximately 3 to 4 m at the Coney Island borrow site and in the reference area. After the last dredging in 1995, and until the last monitoring event (1998), depths of borrow site stations varied from 6 to 15 m, while the average depth of reference area stations did not change during the study period. Prior to dredging, sediments at the borrow site were 55% medium to coarse sands, but by 1995 were fine to medium sands (<20% medium to coarse sand). By 1998, the silt/clay fraction (>20%) of borrow site sediments was significantly higher than in reference area sediments (4%). During each year following the last dredging event, infaunal assemblage composition at the borrow site was numerically dominated by deposit-feeding polychaetes (*Spio setosa* and *Streblospio benedicti*) and mollusks (primarily *Tellina agilis*); none of these species were ever sampled from the reference area. Although hypoxic conditions were never detected at the Coney Island borrow site, bathymetric alteration and subsequent deposition of fine sediments resulted in persistent alteration of the natural assemblage composition.

While the initial impact to benthic assemblages would increase with increasing surface area of sand removal, the persistence of ecological impact that would occur with a relatively shallow excavation would be less than that of a deep pit. A maximum excavation of 3 m (Areas A2, C1, F2, G2, and G3) or 4 m (Areas A1 and G1) with a larger area of sand removal would result in less long-term impact because a more smoothly-graded, trough-like feature would allow greater bottom current flow than would an abrupt pit. New Jersey sand resource areas exhibit natural inter-ridge trough features. These bathymetric depressions can be depositional areas for finer sediments, and they often support benthic assemblages that are different from nearby assemblages inhabiting gravel and sand.

The length of time required for reestablishment of infaunal assemblages within excavated areas partly depends on the length of time required for refilling of those mined areas. The relatively shallow water benthic habitats of the New Jersey inner shelf are strongly influenced by factors such as tidal currents and circulation, and storms (Stubblefield et al., 1975). These same forces would tend to modify impacted areas in the direction of pre-dredging conditions. The rate of reestablishment of the natural benthic conditions at dredged sites may depend especially on the extent of storm-induced sediment transport, which can be substantial at relatively shallow depths such as those in the region of the sand resource areas. It is expected that the time required for redevelopment of sand shoals in areas of excavation will be on the order of decades for all New Jersey sand resource areas (Parker, 1996).

The process of sediment refilling and reworking at excavated sites would be accomplished mainly by storm-induced sorting and, to a lesser degree, longshore sediment drift. Movement of shelf sediments in offshore New Jersey waters occurs primarily as a result of the high winds and waves that characterize intense storms (Parker, 1996), while transport of New Jersey shelf sediments due to sand shoal migration appears to be relatively minimal. Tropical and extra-tropical storms impact the offshore New Jersey region on an annual basis and these events would tend to modify seafloor depressions formed by dredging. The rate of the sand shoal reformation process will depend on the frequency and intensity of storms.

Assuming that the depth of sand excavation will not be so great as to substantially alter local hydrological characteristics, removal of benthic organisms along with sediments would quickly be followed by initial recolonization of the dredged areas by opportunistic infaunal taxa. Early-stage succession will begin within days of sediment removal, through settlement of larval recruits, primarily annelids and bivalves. Initial larval recruits likely would be dominated by populations of deposit feeding, opportunistic taxa (e.g., the polychaete *Asabellides oculata* and bivalves *Nucula proxima* and *Tellina agilis*). These species are well adapted to environmental stress and exploit suitable habitat when it becomes available. Later successional stages of benthic recolonization will be more gradual, and involve taxa that generally are less opportunistic and longer lived. Immigration of motile annelids, crustaceans, and echinoderms into impacted areas also would begin soon after excavation.

The length of time required for reestablishment of infaunal assemblages depends in large measure on sediment composition after dredging. Shoal sediments consist of well-sorted sands and gravel and also appear to be vertically uniform in sedimentary regime. In addition, New Jersey sand resource areas are characterized by a limited amount of fine sediments, indicating that they are not depositional in nature. It may be predicted that recolonization of dredged areas in sand resource areas by later colonizing taxa likely will occur in a timely manner and without persistent inhabitation by initial transitional assemblages, not unlike the process that has been documented in comparable regional habitats (Kropp, 1995b; Scott and Kelly, 1998).

Because the sedimentary regime of shoals is vertically uniform within the New Jersey sand resource areas, recolonization of surficial sediments by later successional stages likely will proceed even if dredged shoals are not completely reestablished. Furthermore, dredging of only a small portion of the area within each of the resource areas will ensure that a supply of non-transitional, motile taxa will be available for rapid migration into dredged areas. While community composition may differ for a period of time after the last dredging, the infaunal assemblage type that exists in mined areas will be similar to naturally occurring assemblages in the study area, particularly those assemblages inhabiting inter-ridge troughs. Based on previous observations of infaunal reestablishment in dredged areas, the infaunal community in dredged sites within sand resource areas most likely will become reestablished within 2 years, exhibiting levels of infaunal abundance, diversity, and composition comparable to nearby non-dredged areas.

7.5.4 Atlantic Surfclam

Atlantic surfclam is the most economically important benthic species found in or around the sand resource areas. Primary effects of dredging on Atlantic surfclam would be entrainment, hypoxia/anoxia, and turbidity. The analysis of surfclam distribution from the NMFS surfclam/ocean quahog surveys (see Section 2.3.1.2) showed that Atlantic surfclams are common to abundant throughout the shelf in the vicinity of the sand resource areas. These data demonstrated that the likelihood of encountering Atlantic surfclams in any of the New Jersey sand resource areas is reasonably high.

7.5.4.1 Entrainment

Individuals of the Atlantic surfclam would be very susceptible to entrainment by hydraulic dredges. Adults and juveniles are infaunal and unable to move away from a working dredge. As a result, any of these individuals within a dredging field would be entrained. Pelagic surfclam larvae could be entrained into the suction field of a hydraulic dredge. Entrainment would cause death or physical trauma to individuals.

7.5.4.2 Hypoxia/Anoxia

Dredging can cause local hypoxia/anoxia due to suspension of anoxic materials and decomposition of suspended sediments (LaSalle et al., 1991). Atlantic surfclams are sensitive to low dissolved oxygen concentrations. It is believed that low dissolved oxygen was responsible for a mass mortality that occurred off northern New Jersey in the early 1970s (Weinberg, 1998b). This event caused a shift in commercial fishing effort to more southerly waters for several years. The spatial extent of hypoxia/anoxia around a hydraulic dredge is difficult to predict (LaSalle et al., 1991); however, it should be limited in spatial extent relative to the entire shelf area. Effects on Atlantic surfclams would only be significant if dense beds existed within the dredging field.

7.5.4.3 Turbidity

Elevated turbidity can affect the movements and behavior of adult and larval bivalves (Loosanoff, 1962). Slight changes in turbidity (quantities of silt) affected the rate of water pumping and the character of shell movements in adults held in aquaria. High sediment concentrations can abrade gill and other soft tissues in adults and juvenile bivalves as well (LaSalle et al., 1991).

7.5.4.4 Project Scheduling

Project scheduling would not be useful for avoiding dredging-induced impacts to Atlantic surfclams; however, another approach should be considered. Given the abundance and distribution of Atlantic surfclams in the vicinity of the sand resource areas (as determined from the NMFS survey data for the New Jersey shelf), the likelihood of encountering appreciable numbers of individuals in a given sand resource area is high. Therefore, once an exact borrow site is chosen for dredging, a commercial clam fisher should be hired to evaluate the site for the presence and abundance of Atlantic surfclams. If commercial quantities are found, then the fisher should harvest them from the site prior to dredging. This approach would remove individuals that would be subject to impacts. Studies have demonstrated that juvenile Atlantic surfclams will recruit to dredged borrow sites (Scott and Kelley, 1998).

7.6 PELAGIC ENVIRONMENT

This section discusses the potential effects of hydraulic (cutterhead and hopper) dredging on water column organisms at a borrow site, and seasonal windows that would reduce the effects to particular species or groups. Groups of organisms considered include zooplankton (including eggs and larvae of economically important fish and shellfish species), squids, pelagic fishes, sea turtles, and marine mammals.

7.6.1 Zooplankton

7.6.1.1 Entrainment

Zooplankters encountering the suction field of hydraulic dredges will be easily drawn into the system (i.e., entrained). Entrained zooplankters are assumed to die from abrasion and physical trauma (LaSalle et al., 1991; Reine and Clarke, 1998). The most detrimental consequence of zooplankton entrainment is the death of fish and invertebrate larvae, which ultimately influences the age structure of adult populations.

The rate of zooplankton entrainment by hydraulic dredges depends upon local hydrographic patterns responsible for their transport and the spatial and temporal dynamics of local populations. Hydrographic patterns can be measured, whereas inherently variable zooplankton populations are more difficult to characterize (Sullivan and Hancock, 1977). Because of difficulties in measuring population parameters from field-collected data, direct estimates of zooplankton entrainment (and subsequent population effects) are not available in the dredging literature. An alternative to using field-collected data has been to develop numerical models that predict population effects given specific scenarios (discussed in LaSalle et al., 1991 and Reine and Clarke, 1998). Unfortunately, population effects estimated from models can differ greatly depending upon model assumptions (LaSalle et al., 1991; Reine and Clarke, 1998).

Entrainment rate also depends upon physical aspects of the dredging operation. Because the suction field of hydraulic dredges remains near the seafloor, species most susceptible to entrainment are those occurring in the lower portion of the water column. Taxa or life stages that spend part of their time associated with the benthic environment, such as demersal fish eggs or demersal zooplankton (Hammer and Zimmerman, 1979), would be especially vulnerable. Unfortunately, no information exists on the abundance or composition of demersal zooplankton in the sand resource areas. Several fish species in the region lay demersal eggs. Considering the high reproductive capacity of zooplankton along with the relatively small area of the dredge suction field and the volume of water entrained compared to the overall volume of surrounding waters, it is unlikely that entrainment would greatly affect zooplankton populations or assemblages in the New Jersey sand resource areas.

7.6.1.2 Turbidity

Sediments suspended and dispersed by the action of a working dredge can affect zooplankters by 1) interfering with feeding activity; 2) direct mortality and toxicity; and 3) physiological impairment.

Most crustacean zooplankters are filter feeders capable of filtering and processing particles between 3 and 10 ìm (Nival and Nival, 1976). Inorganic particles in this size range can easily foul the fine structures (setules) on feeding appendages of crustaceans such as copepods, and crab and shrimp larvae (Sullivan and Hancock, 1977). Laboratory studies have shown that mechanical disruption of feeding can affect growth and reproductive success (Kirk,

1992). Plankters feeding by ciliary action (e.g., echinoderm larvae) also would be susceptible to mechanical effects of suspended particles (Sullivan and Hancock, 1977).

Larval fishes are visual feeders that depend on adequate light levels for their foraging success (Blaxter, 1968). High turbidity reduces light levels in the water column, which in turn shortens the reactive distance between a larval fish and its prey. Laboratory studies have demonstrated the negative influence of elevated turbidity on prey capture rates for larvae of the herring *Clupea harengus harengus* (Johnston and Wildish, 1982), striped bass, *Morone saxatilis* (Morgan et al., 1983; Breitburg, 1988), and dolphin, *Coryphaena hippurus* (Jokiel, 1989). In one laboratory study, however, increased turbidity actually enhanced feeding abilities of larval herring *Clupea harengus pallisi* (Boehlert and Morgan, 1985). The authors suggested that suspended sediment may have provided better contrast against which small particles were viewed.

Direct mortality and toxicity caused by elevated turbidity varies with species and the nature of the sediment and sediment-bound contaminants. Crustacean zooplankters will ingest suspended inorganic particles that may or may not contain contaminants. Contamination is expected to be low in all sand resource areas. A laboratory study showed that copepods ingesting high amounts of “red mud” grew slower than control groups feeding only on diatoms (Paffenhofer, 1972). This was attributed to the non-nutritive value of the red mud rather than to any associated toxic compounds. Sediment-bound toxic compounds introduced into the water column may be ingested by zooplankters. These substances can be detrimental to zooplankters. However, studies with copepods exposed to deep sea mine tailings containing trace metals showed minimal effects (Hirota, 1981; Hu, 1981).

High turbidity can cause physiological changes that can kill or retard developing eggs and larvae of fishes and invertebrates (Davis and Hidu, 1969; Rosenthal, 1971). High concentrations of suspended sediment can kill or deform fish eggs (Rosenthal, 1971). Laboratory studies investigating effects of elevated turbidity on eggs and larvae of bivalves show that slight increases in turbidity actually stimulated larval growth, whereas large increases in turbidity caused abnormalities (Loosanoff, 1962; Davis and Hidu, 1969). Hatching success of fish eggs exposed to high suspended concentrations varies, but most studies show minimal effects from acute exposures in the 50 to 500 mg/L range (Auld and Schubel, 1978; Morgan et al., 1983; Jokiel, 1989). In these same studies, artificially high suspended sediment concentrations (1,000 to 8,000 mg/L) were required to induce mortality.

As with entrainment, the effects of suspended sediments on zooplankters is primarily restricted to the lower portion of the water column for a cutterhead dredge because the turbidity plume remains near the cutterhead with little of the plume reaching surface waters (LaSalle et al., 1991). Suspended sediment plumes in near-bottom waters may extend for up to several hundred meters laterally from the cutterhead. In contrast, hopper barges may create turbid surface plumes due to overwash (LaSalle et al., 1991). With either dredge type, the turbidity plume is expected to cover a small portion of the water column relative to the surrounding waters. Due to the limited areal extent and transient nature of the sediment plume, it is unlikely that turbidity would greatly affect zooplankton populations or assemblages in the New Jersey sand resource areas.

7.6.1.3 Project Scheduling

For open ocean environments, Sullivan and Hancock (1977) generalized that dredging effects on zooplankton would be minimal due to high spatial and temporal variability of the populations, whereas significant effects would be expected in enclosed waters with endemic populations. However, accurate prediction of the local effects of entrainment or dredge-

produced turbidity on zooplankton populations of the sand resource areas requires adequate site-specific data. Zooplankton populations in general should not be subject to impacts from dredging, but available regional information (see Section 2.3.2.1) indicates that planktonic larvae, particularly those of fishes, occur in the project area during summer and fall months (Able and Fahay, 1998). Because adults of these species spawn offshore and larval and juvenile forms make their way back to inshore nursery areas such as Great Egg Bay, Sand Resource Areas G1, G2, and G3 could be construed as lying in an important recruitment corridor. The other sand resource areas are not within such an important position relative to coastal inlets and therefore should not require any special project scheduling consideration.

When data are inadequate to accurately predict the magnitude of dredging effects, environmental windows have been required to provide a conservative approach and lessen potential effects on key species. However, LaSalle et al. (1991) and Reine et al. (1998) have stressed the need to base future environmental windows on sound evidence, and have argued against subjectively selected environmental windows. Environmental windows delay projects and greatly increase costs (Dickerson et al., 1998), and their use should not be driven by subjective or overly conservative approaches. If borrow sites are used in Areas G1, G2, or G3, an environmental window excluding summer and fall months could be considered to avoid dredging when fish juveniles and larvae are most prevalent, but only if additional data become available to determine the extent of impacts and justify the restriction. Progress toward understanding the real need for environmental windows can only be achieved by reducing the degree of uncertainty surrounding impacts and the means to avoid them (Dickerson et al., 1998).

7.6.2 Squids

7.6.2.1 Entrainment

No information exists regarding impacts of hydraulic dredging on squids. Nevertheless, squids could be entrained if they encountered the suction field of a hydraulic dredge. Some general aspects of squid behavior increase the chance of encountering the bottom-oriented dredge suction field. Adult squids are generally demersal by day and enter the water column at night to feed on zooplankton (Fischer, 1978). In addition, squids lay their eggs in large clusters on the seafloor (Vecchione, 1981).

7.6.2.2 Attraction

Because some squid species are attracted to lights at night (Fischer, 1978), it is likely that squids could be attracted to lights of a working dredge. This could draw them into the suction field and increase the chance of entrainment.

7.6.2.3 Project Scheduling

With no information on local squid populations available, reasonable predictions of demographic effects are difficult to make. As with the other pelagic organisms, dredging is unlikely to significantly impact squid populations in the vicinity of the sand resource areas. This precludes the need for an environmental window or specific project scheduling to protect squid resources.

7.6.3 Fishes

7.6.3.1 Entrainment

Entrainment of adult fishes by hydraulic dredging has been reported for several projects (Larson and Moehl, 1988; McGraw and Armstrong, 1988; Reine and Clarke, 1998). The most comprehensive study of fish entrainment took place in Grays Harbor, Washington during a 10-year period when 27 fish taxa were entrained (McGraw and Armstrong, 1988). Most entrained fishes were demersal species such as flatfishes, sand lance, and sculpin; however, three pelagic species (anchovy, herring, and smelt) were recorded. Entrainment rates for the pelagic species were very low, ranging from 1 to 18 fishes/1,000 cy (McGraw and Armstrong, 1988). Comparisons between relative numbers of entrained fishes with numbers captured by trawling showed that some pelagic species were avoiding the dredge. Another entrainment study conducted near the mouth of the Columbia River, Washington reported 14 fish taxa entrained at an average rate of 0.008 to 0.341 fishes/cy (Larson and Moehl, 1988). Few of the coastal pelagic fishes occurring offshore of New Jersey should become entrained because the dredge's suction field exists near the bottom and many pelagic species have sufficient mobility to avoid the suction field.

7.6.3.2 Attraction

Even though dredges are temporary structures, they still can attract roving pelagic species. This may temporarily disrupt a migratory route for some members of the stock, but it is unlikely that there would be an appreciable negative effect.

7.6.3.3 Turbidity

Turbidity can cause feeding impairment, avoidance and attraction movements, and physiological changes in adult pelagic fishes. As discussed for larval fishes, pelagic species are primarily visual feeders and when turbidity reduces light penetration, the fishes reactive distance decreases (Vinyard and O' Brien, 1976). Light scattering caused by suspended sediment also can affect a visual predator's ability to perceive and capture prey (Benfield and Minello, 1996).

Some species will actively avoid or be attracted to turbid water. Experiments with pelagic kawakawa (*Euthynnus affinis*) and yellowfin tuna (*Thunnus albacares*) demonstrated that these species would actively avoid experimental turbidity clouds, but also would swim directly through them during some trials (Barry, 1978). Turbidity plumes emanating from coastal rivers may retard or affect movements of some pelagic species.

Gill cavities can be clogged by suspended sediment preventing normal respiration and mechanically affecting food gathering in planktivorous species (Bruton, 1985). High suspended sediment levels generated by storms have contributed to the death of nearshore and offshore fishes by clogging gill cavities and eroding gill lamellae (Robins, 1957).

The limited spatial and temporal extents of turbidity plumes from either cutterhead or hopper dredges are expected to be limited. Therefore, there should be no significant impact on adult pelagic fishes.

7.6.3.4 Project Scheduling

Hydraulic dredging should not present a significant problem for pelagic fishes offshore of New Jersey. If an environmental window is sought to protect pelagic fishes from dredging impacts, the spring to fall period would encompass the peak seasons for the economically important species. Temporal scheduling as a means to avoid impacts is practical if the organism in question is highly concentrated in waters of the area during some specific time

1801(10)]. The EFH interim final rule summarizing EFH regulations (62 FR 66531-66559) outlines additional interpretation of the EFH definition. Waters, as defined previously, include "aquatic areas and their associated physical, chemical, and biological properties that are used by fish, and may include aquatic areas historically used by fish where appropriate." Substrate includes “sediment, hard bottom, structures underlying the waters, and associated biological communities.” Necessary is defined as "the habitat required to support a sustainable fishery and the managed species' contribution to a healthy ecosystem." “Fish” includes "finfish, mollusks, crustaceans, and all other forms of marine animal and plant life other than marine mammals and birds," whereas "spawning, breeding, feeding or growth to maturity" cover the complete life cycle of those species of interest.

The Mid-Atlantic Fishery Management Council (MAFMC) has produced several FMPs for single and mixed groups of species that inhabit New Jersey offshore waters. All of these FMPs (including those for Atlantic surfclam and ocean quahog [MAFMC, 1998a]; Atlantic mackerel, squids, and butterfish [MAFMC, 1998b]; summer flounder, scup, and black seabass [MAFMC, 1998c]; bluefish [MAFMC, 1998d]; and spiny dogfish [MAFMC, 1999]) were recently amended to address EFH. The amendments identified and described EFH for all life stages of managed species. Some species that occur in New Jersey waters such as sea scallop and winter flounder are under the jurisdiction of the New England Fishery Management Council (NEFMC). The NEFMC also has amended previous FMPs to address EFH (NEFMC, 1998a,b). In addition to the FMPs prepared by the MAFMC and NEFMC, highly migratory species (tunas, sharks, and swordfish) are managed by NMFS (NMFS, 1999). EFH for several of the species (and life stages) covered in these FMPs overlapped the eight sand resource areas offshore New Jersey. EFH characteristics for these overlapping species are presented in Table 7-2.

The area encompassed by the eight sand resource areas is very small relative to the mapped EFH characteristics. For this reason, the effect of dredging on EFH for the managed species is expected to be minimal.

7.6.4 Sea Turtles

7.6.4.1 Entrainment

The main potential effect of dredging on sea turtles is physical injury or death caused by the suction and/or cutting action of the dredge head and subsequent entrainment. Numerous sea turtle injuries and mortalities have been documented during dredging projects, particularly along Florida’s east coast (Studt, 1987; Dickerson et al., 1992; Slay, 1995). Impacts typically have been minimized by some combination of project scheduling and equipment selection,

Table 7-2. Invertebrate and fish species for which Essential Fish Habitat has been identified in the vicinity of the eight sand resource areas offshore New Jersey (adapted from Mid-Atlantic Fishery Management Council, 1998a,b,c,d, 1999; New England Fishery Management Council, 1998a,b; National Marine Fisheries Service, 1999).

Species (Phylogenetic Order)	Life Stage
Invertebrates	
Sea scallop (*Placopecten magellenicus*)	Adults and juveniles
Surfclam (*Spisula solidissima*)	Adults and juveniles
Ocean quahog (*Arctica islandica*)	Adults and juveniles
Long-finned squid (*Loligo pealei*)	Adults and juveniles
Short-finned squid (*Illex illecebrosus*)	Adults and juveniles
Fishes	
Spiny dogfish (*Squalus acanthias*)	Adults and juveniles
Dusky shark (*Carcharhinus obscurus*)	Late juveniles/subadults, neonates/early juveniles
Sandbar shark (*Carcharhinus plumbeus*)	Adults, late juveniles/subadults, neonates/early juveniles
Tiger shark (*Gaelocerdo cuvieri*)	Adults, late juveniles/subadults, neonates/early juveniles
Bluefish (*Pomatomus saltatrix*)	Adults, juveniles, larvae, and eggs
Atlantic Butterfish (*Peprilus triacanthus*)	Adults, juveniles, larvae, and eggs
Scup (*Stenotomus chrysops*)	Adults and juveniles
Black seabass (*Centropristis striata*)	Adults, juveniles, and larvae
Atlantic mackerel (*Scomber scombrus*)	Adults, juveniles, larvae, and eggs
Winter flounder (*Paralichthys lethostigma*)	Adults, juveniles, larvae, and eggs
Summer flounder (*Paralichthys dentatus*)	Adults, juveniles, larvae, and eggs

accompanied if necessary by turtle removal and/or monitoring. Several turtles have been taken during dredging operations in New Jersey and Delaware during recent years (NMFS, 1996). However, dredging has not been implicated as a major cause of death or injury to sea turtles in the region (NMFS, 1996).

Of the four turtle species that typically occur off New Jersey, three (loggerhead, green, and Kemp's ridley) are considered to be at risk from dredging activities because of their benthic feeding habits (Dickerson et al., 1992). Loggerheads are the most abundant turtles in the project area, and historically, they have been the species most frequently entrained during hopper dredging, possibly accounting for up to 86% of the total (Reine and Clarke, 1998). Green and Kemp's ridley turtles historically have accounted for much smaller portions of the total. Leatherbacks, which also occur in New Jersey waters, are unlikely to be affected by dredging because they feed in the water column rather than on the bottom (NMFS, 1996).

Physical impact can occur when a turtle feeding or resting on the seafloor is contacted by the dredge head. Two types of dredges may be used on the proposed project. Cutterhead suction dredges are considered unlikely to kill or injure turtles, perhaps because the cutterhead encounters a smaller area of seafloor per unit time, allowing more opportunity for turtles to escape (Palermo, 1990). Hopper dredges are believed to pose the greatest risk to sea turtles (Dickerson, 1990; NMFS, 1997). There has been considerable research into designing modified hopper dredges with turtle deflectors that reduce the likelihood of entraining sea turtles (Studt, 1987; Berry, 1990; Dickerson et al., 1992; Banks and Alexander, 1994; USACE, 1999). If a

hopper dredge is used on this project during the turtle season of June through November, the NMFS may require turtle monitoring and use of a turtle-deflecting draghead (NMFS, 1996).

Studies in New York waters have shown that chelonid sea turtles (i.e., those other than leatherbacks) feed primarily in depths of 15 m or less (NMFS, 1996). The risk of physical impacts to turtles would appear to be greatest in these shallow water depths, which are present in all of the potential sand resource areas except Area F1. However, there also is risk in deeper water because when turtles feed there, they tend to stay on the bottom longer (NMFS, 1996).

7.6.4.2 Habitat Modification

Juvenile and subadult loggerheads, greens, and Kemp's ridleys use northeastern coastal waters as developmental habit, foraging on benthic organisms (see Section 2.3.2.4). Therefore, when borrow sites have significant concentrations of benthic resources, dredging can reduce food availability both by removing potential food items and altering the benthic habitat (NMFS, 1996). Effects would be temporary, as benthic populations would be expected to recover over a period of months to years (see Section 7.5.3). In addition, borrow sites represent only a small portion of the shallow benthic habitat available off New Jersey. Trawl sampling in support of this document showed that potential turtle food such as various benthic crustaceans, mollusks, and echinoderms are present in the borrow sites, but not in especially dense concentrations (see Section 6.3.4).

7.6.4.3 Turbidity

Sea turtles in and near the project area may encounter turbid water that could temporarily interfere with feeding. However, due to the limited areal extent and transient occurrence of the sediment plume (see Section 7.5.1.2), turbidity is considered unlikely to significantly affect turtle behavior or survival.

7.6.4.4 Hypoxia/Anoxia

Dredging may produce localized hypoxia/anoxia in the water column due to oxygen consumption of the suspended sediments (LaSalle et al., 1991). In general, oxygen levels in the plume and near-bottom waters may approach zero, but levels in adjacent waters outside the plume are at or near normal. Due to the limited extent and transient occurrence of hypoxia/anoxia, no significant effects on turtles are expected.

7.6.4.5 Noise

Dredging is one of many human activities in the marine environment that produce underwater noise. Sea turtles have limited hearing ability (Ridgway et al., 1969; Lenhardt, 1994), and its role in their life cycle and behavior is poorly known. It is believed that sea turtles do not rely on sound to any significant degree for communication or food location, although it has been suggested that low frequency sound may be involved in natal beach homing behavior (Dodd, 1988). The latter would not be a consideration in this case because the project area is not near any significant nesting beach.

There are indications that underwater noise is unlikely to significantly affect turtles. First, studies in the Gulf of Mexico have shown some evidence for positive association of sea turtles with petroleum platforms (Rosman et al., 1987; Lohoefener et al., 1990) despite the industrial noise associated with these structures. Second, experiments testing the use of seismic airguns to repel turtles from dredging activities indicate that even loud noises cause avoidance only at very close range (e.g., 100 m or less) (Zawila, 1994). Turtles became habituated to the noise

after repeated exposure to the airguns (Moein et al., 1994). Therefore, if noise does have any impact on turtles, it would most likely be positive by encouraging avoidance of the dredge.

7.6.4.6 Project Scheduling Considerations

Project scheduling is one way to avoid or minimize turtle impacts during dredging (Studt, 1987; Arnold, 1992). If a cutterhead suction dredge is used, seasonal or other restrictions are considered unnecessary because there is little likelihood of killing or injuring sea turtles. If a hopper dredge is used, then it would be best to avoid the June through November turtle season. However, the NMFS (1996) has recognized that the vagaries of winter weather off New Jersey make it infeasible to prohibit dredging during these months. If use of a hopper dredge during this season cannot be avoided, then other mitigation and monitoring requirements are likely to be imposed, such as turtle monitoring and use of a turtle-deflecting draghead (NMFS, 1996).

7.6.5 Marine Mammals

7.6.5.1 Physical Injury

Unlike sea turtles, most marine mammals are unlikely to be physically injured by dredging *per se* because they generally do not rest on the bottom and they can easily avoid contact with dredging vessels and equipment. The odontocete marine mammals most likely to be found on the continental shelf off New Jersey, such as bottlenose dolphin and common dolphin, are agile swimmers that are presumed capable of avoiding physical injury during dredging.

However, physical injury from vessel strikes is a serious concern for three endangered species of mysticetes: northern right whale, fin whale, and humpback whale. Recovery plans for these three species identify vessel strikes as a contributing factor impeding their recovery (NMFS, 1991a,b; Reeves et al., 1998). Vessel strikes are an especially serious concern for northern right whales. NMFS published regulations in February 1997 restricting vessel approaches of right whales. These regulations prohibit all approaches within 460 m of any right whale, whether by boat, aircraft, or other means (NMFS, 1998b). It is likely that measures to minimize the potential for vessel strikes of endangered whales would be part of any Biological Opinion issued by the NMFS for dredging off New Jersey (e.g., NMFS, 1996).

The harbor porpoise, which has been proposed for listing as a threatened species, is unlikely to be injured by dredging vessels or equipment. The major threat to the recovery of this species is gillnetting (NMFS, 1998b). The NMFS has indicated that interactions of this species with dredging are unlikely (USEPA, 1997).

7.6.5.2 Turbidity

Marine mammals in and near the project area may encounter turbid water during dredging. This turbidity could temporarily interfere with feeding or other activities, but the animals could easily swim to avoid turbid areas. Due to the limited aerial extent and transient occurrence of the sediment plume (see Section 7.5.1.2), turbidity is considered unlikely to significantly affect marine mammal behavior or survival.

7.6.5.3 Noise

Dredging can be a significant source of continuous underwater noise in nearshore areas, particularly in low frequencies (<1,000 Hz) (Richardson et al., 1995). This noise typically diminishes to background levels within about 20 to 25 km of the source (Richardson et al., 1995). Noise levels are not sufficient to cause hearing loss or other auditory damage to marine mammals (Richardson et al., 1995). However, some observations in the vicinity of dredging

operations and other industrial activities have documented avoidance behavior, while in other cases, animals seem to develop a tolerance for the industrial noise (Malme et al., 1983; Richardson et al., 1995). Due to the frequency range of their hearing, mysticetes (baleen whales) are more likely to be affected by low frequency noise than are odontocetes. It is possible that dredging noise could cause avoidance of the project area during humpback whale and northern right whale migrations.

7.6.5.4 Project Scheduling Considerations

Common shelf species such as bottlenose dolphin and common dolphin may be present year-round and, as noted above, are unlikely to be adversely affected by dredging. Harbor porpoise occurrence is more seasonal, but the likelihood of impact is so low that it does not warrant seasonal restrictions on dredging.

Fin and humpback whales would be most likely to occur during winter or spring, and right whales as transients during spring and fall. There is no “resident” population of any of these whales in the study area; rather, they would be temporary inhabitants, or would be transiting the area during seasonal migrations. Generally, the probability of encountering these species in the project area would be lowest during summer. However, due to the low likelihood of impact, seasonal restrictions on dredging probably are not warranted. Instead, measures to minimize possible vessel interactions with these endangered species are likely to be required by the NMFS.

7.7 POTENTIAL CUMULATIVE EFFECTS

Cumulative physical environmental impacts from multiple sand extraction scenarios at one or all sand borrow sites within the study area were evaluated to assess long-term effects at potential borrow sites and along the coastline. Results presented above for wave and sediment transport processes reflect the impact of large extraction scenarios that are expected to be within the cumulative sand resource needs of the State for the next 10 years. Therefore, the cumulative impacts of sand mining offshore New Jersey on wave propagation and sediment transport processes are expected to be negligible under the conditions imposed. Unless substantially larger borrow sites and extraction volumes are selected for sand mining, no significant impacts to normal and storm physical processes are expected.

Cumulative impacts resulting from multiple sand mining operations within sand resource area are a concern when evaluating potential long-term effects on benthic and pelagic assemblages. Given that the expected beach replenishment interval is on the order of 5 to 10 years, and that the expected recovery time of the affected benthic community after sand removal is anticipated to be much less than that (within 2 years), the potential for significant cumulative benthic impacts is remote. No cumulative impacts to the pelagic environment, including zooplankton, squids, fishes, sea turtles, and marine mammals, are expected from multiple sand mining operations within the sand resource areas.

8.0 CONCLUSIONS

The primary purpose of this study was to address environmental concerns raised by the potential for dredging sand from the OCS offshore New Jersey for beach replenishment. Primary concerns focused on physical and biological components of the environment at eight proposed sand resource areas. Biological and physical processes data were analyzed to assess the potential impacts of offshore dredging activities within the study area to minimize or preclude long-term adverse environmental impacts at potential borrow sites and along the coastline landward of borrow sites. Furthermore, wave transformation and sediment transport numerical modeling were employed to simulate the physical environmental effects of proposed sand dredging operations to ensure that offshore sand resources are developed in an environmentally sound manner. Of the eight potential sand resource areas, seven were chosen for evaluating sand extraction scenarios based on historical beach replenishment needs and resource information from the NJGS. Area F1 in the northern portion of the study area was not evaluated as a sand borrow source because potential resource volumes are below 1 MCM.

The following provides a summary of results and conclusions regarding the potential environmental effects of sand mining on the OCS for replenishing sand to eroding beaches. Because benthic and pelagic biological characteristics are in part determined by spatially varying physical processes throughout the study area, physical processes analyses are summarized first.

8.1 WAVE TRANSFORMATION MODELING

A primary component of any physical environmental effects analysis related to sand mining from the OCS must include numerical wave transformation modeling. Potentially rapid and significant changes in bathymetry due to sand extraction on the OCS may have substantial impact on wave propagation patterns on the continental shelf and at the shoreline. In turn, sediment transport patterns may be altered so as to adversely impact beach erosion or accretion problems. As such, substantial effort was spent understanding existing wave propagation patterns relative to those resulting from potential sand extraction scenarios.

The spectral wave transformation model REF/DIF S was used to evaluate changes in wave approach resulting from potential sand dredging activities. REF/DIF S is a combined refraction and diffraction spectral wave model, which can simulate the behavior of a random sea and incorporates the effects of shoaling, wave breaking, refraction, diffraction, and energy dissipation. A spectral wave model was selected to simulate wave transformation because of its ability to propagate realistic wave components (a spectrum) simultaneously across the continental shelf surface. By simulating several wave components together, a spectral wave model represents nature more closely.

Wave transformation results identify key areas of wave convergence, wave divergence, and shadow zones offshore New Jersey. Non-storm significant wave heights and wave angles experience little variation to the 20-m depth contour where the wave field begins to feel the influence of bathymetry. The region offshore of Townsends and Corsons Inlets (Grid A) has a relatively consistent longshore wave height distribution. Several areas of wave convergence and divergence were caused by the shoals surrounding Sand Resource Areas A1 and A2. These features focus wave energy at various locations along the coast depending on the wave approach direction. The area to the south of Barnegat Inlet (Grid B1) experiences mild shoreline retreat and a consistent wave height distribution along the shoreline. Shoals and depressions south of Area C1, as well as offshore linear ridges to the north, can produce significant wave transformation within the modeling domain. Wave energy focused by these features most often impact the Harvey Cedars and Loveladies regions. Offshore Little Egg and

Brigantine Inlets (Grid B2), wave transformation again is influenced by numerous linear ridges. Increased wave heights appear most frequently near Brigantine Inlet. The area seaward of northern Barnegat Bay (Grid C) also experiences wave height changes produced by offshore shoals and depressions within the modeling domain. Consistent wave focusing is observed by the shoal within Area F2, as well as the shoals to the south and southeast of F2. Wave energy focused by these features may impact regions from Seaside Park north to Bay Head, depending on approach direction.

For the 50-yr hurricane and northeast storm, wave patterns are similar to the directional approach results. An increase in wave height is documented in many areas where wave convergence occurs. For example, the shoal present in Area F2 produces wave convergence that results in 6.0 m wave heights during a typical 50-yr northeast storm. The 50-yr hurricane and northeast storm simulated in the present study represents a major storm that could have impact on the approaching wave field and sediment transport patterns.

Differences in wave height between pre- and post-dredging scenarios offshore New Jersey indicate maximum wave height changes for directional approach simulations ranging from 0.1 to 0.25 m (7 to 16% of the initial wave height). The magnitude of modifications increase as the magnitude of waves increase or when the orientation of potential borrow sites aligns with waves to produce maximum impact (e.g., southeast approach at Grid A). In Grids A and B2, which are the southernmost grids, maximum wave height changes dissipate relatively quickly as waves advance towards the coast and break. In Grids B1 and C, maximum changes do not dissipate as readily. At potential impact areas along the coast, wave height changes average ±0.13, ±0.11, ±0.15, and ±0.10 m for Grids A, B1, B2, and C, respectively. These modifications represent changes of approximately ±3 to 15% when compared with wave heights for existing conditions. Overall, there is minimal to no impact caused by potential offshore dredging during normal conditions.

During extreme wave conditions (e.g., a 50-yr storm), wave heights are increased from 0.4 to 1.4 m, suggesting a rather significant change. However, as a result of the increased magnitude of the incoming waves, this generally represents a change of less than 10%. Due to the orientation of the shoreline and the proposed borrow sites, a hurricane has more significant impacts on Grids A and B2 (Areas A1, A2, G1, G2, and G3), while a northeast storm more significantly impacts Grids B1 and C (Areas C1 and F2). For most of the sand borrow sites, a significant amount of wave energy is dissipated before waves reach the coast, especially for Grids A and B2. As such, wave height increases are less than 0.4 m along most of the coast. A maximum change of 0.4 m in wave height is not expected to increase nearshore erosion above existing conditions during a storm event.

Borrow sites within Areas A1 and A2, located offshore of Townsends Inlet, have a greater impact on the wave field due to the larger extraction volumes (8.8 and 8.6 MCM, respectively). In addition, regions with multiple borrow sites (Grids A and B2) indicate a greater potential for wave modifications with simultaneous dredging. Overall, wave transformation impacted by potential borrow sites is minimal during normal and storm conditions.

8.2 CIRCULATION AND SEDIMENT TRANSPORT DYNAMICS

Current measurements and analyses, and wave transformation modeling, provide baseline information on incident processes impacting coastal environments under existing conditions and with respect to proposed sand mining activities for beach replenishment. Ultimately, the most important data set for understanding physical processes impacts from offshore sand extraction is changes in sediment transport dynamics resulting from potential sand extraction scenarios relative to existing conditions.

While no large-scale predictive circulation models were developed to quantify the effects of dredging in sand resource areas, the analysis of current patterns resulting from this study suggests proposed sand mining will have negligible impact on large-scale shelf circulation. Measurement of bottom currents offshore New Jersey (seaward of Little Egg Inlet) throughout an approximate two-year period (1993 to 1995) revealed considerable variability in flow speed and direction. The mean flow was to the southwest along the inner shelf bathymetric contours. Strongest flow was observed in the along-shelf direction, with peak velocities of nearly 50 cm/sec (1 knot) to the south; maximum northward currents reached 37 cm/sec. Flow reversals were noted frequently.

In the cross-shelf direction, mean flow was oriented onshore, consistent with upwelling processes that push bottom waters up onto the shelf. Maximum cross-shelf flow was 31 cm/sec (directed onshore); minimum flow was -13 cm/sec (directed offshore). Cross-shelf bottom currents were affected most significantly by semi-diurnal tides, with a mean onshore flow. Wind-driven currents were found to be less significant in the cross-shelf direction. Seasonal variability was most significant for wind-driven currents. Winter and autumn data records were most energetic, with summer and spring data sets possessing smaller energy values.

These data suggest that along-shelf currents possess higher energy than cross-shelf flows. Along-shelf currents were dominated by wind-driven processes, accounting for as much as 70% of the total current energy. Wind-driven processes were greatest in winter; however, wind-driven flows appeared strongly biased by singular events, such as local responses to storm winds or non-locally generated free waves that influenced the magnitude of wind-driven current energy. This evidence suggests that these singular events, with corresponding higher currents, have the greatest potential to transport sand. If so, sediment transport patterns are predominately in the along-shelf direction, with a net transport oriented in the direction of the mean southerly flow. The data also show that singular events had little impact on cross-shelf currents, indicating that cross-shelf sediment transport due to currents is weak. Because proposed sand mining locations are small relative to the entire shelf area, it is anticipated that proposed dredging will not remove enough material to significantly alter major bathymetric features in the region. Therefore, the forces and geometric features that principally affect circulation patterns will remain relatively unchanged.

Three independent sediment transport analyses were completed to evaluate physical environmental impacts due to sand mining. First, historical sediment transport trends were quantified to document regional, long-term sediment movement throughout the study area using historical bathymetric data. Erosion and accretion patterns were documented, and sediment transport rates in the littoral zone and at offshore borrow sites were evaluated to assess potential changes due to offshore sand dredging activities. Second, sediment transport patterns at proposed offshore borrow sites were evaluated using wave modeling results and current measurements. Post-dredging wave model results were integrated with regional current measurements to estimate sediment transport trends for predicting borrow site infilling rates. Third, nearshore currents and sediment transport were modeled using wave transformation modeling output to estimate potential impacts to the longshore sand transport system (beach erosion and accretion). All three methods were compared for documenting consistency of measurements relative to predictions, and potential physical environmental impacts were identified.

8.2.1 Historical Sediment Transport Patterns

Regional geomorphic changes for the period 1843/91 to 1934/77 were analyzed to assess long-term, net coastal sediment dynamics. Although these data did not provide information on the potential impacts of sand dredging from proposed borrow sites, they do provide a means of

calibrating predictive sediment transport models relative to infilling rates at borrow sites and longshore sand transport.

Shoreline position and nearshore bathymetric change document four important sediment transport trends. First, the predominant direction of transport throughout the study area is north to south. Southern Long Beach Island (north of Little Egg Inlet) and southern Island Beach (north of Barnegat Inlet) have migrated at a rate of about 14 m/yr to the south since 1839/42. The ebb-tidal shoals at all inlets in the study area are skewed to the south, and the channels are aligned in a northwest-southeast direction.

Second, the most dynamic features within the study area, in terms of nearshore sediment transport, are the ebb-tidal shoals associated with inlets along the southeastern barrier island chain. Areas of significant erosion and accretion are documented for the period 1843/91 to 1934/77, reflecting wave and current dynamics at entrances, the influence of engineering structures on morphologic change, and the contribution of littoral sand transport from the north to sediment bypassing and shoal migration.

Third, alternating bands of erosion and accretion on the continental shelf east of the Federal-State boundary illustrate relatively slow but steady reworking of the upper shelf surface as sand ridges migrate from north to south. The process by which this is occurring at Areas G1, G2, and G3 suggests that a borrow site in this region would fill with sand transported from an adjacent site at a rate of about 62,000 to 125,000 m^3/yr. At Areas A1 and A2, the potential sand transport rate increases to 160,000 to 200,000 m^3/yr. This increase in potential transport rate reflects a more dynamic offshore environment seaward of the southern barrier island chain.

Finally, net longshore transport rates determined from seafloor changes in the littoral zone between Little Egg Inlet and the beach south of Hereford Inlet indicate an increasing transport rate to the south from about 70,000 m^3/yr south of Little Egg Inlet to 190,000 to 230,000 m^3/yr at Townsends and Hereford Inlets. It appears that areas of largest net transport exist just south of entrances as a result of natural sediment bypassing from updrift to downdrift barrier beaches. These rates compare well and provide a measured level of confidence in wave and sediment transport modeling predictions relative to impacts associated with sand dredging from proposed borrow sites.

8.2.2 Sediment Transport at Potential Borrow Sites

In addition to predicted modifications to the wave field, potential sand mining at offshore borrow sites results in minor changes in sediment transport pathways in and around the dredged regions. The modifications to bathymetry caused by sand mining only influence local hydrodynamic and sediment transport processes in the offshore area. Although wave heights may change at the dredged borrow sites, areas adjacent to the sites do not experience dramatic changes in wave or sediment transport characteristics.

Initially, sediment transport at borrow sites will experience rapid changes after sand dredging is complete. Given the water depths at the proposed borrow sites, it is expected that minimal impacts to waves and regional sediment transport processes will occur during infilling. Sediment that replaces the dredged material will fluctuate based on location, time of dredging, and storm characteristics following dredging episodes. Average transport rates range from a minimum of 28 m^3/day (about 10,000 m^3/yr; Area F2) to a high of 450 m^3/day (about 164,000 m^3/yr; Area A1), while the infilling rate varies between 54 (Area A1) to 303 years (Area C1). This range of infilling times is based on the volume of sand numerically dredged from a borrow site as well as the sediment transport rate. Predicted nearshore sediment transport rates are slightly lower than those determined from historical data sets, but the two rate estimates are within the same order of magnitude (10,000 to 160,000 m^3/yr versus 62,000 to 200,000 m^3/yr,

respectively). Calculated infilling times would be reduced if storm events were incorporated into the analysis.

8.2.3 Nearshore Sediment Transport Modeling

The potential effects of offshore sand mining on nearshore sediment transport patterns are of interest because dredged holes can intensify wave energy at the shoreline and create erosional hot-spots. Sand dredging impacts for Areas A1 and A2 illustrate that there is a defined, but minor, change in littoral transport. Due to relatively high transport rates along the southern portion of the New Jersey coast, the percent difference in transport rates associated with dredging was smallest within this area (the maximum variation in annual longshore sand transport rate was approximately 7% of the existing value). The shadow zones landward of Areas A1 and A2 are located approximately 5 km and 1 km north of Townsends Inlet, respectively. These shadow zones are indicated by a significant reduction in south-directed wave energy. Likewise, the largest increase in south-directed transport occurs between the shadow zones (3 km north of Townsends Inlet), where both borrow sites in Areas A1 and A2 have wave energy refracted to the south and north, respectively. This increase in wave energy at the shoreline is responsible for the increased south-directed transport between the shadow zones.

Because the offshore distance to Resource Areas G2 and G3 is relatively small (approximately 5 km offshore), the region of potential impacts is more confined than the area defined for Area A2. For the borrow sites in Areas G2 and G3, the maximum variation in annual longshore sand transport rate is approximately 9% of the existing value. Only a single shadow zone landward of Resource Areas G2 and G3 exists approximately 1 km south of Brigantine Inlet. This shadow zone is indicated by a significant reduction in south-directed wave energy. The largest increase in south-directed transport occurs south of the shadow zone (approximately 2 km south of Brigantine Inlet). However, it is unclear whether the shadow zone or the region of increased south-directed wave energy are a result of dredging in Areas G2 (one potential borrow site), G3 (two potential borrow sites), or a combination of the three potential borrow sites.

For Resource Area C1, the combined effect of various wave conditions tends to mute the increase in south-directed sediment transport, where the largest increase is approximately 3,000 m^3/yr. Although the maximum variation in annual longshore sand transport rate is approximately 20% of the existing average value, the relatively high percentage of the 45,000 m^3/yr net transport indicates similar impacts as those predicted for Grids A and B2. A series of shadow zones landward of Area C1 occurs as a result of wave refraction generated by the series of wave conditions modeled. The largest shadow zone exists at approximately UTM Northing coordinate 4,394,000 m due to waves propagating from the east. In addition to this shadow zone, waves propagating from the east-southeast cause a reduction in the south-directed transport at UTM Northing coordinate 4,396,000 m, and waves propagating from the southeast cause a shadow zone at UTM Northing coordinate 4,398,500 m.

For the borrow site in Area F2, the maximum variation in annual longshore sand transport rate is approximately 17% of the existing value. Similar to Grid B1, the relatively low net sediment transport indicates a high percentage of impact to the transport rate; however, the maximum change of approximately 12,700 m^3/yr is similar to the modeled change for Grids A, B2, and B1. The shadow zone landward of Area F2 is located approximately 6 km south of Manasquan Inlet. Likewise, the largest increase in north-directed transport occurs to either side of the shadow zone (approximately 4 and 8 km south of Manasquan Inlet, respectively). This increase in wave energy at the shoreline is responsible for the increased north-directed transport both north and south of the primary shadow zone.

For average annual conditions, mean longshore sand transport rates were approximately equal landward of borrow sites in resource areas along the New Jersey coast. The absolute value of the mean difference between existing and post-dredging conditions was relatively consistent, ranging between 9,000 (20.0%) and 14,900 m^3/yr (7.2%) along the New Jersey shoreline. Although the percent difference computed for the northern two grids (Grids B1 and C) was larger than that calculated farther south, this trend is a result of the low relative net transport rates along the northern beaches rather than an increase in impacts associated with dredging.

8.3 BENTHIC ENVIRONMENT

Results of the biological field surveys agree well with previous descriptions concerning benthic assemblages associated with shallow shelf habitats offshore New Jersey. Benthic assemblages surveyed from the proposed sand resource areas consisted of members of the major invertebrate and vertebrate groups commonly found in the study area. Numerically dominant infaunal groups included numerous crustaceans, echinoderms, molluscans, and polychaetes, while epifaunal taxa consisted primarily of decapod crustaceans, sand dollars, moon snails, and squid. Biological surveys of the sand resource areas support the findings of numerous investigations in the region that have found strong associations of infaunal taxa with particular sedimentary habitats. Canonical correlation analysis indicated that the composition of benthic assemblages inhabiting New Jersey resource area stations was affected mostly by the percentage of gravel composition of surficial sediments. Infaunal assemblage distributions reflected sediment type distributions. Trough and sand ridge features further contributed to the prominent spatial variability exhibited by benthic assemblages in the sand resource areas. Seasonal differences in infaunal assemblages were apparent as well. Nearly half of the infaunal taxa sampled over the entire project were included in both the May and September surveys; however, most (68%) of the remainder of censused taxa were collected only during the September cruise. Also, overall infaunal abundance was higher during the May survey than was observed in September. Both the number of epifaunal taxa and overall epifaunal abundance were greater in September as compared to the May survey, as well, and this temporal abundance pattern also is characteristic of the study area.

Numerically dominant fishes collected during the 1998 sand resource area surveys are typical components of demersal assemblages in the study area. Fishes such as bay anchovy (*Anchoa mitchilli*), clearnose skate (*Raja eglanteria*), northern searobin (*Prionotus carolinus*), scup (*Stenotomus chrysops*), and windowpane (*Scophthalmus aquosus*) were numerical dominants during the 1998 biological surveys and these species consistently are among the most ubiquitous and abundant demersal taxa in the region. Despite inherent spatial and temporal heterogeneity in the distribution and abundance of demersal fishes and low numbers in trawls, results of the 1998 surveys of the sand resource areas generally are consistent with results of historical demersal survey results in the region.

Potential benthic effects from dredging will result from sediment removal, suspension/dispersion, and deposition. Primary effects to infaunal populations will be through removal of individuals along with sediments. Effects are expected to be short-term and localized. Seasonality and recruitment patterns indicate that removal of sand between late fall and early spring would result in less stress on benthic populations. Early stage succession will begin within days of sand removal, through settlement of larval recruits, primarily annelids and bivalves. Initial larval recruitment will be by the opportunistic taxa that were numerical dominants in trough areas during the biological surveys (e.g., the polychaete *Asabellides oculata* and bivalves *Nucula proxima* and *Tellina agilis*). These species are well adapted to environmental stress and exploit suitable habitat when it becomes available. Later successional

stages of benthic recolonization will be more gradual, involving taxa that generally are less opportunistic and longer lived. Immigration of motile annelids, crustaceans, and echinoderms into impacted areas also will begin soon after excavation.

While community composition may differ for a period of time after the last dredging, the infaunal assemblage type that exists in mined areas will be similar to naturally occurring assemblages in the study area, particularly those assemblages inhabiting inter-ridge troughs. Based on previous observations of infaunal reestablishment in dredged areas, the infaunal community in dredged sites within sand resource areas most likely will become reestablished within 2 years, exhibiting levels of infaunal abundance, diversity, and composition comparable to nearby non-dredged areas. Given that the expected beach replenishment interval is on the order of a decade, and that the expected recovery time of the affected benthic community after sand removal is anticipated to be much less than that, the potential for significant cumulative benthic impacts is remote.

Atlantic surfclam is the most economically important benthic species found in or around the sand resource areas. NMFS data indicate that the likelihood of encountering Atlantic surfclams in any of the New Jersey sand resource areas is reasonably high. Primary effects of dredging on Atlantic surfclam would be entrainment, hypoxia/anoxia, and turbidity. Project scheduling would not be useful for avoiding dredging-induced impacts to Atlantic surfclams. Once an exact borrow site is chosen for dredging, a commercial clam fisher should be hired to evaluate the site for the presence and abundance of Atlantic surfclams. If commercial quantities are found, then the fisher should harvest them from the site prior to dredging. This approach would remove individuals that would be subject to impacts. Studies have demonstrated that juvenile Atlantic surfclams will recruit to dredged borrow sites.

8.4 PELAGIC ENVIRONMENT

Zooplankters could be affected by entrainment and turbidity. Considering the high reproductive capacity of zooplankton along with the relatively small area of the dredge suction field and the volume of water entrained compared to the overall volume of surrounding waters, it is unlikely that entrainment or turbidity would greatly affect zooplankton populations or assemblages in the New Jersey sand resource areas. If borrow sites are used in Areas G1, G2, or G3, an environmental window excluding summer and fall months could be considered to avoid dredging when fish juveniles and larvae are most prevalent, but only if additional data become available to determine the extent of impacts and justify the restriction.

Squids could be entrained if they encountered the suction field of a hydraulic dredge. In addition, squid eggs are laid in large clusters on the seafloor and could be removed with sediments. Dredging is unlikely to significantly impact squid populations in the vicinity of the sand resource areas. This precludes the need for an environmental window or specific project scheduling to protect squid resources.

Dredging should not present a significant problem for pelagic fishes offshore of New Jersey. Potential effects to fishes could occur through entrainment, attraction, and turbidity. If an environmental window is sought to protect pelagic fishes from dredging impacts, the spring to fall period would encompass the peak seasons for the economically important species. Quantitative data are lacking to support the use of an environmental window to lessen effects on pelagic fishes.

EFH for several fish species (and life stages) overlap the eight sand resource areas offshore New Jersey. The area encompassed by the eight sand resource areas is very small relative to the mapped EFH characteristics. For this reason, the effect of dredging on EFH for the managed species is expected to be minimal.

The main potential effect of dredging on sea turtles is physical injury or death caused by the suction and/or cutting action of the dredge head. No significant effects on turtles are expected from turbidity, anoxia, or noise. Three sea turtle species that typically occur off New Jersey (loggerhead, green, and Kemp's ridley) are considered to be at risk because of their benthic feeding habits. Loggerheads are the most abundant turtles in the project area, and historically, they have been the species most frequently entrained during hopper dredging. If a hopper dredge is used, then it would be best to avoid the June through November turtle season. However, the vagaries of winter weather off New Jersey make it infeasible to prohibit dredging during these months. If use of a hopper dredge during this season cannot be avoided, then other mitigation and monitoring requirements may be appropriate, such as turtle monitoring and use of a turtle-deflecting draghead. If a cutterhead suction dredge is used, seasonal or other restrictions are considered unnecessary because there is little likelihood of killing or injuring sea turtles.

Marine mammal species occurring commonly on the shelf, such as bottlenose dolphin and common dolphin, may be present year-round but are unlikely to be adversely affected by dredging due to their agility. Harbor porpoise occurrence is more seasonal, but the likelihood of impact is so low that it does not warrant seasonal restrictions on dredging. Fin and humpback whales would be most likely to occur during winter or spring, and northern right whales as transients during spring and fall. There is no "resident" population of any of these whales in the study area; rather, they would be temporary inhabitants, or would be transiting the area during seasonal migrations. Generally, the probability of encountering these species in the project area would be lowest during summer. However, due to the low likelihood of impact, seasonal restrictions on dredging probably are not warranted. Instead, measures to minimize possible vessel interactions with these endangered species may be appropriate.

Zooplankton, squids, fishes, sea turtles, and marine mammals were groups in the pelagic environment considered to be potentially affected by offshore dredging. No cumulative effects to any of these groups are expected from multiple sand mining operations.

8.5 SYNTHESIS

The data collected, analyses performed, and simulations conducted for this study indicate that proposed sand dredging at sites evaluated on the OCS offshore New Jersey should have minimal environmental impact on fluid and sediment dynamics and biological communities. Short-term impacts to benthic communities are expected due to the physical removal of borrow material, but the potential for significant cumulative benthic impacts is remote. Additionally, no cumulative effects to any of the pelagic groups are expected from potential sand mining operations.

Minimal physical environmental impacts due to potential sand dredging operations have been identified through wave and sediment transport simulations. However, under normal wave conditions, the average change in longshore sand transport is about 13% of existing conditions. Because wave and sediment transport predictions are only reliable to within about ±35% (see Rosati and Kraus, 1991), predicted changes are not deemed significant. Although changes during storm conditions illustrate greater variation, the ability of models to predict storm wave transformation and resultant sediment transport is less certain. Because minor impacts to wave and sediment transport dynamics and biology may occur under conditions similar to those imposed in the present study, additional data collection and analysis may be required for a specific sand extraction scenario to determine the extent of impacts.

9.0 LITERATURE CITED

Able, K.W. and S.M. Hagen, 1995. Fishes in the vicinity of Beach Haven Ridge: Annual and Seasonal Patterns of Abundance During the Early 1970s. Institute of Marine and Coastal Sciences, Rutgers University, NJ, Technical Report #95-24, 36 pp.

Able, K.W. and M.P. Fahay, 1998. The First Year in the Life of Estuarine Fishes in the Middle Atlantic Bight. Rutgers University Press, New Brunswick, NJ, 343 pp.

Adams, K.T., 1942. Hydrographic Manual. U.S. Department of Commerce, Coast and Geodetic Survey, Special Publication 143, 940 pp.

Alpine Ocean Seismic Survey, 1988. Identification and Delineation of Potential Borrow Areas for the Atlantic Coast of New Jersey, Asbury Park to Manasquan: Detailed Investigation of the Sea Bright Sand Borrow Areas. Final Report to the U.S. Army Corps of Engineers, Contract #DACW51-87-C-0011, New York District, NY.

Alpine Ocean Seismic Survey, 1997. Absecon Inlet to Manasquan Inlet, New Jersey: Vibracore Sampling. Final Report to the New Jersey Geological Survey, Trenton, NJ, 46 pp.

Amato, R.V., 1994. Sand and Gravel Maps of the Atlantic Continental Shelf with Explanatory Text. U.S. Minerals Management Service, OCS Monograph, MMS 93-0037, 35 pp. + 4 maps.

Anders, F.J. and M.R. Byrnes, 1991. Accuracy of shoreline change rates as determined from maps and aerial photographs. Shore and Beach, 59(1): 17-26.

Applied Biology, Inc., 1979. Biological Studies Concerning Dredging and Beach Nourishment at Duval County, Florida with a Review of Pertinent Literature. U.S. Army Corps of Engineers, Jacksonville District, Jacksonville, FL.

Arnold, D.W., 1992. The Scientific Rationale for Restricting Coastal Construction Activities During the Marine Turtle Nesting Season. In: L.S. Tait (comp.), New Directions in Beach Management. Proceedings of the 5th Annual National Conference on Beach Preservation Technology, St. Petersburg, FL, February 12-14, 1992, pp. 374-380.

Ashley, G.M., 1987. Recommendations for Inlet Dredge Channel Placement Based on Analysis of Historic Change: Townsends and Hereford Inlets, New Jersey. Final Report to New Jersey Department of Environmental Protection, Rutgers University, New Brunswick, NJ, 64 pp.

Ashley, G.M., S.D. Halsey, and C.B. Buteux, 1986. New Jersey's Longshore Current Pattern. Journal of Coastal Research, 2(4): 453-463.

Ashley, G.M., R.W. Wellner, D. Esker, and R.E. Sheridan, 1991. Clastic sequences developed during late-Quaternary glacio-eustatic sea-level fluctuations on a passive margin: Example from the inner continental shelf near Barnegat Inlet, New Jersey. Geological Society of America Bulletin, 103: 1607-1621.

Auld, A.H. and J.R. Schubel, 1978. Effects of suspended sediment on fish eggs and larvae: A laboratory assessment. Estuarine and Coastal Marine Science, 6: 153-164.

Bakker, W.T., 1974. Sand concentration in an oscillatory flow. Proceedings of the 14th Conference on Coastal Engineering, ASCE, New York, pp. 1,129-1,148.

Bakker, W.T. and Th. Van Doorn, 1978. Near-bottom velocities in waves with a current. Proceedings of the 16th Conference on Coastal Engineering, ASCE, New York, pp. 1,394-1,413.

Banks, G.E. and M.P. Alexander, 1994. Development and Evaluation of a Sea Turtle-Deflecting Hopper Dredge Draghead. U.S. Army Engineer Waterways Experiment Station, Vicksburg, MS, Miscellaneous Paper HL-94-5.

Barry A. Vittor & Associates, Inc., 1985. Tuscaloosa Trend Regional Data Search and Synthesis Study, Synthesis Report, Volume I. U.S. Department of the Interior, Minerals Management Service, New Orleans, LA, OCS Study MMS 85-0056.

Barry A. Vittor & Associates, Inc., 1999a. Post-construction Monitoring, Borrow Area Finfish Sampling (BAFS) Summary Report, Section II, Asbury Park to Manasquan, New Jersey. Beach Erosion Control Project Biological Monitoring Program, Prepared for the U.S. Corps of Engineers, New York District.

Barry A. Vittor & Associates, Inc., 1999b. Pre- and Post-dredging Monitoring of Macroinvertebrate Assemblages at a Borrow Area Located Offshore of Coney Island, New York: 1992-1998 Data Synthesis. Prepared for the U.S. Corps of Engineers, New York District, 10 pp. + app.

Barry, M., 1978. Behavioral Response of Yellowfin Tuna, *Thunnus albacares*, and Kawakawa, *Euthynnus affinis*, to Turbidity. U.S. Department of Commerce, National Oceanic and Atmospheric Administration, Environmental Research Laboratories, Pacific Marine Environmental Laboratory, Seattle, WA. Deep Ocean Mining Environmental Study (DOMES), Unpublished Manuscript Number 31. National Technical Information Service No. PB-297, 106 pp.

Beardsley, R. C. and W. C. Boicourt, 1981. On estuarine and continental shelf circulation in the Middle Atlantic Bight. In: B. A. Warren and C. Wunsch, eds., Evolution of Physical Oceanography, The MIT Press, pp. 198-233.

Benfield, M.C. and T.J. Minello, 1996. Relative effects of turbidity and light intensity on reactive distance and feeding of an estuarine fish. Environmental Biology of Fishes, 46: 211-216.

Berkhoff, J.C.W., N. Booij, and A.C. Radder, 1972. Verification of numerical wave propagation models for simple harmonic linear waves. Coastal Engineering, 6: 255-279.

Berry, S.A., 1990. Canaveral Harbor Entrance Channel Operational Measures to Protect Sea Turtles. In: D.D. Dickerson and D.A. Nelson (comps.), Proceedings of the National Workshop on Methods to Minimize Dredging Impacts on Sea Turtles, Jacksonville, Florida. U.S. Army Engineer Waterways Experiment Station, Environmental Effects Laboratory, Vicksburg, MS, Miscellaneous Paper EL-90-5, pp. 49-52.

Biggs, R.B., 1968. Environmental Effects of Overboard Spoil Disposal. Journal of Sanitary Engineering Division 94, No. SA3, Proceeding Paper 5979, pp. 477-478.

Birkemeier, W.A. and R.A. Dalrymple, 1976. Numerical Models for the Prediction of Wave Set-up and Nearshore Circulation. Ocean Engineering Report No. 3, Department of Civil Engineering, University of Delaware, Newark, DE.

Blake, N.J., L.J. Doyle, and J.J. Culter, 1995. Impacts and Direct Effects of Sand Dredging for Beach Renourishment on the Benthic Organisms and Geology of the West Florida Shelf. U.S. Department of the Interior, Minerals Management Service, Office of International Activities and Marine Minerals, Herndon, VA. Executive Summary, OCS Report MMS 95-0004, 23 pp. Final Report, OCS Report MMS 95-0005, 109 pp. Appendices, OCS Report MMS 95-0005.

Blaxter, J.H.S., 1968. Visual thresholds and spectral sensitivity of herring larvae. Journal of Experimental Biology, 48: 39-53.

Blaylock, R.A., J.W. Hain, L.J. Hansen, D.L. Palka, and G.T. Waring, 1995. U.S. Atlantic and Gulf of Mexico Marine Mammal Stock Assessments. NOAA Tech. Mem. NMFS-SEFSC-363, 211 pp.

Bodge, K.R, 1986. Short Term Impoundment of Longshore Sediment Transport. Ph.D. Dissertation, Department of Coastal and Ocean Engineering, University of Florida, Gainesville, FL, 346 pp.

Bodge, K.R., 1989. A literature review of the distribution of longshore sediment transport across the surf zone. Journal of Coastal Research, 5(2): 307-328.

Bodge, K.R. and R.G. Dean, 1987. Short-term Impoundment of Longshore Transport. Proceedings of Coastal Sediments '87, ASCE, pp. 468-483.

Boehlert, G.W. and J. B. Morgan, 1985. Turbidity enhances feeding abilities of larval Pacific herring, *Clupea harengus pallasi*. Hydrobiologia,123: 161-170.

Boesch, D.F., 1972. Species diversity of marine macrobenthos in the Virginia area. Chesapeake Science, 13(3): 206-211.

Boesch, D.F., 1973. Classification and community structure of macrobenthos in the Hampton Roads area, Virginia. Marine Biology, 21: 226-244.

Boicourt, W.C., 1981. Circulation in the Chesapeake Bay entrance region: estuary-shelf interaction. In: J. W. Campbell and J. P. Thomas, eds., Chesapeake Bay Plume Study: Superflux 1980. NASA Conference Publication 2188, pp. 61-78.

Boicourt, W.C., 1982. Estuarine larval retention mechanisms on two scales. In: V. S. Kennedy, ed., Estuarine Comparisons. Academic Press, pp. 445-457.

Bonsdorff, E., 1983. Recovery Potential of Macrozoobenthos from Dredging in Shallow Brackish Waters. In: L. Cabioch et al. (eds.), Fluctuations and Succession in Marine Ecosystems: Proceedings of the 17th European Symposium on Marine Biology, Brest: Oceanologica Acta, pp. 27-32.

Bonsdorff, E., R.J. Diaz, R. Rosenberg, A. Norkko, and G.R. Cutter, 1996. Characterization of soft-bottom benthic habitats of the Åland Islands, northern Baltic Sea. Mar. Ecol. Prog. Ser., 142: 235-245.

Booij, N., 1983. A note on the accuracy of the mild-slope equation. Coastal Engineering, 7:191-203.

Borgman, L.E., 1985. Directional Spectrum Estimation for the S_{xy} Gauges. Technical Report, U.S. Army Engineer Waterways Experiment Station, Coastal Engineering Research Center, Vicksburg, MS, pp. 1-104.

Bowen, P.R. and G.A. Marsh, 1988. Benthic Faunal Colonization of an Offshore Borrow Pit in Southeastern Florida. U.S. Army Engineer Waterways Experiment Station, Vicksburg, MS, Miscellaneous Paper D-88-5.

Breitburg, D.L., 1988. Effects of turbidity on prey consumption by striped bass larvae. Transactions of the American Fisheries Society, 117:72-77.

Bretschneider, C.L., 1968. Significant waves and wave spectrum. Ocean Industry, pp. 40-46.

Brodziak, J.K.T. and W.K. Macy III, 1996. Growth of longfinned squid, *Loligo pealei*, in the northwest Atlantic. Fishery Bulletin, 94:212-236.

Brodziak, J. and L. Hendrickson, 1999. An analysis of environmental effects on survey catches of squids *Loligo pealei* and *Illex illecebrosus* in the northwest Atlantic. Fishery Bulletin, 97:9-24.

Brooks, R.M. and W.D. Corson, 1984. Summary of Archived Study Pressure, Wind, Wave, and Water Level Data. U.S. Army Engineer Waterways Experiment Station, Wave Information Study, Vicksburg, MS, WIS Report 13.

Bruton, M.N., 1985. The effects of suspensoids on fish. Hydrobiologia, 125: 221-241.

Bumpus, D. F., 1973. A description of the circulation on the continental shelf of the east coast of the United States. Progress in Oceanography, 6: 111-157.

Burke, V.J., S.J. Morreale, P. Logan, and E.A. Standora, 1992. Diet of Green Turtles (*Chelonia mydas*) in the Waters of Long Island, New York. In: M. Salmon and J. Wyneken (eds.), Proceedings of the Eleventh Annual Workshop on Sea Turtle Biology and Conservation, NOAA Tech. Memo. NMFS-SEFC-302, pp. 140-142.

Burke, V.J., E.A. Standora, and S.J. Morreale, 1993. Diet of juvenile Kemp's ridley and loggerhead sea turtles from Long Island, New York. Copeia, 1993: 1,176-1,180.

Buteux, C.B., 1982. Variations In Magnitude And Direction Of Longshore Currents Along The Central New Jersey Coast. M.S. Thesis, Rutgers University, New Brunswick, 132 pp.

Byles, R.A., 1988. Satellite Telemetry of Kemp's Ridley Sea Turtle, *Lepidochelys kempii*, in the Gulf of Mexico. Report to the National Fish and Wildlife Foundation, 40 pp.

Byrnes, M.R. and C.G. Groat, 1991. Characterization of the Development Potential of Ship Shoal Sand for Beach Replenishment of Isles Dernieres. Final Report, U.S. Department of the Interior, Minerals Management Service, Office of International Activities and Marine Minerals, Herndon, VA, 164 pp.

Byrnes, M.R. and M.W. Hiland, 1994. Compilation and analysis of shoreline and bathymetry data (Appendix B). In: N.C. Kraus, L.T. Gorman, and J. Pope (editors), Kings Bay Coastal and Estuarine Monitoring and Evaluation Program: Coastal Studies. Technical Report CERC-94-09, U.S. Army Engineer Waterways Experiment Station, Coastal Engineering Research Center, Vicksburg, MS, pp. B1-B89.

Byrnes, M.R., R.M. Hammer, B.A. Vittor, J.S. Ramsey, D.B. Snyder, K.F. Bosma, J.D. Wood, T.D. Thibaut, and N.W. Phillips, 1999. Environmental Study of Identified Sand Resource Areas Offshore Alabama: Volume I: Main Text, Volume II: Appendices. U.S. Department of the Interior, Minerals Management Service, International Activities and Marine Minerals Division (INTERMAR), Herndon, VA. OCS Report MMS 99-0052, 326 pp. + 132 pp. appendices.

Cadrin, S.X., 1998. Longfin Inshore Squid. In: S.H. Clark (ed.), Status of Fishery Resources off the Northeastern United States for 1998. U.S. Department of Commerce, NOAA Tech Mem. NMFS-NE-115, pp. 118-119.

Caldwell, J.M., 1966. Coastal Processes and Beach Erosion. Journal of the Society of Civil Engineers, 53(2):142-157.

Carr, A., 1987. New perspectives on the pelagic stage of sea turtle development. Conservation Biology, 1: 103-121.

Centre for Cold Ocean Resources Engineering (C-CORE), 1995. Proposed Marine Mining Technologies and Mitigation Techniques: A Detailed Analysis With Respect to the Mining of Specific Offshore Mineral Commodities. Contract report for U.S. Department of the

Interior, Minerals Management Service, OCS Report MMS 95-0003, C-CORE Publication 96-C15, 280 pp. + apps.

Chaillou, J.C. and L.C. Scott, 1997. Evaluation of Benthic Macrofaunal Resources at Potential Sand Borrow Sources: Brigantine Inlet to Great Egg Harbor Inlet, Atlantic County, New Jersey. Prepared by Versar, Inc. for the U.S. Army Corps of Engineers, Environmental Resources Branch, Philadelphia District, Philadelphia, PA, Contract No. DACW61-95-D-0011.

Chang, S., F.W. Steimle, Jr., R.N. Reid, S.A. Fromm, V.S. Zdanowicz, and R.A. Pikanowski, 1992. Association of benthic macrofauna with habitat types and quality in the New York Bight. Marine Ecology Progress Series, 89: 237-251.

Chuang, W. S., D. P. Wang and W. C. Boicourt, 1979. Low-Frequency current variability on the southern Mid-Atlantic Bight, Journal Physical Oceanography, 9: 1144-1154.

Coastal Oceanographics, 1996. Hypack Navigation Software Version 6.4.

Coastline Surveys Limited, 1998. Marine Aggregate Mining Benthic and Surface Plume Study. Final report to the U.S. Department of the Interior, Minerals Management Service and Plume Research Group, Report 98/555/03, 168 pp.

Cowen, R.K., J.A. Hare, and M.P. Fahay, 1993. Beyond hydrography: Can physical processes explain larval fish assemblages within the Middle Atlantic Bight? Bulletin of Marine Science, 53(2): 567-587.

Crowell, M., S.P. Leatherman, and M.K. Buckley, 1991. Historical shoreline change: Error analysis and mapping accuracy. Journal of Coastal Research, 7(3): 839-852.

Cruickshank, M.J., J.P. Flanagan, B. Holt, and J.W. Padan, 1987. Marine Mining on the Outer Continental Shelf: Environmental Effects Overview. U.S. Department of the Interior, Minerals Management Service, OCS Report 87-0035, 66 pp.

Csanady, G. T., 1982. Circulation in the Coastal Ocean. D. Reidel Publishing Company, Dordrecht, Holland, 279 pp.

Cutter, G.R., Jr. and R.J. Diaz, 1998. Environmental Studies Relative to Potential Sand Mining in the Vicinity of the City of Virginia Beach, Virginia. Part 1: Benthic Habitats and Biological Resources Off the Virginia Coast 1996 and 1997. Prepared under MMS Cooperative Agreement 14-35-0001-3087 through Virginia Institute of Marine Science, College of William & Mary. 26 pp. + appendices.

Davis, H.C. and H. Hidu, 1969. Effects of turbidity-producing substances in sea water on eggs and larvae of three genera of bivalve mollusks. Veliger, 11(4): 316-323.

Day, M.E., L.C. Schaffner, and R.J. Diaz. 1988. Long Island Sound sediment quality survey and analyses. Tetra Tec, Rpt. to NOAA, NOS, OMA, Rockville, MD. 113 pp.

Diaz, R.J. and L.C. Schaffner, 1988. Comparison of sediment landscapes in the Chesapeake Bay as seen by surface and profile imaging. In: M. P. Lynch and E. C. Krome, eds. Understanding the estuary; Advances in Chesapeake Bay research. Chesapeake Res. Consort. Pub. 129, CBP/TRS 24/88, pp. 222-240.

Dickerson, D.D., 1990. Workgroup 1 Summary. In: D.D. Dickerson and D.A. Nelson (comps.), Proceedings of the National Workshop on Methods to Minimize Dredging Impacts on Sea Turtles, Jacksonville, FL. U.S. Army Engineer Waterways Experiment Station, Vicksburg, MS, Miscellaneous Paper EL-90-5, 89 pp.

Dickerson, D.D., D.A. Nelson, M. Wolff, and L. Manners, 1992. Summary of Dredging Impacts on Sea Turtles: Kings Bay, Georgia and Cape Canaveral, Florida. In: M. Salmon and J. Wyneken (comps.), Proceedings of the Eleventh Annual Workshop on Sea Turtle Biology and Conservation, Jekyll Island, GA. NOAA Tech. Mem. NMFS-SEFSC-302, pp. 148-151.

Dickerson, D.D., K.J. Reine, and D.G. Clarke, 1998. Economic Impacts of Environmental Windows Associated with Dredging Operations. U.S. Army Engineer Waterways Experiment Station, Research and Development Center, Vicksburg, MS. DOER Tech. Note: Collection (TN DOER-E3).

Dill, C.E. and H.J. Miller, 1982. Bathymetric and geologic study of a proposed outfall at Avalon, New Jersey. In: Waterway Handling Facilities, Cape May County, Appendix C, 17: 1-18.

Dodd, C.K., Jr., 1988. Synopsis of the Biological Data on the Loggerhead Sea Turtle *Caretta caretta* (Linnaeus 1758). U.S. Fish and Wildlife Service Biological Report 88(4), 110 pp.

Donahue, J.J., R.C. Allen, and B.C. Heezen, 1966. Sediment size determining profile on the continental shelf off New Jersey. Sedimentology, 7: 155-159.

Doyle, M.J., W.W. Morse, and A.W. Kendall, Jr., 1993. A comparison of larval fish assemblages in the temperate zone of the northeast Pacific and northwest Atlantic oceans. Bulletin of Marine Science, 53(2): 588-644.

Duane, D.B., M.E. Field, E.P. Meisburger, D.J.P. Swift, and S.J. Williams, 1972. Linear shoals on the Atlantic inner continental shelf, Florida to Long Island. In: D.J.P. Swift, D.B Duane, and O.H. Pilkey (editors), Shelf Sediment Transport: Process and Pattern. Dowden Hutchinson, and Ross. Stroudsburg, PA, pp. 447-498.

Duane, D.B. and W.L. Stubblefield, 1988. Sand and gravel resources: U.S. Atlantic Continental Shelf. In: R.E. Sheridan and J.A. Grow (editors), The Atlantic Continental Margin: U.S., Volume I-2, The Geology of North America, Geological Society of America, Boulder, CO, pp. 481-500.

Ebersole, B.A. and R.A. Dalrymple, 1979. A Numerical Model for Nearshore Circulation Including Convective Acceleration and Lateral Mixing. Ocean Engineering Report No. 21, Department of Civil Engineering, University of Delaware, Newark, DE.

Ebersole, B.A. and R.A. Dalrymple, 1980. Numerical Modeling of Nearshore Circulation. Proceedings of the 17th Coastal Engineering Conference, Sydney, pp. 2,710-2,725.

Eckert, K.L., 1995. Leatherback Sea Turtle, *Dermochelys coriacea*. In: P.T. Plotkin (ed.), National Marine Fisheries Service and U. S. Fish and Wildlife Service Status Reviews for Sea Turtles Listed Under the Endangered Species Act of 1973, Silver Spring, MD.

Eckert, S.A., D.W. Nellis, K.L. Eckert, and G.L. Kooyman, 1986. Diving patterns of two leatherback sea turtles (*Dermochelys coriacea*) during internesting intervals at Sandy Point, St. Croix, U.S. Virgin Islands. Herpetologica, 42(3): 381-388.

Ellis, M.Y., 1978. Coastal Mapping Handbook. U.S. Department of the Interior, Geological Survey, U.S. Department of Commerce, National Ocean Service, U.S. Government Printing Office, Washington, D.C., 199 pp.

Emery, K.O. and E. Uchupi, 1965. Structure of Georges Bank. Marine Geology, 3: 349-358.

Emery, K.O., R.L. Wigley, A.S. Barlett, M. Rubin, and E.S. Barghoorn, 1967. Freshwater peat on the continental shelf. Science, 158: 1301-1307.

Farrell, S.C. and S.P. Leatherman, 1989. Computer-based Coastal Erosion Rate Maps for the State of New Jersey and Its Inlets. New Jersey Department of Environmental Protection, Coastal Resources, Contract # C29059 and 29312, Trenton, NJ, 43 pp., 143 maps.

Fauchald, K. and P. Jumars, 1979. The diet of worms: a study of polychaete feeding guilds. Oceanography and Marine Biology Annual Review, 17: 193-284.

Fenchel, T., 1969. The ecology of marine microbenthos. IV. Structure and function of the benthic ecosystem, its chemical and physical factors and microfauna communities with special reference to the ciliated Protozoa. Ophelia 6:1-182.

Field, M.E. and D.B Duane, 1976. Post Pleistocene history of the United States inner continental shelf: Significance to the origin of barrier islands. Geological Society of America Bulletin, 87: 691-702.

Fischer, W. (ed.), 1978. FAO Species Identification Sheets for Fishery Purposes, Western Central Atlantic (Fishing Area 31), Volume VI.

Flagg, C.N., 1977. The kinematics and dynamics of the New England continental shelf and shelf/slope front. Ph.D. Thesis, Massachusetts Institute of Technology/Woods Hole Oceanographic Institution, WHOI Ref. 77-67, 207 pp.

Folk, R.L., 1974. Petrology of sedimentary rocks. Hemphill's, Austin, Texas, 170 pp.

Frank, W.M. and G.M. Friedman, 1973. Continental shelf sediments off New Jersey. Journal of Sedimentary Petrology, 43(1): 224-237.

Frazier, N.B., 1995. Loggerhead sea turtle, *Caretta caretta*. In: P.T. Plotkin (ed.), National Marine Fisheries Service and U. S. Fish and Wildlife Service Status Reviews for Sea Turtles Listed under the Endangered Species Act of 1973. Silver Spring, MD.

Fredsoe, J. and R. Deigaard, 1992. Mechanics of Coastal Sediment Transport. World Scientific, New Jersey, 392 pp.

Garlo, E. and N. Saffian, 1976. Ponar grab. In: C.B. Milstein and D.L. Thomas (eds.), Ecological Studies in the Bays and Other Waterways Near Little Egg Inlet and in the Ocean in the Vicinity of the Proposed Site for the Atlantic Generating Station, New Jersey. Progress Report January-December 1975, Ichthyological Associates, Inc., Absecon, NJ., pp. 69-80, 239-249.

Gaskin, D.E, 1992. The status of the harbour porpoise. Canadian Field-Naturalist, 106: 36-54.

Gilbert, R.O., 1987. Statistical Methods for Environmental Pollution Monitoring. Van Nostrand Reinhold, New York, NY, 320 pp.

Goldberg, W.M., 1989. Biological Effects of Beach Nourishment in South Florida: The Good, the Bad, and the Ugly. Proceedings of Beach Preservation Technology, 1988, Shore and Beach Preservation Association, Tallahassee, FL.

Graf, G., 1992. Pelagic-benthic coupling: a benthic perspective. Oceanogr. Mar. Biol. Annu. Rev., 30:149-190.

Grant, G.C., 1991. Chaetognatha from the central and southern Middle Atlantic Bight: Species composition, temperature salinity relationships, and interspecific associations. Fishery Bulletin, 89(1): 33-40.

Grant, U.S., 1943. Waves as a transporting agent. American Journal of Science, 241: 117-123.

Grant, W.D. and O.S. Madsen, 1978. Bottom Friction Under Waves in the Presence of a Weak Current. NOAA Tech Rep. ERL-MESA-29, 150 pp.

Grant, W.D. and O.S. Madsen, 1979. Combined wave and current interaction with a rough bottom. Journal of Geophysical Research, 84 (C4): 1,797-1,808.

Grassle, J.F. and J.P. Grassle, 1974. Opportunistic life histories and genetic systems in marine benthic polychaetes. Journal of Marine Research, 32: 253-284.

Gray, J.S., 1974. Animal-sediment relationships. Oceanography and Marine Biology Annual Review, 12: 223-261.

Grober, L.E., 1992. The Ecological Effects of Beach Replenishment. M.S. Thesis, Duke University, School of the Environment, NC, 109 pp.

Grosslein, M.D., 1976. Some Results of Fish Surveys in the Mid-Atlantic Important for Assessing Environmental Impacts. In: G. Gross (ed.), Middle Atlantic Continental Shelf and the New York Bight, Proceedings of the Symposium, American Museum of Natural History, New York City, 1975, American Society of Limnology and Oceanography, Inc., Allen Press, Inc., Lawrence, KS, pp. 312-328

Hales, L.S., Jr., R.S. McBride, E.A. Bender, R.L. Hoden, and K.W. Able, 1995. Characterization of Non-Target Invertebrates and Substrates from Trawl Collections During 1991-92 at Beach Haven Ridge (LEO-15) and Adjacent Sites in Great Bay and on the Inner Continental Shelf Off New Jersey. Institute of Marine and Coastal Sciences, Rutgers University, NJ, Contribution No. 95-09, 34 pp.

Hall, S.J., 1994. Physical disturbance and marine benthic communities: Life in unconsolidated sediments. Oceanography and Marine Biology Annual Review, 32: 179-239.

Hallermeier, R.J., 1981. A profile zonation for seasonal sand beaches from wave climate. Coastal Engineering, 4: 253-277.

Hammer, R.M., 1981. Day-night differences in the emergence of demersal zooplankton from a sand substrate in a kelp forest. Marine Biology, 62: 275-280.

Hammer, R.M. and R.C. Zimmerman, 1979. Species of demersal zooplankton inhabiting a kelp forest ecosystem off Santa Catalina Island, California. Bulletin of Southern California Academy of Sciences, 78(3): 199-206.

Hammer, R.M., B.J. Balcom, M.J. Cruickshank, and C.L. Morgan, 1993. Synthesis and Analysis of Existing Information Regarding Environmental Effects of Marine Mining. Final Report by Continental Shelf Associates, Inc. for the U.S. Department of the Interior, Minerals Management Service, Office of International Activities and Marine Minerals, Herndon, VA, OCS Study MMS 93-0006, 392 pp.

Harris, T.F.W., J.M. Jordan, W.R. McMurray, C.J. Verwey, and F. P. Anderson, 1963. Mixing in the surf zone. International Journal of Air and Water Pollution, 7: 649-667.

Hasselmann, K.T., Barnett, E. Bouws, H. Carlson, D. Cartwright, K. Enke, J. Ewing, H. Gienapp, D. Hasselmann, P. Kruseman, A. Meerburgh, P. Muller, D. Olbers, K. Richter, W. Sell, and H. Walden, 1973. Measurement of wind-wave growth and swell decay during the joint north sea wave project (JONSWAP). Deutsches Hydrographisches Zeitschrift Reihe A (8^0), No. 12.

Hendrickson, L., 1998. Northern Shortfin Squid. In: S.H. Clark (ed.), Status of Fishery Resources Off the Northeastern United States for 1998. U.S. Department of Commerce, NOAA Tech Mem. NMFS-NE-115, pp. 116-117.

Herbich, J.B., 1992. Handbook of Dredging Engineering. McGraw-Hill, Inc., NY, NY, 740 pp.

Herbich, J.B. and S.B. Brahme, 1991. Literature Review and Technical Evaluation of Sediment Resuspension During Dredging. U.S. Army Engineer Waterways Experiment Station, Vicksburg, MS., Contract Report HL-91-1.

Hirota, J., 1981. Potential effects of deep-sea minerals mining on macrozooplankton in the north equatorial Pacific. Marine Mining, 3(1/2): 19-57.

Houston, J.R., 1995. Beach nourishment, coastal forum. Shore and Beach, January, 21-24.

Hrabovsky, L., 1990. Hydraulic Cutterhead Pipeline Dredging. In: D.D. Dickerson and D.A. Nelson (comps.), Proceedings of the National Workshop on Methods to Minimize Dredging Impacts on Sea Turtles, Jacksonville, FL. U.S. Army Engineer Waterways Experiment Station, Vicksburg, MS, Miscellaneous Paper EL-90-5, pp. 56-58. http://bigfoot.wes.army.mil/cetn.index.html#part2.

Hu, V.J.H., 1981. Ingestion of deep-sea mining discharge by five species of tropical copepods. Water, Air, and Soil Pollution, 15: 433-440.

Hubertz, J.M., R.M. Brooks, W.A. Brandon, and B.A. Tracy, 1993. Hindcast Wave Information for the U.S. Atlantic Coast. WIS Report 30, U.S. Army Engineer Waterways Experiment Station, Coastal Engineering Research Center, Wave Information Study, Vicksburg, MS.

Hughes, S.A., 1984. The TMA Shallow-water Spectrum Description and Applications. Technical Report, CERC-84-7, U.S. Army Engineer Waterways Experiment Station, Coastal Engineering Research Center, Vicksburg, MS.

Ingle, R.M., 1952. Studies on the Effect of Dredging Operations Upon Fish and Shellfish. Florida State Board of Conservation, Technical Series 5, 26 pp.

Jefferson, T.A., S. Leatherwood, and M.A. Webber, 1993. FAO Species Identification Guide. Marine Mammals of the World. Rome, FAO, 320 pp.

Johnson, R.O. and W.G. Nelson, 1985. Biological effects of dredging in an offshore borrow area. Florida Scientist, 48: 166-188.

Johnston, D.D. and D.J. Wildish, 1982. Effect of suspended sediment on feeding by larval herring (*Clupea harengus harengus L*.). Bulletin of Environmental Contamination and Toxicology, 29: 61-67.

Jokiel, P.L., 1989. Effects of marine mining dredge spoils on eggs and larvae of a commercially important species of fish, the Mahimahi (*Coryphaena hippurus*). Marine Minerals, 8: 305-315.

Jones, D.S., I. Thompson, and W. Ambrose, 1978. Age and growth rate determinations for the Atlantic surf clam *Spisula solidissima* (Bivalvia: Mactracea), based on internal growth lines in shell cross-sections. Marine Biology, 47: 63-70.

Jones, G. and S. Candy, 1981. Effects of dredging on the macrobenthic infauna of Botany Bay. Australian Journal of Marine and Freshwater Research, 32: 379-399.

Jonsson, I.G., 1966. Wave boundary layers and friction factors. Proceedings of the 10th Conference on Coastal Engineering, Tokyo, ASCE, New York, NY, pp. 1: 127-148.

Jonsson, I.G., 1980. A new approach to oscillatory rough turbulent boundary layers. Ocean Engineering, 7: 109-152.

Judkins, D.C., C.D. Wirick, and W.E. Esaias, 1980. Composition, abundance, and distribution of zooplankton in the New York Bight, September 1974-September 1975. Fishery Bulletin, 77(3): 669-684.

Kajiura, K., 1964. On the bottom friction in an oscillatory current. Bulletin of Earthquake Research, Inst. Tokyo University, 42(99): 147-174.

Kajiura, K., 1968. A model for the bottom boundary layer in water waves. Bulletin of Earthquake Research, Inst. Tokyo University, 46: 75-123.

Kamphuis, J.W., 1975. Friction under oscillatory waves. Journal of Waterways and Harbors, Coastal Engineering Division, ASCE, 101: 135-144.

Kane, J., 1997. Persistent spatial and temporal abundance patterns for late-stage copepodites of *Centropages hamatus* (Copepoda: Calanoida) in the U.S. northeast continental shelf ecosystem. Fishery Bulletin, 95 (1): 85-98.

Kenney, R.D., 1990. Bottlenose Dolphins off the Northeastern United States. In: S. Leatherwood and R. R. Reeves (eds.), The Bottlenose Dolphin. Academic Press, San Diego, CA, pp. 369-386.

Kerr, S.J., 1995. Silt, Turbidity and Suspended Sediments in the Aquatic Environment: An Annotated Bibliography and Literature Review. Ontario Ministry of Natural Resources, Southern Region Science and Technology Transfer Unit, Technical Report TR-008, 277 pp.

Kirby, J.T., 1983. Propagation of weakly-nonlinear surface water waves in regions with varying depth and current. ONR Tech. Rept. 14, Res. Rept. CE-83-37, Department of Civil Engineering University of Delaware, Newark.

Kirby, J.T., 1984. A note on linear surface wave-current interaction. Journal of Geophysical Research, 89: 745-747.

Kirby, J.T. and R.A. Dalrymple, 1983a. A parabolic equation for the combined refraction-diffraction of stokes waves by mildly varying topography. Journal of Fluid Mechanics 136: 543-566.

Kirby, J.T. and R.A. Dalrymple, 1983b. The propagation of weakly nonlinear waves in the presence of varying depth and currents. Proceedings of the 20th Congress I.A.H.R., Moscow.

Kirby, J.T. and R.A. Dalrymple, 1984. Verification of a parabolic equation for propagation of weakly non-linear waves. Coastal Engineering, 8: 219-232.

Kirby, J.T. and H.T. Özkan, 1994. Combined refraction/diffraction model for spectral wave conditions, REF/DIF S. v. 1.1, no. CACR-94-04, Center for Applied Coastal Research, Newark, DE.

Kirk, K. L., 1992. Effects of suspended clay on Daphnia body growth and fitness. Freshwater Biology, 28: 102-109.

Klitgord, K.D., D.R. Hutchinson, and H. Schouten, 1988. U.S. Atlantic continental margin: structural and tectonic framework. In: R.E. Sheridan and J.A. Grow (editors), The Atlantic Continental Margin: U.S., Volume I-2, The Geology of North America, Geological Society of America, Boulder, CO, pp. 19-55.

Knebel, H.J., 1981. Processes controlling the characteristics of the surficial sand sheet, U.S. Atlantic outer continental shelf. Marine Geology, 42: 349-368.

Knebel, H.J. and E.C. Spiker, 1977. Thickness and age of surficial sand sheet, Baltimore Canyon Trough area. American Association of Petroleum Geologists Bulletin, 61:861-871.

Knight, D.W., 1978. Review of oscillatory boundary layer flow. Journal of the Hydraulics Division, ASCE, 104(HY6): 839-855.

Kocik, J., 1998a. River Herring. In: S.H. Clark (ed.), Status of Fishery Resources off the Northeastern United States for 1998. U.S. Department of Commerce, NOAA Tech Mem. NMFS-NE-115, pp. 134-135.

Kocik, J., 1998b. American Shad. In: S.H. Clark (ed.), Status of Fishery Resources off the Northeastern United States for 1998. U.S. Department of Commerce, NOAA Tech Mem. NMFS-NE-115, pp. 136-137.

Komar, P.D. and D.L. Inman, 1970. Longshore sand transport on beaches. Journal of Geophysical Research, 75(30): 5,914-5,927.

Kraus, N.C. and T.O. Sasaki, 1979. Influence of wave angle and lateral mixing on the longshore current. Marine Science Communications, 5(2): 91-126.

Kraus, N.C., N.W. Scheffner, H. Hanson, L.W. Chou, M.A. Cialone, J.M. Smith, and T.A. Hardy, 1988. Coastal Processes at Sea Bright to Ocean Township, New Jersey. Miscellaneous Paper CERC-88-2, U.S. Army Corps of Engineers, Waterways Experiment Station, Coastal Engineering Research Center, Vicksburg, MS, 142 p.

Kraus, N.C. and M. Larson, 1991. NMLONG: Numerical Model for Simulating the Longshore Current; Report 1, Model Development and Tests. Technical Report DRP-91-1, U.S. Army Engineer Waterways Experiment Station, Dredged Material Research Program, Vicksburg, MS, 166 pp.

Kraus, S.D., A.R. Knowlton, and J.H. Prescott, 1988. Surveys for Wintering Right Whales (*Eubalaena glacialis*) Along the Southeastern United States, 1984-1988. Final report to the Department of the Interior, Minerals Management Service, Branch of Environmental Studies, Washington, DC, 19 pp. + app.

Kraus, S.D., R.D. Kenney, A.R. Knowlton, and J.N. Ciano, 1993. Endangered Right Whales of the Southwestern North Atlantic. Final report to the Department of the Interior, Minerals Management Service, Atlantic OCS Region, Herndon, VA, 69 pp.

Kropp, R.K., 1995a. Brigantine Inlet to Great Egg Harbor Inlet, Atlantic County, New Jersey: Benthic Animal Assessment of Potential Borrow Source. Report prepared for the U.S. Army Corps of Engineers, Philadelphia District, Philadelphia, PA, Contract No. DAAL03-91-C-0034.

Kropp, R.K., 1995b. Environmental Post-dredge Monitoring, Great Egg Harbor Inlet and Peck Beach, Ocean City, New Jersey. Prepared for the U.S. Army Corps of Engineers, Philadelphia District, Philadelphia, PA by Battelle Ocean Sciences, Duxbury, MA, Contract DACW61-95-C-001, 44 pp. + app.

Lange, A.M.T. and M.P. Sissenwine, 1980. Biological considerations relevant to the management of squid (*Loligo pealei* and *Illex illecebrosus*) of the northwest Atlantic Mar. Fish. Rev., 42(7-8): 23-38.

Larson, K.W. and C.E. Moehl, 1988. Entrainment of Anadromous Fish by Hopper Dredge at the Mouth of the Columbia River. In: C.A. Simenstad (ed.), Effects of Dredging on Anadromous Pacific Coast Fishes, Workshop Proceedings, University of Washington Sea Grant, pp. 102-112.

Larson, M. and N.C. Kraus, 1995. Prediction of Cross-shore Sediment Transport at Different Spatial and Temporal Scales. In: J.H. List and J.H.J. Terwindt (eds.), Large-Scale Coastal Behavior, Marine Geology Special Issue, 126(1/4): 111-128.

LaSalle, M.W., D.G. Clarke, J. Homziak, J.D. Lunz, and T.J. Fredette, 1991. A Framework for Assessing the Need for Seasonal Restrictions on Dredging and Disposal Operations. U.S. Army Engineer Waterways Experiment Station, Vicksburg, MS, Technical Report D-91-1, 74 pp.

Lenhardt, M.L., 1994. Seismic and Very Low Frequency Sound Induced Behaviors in Captive Loggerhead Marine Turtles (*Caretta caretta*). In: K.A. Bjorndal, A.B. Bolten, D.A. Johnson, and P.J. Eliazar (comps.), Proceedings of the Fourteenth Annual Symposium on Sea Turtle Biology and Conservation, Hilton Head, SC, U.S. Department of Commerce, National Oceanic and Oceanographic Administration, National Marine Fisheries Service, Southeast Fisheries Science Center, Miami, FL.

Lohoefener, R., W. Hoggard, K. Mullin, C. Roden, and C. Rogers, 1990. Association of Sea Turtles with Petroleum Platforms in the North-central Gulf of Mexico. U.S. Department of the Interior, Minerals Management Service, Gulf of Mexico OCS Region, New Orleans, LA, OCS Study MMS 90-0025, 90 pp.

Longuet-Higgins, M.S., 1970. Longshore currents generated by obliquely incident sea waves, parts 1 and 2. Journal of Geophysical Research, 75(33): 6,778-6,801.

Loosanoff, V.L., 1962. Effects of turbidity on some larval and adult bivalves. Proceedings of the 14th Annual Session, Gulf and Caribbean Fisheries Institute, pp. 80-95.

Louis Berger Group, 1999. Use of Federal Offshore Sand Resources for Beach and Coastal Restoration in New Jersey, Maryland, Delaware, and Virgina. U.S. Department of the Interior, Minerals Management, OCS Study MMS 99-0036, 355 pp.

Lozano, C.J. and P.L.F. Liu, 1980. Refraction-diffraction model for linear surface water waves. Journal of Fluid Mechanics, 101(4): 705-720.

Lutcavage, M. and J.A. Musick, 1985. Aspects of the biology of sea turtles in Virginia. Copeia, 1985(2): 449-456.

MacArthur, R.H., 1960. On the relative abundance of species. American Naturalist, 94: 25-36.

MacArthur, R.H. and E.O. Wilson, 1967. Theory of Island Biogeography. Princeton University Press, Princeton, NJ, 203 pp.

Madsen, O.S. and W.D. Grant, 1976. Sediment Transport in the Coastal Environment. Report No. 209, MIT, Department of Civil Engineering, Cambridge, MA, 105 pp.

Madsen, O.S. and W.D. Grant, 1977. Quantitative description of sediment transport by waves. Proceedings 15th International Coastal Engineering Conference, ASCE, New York, NY, pp. 1,093-1,112.

Malme, C.I., P.R. Miles, C.W. Clark, P. Tyack, and J.E. Bird, 1983. Investigations of the Potential Effects of Underwater Noise from Petroleum Industry Activities on Migrating Gray Whale Behavior. Report by Bolt, Beranek and Newman, Inc., Cambridge, MA, for the U.S. Department of the Interior, Minerals Management Service, Anchorage, AK, BBN Rep. 5366.

Marine Turtle Expert Working Group, 1996a. Status of the Loggerhead Turtle Population (*Caretta caretta*) in the Western North Atlantic. 50 pp.

Marine Turtle Expert Working Group, 1996b. Kemp's Ridley Sea Turtle (*Lepidochelys kempii*) Status Report. 49 pp.

Marquez, R.M., 1990. Sea Turtles of the World. FAO Species Catalogue, Volume 11. FAO, Rome, 81 pp.

Marsh, G.A. and D.B. Turbeville, 1981. The environmental impact of beach nourishment: Two studies in southeastern Florida. Shore and Beach, 1981: 40-44.

Maurer, D., R.T. Keck, J.C. Tinsman, W.A. Leathem, C. Wethe, C. Lord, and T.M. Church, 1986. Vertical migration and mortality of marine benthos in dredged material: A synthesis. Internationale Revue der gesamten Hydrobiologie, 71: 49-63.

Mauriello, M.N., 1991. Beach nourishment and dredging: New Jersey's policies. Shore and Beach, 59(3):25-28.

Mayer, D. A., 1982. The structure of circulation: MESA physical oceanographic studies in New York Bight. Journal Geophysical Research, 87: 9579-9588.

Mayer, D. A., D. V. Hansen, and D. A. Ortman, 1979. Long-term current and temperature observations on the Middle Atlantic shelf. Journal Geophysical Research, 84: 1776-1792.

McBride, R.A. and T.F. Moslow, 1991. Origin, evolution, and distribution of shoreface sand ridges, Atlantic inner shelf, U.S.A. Marine Geology, 97: 57-85.

McCaully, J.E., R.A. Parr, and D.R. Hancock, 1977. Benthic infauna and maintenance dredging: a case study. Water Research, 11: 233-242.

McClennen, C.E., 1983. Middle Atlantic nearshore seismic survey and sidescan sonar survey: Potential geologic hazards off the New Jersey coastline. U.S. Geological Survey Open File Report 83-824, Reston, VA, 30 pp.

McClennen, C.E. and R.L. McMaster, 1971. Probably transgressive effects on the geomorphic features of the continental shelf off New Jersey, United States. Journal of Sedimentary Petrology, 7: 69-72.

McGraw, K.A. and D.A. Armstrong, 1988. Fish Entrainment by Dredges in Grays Harbor, Washington. In: C.A. Simenstad (ed.), Effects of Dredging on Anadromous Pacific Coast Fishes, Workshop Proceedings, University of Washington Sea Grant, pp. 113-131.

McKinney, T.F. and G.M. Friedman, 1970. Continental shelf sediments of Long Island, New York. Journal of Sedimentary Petrology, 40: 213-248.

McKinney, T.G., W.L. Stubblefield, and D.J.P. Swift, 1974. Large-scale current lineations, central New Jersey shelf: Investigations by sidescan sonar. Marine Geology, 17: 79-102.

McMaster, R.L., 1954. Petrography and genesis of the New Jersey beach sands. New Jersey Department of Conservation and Economic Development, Geological Survey Bulletin No. 63, 239 pp.

McNulty, J.K., R.C. Work, and H.B. Moore, 1962. Some relationships between the infauna of the level bottom and the sediment in South Florida. Bulletin of Marine Science in the Gulf and Caribbean, 12: 322-332.

Meisburger, E.P. and S.J. Williams, 1980. Sand Resources on the Inner Continental Shelf of Cape May Region, New Jersey. U.S. Army Corps of Engineers, Coastal Engineering Research Center, Miscellaneous Report 80-4, Fort Belvoir, VA, 40 pp.

Meisburger, E.P. and S.J. Williams, 1982. Sand Resources on the Inner Continental Shelf off the Central New Jersey Coast. U.S. Army Corps of Engineers, Coastal Engineering Research Center, Miscellaneous Report 80-4, Fort Belvoir, VA, 48 pp.

Mid-Atlantic Fishery Management Council, 1988. Amendment #8 to the Fishery Management Plan for the Atlantic Surf Clam and Ocean Quahog Fishery Management Plan. Dover, DE.

Mid-Atlantic Fishery Management Council, 1998. Amendment #12 to the Fishery Management Plan for the Atlantic Surf Clam and Ocean Quahog Fishery Management Plan. Dover, DE.

Mid-Atlantic Fishery Management Council, 1998a. Amendment #12 to the Atlantic Surfclam and Ocean Quahog Fishery Management Plan. Mid-Atlantic Fishery Management Council, Dover, DE, 249 pp.

Mid-Atlantic Fishery Management Council, 1998b. Amendment 8 to the Atlantic Mackerel, Squid, and Butterfish Fishery Management Plan. Mid-Atlantic Fishery Management Council, Dover, DE, 351 pp. + apps.

Mid-Atlantic Fishery Management Council, 1998c. Amendment 12 to the Summer Flounder, Scup, and Black Sea Bass Fishery Management Plan. Mid-Atlantic Fishery Management Council, Dover, DE, 398 pp. + apps.

Mid-Atlantic Fishery Management Council, 1998d. Amendment 1 to the Bluefish Fishery Management Plan. Mid-Atlantic Fishery Management Council, 2 Vols., Dover, DE, 341 pp. + apps.

Mid-Atlantic Fishery Management Council, 1999. The Spiny Dogfish Fishery Management Plan. Mid-Atlantic Fishery Management Council, 292 pp. + apps.

Miller, H.J., C.E. Dill, and G.B. Tirey, 1973. Geophysical Investigation of the Atlantic Generating Station Site and Region. Alpine Geophysical Association Technical Report, Norwood, NJ, 56 pp.

Miller, M.L., 1993. The rise of coastal marine tourism. Ocean and Coastal Management, 20: 181-199.

Milliman, J.D., 1972. Atlantic Continental Shelf and Slope of the United States – Petrology and Sand Fraction of Sediments, Northern New Jersey to Florida. U.S. Geological Survey Professional Paper 529-J, 39 pp.

MMS, 1989. Description of the Mid-Atlantic Environment. In: S.A. Abernathy (ed.), Atlantic OCS Region, MMS 89-0064.

Moein, S.E., J.A. Musick, J.A. Keinath, D.E. Barnard, M.L. Lenhardt, and R. George, 1994. Evaluation of Seismic Sources for Repelling Sea Turtles from Hopper Dredges. Virginia Institute of Marine Science, College of William and Mary, Gloucester Point, VA, final contract report to U.S. Army Engineer Waterways Experiment Station. As excerpted in: Sea Turtle Research Program Summary Report. Prepared by U.S. Army Engineer Waterways Experiment Station, Vicksburg, MS for U.S. Army Engineer Division, South Atlantic, Atlanta, GA and U.S. Naval Submarine Base, Kings Bay, GA, Technical Report CHL-97-31, NTIS ADA332588, 147 pp.

Moody, J. A., B. Butman, R.C. Beardsley, W.S. Brown, P. Daifuku, J.D. Irish, D.A. Mayer, H.O. Mofjeld, B. Petrie, S. Ramp, P. Smith, and W.R. Wright, 1983. Atlas of Tidal Elevation and Current Observations on the Northeast American Continental Shelf and Slope. U.S. Geological Survey Bulletin Survey Bulletin 1611, 122 pp.

Moore, P.G., 1977. Inorganic particulate suspensions in the sea and their effects on marine animals. Oceanography and Marine Biology Annual Review, 15: 225-363.

Morgan, R.P., V.J. Rasin, Jr., and L.A. Noe, 1983. Sediment effects on eggs and larvae of striped bass and white perch. Transactions of the American Fisheries Society, 112: 220-224.

Mortimer, J.A., 1982. Feeding Ecology of Sea Turtles. In: K.A. Bjorndal (ed.), Biology and Conservation of Sea Turtles. Smithsonian Institution Press, Washington, DC, pp. 103-109.

Murawski, W.S., 1969. A Study of Submerged Dredge Holes in New Jersey Estuaries with Respect to their Fitness as Finfish Habitat. New Jersey Department of Conservation and Economic Development, Division of Fish and Game, Miscellaneous Report No. 2M, 32 pp.

Naqvi, S. and E. Pullen, 1982. Effects of Beach Nourishment and Borrowing on Marine Organisms. U.S. Army Corps of Engineers, Coastal Engineering Research Center, Fort Belvoir, VA, Miscellaneous Report No. 82-14.

National Research Council, 1995. Beach Nourishment and Protection. National Academy Press, 334 pp.

Nelson, W.G., 1985. Physical and Biological Guidelines for Beach Restoration Projects. Part 1. Biological Guidelines. Florida Sea Grant College Program, Report No. 76.

New England Fishery Management Council, 1998a. Final Amendment 9 to the Northeast Multispecies Fishery Management Plan. New England Fishery Management Council, Saugus, MA.

New England Fishery Management Council, 1998b. Final Amendment 11 to the Northeast Multispecies Fishery Management Plan. New England Fishery Management Council, Saugus, MA.

Newell, R.C., L.J. Seiderer, and D.R. Hitchcock, 1998. The impact of dredging works in coastal waters: A review of the sensitivity to disturbance and subsequent recovery of biological resources on the seabed. Oceanography and Marine Biology Annual Review, 36: 127-178.

Nilsson, H.C. and R. Rosenberg, 1997. Benthic habitat quality assessment of an oxygen stressed fjord by surface and sediment profile images. Journal Marine Systems, 11: 249-264.

Nival, P. and S. Nival, 1976. Particle retention efficiencies of an herbivorous copepod, *Acartia clausi* (adult and copepodite stages): effects of grazing. Limnology and Oceanography, 21(1): 24-38.

NMFS, 1991a. Recovery Plan for the Humpback Whale (*Megaptera novaeangliae*). Prepared by the Humpback Whale Recovery Team for the National Marine Fisheries Service, Silver Spring, MD, 105 pp.

NMFS, 1991b. Recovery Plan for the Northern Right Whale (*Eubalaena glacialis*). Prepared by the Right Whale Recovery Team for the National Marine Fisheries Service, Silver Spring, MD, 86 pp.

NMFS, 1996. Endangered Species Act, Section 7 Consultation, Biological Opinion Concerning Dredging Activities Within the Philadelphia District of the U.S. Department of the Army. Prepared by the National Marine Fisheries Service, Northeast Regional Office, 43 pp.

NMFS, 1997. Regional Biological Opinion for Hopper Dredging of Channels and Beach Nourishment Activities in the Southeastern United States from North Carolina through Florida East Coast. October 1997.

NMFS, 1998a. Unpublished Surfclam/Ocean Quahog Survey Data. Northeast Fisheries Science Center, Woods Hole, MA.

NMFS, 1998b. Marine Mammal Protection Act of 1972 Annual Report, January 1, 1997 to December 31, 1997. Office of Protected Resources, National Marine Fisheries Service, Silver Spring, MD.

NMFS, 1999. Fishery Management Plan for Atlantic Tunas, Swordfish, and Sharks, Volume II . National Marine Fisheries Service Division of Highly Migratory Species, Office of Sustainable Fisheries, Silver Spring, MD, 302 pp.

NMFS and USFWS, 1991. Recovery Plan for U.S. Population of Atlantic Green Turtle. National Marine Fisheries Service, Washington, DC, 52 pp.

NMFS and USFWS, 1992. Recovery Plan for the Kemp's Ridley Sea Turtle (*Lepidochelys kempii*). National Marine Fisheries Service, St. Petersburg, FL, 40 pp.

Noble, M., and B. Butman, 1979. Low-frequency wind-induced sea level oscillations along the East Coast of North America. Journal Geophysical Research, 84(C6): 3227-3236.

Noble, M., B. Butman, and E. Williams, 1983. On the longshelf structure and dynamics of subtidal currents on the eastern United States Continental Shelf. Journal Physical Oceanography, 13(12): 2125-2147.

Noble, M., B. Butman, and M. Wimbush, 1985. Wind-current coupling on the southern flank of Georges Bank: Variation with season and frequency. Journal Physical Oceanography, 15 (5): 604-620.

Nyman, R.M. and D.O. Conover, 1988. The relation between spawning season and the recruitment of young-of-the-year bluefish, *Pomatomus saltatrix*, to New York. Fishery Bulletin, 86(2): 237-250.

Oakwood Environmental, Ltd., 1999. Strategic Cumulative Effects of Marine Aggregates Dredging (SCEMAD). Prepared for the U.S. Department of the Interior, Minerals Management Service, 175 pp.

Odum, E.P., 1969. The strategy of ecosystem development. Science, 164: 262-270.

Ou, H. W., R. C. Beardsley, D. Mayer, W. C. Boicourt, and B. Butman, 1981. An analysis of subtidal current fluctuations in the Middle Atlantic Bight. Journal Physical Oceanography, 11(10): 1383-1392.

Overholtz, W., 1998a. Atlantic Mackerel. In: S.H. Clark (ed.), Status of Fishery Resources off the Northeastern United States for 1998. U.S. Department of Commerce, NOAA Tech Mem. NMFS-NE-115, pp. 106-107.

Overholtz, W., 1998b. Butterfish. In: S.H. Clark (ed.), Status of Fishery Resources off the Northeastern United States for 1998. U.S. Department of Commerce, NOAA Tech Mem. NMFS-NE-115, pp. 108-109.

Oviatt, C.A., C.D. Hunt, G.A. Vargo, and K.W. Kopchynski, 1982. Simulation of a storm event in a marine microcosm. Journal of Marine Research, 39: 605-618.

Paffenhofer, G.A., 1972. The effects of “red mud” on mortality, body weight, and growth of marine planktonic copepod, Calanus helgolandicus. Water, Air, and Soil Pollution, 1: 314-321.

Palermo, M.R., 1990. Workgroup 2 Summary. In: D.D. Dickerson and D.A. Nelson (comps.), Proceedings of the National Workshop on Methods to Minimize Dredging Impacts on Sea Turtles, Jacksonville, FL. U.S. Army Engineer Waterways Experiment Station, Vicksburg, MS, Miscellaneous Paper EL-90-5, pp. 76-80.

Parker, P., 1967. Clam survey, Ocean City, Maryland to Cape Charles, Virginia. Commercial Fisheries Review, 29(5): 53-77.

Parker, P. and L. Fahlen, 1968. Clam survey off Virginia (Cape Charles to False Cape). Commercial Fisheries Review, 30(1): 25-36.

Parker, P.C., 1996. Nearshore Ridges and Underlying Upper Pleistocene Sediments on the Inner Continental Shelf of New Jersey. M.S. thesis, Rutgers University, NJ, 157 pp.

Pearce, J., 1974. Environmental Impact of the Construction Phase of Offshore Floating or Barge Mounted Nuclear Power Plants to be Sited Between Sandy Hook and Atlantic City, N.J. In: J. Peres (ed.), Modifications Thermiques et Equilibres Biologiques, North-Holland Publishing Company, Amsterdam, Netherlands, pp. 395-408.

Pearce, J.B., J.V. Caracciolo, M.B. Halsey, and L.H. Rogers, 1976. Temporal and Spatial Distributions of Benthic Macroinvertebrates in the New York Bight. In: G. Gross (ed.), Middle Atlantic Continental Shelf and New York Bight, Proceedings of the Symposium, American Museum of Natural History, New York City, 1975. American Society of Limnology and Oceanography, Inc., Allen Press, Inc., Lawrence, KS, pp. 394-403.

Pearce, J.B., D.J. Radosh, J.V. Caracciolo, and F.W. Steimle, Jr., 1981. Benthic Fauna: Marine EcoSystems Analysis (MESA) Program, MESA New York Bight Project. MESA New York Bight Atlas Monograph 14, New York Sea Grant Institute, Albany, NY, 79 pp.

Peddicord, R.K. and V.A. McFarland, 1978. Effects of Suspended Dredged Material on Aquatic Animals. U.S. Army Engineer Waterways Experiment Station, Vicksburg, MS, Technical Report D-78-29, 102 pp. + app.

Peterson, C.G.J., 1913. Valuation of the Sea. II. The Animal Communities of the Sea-bottom and Their Importance for Marine Zoogeography. Report of the Danish Biological Station to the Board of Agriculture, 21: 1-44.

Pettibone, M.H., 1963. Marine Polychaete Worms of New England. Part I, Aphroditidae through Trochochaetidae. Smithsonian Institution, Washington, D.C., Government Printing Office, 360 pp.

Phillips, P.J., W.D. Burke, and E.J. Keener, 1969. Observations on the trophic significance of jellyfishes in Mississippi Sound with quantitative data on the associative behavior of small fishes with medusae. Transactions of the American Fisheries Society, 98(4): 703-712.

Pianka, E.R., 1970. On r- and K-selection. American Naturalist, 104: 592-597.

Pielou, E.C., 1966. Species-diversity and pattern-diversity in the study of ecological succession. Journal of Theoretical Biology, 10: 370-383.

Poiner, I.R. and R. Kennedy, 1984. Complex pattern of change in the macrobenthos of a large sandbank following dredging. I. Community analysis. Marine Biology, 78: 335-352.

Poppe, L.J., J.S. Schlee, and H.J. Knebel,1994. Map Showing Distribution of Surficial Sediment on the Mid-Atlantic Continental Margin, Cape Cod to Ablemarle Sound. U.S. Geological Survey, Miscellaneous Investigations Series, Map I-1987-D.

Quinn, M.-L., 1977. The History of the Beach Erosion Board. U.S. Army Corps of Engineers, Coastal Engineering Research Center, Miscellaneous Report 77-9, Vicksburg, MS, 181 p.

Radder, A.C., 1979. On the parabolic equation method for water-wave propagation. Journal of Fluid Mechanics, 95: 159-176.

Ramsey, J.S., 1991. A Study of Wave-Induced Currents Behind Shore Parallel Breakwaters. M.C.E. Thesis, Dept. of Civil Engineering, University of Delaware, Newark, DE, 101 pp.

Raudkivi, A.J., 1990. Loose Boundary Hydraulics. 3rd Edition, Pergamon Press, Oxford.

Reeves, R. R., G. K. Silber, and P. M. Payne, 1998. Draft recovery plan for the fin whale, *Balaenoptera physalus* and sei whale, *Balaenoptera borealis*. Prepared for the Office of Protected Resources, National Marine Fisheries Service, Silver Spring, MD, 65 pp.

Reid, R.N., D.J. Radosh, A. B. Frame, and S.A. Fromm, 1991. Benthic Macrofauna of the New York Bight. U.S. Department of Commerce, National Marine Fisheries Service, NOAA Technical Report NMFS 103, 50 pp.

Reine, K. and D. Clarke, 1998. Entrainment by hydraulic dredges–A review of potential impacts. U.S. Army Engineer Research and Development Center, Vicksburg, MS, Technical Note DOER-E1, 14 pp.

Reine, K.J., D.D. Dickerson, and D.G. Clarke, 1998. Environmental windows associated with dredging operations. U. S. Army Engineer Research and Development Center, Vicksburg, MS, DOER Tech. Notes Collection (TN DOER-E2).

Resio, D.T., and B.A. Tracy, 1983. A Numerical Model for Wind-Wave Prediction in Deepwater. WIS Report 12, U.S. Army Engineer Waterways Experiment Station, Coastal Engineering Research Center, Wave Information Study, Vicksburg, MS.

Revelas, E.C., D.C. Rhoads, and J.D. Germano. 1987. San Francisco Bay sediment quality survey and analysis. NOAA Tech. Memor. NOS OMA 35. Rockville, MD. 127 pp.

Rhoads, D.C. 1974. Organism sediment relations on the muddy sea floor. Oceanography and Marine Biology Annual Review 12:263-300.

Rhoads, D.C., P.L. McCall, and J.Y. Yingst, 1978. Disturbance and production on the estuarine seafloor. American Science, 66: 577-586.

Rhoads, D.C. and J.D. Germano, 1982. Characterization of organism-sediment relations using sediment profile imaging: An efficient method of remote ecological monitoring of the seafloor (REMOTS system). Mar. Ecol. Prog. Ser. 8:115-128.

Rhoads, D.C. and L.F. Boyer, 1982. The effects of Marine Benthos on Physical Properties of Sediments: A Successional Perspective. In: P.L. McCall and M.J.S. Tevesz (eds.), Animal-Sediment Relations, The Biogenic Alteration of Sediments. Plenum Press, New York, NY, pp. 3-52.

Rhoads, D.C. and J.D. Germano, 1986. Interpreting long-term changes in benthic community structure: a new protocol. Hydrobiologia, 142: 291-308.

Richardson, W. J., C. R. Greene, Jr., C. I. Malme, and D. H. Thomson, 1995. Marine Mammals and Noise. Academic Press, San Diego, 576 pp.

Ridgway, S.H., E.G. Wever, J.G. McCormick, J. Palin, and J.H. Anderson, 1969. Hearing in the giant sea turtle, *Chelonia mydas*. Proceedings of the National Academy of Sciences, 64(3): 884-890.

Rine, J.M., R.W. Tillman, W.L. Stubblefield, and D.J.P. Swift, 1986. Lithostratigraphy of Holocene sand ridges from the nearshore and middle continental shelf of New Jersey, U.S.A. In: T.F. Moslow and E.G. Rhodes (editors), Modern and Ancient Shelf Clastics: A Core Workshop. SEPM Core Workshop No. 9, Tulsa, OK, p. 1-72.

Rine, J.M., R.W. Tillman, S.J. Culver, and D.J.P. Swift, 1991. Generation of Late Holocene ridges on the middle continental shelf of New Jersey, USA – evidence for formation in a mid-shelf setting based upon comparison with a nearshore ridge. In: D.J.P. Swift, G.F. Oertel, and R.W. Tillman (editors), Shelf Sand and Sandstone: Geometry, Facies, and Sequence Stratigraphy. International Association of Sedimentologists, Special Publication 14, p. 395-426.

Robins, C.R., 1957. Effects of storms on the shallow-water fish fauna of southern Florida with records of fishes from Florida. Bulletin of Marine Science in the Gulf and Caribbean, 7(3): 266-275.

Roden, C., 1998. Cruise results: Summer Atlantic Marine Mammal Survey, NOAA Ship Relentless Cruise RS 98-01(3). National Marine Fisheries Service, Southeast Fisheries Science Center, Mississippi Laboratories, Pascagoula Facility, Pascagoula, MS.

Rogers, R.M., 1977. Trophic Interrelationships of Selected Fishes on the Continental Shelf of the Northern Gulf of Mexico. Ph.D. dissertation, Texas A&M University, College Station, TX, 244 pp.

Rosati, J.D. and N.C. Kraus, 1991. Practical Considerations in Longshore Transport Calculations. CETN II-24, U.S. Army Engineer Waterways Experiment Station, Coastal and Hydraulics Laboratory, Vicksburg, MS, 6 pp.

Rosenthal, H.S., 1971. Effects of “red mud” on embryos and larvae of the herring *Clupea harengus*. Helgolaender Wiss. Meeresuntersuchungen, 22: 366-376.

Rosman, I., G.S. Boland, L. Martin, and C. Chandler, 1987. Underwater Sightings of Sea Turtles in the Northern Gulf of Mexico. U.S. Department of the Interior, Minerals Management Service, Gulf of Mexico OCS Region, New Orleans, LA, OCS Study MMS 87-0107, 37 pp.

Rotunno, T. and R.K. Cowen, 1997. Temporal and spatial spawning patterns of the Atlantic butterfish, *Peprilus triacanthus*, in the South and Middle Atlantic Bights. Fishery Bulletin, 95(4): 785-799.

Saloman, C.H., 1974. Physical, Chemical, and Biological Characteristics of Nearshore Zone of Sand Key, Florida, Prior to Beach Restoration. National Marine Fisheries Service, Gulf Coastal Fisheries Center, Panama City Laboratory, Panama City, FL.

Saloman, C.H., S.P. Naughton, and J.L. Taylor, 1982. Benthic Community Response to Dredging Borrow Pits, Panama City Beach, Florida. U.S. Army Corps of Engineers, Coastal Engineering Research Center, Fort Belvoir, VA, Miscellaneous Report No. 82-3, 138 pp.

Sanders, H.L., 1958. Benthic studies of Buzzards Bay. I. Animal-sediment relationships. Limnology and Oceanography, 3: 245-258.

Sanders, J.E. and N. Kumar, 1975. Holocene shoestring sand on the inner continental shelf off Long Island, New York. American Association of Petroleum Geologists Bulletin, 59: 997-1009.

SAS Institute Inc., 1989. SAS/STAT Users Guide, Version 6, Fourth Edition, Volume 1. SAS Institute Inc., Cary, NC, 943 pp.

Sawaragi, T. and I. Deguchi, 1978. Distribution of Sand Transport Rate Across a Surf Zone. Proceedings, 16th International Conference on Coastal Engineering, ASCE, pp. 1,596-1,613.

Schaeff, C.M., S.D. Kraus, M.W. Brown, and B.N. White, 1993. Assessment of the population structure of western North Atlantic right whales (*Eubalaena glacialis*) based on sighting and mtDNA data. Canadian Journal of Zoology, 71(2): 339-345.

Schlee, J.S., 1964. New Jersey offshore gravel deposit. Pit and Quarry, 57: 80-81.

Scott, L.C. and F.S. Kelley, 1998. An Evaluation and Comparison of Benthic Community Assemblages and Surf Clam Populations Within the Offshore Sand Borrow Site for the Great Egg Harbor Inlet and Peck Beach, Ocean City, New Jersey Project. Prepared for the U.S. Army Corps of Engineers, Philadelphia District, Philadelphia, PA by Versar, Inc., Columbia, MD, 36 pp. + app.

Shalowitz, A.L., 1964. Shoreline and Sea Boundaries, Volume 2. U.S. Department of Commerce Publication 10-1, U.S. Coast and Geodetic Survey, U.S. Government Printing Office, Washington, DC, 420 pp.

Shaver, D.J., 1991. Feeding ecology of wild and headstarted Kemp's ridley sea turtles in South Texas waters. Journal of Herpetology, 25(3): 327-334.

Sherk, J.A., Jr., 1971. The Effects of Suspended and Deposited Sediment on Estuarine Organisms: Literature Summary and Research Needs. University of Maryland, Natural Resources Institute, Chesapeake Biological Laboratory Contribution No. 43, 73 pp.

Sherk, J.A., Jr., 1972. Current status of the knowledge of the biological effects of suspended and deposited sediments in Chesapeake Bay. Chesapeake Science 13 (Suppl.): S137-S144.

Sherk, J.A., Jr. and L.E. Cronin, 1970 The Effects of Suspended and Deposited Sediments on Estuarine Organisms, an Annotated Bibliography of Selected References. University of Maryland, Chesapeake Biological Laboratory, Natural Resources Institute, Reference No. 70-19, 62 pp.

Sherk, J.A., J.M. O'Connor, and D.A. Newman, 1975. Effects of Suspended and Deposited Sediments on Estuarine Environments. In: L.F. Cronin (ed.), Estuarine Research Volume 2. Academic Press, New York, NY, pp. 541-558.

Sherman, K., R.J. Green, J.R. Goulet, and L. Ejsymont, 1983. Coherence in zooplankton of a large northwest Atlantic ecosystem. Fishery Bulletin, 81(4): 855-862.

Sherman, K., W. Smith, W. Morse, M. Berman, J. Green, and L. Ejsymont, 1984. Spawning strategies of fishes in relation to circulation, phytoplankton production, and pulses in zooplankton off the northeastern United States. Marine Ecology Progress Series, 18: 1-19.

Shields, I.A., 1936. Application of similarity principles and turbulence research to bed-load movement (in German). Mitteilunden der Preoss. Versuchsanst. Fur Wasserbau and Schiffbau, Berlin, No. 26.

Slay, C.K., 1995. Sea Turtle Mortality Related to Dredging Activities in the Southeastern U.S.: 1991. In: J.I. Richardson and T.H. Richardson (comps.), Proceedings of the Twelfth Annual Workshop on Sea Turtle Biology and Conservation, Jekyll Island, GA, NOAA Technical Memorandum NMFS-SEFSC-361, pp. 132-133.

Smith, J.D., 1977. Modeling of Sediment Transport on Continental Shelves. In: The Sea, Volume 6, Edited by Goldberg, E.D., McCave, I.N., O'Brien, J.J., and Steele, J.H., Wiley-Interscience, New York, NY.

Smith, P.C., 1996. Nearshore Ridges and Underlying Upper Pleistocene Sediments on the Inner Continental Shelf of New Jersey. Masters Thesis, Rutgers University, Geological Sciences, New Brunswick, NJ, 157 p.

Smith, W.G. (ed.), 1988. Analysis and Evaluation of Ichthyoplankton Survey Data from the Northeast Continental Shelf Ecosystem. NOAA-TM-NMFS-F/NEC-57, 133 pp.

Smith, W. and W. Morse, 1988. Seasonal Distribution, Abundance, and Diversity Patterns of Fish Eggs and Larvae in the Middle Atlantic Bight. In: A.L. Pacheco (ed.), Characterization of the Middle Atlantic Water Management Unit of the Northeast Regional Action Plan. NOAA-TM-NMFS-F/NEC- 56, pp. 177-189.

Smith, W., P. Berrien, and T. Potthoff, 1994. Spawning patterns of bluefish, *Pomatomus saltatrix*, in the northeast continental shelf ecosystem. Bulletin of Marine Science, 54(1): 8-15.

Snedden, J.W., R.W. Tillman, R.D. Kreisa, W.J. Schweller, S.J. Culver, and R.D. Winn, 1994. Stratigraphy and genesis of a modern shoreface-attached sand ridge, Peahala Ridge, New Jersey. Journal of Sedimentary Research, Section B: Stratigaphy and Global Studies, B64(4): 560-581.

Snelgrove, P.V.R. and C.A. Butman. 1994. Animal-sediment relationships revisited: Cause versus effect. Oceanography and Marine Biology Annual Review, 32: 111-177.

Stephenson, W.W.T., S.D. Cook, and S.J. Newlands, 1978. The macrobenthos of the Middle Banks of Moreton Bay. Mem. Queensl. Mus., 18: 95-118.

Stern, E.M. and W.B. Stickle, 1978. Effects of Turbidity and Suspended Material in Aquatic Environments: Literature Review. U.S. Army Engineer Waterways Experiment Station, Vicksburg, MS, Technical Report D-78-21, 117 pp.

Stubblefield, W.L., J.W. Lavelle, D.J.P. Swift, and T.F. McKinney, 1975. Sediment response to the present hydraulic regime on the central New Jersey shelf. Journal of Sediment Petrology, 45: 337-358.

Stubblefield, W.L. and D.J.P. Swift, 1981. Grain size variations across sand ridges, New Jersey continental shelf, U.S.A. Geo-Marine Letters, 1: 45-48.

Stubblefield, W.L., D.W. McGrail, and D.G. Kersey, 1984. Recognition of transgressive and post-transgressive sand ridges on the New Jersey continental shelf. In: R.W. Tillman and C.T. Siemers (editors), Siliclastic Shelf Sediments, Society of Economic Paleontologists and Mineralogists, Special Publication 34, p. 1-23.

Studt, J.F., 1987. Amelioration of Maintenance Dredging Impacts on Sea Turtles, Canaveral Harbor, Florida. In: W. Witzell (ed.), Ecology of East Florida Sea Turtles. Proceedings of the Cape Canaveral, Florida Sea Turtle Workshop, Miami, FL, NOAA Technical Report NMFS 53, pp. 55-58.

Sullivan, B.K. and D. Hancock, 1977. Zooplankton and dredging: Research perspectives from a critical review. Water Research Bulletin, 13(3): 461-468.

Svendson, I.A., and I.G. Jonsson, 1976. Hydrodynamics of Coastal Regions. Technical University of Denmark, 285 pp.

Swift, D.J.P., 1976. Continental shelf sedimentation. In: D.J. Stanley and D.J.P. Swift (editors), Marine Sediment Transport and Environmental Management. Wiley and Sons, New York, NY, p. 311-350.

Swift, D.J.P., J.W. Kofoed, F.P. Salsbury, and P. Sears, 1972. Holocene evolution of the shelf surface, central and southern Atlantic shelf of North America. In: D.J.P. Swift, D.B Duane, and O.H. Pilkey (editors), Shelf Sediment Transport: Process and Pattern. Dowden Hutchinson, and Ross. Stroudsburg, PA, p. 499-575.

Swift, D.J.P., D.B. Duane, and T.F. McKinney, 1973. Ridge and swale topography of the Middle Atlantic Bight, North America: Secular response to the Holocene hydraulic regime. Marine Geology, 15: 227-247.

Swift, D.J.P and M.E. Field, 1981. Evolution of a classic sand ridge field: Maryland sector, North American inner shelf. Sedimentology, 28: 461-482.

Swift, D.J.P. and A.W. Niedoroda, 1985. Fluid and Sediment Dynamics on Continental Shelves. In: Tillman, R.W., D.J.P. Swift, and R.G. Walker (editors), Shelf Sands and Sandstone Reservoirs, SEPM Short Course No. 13, Tulsa, OK, pp. 47-133.

Swingle, W.M., S.G. Barco, T.D. Pitchford, W.A. McLellan, and D.A. Pabst, 1993. Appearance of juvenile humpback whales feeding in the nearshore waters of Virginia. Mar. Mamm. Sci., 9(3): 309-315.

Tanaka H. and N. Shuto, 1981. Friction coefficient for a wave-current coexisting system. Coastal Engineering of Japan, 24: 105-128.

Taylor, A.S., 1990. The Hopper Dredge. In: D.D. Dickerson and D.A. Nelson (comps.), Proceedings of the National Workshop on Methods to Minimize Dredging Impacts on Sea Turtles, Jacksonville, FL, U.S. Army Engineer Waterways Experiment Station, Vicksburg, MS, Miscellaneous Paper EL-90-5, pp. 59-63.

Taylor, A.S., 1999. Personal communication with Mark Byrnes.

Terceiro, M., 1998. Bluefish. In: S.H. Clark (ed.), Status of Fishery Resources off the Northeastern United States for 1998. U.S. Department of Commerce, NOAA Tech. Mem. NMFS-NE-115, pp. 110-111.

Thayer, C.W., 1983. Sediment-mediated Biological Disturbance and the Evolution of Marine Benthos. In: M.J.S. Tevesz and P.L. McCall (eds.), Biotic Interactions in Recent and Fossil Benthic Communities. Plenum Press, NY, pp. 479-625.

Theroux, R.B. and R.L. Wigley, 1998. Quantitative Composition and Distribution of the Macrobenthic Invertebrate Fauna of the Continental Shelf Ecosystems of the Northeastern United States. U.S. Department of Commerce, Seattle, WA, NOAA Technical Report NMFS 140, 240 pp.

Thistle, D., 1981. Natural physical disturbances and communities of marine soft bottoms. Marine Ecology Progress Series, 6: 223-228.

Thompson, J.R., 1973. Ecological Effects of Offshore Dredging and Beach Nourishment: A Review. U.S. Army Engineer Waterways Experiment Station MP 1-73, U.S. Army Corps of Engineers, Coastal Engineering Research Center, Fort Belvoir, VA, Report 1-73.

Thornton, E.B. and R.T. Guza, 1983. Transformation of wave height distribution. Journal of Geophysical Research, 88: 5,925-5,938.

Thornton, E.B. and R.T. Guza, 1989. Models for Surf Zone Dynamics. In: Nearshore Sediment Transport, R.J. Seymour, (ed.), Plenum Press, New York, NY, pp. 337-369.

Thorson, G., 1957. Bottom communities (sublittoral or shallow shelf). Geological Society of America Memoir, 67: 461-534.

Thorson, G., 1966. Some factors influencing the recruitment and establishment of marine benthic communities. Netherlands Journal of Sea Research, 3(2): 267-293.

Trowbridge, J. and O. Madsen, 1984. Turbulent wave boundary layers, 1. model formulation and first-order solution. Journal of Geophysical Research, 89: 7,989-7,997.

Trowbridge, J. and V.C. Agrawal, 1995. Glimpses of a wave boundary layer. Journal of Geophysical Research, 100: 729-744.

Turbeville, D.B. and G.A. Marsh, 1982. Benthic Fauna of an Offshore Borrow Area in Broward County, Florida. U.S. Army Corps of Engineers, Coastal Engineering Research Center, Miscellaneous Report 82-1, 43 pp.

Uchupi, E., 1968. Atlantic Continental Shelf and Slope of the United States – Physiography. U.S. Geological Survey Professional Paper 529-C, 30 p.

Uchupi, E., 1970. Atlantic Continental Shelf and Slope of the U.S. – Shallow Structure. U.S. Geological Survey Professional Paper 529-I, 44 p.

Uptegrove, J., L.G. Mulliken, J.S. Waldner, G.M. Ashley, R.E. Sheridan, D.W. Hall, J. Gillroy, and S. Farrell, 1995. Characterization of Offshore Sediments in Federal Waters as Potential Sources of Beach Replenishment Sand – Phase I. Open File Report OFR 95-1, New Jersey Geological Survey, Trenton, NJ, 148 p.

Uptegrove, J., J.S. Waldner, D.W. Hall, P.C. Smith, G.M. Ashley, R.E. Sheridan, Z. Allen-Lafayette, M.C. Goss, F.L. Muller, and E. Keller, 1997. Characterization of Offshore Sediments in Federal Waters as Potential Sources of Beach Replenishment Sand – Phase II. Final Report to U.S. Minerals Management Service, Cooperative #14-35-0001-30751, New Jersey Geological Survey, Trenton, NJ, 28 p.

USACE, 1984. Shore Protection Manual. U.S. Army Engineer Waterways Experiment Station, Coastal Engineering Research Center, Vicksburg MS.

USACE, 1996. Brigantine Inlet to Great Egg Harbor Inlet Absecon Island Interim Feasibility Study, Volume I. U.S. Army Corps of Engineers New Jersey Protection Study, Philadelphia District, Philadelphia, PA.

USACE, 1997. Townsends Inlet to Cape May Inlet Feasibility Study. U.S. Army Corps of Engineers New Jersey Shore Protection Study, Philadelphia District, Philadelphia, PA.

USACE, 1999. Hopper dredge sea turtle deflector draghead and operational requirements. Web page http://www.saj.usace.army.mil/pd/turtle.htm.

USEPA, 1997. Supplement to the Environmental Impact Statement on the New York Dredged Material Disposal Site Designation for the Designation of the Historic Area Remediation Site (HARS) in the New York Bight apex. Prepared by U.S. Environmental Protection Agency, Region 2, New York, NY with the assistance of Battelle, Duxbury, MA.

Valente, R.M., D.C. Rhoads, J.D. Germano and V.J. Cabelli. 1992. Mapping of benthic enrichment patterns in Narragansett Bay, Rhode Island. Estuaries 15:1-17.

Van Dolah, R.F., 1996. Impacts of Beach Nourishment on the Benthos: What Have We Learned? Proceedings of the Twenty-fourth Annual Benthic Ecology Meeting, Columbia, SC, p. 82.

Van Dolah, R.F., D.R. Calder, and D.M. Knott, 1984. Effects of dredging and open-water disposal on benthic macroinvertebrates in a South Carolina estuary. Estuaries, 7: 28-37.

Van Dolah, R.F., P.H. Wendt, R.M. Martore, M.V. Levisen, and W.A. Roumillat, 1992. A Physical and Biological Monitoring Study of the Hilton Head Beach Nourishment Project. Final Report submitted to the Town of Hilton Head Island and South Carolina Coastal Council by the South Carolina Wildlife and Marine Resources Department, Marine Resource Research Institute, 159 pp.

Van Dolah, R.F., R.M. Martore, and M.V. Levisen, 1993. Supplemental Report for the Physical and Biological Monitoring Study of the Hilton Head Beach Nourishment Project. Prepared by the South Carolina Marine Resources Division, Marine Resources Research Institute for the for the Town of Hilton Head Island, SC.

Van Dolah, R.F., B.J. Digre, P.T. Gayes, P. Donovan-Ealy, and M.W. Dowd, 1998. An Evaluation of Physical Recovery Rates in Sand Borrow Sites Used for Beach Nourishment Projects in South Carolina. Final report to the U.S. Department of the Interior, Minerals Management Service, Office of International Activities and Marine Minerals by the South Carolina Department of Natural Resources, Marine Resources Research Institute, 76 pp. + app.

Vecchione, M., 1981. Aspects of the early life history of *Loligo pealei* (Cephalopoda; Myopsida). Journal of Shellfish Research, 1: 171-180.

Versar, Inc., 1997. An Evaluation and Assessment of the Benthic Macroinvertebrate Resources of the Proposed Sand Borrow Areas for Lower Cape May Meadows, New Jersey. Report prepared for the U.S. Army Corps of Engineers, Philadelphia District, Philadelphia, PA, Contract No. DACW61-95-D-0011.

Viles, C. and R.J. Diaz, 1991. Bencore, an image analysis system for measuring sediment profile camera slides. School of Marine Science, Virginia Institute of Marine Science, College of William and Mary, Gloucester Pt. VA. 13 pp.

Vincent, C.L. and M.J. Briggs, 1989. Refraction-diffraction of irregular waves over a mound. Journal of Waterway Port, Coastal And Ocean Engineering, 115(2): 269-284.

Vinyard, G.L. and J.W. O'Brien, 1976. Effects of light and turbidity on the reactive distance of bluegill (*Lepomis macrochirus*). Journal of the Fisheries Research Board of Canada, 33: 2,845-2,849.

Viscido, S.V., D.E. Stearns, and K.W. Able, 1997. Seasonal and spatial patterns of an epibenthic crustacean assemblage in northwest Atlantic Continental Shelf waters. Estuarine, Coastal, and Shelf Science, 45: 377-392.

Vismann, B., 1991. Sulfide tolerance: Physiological mechanisms and ecological implications. Ophelia 34:1-27.

Walker, T.A. and G. O'Donnell, 1981. Observations on nitrate, phosphate and silicate in Cleveland Bay, Northern Queensland. Australian Journal of Marine and Freshwater Research, 32: 877-887.

Weber, M., 1995. Kemp's Ridley Sea Turtle, *Lepidochelys kempii*. In: P.T. Plotkin (ed.), National Marine Fisheries Service and U. S. Fish and Wildlife Service Status Reviews for Sea Turtles Listed under the Endangered Species Act of 1973. Silver Spring, MD.

Weinberg, J.R., 1998a. Altantic Surfclam. In: S.H. Clark (ed.), Status of Fishery Resources off the Northeastern United States for 1998. U.S. Department of Commerce, NOAA Tech Mem. NMFS-NE-115, pp. 125-127

Weinberg, J.R., 1998b. Density-dependent growth in the Atlantic surfclam, *Spisula solidissima*, off the coast of the Delmarva Peninsula, USA. Marine Biology, 130: 621-630.

Werner, S.A. and A.M. Landry, Jr., 1994. Feeding ecology of Wild and Head Started Kemp's Ridley Sea Turtles (*Lepidochelys kempii*). In: K.A. Bjorndal, A.B. Bolten, D.A. Johnson, and P.J. Eliazar (comps.), Proceedings of the Fourteenth Annual Symposium on Sea Turtle Biology and Conservation, NOAA Tech. Memo. NMFS-SEFSC-351, U.S. Department of Commerce, Miami, FL, p. 163.

Wicker, C.F., 1951. History of the New Jersey Coastline. Proceeding of the 1st Conference on Coastal Engineering, Long Beach, CA, p. 299-319.

Wiegel, R.L. and T. Saville, 1996. History of coastal engineering in the USA. In: N.C. Kraus (editor), History and Heritage of Coastal Engineering, American Society of Civil Engineers, New York, NY, p. 513-600.

Wigley, R.L. and R.B. Theroux, 1981. Atlantic Continental Shelf and Slope of the United States-Macrobenthic Invertebrate Fauna of the Middle Atlantic Bight Region-Faunal Composition and Quantitative Distribution. U.S. Geological Survey Professional Paper 529-N, 198 pp.

Wilber, P. and M. Stern, 1992. A Re-examination of Infaunal Studies That Accompany Beach Nourishment Projects. In: New Directions in Beach Management: Proceedings of the 5th Annual National Conference on Beach Preservation Technology, Florida Shore and Beach Preservation Association, Tallahassee, FL, pp. 242-257.

Wiley, D.N., R.A. Asmutis, T.D. Pitchford, and D.P. Gannon, 1995. Stranding and mortality of humpback whales, Megaptera novaeangliae, in the mid-Atlantic and southeast United States, 1985-1992. Fishery Bulletin, 93: 196-205.

Williams, R.G., and F. A. Godshall, 1977. Summarization and interpretation of historical physical oceanographic and meteorological information for the mid-Atlantic region. Interagency Agreement AA550-IA6-12. Prepared by NOAA for the Bureau of Land Management. 295 pp.

Williams, S.J., 1992. Coasts in Crisis. U.S. Geological Survey Circular 1075, 32 pp.

Winer, H., 1988. Numerical Modeling of Wave-Induced Currents Using a Parabolic Wave Equation. Technical Report No. 80, Dept. of Coastal and Oceanographic Engineering, University of Florida, Gainesville, FL.

Winn, H.E. (ed.), 1982. A Characterization of Marine Mammals and Turtles in the Mid- and North Atlantic Areas of the U.S. Outer Continental Shelf. Final report of the Cetacean and Turtle Assessment Program. University of Rhode Island, Kingston, RI, Prepared for U.S. Department of the Interior, Bureau of Land Management, Washington, DC, Available through National Technical Information Service, Springfield, VA, PB83-215855.

Woodworth-Lynas, C. and L. Davis, 1996. Proposed Marine Mining Technologies and Mitigation Techniques: A Detailed Analysis with Respect to the Mining of Specific Offshore Mineral Commodities. Final Report. Prepared by the Centre for Cold Ocean Resources Engineering for the U.S. Department of the Interior, Minerals Management Service. Contract No. 14-35-0001-30723, OCS Report MMS 95-0003, 279 pp. + 6 Appendices.

Wright, D.G., 1977. Artificial Islands in the Beaufort Sea: A Review of Potential Impacts. Department of Fisheries and Environment, Winnipeg, Manitoba, 38 pp.

Yan, Y., 1987. Numerical Modeling of Current and Wave Interactions on an Inlet-beach System. Technical Report No. 73, Dept. of Coastal and Oceanographic Engineering, University of Florida, Gainesville, FL.

Young D. and D. Rhoads, 1971. Animal-sediment relations in Cape Cod Bay, Massachusetts. I. A transect study. Marine Biology, 11: 242-54.

Zajac, R.N. and R.B. Whitlatch, 1982. Responses of estuarine infauna to disturbance. I. Spatial and temporal variation of initial recolonization. Marine Ecology Progress Series, 10: 1-14.

Zawila, J. S., 1994. Analysis of a Seismic Air Gun Acoustic Dispersal Technique at the Fort Pierce Sea Turtle Trial Site. Contract report to U.S. Army Engineer Waterways Experiment Station, as excerpted in: Sea Turtle Research Program Summary Report. Prepared by U.S. Army Engineer Waterways Experiment Station, Vicksburg, MS for U.S. Army Engineer Division, South Atlantic, Atlanta, GA and U.S. Naval Submarine Base, Kings Bay, GA, Technical Report CHL-97-31, NTIS ADA332588, 147 pp.